Concentrations and fluxes of atmospheric biogenic volatile organic compounds by proton transfer reaction mass spectrometry

Pawel K. Misztal

This thesis has been submitted in fulfilment of university requirements to the School of Chemistry, College of Science and Engineering at the University of Edinburgh for the degree of Doctor of Philosophy.

A copy of this thesis has been sent to Danum Valley Field Centre Library and the Sabahmas Oil Palm Plantation.

2010

Declaration

I, Pawel Misztal, declare that this thesis contains only my genuine work except where stated otherwise in the text and it has not been presented either in whole or in part for a degree at any other university. If any portion of the work was done in a collaborative effort then the degree and means of my personal contribution are acknowledged.

Acknowledgements

I would like first to express enormous gratitude to my supervisors: Prof. Neil Cape and Dr. Mat Heal, for their excellent guidance, suggestions, expertise, mentoring, friendship, the financial support of my PhD, and greatly appreciated generosity in supporting my attendances to various conferences, meetings, campaigns, and workshops. Secondly a huge thank-you I send to my informal co-supervisor Dr. Eiko Nemitz for his exceptionally inspireful mastermind leadership in the jungle and oil palm, excellent solutions to obstacles in programming, troubleshooting and data analysis, and sharing his fascination and expertise in atmospheric sciences.

Then I would like to thank Dr. Ben Langford for sharing his genial experience in LabVIEW programming and for his fruitful collaboration and friendship throughout my entire PhD. It was a huge fun to work closely on various fascinating ideas. Many thanks to Dr. Emily House for giving me an intensive, thorough and inspireful training in PTR-MS in the first few months of my PhD. Special gratefulness I owe to Dr. Susan Owen, the queen of gas chromatography, for the skill-transfer and teaching me the royal etiquette; to Dr. Tony Dore for his encouragement, mentoring, and raising my scientific confidence and research skills.

In addition, I would like to acknowledge the following CEH colleagues, who have helped me during realisation of my PhD: Prof. David Fowler, Dr. Mike Billett, Dr. Mark Sutton, Mrs Davis Innes, Dr. Chiara DiMarco, Dr. Gavin Phillips, Frank Harvey, Dr. Mhairi Coyle, Dr. Carole Helfter, John Kentisbeer, Dr. Daniela Famulari, Robert Storeton-West, Dr. Daniel Chapman, Dr. Adam Vanbergen, Dr. Laurence Carvalho, Dr. Lucy Sheppard, Dr. Witold Wachowiak, Dr. Julia Drewer, Dr. Sarah Burthe and others.

I am also grateful to all my fellow PhD students at CEH and Chemistry department who were a brilliant laugh, entertainment and part of nice social experiences.

Acknowledgements

Particularly I would like to thank James Ryder, with whom I shared three different offices, for his help on various aspects of life in Britain, helpfulness and collaboration in Griffin Forest and in the jungle in Borneo. I shall mention also the following students from CEH and Chemistry at the University of Edinburgh who had particular significance in my PhD life: Dr. Juan Manuel Gonzalez-Benitez, Dr. David Galbraith, Matti Salmela, Emily Barlow, Iain Proctor, Debbie Polson, Sanna Kivimaki, Esther Vogt, Lara Salido, Nichola Copeland, Susanne Steinle, Ying Zhang, Dr. Catherine Hardacre, Dr. Emanuel Blei, Mark Hammonds, and Jambery Siong.

Many thanks to ACCENT, OP3 and ACES groups, and particularly to:
Lancaster: Prof. Nick Hewitt, Dr. Annette Ryan, Dr. Brian Davison, Tom Pugh, Kirsti Ashworth, Dr. Malcolm Possel, Prof. Nick Chapel, Dr. Rob MacKenzie, Dr. Annette Ryan and others.
Leeds: Dr. Kate Furneaux, Pete Edwards, Dwayne Heard, Dave Edwards
Manchester: Dr. Niall Robinson, Dr. James Dorsey, Prof. Gordon McFiggans
Cambridge: Rachel Pike, Dr. Andrew Robinson, Prof. John Pyle, Paul Young, Nicola Warwick
Leicester: Prof. Paul Monks, Dr. Virginia Nicolas-Perea, Arunasalam Karunaharan
York: Jim Hopkins, James Lee
Norwich: Prof. Dave Oram, Dr. Graham Mills, Hanna Newton
Italian team: Prof. Francesco Loreto, Dr. Stan Cieslik, Dr. Silvano Farez,
I wish to thank all the people in Sabah, Malaysia, who helped me during my time spent there. Especially Glen Reynolds, Alex Karolus, Johnny, Danum Valley Field Centre and the management of Sabahmas oil palm plantation, particularly Mr Foo, Mr. Chiang, Mr. Yap for hospitality.

Special gratefulness I would like to express to the American team: Alex Guenther for his brilliant ideas and expertise in BVOC, Chris Geron for nice suggestions, Rei Rasmussen for his help in anisole chemistry, Peter Harley for sharing his monoterpene standard.

Finally, I would like to enormously thank my family: my wife Gosia and my daughter Claudia for their continuing support throughout.

Thesis abstract

There are few published direct measurements of the atmosphere-surface exchange of volatile organic compounds (VOCs), particularly for biogenic VOCs (BVOCs). Global modelling of atmospheric chemistry and transport of BVOCs has large uncertainties due to the very small number of measurements in tropical regions, which are responsible for half the global BVOC emissions.

This thesis presents direct measurements of concentrations and ecosystem fluxes of BVOCs in different regions (Tropics, Mediterranean) using the approach of virtual disjunct eddy covariance (vDEC) combined with proton transfer reaction mass spectrometry (PTR-MS) – a real-time BVOC sensor. The field measurements also included methodological developments of the vDEC/PTR-MS approach, which will be of value to the wider flux measurement community. A novel approach to determining the lag time between the vertical wind measurement and the air concentration measurement has been developed that will greatly reduce the uncertainty in the derived flux measurements. In the laboratory, the selectivity of PTR-MS was investigated by designing an alternating drift-voltage mode (AD-PTR-MS) to discriminate between structural isomers detected at the same *m/z* channel, with monoterpenes used as model compounds.

The results of the measurements, particularly from the rainforest and oil palm plantations in Borneo, are novel and therefore provide important experimental constraints on models of atmospheric emissions, chemistry and transport. For example, although parameters which work reasonably well can be derived for model algorithms for the emission of isoprene from the rainforest, their performance over oil palms was less good, because of circadian controls of emissions from oil palms. However, the larger problem is the measured basal emission rates (BERs) which are significantly smaller than those used by default in the global MEGAN model.

Another novel finding was the high deposition velocities of MVK and MACR (isoprene first order oxidation products) which at the oil palm plantation commonly exceeded 1 cm s^{-1}; this result has implications for atmospheric modelling. The successful field results relied on significant developments in software for data acquisition and processing, and operational optimisation of the PTR-MS instruments in the extreme humidity encountered during the fieldwork in Borneo.

Table of contents

List of Tables

List of Figures

List of acronyms

ACCENT	Atmospheric Composition Change the European Network of Excellence
ACES	Aerosol Coupling in the Earth System
AD	Alternating Drift-Voltage
AMOB	1-Allyl-4-MethOxyBenzene
AMS	Aerosol Mass Spectrometry
ANVOCs	Anthropogenic Volatile Organic Compounds
ATP	Adenosine-5'-triphosphate
AVG	Average peak location in the CC function
AVOCs	Anthropogenic Volatile Organic Compounds
BER	Basal Emission Rate
BSOA	Biogenic Secondary Organic Aerosol
BVOC	Biogenic Volatile Compound
CALC	Calculated lag time
CC	Cross-Correlation function; covariance function
CEH	Centre for Ecology & Hydrology
CID	Collision Induced Dissociation
CIMS	Chemical Ionisation Mas Spectrometry
DDE	Dynamic Data Exchange
DEC	Disjunct Eddy Covariance
DMAPP	Dimethylallyl pyrophosphate
DMS	Dimethyl sulphide
EC	Eddy Covariance
ECHO	Emission and CHemical Transformation of Biogenic Volatile Organic Compounds
EDGAR	Emissions Database for Global Atmospheric Research
EPA	Environmental Protection Agency
FID	Flame Ionisation Detection
FIS	Fast Isoprene Sensor
FSG	The Fuller, Schettler and Giddings method of estimating diffusion coefficients in air
FSG/LaBas	FSG method using molar volume LaBas estimates for calculating diffusivities
FTIR	Fourier transform infrared spectroscopy
G06	Guenther et al. (2006) algorithm
G95	Guenther et al. (1995) algorithm
GABRIEL	Guyanas Atmosphere-Biosphere exchange and Radicals Intensive Experiment with the Learjet
GAW	Global Atmospheric Watch
GC	Gas Chromatography
GC-FID	Gas Chromatography with Flame Ionisation Detection
GC-MS	Gas Chromatography – Mass Spectrometry
GEIA	Global Emissions Inventory Activity
GMT	Greenwich Mean Time
HA	Hydroxyacetone

HS	High Sensitivity
ID	Internal diameter
IEPOX	Isoprene epoxides
IMED	Internal Median lag time method
IPCC	Intergovernmental Panel on Climate Change
IRGA	Infra Red Gas Analyser
ISOPOOH	Isoprene hydroxyhydroperoxides
IUPAC	International Union of Pure and Applied Chemistry
LAI	Leaf Area Index
LOD	Limit of Detection
LT	Lag Time
LTV	Lag Time Validity
LU	Lancaster University
MACR	Methacrolein
MAX	Lag time derived from the absolute maximum in the CC function
MBO	2-Methyl-3-buten-2-ol
MCM	Master Chemical Mechanism
MEGAN	Model of Emissions of Gases and Aerosols from Nature
MID	Multiple Ion Detection
MIM2	Mainz Isoprene Mechanism 2
MPAN	Peroxymethacryloyl nitrate
MS	Mass spectrometry
MT	Monoterpene
MVK	Methyl Vinyl Ketone
MW	Molecular Weight
N99	Niinemets et al. (1999) model
NADPH	Reduced form of nicotinamide adenine dinucleotide phosphate
NCAR	The National Center for Atmospheric Research
NEAQS	New England Air Quality Study
NERC	Natural Environment Research Council
NMHC	Non-methane hydrocarbons
NMR	Nuclear Magnetic Resonance
NNMF	Non-Negative Matrix Factorisation
NVOCs	Natural Volatile Organic Compounds
OD	Outer diameter
OP3	Oxidant and Particle Photochemical Processes above a South-East Asian tropical rain forest
OVOC	Oxygenated Volatile Organic Compounds
PAN	Peroxy acetyl nitrate
PAR	Photosynthetically Active Radiation
PA	Proton affinity
PBL	Planetary Boundary Layer
PCA	Principal Component Analysis
PF	Peak Finder
PFT	Plant Functional Type
PIT-MS	Proton-Transfer-Reaction Ion Trap Mass Spectrometer
PMF	Positive Matrix Factorization
POCP	Photochemical Ozone Creation Potential

PTFE	Polytetrafluoroethylene
PTR-MS	Proton Transfer Reaction Mass Spectrometry
TOF-PTR-MS	Time of Flight Proton Transfer Reaction Mass Spectrometry
QMS	Quadrupole Mas Spectrometer
QS422	Quadstar program
REA	Relaxed Eddy Accumulation
RH	Relative Humidity
RMM	Relative Molecular Mas
SEM	Secondary Electron Multiplier
SIFT-MS	Selected Ion Flow Tube Mass Spectrometry
SOA	Secondary Organic Aerosol
SQT	Sesquiterpenes
SVOC	Semi-Volatile Organic Compounds
TOF-AMS	Time-of-Flight-Aerosol Mass Spectrometer
UTC	Coordinated Universal Time
VIS	Lag time method based on a visual assessment of the CC function
VMR	Volume Mixing Ratio
VOC	Volatile Organic Compound
WL	The Wilke and Lee method of estimating diffusion coefficients in air
WVP	Water Vapour Pressure
ZA	Zero Air

Preface

"Panta Rei" (Everything is changing)

"…everything is in flux and nothing abides
everything flows and nothing stays fixed
everything is constantly changing and nothing stays the same"

Heraclitus (500 B.C.)

In the environment, in which we humans live, there is a continuous exchange of energy and the entropy of our universe is constantly growing. There is also a continuous flux of matter within a huge and constantly mixed environmental reactor which is our Earth.

The chemical composition of the atmosphere has a great influence on most fundamental physical parameters of the Earth's surface enabling life. This composition, when disturbed by human activity, can have a huge impact on the environment ranging in diversity from the increase in malignant tumours attributed to changes in UV irradiation to global warming and even severe local and global climate anomalies. In the end the superposition of all factors, biogenic and anthropogenic, counts towards climate changes. Despite increasing awareness of environmental concerns caused by greenhouse gas emissions the importance of natural volatile compounds released from living plants is not yet widely established in the general community.

Globally, biogenic volatile organic compounds (BVOCs) constitute approximately 90% of all volatile organic compounds (VOCs) (hydrocarbons excluding methane) emitted to the atmosphere. Although their importance had been noted five decades ago in the blue-haze phenomenon, initially only a very basic suite of chemical compounds was measured, and the analysis time offered by available analytical

instrumentation was far too short to fulfil the requirements for eddy correlation methods used in micrometeorology for direct determination of surface atmosphere exchange. With the advent of fast spectrometric methods, such as PTR-MS about a decade ago, a more precise flux of a much wider range of compounds could be measured although the methodologies are still in the process of development in, for example, studies like this PhD. BVOCs have recently been recognised to play important roles in atmospheric chemistry and climate. For example, they compete with greenhouse gases and pollutants for hydroxyl radicals; are capable of generating biogenic secondary organic aerosols (BSOA); and can form tropospheric pollutants such as ozone, peroxyacyl nitrates (PANs) and a series of epoxides and hydroxyepoxides. Various mechanisms have been proposed for VOC photooxidation, ozonolysis, and the reactions of VOC and their oxygenation-product radicals in nitrogen oxide-rich and –low environments. There are currently contradicting reports on the effect of BVOCs on OH concentration and lifetimes especially at high VOC and low NO_x levels but there is a very small number of OH and VOC measurements in tropical regions which contribute over half of total BVOC emissions. Currently the total emissions from only tropical forests are estimated at 1,300 Tg of carbon per year. Including deposition of some oxygenated products of isoprene (and likely those of monoterpenes) would make a large impact on these estimates. For those reasons it is essential to conduct more atmospheric measurements from all vegetation ecosystems using these most direct approaches in order to gain more confidence in atmospheric modelling and it may be important to include deposition which is currently weakly evidenced in measurements. The author measured high deposition velocities of MVK and MACR which at an oil palm plantation exceeded 1 cm s^{-1}.

Although it is relatively easy to apply classical analytical approaches such as gas chromatography to obtain leaf level basal emission rates (BERs) from vegetative monocultures, it can be extremely difficult to obtain unbiased superposition of BERs from all species making up heterogeneous environments, especially as dense as tropical rainforests, where one of the approaches is to derive the rates for the most representative plants. Even then a bottom-up estimate can be highly uncertain

without corroboration from direct flux measurements from above canopy. On the other hand PTR-MS approaches need concurrently analytical gold standards for excluding interferences at mass spectra from isobaric or fragmented compounds. The goals of this PhD were enormously facilitated by development of substantial software for data acquisition and processing, and operational optimisation of the PTR-MS instruments in extreme humidity, as encountered in Borneo. The first part of the thesis aims to provide the general background in understanding the key concepts of atmospheric chemistry, PTR-MS, micrometeorology and the ecological significance of VOCs.

The practical part of the thesis contains scientific reports of findings, which either have been submitted or are being written for publications. Numerous collaborative publications, to which the author has contributed, are assembled at the end of the thesis in appendices. The author collected more data/ideas than it was possible to thoroughly describe in the timescales prescribed for the PhD. However, these will be further researched as part of future postdoctoral plans, for example exploring the ecological significance of BVOCs in plant and insect communication and VOC signalling in birds, despite the principal interest in atmospheric chemistry, particularly exploring VOCs at gas/aerosol interfaces.

1 Theoretical Part

1.1 Volatile Organic Compounds (VOCs)

1.1.1 Definitions and classifications

There are certain discrepancies in notations used to describe volatile organic compounds (VOCs) in the literature. One of the first terms used to describe them was non-methane hydrocarbons (NMHC) for the purpose of distinction from methane. However, since the word hydrocarbon clearly denotes a molecule consisting of carbon and hydrogen atoms, it seems to exclude oxygenated species such as alcohols, aldehydes, esters, acids as well as compounds containing other heteroatoms. The term VOCs is therefore appropriate to embrace all of these, but the exact definition is still not precise. The US Environmental Protection Agency (EPA) defined a VOC as any compound participating in atmospheric photochemical reactions. In another slightly more quantitative definition VOCs are regarded as those organic species that have a vapour pressure greater than 10 Pa at 25°C, a boiling point of up to 260°C at atmospheric pressure and 15 or less carbon atoms. The remaining compounds are termed semi-volatile organic compounds (SVOCs). This distinction seem sensible, as the semi-volatile compounds, which are more likely to partition into the particle phase, exhibit different transport and chemistry in contrast to volatile gas species.

A separate notion is used for referring to oxygenated volatile organic compounds (OVOCs), which seems right in order to describe oxygen-containing volatile species that, for example, have important roles in atmospheric chemistry, but on the other hand it is not consistent with VOC and SVOC definitions. In addition, one can frequently encounter acronyms like AVOCs or ANVOCs standing for anthropogenic volatile organic compounds in contrast to BVOCs or NVOCs expressing biogenic or natural volatile compounds. In this thesis the term VOC is used for referring to all non-methane volatile organic compounds including oxygenates, while the term

OVOC will be used to specifically emphasise the oxygenated nature of a given compound. The author also likes using the BVOC acronym, when referring to vegetative organic compounds but it must be noted that not all BVOCs are purely biogenic, as some of them can be contained in anthropogenic classifications even though they can also be emitted from vegetation.

1.1.2 VOCs in the environment

Figure 1 is a general schematic of the behaviour of VOCs in the environment.

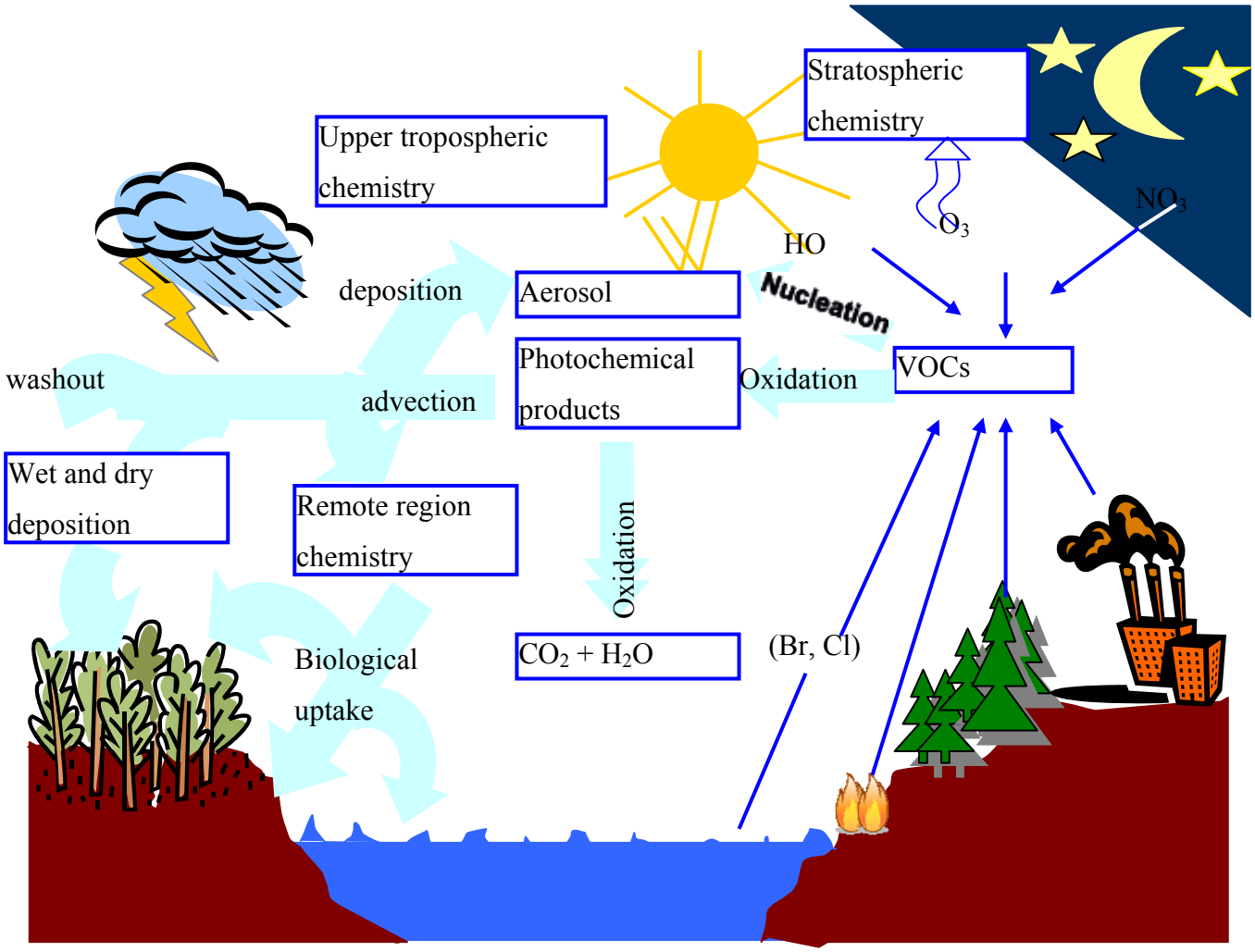

Figure 1.1-1 Sketch of interactions of VOCs in physical and chemical processes in the environment (derived from Koppmann 2007).

VOCs have numerous sources and sinks. Some of them are important pollutants; for example those which arise in combustion processes and also halogenated hydrocarbons. Many of the anthropogenic VOCs are emitted from industrial processes, from heavy traffic in large cities, and from different types of fires. It is still a matter of debate whether biomass burning should be classified as an anthropogenic or a natural process. As biomass burning is often difficult to predict it is quite challenging for modellers to take it into account. For instance, extensive forest fires can instantly introduce copious VOC content into the atmosphere. From satellite observations emissions of this type are estimated as 38 Tg y^{-1} (Ito and Penner, 2004) while current global models estimate the total anthropogenic VOC emissions to amount to 186 Tg y^{-1} (EDGAR, 2005). However, biogenic emissions are estimated to be one order of magnitude higher i.e. 1150 TgC yr^{-1} (Guenther et al., 1995), the main contribution to which is from vegetation and only a small portion is from oceans and soils.

Regardless of their origin, VOCs are known to impact on tropospheric radical chemistry, contributing to ozone as well as secondary organic aerosol formation. By competing with hydrogen oxide radicals they prolong lifetimes of greenhouse gases and other pollutants. Therefore, they can indirectly impact local and global climate changes and can also have influence on global warming potentials. Their degradation pathways are mainly through photooxidation and reacting with OH radicals during the day, and reacting with NO_3 during the night. Ozonolysis and reactions with peroxyradicals can also be important processes in VOC oxidation and degradation. Therefore, vegetative emissions can amplify the detrimental effects of anthropogenic contributions through reaction with NO_x leading to ozone formation. However, not all reactions that VOCs undergo in the atmosphere have been verified experimentally, including partitioning of some them into the aqueous phase and the effects of various nitrogen oxide concentrations on these reactions. One of many examples is the experimental verification of nitrophenol formation by Heal et al. (2007). Nevertheless, only a combination of different-scale field measurements,

aircraft and lab studies can guarantee the most accurate picture and understanding of atmospheric chemistry.

1.1.3 Commonly used analytical techniques

BVOCs can be measured by a range of analytical techniques and over different scales (i.e. leaf, canopy, landscape and regional scale). The most commonly used analytical methods of BVOC concentrations and fluxes have been recently generally reviewed by Misztal et al. (2007) (Appendix II-G).

1.1.3.1 Concentrations

For determination of concentration the most commonly used method is capillary gas chromatography (GC) with flame ionisation detection (FID), and/or mass spectrometry (MS) detection. Such analysis is relatively slow (~30 minutes) but gives both qualitative and quantitative results (e.g. Cape, 1986). To achieve a detection limit as low as part per trillion mixing ratio (ppt), the sample must first be preconcentrated, for example using cryogenic or sorbent principles (Wang and Austin, 2006). Some recent variants of chromatographic instrumentation with better detection and speciation of biogenic compounds involve gas chromatography-time of flight mass spectrometry (GC-TOF/MS) or comprehensive gas chromatography-time of flight mass spectrometry (GCxGC-TOF/MS) (e.g. Saxton et al., 2007)

Another analytical method is Proton Transfer Reaction Mass Spectrometry (PTR-MS), which has been extensively used over the past decade for the quantification of many BVOC (e.g. Warneke et al., 2001; Grabmer et al., 2003; Ammann et al., 2004; Karl and Guenther, 2004; Warneke et al., 2005; Velasco et al., 2007; Langford et al., 2009b; Kim et al., 2010). The advantage of this method is that it has very fast analysis time, of the order of seconds, and sensitivity in the ppt range. However, this method often requires combination with other techniques in order to validate what compounds are contributing to which particular *m/z* channels (e.g. de Gouw et al.,

2003c; de Gouw and Warneke, 2007; Ambrose et al., 2010). On the other hand, the recent development of the Proton Transfer Reaction - Time of Flight - Mass Spectrometer (PTR-TOF-MS) enables much higher mass resolution, thus allowing for the separation and detection of the majority of isobars (Blake et al., 2004; Blake et al., 2009).

1.1.3.2 Fluxes

In order to determine how much of a particular biogenic compound is emitted to the atmosphere or how much is deposited to the surface (which may be in part taken up by plants), it is required to measure and calculate the flux. This can be done by several currently used methods, which include:

1. Leaf cuvettes, which are temperature controlled and connected to a measurement and control system (e.g. Harley et al., 1996). Constituting a leaf gas exchange measurement system, they can be widely used for evaluations of photosynthesis, transpiration and stomatal function of a leaf (e.g. Loreto and Fares, 2007). In order to obtain an estimate of the flux to the atmosphere extrapolated from such leaf-level measurements a canopy model must be applied (Owen et al., 1998). For example, the conifer cuvettes are the type of a leaf cuvette designated for needle studies in conifer species (e.g. Hayward et al., 2004).

2. Branch enclosures. These rely on sampling and analysis of enclosed individual branches of trees with light-transparent Teflon® or Tedlar® bags for a certain period of time. Subsequently, using an extrapolation method a canopy flux can be estimated (e.g. Owen and Hewitt, 2000; Helmig et al., 2006).

3. Flux towers. For the purpose of flux measurements in- and over-canopy scale, a flux tower is usually deployed. There are many flux measurement approaches, most common of which is the aerodynamic gradient method (e.g. Nemitz et al., 2002), where the concentrations are measured at two or more different heights. Another example is the eddy covariance (EC) technique (Greenberg et al., 2003; Rinne et al.,

2001), which is one of the most direct methods in measuring trace gas exchange between vegetation and the atmosphere. The general principle of EC flux is the covariance of the instantaneous deviation in the concentration of a tracer and the corresponding instantaneous deviation in the vertical wind speed. In order to fulfil the requirements for this method, fast sensors (~ 10 Hz) are normally required. Owing to the high frequency of concentration measurements by PTR-MS, it is possible to achieve direct BVOC flux determination by EC (e.g. Karl and Guenther, 2004; Rinne et al., 2001). However, only one compound can be monitored in the continuous EC. The EC sub-variant is the disjunct eddy covariance (DEC) where air samples are grabbed and analysed at high frequency but not simultaneously for each analysed compound. In this mode typically up to 10 compounds can normally be monitored close to real time as the disjunct error is proportional to the gaps between the timeseries, and thus to number of *m/z*, but is inversely proportional to the integration time (Rinne et al., 2001; Karl, 2002; Grabmer et al., 2004; Turnipseed et al., 2009). Apart from PTR-MS, a Fast Isoprene Sensor (FIS) (Guenther and Hills, 1998) is also capable of such high frequency sensing, and thus has also been suitable for inclusion in an eddy covariance flux system.

4. Aircraft studies. The previously-listed methods are very useful for studying processes occurring in the boundary layer close to the ground. However, VOCs differ in atmospheric lifetimes and have different Henry's Law constants so vertical flux divergence can be high. Therefore coupling of aircraft and ground measurement is required both for constraining the bottom-up estimates and for verifying the performance of top-down modelling approaches. Recently, aircraft atmospheric studies have become more and more common, including airborne eddy covariance (Cronn and Nutmagul, 1982; Khelif et al., 1999; Karl et al., 2007; Oram, 2008; Fowler et al., 2009; Karl et al., 2009a; Murphy et al., 2010). Another advantage of airborne measurements is the capability of spatial and latitudinal characterisation of the atmosphere which is essential for understanding sources and reactions of BVOCs across all dimensions.

1.2 Proton Transfer Reaction Mass Spectrometer (PTR-MS)

1.2.1 Description and history

The Proton-Transfer-Reaction Mass Spectrometer (PTR-MS) is a fairly recent but enormously useful tool to quantify VOCs at close to real-time resolution. Because of the advantages it offers (see chapter 1.2.3) such as ultra-low detection limit (in the order of ppt) and a very fast response time (less than 0.2 s) it has found numerous applications since its first use about a decade ago, mainly in environmental sciences, chemistry, biology, medicine, and food control. Examples of specific applications include: atmospheric VOC measurements (e.g. Karl and Guenther, 2004; de Gouw, 2007; de Gouw et al., 2003c; Hanson et al., 2004; Hewitt et al., 2003; Langford et al., 2009a); pollution monitoring over cities (Filella and Penuelas, 2006; Velasco et al., 2007; Warneke et al., 2001); biogenic emissions from forests, croplands, and grasslands (Davison et al., 2008; Folkers et al., 2008; Grabmer et al., 2004; Guenther et al., 1996; Hakola et al., 2006; Tarvainen et al., 2005; Warneke, 2002); medicine e.g.: breath analysis, medical screening incl. cancer diagnosis (Amann et al., 2004; Lirk et al., 2004; Taucher et al., 1995; Wehinger et al., 2007); or in food quality applications such as fermentation processes, geographical origin testing of wine and recently also olive oil (Araghipour et al., 2008; Boamfa et al., 2004; Boscaini et al., 2004). Some interesting uses of PTR-MS are in BVOC emissions from ornamental trees in cities (Owen, 2003; Noe et al., 2008) or in odour studies/detection (Biasioli et al., 2004; Hartungen et al., 2004), but theoretically the potential number of applications is almost infinite, anywhere there is a need for fast online measurements of trace gas constituents. Recently, the applicability of PTR-MS has been extended to measurement of ammonia (Norman et al., 2007) and to measurements of semi-volatile and aerosol VOCs (Hellén et al., 2008; Holzinger et al., 2010).

The technical details of PTR-MS and operational description are presented in detail by Lindinger et al. (1998). In addition, this analytical technique has been further

improved by different research teams (e.g. Ammann et al., 2006; de Gouw et al., 2003b; de Gouw et al., 2003c; Hartungen et al., 2004; Maleknia et al., 2007; Steinbacher et al., 2004; Tani et al., 2004; Wang et al., 2004). For the purpose of this thesis only the main concepts will be given. A detailed review of PTR-MS has recently been provided by Blake et al. (2009) and de Gouw and Warneke (2007).

Figure 1.2-1 shows the external appearance of a high-sensitivity PTR-MS widely used in environmental studies. A much smaller compact model is not appropriate for environmental applications due to a lower sensitivity.

Figure 1.2-1. High sensitivity commercial PTR-MS (weight: 150 kg, dimentions 560x780x860 mm WLH).

1.2.2 Principle of operation

The chemical principle of operation is the reaction of proton transfer from the protonated water molecule (H_3O^+) to the investigated species (Reaction 1.2-1).

Therefore the recorded mass to charge ratio (*m/z*) will be higher by 1 in relation to the relative molecular mass (RMM) divided by *z*. In the PTR-MS the charge of the detected protonated ions is normally always equal to +1, in contrast to common electron ionisation techniques where *z* can have several values and also negative sign. Descriptors such as 'masses' or 'protonated masses' are in common use in PTR-MS jargon but the *m/z* ratio is the most appropriate name, since PTR-MS detection is not of a mass but a mass-to-charge ratio.

$$H_3O^+ + R \xrightarrow{k} RH^+ + H_2O \qquad \text{(R 1.2-1)}$$

Chemical species which can be measured by PTR-MS extend to a broad range of all those compounds which have proton affinities (PAs) greater than the PA of water, as only for these reactions is proton transfer exoergic and spontaneous ($\Delta G<0$) at speeds close to the collision rate. In the VOC detection the major constituents of air do not disturb as their proton affinities (PAs) are lower than that of water, so cannot be protonated. The list of PAs for example common compounds is presented in Table 1.2-1. However, since one can only record counts at particular *m/z* channels, it can be difficult to distinguish between isobars, which can be either parent or fragment ions. However, in the process of soft ionisation the majority of detected ions are molecular ions with little or, in some cases, no fragment ion. The degree of fragmentation depends on the *E/N* ratio (i.e., electrical field density divided by buffer gas number density) characterising the drift tube conditions. In order to gain confidence that a given ion mass corresponds to the particular VOC, PTR-MS may additionally require combination with other analytical technique such as GC-FID/MS, which does not have to be as fast as PTR-MS. Nevertheless, most *m/z* ratios have been extensively validated during various atmospheric VOC measurements by PTR-MS (e.g. de Gouw et al., 2003c; de Gouw, 2007; Ambrose et al., 2010).

Table 1.2-1 List of proton affinities for example atmospheric compounds. Data extracted from Ionicon's compilation of proton affinities (available online at www.ionicon.com).

Compound	Proton affinity (kcal mol^{-1})
Water	165.2
Species of PA lower than water	
Helium	43
Neon	49
Argon	88
Oxygen	101
Nitrogen	118
Carbon dioxide	129
Methane	130
Species of PA higher than water	
Formaldehyde	171
Methanol	180
Benzene	180
Acetaldehyde	184
Acetonitrile	186
Toluene	187
Acetone	194
MACR	194
Isoprene	199
MVK	200

The PTR-MS vacuum system and the electrical schematic are illustrated in Figure 1.2-2 and Figure 1.2-3, respectively. Hydronium ions, which serve as the primary ions, are formed from the electrical discharge in the hollow cathode of the ion source, to which water vapour flows at a constant rate (typically 6-8 sccm) from the water reservoir. These primary ions (H_3O^+) are focused on the tiny aperture, and enter the relatively high pressure drift region (typically 2 mbar), where buffer gas (air from the inlet) contains VOCs under study. Those molecules with higher PA than 7.2 eV (i.e. the PA of water) get protonated in the collisions with the primary ions accelerated by the electric field. Generally, with the energies close to the collision energies of VOCs, the proton is transferred from the hydronium ion to the VOC softly without causing fragmentation but increasing its RMM by 1 before being detected in the detection region.

The *E/N* ratio is an important parameter which governs the relative proportion between ion fragmentation and ion clustering in the reaction chamber (drift tube). Typically a measurement is conducted at a constant value of *E/N*, commonly in the range of 120 - 140 Td (Townsend) (1 Td = 1×10^{-17} V cm^{-2}). At high *E/N* ratios fragmentation is favoured and clustering is minimised, whereas at the low ratios fragmentation is reduced but clustering is enhanced. The latter is manifested by elevated levels of water clusters (*m/z* 37, 55, 73, 91, etc.). Other VOCs can cluster with water clusters or form dimers or trimers at the low *E/N* ratios. Therefore the optimal *E/N* ratio should be a best compromise between fragmentation and clustering. At high ambient relative humidity it is sensible to run at elevated *E/N* ratios to minimise excessive clustering from highly abundant $H_3O(H_2O)_n$ species (n = 1, 2, 3 …).

The third vacuum section of a PTR-MS instrument comprises the detection region, in which the combination of the secondary electron multiplier (SEM) and quadrupole mass spectrometer (QMS) is used as an ion detector. The pressure is much lower than in the drift region and is normally in the order of 10^{-5} mbar during measurement. As has been observed by the author and other researchers, high signals for O_2^+ (*m/z* 32), NO^+ (*m/z* 30), and also water-cluster ions, can impact on the sensitivity and instrumental background and thus on detection limits. In addition, these ions are suspected to reduce the SEM lifetime. The modification of a standard PTR-MS by incorporation of an additional turbo-molecular pump to the detection region has been a step forward to achieving a higher sensitivity because of the higher ion-extraction efficiency compared to the former standard PTR-MS models. Replacements of Viton® by Teflon® rings in the drift-tube have largely minimised memory effects and response times. Therefore the high-sensitivity instrument (as used at CEH Edinburgh) has a response time of less than 0.2 s for most of the compounds and consequently requires no frequency corrections to the flux in this respect.

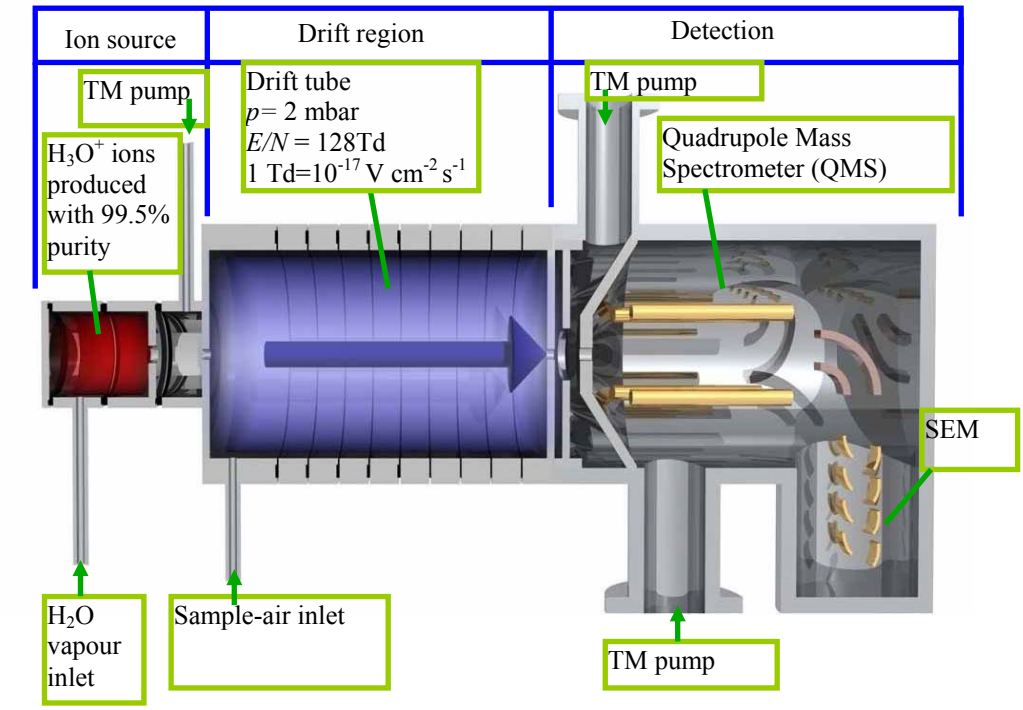

Figure 1.2-2. Schematic presenting the major vacuum components of the ion source, drift, and detection regions in a standard quad-PTR-MS.

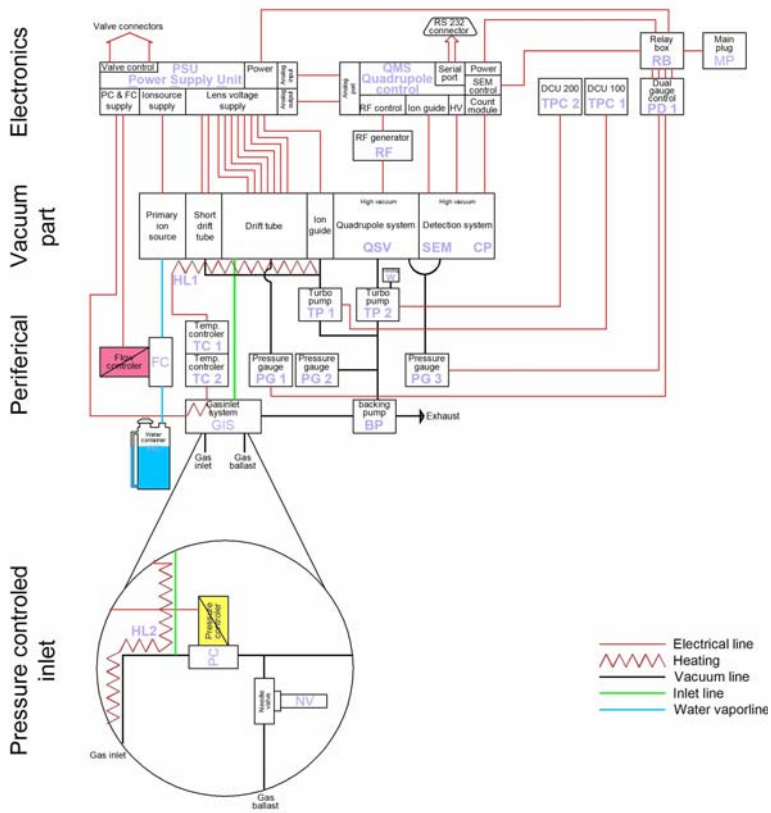

Figure 1.2-3. Electrical schematic of PTR-MS (Haidacher et al., 2007)

1.2.3 Advantages and disadvantages

The general advantages of PTR-MS are the high sensitivity (down to 10 pptv), linearity (up to 10 ppmv) and fast response time (as short as 100 ms in the high sensitivity (HS) model. These advantages make the instrument ideal for both concentration monitoring and direct eddy flux measurements of volatiles whose RMM falls in the range between 17 and 512 amu. Such good specifications are possible owing to the efficient soft ionisation process during the proton transfer reaction at reaction rates of about 2×10^{-9} cm^3 s^{-1}. The proton reaction rate constants for numerous VOCs have been experimentally derived by Zhao and Zhang (2004), allowing for the determination of the volume mixing ratios from the instrument's transmission curve when calibration standard for a particular VOC is not available (see. chapter 1.5.1) One further advantage is direct sampling without the need for sample preparation or pre-concentration, which can introduce artefacts.

However, until now PTR-MS has been unable to provide speciation of isomers so additional qualitative analysis is commonly required for compound validation. The author has made a development of expanding the specificity of PTR-MS by designing and running measurements at alternating drift voltage (*E/N* ratio) coupled with an appropriate analysis of fragmentation patterns (see chapter 2.6).

A general disadvantage of PTR-MS can be the relatively high cost of running the equipment, which is related to the fast ageing of an expensive SEM, and other sporadic maintenance cost such as turbopump replacement. To extend the SEM lifetime, the voltage must not be set too high and not too early after starting up the vacuum system. One has to make sure that no sparking or arcing in the drift tube is present and try to minimise the exposure to high concentrations (>10 ppm) of "sticky" VOCs such as xylene, toluene, benzene, etc. Humidity extraction by fully functional bypass flow, which removes the excess air from the T-junction between the inlet and the capillary leading to the drift-tube, is also essential, and ensuring

good vacuum at all times. During transport the system either should be capable of retaining the vacuum or nitrogen gas should be used for filling the system so that no oxidising agent is present. Finally, SEM exchange optimally should be performed in extremely clean atmospheres, which can be challenging in field campaigns where dust and particles can be very high.

Although the logging software provided by the manufacturer has improved in recent models, it is still not perfect for flux measurements. This is why unofficial programs are commonly used. For example the Quadstar program managing the QMS is lacking many useful features, for example logging additional signals (e.g. from an anemometer) at frequency higher than a cycle length. For this reason many researchers have logged separately the PTR-MS data and the wind data, which introduced extra time needed to synchronise the timeseries. However, at CEH Edinburgh and Lancaster University a concept of using the dynamic data exchange server (DDE) to share the online PTR-MS data and log synchronised data to one file using fast LabVIEW acquisition has been adopted. Further insight into PTR-MS data processing is made in chapter 1.5.

The author's logging and processing software developments are described in Appendix I.

1.2.4 Further developments of PTR-MS

Even the state-of-the-art analytical techniques cannot guarantee that all less abundant or short-lived compounds have been detected. It would be really useful if a device was capable of identifying and quantifying all isomeric species, including optical isomers, in real time and obtain their fluxes. Recent progress in ToF-PTR-MS makes this quite likely. For example, until recently, measurements of direct eddy fluxes of ammonia have been lacking the fast sensors so only indirect methods such as relaxed eddy accumulation (REA) have been possible (Fowler et al., 2001; Nemitz et al., 2001). Nowadays, it is possible to measure the continuous flux of ammonia with PTR-MS, whose ion source can be easily modified to produce O_2^+ from oxygen

cylinder, instead of the water reservoir. Such change of a proton transfer into electron transfer reaction mass spectrometer enables fast and precise detection of ammonia which has electron affinity lower than oxygen (Norman et al., 2007). A similar situation concerns other VOCs such as e.g. formic acid or formaldehyde which are not measured very reliably by PTR-MS due to their low PAs but where future developments in chemical ionisation mass spectrometry (CIMS) with other primary ions can extend the range of detectable compounds (e.g. peroxy radicals).

The Time-of-Flight PTR-MS (TOF-PTR-MS), in distinction from Quad-PTR-MS offers much better mass resolution (~0.005 of amu as opposed to 1 amu in Quad type PTR-MS), so it enables differentiation of isobars and it also does not have any mass range limitation (Tanimoto et al., 2007). For these reasons a potential to apply this instrument for fast fingerprinting of arson accelerants has been already reported (Whyte et al., 2007). However, it still cannot speciate isomers, and the lack of software for running it has probably been the biggest limiting factor until very recently (Müller et al., 2010); previously the whole range of data had to be recorded with no option for selective mass (selective narrow mass ranges) acquisition, which in turn produced enormous amounts of raw data.

However, ToF-PTR-MS is still very expensive so it remains desirable for a conventional PTR-MS capable of separating isomers e.g. monoterpenes. At the GRC conference on Floral and Vegetative Volatiles 2007, and later at the PTR-MS conference 2009, the design of a Triplequad-PTR-MS has been presented. It comprised 3 quadrupole spectrometers connected in an array and from subtraction of collision energies and from fragmentation examination the final structure could be obtained. However, not only is such a design expensive but it still requires tests before it can be widely available.

The author of this thesis has thought of a similar approach but without the need for a triplequad in order to deliver more qualitative information about the VOCs. The results of the first successful discrimination experiment using a conventional PTR-MS but in the alternating drift mode are presented in chapter 2.6. The theory behind

this design was the creation of several completely different fragmentation states repeated in the alternated drift (AD) voltage (and therefore *E/N* ratio; at a constant drift pressure). The assumption was made that each isomer differs less or more in the energy required to produce a specific fragment or energy to cluster specific fragment/s. This has been demonstrated for several pure monoterpene standards differing in structure. In addition this required modification of the Quadstar sequence and writing a LabVIEW program which processed the AD data. Some guiding information was available in the prior literature (Maleknia et al., 2007; Tani et al., 2003), which indicated different relative abundances of parent and fragment ions at different *E/N* ratios. These authors determined different optimal drift voltages for detection of various parent ions of individual monoterpenes and suggested to use the sum of *m/z* 81 and *m/z* 137. Fragmentation patterns of monoterpenes in PTR-MS and also their dependence on water vapour pressure (WVP) have been a subject of investigation by Tani et al. (2004; 2003). However, no AD mode for monoterpene measurement has been proposed. The author of the thesis thought that although the sum of the main monoterpene ions (i.e. *m/z* 81 and *m/z* 137) could give a quantitative agreement for all the monoterpene isomers, it is the ratio of the two *m/z* which could provide qualitative isomeric information. However, at a constant *E/N* ratio this monoterpene *m/z* ratio may not necessarily be specific, so the AD mode was required in order to integrate the ratio over a range of drift voltages (see chapter 2.6 for details).

1.3 Fluxes of VOCs

1.3.1 Current methods of flux determination

The principles of turbulence, advection and transport of chemical species from the surface to the atmosphere have been widely described in the literature and micrometeorological handbooks (e.g. Arya 1988, Lee et al. 2004, Garstang and Fitzjarrald 1999, Fowler et al. 2001, Monteith and Unsworth 2001). A full description of the theory is beyond the scope of the thesis so only a general overview and the most relevant aspects are presented here. The main focus is on the disjunct technique particularly suitable for PTR-MS (chapter 1.4). For small-scale studies the chamber technique (chapter 1.3.3) is frequently used, while for canopy, landscape and regional scales other techniques are described such as gradient method (chapter 1.3.2), or eddy correlation techniques (chapter 1.3.4). Each method has its own advantages and disadvantages and therefore their selection depends on the particular application, availability of sufficiently fast sensors/samplers and whether one point (e.g. on a tower) or several points (e.g. several heights as in gradient methods) can be considered.

1.3.2 Gradient Method

The gradient method relies on measurements at two or more different heights in the surface layer. It is fairly easy to set-up and does not require a knowledge of the surface roughness or surface temperature, which are necessary to know in, for example, the. bulk aerodynamic method (not described here). This method can be suitable when the turbulence is not sufficient for eddy correlation derivation or when the sensor frequency is not sufficiently high for eddy covariance methods. The Richardson number must not be larger than 0.2 in accordance with Monin-Obukhov similarity theory (Monin and Obukhov, 1954). In general, this theory states that in a

horizontally homogenous terrain the mean flow and turbulent characteristics depend only on the four independent variables, namely the height, friction velocity, surface heat flux and the buoyancy variable. The distance between the heights should be appropriately chosen (generally z_1/z_2 should fall between 2 and 4). The concentration gradients ($\partial C/\partial z$) can be calculated and the flux derived as from Equation 1.3-1:

Equation 1.3-1

$$F = -K\frac{\partial C}{\partial z}$$

where K is the eddy diffusivity or turbulent exchange coefficient ($m^2\ s^{-1}$). From analogy to Fick's 1st law the K coefficient needed for the flux calculation can either be obtained by using the concentration of a tracer, e.g. H_2O or CO_2, (modified Bowen-ratio technique) or by surface layer similarity theories. Theoretically, if the measurements at each height are fast enough and there is no advection then it is possible to gather information about chemical reactions if appropriate compounds are measured. The disadvantages of this method are different footprint characteristics of various heights, quite large error (normally ~30%), measurements at more than one height can be sometimes difficult as in aircraft measurements, requirement for quite complex uncertainty evaluation, and difficulties in obtaining appropriate values of eddy diffusivities in strongly stratified conditions. A more precise derivative of this method is the profile method, or gradient profiling, where for example the sampling inlet is moved up and down (e.g. Karl and Guenther, 2004). In addition, for reactive VOCs (isoprenoids, sesquiterpenes) photochemical destruction can provoke misleading conclusions about the flux.

1.3.3 Chamber Method

The chamber method is probably the least sophisticated method and very useful for obtaining long-term flux e.g. seasonal flux. It is a particularly valuable method to determine an uptake or emission from a given plant, leaf or branch in enclosure studies. Since the derived flux is an average over a relatively long time, it may not be appropriate for recording short-scale temporal variations. In a closed-chamber

technique, for example, the ground surface area is enclosed for a given amount of time. Because the physical parameters of the chamber are known after analysis of concentration (online or offline) one can compute the flux. It is, however, worth noting difficulties frequently experienced in this type of indirect method (which are common in the indirect eddy correlation methods as well). These include reactions with surface ozone and other reactive species (compound conversion), memory effects, as well as humidity and condensation interferences.

1.3.4 Eddy accumulation (EA) and eddy covariance (EC) techniques

Eddy accumulation and eddy correlation methods are advanced and relatively complex methods often requiring novel gas/particle and wind instrumentation. However, the benefits largely exceed the ones from previously mentioned methods. In addition all these techniques are appropriate for ecosystem measurements of surface-atmosphere exchange of VOCs. These techniques can be either indirect or direct.

Eddy accumulation (EA) techniques involve sampling air into two reservoirs depending on the sign of the vertical wind speed. In the true eddy accumulation method developed by Desjardins (1977) the air is sampled proportionally to the vertical wind speed. The biggest practical difficulty in realisation of this system has been maintaining constant and fast enough flow. This difficulty has been overcome in the Relaxed Eddy Accumulation (REA), known also as the conditional sampling technique, first presented by Businger and Oncley (1990), and this approach is presented here in more detail. The REA is quite widely used in the quantification of organic species emitted over ecosystem scale (e.g. Nemitz et al., 2001; Graus et al., 2006). Even though this technique is indirect, requiring parameterisations, it has proven useful. The principle of the REA method is sampling into two reservoirs (e.g. 0.5 l each), one of which is an up-draught reservoir sampling when vertical wind

speed (w) is positive, while the other is a down-draught reservoir collecting air parcels travelling downwards (w <0). After an averaging time (typically 30 min) the reservoirs are analysed for the accumulated concentrations (c^+ and c^-). In terms of VOCs, PTR-MS, GC-FID/MS or PTR-MS coupled to GC-FID can for example be used (analytical techniques of VOCs have been described in chapter 1.1.3) but the sensor does not have to be as fast as in continuous methods described later in this chapter. In the REA the relaxation technique allows flows into both reservoirs independent of the absolute value of the vertical wind speed. Thus, the vertical flux (Equation 1.3-2) is proportional to the concentration difference between c^+ and c^-, the standard deviation of the vertical wind speed σ_w and the dimensionless Businger Oncley parameter, b, which is dependent on the atmospheric stability conditions.

Equation 1.3-2

$$F_c = b\sigma_w(c_+ - c_-)$$

In contrast to the gradient methods, this technique offers one point measurement which has many practical advantages but is not optimal when advection or flux divergence is present.

Another group of these measurement techniques consists of direct eddy correlation methods, which rely on correlation of fluctuations in vertical wind speed with those of the components whose flux is to be determined (e.g. temperature, water, CO_2 and VOCs). In other words, at the surface the mean vertical wind speed is assumed to be zero, as the ground is neither source nor sink for air. What it signifies is that when any flux of a scalar, suppose water for example, is greater than zero, then more of the positive deviations from the mean value of w were "wetter" than negative portions of the fluctuations, while mean w is still 0. This implies that if there is no correlation between the measured scalar and vertical wind velocity, there is no flux. As the substantial flux in the turbulent Planetary Boundary Layer (PBL) is carried by small eddies, which can only be recorded by either fast sensors (10 Hz) or fast samplers combined with slower sensors, these methods are most suitable for quantification of VOC surface-atmosphere exchange.

The eddy correlation methods include (continuous) eddy covariance (EC), disjunct eddy covariance (DEC) and most recently virtual disjunct eddy covariance (vDEC), which all are direct methods. The principles of eddy covariance have been described in detail by Arya (1988), Dabberdt et al. (1993), and more recently by Moncrieff et al. (1997) and Guenther (2002). In general, the eddy flux of any scalar can be written as in Equation 1.3-3.

Equation 1.3-3

$$F_c = \overline{w\rho_c}$$

where F_c is the flux density of scalar c, w is the vertical wind velocity, ρ_c is the density (or concentration) of the scalar. The overbar represents the mean of the product over the sampling interval. As the records from a sonic anemometer and a fast sensor for concentration of a compound have irregular patterns, it is suitable to regard these variables as a sum of the mean and fluctuating part. Such process is called Reynolds decomposition (Arya, 1988), which for wind speeds and concentrations can be presented as in Equation 1.3-4 and Equation 1.3-5, respectively:

Equation 1.3-4

$$w = \overline{w} + w'$$

Equation 1.3-5

$$\rho_c = \overline{\rho_c} + \rho_c'$$

where the primes represent the fluctuations around the mean. Equation 1.3-3 can further be represented as in Equation 1.3-6:

Equation 1.3-6

$$F_c = \overline{w\rho_c} + \overline{w'\rho_c'}$$

As the assumption is made that $\overline{w} = 0$, the final practical equation is

Equation 1.3-7

$$F_c = \overline{w' \rho_c'} + \text{correction terms}$$

Over a given integration time, eddy covariance flux can be calculated using the following formula:

Equation 1.3-8

$$F_c = \frac{1}{t_2 - t_1} \int_{t_1}^{t_2} w'(t) \rho_c'(t) dt$$

Because the flux is defined as a covariance of eddy components it can be derived from a subset of fast-grabbed but time-separated samples. This is done in the so-called disjunct approach, which is a good approximation of a continuous eddy covariance, where Equation 1.3-8 could be simplified as follows:

Equation 1.3-9

$$F_c = \frac{1}{N} \sum_{i=1}^{N} w'(i\Delta t) \rho_c'(i\Delta t)$$

where Δt is the time of the gap (usually up to a few seconds). The considerable benefit of using the disjunct method is that it allows for relatively slower sensors to be used in conjunction with a fast sampler. The variant of this method is a virtual disjunct eddy covariance, which takes advantage of the PTR-MS as both the fast sampler and analyser (dwell time is typically adjusted between 0.2 and 1.0 s). This method is reviewed in more detail in the next chapter (1.4).

1.4 Introduction to the Virtual Disjunct Eddy Covariance (vDEC) technique using PTR-MS as VOC sensor

1.4.1 Description of the method

The virtual disjunct eddy covariance (vDEC) technique was demonstrated for the first time by Karl et al. (2002). The method is a variant of disjunct eddy covariance, which had been previously demonstrated with PTR-MS by Rinne et al. (2001), but in conjunction with a disjunct sampler. This sampler grabbed air samples almost instantaneously (0.1 s) which were subsequently analysed during a relatively long period (10-30 s) by PTR-MS and thus a continuous subset of 10 Hz data series was obtained. Karl et al. (2001a) increased the set of compounds measured, recording OVOC fluxes over croplands in the DEC mode, by redesigning the PTR-MS i.e. ion source gaskets and drift tube segment were exchanged for Teflon; this increased sensitivity by a factor of three and enabled an improvement in eddy covariance sampling frequency up to 8 Hz.

Before the introduction of a disjunct sampler (Rinne et al., 2000), there had been an obstacle to using PTR-MS for direct EC flux measurements in that the quadrupole mass spectrometer (QMS) used for PTR-MS was thought to be unable to make fast measurements for more than a few compounds simultaneously.

In the vDEC system the disjunct concept has been adopted, but the need for using a physical grab sampler has been eliminated, making the inlet system much simpler. The QMS, operating in multiple ion detection (MID) mode cycles through 10-20 compounds under study at 0.2 s integration time (dwell time). In the MID mode the QMS assigns this integration time per each compound that is specified in a configuration file, analysing them one after another. Therefore it produces virtually disjunct series for each VOC. For example, if 8 compounds are measured at 0.2 s dwell time, the analysis time for one full cycle is ~ 1.6 s plus a short time (10 ms) for switching from one *m/z* ratio to another. This example is visualised in Figure 1.4-1.

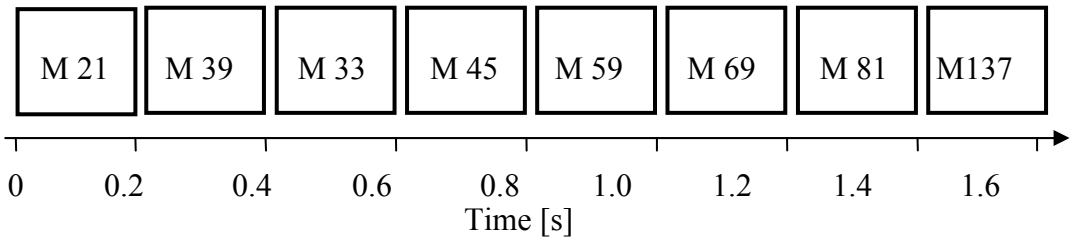

Figure 1.4-1. Example of a vDEC duty cycle for 0.2 dwell time.

As many non PTR-MS disjunct systems have been previously described (e.g. Fowler et al., 2001; Moncrieff et al., 1997; Rinne et al., 2000), the many advances in these methods could be further adopted without the need for "reinventing the wheel". However, there are some specificities about PTR-MS, being a virtual disjunct sampler, which include additional challenges such as identification of the precise lag-time and the noisier covariance functions (see chapter devoted to lag-time development; Chapter 2.5). In the processing analysis of such disjunct time series, there have been two major approaches, generally using different software, developed independently by different teams within the PTR-MS flux research community. For an example case, the final output results acquired with 0.2 s dwell time and with 8 masses specified in the MID will contain 5 Hz lines of counts per second, separated by 0.625 Hz gaps. For consecutive processing, one could either cut out the gaps, obtaining a subset of continuous 5 Hz series, or one could fill these gaps with the previous value from the last line until the next one is available, and then repeat the procedure throughout the whole dataset. This latter approach has been proposed by Spirig et al. (2005). Another (third approach) is optimal as it retains the vertical wind speed data in its full frequency (e.g. 20 Hz), and rather than filling the gaps with the previous number it fills the gaps with "NaNs" – not a number parameter. This can be done using software such as PawEddy written in LabVIEW (see Appendix I).
In order to calculate the flux i.e. a covariance of instantaneous deviation in vertical wind velocity and the corresponding instantaneous deviation in concentration of a given VOC one has to take into account the lag time caused by a residence time of the measured compound in the tubing system, as in the following equation:

Equation 1.4-1

$$F_c(\tau_{eff}) = \frac{1}{N}\sum_{i=1}^{N}(w_i - \overline{w}) \times (c_{\,i+\frac{\tau_{eff}}{\Delta t}} - \overline{c})$$

where τ_{eff} is the time lag between the two series $w(t)$ and $c(t)$. The lag time determination is described in chapter 1.4.3.

Currently this vDEC technique is gaining large appreciation by researchers using PTR-MS for measuring surface–atmosphere exchange of VOCs. For example, Grabmer et al. (2004) measured monoterpene fluxes from a Norway spruce forest, while Rinne et al. (2007a) measured VOC fluxes above a Scots pine forest canopy and Karl et al. (2004) from above a tropical rain forest. Flux estimates and OH reaction potential of reactive biogenic volatile organic compounds (BVOCs) from a mixed northern hardwood forest have been reported by using this flux method (Ortega et al., 2007), and flux of BVOCs from Mopane woodlands of Botswana has been delivered (Hewitt et al., 2003). Recently, Custer and Schade (2007) obtained fluxes of methanol and acetaldehyde over ryegrass, while Davison et al. (2008) investigated green leaf volatile fluxes over grasslands. Nevertheless the community using vDEC is still quite small. Measurements using vDEC are thought to be the most appropriate for validation of atmospheric models but the number of measurements should be increased, especially in the tropical regions.

1.4.2 Major assumptions and error sources

The following assumptions are made in DEC, which are also common for other EC techniques:
1. Flux is fully turbulent, i.e. most of the vertical flux is carried out by eddies; 2 the footprint is adequate; 3. the terrain is horizontal and uniform; 4. the flow convergence and divergence are negligible; 5. measurements at a point can represent an upwind area.

There are many sources of uncertainty in the eddy flux techniques. However, the main source of errors specific to the vDEC method involve counting statistics errors at small dwell times of the QMS. Therefore appropriately long integration times should be chosen, at some cases even at the cost of frequency corrections. It is essential to optimise the PTR-MS to the highest possible sensitivity for the purpose of obtaining clear peaks in the cross-correlation (CC) functions distinct from the noise.

Other errors common to other EC techniques comprise frequency response errors due to: time response; sensor separation; scalar path averaging; tube attenuation; high and low pass filtering; sensor response mismatch; digital sampling. In addition one should take into account: time delays (e.g. DDE server used for mediating the PTR-MS and the wind data, QMS switching); spikes and noise; density fluctuations (Webb-Pearman-Leuning); sonic heat flux errors; band-broadening; oxygen in the path; unlevelled sonic anemometer; data filling. Each of these may introduce from 0-30% error, and altogether may even combine to 100% uncertainty in the measured flux.

There are ways to correct for most of these errors, i.e. frequency response corrections; adjusting for delay; spike removal; coordinate rotation; WPL corrections; sonic temperature corrections; band-broadening corrections; oxygen corrections and data-filling by Monte-Carlo or by emission algorithms, etc. Flux losses associated with signal damping due to residence time in the tubing can be assessed by comparing latent heat fluxes derived from *m/z* 37, calibrated using specific humidity converted from relative humidity (measured by a separate sensor; e.g. Vaisala sensor), with latent heat fluxes from an open path gas analyser.

However, because of so many potential errors, the flux quality control procedures are very important. Most of them have been included in the FLUXNET criteria which set the guidelines and rank the data quality according to the stationarity test, test for

similarity with ideal conditions, and the degree of sonic tilt. These procedures and ranking were described in detail by Foken et al.(2004).

As outlined by the author in the individual practical chapters, the flux data presented here were labelled according to routine tests commonly used in eddy covariance for filtering purposes (Clement et al., 2009; Foken and Wichura, 1996; Langford et al., 2009a; Moncrieff et al., 1997). However, the errors derived from lack or misidentification of the lag time can be high. Previously it was thought that an erroneous lag time would lead to flux underestimation, but significant overestimations can be made when using the common method of finding the lag time on the absolute maximum in the covariance function (Taipale et al., 2010), and can lead to erroneous sign of the flux in small-concentration compounds (see Chapter 2.5). Since errors from lag-time misidentification can be large, but have been under-discussed in the literature, a method for validating the lag-time was desired. The author developed a lag-time validation method which can assess the lag-time quality which is useful for excluding the instances of erroneous lag times or lag times which would lead to a lower flux quality (Chapter 2.5).

The lower limit for the friction velocity is normally set to 0.2 m s^{-1} and points below this threshold should not be included in analyses unless for specific tests. According to the tests proposed by Foken and Wichura (1996) the data should not be included in further analysis if the deviation from the ideal integral similarity characteristics is higher than 60%, and are labelled lower quality if they are within 30-60% of the ideal. A stationarity test (the value for the flux integrated over 25 min compared with the average of 5 values of fluxes integrated over 5 min segments of the same averaging period) is used to exclude non-stationary data when the difference is above 60% and to label as low quality periods with differences between 30 and 60%. The author proposes that the lag-time validation method should also be included to the FLUXNET criteria.

1.4.3 Common problems and their solutions

One of the most fundamental problems in the vDEC system has been shown to be the lag-time determination, which usually must be done for each integration period (commonly 30 min). The lag-time theory and development is described in Chapter 2.5. There can be various reasons for difficulties in lag-time determination, a part of which is associated with the data logging strategy and software. If the wind data and PTR-MS data are logged into separate files (e.g. Rinne et al., 2007a), then a variable lag time can be caused by clock variations and, for example, delay in the first start of the cycle. The way to overcome these are frequent time synchronisations as well as connecting an additional sonic anemometer signal to one of the PTR-MS analog inputs, so that the approximate magnitude of the lag time is known. The covariance of w and c as a function of the lag (τ) is called the cross-correlation function (CC function) or just covariance function $F_c(\tau)$. If both the sonic anemometer and PTR-MS data have the same frequencies, e.g. after filling the disjunct gaps by adding the lines until next available is present (Spirig et al., 2005), then the effective lag time can be efficiently calculated via transformation of the time series into the frequency domain by application of fast Fourier transformations, multiplication of the Fourier spectra and subsequent reverse transformation. Provided that there is a flux, the absolute maximum in the CC function denotes the effective time lag. It is not always necessary to perform Fourier transformation, and generally the disadvantage of frequency correction is the attenuation of high frequency fluxes. It may also not be possible to perform a Fourier transformation if the disjunct gaps are variable. Both at CEH and Lancaster University another approach has been adopted which logs the two data series of wind and VOC concentrations to the same file. This automatically eliminates the clock synchronisation issue and the lag caused by that, so the data are only shifted by the true residence time of a compound plus/minus the length of the PTR-MS cycle. However, the effective lag time needs to be found individually for each integration period, which puts constraints on processing time (see software developments in the practical section: Appendix I). The feature in the LabVIEW program calculates the CC function and then if the lag time is found, it is further applied to calculations for each half-hour period and each compound separately.

Different methods of lag-time determination are described in the lag-time development chapter (2.5). The reasons for relatively different lag times for various compounds in vDEC are delays due to QMS switching, chromatographic effects for sticky compounds and delays in DDE server or other mediating process(es). The lag time may not be the same in each integration time, but it should be at least relatively constant within the integration period.

Other problems that can be encountered in vDEC are generally common to other EC techniques, previously described. They include among others insufficient counting statistics for too short acquisition times, high detection limits, and water condensation issues.

1.5 Theoretical challenges

This chapter presents an outline of selected challenges typically faced with PTR-MS.

1.5.1 Calibration

The calibration of the PTR-MS instrument is fundamental for reporting standardised absolute concentrations (or mixing ratios) as well as arriving at correct absolute flux values. Although the calibration itself concerns correlation of the instrument's response (normalised counts per second) with absolute measured concentrations, in terms of the PTR-MS also the transmission measurements are very important as they enable calculation of concentrations quickly, although less precisely, but when standards are not available.

Calibration is normally done by using gas calibration standards, diffusion or permeation systems. The resulting calibration equation can be used to determine calibration coefficients and thus sensitivities for given compounds. Although PTR-MS has well-defined parameters, which makes online calculations of concentrations from instrumental transmission feasible, it is essential to make frequent calibrations for as many as possible compounds to increase the precision. The calculation of the concentration for a given VOC by the use of only the transmission coefficients can be performed by using Equation 1.5-2, expanded from Equation 1.5-1. Since the proton transfer reaction (R 1.2-1) exhibits a pseudo-first order kinetics, for the neutral concentration, it can be written:

Equation 1.5-1

$$[R] \cong \frac{1}{k \times t} \times \frac{RH^+[cps]}{H_3O^+[cps]}$$

and then

Equation 1.5-2

$$c_i\left[\text{ppb}\right] = 1\times10^9 \times \frac{(\text{RH}^+[\text{cps}])\times p_0 \times V_0 \times T_{\text{drift}} \times Tr_{\text{H}_3\text{O}^+}}{k \times t \times (\text{H}_3\text{O}^+[\text{cps}]) \times p_{\text{drift}} \times N_a \times T_0 \times Tr_{\text{RH}^+}}$$

where k is reaction rate constant, t is reaction time, $Tr_{\text{H3O+}}$ is the transmission coefficient of the primary ions, $Tr_{\text{RH+}}$ is the transmission coefficient for RH^+, p_0 is standard pressure in hPa, p_{drift} is drift-tube pressure in hPa, V_0 is the volume of one mole of ideal gas under standard conditions in cm^3, N_a is Avogadro number, T_0 and T_{drift} are the standard and drift-tube temperature, respectively.

Before the concentration is calculated the counts for each *m/z* channel of interest should be normalised to account for internal variability in primary ions, water vapour and drift pressure. The process of normalising the counts to one million primary ion counts and to 2 mbar of the drift tube pressure, and water vapour can facilitate comparisons between instruments even at different operating conditions (Equation 1.5-3).

Provided that a transmission measurement has been performed relatively recently, and after normalising the cps, the error attributed to this calculation is up to 100% (Steinbacher et al., 2004) which mainly derives from uncertainty in the reaction rate constant, which is increasing for the compounds of higher *m/z*. The accuracy can be significantly improved by using calculations relying on current calibration coefficients. This can be undertaken using the following equation (e.g. de Gouw et al., 2003c; Rinne et al., 2007a):

Equation 1.5-3

$$c_i = \alpha_i \left[\frac{S_i}{\left(\delta_{\text{M21/M19}}^{-1} S_{\text{M21}} + S_{\text{M37}}\right)} - \frac{S_{i,\text{zero}}}{\left(\delta_{\text{M21/M19}}^{-1} S_{\text{M21,zero}} + S_{\text{M37,zero}}\right)} \right]$$

where α_i is the calibration coefficient, S_i is the signal of the VOC in cps, $S_{i,zero}$ is the signal of the VOC-free air, $\delta_{M21/M19}$ is the ratio of $H_3{}^{18}O^+$ to $H_3{}^{16}O^+$ which equals 0.002. The calibration coefficients can be obtained during the calibration process and calculated by inverting the equation to yield α_i. The reciprocal of α_i is normalised sensitivity (S_{norm}). Recently an approach of combining the two calculation methods (as in Equation 1.5-2 and Equation 1.5-3) was highlighted by Taipale et al. (2008). Based on calibration of non-fragmenting compounds it is possible to derive transmission coefficients. The relative transmission curve can be subsequently used to optain empirical sensitivities of compounds that were not present in the calibration mixture. This approach can decrease the uncertainty by a factor of three compared to the classical derivation of transmission (e.g., Steinbacher , 2004). The relative transmission approach has been used by the author of this thesis in Italy and in Borneo and whenever the calibration standard for a compound was not available. The example is shown in Figure 1.5-1.

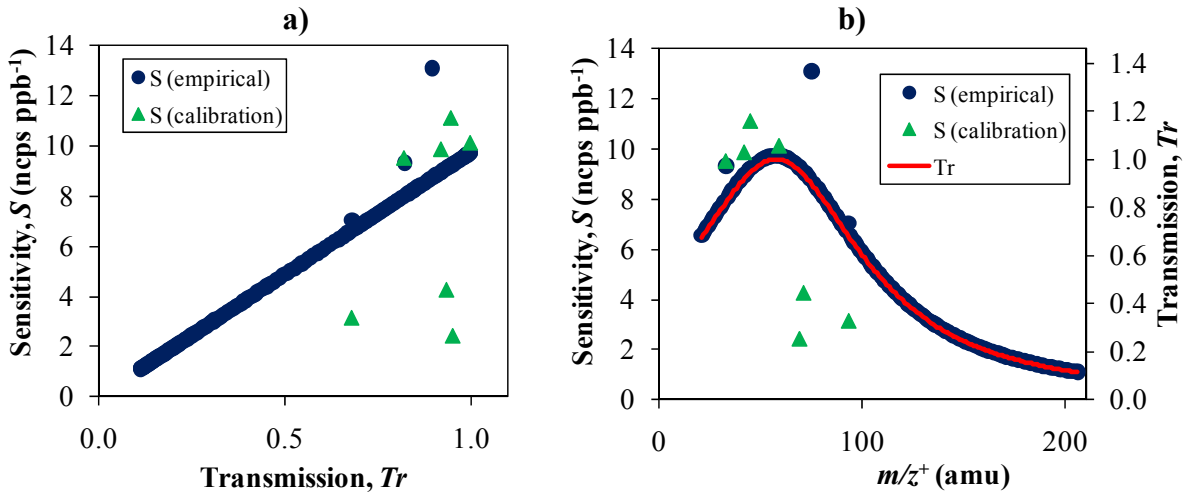

Figure 1.5-1 Example of an application of the relative transmission approach: a) relationship between the sensitivity and transmission curves obtained in the calibration of nonfragmenting compounds; b) Sensitivity and transmission curves (Lorentzian fit). Note that the calibration here was made under highly fragmenting conditions (140 Td) so the calibrated sensitivities of higher masses deviated from the curve and were not included in the relative transmission derivation. The blue outliers come from application of adjusted proton transfer reaction rate constants (Zhao and Zhang, 2004).

A very important issue that needs to be taken into accounted is humidity. For example, the zero air and/or standards optimally should not be dry, if a measurement is done in humid conditions. Dry standards should be appropriately enriched in water vapour in order to derive the humidity dependent sensitivities. A zero air generator which does not dry air seems therefore appropriate to provide the gas for the standard dilution. Example of such zero-air generator contains a Pt/Al_2O_3 catalyst heated to 200ºC. If the high concentration standard is dry it can be diluted using the zero-air source of similar to ambient humidity. In any case errors may arise if no corrections for humidity are made in concentration calculations. Ideally, calibration should be made at the dew point similar to that of the measured sample. However, even then the correction for the water cluster at *m/z* 37 should always be done in calculations regarding all the compounds (except highly hydrophobic aromatics e.g. toluene). The effect of water vapour pressure on monoterpene measurements by PTR-MS has been investigated by Tani et al. (2004), while validation of PTR-MS for measuring water vapour concentration and flux has been reported by Ammann et al. (2006)

1.5.2 Data processing

Processing the data is the most important part of delivering final and unbiased results. In order to prevent potential problems, one must make an effort at the logging stage and ensure that the data acquisition phase is correctly designed and set up. It has already been mentioned that two logging approaches have been used, i.e. logging the wind and concentration data either to one file or to independent files (e.g. on different computers). Processing the data online during a measurement can be useful for overview purposes, but should be limited since the use of excessive resources may lead to possible delays in the logging. Therefore usually a more or less sophisticated program can be written to facilitate the post-processing. Typically, data first need to be assessed for periods of known disturbances (i.e. checked with the log-book). The data from the valid period need to be then checked for spikes and in some cases should be despiked and/or detrended. Flux data processing which includes precise lag-time analysis for each compound and integration period may require

substantial numerical resources, in order to process the data quickly. Before the lag-time determination, the wind data should be corrected for sonic tilts. This can be done using a single, double, triple or planar fit rotation.

Subsequently, the raw data from PTR-MS should be normalised and converted to concentrations as previously described. As the zero air subtraction does not matter for the flux, the process of zero air subtraction can be done in parallel for obtaining the concentrations. The data containing zero air files should be checked for the presence of diurnal trends and spikes and can be converted to concentrations using exactly the same process as for measurement files. Sometimes the subtraction is more conveniently performed separately for example using a running median ZA, instantaneous ZA, or the lower 10^{th} percentile of ZA. Comparisons with the raw files unaffected by the additional white noise from ZA subtraction can be useful in addition to the ZA subtracted concentrations. Once the concentration array has been derived it can be used to calculate the covariance function and determine the lag time. Simultaneously the limit of flux detection is derived from 3 times the standard deviation of the covariance of the noise (i.e. sufficiently far away from the lag time). For the different methods of lag-time determination the reader is referred to Chapter 2.5. The time series should be shifted by the calculated lag time and the covariance should be computed, which is the flux. Before this, usually the conversion of concentration data (typically in ppb) to mg m^{-3} or µmol m^{-3} is required. Finally the validation tests results should be saved along with the flux value. Rather than discarding the data which did not pass the validation criteria, all data are saved but the appropriate quality tags can later be used for filtering. The whole process needs to be repeated for each half hour file and for each compound.

1.5.3 Interpretation of PTR-MS data

One has to be very critical and careful when referring to a compound based only on the *m/z*. This is because any *m/z* can have an unknown number of potential contributions from external sources or from internal fragmentation. It is sensible to

make the interpretation of data by firstly validating the actual *m/z*. The optimal situation is when a complementary measurement is run at the same time, for example GC-FID. If the data can be validated then the derived flux can be assumed valid. However, validation may not be possible during the measurements. In such cases all known possible known contributions should be considered as a potential contribution. Thanks to the growing PTR-MS community, and various validation field and lab studies, most commonly-encountered compounds have been validated, but unknown contributions must also be considered. The database of compounds contributing to different *m/z* has been constructed by Ionicon on the basis of literature data and theoretical studies of proton affinities and is available on the Ionicon website. In addition the interpretation of the results must be sensible, so it must be done in conjunction with the current background knowledge concerning the type of vegetation, mechanisms for release of the compounds, interactions with herbivores, stresses, possibility of anthropogenic compounds and any artefacts that could have been present.

1.6 References

Amann, A., Poupart, G., Telser, S., Ledochowski, M., Schmid, A., and Mechtcheriakov, S.: Applications of breath gas analysis in medicine, International Journal of Mass Spectrometry, 239, 227-233, 2004.

Ambrose, J. L., Haase, K., Russo, R. S., Zhou, Y., White, M. L., Frinak, E. K., Jordan, C., Mayne, H. R., Talbot, R., and Sive, B. C.: An intercomparison of GC-FID and PTR-MS toluene measurements in ambient air under conditions of enhanced monoterpene loading, Atmos. Meas. Tech. Discuss., 3, 1-54, 10.5194/amtd-3-1-2010, 2010.

Ammann, C., Spirig, C., Neftel, A., Steinbacher, M., Komenda, M., and Schaub, A.: Application of PTR-MS for measurements of biogenic VOC in a deciduous forest, International Journal of Mass Spectrometry, 239, 87-101, 2004.

Ammann, C., Brunner, A., Spirig, C., and Neftel, A.: Technical note: Water vapour concentration and flux measurements with PTR-MS, Atmospheric Chemistry and Physics, 6, 4643-4651, 2006.

Araghipour, N., Colineau, J., Koot, A., Akkermans, W., Rojas, J. M. M., Beauchamp, J., Wisthaler, A., Mark, T. D., Downey, G., Guillou, C., Mannina, L., and Ruth, S. v.: Geographical origin classification of olive oils by PTR-MS, Food Chemistry, 108, 374-383, 2008.

Biasioli, F., Gasperi, F., Odorizzi, G., Aprea, E., Mott, D., Marini, F., Autiero, G., Rotondo, G., and Mark, T. D.: PTR-MS monitoring of odour emissions from composting plants, International Journal of Mass Spectrometry, 239, 103-109, 2004.

Blake, R. S., Whyte, C., Hughes, C. O., Ellis, A. M., and Monks, P. S.: Demonstration of Proton-Transfer Reaction Time-of-Flight Mass Spectrometry for Real-Time Analysis of Trace Volatile Organic Compounds, Anal. Chem., 76, 3841-3845, 2004.

Blake, R. S., Monks, P. S., and Ellis, A. M.: Proton-Transfer Reaction Mass Spectrometry, Chemical Reviews, 109, 861-896, doi:10.1021/cr800364q, 2009.

Boamfa, E. I., Steeghs, M. M. L., Cristescu, S. M., and Harren, F. J. M.: Trace gas detection from fermentation processes in apples; an intercomparison study

between proton-transfer-reaction mass spectrometry and laser photoacoustics, International Journal of Mass Spectrometry, 239, 193-201, 2004.

Boscaini, E., Mikoviny, T., Wisthaler, A., Hartungen, E. v., and Mark, T. D.: Characterization of wine with PTR-MS, International Journal of Mass Spectrometry, 239, 215-219, 2004.

Cape, J. N.: Effects of air-pollution on the chemistry of surface waxes of scots pine, Water Air Soil Pollut., 31, 393-399, 1986.

Clement, R. J., Burba, G. G., Grelle, A., Anderson, D. J., and Moncrieff, J. B.: Improved trace gas flux estimation through IRGA sampling optimization, Agric. For. Meteorol., 149, 623-638, 10.1016/j.agrformet.2008.10.008, 2009.

Cronn, D. R., and Nutmagul, W.: Analysis of atmospheric hydrocarbons during winter MONEX, Tellus, 34, 159-165, 1982.

Custer, T., and Schade, G.: Methanol and acetaldehyde fluxes over ryegrass, Tellus B, 59, 673-684, doi:10.1111/j.1600-0889.2007.00294.x, 2007.

Davison, B., Brunner, A., Ammann, C., Spirig, C., Jocher, M., and Neftel, A.: Cut-induced VOC emissions from agricultural grasslands, Plant Biology, 10, 76-85, doi:10.1055/s-2007-965043, 2008.

de Gouw, J., and Warneke, C.: Measurements of volatile organic compounds in the earths atmosphere using proton-transfer-reaction mass spectrometry, Mass Spectrom. Rev., 26, 223-257, 10.1002/mas.20119, 2007.

de Gouw, J. A., Goldan, P. D., Warneke, C., Kuster, W. C., Roberts, J. M., Marchewka, M., Bertman, S. B., Pszenny, A. A. P., and Keene, W. C.: Validation of proton transfer reaction-mass spectrometry (PTR-MS) measurements of gas-phase organic compounds in the atmosphere during the New England Air Quality Study (NEAQS) in 2002, J. Geophys. Res.-Atmos., 108, 2003a.

de Gouw, J. A., Warneke, C., Kuster, W. C., Goldan, P. D., and Fall, R.: Validation of Atmospheric VOC Measurements by Proton-Transfer- Reaction Mass Spectrometry Using a Gas-Chromatographic Preseparation Method, Environ. Sci. Technol., 37, 2494-2501, 2003b.

de Gouw, J. W., Carsten: Measurements of Volatile Organic Compounds in the Earth's Atmosphere using Proton-Transfer-Reaction Mass Spectrometry, Mass Spectrometry Reviews, 26, 223-257, 2007.

EDGAR: EDGAR 3.2 Fast Track 2000 (32FT2000) dataset, http://www.mnp.nl/edgar/model/v32ft2000edgar/index.jsp, 2005.

Filella, I., and Penuelas, J.: Daily, weekly, and seasonal time courses of VOC concentrations in a semi-urban area near Barcelona, Atmospheric Environment, 40, 7752-7769, 2006.

Foken, T., and Wichura, B.: Tools for quality assessment of surface-based flux measurements, Agric. For. Meteorol., 78, 83-105, 1996.

Foken, T., Göckede, M., Mauder, M., Mahrt, L., Amiro, B., and Munger, W.: Post-field data quality control, in: Handbook of Micrometeorology: A guide for surface flux measurement and analysis., edited by: Lee, W. M. X., and Law, B., Kluwer Academic Publishers, Dordrecht, 181-203, 2004.

Folkers, A., Huve, K., Ammann, C., Dindorf, T., Kesselmeier, J., Kleist, E., Kuhn, U., Uerlings, R., and Wildt, J.: Methanol emissions from deciduous tree species: dependence on temperature and light intensity, Plant Biology, 10, 65-75, doi:10.1111/j.1438-8677.2007.00012.x, 2008.

Fowler, D., Coyle, M., Flechard, C., Hargreaves, K., Nemitz, E., Storeton-West, R., Sutton, M., and Erisman, J. W.: Advances in micrometeorological methods for the measurement and interpretation of gas and particle nitrogen fluxes, Plant and Soil, 228, 117-129, 2001.

Fowler, D., Pilegaard, K., Sutton, M. A., Ambus, P., Raivonen, M., Duyzer, J., Simpson, D., Fagerli, H., Fuzzi, S., Schjoerring, J. K., Granier, C., Neftel, A., Isaksen, I. S. A., Laj, P., Maione, M., Monks, P. S., Burkhardt, J., Daemmgen, U., Neirynck, J., Personne, E., Wichink-Kruit, R., Butterbach-Bahl, K., Flechard, C., Tuovinen, J. P., Coyle, M., Gerosa, G., Loubet, B., Altimir, N., Gruenhage, L., Ammann, C., Cieslik, S., Paoletti, E., Mikkelsen, T. N., Ro-Poulsen, H., Cellier, P., Cape, J. N., Horvath, L., Loreto, F., Niinemets, U., Palmer, P. I., Rinne, J., Misztal, P., Nemitz, E., Nilsson, D., Pryor, S., Gallagher, M. W., Vesala, T., Skiba, U., Brueggemann, N., Zechmeister-Boltenstern, S., Williams, J., O'Dowd, C., Facchini, M. C., de Leeuw, G.,

Flossman, A., Chaumerliac, N., and Erisman, J. W.: Atmospheric composition change: Ecosystems-Atmosphere interactions, Atmospheric Environment, 43, 5193-5267, 10.1016/j.atmosenv.2009.07.068, 2009.

Grabmer, W., Graus, M., Lindinger, C., Wisthaler, A., Rappengluck, B., Steinbrecher, R., and Hansel, A.: Disjunct eddy covariance measurements of monoterpene fluxes from a Norway spruce forest using PTR-MS, 1st International Conference on Proton Transfer Mass Spectrometry, Igls, AUSTRIA, 2003, ISI:000225902200005, 111-115,

Grabmer, W., Graus, M., Lindinger, C., Wisthaler, A., Rappengluck, B., Steinbrecher, R., and Hansel, A.: Disjunct eddy covariance measurements of monoterpene fluxes from a Norway spruce forest using PTR-MS, International Journal of Mass Spectrometry, 239, 111-115, 2004.

Graus, M., Hansel, A., Wisthaler, A., Lindinger, C., Forkel, R., Hauff, K., Klauer, M., Pfichner, A., Rappengluck, B., Steigner, D., and Steinbrecher, R.: A relaxed-eddy-accumulation method for the measurement of isoprenoid canopy-fluxes using an online gas-chromatographic technique and PTR-MS simultaneously, Atmospheric Environment, 40, S43-S54, 2006.

Greenberg, J. P., Guenther, A., Harley, P., Otter, L., Veenendaal, E. M., Hewitt, C. N., James, A. E., and Owen, S. M.: Eddy flux and leaf-level measurements of biogenic VOC emissions from mopane woodland of Botswana, J. Geophys. Res.-Atmos., 108, 9, 8466

10.1029/2002jd002317, 2003.

Guenther, A., Hewitt, C. N., Erickson, D., Fall, R., Geron, C., Graedel, T., Harley, P., Klinger, L., Lerdau, M., McKay, W. A., Pierce, T., Scholes, B., Steinbrecher, R., Tallamraju, R., Taylor, J., and Zimmerman, P.: A global-model o fnatural volatile organic-compound emissions, J. Geophys. Res.-Atmos., 100, 8873-8892, 1995.

Guenther, A., Greenberg, J., Harley, P., Helmig, D., Klinger, L., Vierling, L., Zimmerman, P., and Geron, C.: Leaf, branch, stand and landscape scale measurements of volatile organic compound fluxes from U.S. woodlands, 16, 17-24, 1996.

Guenther, A. B., and Hills, A. J.: Eddy covariance measurement of isoprene fluxes, J. Geophys. Res.-Atmos., 103, 13145-13152, 1998.

Haidacher, S., Hartungen, E. V., and Schottkowsky, R.: Ionicon PTR-MS Manual v 1.8.2., 2007.

Hakola, H., Tarvainen, V., Back, J., Ranta, H., Bonn, B., Rinne, J., and Kulmala, M.: Seasonal variation of mono- and sesquiterpene emission rates of Scots pine, Biogeosciences, 3, 93-101, 2006.

Hanson, D., Orlando, J., Noziere, B., and Kosciuch, E.: Proton transfer mass spectrometry studies of peroxy radicals, International Journal of Mass Spectrometry, 239, 147-159, 2004.

Harley, P., Guenther, A., and Zimmerman, P.: Effects of light, temperature and canopy position on net photosynthesis and isoprene emission from sweetgum (Liquidambar styraciflua) leaves, 16, 25-32, 1996.

Hartungen, E. v., Wisthaler, A., Mikoviny, T., Jaksch, D., Boscaini, E., Dunphy, P. J., and Mark, T. D.: Proton-transfer-reaction mass spectrometry (PTR-MS) of carboxylic acids: Determination of Henry's law constants and axillary odour investigations, International Journal of Mass Spectrometry, 239, 243-248, 2004.

Hayward, S., Tani, A., Owen, S. M., and Hewitt, C. N.: Online analysis of volatile organic compound emissions from Sitka spruce (Picea sitchensis), 24, 721-728, 2004.

Heal, M. R., Harrison, M. A. J., and Cape, J. N.: Aqueous-phase nitration of phenol by N2O5 and ClNO2, Atmospheric Environment, 41, 3515-3520, 10.1016/j.atmosenv.2007.02.003, 2007.

Hellén, H., Dommen, J., Metzger, A., Gascho, A., Duplissy, J., Tritscher, T., Prevot, A. S. H., and Baltensperger, U.: Using Proton Transfer Reaction Mass Spectrometry for Online Analysis of Secondary Organic Aerosols, Environ. Sci. Technol., 42, 7347-7353, 10.1021/es801279m, 2008.

Helmig, D., Ortega, J., Guenther, A., Herrick, J. D., and Geron, C.: Sesquiterpene emissions from loblolly pine and their potential contribution to biogenic aerosol formation in the Southeastern US, Atmospheric Environment, 40, 4150-4157, 2006.

Hewitt C.N., J. A., Owen S. M.: Eddy flux and leaf-level measurements of biogenic VOC emissions from Mopane woodlands of Botswana, Journal of Geophysical Research-Atmospheres, 108, 8466-8474 2003.

Hewitt, C. N., Hayward, S., and Tani, A.: The application of proton transfer reaction-mass spectrometry (PTR-MS) to the monitoring and analysis of volatile organic compounds in the atmosphere, Journal of Environmental Monitoring, 5, 1-7, 2003.

Holzinger, R., Williams, J., Herrmann, F., Lelieveld, J., Donahue, N. M., and Röckmann, T.: Aerosol analysis using a Thermal-Desorption Proton-Transfer-Reaction Mass Spectrometer (TD-PTR-MS): a new approach to study processing of organic aerosols, Atmos. Chem. Phys., 10, 2257-2267, 2010.

Karl, T., Guenther, A., Jordan, A., Fall, R., and Lindinger, W.: Eddy covariance measurement of biogenic oxygenated VOC emissions from hay harvesting, Atmos Environ, 35, 491-495, 2001.

Karl, T., and Guenther, A.: Atmospheric variability of biogenic VOCs in the surface layer measured by proton-transfer-reaction mass spectrometry, International Journal of Mass Spectrometry, 239, 77-86, 2004.

Karl, T., Guenther, A., Yokelson, R. J., Greenberg, J., Potosnak, M., Blake, D. R., and Artaxo, P.: The tropical forest and fire emissions experiment: Emission, chemistry, and transport of biogenic volatile organic compounds in the lower atmosphere over Amazonia, J. Geophys. Res.-Atmos., 112, 17, D18302 10.1029/2007jd008539, 2007.

Karl, T., Apel, E., Hodzic, A., Riemer, D. D., Blake, D. R., and Wiedinmyer, C.: Emissions of volatile organic compounds inferred from airborne flux measurements over a megacity, Atmospheric Chemistry and Physics, 9, 271-285, 2009.

Karl, T., M. Potosnak, et al.: Exchange processes of volatile organic compounds above a tropical rain forest: Implications for modeling tropospheric chemistry above dense vegetation, J. Geophys. Res.-Atmos., 109, 2004.

Karl, T. G., C. Spirig, et al.: Virtual disjunct eddy covariance measurements of organic compound fluxes from a subalpine forest using proton transfer reaction mass spectrometry, Atmospheric Chemistry and Physics, 2, 279-291, 2002.

Khelif, D., Burns, S. P., and Friehe, C. A.: Improved wind measurements on research aircraft, Journal of Atmospheric and Oceanic Technology, 16, 860-875, 1999.

Kim, S., Karl, T., Guenther, A., Tyndall, G., Orlando, J., Harley, P., Rasmussen, R., and Apel, E.: Emissions and ambient distributions of Biogenic Volatile Organic Compounds (BVOC) in a ponderosa pine ecosystem: interpretation of PTR-MS mass spectra, Atmos. Chem. Phys., 10, 1759-1771, 10.5194/acp-10-1759-2010, 2010.

Langford, B., Davison, B., Nemitz, E., and Hewitt, C. N.: Mixing ratios and eddy covariance flux measurements of volatile organic compounds from an urban canopy (Manchester, UK), Atmos. Chem. Phys., 9, 1971-1987, 2009a.

Langford, B., Nemitz, E., House, E., Phillips, G. J., Famulari, D., Davison, B., Hopkins, J. R., Lewis, A. C., and Hewitt, C. N.: Fluxes and concentrations of volatile organic compounds above central London, UK, Atmos. Chem. Phys. Discuss., 9, 17297-17333, 2009b.

Lindinger, W., Hansel, A., and Jordan, A.: On-line monitoring of volatile organic compounds at pptv levels by means of proton-transfer-reaction mass spectrometry (PTR-MS) - Medical applications, food control and environmental research, International Journal of Mass Spectrometry, 173, 191-241, 1998.

Lirk, P., Bodrogi, F., and Rieder, J.: Medical applications of proton transfer reaction-mass spectrometry: ambient air monitoring and breath analysis, International Journal of Mass Spectrometry, 239, 221-226, 2004.

Loreto, F., and Fares, S.: Is Ozone Flux Inside Leaves Only a Damage Indicator? Clues from Volatile Isoprenoid Studies, Plant Physiol., 143, 1096-1100, 10.1104/pp.106.091892, 2007.

Maleknia, S. D., Bell, T. L., and Adams, M. A.: PTR-MS analysis of reference and plant-emitted volatile organic compounds, International Journal of Mass Spectrometry, 262, 203-210, 2007.

Misztal, P., Fares, S., and Taraborrelli, D.: Report on an e-working module on biogenic emissions, in:Report on Surface Emissions and Prediction of Atmospheric Composition Changes - Summer School Ile d'Oleron, France, 44-48, 2007.

Moncrieff, J., Valentini, R., Greco, S., Guenther, S., and Ciccioli, P.: Trace gas exchange over terrestrial ecosystems: methods and perspectives in micrometeorology, J. Exp. Bot., 48, 1133-1142, 10.1093/jxb/48.5.1133, 1997.

Monin, A., and Obukhov, A.: Basic laws of turbulent mixing in the ground layer of the atmosphere, Trudy Geofiz. Inst. Akad. Nauk SSSR, 151 (A 1959 translation (under auspices of American Meteorological Society) is available from Defense Technical Information Center (http://handle.dtic.mil/100.2/AD672723)), 163-187, 1954.

Müller, M., Graus, M., Ruuskanen, T. M., Schnitzhofer, R., Bamberger, I., Kaser, L., Titzmann, T., Hörtnagl, L., Wohlfahrt, G., Karl, T., and Hansel, A.: First eddy covariance flux measurements by PTR-TOF, Atmos. Meas. Tech., 3, 387-395, 10.5194/amt-3-387-2010, 2010.

Murphy, J. G., Oram, D. E., and Reeves, C. E.: Measurements of volatile organic compounds over West Africa, Atmos. Chem. Phys. Discuss., 10, 3861-3892, 10.5194/acpd-10-3861-2010, 2010.

Nemitz, E., Flynn, M., Williams, P. I., Milford, C., Theobald, M. R., Blatter, A., Gallagher, M. W., and Sutton, M. A.: A Relaxed Eddy Accumulation System for the Automated Measurement of Atmospheric Ammonia Fluxes, Water, Air, & Soil Pollution: Focus, 1, 189-202, 2001.

Nemitz, E., Hargreaves, K. J., McDonald, A. G., Dorsey, J. R., and Fowler, D.: Meteorological measurements of the urban heat budget and CO2 emissions on a city scale, Environ. Sci. Technol., 36, 3139-3146, 10.1021/es010277e, 2002.

Noe, S. M., Penuelas, J., and Niinemets, U.: Monoterpene emissions from ornamental trees in urban areas: a case study of Barcelona, Spain, Plant Biology, 10, 163-169, doi:10.1111/j.1438-8677.2007.00014.x, 2008.

Norman, M., Hansel, A., and Wisthaler, A.: O2+ as reagent ion in the PTR-MS instrument: Detection of gas-phase ammonia, International Journal of Mass Spectrometry, 265, 382-387, 2007.

Oram, D.: Aircraft PTR measurements of VOC, OP3 Science Meeting, University of Leeds, 27-29 November 2008, 2008.

Ortega, J., Helmig, D., Guenther, A., Harley, P., Pressley, S., and Vogel, C.: Flux estimates and OH reaction potential of reactive biogenic volatile organic

compounds (BVOCs) from a mixed northern hardwood forest, Atmospheric Environment, 41, 5479-5495, 2007.

Owen, S. M., Boissard, C., Hagenlocher, B., and Hewitt, C. N.: Field studies of isoprene emissions from vegetation in the Northwest Mediterranean region, J. Geophys. Res.-Atmos., 103, 25499-25511, 1998.

Owen, S. M., and Hewitt, C. N.: Extrapolating branch enclosure measurements to estimates of regional scale biogenic VOC fluxes in the northwestern Mediterranean basin, J. Geophys. Res., 105, 11573-11583, 2000.

Owen, S. M., MacKenzie, A. R., Stewart, H., Donovan, R., Hewitta, C. N., : BIOGENIC VOLATILE ORGANIC COMPOUND (VOC) EMISSION ESTIMATES FROM AN URBAN TREE CANOPY, Ecol. Appl., 13, 927-938, 2003.

Rinne, H. J. I., Delany, A. C., Greenberg, J. P., and Guenther, A. B.: A true eddy accumulation system for trace gas fluxes using disjunct eddy sampling method, Journal of Geophysical Research-Atmospheres, 105, 24791-24798, 2000.

Rinne, H. J. I., Guenther, A. B., Warneke, C., de Gouw, J. A., and Luxembourg, S. L.: Disjunct eddy covariance technique for trace gas flux measurements, Geophys. Res. Lett., 28, 3139-3142, 2001.

Rinne, J., Taipale, R., Markkanen, T., Ruuskanen, T. M., HellÃ©n, H., Kajos, M. K., Vesala, T., and Kulmala, M.: Hydrocarbon fluxes above a Scots pine forest canopy: measurements and modeling, Atmos. Chem. Phys., 7, 3361-3372, 2007.

Saxton, J. E., Lewis, A. C., Kettlewell, J. H., Ozel, M. Z., Gogus, F., Boni, Y., Korogone, S. O. U., and Serca, D.: Isoprene and monoterpene measurements in a secondary forest in northern Benin, Atmospheric Chemistry and Physics, 7, 4095-4106, 2007.

Spirig, C., Neftel, A., Ammann, C., Dommen, J., Grabmer, W., Thielmann, A., Schaub, A., Beauchamp, J., Wisthaler, A., and Hansel, A.: Eddy covariance flux measurements of biogenic VOCs during ECHO 2003 using proton transfer reaction mass spectrometry, Atmospheric Chemistry and Physics, 5, 465-481, 2005.

Steinbacher, M., Dommen, J., Ammann, C., Spirig, C., Neftel, A., and Prevot, A. S. H.: Performance characteristics of a proton-transfer-reaction mass spectrometer

(PTR-MS) derived from laboratory and field measurements, International Journal of Mass Spectrometry, 239, 117-128, 2004.

Taipale, R., Ruuskanen, T. M., and Rinne, J.: Lag time determination in DEC measurements with PTR-MS, Atmos. Meas. Tech. Discuss., 3, 405-429, 10.5194/amtd-3-405-2010, 2010.

Tani, A., Hayward, S., and Hewitt, C. N.: Measurement of monoterpenes and related compounds by proton transfer reaction-mass spectrometry (PTR-MS), International Journal of Mass Spectrometry, 223, 561-578, 2003.

Tani, A., Hayward, S., Hansel, A., and Hewitt, C. N.: Effect of water vapour pressure on monoterpene measurements using proton transfer reaction-mass spectrometry (PTR-MS), International Journal of Mass Spectrometry, 239, 161-169, 2004.

Tanimoto, H., Aoki, N., Inomata, S., Hirokawa, J., and Sadanaga, Y.: Development of a PTR-TOFMS instrument for real-time measurements of volatile organic compounds in air, International Journal of Mass Spectrometry, 263, 1-11, 2007.

Tarvainen, V., Hakola, H., Hellen, H., Back, J., Hari, P., and Kulmala, M.: Temperature and light dependence of the VOC emissions of Scots pine, Atmospheric Chemistry and Physics, 5, 989-998, 2005.

Taucher, J., Lagg, A., Hansel, A., Vogel, W., and Lindinger, W.: Methanol in Human Breath, Alcoholism-Clinical and Experimental Research, 19, 1147-1150, 1995.

Turnipseed, A. A., Pressley, S. N., Karl, T., Lamb, B., Nemitz, E., Allwine, E., Cooper, W. A., Shertz, S., and Guenther, A. B.: The use of disjunct eddy sampling methods for the determination of ecosystem level fluxes of trace gases, Atmos. Chem. Phys., 9, 981-994, 10.5194/acp-9-981-2009, 2009.

Velasco, E., Lamb, B., Westberg, H., Allwine, E., Sosa, G., Arriaga-Colina, J. L., Jobson, B. T., Alexander, M. L., Prazeller, P., Knighton, W. B., Rogers, T. M., Grutter, M., Herndon, S. C., Kolb, C. E., Zavala, M., de Foy, B., Volkamer, R., Molina, L. T., and Molina, M. J.: Distribution, magnitudes, reactivities, ratios and diurnal patterns of volatile organic compounds in the Valley of Mexico during the MCMA 2002 & 2003 field campaigns, Atmospheric Chemistry and Physics, 7, 329-353, 2007.

Wang, D. K. W., and Austin, C. C.: Determination of complex mixtures of volatile organic compounds in ambient air: an overview, Anal. Bioanal. Chem., 386, 1089-1098, 10.1007/s00216-006-0475-5, 2006.

Wang, T., Spanel, P., and Smith, D.: A selected ion flow tube study of the reactions of H3O+, NO+ and O2+- with some phenols, phenyl alcohols and cyclic carbonyl compounds in support of SIFT-MS and PTR-MS, International Journal of Mass Spectrometry, 239, 139-146, 2004.

Warneke, C., van der Veen, C., Luxembourg, S., de Gouw, J. A., and Kok, A.: Measurements of benzene and toluene in ambient air using proton-transfer-reaction mass spectrometry: calibration, humidity dependence, and field intercomparison, International Journal of Mass Spectrometry, 207, 167-182, 2001.

Warneke, C., Kato, S., De Gouw, J. A., Goldan, P. D., Kuster, W. C., Shao, M., Lovejoy, E. R., Fall, R., and Fehsenfeld, F. C.: Online volatile organic compound measurements using a newly developed proton-transfer ion-trap mass spectrometry instrument during New England Air Quality Study - Intercontinental Transport and Chemical Transformation 2004: Performance, intercomparison, and compound identification, Environ. Sci. Technol., 39, 5390-5397, 10.1021/es050602o, 2005.

Warneke, C., S. L. Luxembourg, et al.: Disjunct eddy covariance measurements of oxygenated volatile organic compounds fluxes from an alfalfa field before and after cutting, J. Geophys. Res.-Atmos., 107, 2002.

Wehinger, A., Schmid, A., Mechtcheriakov, S., Ledochowski, M., Grabmer, C., Gastl, G. A., and Amann, A.: Lung cancer detection by proton transfer reaction mass-spectrometric analysis of human breath gas, International Journal of Mass Spectrometry, 265, 49-59, 2007.

Whyte, C., Wyche, K. P., Kholia, M., Ellis, A. M., and Monks, P. S.: Fast fingerprinting of arson accelerants by proton transfer reaction time-of-flight mass spectrometry, International Journal of Mass Spectrometry, 263, 222-232, 2007.

Zhao, J., and Zhang, R.: Proton transfer reaction rate constants between hydronium ion (H3O+) and volatile organic compounds, Atmospheric Environment, 38, 2177-2185, 2004.

2 Practical Part

2.1 Introduction to practical part

This part comprises measurements, analyses and method developments.

The first three chapters (2.2 – 2.4) describe fieldwork-derived high frequency measurements of concentrations and fluxes above two different vegetation types (Mediterranean Macchia vegetation, and oil palm in S.E. Asia) using the capabilities of the PTR-MS coupled to virtual disjunct eddy covariance technique (vDEC).

Chapter 2.2 deals with an example of Mediterranean coastal dune habitat, with a marked day/night change in wind directions and therefore VOC transport. During the early stage of Macchia growth in late spring, the vegetation was found to be a large methanol emitter but isoprene and monoterpene were mainly advected from outside the measurement area.

In contrast, chapter 2.3 presents findings from a tropical oil palm plantation. This chapter is the most comprehensive since it deals with multi-directional effects of particularly high VOC fluxes, which were several times higher than from a nearby rainforest location. Although references to rainforest are made, the author's work from the rainforest location is not included in the thesis, but the reader is referred to a paper written in collaboration (Appendix II-F).

Estragole, which was the second most abundantly emitted compound after isoprene at the oil palm plantation, was emitted from flowers. Since estragole can be more important for atmospheric chemistry and aerosol formation than isoprene and has an important ecological significance, a separate chapter (2.4) has been devoted to describing this globally significant floral VOC in more detail. This work has been published in a collaborative paper led by the author (Appendix II-H) but only the author's contribution has been retained in the chapter.

The remaining chapters (2.5 – 2.6) show the author's developments of software and analytical methods.Chapter 2.5 focuses on eddy covariance flux processing, for which a novel lag-time validation and determination methods are proposed.

Chapter 2.6 shows a technical development which extends the selectivity of a standard PTR-MS. This development tested and enabled discrimination of common monoterpenes under alternating drift voltage.

2.2 Ecosystem VOC fluxes from Mediterranean Macchia

This work was the part of my involvement in the ACCENT-VOCBAS-BIAFLUX campaign at the Castelporziano presidential estate near Rome 2007.

Collaborating persons:
CEH: Neil Cape, David Fowler, Eiko Nemitz
University of Lancaster: Ben Langford, Brian Davison, Annette Ryan, Nick Hewitt
University of Rome: Francesco Loreto, Silvano Farez
European Commission Joint Research Centre: Stan Cieslik
Catholic University of Brescia: Angelo Finco, Giacomo Gerosa

Please also refer to my articles as a co-author (approximate contribution in parentheses):

Appendix II-B: Davison, B., ..., Misztal, P., et al.: Concentrations and fluxes of biogenic volatile organic compounds above a Mediterranean macchia ecosystem in western Italy, Biogeosciences, 6, 1655-1670, 2009. (~30% measurement, data processing, lag-time approaches, instrument intercomparison)

Appendix II-A: Cieslik, ..., and Misztal, P.: Turbulence in a coastal Mediterranean area: surface fluxes and related parameters at Castel Porziano, Italy, Biogeosciences Discuss., 6, 3355-3372, 2009. (~5% contribution: wind data processing; footprint analysis which was meant to be included in the revised paper)

Appendix II-C: Fowler, D., ..., Misztal, P., et al.: Atmospheric composition change: Ecosystems-Atmosphere interactions, Atmospheric Environment, 43, 5193-5267, 10.1016/j.atmosenv.2009.07.068, 2009. (less than 1%; part of the synthesis paper)

Table of contents

2.2.1 Abstract

Two PTR-MS instruments were employed in a field campaign at Castelporziano in Italy during early May 2007. The spatial distribution of sources is estimated from the dependence on wind direction of VOC concentrations multiplied by wind velocity, separately for day and night times and presented on polar graphs. During the continuous measurements, a clear diurnal trend of VOC concentrations could be observed, which was consistent for both PTR-MS instruments. Sonic anemometer measurements were synchronised in time with the PTR-MS. Advection from the vegetation source (SW and NE), occurring mostly during the night, correlated well with increased concentrations of monoterpenes and isoprene, while levels of methanol, acetaldehyde and acetone were low. However, the opposite pattern was recorded during the daytime when the wind direction changed to SE and NW, revealing low levels of monoterpenes and isoprene while levels of other measured VOCs exhibited marked enhancement. This must be attributed to specific diurnal and nocturnal wind patterns. The fluxes are presented and comparison with another PTR-MS instrument is made. The results serve to illustrate plant volatiles transport patterns, which can be compared with other measurements or create a basis for the elaboration of terrestrial models. Intercomparisons between PTR-MS instruments are

very scarce in the literature, not only of concentrations but in particular of virtual disjunct eddy covariance fluxes. For example, it has not been known how a different lag-time processing can impact on the flux.

2.2.2 Site description

The measurement campaign took place in Castelporziano, Italy (41°41'58.21" N; 12°21'5.95" E) located over Macchia dune vegetation, between a moderately trafficked road approx. 100 m to the NE and the Tyrrhenian Sea approx. 300 m to the SW. The measurements were part of the ACCENT-VOCBAS campaign. The site characteristics and overview of the campaign have been presented by Fares et al. (2009) and the processes involved in trace-gas and aerosol exchange based on ACCENT measurements were synthesised by Fowler et al. (2009).

2.2.3 Methodology

2.2.3.1 Setup

An Ionicon High Sensitivity PTR-MS (PTRMS1) was run by the team from CEH Edinburgh (Pawel Misztal, Neil Cape) while a standard Ionicon PTR-MS (PTRMS2) was operated by the Lancaster team (Ben Langford, Brian Davison).

The vacuum system in the Edinburgh instrument comprised a Varian V70 turbo pump for the drift tube and another Varian V301 for the detection chamber. There was also an additional Varian V70 turbo pump attached to the detection chamber for the purpose of achieving better vacuum conditions and a better sensitivity to noise ratio, compared to the standard PTR-MS.

The parameters of both PTR-MS instruments were unified as follows: the *E*/*N* ratio was maintained at 128.2 Td with the drift tube voltage of 546 V, pressure of 2.0 mbar and temperature of 50°C. The water flow was set to a maximum of 10 sccm to reduce

the level of background O_2^+ ions to less than 1% of the primary ion counts throughout the experiment.

A sonic anemometer (Gill Solent R2 with 20.83 Hz logging frequency) was deployed to record wind speed vectors and temperature. Sonic anemometer measurements were synchronised with the PTR-MS and logged into one file, separately on two PCs. This resulted in the two identical copies of wind data and two PTR-MS data sets which were specific to a particular PTR-MS instrument. The inlet of the 3/8" PTFE sampling tube was attached close to the sonic anemometer on a tower, which was at 5 m above the ground surface.

A diagram of the setup and photographs of the tower and inlets are presented in Figure 2.2-1a-d. Eight *m/z* channels were measured in the MID mode of the virtual disjunct eddy covariance technique. The duty cycle used during this campaign is presented in Figure 1.4-1 of the theoretical section. The five compounds monitored in vDEC were: methanol (*m/z* 33), acetaldehyde (*m/z* 45), acetone (*m/z* 59), isoprene (*m/z* 69), and monoterpenes (*m/z* 81, *m/z* 137). All these compounds were present in the calibration mixture except for isoprene and monoterpenes. The calibration was performed separately for two instruments during the same interruption period towards the end of campaign. The empirical calibration factors for isoprene and monoterpenes were derived from the fit of the transmission coefficients and calibrated coefficients for the remaining compounds, yielding empirical coefficients. This approach has been described in Davison et al. (2009) and extended by Taipale et al. (2008) in the relative transmission approach.

In addition, every hour a 5-min mass scan was performed, which included an extended suite of 8 compounds other than those included in the flux mode.

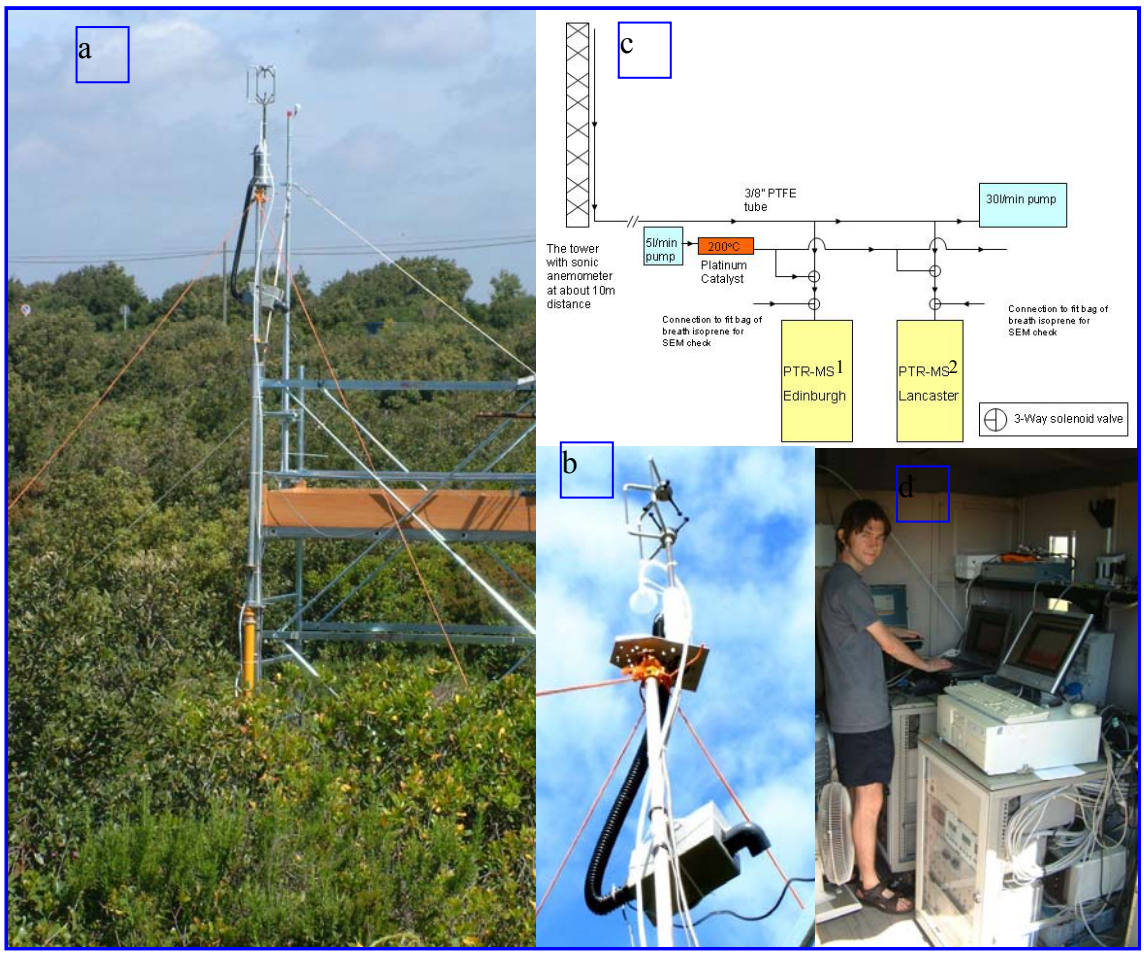

Figure 2.2-1. The setup in Castel Porziano: a) tower with sonic anemometer and the sampling inlet tubing (photo by Neil Cape); b) close-up of the sonic anemometer (photo by Neil Cape); c) schematic of the setup d) data acquisition by two PTR-MS instruments – Pawel Misztal running Edinburgh PTR-MS (photo by Neil Cape).

2.2.3.2 Lag-time approaches tested

As both the PTR-MS instruments were subsampling from the same line the measurements could serve as an intercomparison of the two instruments. Provided that an agreement in concentrations is close for a compound then the two independent flux methods can be compared. For consistency in these comparisons all validation criteria and quality control procedures were exactly the same for the flux data from the CEH instrument processed by the author and the flux data from the Lancaster University (LU) instrument processed by Ben Langford. Details of the

common protocol used are described elsewhere (Davison et al., 2009; Appendix II-B). The only difference was in the technicality of lag-time derivation, which is described below.

Two different processing programs were used relying on similar common procedures and were checked by deriving very similar (almost identical) sensible heat fluxes. The lag time in both programs was derived independently for each half-hour period and compound. The approach used by the author relied on a combination of the MAX and the VIS methods, which were recently described by Taipale et al. (2010). In the MAX method the lag time is obtained from the maximum point in the covariance function. Although this approach worked well for abundant species such as methanol, the peak was not always obvious in the case of other compounds, so the MAX method could lead to a wrongly identified lag time. The LabVIEW routine was designed by the author in order to enable the VIS method to aid the MAX method. For each half hour the program prompted the user for an input of the lag time based on the displayed covariance function. In obvious cases the user could simply press the button which passes the value from the MAX method or could input the same value manually. In the cases where the MAX method was evidently erroneous (e.g., when a spike on the covariance function rather than the true peak was selected) the user could input the correct value. Finally, in the ambiguous cases the user could press the "reject" button which would mark the flux point as invalid.

The approach used by the Lancaster team was different in the sense that a MAX method was constrained by a lag time derived from the humidity sensor mounted inside the tube just before the PTR-MS2 inlet and further accounted for the time of the cycle length and an approximated travel time in the internal tubing. The VIS method was not used.

2.2.4 Results and discussion

2.2.4.1 Concentration Timeseries

The VOC concentrations from both the PTR-MS instruments are presented in Figure 2.2-2a-e. An excellent agreement was found for methanol concentrations, which were the highest of all VOCs and were quantitatively within a 6% error (r^2 =0.99). Slightly less good agreement was shown for concentrations of acetaldehyde; 14% error (r^2 = 0.92). However, discrepancies in acetaldehyde measurements have been known to be significant (de Gouw and Warneke, 2007; de Gouw et al., 2003b), so the agreement at Castelporziano is thought to be rather impressive. The main discrepancy in acetaldehyde concentrations affecting the overall agreement is just after restarting PTR-MS1 measurements after the turbo-pump switched off because of overheating. As mentioned before, the turbo-pumps of the PTR-MS2 instrument were made by a different manufacturer and were more resistant to heat but less to shocks. One explanation for the discrepancy after the start-up could be a transient increase in O_2^+ and NO^+ ions, which were not monitored.

The slope in acetone concentrations was 1.00 but the quality of correlation was not as good as for methanol (r^2 = 0.95). There was an evident offset in the latter part of the campaign which was not fully compensated by the zero-air subtraction. This could be attributed to the small change in sensitivity for acetone in one of the instruments. Isoprene was the least abundant VOC, but the concentration agreement was nevertheless still quite good (r^2 = 0.92; slope = 0.85). Since the calibration factors were empirical the difference falls well within the uncertainty in the transmission approach. However, towards the end of campaign, when the concentrations were particularly small, it could be seen that the less sensitive PTR-MS2 was prone to underestimation due to more zeros counted when the concentrations were low, even though the same instrument was reporting higher concentrations previously. Finally the agreement in the concentrations of total monoterpenes (derived from the sum of

m/z 81 and *m/z* 137) was qualitatively good (r^2 = 0.93) but the difference in the absolute values was almost a factor of 2 (slope = 0.52). Clearly this can come from uncertainty in the transmission approach, which can be very high, particularly for higher *m/z* region. This is still within the limit of 100% provided by Steinbacher et al.(2004). Since both instruments used the same transmission approach the maximal cumulative uncertainty would be 200%. For example it could happen that the relative transmission approach led to overestimated sensitivities for the PTR-MS1 and/or underestimated sensitivities for the PTR-MS2. Because of these discrepancies monoterpene flux comparisons should be treated with caution.

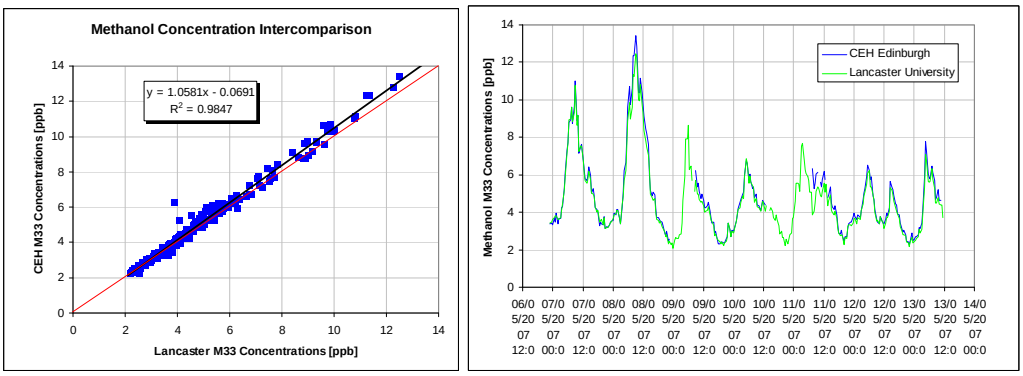

a)

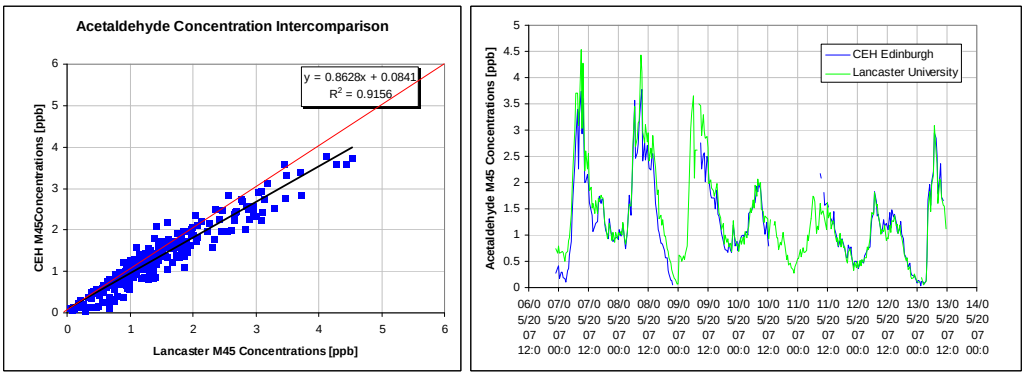

b)

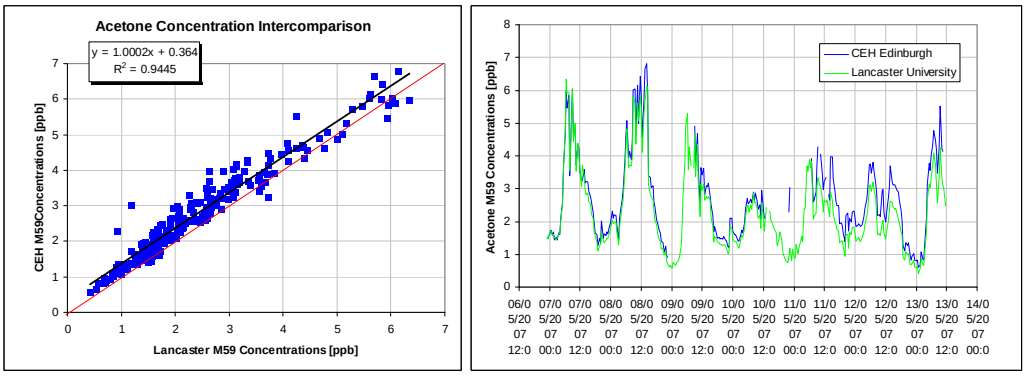

c)

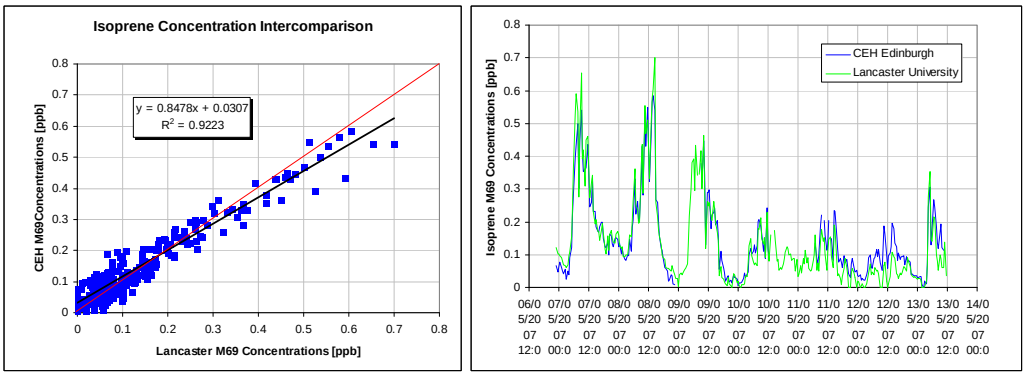

d)

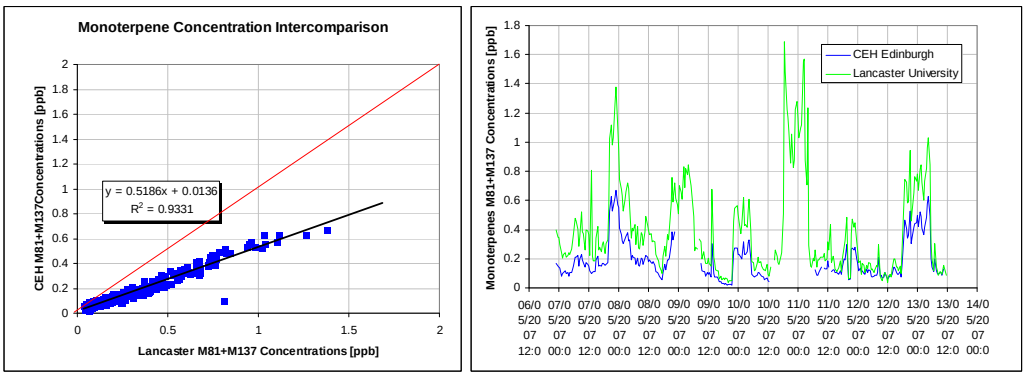

e)

Figure 2.2-2. Intercomparison of both Lancaster and Edinburgh concentration data for a) methanol, b) acetaldehyde c) acetone d) isoprene and e) the sum of monoterpenes.

Overall, a very close agreement can be seen in the summary of basic statistical parameters of the concentration data (Table 2.2-1) except for monoterpenes. The average values were very slightly higher from the PTR-MS1 instrument in the case of methanol, acetone and isoprene, but mean concentrations of acetaldehyde were

higher in PTR-MS2. For the reasons discussed earlier, PTR-MS2 reported a factor two higher monoterpene concentrations than PTR-MS1.

Table 2.2-1. The summary statistics for concentrations (ppb) derived from CEH and Lancaster PTR-MS instruments. Only the CEH data have been derived by the author. The LU data are courtesy of Ben Langford.

	Methanol (*m/z* 33)		Acetaldehyde (*m/z* 45)		Acetone (*m/z* 59)		Isoprene (*m/z* 69)		Monoterpenes (*m/z* 81+137)	
	CEH	LU	CEH	LU	CEH	LU	CEH	LU	CEH	LU
Mean	4.89	4.64	1.29	1.34	2.71	2.28	0.15	0.13	0.19	0.40
Median	4.29	4.11	1.14	1.12	2.48	1.96	0.11	0.09	0.14	0.28
SD	2.16	1.97	0.80	0.88	1.30	1.26	0.12	0.13	0.14	0.32
Max	13.4	12.5	3.78	4.53	6.80	6.35	0.59	0.70	0.67	1.69
Min	2.29	2.10	0.03	0.05	0.60	0.42	0.00	0.00	0.02	0.04
95^{th}	9.69	8.98	2.76	3.09	5.48	5.04	0.43	0.44	0.49	1.09
5^{th}	2.52	2.42	0.16	0.27	1.05	0.74	0.02	0.00	0.06	0.07

2.2.4.2 Windroses

The spatial distribution of VOC sources can be estimated from the dependence on wind direction of VOC concentrations (C_{VOC}) multiplied by wind velocity (v_w). Figure 2.2-3 presents polar graphs of such dependences for the measured VOCs, separately for the day (8:00 – 18:00 GMT) and night (18:00 – 8:00 GMT). The site was characterised by a sea breeze during the day time, and a land breeze (bringing polluted air from Rome) at night. The wind direction changed sometime in the morning, so a clearer effect would be observed if only 5 hours past noon were plotted for the day and 5 hours after midnight for the night. This was done in the paper by Davison et al. (2009) (see Appendix II-B) but the concentrations were not multiplied by the wind speed. In comparison, Figure 2.2-3 shows the complete data separated

equally into 12-h day and night (although the actual day-time was longer than night-time). During the day-time the sources of all VOCs were distributed rather similarly since they were well within the Macchia footprint (see Chapter 2.2.4.4). However, during the night advection was possibly the highest contributor to the approximated source strengths since the turbulence was very small. The night advection was particularly evident in the case of monoterpenes which were carried from an oak and pine forest from the NW. Night time monoterpenes may indicate that monoterpene forest emissions were only temperature dependent, rather than light dependent also, unless the advection was from monoterpenes released during the day but residing in the shallow night-time boundary layer. However, the night time isoprene concentration was very small.

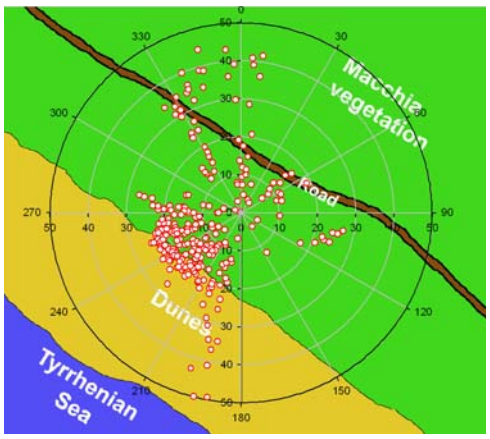

Methanol *m/z* 33 day

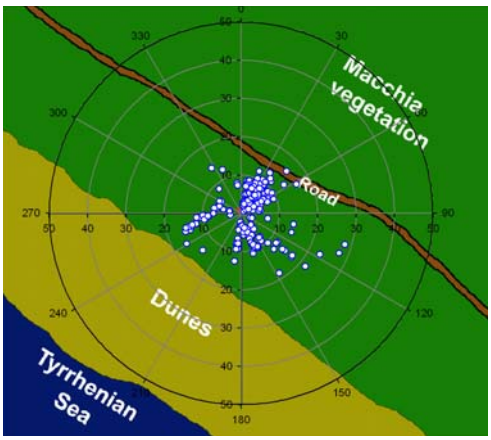

Methanol *m/z* 33 night

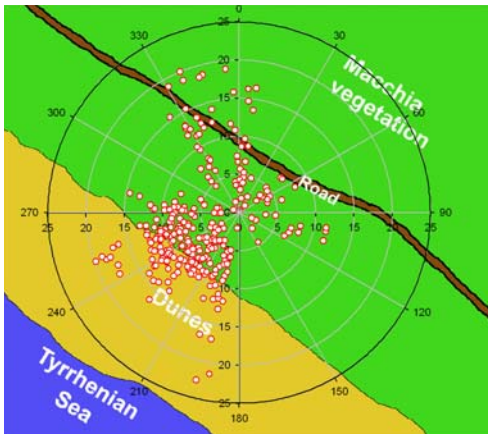

Acetaldehyde *m/z* 45 day

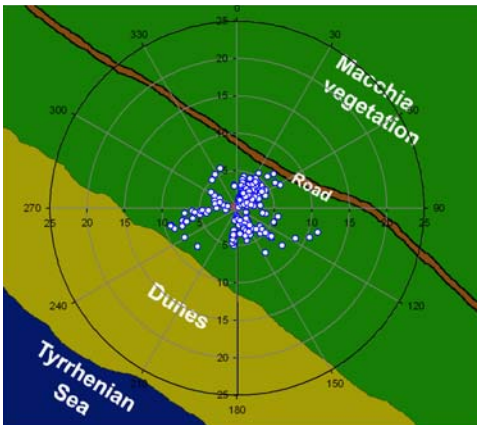

Acetaldehyde *m/z* 45 night

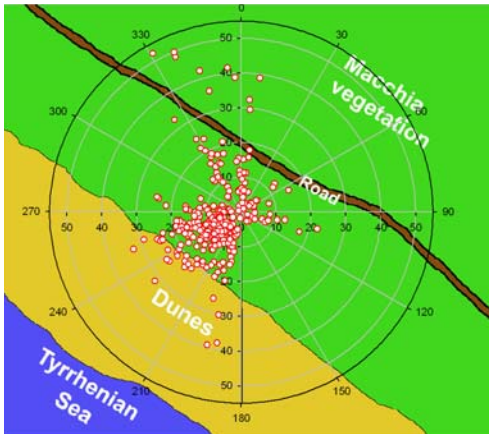

Acetone *m/z* 59 day

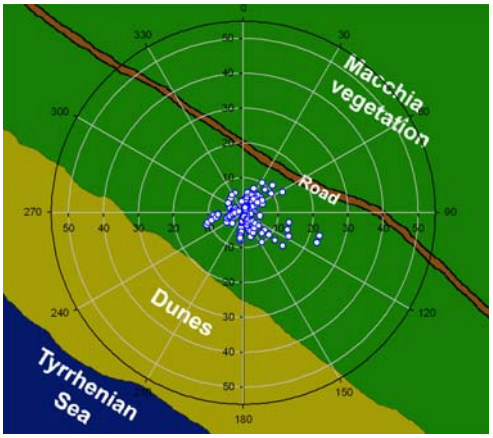

Acetone *m/z* 59 night

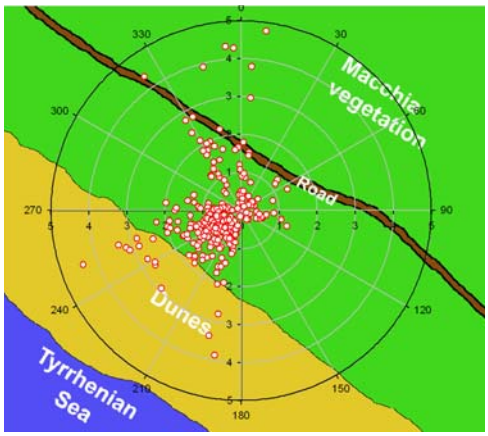

Isoprene *m/z* 69 day

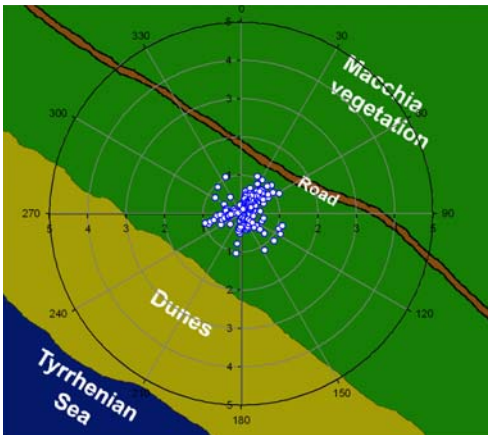

Isoprene *m/z* 69 night

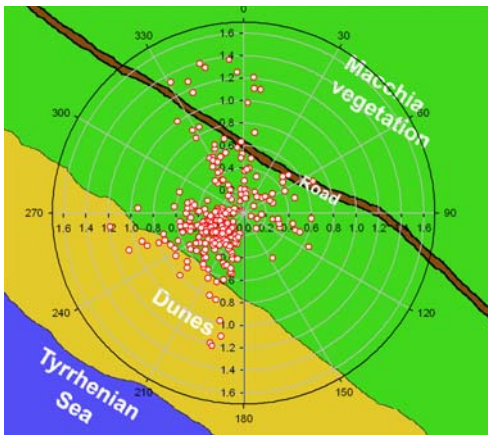

Monoterpenes *m/z* 81 day

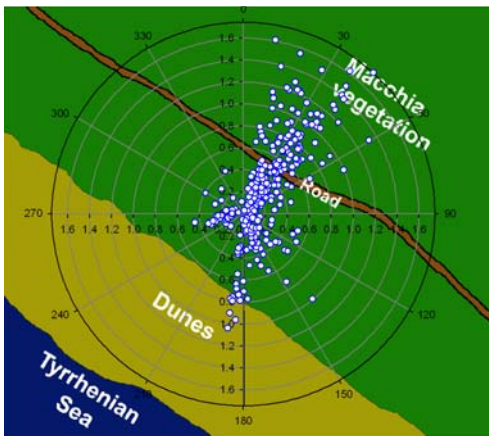

Monoterpenes *m/z* 81 night

Figure 2.2-3. Polar graphs presenting the concentrations of VOCs multiplied by wind speed (ppb m s^{-1}) and plotted against the wind direction.

2.2.4.3 Flux results and intercomparison

The fluxes measured by the Edinburgh and Lancaster PTR-MS instruments were processed independently, by different LabVIEW programs, but using similar principles and differing only in the lag-time approach (as discussed in Chapter 2.2.3.2). The flux inter-comparisons are presented in Figure 2.2-4 a-e. The agreements in the fluxes were generally not as good as in the concentrations. However, flux processing is much more challenging. The main factors that could play a role were: sensitivity, noise of the covariance, and most importantly the lag-time approach. The first two could be attributed to the different response times of the standard and high-sensitivity instruments. The former instrument would be prone to losses in the high frequency region. The remaining difference would most probably result from the different lag-time approach used. Bearing these in mind the agreement in fluxes was quite good with slopes of 1.1, 1.2, 1.4, 1.2 and 1.0 for methanol, acetone, isoprene, acetaldehyde and monoterpene fluxes, respectively. The goodness of fit values measured as r^2 were 0.67, 0.70, 0.72, 0.52 and 0.38, respectively. The correlation coefficients can be significantly degraded if just a few flux sign errors made by either method were present. This was particularly the case for monoterpenes, where the author's method derived mainly deposition at night but

the method of the collaborating colleague showed small emission. The lag validity method and the internal median lag-method, which the author introduces in Chapter 2.5, had not been developed at the time of the processing of the data for this campaign but could serve as a more thorough validation of the lag times. It seems that all the fluxes reported by the author's method were slightly higher than the fluxes reported by the other researcher. Just the high frequency losses due to different response times of the instruments could explain these differences although they would be expected to be similar for the same compounds. However, discrepancies seem to be particularly exacerbated at small concentrations or with potentially depositing compounds. It would be possible that the fluxes from PTR-MS1 had been overestimated if the MAX method had been used with only one data set, but as it was used in both the only difference was that one method was aided by the VIS method and the second was constrained by the lag time of the humidity sensor. However the latter method could potentially be prone to lag-time errors for the portion of data where the lag time was different from that of water. The results of lag-time developments by the author (chapter 2.5) and other researchers (e.g. Taipale et al., 2010) suggest that the lag-time can vary significantly from one integration period to another, which can be more due to the start of a QMS cycle than the effective residence time. In addition, the travel time from the inlet to the detector can be relatively long. The consequences of a mis-identified lag-time are underestimation or errors of the flux sign. Nevertheless, the overall agreement was quite good, which can be seen in the summary statistics presented in Table 2.2-2.

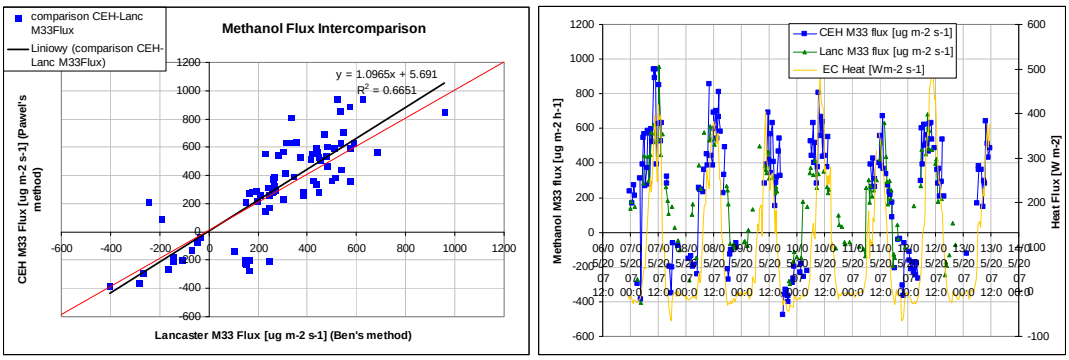

a)

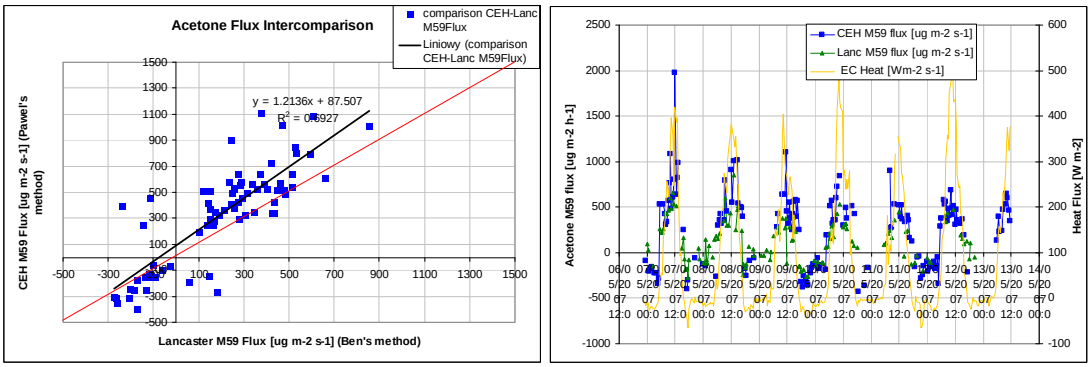

b)

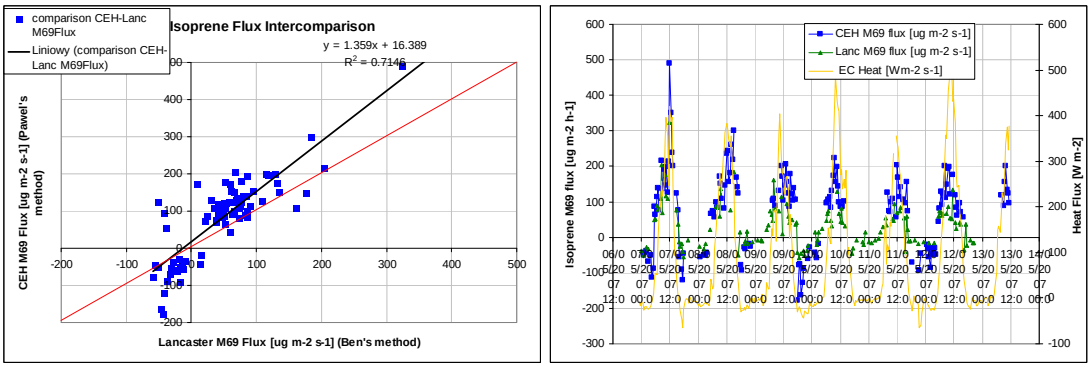

c)

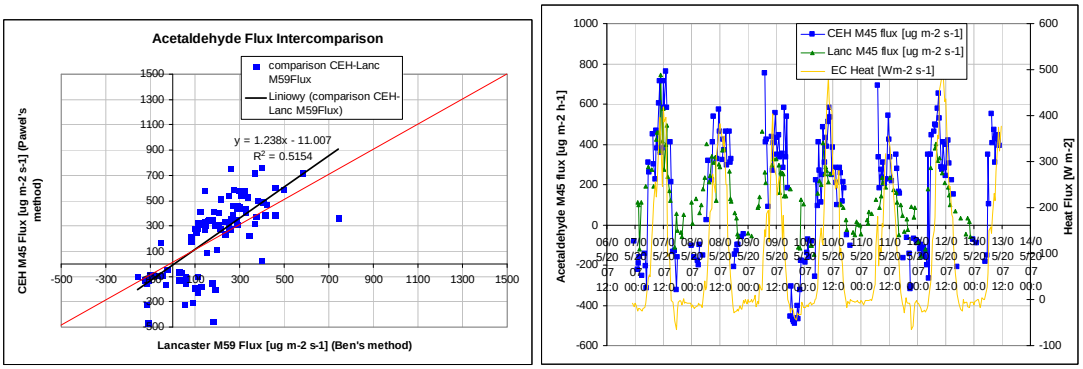

d)

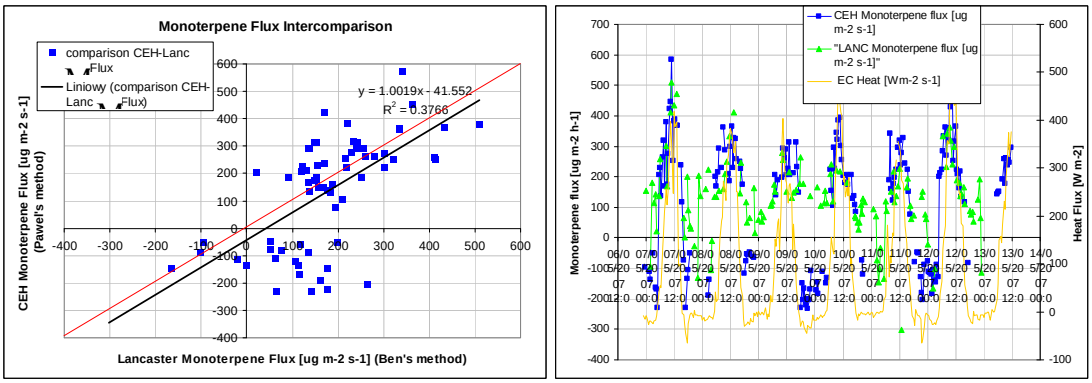

e)

Figure 2.2-4. Intercomparison of both Lancaster and Edinburgh flux data for a) methanol, b) acetone c) isoprene d) acetaldehyde and e) the sum of monoterpenes.

The summary statistics for fluxes derived by the two methods are shown in Table 2.2-1. Despite the good correlations, mean fluxes derived by the author's method were higher than the fluxes derived by the other method by 29%, 13%, 96%, 250%, and 1% for methanol, acetaldehyde, acetone, isoprene and monoterpenes, respectively. Methanol and acetaldehyde seem to be therefore well within the flux uncertainty, but the difference in the mean fluxes for acetone and isoprene was very high. Paradoxically, monoterpene mean values were almost identical, since the difference in the concentrations reported earlier was compensated. However the last three compounds had the most challenging lag times to identify, and this was one of the reasons why the VIS approach or the humidity-sensor approach were used. Since the latter approach was automatic (i.e. the covariance function was not inspected manually) it would be very susceptible to misidentifications, in particular as there was no guarantee that the lag time of low concentration species would be similar to the lag time of water vapour. However, the author's method was not perfect either, as it relied on the MAX method which can overestimate the small fluxes. The ideal solution would be the IMED method validated by the LTV test (see chapter 2.5). The expected fluxes could be somewhere in between the two methods. These methods could also answer the question whether the deposition of night time monoterpenes reported by the author was real. However, high concentrations of monoterpenes at night clearly advected from the forest imply that deposition was more likely. Since Macchia vegetation in its early phenological stage was a small monoterpene emitter during the day it would be unlikely to expect that it was emitting monoterpenes at night.

Table 2.2-2. The basic statistics for LU and CEH fluxes (µg m^{-2} h^{-1}). Only the CEH data have been processed by the author. The LU data are courtesy of Ben Langford.

	Methanol (*m/z* 33)		Acetaldehyde (*m/z* 45)		Acetone (*m/z* 59)		Isoprene (*m/z* 69)		Monoterpenes (*m/z* 81+137)	
	CEH	LU	CEH	LU	CEH	LU	CEH	LU	CEH	LU
Mean	256	199	171	151	263	134	80.5	31.5	132	133
Median	326	235	256	131	343	138	99.2	31.6	197	134
SD	340	261	302	164	394	232	107	60	198	130
Max	942	957	761	744	1980	854	490	324	585	509
Min	-477	-404	-489	-156	-425	-273	-177	-58.3	-232	-302
95^{th}	693	575	581	414	862	514	220	130	385	349
5^{th}	-324	-193	-317	-104	-324	-186	-88.7	-44.5	-192	-104

2.2.4.4 Footprint analysis

The footprint analysis was made following the theory described in detail by Kormann and Meixner (2001). Intercomparison of turbulence parameters and footprints of different collocated sampling sites during the ACCENT campaign were the goals of the paper led by Cieslik et al. (2009; Appendix II-A). The key point of analysis performed by the author (Figure 2.2-5) is that 70% of the day-time flux was well within the Macchia footprint, so the day-time flux values reported by Davison et al. (2009; Appendix II-B) and the author can be regarded as representative for the Macchia area. The distance to the maximal flux (xmaxf) was completely within the Macchia area. The Korman and Meixner footprint model for non-neutral stratification was chosen as it was relatively simple and was valid under all atmospheric stability conditions.

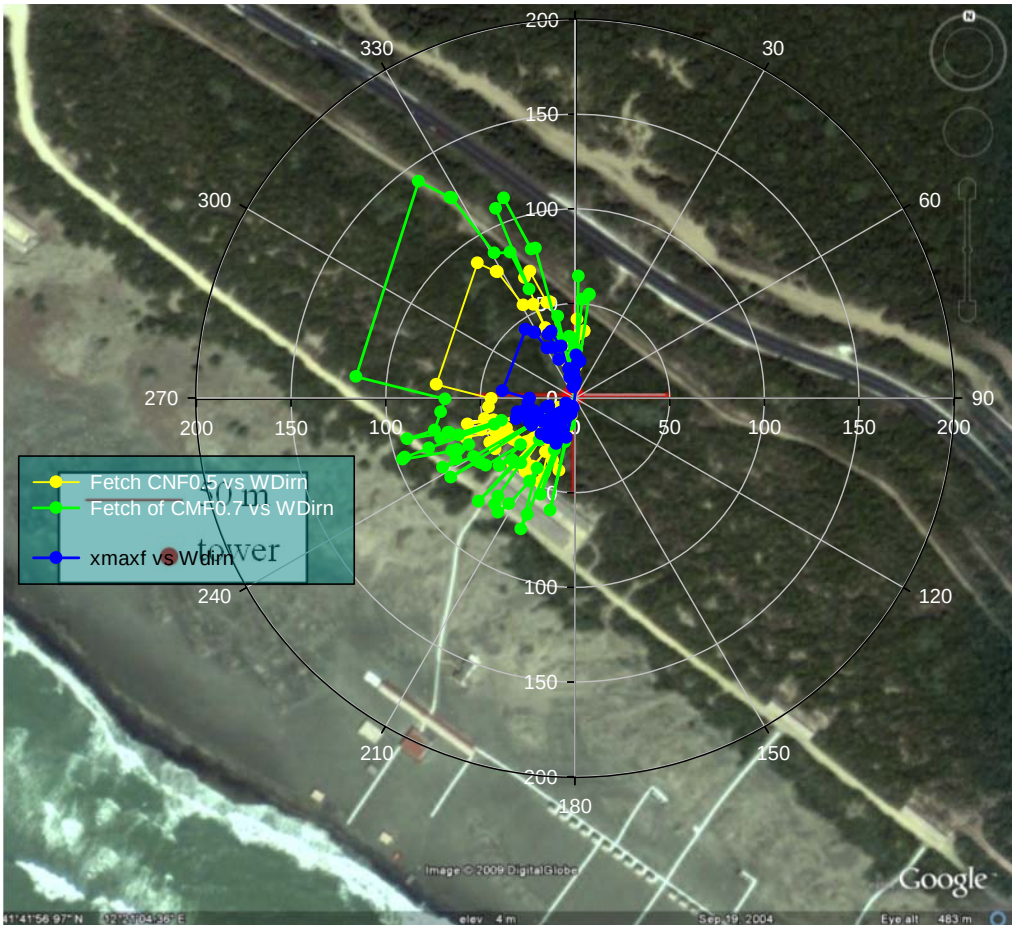

Figure 2.2-5 Cumulative normalised footprints derived from the CEH sonic anemometer. The blue line represents the distance to the maximum in the footprint and the yellow and blue lines correspond to the fetches of 50% and 70% of the footprint, respectively.

2.2.4.5 VOCs derived from mass scans

Concentrations of a further eight compounds, which were not included in the flux mode, were measured for 5 minutes every hour. The timeseries for these compounds, as volume mixing ratios (VMRs), are shown in Figure 2.2-6. Elevated VMRs of dimethyl sulphide (DMS) were noted during the middle of the day, particularly on the 10th and 12th of May 2007. However, in the first three days the level of DMS was low.

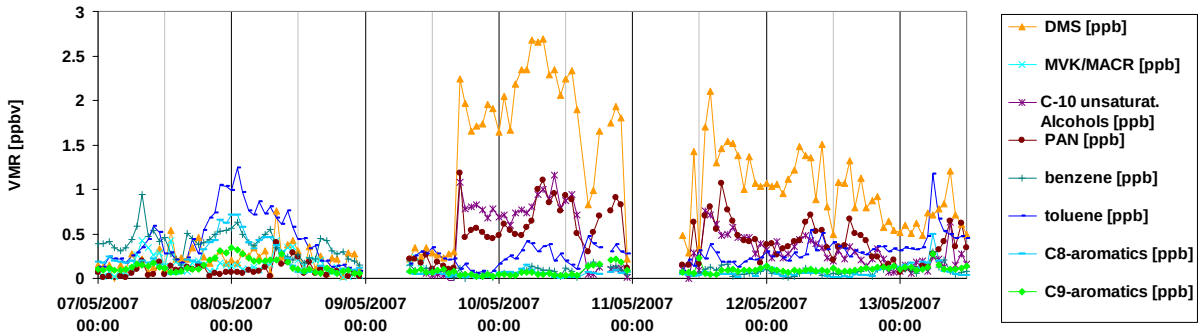

Figure 2.2-6 Timeseries for concentrations of additional compounds monitored in the 5-min scans.

The wind roses for these compounds (Figure 2.2-7) indicate that the elevated DMS was coming from the sea. Peroxyacyl nitrates (PAN) were elevated during the day, skewed towards evening and similar in trend to C-10 unsaturated alcohols and toluene, which may correspond to aged polluted air masses advected from Rome. This can also be seen in the windrose for the toluene-to-benzene ratio. Since the direction was similar to the direction of the forest, one could argue whether the elevated *m/z* 93 could not correspond to p-cymene or monoterpenes. This is not likely since the highest benzene-to-toluene ratios were observed from this direction. The recent research by Ambrose et al. (2010) suggested that the contribution from a high loading of monoterpenes to *m/z* 93 is insignificant.

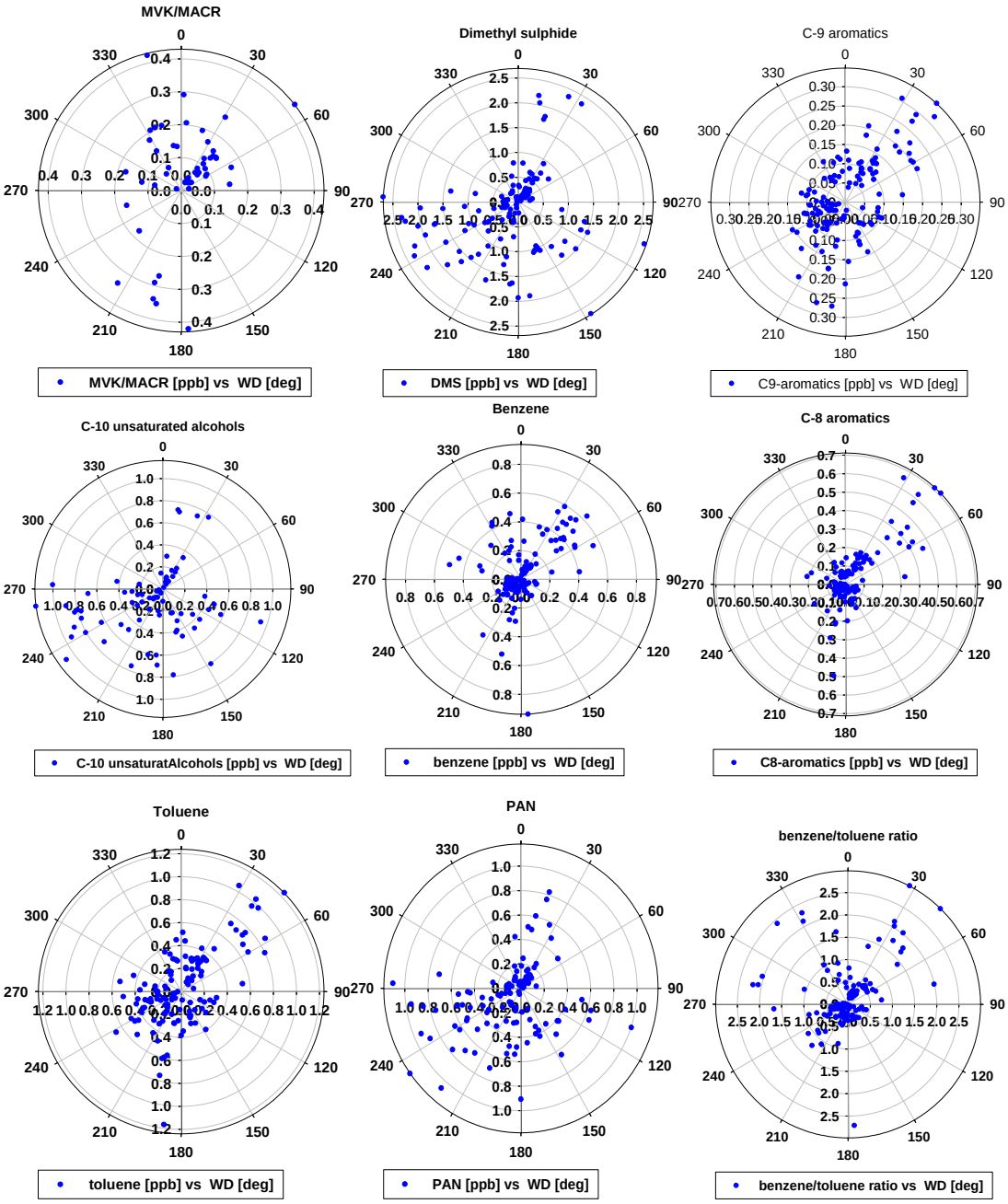

Figure 2.2-7 Windroses of concentrations (as ppbv) of 8 additional compounds.

2.2.5 Conclusions

The results presented in this chapter complement the findings reported elsewhere (Cieslik et al., 2009; Davison et al., 2009; Chapters II-A, II-B). PTR-MS instruments, which differed in response times, were able to provide almost identical results in terms of concentrations of the compounds that were calibrated by the use of an external standard. The difference in the absolute values of monoterpene concentrations was almost 100% even though the agreement in the pattern was very good. This suggests that the approach of deriving the concentrations from the transmission can be prone to a high error which has been known to be the case for compounds of high molecular weight.

The use of the two flux methods differing in the type of lag-time approach used and type of PTR-MS suggested that the identification of the correct lag-time could be crucial for the precision of the absolute flux measurement.

The coastal location at Castelporziano provides an example of a clear shore effect which has an impact on the transport of VOCs. The data suggest that deposition of monoterpenes was probable at night but the data were on the limit of the validation criteria which is typical for night times when the turbulence is low.

Nevertheless, the results show the contribution of this vegetation type to atmospheric VOC concentrations, with implications for ozone formation downwind.

References

Ambrose, J. L., Haase, K., Russo, R. S., Zhou, Y., White, M. L., Frinak, E. K., Jordan, C., Mayne, H. R., Talbot, R., and Sive, B. C.: An intercomparison of GC-FID and PTR-MS toluene measurements in ambient air under conditions of enhanced monoterpene loading, Atmos. Meas. Tech. Discuss., 3, 1-54, 10.5194/amtd-3-1-2010, 2010.

Cieslik, S. A., Gerosa, G., Finco, A., Matteucci, G., Cape, N., and Misztal, P.: Turbulence in a coastal Mediterranean area: surface fluxes and related parameters at Castel Porziano, Italy, Biogeosciences Discuss., 6, 3355-3372, 2009.

Davison, B., Taipale, R., Langford, B., Misztal, P., Fares, S., Matteucci, G., Loreto, F., Cape, J. N., Rinne, J., and Hewitt, C. N.: Concentrations and fluxes of biogenic volatile organic compounds above a Mediterranean macchia ecosystem in western Italy, Biogeosciences, 6, 1655-1670, 2009.

de Gouw, J., and Warneke, C.: Measurements of volatile organic compounds in the earths atmosphere using proton-transfer-reaction mass spectrometry, Mass Spectrom. Rev., 26, 223-257, 10.1002/mas.20119, 2007.

de Gouw, J. A., Goldan, P. D., Warneke, C., Kuster, W. C., Roberts, J. M., Marchewka, M., Bertman, S. B., Pszenny, A. A. P., and Keene, W. C.: Validation of proton transfer reaction-mass spectrometry (PTR-MS) measurements of gas-phase organic compounds in the atmosphere during the New England Air Quality Study (NEAQS) in 2002, J. Geophys. Res.-Atmos., 108, 2003.

Fares, S., Mereu, S., Scarascia Mugnozza, G., Vitale, M., Manes, F., Frattoni, M., Ciccioli, P., Gerosa, G., and Loreto, F.: The ACCENT-VOCBAS field campaign on biosphere-atmosphere interactions in a Mediterranean ecosystem of Castelporziano (Rome): site characteristics, climatic and meteorological conditions, and eco-physiology of vegetation, Biogeosciences, 6, 1043-1058, 10.5194/bg-6-1043-2009, 2009.

Fowler, D., Pilegaard, K., Sutton, M. A., Ambus, P., Raivonen, M., Duyzer, J., Simpson, D., Fagerli, H., Fuzzi, S., Schjoerring, J. K., Granier, C., Neftel, A., Isaksen, I. S. A., Laj, P., Maione, M., Monks, P. S., Burkhardt, J., Daemmgen, U., Neirynck, J., Personne, E., Wichink-Kruit, R., Butterbach-Bahl, K., Flechard, C., Tuovinen, J. P., Coyle, M., Gerosa, G., Loubet, B., Altimir, N., Gruenhage, L., Ammann, C., Cieslik, S., Paoletti, E., Mikkelsen, T. N., Ro-Poulsen, H., Cellier, P., Cape, J. N., Horvath, L., Loreto, F., Niinemets, U., Palmer, P. I., Rinne, J., Misztal, P., Nemitz, E., Nilsson, D., Pryor, S., Gallagher, M. W., Vesala, T., Skiba, U., Brueggemann, N., Zechmeister-Boltenstern, S., Williams, J., O'Dowd, C., Facchini, M. C., de Leeuw, G., Flossman, A., Chaumerliac, N., and Erisman, J. W.: Atmospheric composition change: Ecosystems-Atmosphere interactions, Atmospheric Environment, 43, 5193-5267, 10.1016/j.atmosenv.2009.07.068, 2009.

Kormann, R., and Meixner, F. X.: An analytical footprint model for non-neutral stratification, Bound.-Layer Meteor., 99, 207-224, 2001.

Steinbacher, M., Dommen, J., Ammann, C., Spirig, C., Neftel, A., and Prevot, A. S. H.: Performance characteristics of a proton-transfer-reaction mass spectrometer (PTR-MS) derived from laboratory and field measurements, International Journal of Mass Spectrometry, 239, 117-128, 2004.

Taipale, R., Ruuskanen, T. M., Rinne, J., Kajos, M. K., Hakola, H., Pohja, T., and Kulmala, M.: Technical Note: Quantitative long-term measurements of VOC concentrations by PTR-MS - measurement, calibration, and volume mixing ratio calculation methods, Atmospheric Chemistry and Physics, 8, 6681-6698, 2008.

Taipale, R., Ruuskanen, T. M., and Rinne, J.: Lag time determination in DEC measurements with PTR-MS, Atmos. Meas. Tech. Discuss., 3, 405-429, 10.5194/amtd-3-405-2010, 2010.

2.3 First direct ecosystem fluxes of BVOCs from oil palms

This work was the part of my involvement in OP3/ACES campaign at oil palm plantation May/June 2008. It contains my work, which was inspired by myself and by suggestions/ discussions with the collaborating/participating team.For this chapter, only the data and analysis performed by the author is presented, otherwise the reference is clearly cited, for example if a comparison is made (i.e. other studies such as at the rainforest). Although deriving the micrometeorological parameters (such as u_*),from the sonic anemometer and the latent fluxes from the LiCOR were not the responsibility of the author, they were derived independently by the author. These were later checked and found consistent with the official data.

Collaborating persons:
CEH: Neil Cape, David Fowler, Eiko Nemitz, Sue Owen
The University of Edinburgh: Mat Heal
University of Lancaster: Ben Langford, Annette Ryan, Nick Hewitt
NCAR: Alex Guenther, Peter Harley
EPA USA: Chris Geron
Oregon Graduate Institute: Rei Rasmussen

This chapter corresponds to a draft of an article to be published in ACP 2010: Please also refer to my articles as a co-author in appendix II (approximate contribution in parentheses):
Appendix II-D: Hewitt, C. N., ..., Misztal, P., et al.: Nitrogen management is essential to prevent tropical oil palm plantations from causing ground-level ozone pollution, Proceedings of the National Academy of Sciences, 106, 18447-18451, 10.1073/pnas.0907541106, 2009. (10%; data collection and processing)

Appendix II-E Hewitt, C. N., ... , Misztal, P., et al.: Overview: oxidant and particle photochemical processes above a south-east Asian tropical rainforest (the OP3 project): introduction, rationale, location characteristics and tools, Atmos. Chem. Phys., 10, 169-199, 20 (10%: writing, data collection, data processing)

The author has been also contributing to the following papers in preparation:

a) *MacKenzie, ... Misztal ... , et al. The atmospheric chemistry of trace gases and particulate matter emitted by different land uses in Borneo, Phil.Trans, in preparation 2010 (10% contribution with data analysis and results)*
b) *Fowler, Nemitz, Misztal, ...et al. Effects of land use on trace gas emissions and deposition in Borneo: comparing atmosphere-surface exchange over oil palm plantations with a rain forest. Phil. Trans. 2010 in preparation(25% contribution)*
c) *Hewitt, ..., Misztal..., et al. Isoprene emissions from tropical tree canopies are under circadian control (30% contribution), Nature, 2010 in preparation.*

Table of contents

2.3.1 Abstract

This chapter reports for the first time in South East Asia direct eddy covariance fluxes of reactive volatile organic compounds (VOCs) from oil palms to the atmosphere using proton-transfer-reaction mass spectrometry (PTR-MS). Net midday isoprene eddy covariance flux constituted the largest fraction (84%) of all VOCs emitted, peaking at up to 30 mg m^{-2} h^{-1}. For isoprene mostly upward fluxes were recorded, while oxidation products such as methyl vinyl ketone (MVK) and methacrolein (MACR) exhibited clear deposition. Approximately 15% of the VOC flux from oil palm trees can be related to floral emissions, which are thought to be the highest biogenic source of estragole and possibly also toluene. The basal emission rate for isoprene is adjusted in the Guenther et al. 2006 algorithm for MEGAN using oil palm canopy data and the parameterisation is performed for isoprene and other emitted VOCs driven by temperature and PAR. Upscaling oil palm VOC emissions to global contributions from oil palm plantations to the atmosphere yielded the value of 5 Tg a^{-1}. This means that the high isoprene emissions constitute currently only 1% of global vegetative emissions. However, using the Niinemets et al. 2007 process-based model and predictions in the cultivation area, temperature rise and concentrations of CO_2 it is shown that the

emissions can triple in the next 5 decades. We parameterise fluxes of depositing compounds using the Nemitz et al. 2009 resistance approach using direct canopy measurements of deposition. We propose that it is important to include deposition in models, especially for secondary oxidation products, in order to prevent flux overestimation. Nevertheless, the overall equivalent aerosol contribution from VOCs is high (1 mg m^{-2} h^{-1}) which is exceeding that of the rainforest approximately by the factor of 3.

2.3.2 Introduction

Emissions of biogenic volatile organic compounds (BVOCs) constitute approximately 90% of all atmospheric volatile organic compounds (VOCs), half of which are contributed by one compound – isoprene, which has an estimated global annual emission from vegetation of ~ 600 Tg (Guenther et al., 2006). VOCs play many important roles in atmospheric chemistry, for example serving as sinks for OH radicals, and thus indirectly prolonging the lifetime of pollutants and greenhouse gases in the troposphere. They also contribute to the formation of tropospheric ozone and secondary organic aerosol, and thus indirectly impact regional and global climate.

However, their representation in current models has high uncertainties because of the limited number of measurements, particularly in tropical regions, which are thought to contribute half of the global VOC emissions (Karl et al., 2004). In particular, there are practically no VOC data from South East Asia, where there are large land-use changes with rainforest being converted to oil palm plantations. It has only recently been found that oil palms (*Elaeis guineensis*) are very high isoprene emitters (Wilkinson et al., 2006).

This thesis chapter presents the first above-canopy eddy-covariance measurements of BVOC fluxes from oil palms, by proton-transfer-reaction mass spectrometry (PTR-MS), which were part of author's involvement in two overlapping projects: Oxidant

and Particle Photochemical Processes (OP3) and Aerosol Coupling in the Earth System (ACES). These projects made VOC flux and other atmospheric measurements at two contrasting sites: a secondary rainforest, and an oil palm plantation, about 80 km apart. The detailed list of measurements can be found in the introductory paper of the special issue of *Atmospheric Chemistry and Physics* (Hewitt et al., 2010).

There are currently 14 million ha of oil palm plantations worldwide (FAO, 2009), nearly 9 million ha of which are located in South East Asia. It is consequently important to understand the atmospheric chemistry occurring in this ecosystem, and the potential impacts on climate, following the change in land-use from rainforest. Although this paper focuses on oil palm, VOC fluxes from the rainforest are reported in the special issue by Langford et al. (2010). The lack of measured emission rates of BVOCs, especially from tropical regions, leads to significant uncertainties in modelling future global climate scenarios.

Global modelling often has to rely on up-scaling from leaf level emissions without the constraints imposed by the corresponding ecosystem-scale measurements. Uncertainties arise not simply because of a lack of knowledge of leaf-level emissions, but also of the processes by which BVOCs are transported within and from the forest canopy, the possibility of deposition, and of chemical reactions within the canopy. Oil palms form a monoculture, which is ideal for constraining the scale-up of a frond-level measurement with above-canopy eddy covariance data. This comparison is more difficult for the rainforest, where there is great diversity of vegetation types, and where ecosystem scale measurements are particularly required.

Emission algorithms have not yet been validated for the SE Asian tropics and therefore may need adjustment by parameterisation based on the above-canopy data. Below are presented parameterisations for BVOC emissions from oil palms, including factors to account for the circadian control of emission. The oil palm (*Elaeis guineensis*) has an unusual emission response to radiation and temperature in that emission rates exhibit an internal circadian cycle. Although most plants probably

do not follow circadian rhythms, Wilkinson et al. (2006) reported that the circadian rhythm in oil palms is particularly strong. It is likely, therefore, that use of a constant basal emission rate (BER) might lead to either overestimation or underestimation of emission rates depending on the time that a leaf-level BER is taken.
It is also shown here that parameterisation of the G06 algorithm (Guenther et al., 2006) can compensate for a circadian rhythm, even with a constant BER. However, variabilities in BERs (Niinemets et al., 2010a; Niinemets et al., 2010b) regarded as a range of representative values, can be an issue for precise modelling, in particular because *Elaeis guineensis* is sensitive to various climatic variations, such as soil water deficit (Legros et al., 2009).

2.3.3 Methodology

2.3.3.1 Site and sampling system

The experiment was conducted in the NE part of Borneo, in the Sabah province of Malaysia, in May-June 2008. The experimental site (5°14'52.67''N latitude, 118°27'14.96''E longitude) was located within a flat 33 ha zone of commercial oil palm plantation surrounded by a much larger oil palm area belonging to the Sabahmas Oil Palm Plantation and owned by Wilmar International Ltd. The nearest town is Lahad Datu at a distance of 28 km NE. The palms were 12 year old *E. guineensis* × *E. oleifera* hybrids of the progeny "Gutherie", with an average height of 12 m, a single-sided leaf area index (LAI) of about 6, and a commercial planting density of 150 trees ha^{-1}. A summary of atmospheric measurements as part of the OP3 and ACES projects at this site was presented in the introductory paper of the special issue (Hewitt et al., 2010). The instrumentation was as described by Misztal et al. (2010c) (see also chapter 2.7). The sampling inlet of a 20 m PTFE tube (1/4" OD) was attached at a height of 15 m, close to a 20 Hz Solent Gill R3 sonic anemometer, on a pump-up mast. The other end was connected to a 35 L min^{-1} pump and the PTR-MS sub-sampled continuously at a flow rate of 0.4 L min^{-1}. The ground-level section of the tubing, including the solenoid valves, was heated by a resistance heating tape (Omega, UK type SRF3-2C self-regulating heat cable) to 40

ºC and insulated by a polymer foam sleeve in order to prevent water condensation. The high flow rate in the main line had two purposes: (1) to maintain a high Reynold's number ($R_e > 6000$) in the tubing, as required for measuring the turbulent eddy covariance flux, and (2) to ensure low pressure, thereby protecting against condensation.

2.3.3.2 Proton Transfer Reaction Mass Spectrometry (PTR-MS)

The concentrations and eddy fluxes of biogenic volatile organic compounds (BVOCs) were measured by a Proton-Transfer-Reaction Mass Spectrometer (PTR-MS) operated in continuous flow disjunct eddy covariance (cfDEC) mode, or in the virtual disjunct eddy covariance (vDEC) mode, described in the next section. The instrument was the high-sensitivity model (Ionicon, Austria, s/n 04-03) which was equipped with an additional turbomolecular pump for the detection chamber and incorporated Teflon®, instead of Viton®, gaskets in the drift tube. Since the characteristics of instrument design and operation have been thoroughly described in the literature (Blake et al., 2009; de Gouw, 2007; Hansel et al., 1995; Lindinger et al., 1998; Warneke et al., 2001), only a general overview specific to running at high humidity will be given here.

The principle of PTR-MS is the soft ionisation of VOCs by hydronium ions formed in a hollow cathode ion-source from pure water vapour; these effectively transfer protons to all molecules with proton affinities (PA) greater than that of water. Most VOCs have sufficiently large PA for effective ion transfer, but a few low-weight molecular compounds, with PA only slightly higher than water (e.g. formaldehyde), may require specific optimisation to minimise the impact on sensitivity of humidity dependent back-reactions. The conditions inside the reaction chamber are dependent on both electric field (E) and the number density of the buffer gas (N) and the ratio of these (E/N) determines the degree of fragmentation and clustering. At typical ambient conditions this ratio is kept in the range 120 – 140 Td (1 Td = 10^{-17} V cm^2). However, for a constant E/N ratio the sensitivity is proportional to N and thus operation at 2 mbar or larger is recommended (Warneke et al., 2001). The protonated ions are filtered through a quadrupole mass filter (QMA 400) and counted with a

Secondary Electron Multiplier (Pfeiffer SEM-217) coupled to an ion-count pre-amplifier (Pfeiffer CP-400). The radio-frequency and direct current is generated from an RF box (Pfeiffer QMH400). Since the sampled VOCs undergo protonation, they are detected at a mass to charge (*m/z*) ratio equal to one unit greater than their molecular weight. The soft ionisation method means that most compounds can be detected as their parent ion. For heavier compounds (*m/z* >100) two or more protonated masses may need to be taken into account. This is the case, for example, for monoterpenes (*m/z* 137, 81) (e.g. Tani et al., 2003) and sesquiterpenes (*m/z* 205, 149) (Kim et al., 2009). Because some compounds fragment more than others, appropriate calibration and calculation approaches have to be applied (sections 2.3.3.3 and 2.3.3.4).

The optimisation of the PTR-MS and the sampling system sought a compromise between reliable measurements at very high humidity and sensitivity for VOCs. Tani et al. (2004) showed that sample humidity has a significant impact on fragmentation patterns at normal *E/N* ratios, but has no influence if *E/N* is kept around 140 Td. The range of water vapour pressures tested by these authors was from 0.59 to 2.4 kPa. However, the vapour pressures encountered at the oil palm site were much higher, ranging from 2.5 to 3.2 kPa (2.75 kPa on average) due to high relative humidity (88% on average) accompanied by high temperatures (22 – 31 °C). Humidity effects on PTR-MS measurements were also studied by Warneke et al. (2001), who noted decreasing sensitivities at higher humidities, although again the levels of specific humidity encountered in Borneo were not tested by these authors. Although the sensitivity could be enhanced by increasing the drift tube pressure to 2 - 3 mbar this approach was not possible for the conditions here, because the high flow in the sampling line and the high specific humidity would have required operation at a detection pressure close to or above the set points of the instrument. In addition, higher drift tube pressure would have increased the likelihood of internal condensation.

Therefore, the optimal operating conditions were determined experimentally to be a drift tube pressure of 1.6 mbar, inlet and drift-tube temperatures of 45 ºC and drift

voltage of 485 V, giving an *E/N* value of 140 Td. This was maintained constant throughout the experiment. Our subsequent measurements in the laboratory revealed less than 5% reduction in sensitivity when operating at 1.6 mbar drift tube pressure, compared to 2.2 mbar at the same *E/N* ratio. However, high ambient water vapour pressure had an impact on the sensitivities, and normalisation for the presence of water clusters was required (Davison et al., 2009; Tani et al., 2004). The overall reduction in sensitivity was estimated at 20% with respect to operation at temperate humidities.

The system was automated to run continuously in 3 modes: (1) *m/z* 21-206 scan of ambient air; (2) multiple ion detection (MID) of 11 pre-selected VOCs at 0.5 s dwell time each (0.2 s for additional *m/z* 21 and 37 corresponding to $H_3{}^{18}O^+$ and $H_3{}^{16}O(H_2{}^{16}O)^+$, respectively; and (3) *m/z* 21-206 background measurement of humid VOC-free air. Mode 1 was set to run for the first 5 minutes of each hour, then 25 min was devoted to mode 2, then mode 3 for 5 min and again mode 2 for the remaining 25 min. The switching between modes was automated through a solenoid valve system operated from the 12 V DC power port of the PTR-MS power supply unit and managed through a QS422 sequence. The online preview and logging of volume mixing ratios and fluxes was done using the DDE feature of the Balzer sequencer communicating with a LabVIEW program which logged the sonic anemometer data together with the PTR-MS data to one file, so that each 25-min file contained 30000 wind rows and 210 PTR-MS rows of data synchronised in time, but not yet corrected for the lag-time associated with the residence time in the tubing (see Sect. 2.3.3.4).

Direct calibration used a VOC gas mixture supplied by Apel-Riemer Environmental Inc., USA, which contained methanol, acetaldehyde, acetone, isoprene, acetonitrile and formaldehyde, each at 1 ppmv, and d-limonene at 0.18 ppmv. This standard was checked after the campaign by reference to a GC-MS calibrated with a different isoprene standard (BOC gases, UK) and a d-limonene standard prepared from a diluted (with methanol) liquid standard (Sigma Aldrich, UK) injected directly onto the column. Agreement for isoprene was within 4% and about 10% for monoterpenes. Other VOC were compared with another gas standard delivered by

Apel-Riemer (at 0.5 ppm concentration per VOC) which was 2 years older and contained the same VOCs plus MVK, and other organics. The agreement was within 18%; the older standard showed 8-18% smaller concentrations for all VOCs except for acetaldehyde, which was 8% higher possibly through contributions of fragments from other organic species (e.g. MVK) that were not present in the other mixture. It has been assumed that the calibration standard was within the certified 5% standard precision for isoprene and other VOCs at the time of calibration. A larger uncertainty of 20% has been attributed to MVK sensitivity, which was not present in the calibration standard in the field, but which was inferred from the comparison of the sensitivity curves in the laboratory derived from the MVK containing standard. It was also assumed that the sensitivity for the sum of MVK+MACR is the same as for MVK only.

2.3.3.3 Volume mixing ratios (VMRs)

The signal intensities measured as counts per second I_{mz} (cps) for each of the monitored *m/z* channels were first converted to normalised counts per second I_{mz} (ncps) (Davison et al., 2009; Rinne et al., 2007b; Tani et al., 2004) in order to compensate for fluctuations in the primary ion, water vapour and drift-tube pressure, as presented in Appendix II-H

Equation 2.3-1

$$I_{mz}(ncps) = \frac{I_{mz}(cps) \times 10^6}{I_{21}(cps) \times 500 + I_{37}(cps)} \times \frac{p_{dnorm}}{p_d}$$

where I_{21}, and I_{37} are the instantaneous counts (cps) of $H_3{}^{18}O^+$ (approximately a factor of 500 lower than $H_3{}^{16}O^+$), and $H_3{}^{16}O(H_2{}^{16}O)^+$, respectively. The *m/z* 21 channel instead of *m/z* 19 was selected for monitoring primary ions in order to prevent detector saturation. Generally a ratio of 500 is used in the calculation (Kuhn et al., 2007; Langford et al., 2009a; Rinne et al., 2007b) although the use of a slightly lower precise ratio of 487 was proposed (Taipale et al., 2008). In fact, the true ratio might differ slightly depending on the location (e.g. close to oceanic waters) and one of the purposes of normalisation is to make the results uniform for comparisons with other results, where the level of primary ions used was different. In our case the level

of primary ion counts was 6.5-7.5 x 10^6 cps. The volume mixing ratios (χ) were obtained for each VOC as in Equation 2.3-2

.

$$\chi_{VOC} = \frac{I_{mz}(\text{ncps}) - I_{mz(zero)}(\text{ncps})}{S_{mz}(\text{ncps/ppbv})}$$

Equation 2.3-2

Here, $I_{mz(zero)}$(ncps) is the background normalised count rate for the given *m/z* channel, and the S_{mz} (ncps/ppbv) is the normalised sensitivity for a given compound. The S_{mz} for compounds present in the gas standard was obtained from the slope of a 6-point calibration line in the range 0 to 500 ppbv (0 to 90 ppbv for monoterpenes) corrected for background I_{mz} (ncps).

The primary ions were typically maintained at 7×10^6 cps during the whole measurement period and during calibration . The standard was appropriately diluted in clean Tedlar bags using VOC-free air, generated by purging ambient air through a Pt/Al_2O_3 catalyst heated to 200°C. This catalyst removed most VOCs effectively, but did not significantly affect water vapour concentrations, thereby avoiding problems arising from using dry calibration gas. However, normalisation for water clusters was always performed (eqn. Equation 2.3-1). For compounds not present in the standard, the empirical sensitivity S'_{mz} was approximated from the relative transmission curve (RTC) (Davison et al., 2009;Taipale et al., 2008). Only the sensitivities of non-fragmenting compounds which are known not to deviate from the RTC (e.g. methanol, acetaldehyde, acetone, acetonitrile) were used to derive the relationship between the sensitivities and the transmission coefficients from using the reaction rate coefficients for the proton transfer reaction taken from (Zhao and Zhang, 2004). Since no large *m/z* compounds were used in calibration, the RTC approach was limited to the 21-71 range, and was extended later after comparison to the classical transmission coefficients using higher MW compounds such as xylene and camphor. The calibration error using the standard is assumed to be less than 5% while that from using reaction rate constants can be up to 100% (Steinbacher et al., 2004). However, the relative transmission approach used here can offer less than 30% relative error (Taipale et al., 2008).

2.3.3.4 Flux derivation and validation

PTR-MS, with its relatively frequent sampling rate, is a perfect tool for application in direct, eddy covariance, but when more than one *m/z* are monitored the timeseries are not continuous any more, but disjunct. As typically several compounds are selected, the instrument can serve as a disjunct sampler, such that the quadrupole analyses one *m/z* after another during continuous flow. Its use in this manner has been termed 'virtual disjunct eddy covariance' (vDEC) (Karl, 2002) or 'continuous flow disjunct eddy covariance' (cfDEC) (Rinne et al., 2008; Rinne et al., 2002); both names denote the same approach. Files containing 25-min arrays of wind and PTR-MS data were validated for periods of breakdown or other disturbances according to the log file. After a careful examination, no raw data files have been marked for despiking or detrending. Double coordinate rotation has been applied to the wind speed vectors in order to account for tilts of the anemometer. Each data row corresponding to a given VOC was converted to ppbv (as described in section 2.3.3.3) and subsequently to mg m^{-3} using instantaneous pressure values from the Vaisala sensor attached close to the sonic anemometer. For PTR-MS and wind data, the gaps between PTR-MS rows were filled with "NaN"s in order to align the frequency of the two time series, and the covariance function was then obtained by computing separately for each VOC the covariance between the instantaneous deviation in mixing ratio (χ') and the instantaneous deviation in vertical wind velocity (w') (i.e., cov$<w'\chi'>$) for each time lag step (0.05 s) expressed as a shift in the wind row versus concentration row. If a clear maximum in the covariance was found within the time lag window, which was defined as at least twice the theoretical lag time and not less than twice the cycle length, then the time lag was recorded for this 25 min period and applied in the final computation of the flux as below:

$$F_{VOC} = \sum (w_i - \overline{w}) \times (\chi_{i+\tau} - \overline{\chi})$$

Equation 2.3-3

where w_i and $\overline{w}$ are the instantaneous value and mean over an integration period, respectively, for vertical wind velocity, $\chi_{i+\tau}$ is the lag-time adjusted instantaneous

value for the mixing ratio and $\overline{\chi}$ is the mean mixing ratio over the same integration period.

The optimum time lag was found automatically from the maximum covariance using a LabVIEW program. If no acceptable maximum was found, or if the flux value was below the detection limit (defined as 3 times the standard deviation of the covariance for lag times well outside the possible window (Spirig et al., 2005)), then the data point was marked as invalid and was normally not included in further analysis. Finally, the accepted lag times were manually examined in terms of their variability. If the lag time exceeded the theoretical lag time (based on sample flow rates) by the cycle length, or if the lag time found from the covariance functions of shorter integration time periods (e.g. 5 min) was found variable within the 25 min period, then any peak in the covariance found by the program was marked unreal (pseudopeak). However, the lag time value was allowed to be variable by not more than 30% within a 25-min period (as found on 5-min integration times).

In addition, the data were labelled according to routine tests commonly used in eddy covariance for filtering purposes (Clement et al., 2009; Foken and Wichura, 1996; Langford et al., 2009a; Moncrieff et al., 1997). The lower limit for the friction velocity was normally set to 0.15 m s^{-1} and points below this threshold were not included in analyses unless for specific tests. According to the FLUXNET criteria for ideal conditions described by Foken et al.(2004) the turbulence was quite well developed at the site, with 90 % of data in the first 3 classes and no data ranked in 8^{th} or 9^{th} category. However, at night, friction velocities were typically below the threshold of 0.15 m s^{-1}. According to the tests proposed by Foken and Wichura (1996) the data were not included in further analysis if the deviation from the ideal integral similarity characteristics was higher than 60%, and were labelled lower quality if they were within 30-60% of the ideal. A stationarity test (the value for the flux integrated over 25 min compared with the average of 5 values of fluxes integrated over 5 min segments of the same averaging period) was used to exclude non-stationary data when the difference was above 60% and to label as low quality

periods with differences between 30 and 60%. These tests were done on the sensible heat data and the affected periods were also removed from the VOC flux datasets.

Flux losses associated with signal damping due to residence time in the tubing were assessed by comparing latent heat fluxes derived from *m/z* 37, calibrated using specific humidity converted from relative humidity (Vaisala sensor), with latent heat fluxes from the an open path gas analyser (Coyle et al. 2010)[1]. A close agreement (Figure 2.3-1) suggested that no additional corrections (e.g. Webb density correction) were required.

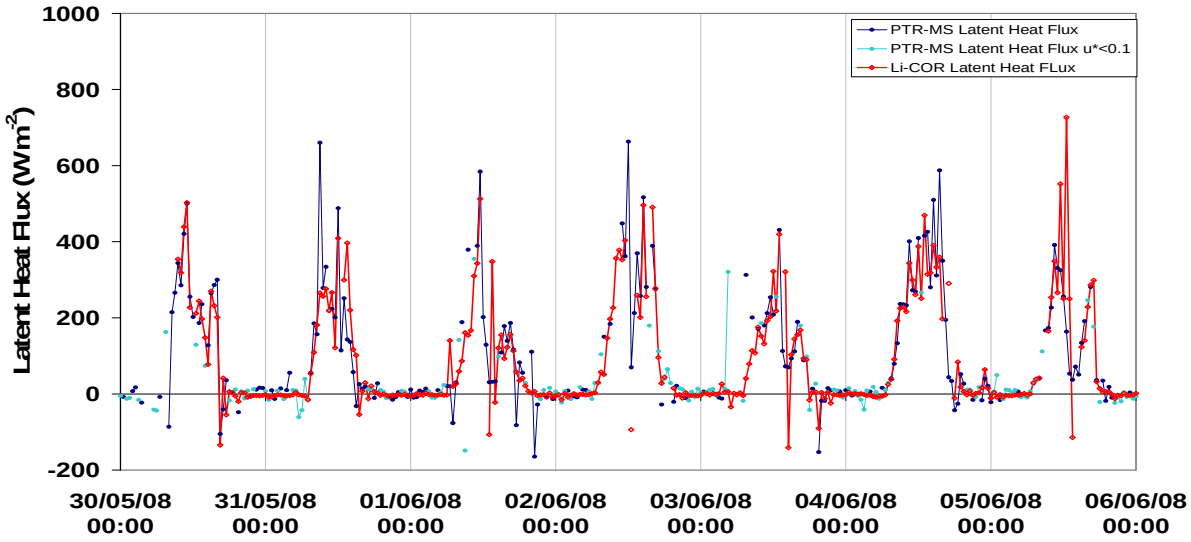

Figure 2.3-1 Comparison of latent heat fluxes derived by PTR-MS and open-path Li-COR

Finally, low frequency losses were examined by comparison with fluxes with longer averaging periods (Langford et al., 2009a) and the error introduced by disjunct sampling was estimated by comparing disjunct series for sensible heat flux (corresponding to times when PTR-MS data were available) with continuous data for sensible heat flux (Langford et al., 2009b). The overall flux losses were found to be below 10% and no corrections have been made.

[1] Coyle et al. in prep.

2.3.3.5 Parameterisation of flux algorithms for oil palms

2.3.3.5.1 Isoprene emission

The isoprene flux was measured by the disjunct eddy covariance technique (continuous flow mode) relatively close to the oil palm canopy and thus it could serve as a validation and constraint tool for emission models for this vegetation type. The G06 algorithm (Guenther et al., 2006) is an empirical model driven by two environmental variables: temperature and photosynthetic active radiation (PAR) and is an improvement of the former G95 model (Guenther et al., 1995) by including data on the past history of those variables. The past history contributes to isoprene emission control through their effect on enzyme (isoprene synthase) kinetics (Fall and Wildermuth, 1998) and substrate (dimethylallyl pyrophosphate (DMAPP)) availability, and allows for a better representation of short- and long-term variability. Normally these algorithms are designed to operate on leaf-level data and hence on leaf temperature. However, measurements by eddy covariance above canopy use the ambient temperature from a sensor close to the sampling inlet. Temperature of the foliage (T_c) can be approximately 2 °C higher than the ambient temperature ($T_a(z_m)$) at the measurement height z_m (Figure 2.3-2). The former temperature should be used in parameterisations of emission and deposition. For the latter the resistance analogy (e.g. Nemitz et al., 2009d; Singles et al., 1998) was used, where the canopy can be regarded as a big leaf.

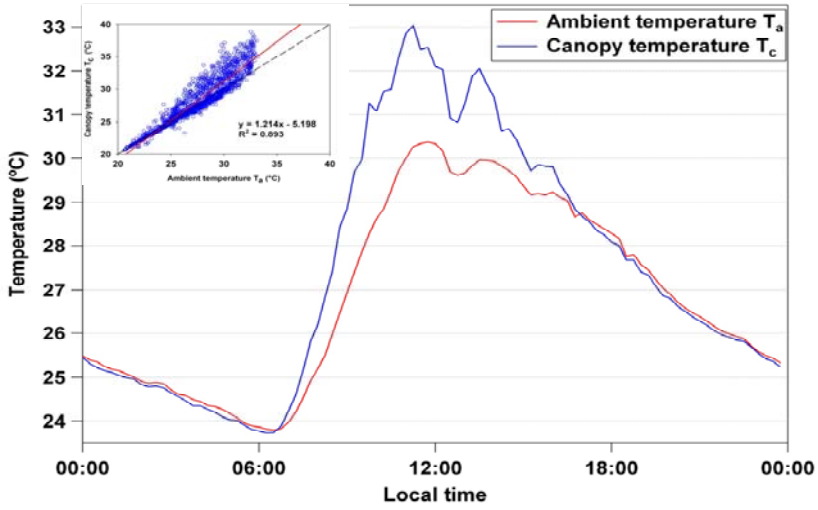

Figure 2.3-2 Comparison between the ambient ($T_a(z_m)$) and canopy (T_c) temperatures. Inset showing regression and higher variability in the upper range.

The Guenther et al. (2006) model (G06) is the most advanced empirical model for terpene emission, which is a significant advancement from previous Guenther et al. models (Guenther et al., 1999; Guenther et al., 1995; Guenther et al., 1993) in that the parameters which used to assume constant values (i.e., α, C_p, T_{opt} and E_{opt}) were extended to simulate variations in enzymatic kinetics andisoprene substrate availability, caused by previous history of temperature and PAR, as tested in a range of field studies (Geron et al., 2000; Hanson and Sharkey, 2001; Monson et al., 1994; Petron et al., 2001; Sharkey et al., 1999). In addition, the algorithm has an incorporated environmental model so it can directly simulate canopy flux (mg m^{-2} h^{-1}). This also makes it convenient for canopy flux measured data, such as from eddy covariance, to be used for model testing, constraining and parameterisation. Ten empirical parameters have been chosen and labelled analogously to those in equations presented for estragole emission parameterisation by Misztal et al. (2010c). These equations for the temperature and PAR dependent activity factors (γ_T and γ_P) were merged together into one equation so the parameterised flux is represented as below (Equation 2.3-4) with the 10 parameters marked as b_1-b_6, $T_{b,}$ P_0, C_{T1} and C_{T2} to be optimised to fit the experimental data from oil palms. The dependent variables were the photosynthetically active radiation (PAR) and the canopy temperature (T) estimated from an ambient temperature using the resistance approach (see Sect. 2.7).

The P_{24} and T_{24} are the 24 h averages of previous PAR and T, respectively; and P_{240} and T_{240} are the previous 10-day averages.

$$F_{G06} = \underbrace{\mathrm{BER} \cdot b_3 \cdot \exp\left[b_2 \cdot (P_{24} - P_0)\right] \cdot (P_{240})^{0.6} \cdot \frac{\left[b_1 - b_2 \ln(P_{240})\right] \cdot \mathrm{PAR}}{\sqrt{1 + \left[b_1 - b_2 \ln(P_{240})\right]^2 \cdot \mathrm{PAR}^2}}}_{\gamma_P} \cdot \underbrace{b_5 \cdot \exp\left[b_6 \cdot (T_{24} - 297)\right] \cdot \exp\left[b_6 \cdot (T_{240} - 297)\right] \cdot \frac{C_{T2} \cdot \exp\left[C_{T1} \cdot \left(\frac{1}{T_{opt}} - \frac{1}{T}\right) \cdot \frac{1}{0.00831}\right]}{C_{T2} - C_{T1} \cdot \left[1 - \exp\left(C_{T2} \cdot \left(\frac{1}{T_{opt}} - \frac{1}{T}\right) \cdot \frac{1}{0.00831}\right)\right]}}_{\gamma_T}$$

Equation 2.3-4

2.3.3.5.2 Methyl vinyl ketone (MVK) and methacrolein (MACR) deposition

MVK and MACR fluxes were measured by the same technique as isoprene fluxes, and were shown to be downwards.
The fluxes presented in Sect. 2.3.4.6.2 have been used to derive MVK+MACR deposition velocity (V_d) using Equation 2.3-5,

Equation 2.3-5

$$V_d\,(z_m) = -\,F \cdot \chi(z_m)^{-1}$$

where F is the measured flux of MVK and MACR, and $\chi(z_m)$ is the measured volume mixing ratio of MVK and MACR at the measurement height (15 m).
The deposition velocity of the sum of MVK and MACR ($V_d(z_m)$) can also be represented as using the resistance approach (Nemitz et al., 2009d; Singles et al., 1998; Sutton et al., 1995) as in Equation 2.3-6.

Equation 2.3-6

$$V_d(z) = \frac{1}{R_a\left(z-d\right) + R_b + R_c}$$

where R_b is the laminar boundary layer resistance close to the surface of the leaves, R_c is the canopy resistance, and d is the displacement height. R_a and R_b were obtained from measured micrometeorological parameters as described by Nemitz et al. (2009c), and the molecular diffusivity in air D_a for MVK (1.00×10^{-6} m^2 s^{-1}), required in the Schmidt number which is part of the Stanton number which in turn is part of the R_b equation, has been obtained from the molecular structure online calculator (EPA, 2007) as the average value of the Wilke and Lee (WL), the Fuller, Schettler and Giddings (FSG) and the FSG with LaBas molar volume (FSG/LaBas) estimation methods of diffusion coefficients in air. For modelling the MVK+MACR flux timeseries the canopy resistance (R_c) is required, which was obtained by substituting $V_d(z)$ in Equation 2.3-6 and rearranging the equation to yield R_c.

The maximal deposition at a leaf surface is constrained by the maximal deposition velocity (V_{max}), (Equation 2.3-7).

Equation 2.3-7

$$V_{d\,max} = (R_a\,(z - d) + R_b)^{-1}$$

2.3.4 Results

2.3.4.1 Volume mixing ratios (VMRs) of dominant VOCs

The diverse VOC mix of compounds recorded by PTR-MS can be seen on an averaged mass scan for the entire measurement period (Figure 2.3-3). In addition, summary statistics of the 10 most dominant compounds selected for the flux mode is tabulated separately for the total period (Table 2.3-1) and for the midday time range (Table 2.3-2) The most abundant compound at the plantation was isoprene, which was released by the fronds in response to temperature and PAR reaching mid-day averages of around 13 ppbv (maximal values peaking at 26 ppbv), which constituted nearly half of the total VOC mixing ratios during the daytime (Figure 2.3-6a) and one third over the entire period (Figure 2.3-6b). The lower latter contribution is because isoprene was not emitted in the dark so due to its short atmospheric lifetime the mixing ratio was close to zero at night.

During the day isoprene oxidation was responsible for the formation of the first-order oxidation products MVK and MACR, which followed a very similar diurnal pattern with a mid-day average of 2.2 ppbv. Their ratio with respect to isoprene was the smallest in the middle of the day amounting to 0.2, when the production rate of isoprene was exceeding the photochemical turnover, whereas ratios as high as 0.4 were observed either in the morning or in the afternoon.

Another important oxidation product of isoprene which derives from MACR is hydroxyacetone (HA), which most probably was reflected in the *m/z* 75 signal. Although attribution of this ion channel to HA has been recently reported as reliable

(Karl et al., 2009, ACP) it is likely that this *m/z* could also receive interferences from propionic acid and/or biogenic esters (mainly propionates), some of which are known kairomones of the oil palm weevil (Gries, 1994), and so may have been present in the air. This could lead to an overestimation of the HA to isoprene ratio, which was 0.1 in the morning, 0.2 during midday and sharply increasing in the afternoon to about 1, when isoprene emissions were small. However HA has a relatively long atmospheric lifetime of 4 days (Orlando et al., 1999) with respect to OH, so can potentially accumulate in the shallow boundary layer after its collapse in the evening.

Although the palm fronds are probably responsible for the majority of VOC emissions, the flowers (thousands on one inflorescence) release estragole with a response of a few hours delayed relative to temperature and PAR (Misztal et al., 2010b). The details of estragole floral emissions by palms are thoroughly described in chapter 2.4, so only a general information is brought forward to here. On account of relatively short lifetime (1 hour) estragole may make a significant contribution to regional photochemistry. Estragole mixing ratios were 3.0 ppbv in the middle of the day but increased further later in the day (3.8 ppbv) and in the evening (4.5 ppbv) which could be the effect of the potential thermogenesis of the flowers and the accumulation in the shallow boundary layer. Estragole is important for the oil palm industry as it attracts the pollinating weevil (Hussein et al., 1989) enhancing the crop yields.

Very high signals (corresponding to 1.7 ppbv) were detected at *m/z* 93, typically assigned to toluene. Earlier biogenic toluene emissions have been reported by Heiden et al. (1999) from sunflowers, and also recently by White et al. (2009) from alfalfa, although the absolute levels were smaller. Although atypical contributions at *m/z* 93 cannot be excluded, the known interferences from p-cymene, hydrated hydroxyacetone, monoterpenes or chloroacetone were tested and found unlikely. However, the analysis of the fluxes (Sect. 2.3.4.6.5) suggests that the source for this *m/z* must be below the canopy and the pattern clearly indicates a biogenic source. Initially it was thought that the emissions of toluene were related to the fungus which is commonly found to live in a symbiosis with the fronds (pinkish spots). Small

levels of toluene were found in some of those fronds which had those spots. However, much higher levels were subsequently found in the flower enclosures which were undertaken for the purpose of estragole source screening (Misztal et al., 2010c).

Toluene was only detected in the adsorbent tubes sampled from male inflorescences although it may have been lost in the much more abundant estragole level of female inflorescences, which saturated the GC-MS detector. Formation of toluene in the CEH desorption system has been noted in the past, so it should be considered as a possible artefact. However, it was not detected in any of the female-flower tubes (run in a female-male-female-male sequence) nor in any other tube from the same batch (e.g. blank, a part of the study at the rainforest)). Another argument is that the diurnal pattern of toluene in Figure 2.3-7 is shifted towards later in the day as is the case for the florally-emitted estragole. Toluene appears to be a known flower component of many other species such as *Anthurium* (Kuanprasert et al., 1998), *Ophrys* orchids (Borgkarlson et al., 1985; Borgkarlson et al., 1987), *Prunus* trees (Baraldi et al., 1999) and kiwi fruit (Tatsuka et al., 1990). However, toluene has not been reported as a constituent of oil palm emissions. As the winds were commonly blowing from the S no evident contributions were identified from either the oil palm mill or residential areas, although (Oram, 2008) noted methanol spikes over a mill plume. Methanol, however, was very low. In addition, acetonitrile, as apparent from the mass scans, lacked spike features typical for anthropogenic occurrences and no *m/z* 79 signal typical for benzene was recorded.

On the other hand, acetone (*m/z* 59) and hexanals (*m/z* 83), both at an average 1.0 ppbv midday level, may have originated outside of the area of measurement, since their relatively high mixing ratios did not perfectly correspond to the flux and well might be subject to deposition and reemission.

Finally, the monoterpenes (MT) and sesquiterpenes (SQT) were frequently below the detection limit for *m/z* 81 (> 50% of data) and m/z 205 (~70% of data), respectively. For that reason the values below the detection limit were replaced by half of the

detection limit value. In addition the signal at *m/z* 81 could have been overestimated by a contribution from hexanals, but statistical comparison of the less sensitive *m/z* 137 showed similar absolute values. Leaf level measurements (Owen et al., 2010) found small levels of monoterpenes but their presence was not confirmed in all fronds, which indicates that oil palms may not be typical monoterpene emitters, although some of the monoterpenes were detected in the flower enclosures.

However, estragole with a similar BSOA yield to that of monoterpenes, and also possibly toluene might be the highest contributors to the aerosol mass at the plantation, whereas isoprene may be not as important in this respect due to its lower aerosol yield, or might even lead to aerosol inhibition by effective scavenging of OH (Kiendler-Sharr, 2009).

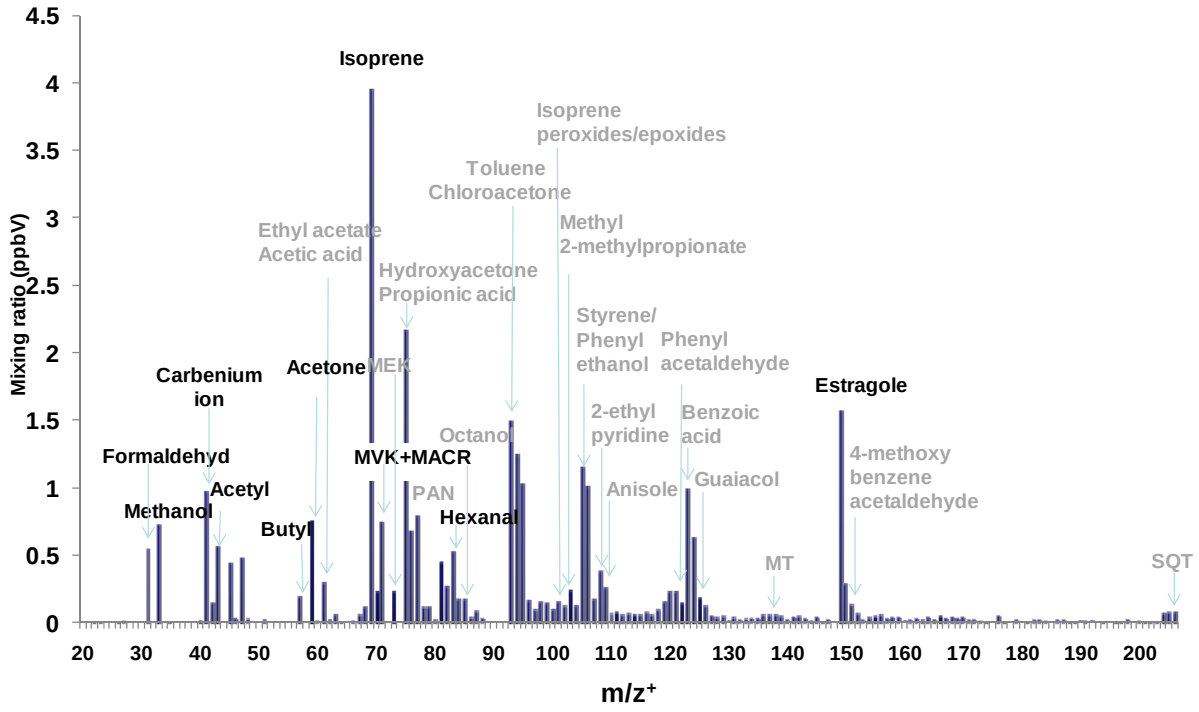

Figure 2.3-3 VOC composition at the oil palm plantation; averaged data of the campaign.

2.3.4.2 Mixing-ratio distributions, detection limits and statistical summary

Reliable reflection on the most representative values of derived volume mixing ratios is only possible when statistically sufficient amount of data covering the entire period is available. Since PTR-MS collects thousands of samples in a half hour, a half hour mean can be considered statistically valid but only if the measured values exceed the limit of detection (LOD). The commonly used approach for the derivation of an LOD (e.g. Davison et al., 2009; Langford et al., 2009a; Langford et al., 2009b; Misztal et al., 2010c; Rinne et al., 2007b; Taipale et al., 2008) is twice the standard deviation of the noise (as normalised counts of the representative zero air measurement divided by the normalised sensitivity).

The detection limits can vary between compounds, and depend also on the instrument and on the given measurement period. Typically, for low weight m/z channels high background can be the most significant factor affecting LOD. High backgrounds for methanol and acetaldehyde, are sometimes encountered by PTR-MS users (Eerdekens et al., 2009; Murphy et al., 2010) and they were relatively high in Borneo both at the rainforest (Langford et al., 2010) and the plantation (this work). However, the same instrument had a very low detection limit for those compounds during the ACCENT-VOCBAS campaign in Italy (Sect.2.3 ;Davison et al. (2009). The cause for these differences is not clear although isotopic O_2^+ signal may be in part responsible for the interference at *m/z* 33. One could speculate about the not highly probable internal generation of methanol in the system at high humidity. More probable is noise from methanol forming adducts with water cluster at high humidity. The backward proton-transfer reactions should also be considered since the proton affinity of methanol is not much higher than that of water. For the higher molecular *m/z* channels (e.g. 137, 149, 205) the background noise variations are not as significant as the reduction in sensitivities caused by the fringing effect of the quadrupole (Kim et al., 2009) related to decreases in transmission efficiency. Nevertheless, the LODs for isoprene, MVK and acetone were very low even despite the relatively high *E/N* ratio used as a compensating measure for high humidity.

The optimal situation is when all data points for a compound exceed the detection limit, but it is quite common for environmental data sets to contain mixing ratios almost at a zero level, for example at night, and how best to treat those data is an under-discussed general problem. For compounds which have a proportion of their concentration data below the LOD, but whose concentration distributions follow normal or lognormal distributions, the data below the LOD value can be replaced by the half the LOD value to produce a reliable average (Caudill et al., 2007; Clarke, 1998; Porter et al., 1988). This approach usually works better than the regression methods to back-estimate the data below LOD from probability plots (e.g. Helsel, 1990), mainly because of the uncertainties of the predictions of the missing distribution. If values lower than LOD were not replaced by the half-LOD value then a calculated mean would be biased downwards by zero values if the data below detection limit were replaced by zeros and biased upwards if the data below LOD were totally disregarded when averaging.

The distributions of mixing ratios of the targeted compounds (i.e., those included in the flux mode) and their detection limits are shown in Figure 2.3-4. Based on this the compounds selected to undergo a statistical treatment of the data below detection limit were methanol, monoterpenes (MT), sesquiterpenes (SQT), acetaldehyde, hexanals, and toluene, whereas acetone, estragole, isoprene and MVK+MACR were considered representative in their full set. It could be argued that isoprene and MVK+MACR whose values decreased practically to zero during the night might have also needed a replacement of their data below detection limits which were in the order of tens of pptv. Those compounds had a multimodal distribution so the method could not be applied. However, the error related to retaining the data below their LOD in their data sets would be less than a percentile and well within the reported uncertainty of 10% for the compounds in the calibration mixture.

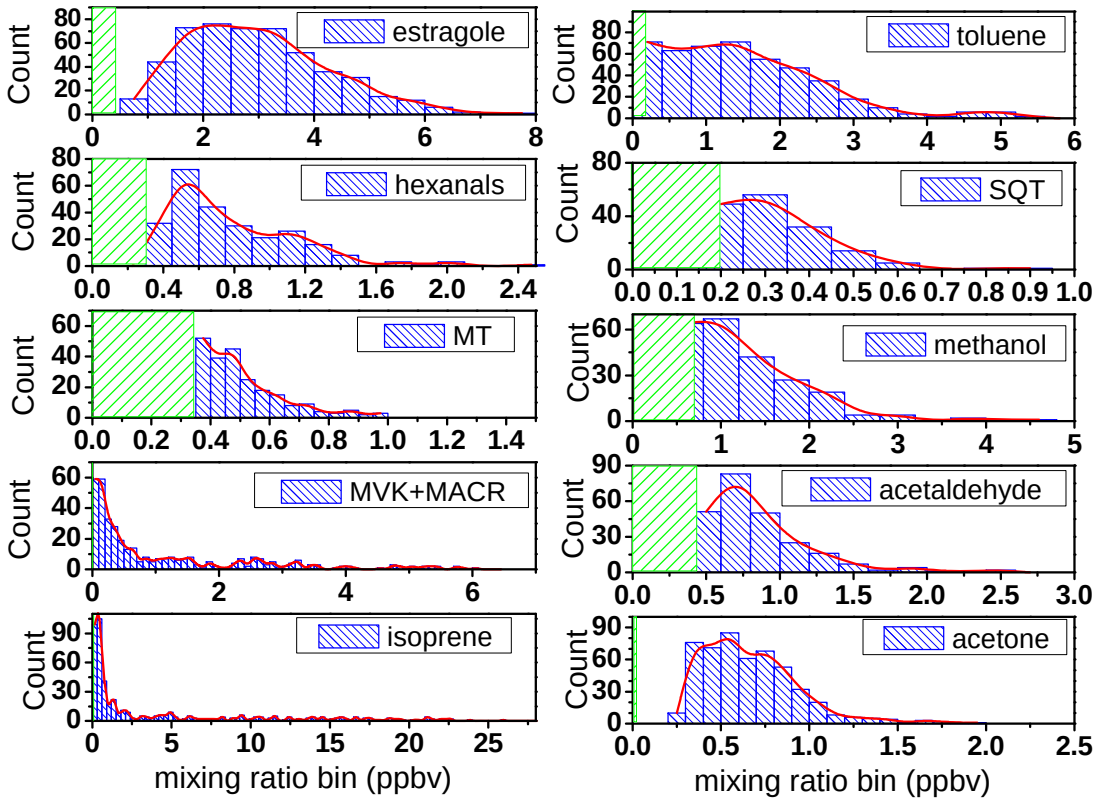

Figure 2.3-4 Distributions of the volume mixing ratio values of the compounds measured in the flux mode. Green areas correspond to detection limits.

In the summary statistics for the whole measurement period (day and night data) (Table 2.3-1) the LOD values, means and standard deviations are compared with those derived from the relationship of the ranked data with standard normal cumulative distributions (example cases in Figure 2.3-5). For the data which had lognormal distribution, which are common for environmental datasets, the exponential of the slope of the lognormal line corresponds to the geometrical mean (and the exponential of the intercept corresponds to the geometrical standard deviation). The geometrical LOD can be found from the exponential of the slope break. For the normally-distributed data, the slope of the line of non-logarithmic VMR values versus normal cumulative distributions corresponds to the arithmetic standard deviation and the intercept to the arithmetic mean. For compounds whose distributions were multimodal (e.g. isoprene, MVK) the graphical methods were not applicable.

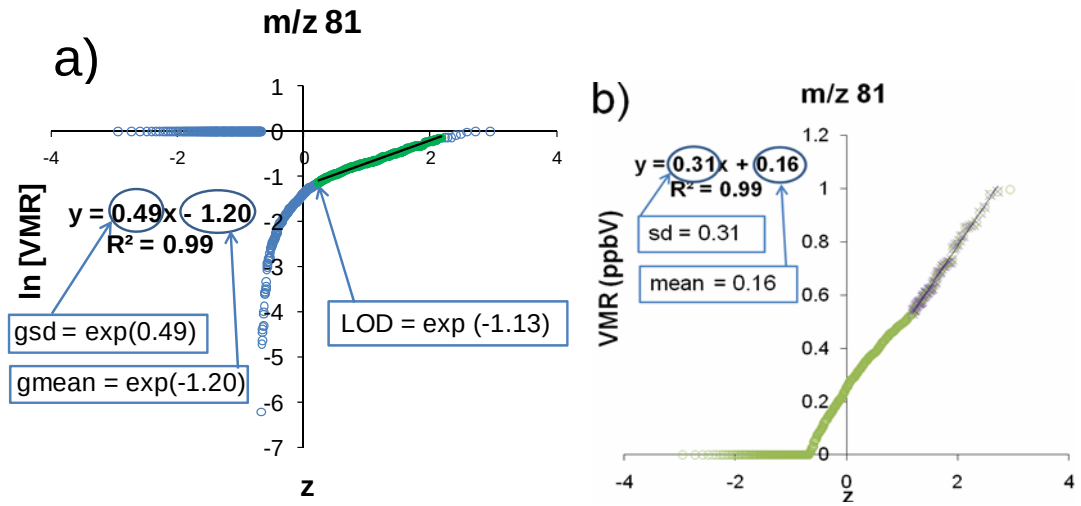

Figure 2.3-5 An example of the graphical estimation of the limit of detection and other statistical parameters from lognormal data values (a) and normal data values (b) plotted against normal cumulative distributions.

The summary statistics for the volume mixing data during the mid-day period (10:00 – 14:00) (Table 2.3-2) shows that most compounds had much higher values during the day and therefore the relative percentage contributions of each compound (Figure 2.3-6)

Table 2.3-1 Statistical summary (11 days 0:00 – 0:00) of volume mixing ratios (ppbv) of 10 targeted VOCs.

m/z	33	45	59	69	71	81*	83	93	137*	149	205
Compound	Methanol	Acet-aldehyde	Acetone	Isoprene	MVK+ MACR	MT	Hexanals	Toluene	MT	Estragole	SQT
Arithmetic mean	0.75	0.54	0.67	4.28	0.86	0.33	0.49	1.62	0.33	2.98	0.17
Arithmetic mean [graphical]	0.79	0.48	0.63	n/a	n/a	0.31	0.40	1.50	0.36	2.84	0.13
Geometric mean	0.59	0.42	0.61	1.29	0.22	0.28	0.34	1.22	0.30	2.70	0.14
Geometric mean [graphical]	0.55	0.48	0.61	n/a	n/a	0.30	0.38	1.73	0.36	2.83	0.18
σ	0.63	0.40	0.28	6.15	1.30	0.19	0.40	1.08	0.19	1.31	0.12
σ [graphical]	0.26	0.40	0.28	n/a	n/a	0.16	0.40	1.14	0.24	1.42	0.15
σ_{geo}	1.88	2.02	1.49	5.10	6.31	1.73	2.47	2.33	1.50	1.59	1.75
σ_{geo} [graphical]	2.14	1.97	1.52	n/a	n/a	1.64	2.56	3.39	1.64	1.72	1.65
Median	0.39	0.48	0.61	0.86	0.22	0.18	0.40	1.51	0.25	2.81	0.10
Max	4.40	2.50	1.90	26.0	6.06	1.00	2.42	5.5	1.08	8.10	0.90
Min	<0.39	<0.20	0.26	0.00	0.00	<0.18	<0.10	<0.20	<0.25	0.51	<0.10
5^{th} percentile	0.39	0.20	0.33	0.17	0.02	0.18	0.10	0.20	0.25	1.23	0.10
95^{th} percentile	2.04	1.28	1.14	18.5	3.73	0.71	1.25	3.47	0.83	5.28	0.42
N	511	511	511	511	511	511	511	511	511	511	511
% filled with 0.5LOD	66.5	43.1	0.00	0.0	0.0	55.2	29.4	8.0	84.9	0.00	67.3
LOD [$2\sigma_{ZA}/S_{norm}$]	1.5	0.50	0.02	0.05	0.04	0.35	0.42	0.43	0.62	0.5	0.28
LOD [graphical]	0.78	0.40	n/a	n/a	n/a	0.32	0.20	0.41	0.46	n/a	0.20

* Monoterpenes (MT) were calibrated to yield absolute concentrations independently at *m/z* 81 and *m/z* 137. A more sensitive signal at m/z 81 was used.

Table 2.3-2 Statistical summary (midday 10:00 – 14:00 LT) of volume mixing ratios (ppbv) of 10 targeted VOC and hydroxyacetone (HA).

m/z	33	45	59	69	71	75*	81	83	93	149	205
	Methanol	Acetaldehyde	Acetone	Isoprene	MVK	HA[1]	MT	Hexanals	Toluene	Estragole	SQT
Arithmetic mean	0.92	0.61	0.93	13.1	2.56	2.35	0.42	0.94	1.81	3.16	0.13
Geometric mean	0.72	0.48	0.91	11.7	2.06	2.22	0.37	0.88	1.66	2.91	0.12
σ	0.68	0.41	0.20	5.35	1.45	0.81	0.21	0.33	0.67	1.00	0.06
Median	0.39	0.57	0.88	13.8	2.52	2.18	0.43	0.95	1.73	2.96	0.10
σ_{geo}	1.99	2.10	1.21	1.70	2.11	1.41	1.74	1.48	1.62	1.49	1.43
5th percentile	0.39	0.20	0.71	4.16	0.41	1.43	0.18	0.49	0.79	1.78	0.10
95th percentile	2.19	1.29	1.39	21.4	5.20	3.92	0.86	1.47	2.84	5.01	0.26
N (N<LOD)	88 (45)	88 (34)	88	88	88	40	88 (28)	88	88 (2)	88	88 (74)

*derived from 5-min hourly mass scans; [1]upper limit due to interferences with propionates at *m/z* 75.

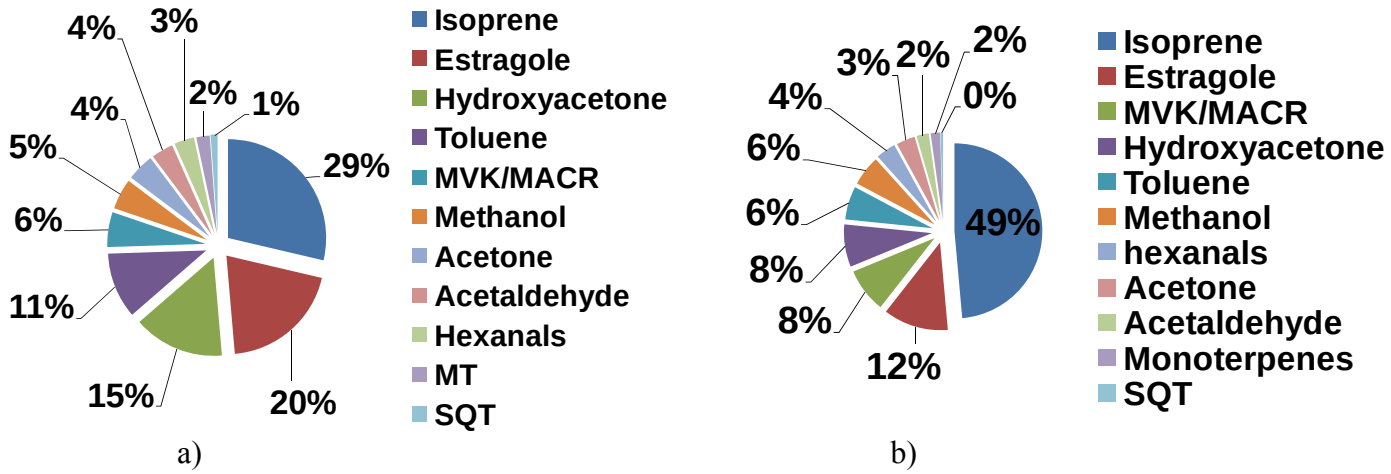

Figure 2.3-6 Composition of VOCs in terms of their 24 h (a) and midday (10:00-14:00 LT) (b) average volume mixing ratios.

2.3.4.3 Diurnal trends of mixing ratios

Campaign-averaged diurnal variations in the volume mixing ratios of the dominant VOCs are presented in Figure 2.3-7a-k. A clear diurnal pattern in mixing ratios was present for isoprene, MVK+MACR, estragole, hydroxyacetone, toluene, acetone and hexanals. In contrast, methanol, acetaldehyde, monoterpenes (MT) and sesquiterpenes (SQT) did not follow a clear diurnal course, which could be because of the higher distance to their sources, small emissions from below the measurement height and the values being in a range close to the detection limits. Isoprene and MVK were very well correlated with temperature and PAR during a day. Estragole had its two main peaks shifted to later in the day with respect to isoprene, as its mixing ratios were also correlated with temperature and PAR but with a few hours delay, which might have been related to the storage of the compound inside the plant before subsequent release (see chapter on estragole). In fact the pattern for toluene also showed a positive time shift and its level increased gradually, similarly to that of estragole, but it had only one broad peak. This might also suggest toluene being a flower component, although its release mechanism may differ from those of estragole or possible may only be released by female inflorescences. Hydroxyacetone starts increasing at the same time as isoprene and MVK+MACR but stays longer elevated, probably due to its longer atmospheric lifetime. A diurnal trend in a ratio of MVK+MACR to isoprene and of hydroxyacetone to isoprene is in addition presented in Figure 2.3-7l. Hexanals and acetone had a similar diurnal pattern, which was different from that for the other compounds. It might suggest that these compounds may be originating from a similar kind of source/process, for example, from leaf wounding, stress from herbivores or growth processes, litter or soil. The trend in methanol mixing ratio was quite noisy but was gradually increasing in the day. As later shown in the flux section it was mainly deposited so may well have formed above as a product of oxidation (e.g. of methane), and as such would be expected to increase in the afternoon.

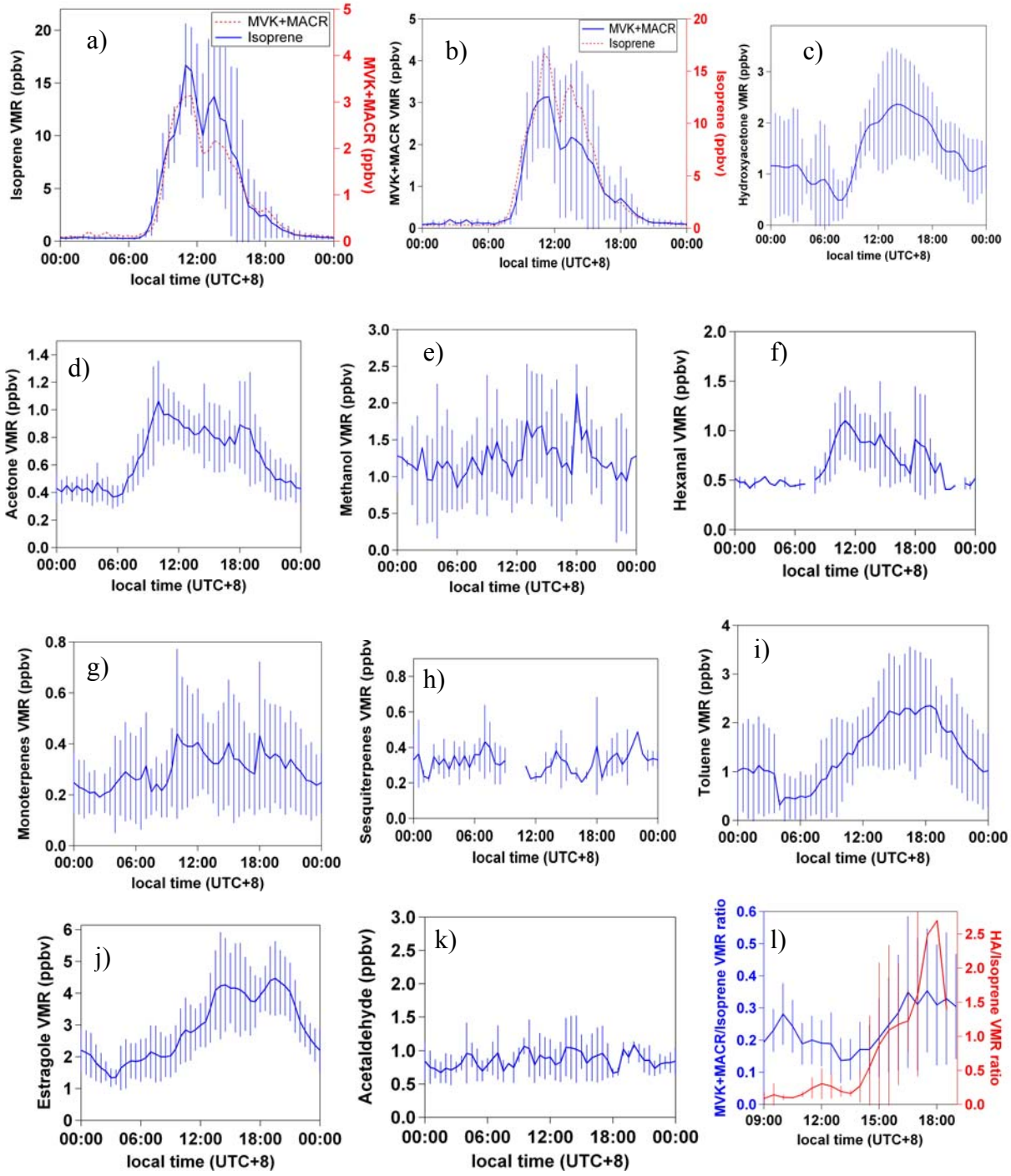

Figure 2.3-7. Daily average diurnal mixing ratios of dominant VOCs (a-k) at the oil palm plantation; ratios of isoprene oxidation products (l). Error bars denote day-to-day variability (1 standard deviation).

2.3.4.4 Fluxes of dominant VOCs

Not all the compounds which were abundant in terms of mixing ratios displayed this abundance in fluxes. The summary statistics for compounds monitored in the flux mode are presented in Table 2.3-3 for the entire period (12 days) and Table 2.3-4 for the midday range (10:00-14:00 LT). In addition, values are given in parenthesis for the gap-filled data with the G06 algorithm optimised specifically for isoprene, estragole and toluene, and with the big-leaf resistance approach for MVK+MACR. The results of the parameterisations are given later in Sect. 2.3.4.8. In some cases gap-filling can change the averaged values quite substantially, since all the near-zero values are taken in the computation. Without the gap-filling only the available data would be averaged so they would be skewed towards larger values such as encountered during a day when there is a higher probability to fulfil the quality criteria for the flux. In this sense the gap-filling approach makes the dataset look more representative, in particular since the agreement of the measurement and optimised models was very good even for floral species such as estragole and possibly floral toluene. On the other hand, gap-filling with an emission-only model does not reflect deposition, which is probably a minor component and could be accounted for as a loss in emission.

The relative percentages of VOC fluxes for the different compounds in relation to the absolute fluxes, emission only or for gap-filled data for the entire period are showed in the pie-charts in Figure 2.3-8 (a-c) and for the midday period (10:00 – 14:00 LT) in Figure 2.3-9 (a-c). Isoprene had the clearest flux with the least number of rejections based on the criteria discussed in Sect. 2.3.3.4. It dominated the fluxes constituting 82% (74% if gap-filled) when considering the entire period, which is nearly 3 (2.5) times more than the relative isoprene share in the mixing ratios. It is clear that some longer lived compounds such as estragole, or toluene could persevere in the shallow nocturnal boundary layer, whereas their fluxes were minimal due to inhibited transport and typically also could not be captured at night conditions due to the low turbulence. However, the high values for isoprene mixing ratios during a day quickly disappeared due to enhanced photooxidation but also owing to the circadian

control of isoprene emissions (Wilkinson et al., 2006), both of which were responsible for a shorter daily peak of isoprene emissions in comparison with those from the rainforest. For VOC measurements of concentrations and fluxes at the rainforest in which the author collaborated with the Lancaster team the reader is referred to Langford et al. (2010).

The second most abundant flux was that of estragole, a floral component, which constituted approximately 10% of total isoprene fluxes (~ 20% if the data were gap-filled). The third highest clear flux was recorded for toluene, a suspected floral component, which was mainly emitted at rates close to those of estragole for the available data but only half of those if the data were gap-filled.

Toluene was only found in the enclosed male inflorescences, but its level found therein probably cannot fully explain the relatively higher values observed in eddy covariance, so it is not certain whether there could be an additional source such as a fungus on the fronds. Methodology used during enclosures is presented in the next chapter (2.4). However, as described later, toluene emission was very closely dependent on temperature and the parameterisation did not change significantly the G06 parameters with respect to those originally designed for isoprene. In other words, isoprene parameterisation resulted in more radical changes to the parameters than that for toluene, which is interesting. Toluene was earlier seen in floral emissions of palm trees (Arecaceae family)(Knudsen et al., 2006) but has not been reported so far from African oil palms (Arecaceae *Elaeis guineensis* Jacq).

Small emissions were noted for acetone, acetaldehyde and hexanals, which altogether would be less than 1 % of total emissions. However it has not been tested whether cutting branches or other stresses could induce enhancement of these emissions. Another finding is the clear deposition of isoprene first order oxidation products (i.e., MVK and MACR) whose downward fluxes less than -1 mg m^{-2} h^{-1} were recorded during enhanced isoprene oxidation. Another almost purely depositing compound was methanol, which constituted approximately one third of the average deposition value for the sum of MVK and MACR. It is expected that hydroxyacetone

could also be subject to deposition but it was not measured in the flux mode. The relatively small number of validated fluxes for monoterpenes suggests that they were mostly deposited, with only a few episodes of emission, giving a net deposition of 0.026 mg m^{-2} h^{-1}. Leaf level measurements suggested that monoterpene emissions from the fronds were small , sometimes not even detected (Owen et al., 2010) but small amounts were found subsequently in the flower enclosures, so it seems that oil palms may be a sink for monoterpenes. Sesquiterpenes were probably emitted at a low rate but the number of validated data points was too small to ensure representativeness so they are omitted from the results section.

Table 2.3-3 Summary statistics for eddy covariance BVOC fluxes at oil palm (total measurement period). In parentheses are given statistics values for fluxes gap-filled using approaches discussed in Sect. 2.3.4.8

m/z	33	45	59	69	71	81	83	93	149
	Methanol	Acetaldehyde	Acetone	Isoprene	MVK+MACR	MT	Hexanals	Toluene	Estragole
Max	0.345	0.473	0.270	28.94 (28.94)	0.398 (0.398)	0.378	0.813	3.390 (3.390)	2.073 (2.119)
Min	-0.360	-0.183	-0.092	-2.392 (-2.392)	-1.423 (-1.423)	-0.966	-0.436	-0.367 (-0.367)	-0.774 (-0.774)
Mean	-0.044	0.010	0.012	4.394 (2.121)	-0.119 (-0.053)	-0.026	0.012	0.353 (0.186)	0.440 (0.398)
Median	-0.024	0.004	0.002	1.104 (0.027)	-0.064 (-0.003)	-0.023	0.014	0.152 (0.009)	0.249 (0.165)
σ	0.107	0.074	0.050	6.369 (4.701)	0.212 (0.144)	0.227	0.180	0.513 (0.382)	0.629 (0.497)
5th percentile	-0.223	-0.102	-0.041	-0.063 (-0.018)	-0.512 (-0.247)	-0.450	-0.264	-0.103 (-0.005)	-0.341 (0.000)
95th percentile	0.100	0.137	0.096	19.22 (12.84)	0.054 (0.008)	0.328	0.255	1.178 (0.990)	1.606 (1.437)
N	163	173	167	213 (633)	205 (529)	81	77	153 (633)	109 (633)

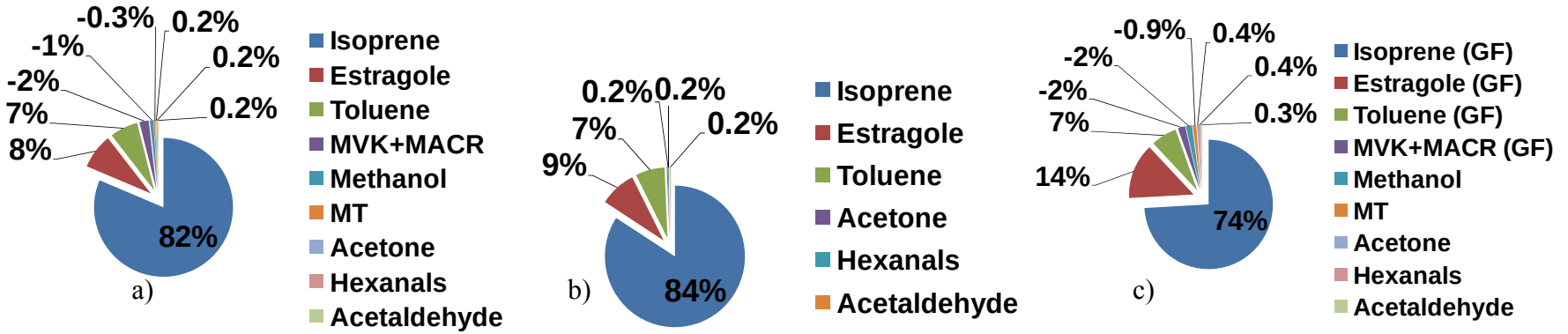

Figure 2.3-8 Relative percentages of the flux averaged over the entire measurement period; (a) for both emission and deposition fluxes (b) for emission only and (c) for fluxes with main VOCs gap-filled using optimised G06 algorithms for isoprene, estragole, toluene and N09 resistance approach for MVK+MACR.

Table 2.3-4 Summary statistics for mid-day fluxes (10:00 – 14:00 LT). In parentheses are given statistics values for fluxes gapfilled using approaches discussed in Sect. 2.3.4.8

m/z	33 Methanol	45 Acetaldehyde	59 Acetone	69 Isoprene	71 MVK+MACR	81 MT	83 Hexanals	93 Toluene	149 Estragole
Max	0.226	0.473	0.194	28.94 (28.94)	0.398 (0.398)	0.373	0.483	3.390 (3.390)	1.635 (1.821)
Min	-0.342	-0.154	-0.076	-2.392 (-2.392)	-0.973 (-0.973)	-0.502	-0.382	0.102 (0.020)	-0.088 (-0.088)
Mean	-0.098	0.041	0.030	9.707 (8.370)	-0.220 (-0.173)	-0.042	0.029	0.763 (0.684)	0.807 (0.920)
Median	-0.098	0.033	0.026	8.446 (7.025)	-0.154 (-0.123)	-0.057	0.043	0.605 (0.560)	0.718 (0.866)
σ	0.120	0.094	0.054	7.185 (6.957)	0.237 (0.210)	0.237	0.234	0.582 (0.551)	0.542 (0.405)
5th percentile	-0.278	-0.052	-0.037	0.862 (0.477)	-0.617 (-0.529)	-0.477	-0.334	0.144 (0.061)	0.003 (0.315)
95th percentile	0.066	0.177	0.120	20.62 (20.03)	0.013 (0.003)	0.351	0.417	1.751 (1.776)	1.601 (1.636)
N	44	52	53	64 (100)	60 (88)	18	20	45 (100)	26 (100)

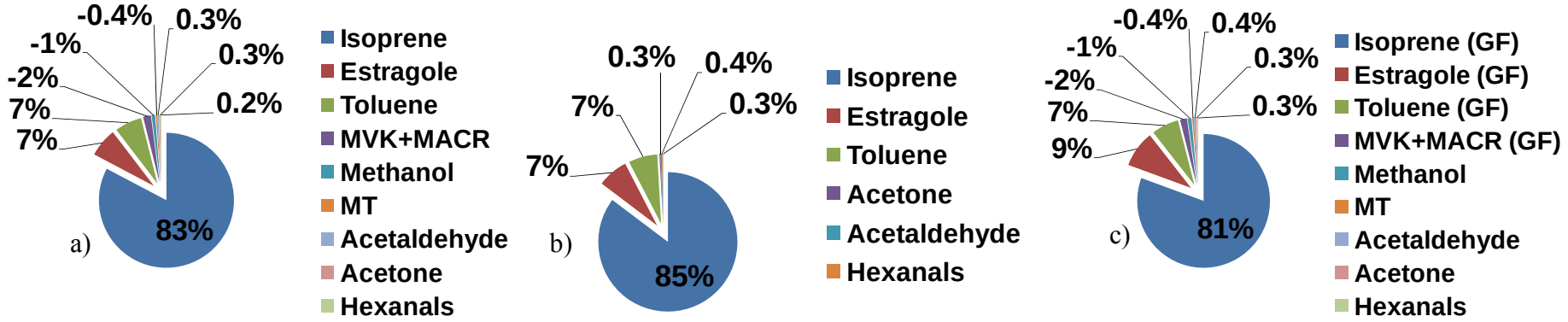

Figure 2.3-9 Relative percentages of the flux averaged over the mid-day periods (10:00 – 14:00 LT); (a) for both emission and deposition fluxes (b) for emission only and (c) for fluxes with main VOCs gap-filled using optimised G06 algorithms for isoprene, estragole, toluene and N09 resistance approach for MVK+MACR.

2.3.4.5 Diurnal trends of fluxes

Fluxes of the most abundant compounds are presented as diurnal time series in Figure 2.3-10. Isoprene fluxes peaked during the middle of the day at around 11:00 LT. It was typical for a heavy rain episode to occur at around 12:00 LT causing a dip in PAR, which also can be seen in the pattern for the isoprene flux. This differed from the rainforest where rain typically occurred in the afternoon (Langford et al., 2010). The second, smaller peak in isoprene flux was observed around 14:00 LT. Despite the very high positive fluxes during the day (peaking close to 30 mg m^{-2} h^{-1}), the isoprene emissions ceased quite early with their fluxes falling below 1 mg m^{-2} h^{-1} at 17:00 LT. This is typical for isoprene emissions when PAR and temperature fall markedly, but an additional narrowing of the peak could be also due to the circadian control (see Sect.2.3.4.9). Estragole had a larger emission peak in the afternoon compared to the morning peak, so typically the flux of estragole exceeded that of isoprene at around 15:00 LT. Toluene flux had a pattern more similar to that of isoprene flux although there was no dip associated with the rain events around noon. There was also no such dip in the toluene mixing ratios, in contrast to both isoprene and estragole, but the mixing ratios seemed skewed towards later in the day which was not reflected in the fluxes. This suggests that emissions of toluene may be only temperature dependent and not PAR dependent. In addition toluene's relatively long atmospheric lifetime may lead to accumulation later in the day, although the flux is not much higher in the afternoon as was the case for estragole. Consequently, another hypothesis is that due to "stickiness" of toluene the prolonged memory effect in the sampling tube may have led to elevated mixing ratios at the end of a day but this does not produce a covariance with vertical wind speed at the same time. Only small emissions of acetone and hexanals were observed despite an evident pattern which can explain only a portion of their mixing ratios. A clear deposition pattern can be observed for the sum of MVK and MACR and methanol. This suggests the primary source for these compounds is in the troposphere from photooxidation, in particular as the deposition of MVK and MACR is enhanced in the late morning coexistent with the highest isoprene emissions. However, methanol seems to be deposited at a more or less constant rate throughout the day and its primary source is most probably

the photooxidation of methane although it could also be direct emission of methanol from decomposing pectin (Fall, 2003) found in oil palm fruits (Henderson et al., 2001) and its subsequent wet deposition due to its high water solubility. Monoterpenes, and to a lesser extent acetaldehyde, exhibited mixed diurnal deposition, which could be due to variable gradients from scattered sources at the edge of the footprint, and oil palms being the net sink for those compounds.

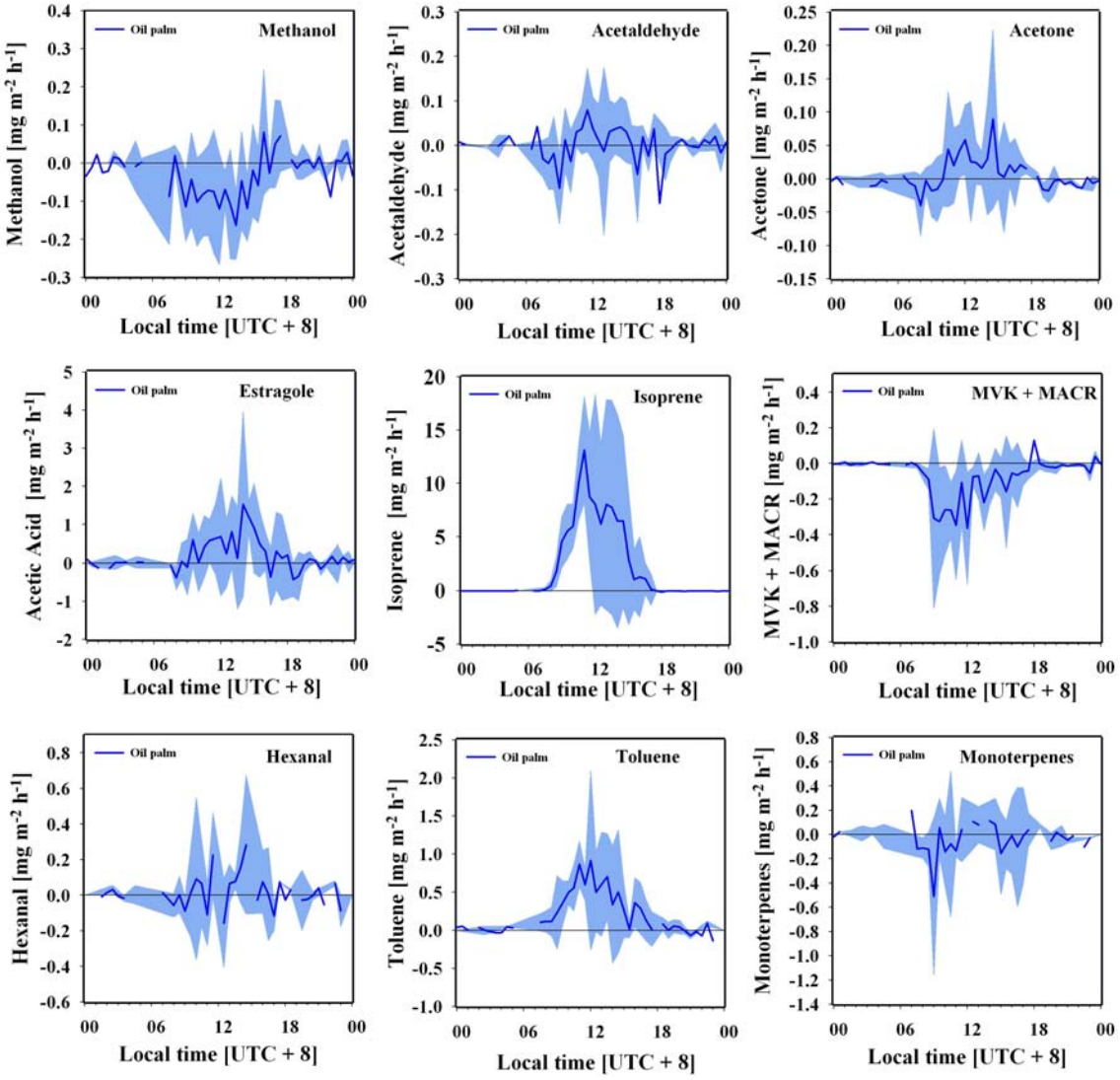

Figure 2.3-10 Daily averages of VOC fluxes with one standard deviation

2.3.4.6 Characterisation of abundant VOCs

2.3.4.6.1 Isoprene (m/z^+ 69) and its oxidation

Isoprene was the most abundant compound measured at the oil palm plantation both in mixing ratios and fluxes during a day but it was not emitted at night. Isoprene also dominated a different VOC mix at the rainforest where its absolute values were several times lower than those presented here (Langford et al., 2010). Oil palm has been known before to be a very high isoprene emitter (Wilkinson et al., 2006) but these are the first direct eddy covariance measurements, using the PTR-MS as a sensor.

It is still not entirely clear why the plant gives off isoprene since it requires substantial metabolic effort of 20 ATP and 14 NADPH molecules per one isoprene molecule (Sharkey et al., 2008). Most probably isoprene emission encountered in oil palm is a result of a specific thermotolerance mechanism (Sharkey and Schrader, 2006) although it could also potentially serve as a protection against herbivores (Laothawornkitkul et al., 2008) or as a stimulant to flowering (Terry et al., 1995). The latter hypothesis would seem consistent with a good correlation with temperature history in floral estragole (Sect. 2.5, Misztal et al. (2010c)). Finally isoprene may be protective against an oxidative stress (Loreto et al., 2001) but on the other hand ozone can inhibit isoprene production (Fares et al., 2010). However, ozone level at the plantation was typically less than 10 ppbv (Coyle, 2010) although other reactive oxygen species could possibly be present.

Isoprene detection by PTR-MS at *m/z* 69 shows a good agreement with GC-MS reported in various studies (de Gouw, 2007; Kuster et al., 2004), despite a notable interference at this *m/z* ratio potentially deriving from a fragment of prenol (2-methyl-3-buten-2-ol) (Holzinger et al., 2005), and/or 1-penten-3-ol (Karl et al., 2001b), both of which can also be detected at *m/z* 87. However, no elevated signal at *m/z* 87 was observed and neither of these compounds were detected in leaf cuvettes air by GC-MS (Owen et al., 2010). Another potential interference could be from

furan, a tracer of biomass burning (Christian et al., 2004) and a few anthropogenic compounds (de Gouw et al., 2003a), but the signal of acetonitrile at *m/z* 42, another biomass burning compound, and of benzene at *m/z* 79, an anthropogenic indicator, were both very low in the mass scans. Therefore considering the magnitude of isoprene emissions and its clear diurnal trends it is extremely unlikely that any interferences were significant.

Isoprene fluxes were mainly emission, and its fluxes were well correlated with canopy temperature (T_c) (r^2 = 0.84 of the exponential fit), PAR (r^2 = 0.91 of the quadratic fit); they were linearly well correlated with sensible heat flux (H) (r^2 = 0.8), in contrast to its first oxidation products MVK and MACR (schematic of oxidation in Figure 2.3-11), which exhibited mainly deposition and negative correlation with H (see Sect. 2.3.4.6.2 below).

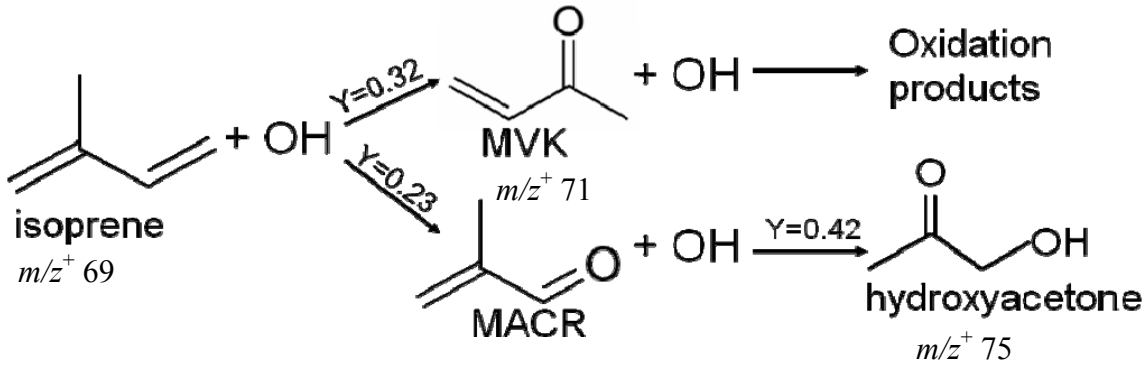

Figure 2.3-11 Basic schematic of isoprene photooxidation with branching ratios (adopted from Karl et al. (2009b)

The timeseries for isoprene volume mixing ratios and fluxes are shown in Figure 2.3-12. The graph presenting the flux timeseries shows the pattern following closely the variation in PAR and temperature. The exponential relationship with temperature can be observed both in the mixing ratios and the fluxes provided that the PAR is greater than zero (Figure 2.3-13 a and b respectively). The isoprene flux-temperature relationship for the rainforest (not presented here) also showed an exponential fit but the line was much steeper for the oil palm, which suggests higher sensitivity of oil palm emissions to temperature. From these dependencies it is clear that an increase

in global temperatures could dramatically increase oil palm emissions (see Sect. 2.3.5.1).

The main oxidation products MVK and MACR, and in addition hydroxyacetone (HA), are discussed below in Sections 2.3.4.6.2 and 2.3.4.6.4, but there are also many other photooxidation products of isoprene such as C5-carbonyls, glycolaldehyde, glyoxal and methylglyoxal (Taraborrelli et al., 2009), but which are not reported here. For example glycol aldehyde might be picked up at *m/z* 61 (Kim et al., 2010) but coinciding with acetic acid or ethyl acetate, which could also be present. Some short lived intermediate compounds may not be detected either, but recent interest sparked by analytical improvements in tandem mass spectrometry with collision-induced dissociation (CID-MS/MS) has been in measurements of isoprene epoxides and peroxides (Paulot et al., 2009), whose inclusion into models of low-NO isoprene chemistry can positively affect their predictive capabilities of OH radical concentrations (Kleindienst, 2009), and which are suspected contributors to isoprene-derived SOA (iSOA). With no negative ion mode, a standard PTR-MS cannot distinguish between isoprene hydroxyhydroperoxides (ISOPOOH) and isoprene dihydroxyepoxides (IEPOX) which are isobaric so both should be detected at *m/z* 101 in the PTR-MS systems which utilise an energetic ion de-clustering phase. Thus, the diurnal pattern of approximate mixing ratios of the sum of these two species might be reflected in Figure 2.3-14, although it cannot be confirmed by any alternative technique. Contribution of isoprene emission to biogenic secondary organic aerosols (BSOA) is discussed in Sect. 2.3.5.2.

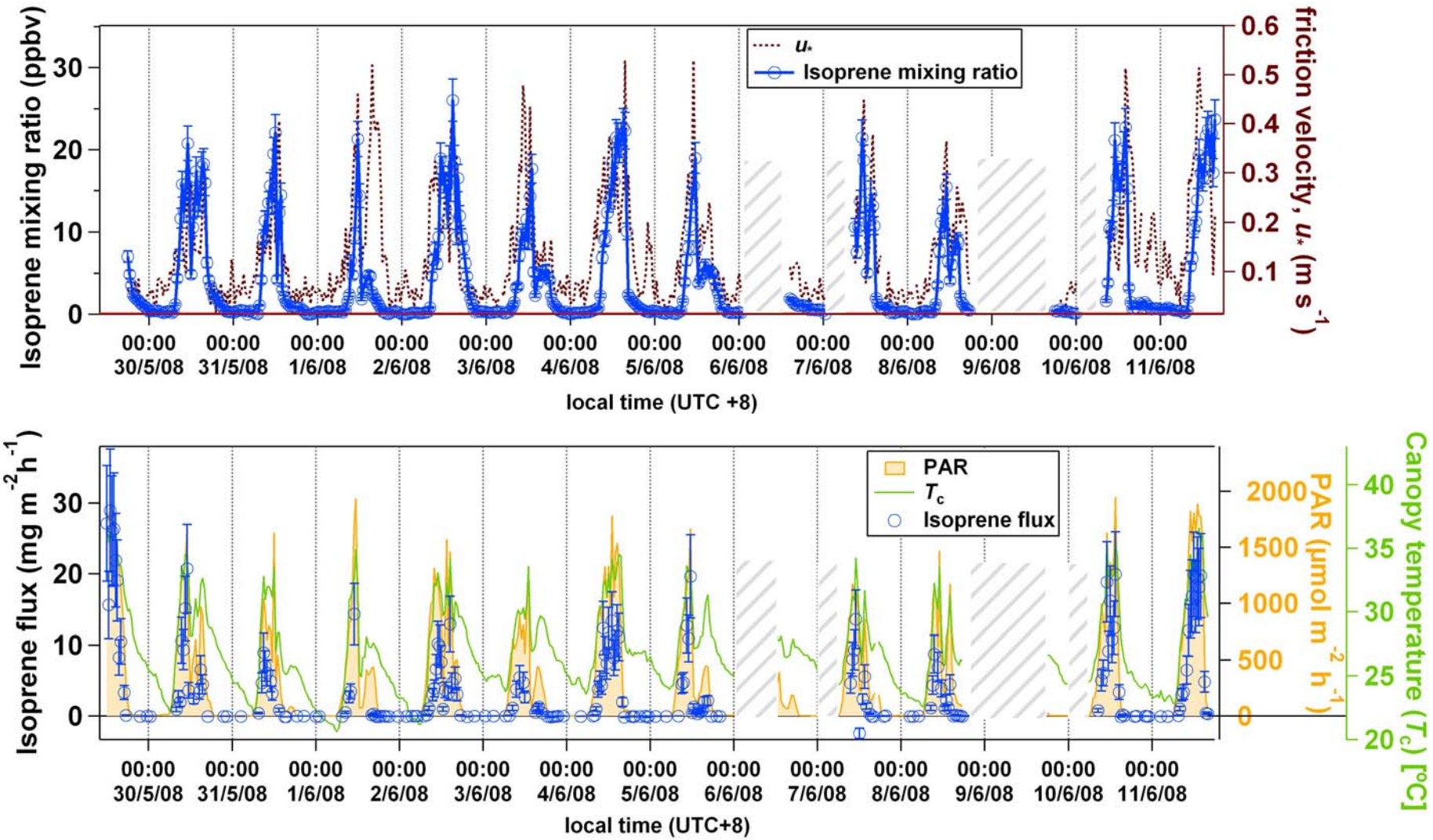

Figure 2.3-12 Isoprene (*m/z* 69) volume mixing ratios (top graph) in relation to u_* and validated flux (bottom graph) in relation to T_c and PAR. Crosshatch zones correspond to power interruptions and a red line to the detection limit.

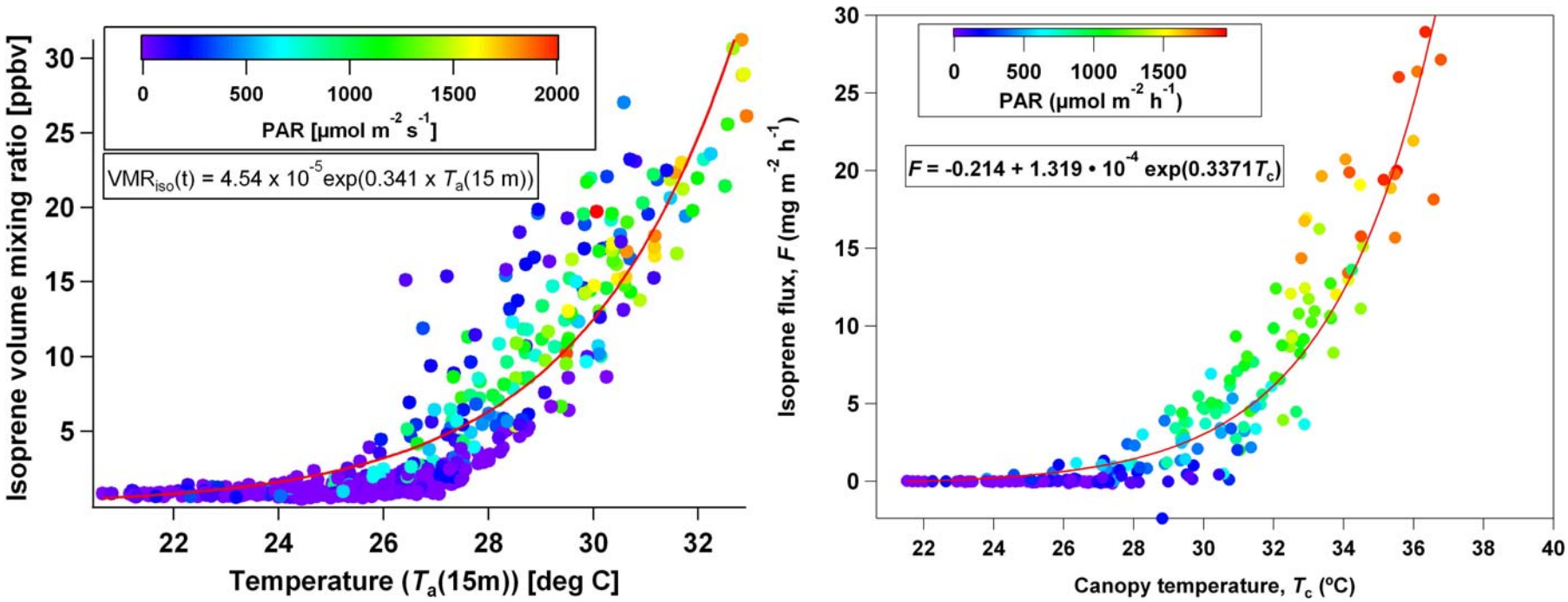

Figure 2.3-13 Exponential relationships between temperature and isoprene mixing ratios (a), and fluxes (b), coloured according to magnitude of PAR.

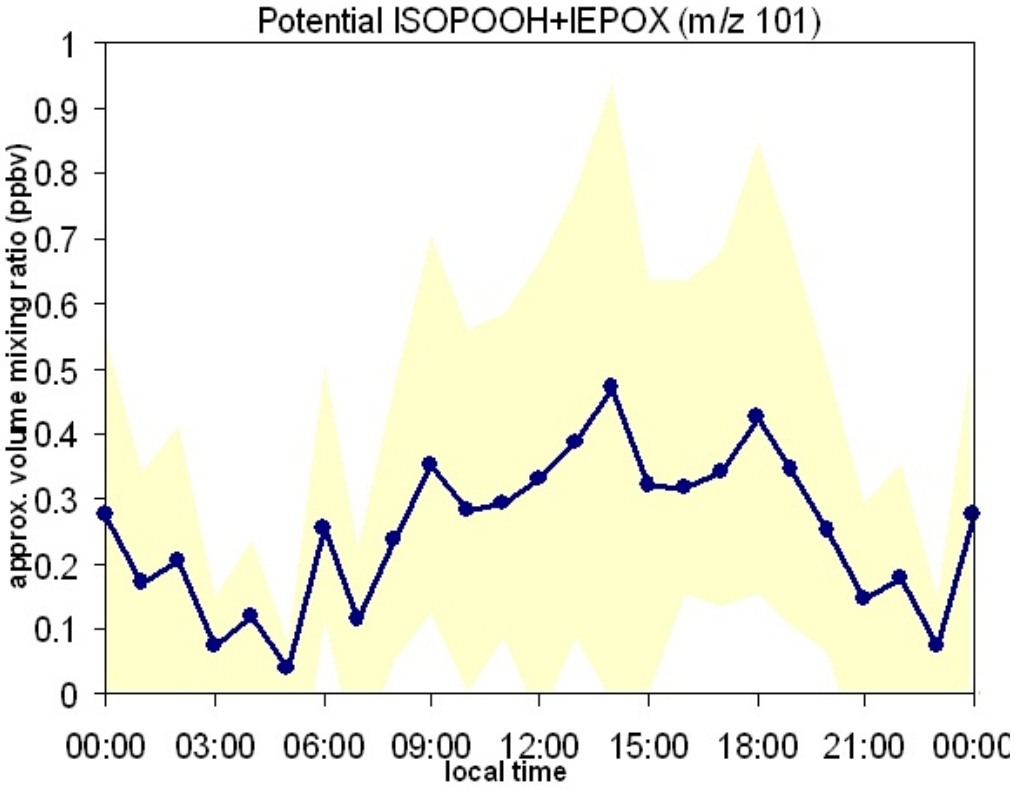

Figure 2.3-14 Suspected isoprene peroxides and epoxides coinciding at 101 m/z ion channel.

2.3.4.6.2 Methyl vinyl ketone (MVK) and methacrolein (MACR) (m/z^+ 71)

MVK and MACR are the first-order oxidation products of isoprene which form the majority (over 50%) of all oxidation products. The sum of those two isomers can be detected reliably at *m/z* 71 and the timeseries of mixing ratios and fluxes are presented in Figure 2.3-15. There was a strong positive correlation of MVK+MACR with isoprene in the mixing ratios (r^2 = 0.80, slope 0.19±0.04). A similar slope of correlation was found at the rainforest (Langford et al., 2010) despite a large difference in the measurement heights. However, the slope of this correlation in measurements from the Amazon (Karl et al., 2009b) was more than two times higher which might indicate a higher oxidative capacity at Amazon, different chemistry

caused by different recycling mechanisms or differences in the oxidation product losses due to the wet deposition. On the other hand, the correlation in the fluxes was negative because more of the MVK and MACR is formed higher in the troposphere so the gradient is such that MVK and MACR can be efficiently deposited to the surfaces of the fronds (Figure 2.3-16) at a deposition velocity ($V_d(z_m)$) exceeding 1 cm s^{-1} during the mid-day and reaching maximal deposition velocity (v_{max}) at times (1.5 to 2 cm s^{-1}).

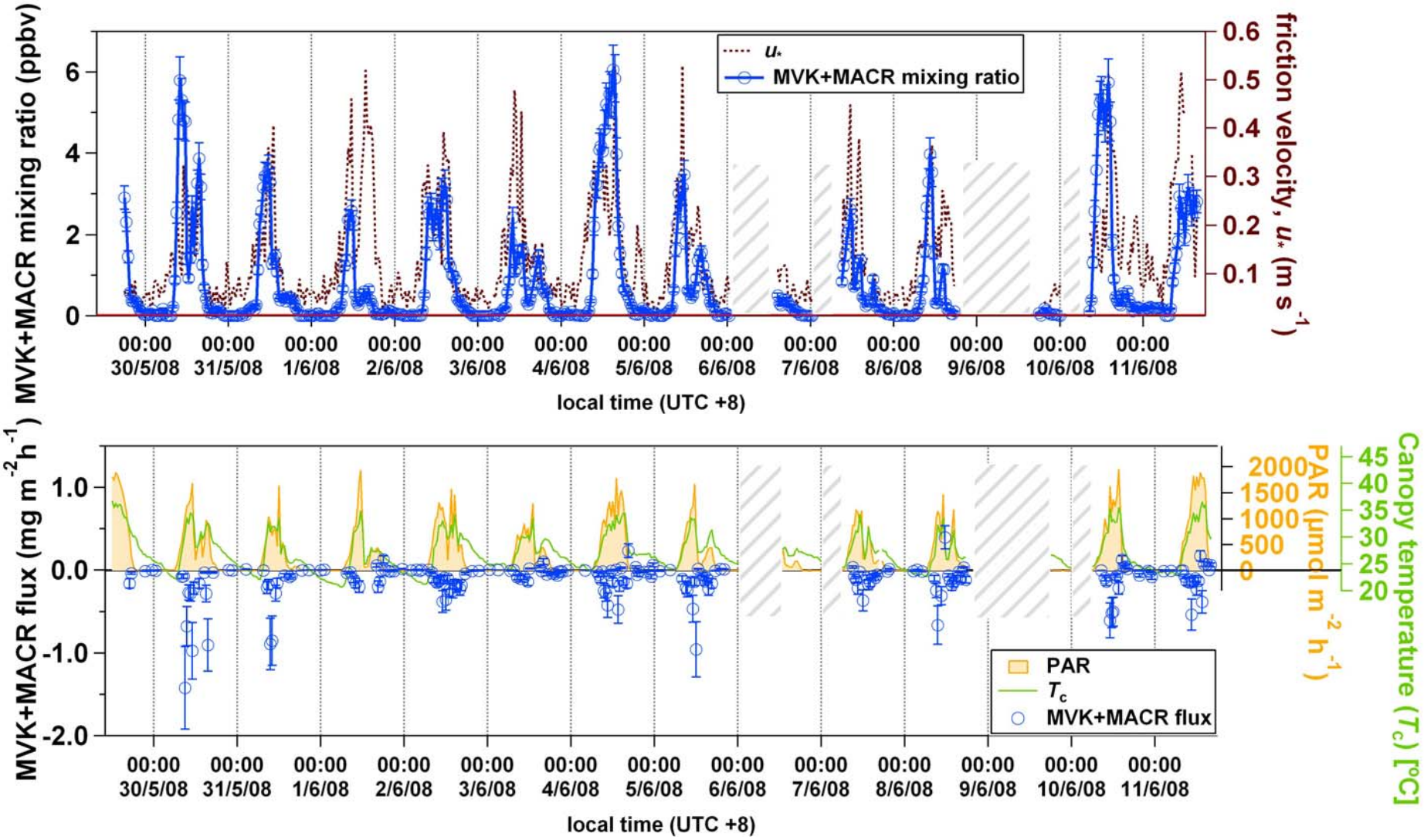

Figure 2.3-15 MVK plus MACR (*m/z* 71) volume mixing ratios (top graph) in relation to u_* and validated flux (bottom graph) in relation to T_c and PAR. Crosshatch zones correspond to power interruptions and a red line to the detection limit.

It is likely that other oxidation products of isoprene are also effectively deposited as was also found in other studies (Karl et al., 2009b; Karl et al., 2007; Kuhn et al., 2007) where the highest deposition was noted at the top of the canopy and the integrated source/sink distribution over the entire canopy indicated that the primary source for these OVOCs was above canopy. Inclusion of such high deposition velocities into models can significantly improve the agreement of model with measurements (Pugh et al., 2010). Eddy covariance measurements of deposition are therefore particularly important, since deposition cannot be measured in the photooxidation chambers. At the nearby rainforest an in-canopy BVOC profile analysis by Ryder et al. (2010) indicated that MVK/MACR were emitted at the top of the canopy but eddy covariance flux measurements at 75 m, integrated over a much larger footprint (Langford et al., 2010), revealed a small net emission in the morning and deposition in the afternoon. From the Henry's law constants listed by Sander (1999), it seems that the constant for MVK is about 20 – 40 M atm^{-1}, which is approximately 3 orders of magnitude larger than the Henry's Law constant for isoprene and 1 order of magnitude smaller than for methanol. Therefore, it could be expected that MVK and MACR are subject to both dry and wet deposition whereas the latter would be the dominant process for methanol deposition (Sect. 2.3.4.6.6.).

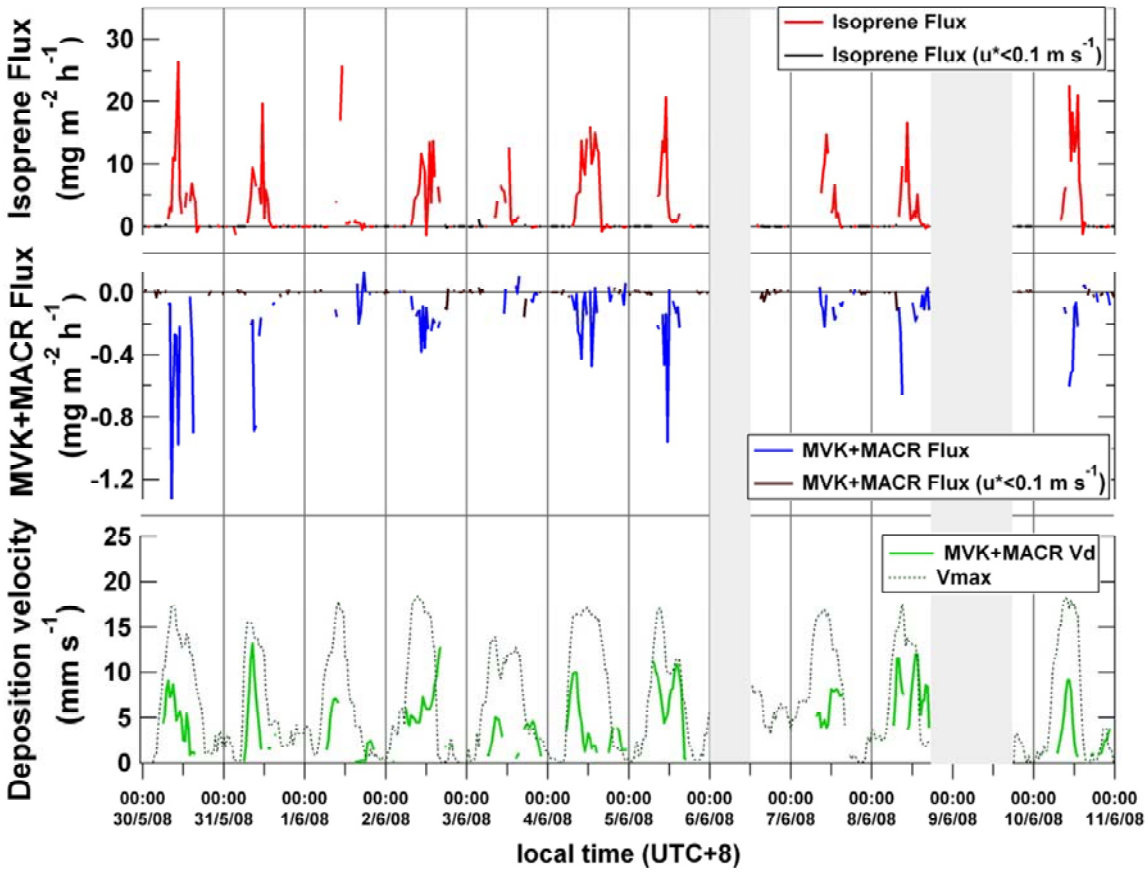

Figure 2.3-16 MVK+MACR downward flux (blue), deposition velocity (green) in relation to maximal theoretical velocity (V_{max}) and the positive isoprene flux (red) for comparison.

2.3.4.6.3 Estragole (m/z^+ 149)

Since estragole (methyl chavicol) emissions are described in detail in Sect. 2.5 and in Misztal et al. (2010c), here only a summary of data is presented for comparison purposes. From the mixing ratio and flux time series (Figure 2.3-17) it can be observed that the elevated mixing ratios still persisted in the low u^* conditions but this is not reflected in the fluxes due to insufficient turbulence. As this compound was found to be a flower component, the late peaking mixing ratios may be the result of thermogenesis which typically turns on when the ambient temperature declines. Thus, estragole could be volatilised later than it was synthesised, which could be seen in the maximal correlations of mixing ratios with the past temperature and PAR history (3.5 h average lag). Estragole was mainly emitted, with occasional deposition

periods in the early morning or in the evening, and its emission can be modelled by the modified Guenther et al. (2006) algorithm (see Sect. 2.3.4.8.4).

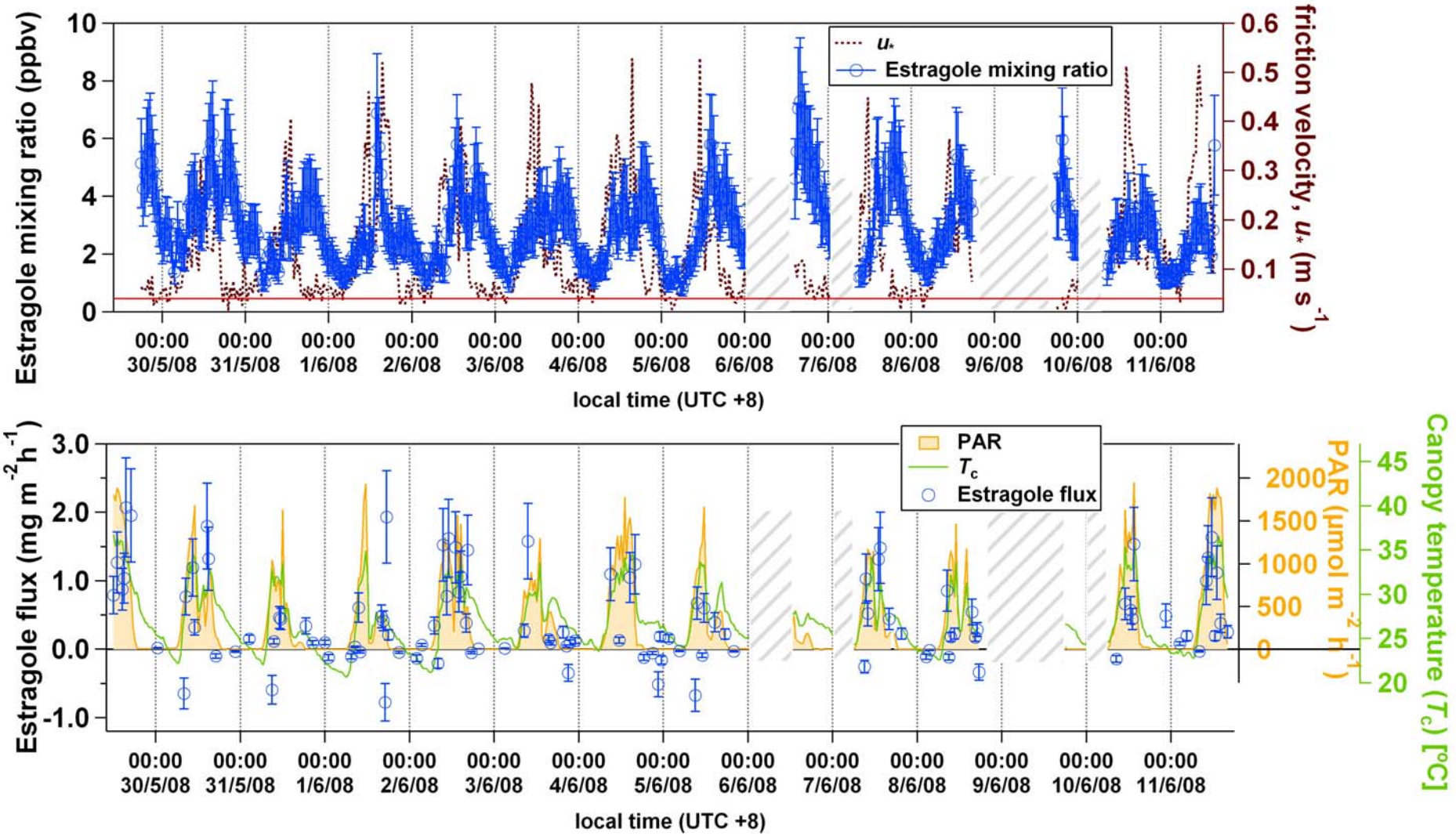

Figure 2.3-17 Estragole (*m/z* 149) volume mixing ratios (top graph) in relation to u_* and validated flux (bottom graph) in relation to T_c and PAR. Crosshatch zones correspond to power interruptions and a red line to the detection limit.

2.3.4.6.4 Hydroxyacetone (HA) (m/z^+ 75)

Due to the limited number of compounds which could be measured in the eddy covariance mode, m/z^+ 75 was not included in the flux mode, so only the results for VMRs, which were derived from the hourly 5 min scan data, are presented (Figure 2.3-18). It should be noted that 5 min corresponds to 3 full-range cycles, giving altogether 1.5 s (3 x 0.5 s) per each *m/z* in an hour so offering only a small fraction of time resolution compared to the other compounds presented here that were included in the flux mode. The major source of HA is the oxidation of MACR (Carter and Atkinson, 1996). However, the correlation with MVK+MACR mixing ratios was quite weak (r^2 = 0.4, slope 0.4±0.1) so it is highly probable that this *m/z* ion channel received contributions from compounds such as biogenic esters which are known to appear at this *m/z* (e.g. propionates or propionic acid). Alternatively there could be a different source of HA other than from MACR oxidation. Karl et al. (2009b) found ten times higher HA/(MVK+MACR) ratios than predicted from the MACR → HA reaction scheme (Figure 2.3-11) and suggested another source within the isoprene oxidation scheme but faster than the MACR production, other sources of HA such as from oxidation of peroxides or from oxidation of acetone. Due to relatively high uncertainties associated with compound attribution to this *m/z* the data should currently be treated with caution in deducing the oxidation rates of MACR.

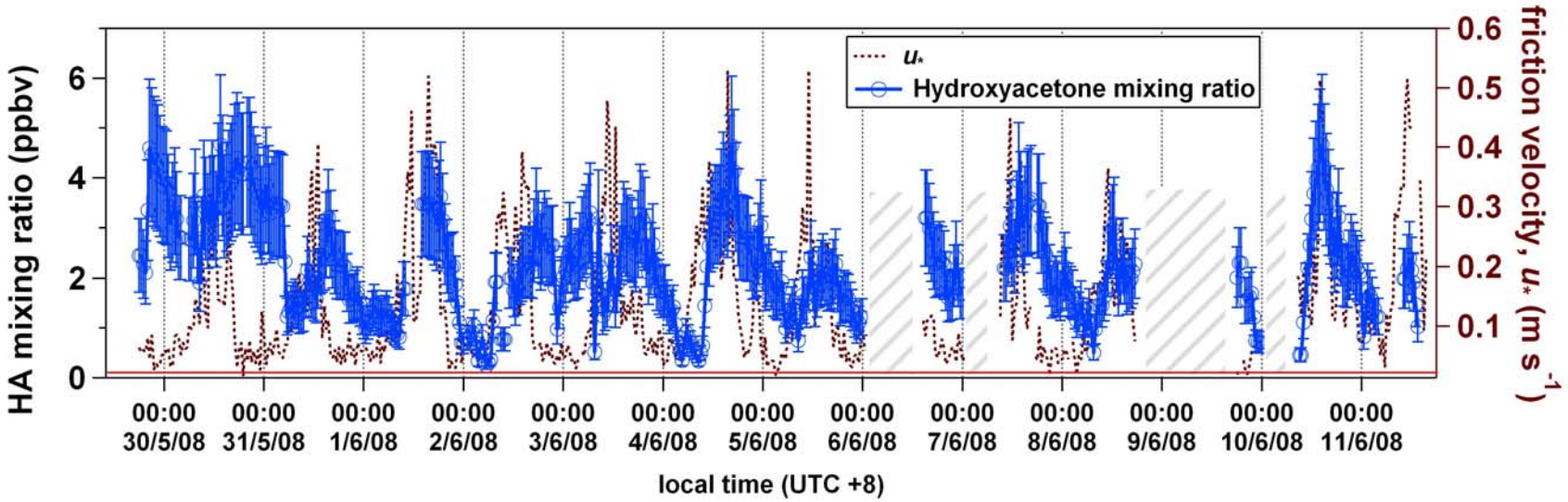

Figure 2.3-18 Hydroxyacetone (*m/z* 75) volume mixing ratios in relation to u_*. The data were retrieved from less frequent mass scans since *m/z* 75 was not included in the flux mode. Crosshatch zones correspond to power interruptions and a red line to the detection limit.

2.3.4.6.5 Toluene (m/z^+ 93)

Although one can never be absolutely certain when relying predominantly on the PTR-MS data of any potential contributions/interferences, it is extremely probable that this ion channel *m/z* 93 received contribution from toluene. The toluene mixing ratio in comparison with u_* and flux time series in comparison withare T_c and PAR are presented in Figure 2.3-19. In various measurement campaigns conducted in conjunction with GC-MS, the *m/z* 93 channel was validated as toluene with good agreement (Apel et al., 2008; de Gouw et al., 2003b; de Gouw et al., 2003c; de Gouw, 2007; Warneke et al., 2001). The only known significant other contribution found so far has been from p-cymene (Maleknia et al., 2007; Tani et al., 2003), a $C_{10}H_{14}$ compound, which is similar in structure to monoterpenes but has an aromatic ring instead of cyclohexanyl, cyclohexenyl or cyclohexadienyl ring. Monoterpenes could also contribute to this *m/z* but the relative abundance at this *m/z* is up to around 1% or less (Tani et al., 2004; Tani et al., 2003) irrespective of the *E/N* values commonly used. The author conducted a detailed experiment with the range of monoterpenes and p-cymene (see Sect. 2.8 on monoterpene discrimination) covering a wide range of *E/N* ratios. The parent ion for p-cymene is detected at *m/z* 135 and no signal was observed at this ion channel at the oil palm plantation. However, p-cymene is so easily fragmented that at higher *E/N* ratios its abundance is close to zero. In this case, however, relatively high signals would have to be present at *m/z* 119, *m/z* 43 and also at other less abundant ions such as *m/z* 53. It is therefore unlikely that p-cymene would appear only on *m/z* 93, unless its mixing ratios were small so the minor fragments would be lost in the noise. No correlations were found at *m/z* 119 and *m/z* 43 with *m/z* 93.

In fact, toluene was detected in GC-MS in the ambient air although its peak was much smaller than that of estragole. Small levels of o-cymene were also detected in the ambient air by collaborators and the levels of toluene of similar abundance to that of estragole were subsequently found in flower enclosures (but only male inflorescences). As previously mentioned, toluene is a known constituent of many floral scents, although usually is only a minor component. However, Hadacek and

Weber (2002) found toluene-rich scents (referred to as 'medicinal odour') in *Sauromatum guttatum* belonging to the same family (Arecaceae) as oil palm. These scents were observed to be attractants of tephridid flies. Considering all pieces of information, the signal at *m/z* 93 was ascribed with the highest probability to toluene, although one cannot totally exclude small contributions from o-cymene. The toluene flux showed good quadratic correlations with temperature ($r^2 = 0.77$) and PAR ($r^2 = 0.69$); the exponential relationships were much worse than those for isoprene flux. A correlation with PAR does not necessarily mean that toluene emission is PAR dependent as both temperature and PAR variables are strongly autocorrelated.

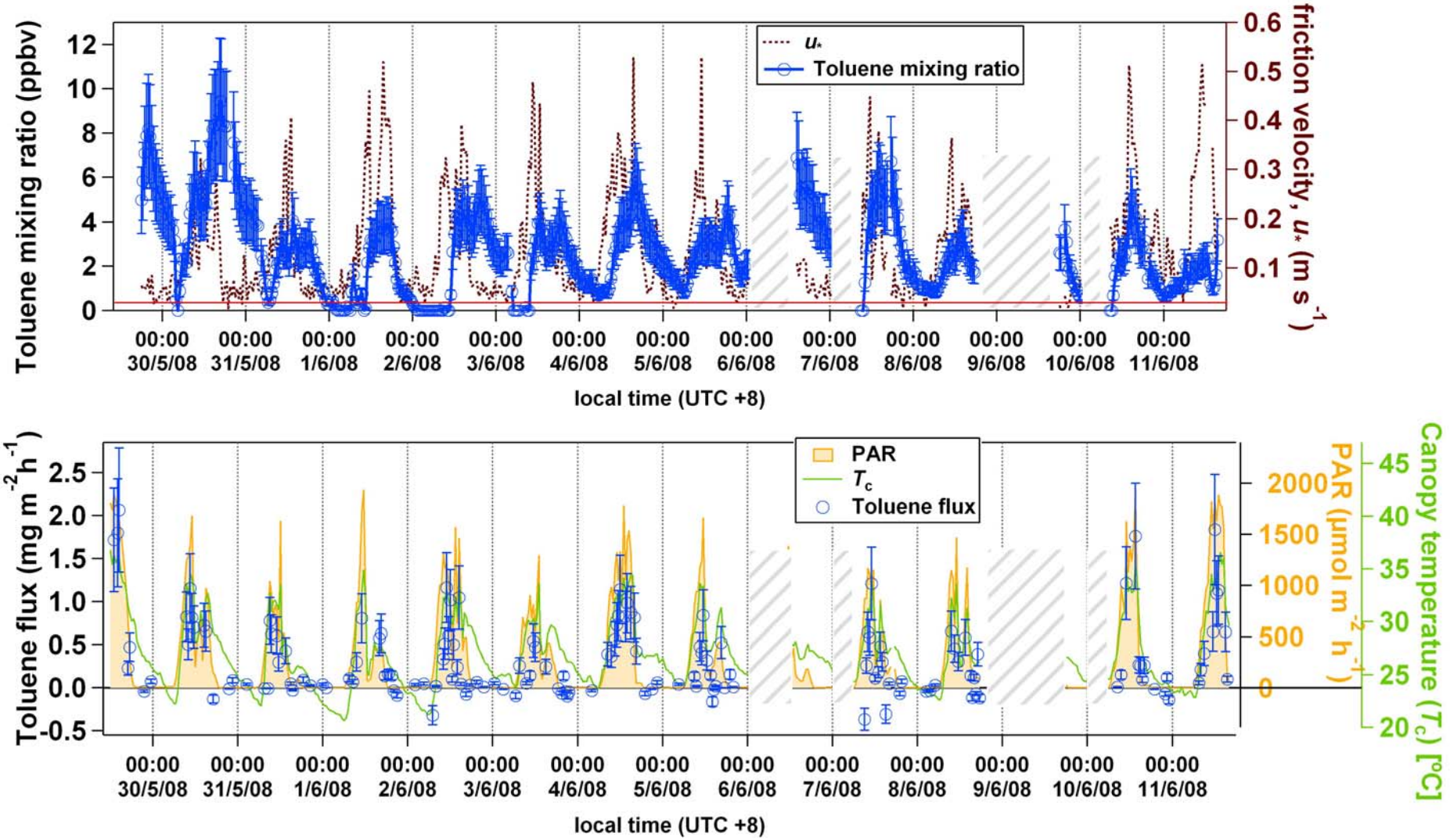

Figure 2.3-19 Toluene (*m/z* 93) volume mixing ratios (top graph) in relation to u_*, and validated flux (bottom graph) in relation to T_c and PAR. Crosshatch zones correspond to power interruptions and a red line to the detection limit.

2.3.4.6.6 Methanol (m/z^+ 33)

Methanol is an oxygenated VOC, which is of interest for atmospheric chemistry and has been widely studied in various environments (Brunner et al., 2007; Custer and Schade, 2007; Seco et al., 2007; Sinha et al., 2007). It is a very important alcohol because of its high impact on tropospheric oxidation (Tie et al., 2003). Due to an unexpectedly high background encountered at this *m/z* value less than a half of the data exceeded the higher than normal detection limit (see explanation in Sect. 2.3.4.2). The timeseries for the mixing ratios and fluxes are presented in Figure 2.3-20. It seems that methanol mixing ratios exceeding LOD were well correlated with friction velocity during the day and that the majority of the vDEC flux was negative, making methanol the second most highly depositing compound after MVK and MACR. However, with its high Henry's law constant methanol is very likely to be wet deposited. Previous studies have found net flux of methanol always positive with only partial deposition, but the high humidity encountered in Borneo could be a factor. Our findings at the rainforest (Langford et al., 2010) also indicated a net deposition of methanol at the rainforest. Most probably the primary source of methanol depositing at the oil palm plantation can be a result of methane oxidation higher in the troposphere, since methane flux was considerable at the site (Siong et al., 2010) although methanol emission due to pectin decomposition from senescing biomass (Fall, 2003) or from leaves as a result of growth or stress (Davison et al., 2009; Folkers et al., 2008) could be responsible for the exchange in the opposite direction. Nevertheless, methanol deposition can be important globally as the conversion rate from methane is currently not known, nor how much is diverted to the surface due to wet deposition, hence a need for more eddy covariance studies.

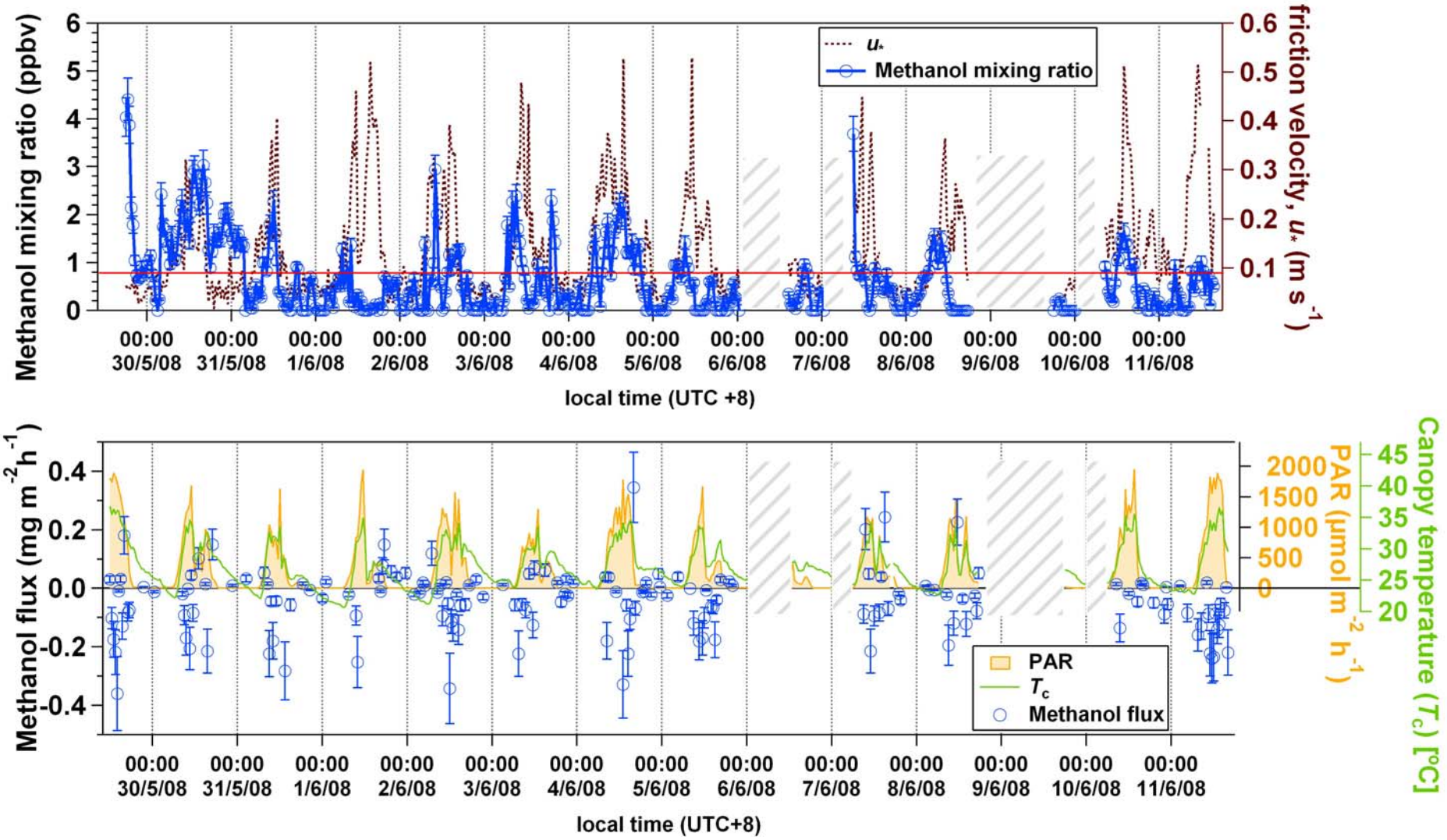

Figure 2.3-20 Methanol (*m/z* 33) volume mixing ratios (top graph) in relation to u_*, and validated flux (bottom graph) in relation to T_c and PAR. Crosshatch zones correspond to power interruptions and a red line to the detection limit.

2.3.4.6.7 Acetaldehyde (m/z^+ 45)

According to recent 3-D modelling (GEOS-Chem) constrained by in-situ and satellite observations, the largest acetaldehyde source in the atmosphere is from hydrocarbon secondary oxidation (128 Tg a^{-1}) with only 23 Tg a^{-1} emitted directly from the biosphere including emission from decaying plants (Millet et al., 2010). In plants acetaldehyde has been shown to derive from ethanol fermentation under anoxic conditions in roots and leaves (Jardine et al., 2008; Winters et al., 2009) with much enhanced emissions after anoxic and wounding stress (Jardine et al., 2009), the latter probably resulting from fatty acid peroxidation by accumulated reactive oxygen species. The exchange of acetaldehyde is bidirectional because it can be taken up and consumed metabolically (Fall, 2003). However, it is suspected that isoprene oxidation can be a significant source of acetaldehyde in high isoprene environments, where it is mainly formed from photolysis of MVK (Atkinson et al., 2006) through propene degradation and could also be generated from the ozonolysis of isoprene (Taraborrelli et al., 2009). Millet et al. (2010) reported that the total acetaldehyde yield from isoprene, depending on low or high NO_x level, respectively, is 1.9% - 2.5% in GEOS-Chem, 4.7% - 4.3% in MCMv3.1 and estimated at 2% by 3-D modelling using the Mainz Isoprene Mechanism 2 (MIM2) (Taraborrelli et al., 2009).

At the plantation, acetaldehyde constituted 4% of VOC mix in mixing ratios and only 0.2% in the flux. The detection limit for this compound was elevated leaving 57% of valid data for the mixing ratios, which are presented along with the fluxes in Figure 2.3-21. Although acetaldehyde was found to be the main compound detected at *m/z* 45 the agreement with GC-MS was not always good quantitatively because of potential artefacts including acetaldehyde generated from ozone (de Gouw, 2007). There were no correlations in the mixing ratios of acetaldehyde with ozone, which was low (less than 6 ppb), or any other VOC, and it was lacking a clear diurnal trend (Figure 2.3-7k) although in the full timeseries periods of correlation with u_* are evident and the data had a clearly lognormal distribution (Figure 2.3-4).

However, a clearer trend could be obtained in the fluxes (Figure 2.3-10i) with prevailing periods of emissions, and with deposition periods in the morning or in the evening or around the rain episode at noon time. The lack of structure in the mixing ratios, but a reasonable small positive flux, could suggest acetaldehyde flux to be possibly originating from ethanol oxidation under the anaerobic soil conditions (soil-moisture dependent) with periods of deposition of photochemically formed acetaldehyde. The acetaldehyde yields from isoprene obtained in the chambers may be overestimated if they do not account for the deposition of this species.

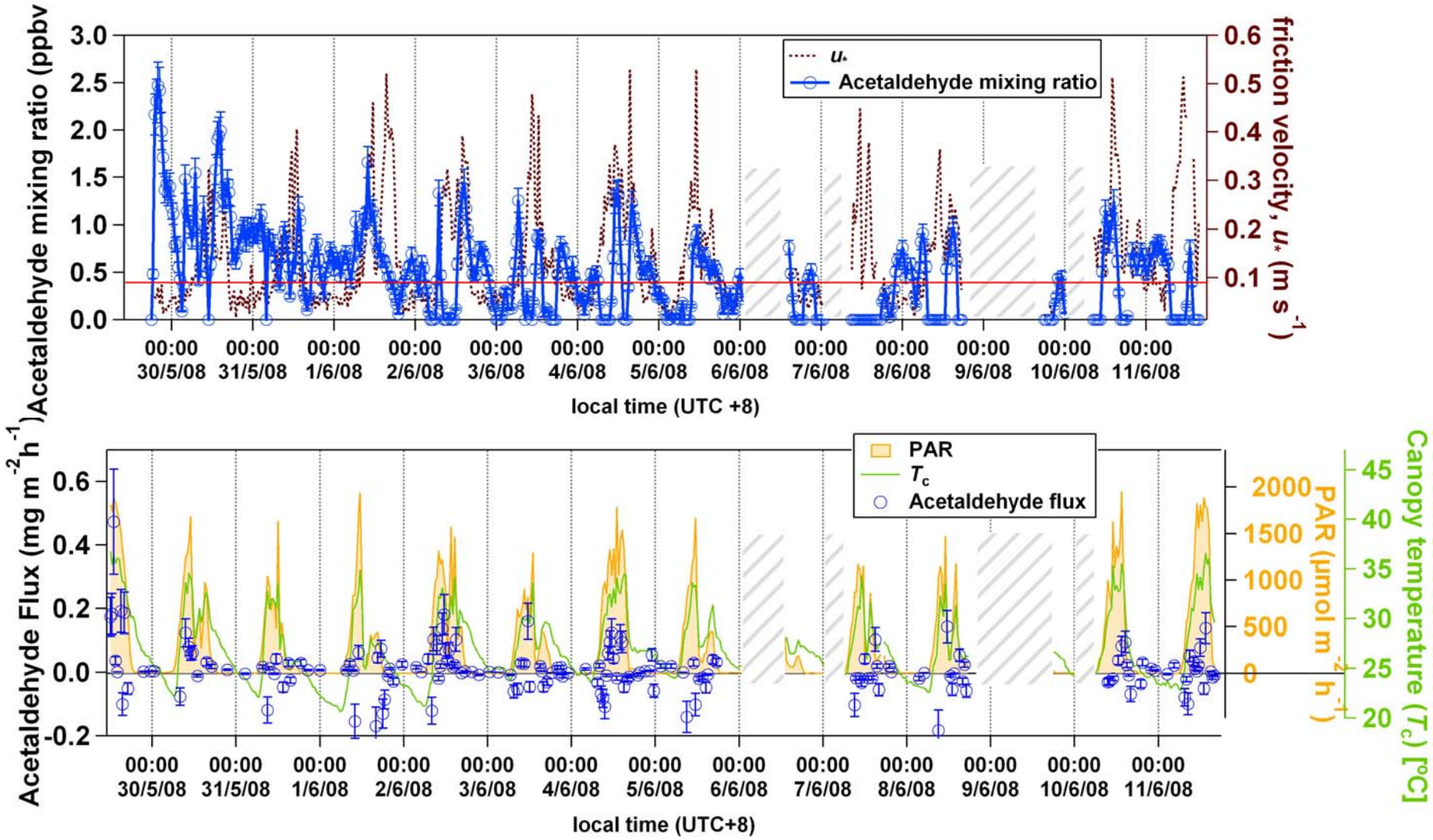

Figure 2.3-21 Acetaldehyde (*m/z* 45) volume mixing ratios (top graph) in relation to u_*, and validated flux (bottom graph) in relation to T_c and PAR. Crosshatch zones correspond to power interruptions and a red line to the detection limit.

2.3.4.6.8 Acetone (m/z^+ 59)

Acetone has been shown to be reliably detected by PTR-MS at *m/z* 59 with a minor (0-10%) possible contribution from propanal (de Gouw, 2007). Potentially, glyoxal could be detected at this *m/z* but its detection would require an aerosol-capturing inlet (Hellén et al., 2008). Acetone is regarded as a dominant VOC in the atmosphere (Singh et al., 1994) with the major source from oxidation of VOC precursors. Various campaigns have reported elevated acetone levels above various vegetation types (Karl et al., 2005; Murphy et al., 2010; Warneke, 2002) and aircraft PTR-MS measurements showed particularly elevated acetone levels above tropical rainforests (Pöschl et al., 2001; Karl et al., 2004). Among other sources are direct emissions from plants, biomass burning and decomposing biomass (Fall, 2003). In plants it is thought that acetone is formed through cyanogenesis and decarboxylation of acetoacetate.

The timeseries for acetone mixing ratios and fluxes from this work are presented in Figure 2.3-22. Acetone mixing ratios were linearly correlated with canopy temperature (r^2 = 0.55), PAR (r^2 = 0.30) and logarithmically with MVK and MACR (r^2 = 0.56) and isoprene mixing ratios (r^2 = 0.55), although surprisingly the highest degree of linear correlation (r^2 = 0.65) was obtained with hexanals (*m/z* 83; Sect. 2.3.4.6.10), which are regarded as wounding stress compounds. Acetone has not yet been reported as a stress compound, but there have been studies which also found agreement of acetone and hexanal mixing ratios. Davison et al. (2008) reported a high correlation in the fluxes, after cutting, of acetone and hexanals (r^2 = 0.73), which was the second highest correlation after hexenals. There is also some scarce evidence suggesting that biogenic production of acetone is enhanced after stress (Bubenheim et al., 2004). Agreement in the fluxes of acetone and hexanals at the plantation was worse, probably due to differences in the deposition. Acetone has a relatively long lifetime and its relatively high mixing ratios may not always result in the high surface flux (Karl et al., 2004). The 95th percentile value for acetone flux was only 0.10 mg m^{-2} h^{-1}, and the mean value was 0.012 which was very similar to the value obtained at the rainforest 0.12 mg m^{-2} h^{-1} and 0.012 mg m^{-2} h^{-1} (Langford et al., 2010). This is somewhat at odds with model estimates from GABRIEL 2005 campaign which was estimated at 0.35 mg m^{-2} h^{-1} (Eerdekens et al., 2009) despite

agreement in the mixing ratios. Physical losses of acetone due to deposition may be responsible for this discrepancy.

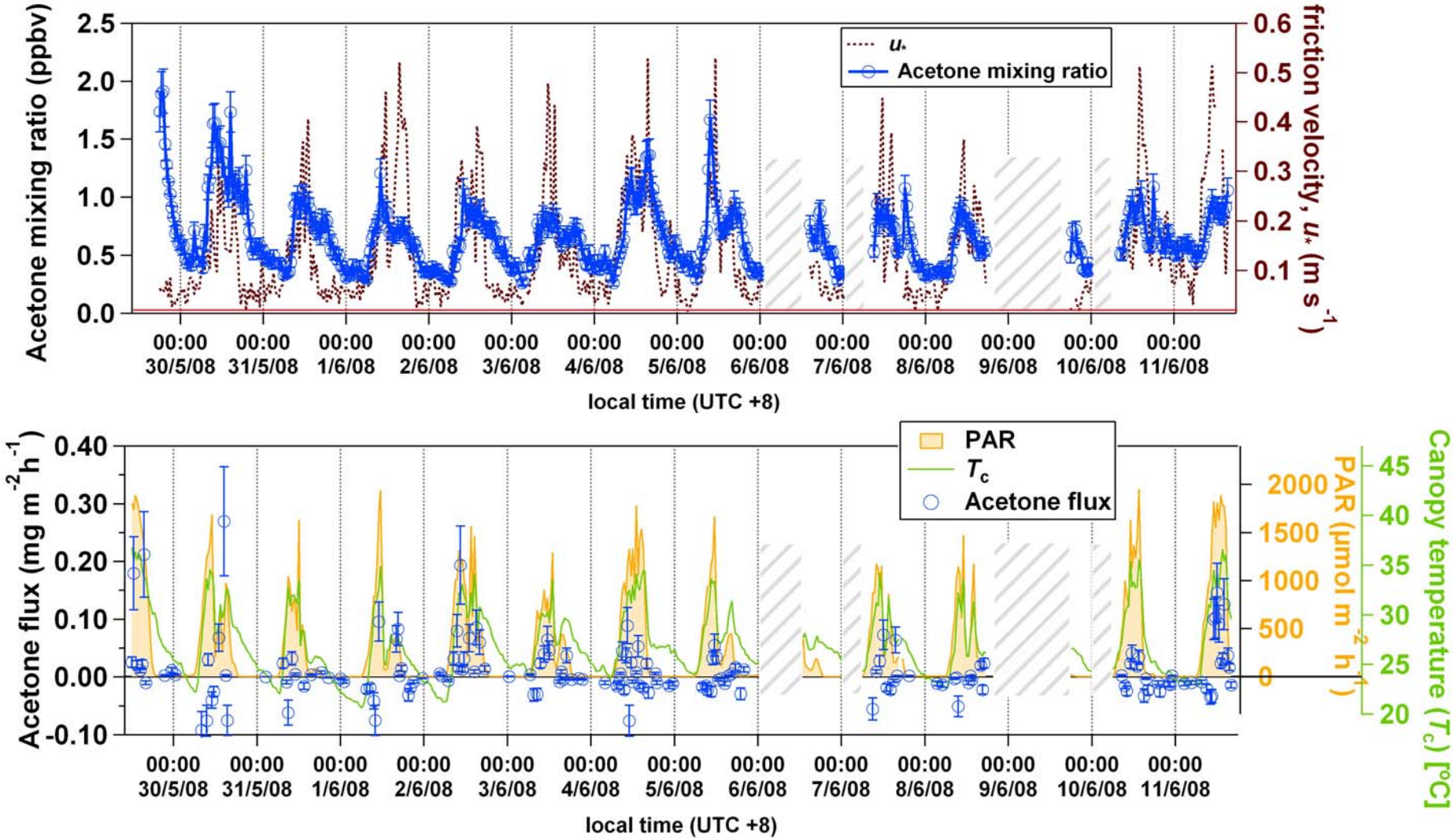

Figure 2.3-22 Acetone (*m/z* 59) volume mixing ratios (top graph) in relation to u_*, and validated flux (bottom graph) in relation to T_c and PAR. Crosshatch zones correspond to power interruptions and a red line to the detection limit.

2.3.4.6.9 Monoterpenes (m/z^+ 81, 137)

Timeseries for monoterpene (*m/z* 81) mixing ratios and fluxes are presented in Figure 2.3-23. Monoterpenes were measured in the flux mode at *m/z* 81 and *m/z* 137. Normally a sum of the signals at these *m/z* ratios is used for quantification of total monoterpenes in order to account for variabilities in the relative proportion between *m/z* 81 and *m/z* 137 signals at variable humidity (Tani et al., 2003). High humidity can have an impact on the sensitivity (Tani et al., 2004), which was much better at *m/z* 81 than at *m/z* 137, and therefore both ions were calibrated separately but the signals were not merged in order to avoid introducing noise from the less sensitive channel. However, the statistical methods presented in Sect. 2.3.4.2 showed good agreement between the absolute values of the total monoterpenes derived from either *m/z*. However, only 45% of the mixing ratios exceeded the detection limit for *m/z* 81, and the rest was filled with half of the detection limit value. Thus the average mixing ratio was found to be 0.33 ppbv which is higher than a corresponding 0.24 ppbv value for the rainforest, although much lower than for isoprene. Nevertheless the value of 0.33 ppbv seems higher than the results from leaf cuvettes (Owen et al., 2010) so it is likely that ambient monoterpenes were originating from flowers as they were subsequently found in the flower enclosures. However, the ambient mixing ratios were not correlated with temperature (r^2 = 0.10) or PAR (r^2 = 0.07). Also the correlation with *m/z* 83 was small (r^2 = 0.16) making contributions from hexenals unlikely. The flux was dominated by deposition periods giving overall net deposition of -0.026 mg m^{-2} h^{-1} which is in contrast with clear emission pattern from rainforest at net average of 0.241 mg m^{-2} h^{-1}.

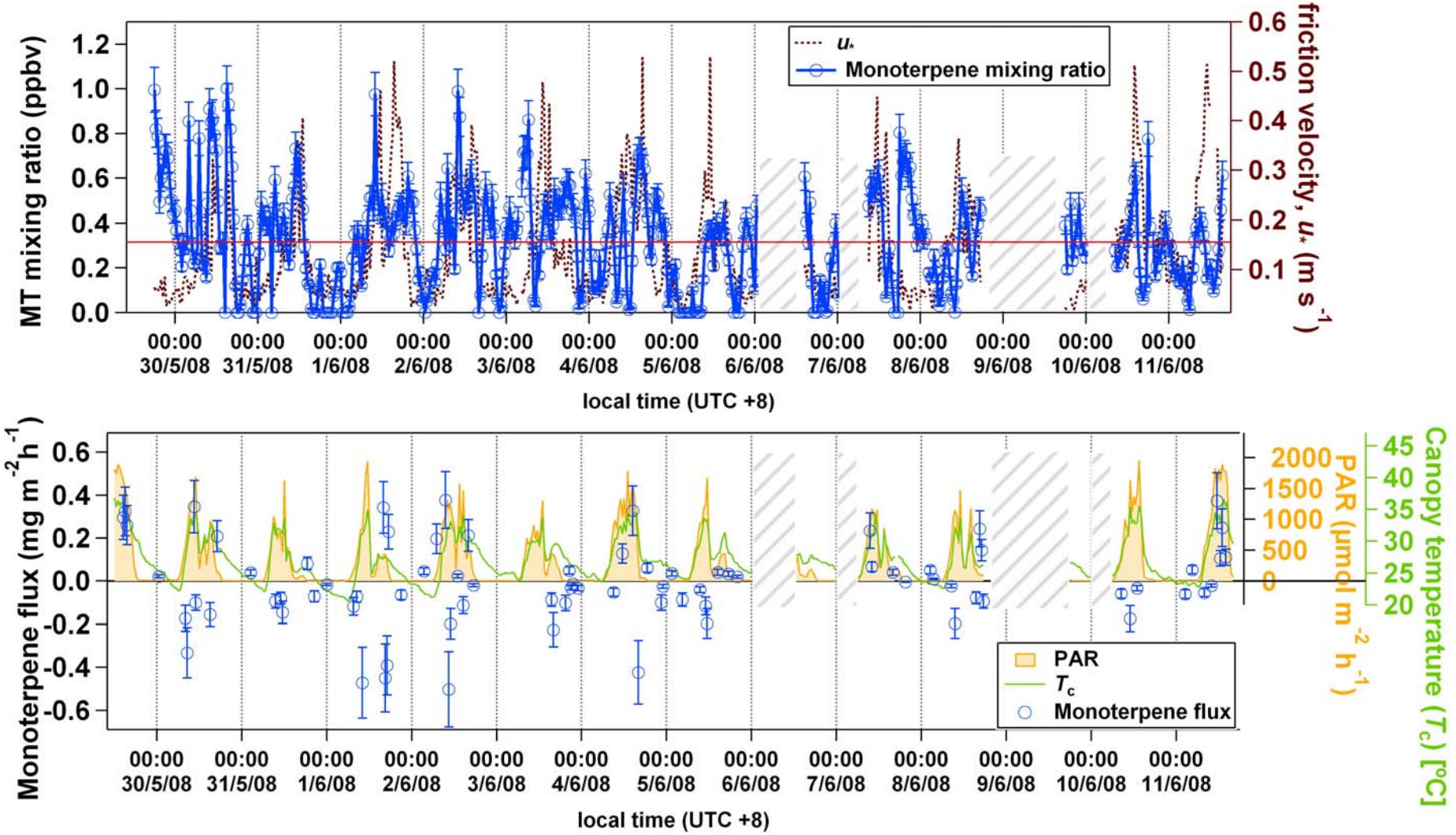

Figure 2.3-23 Monoterpene (*m/z* 81) volume mixing ratios (top graph) in relation to u_*, and validated flux (bottom graph) in relation to T_c and PAR. Crosshatch zones correspond to power interruptions and a red line to the detection limit.

2.3.4.6.10 Hexanals (m/z^+ 83)

Hexanals belong to a green leaf volatile class of compounds which are known to be emitted under stress (e.g. Davison et al., 2008; Filella et al., 2007; Karl et al., 2001b). The timeseries for mixing ratios and fluxes are presented in Figure 2.3-24. The VMRs were characterised by a clear diurnal trend and they were linearly correlated with acetone (r^2 = 0.66), and canopy temperature (r^2 = 0.51) and weakly with PAR (r^2 = 0.38). Interestingly this *m/z* was logarithmically correlated with MVK+MACR (r^2 = 0.57) and isoprene (r^2 = 0.54), which was similar to what was earlier observed for acetone so it might suggest that acetone and hexanals might be formed in the isoprene oxidation chain or/and may be emitted in response to the depositing oxidation products.

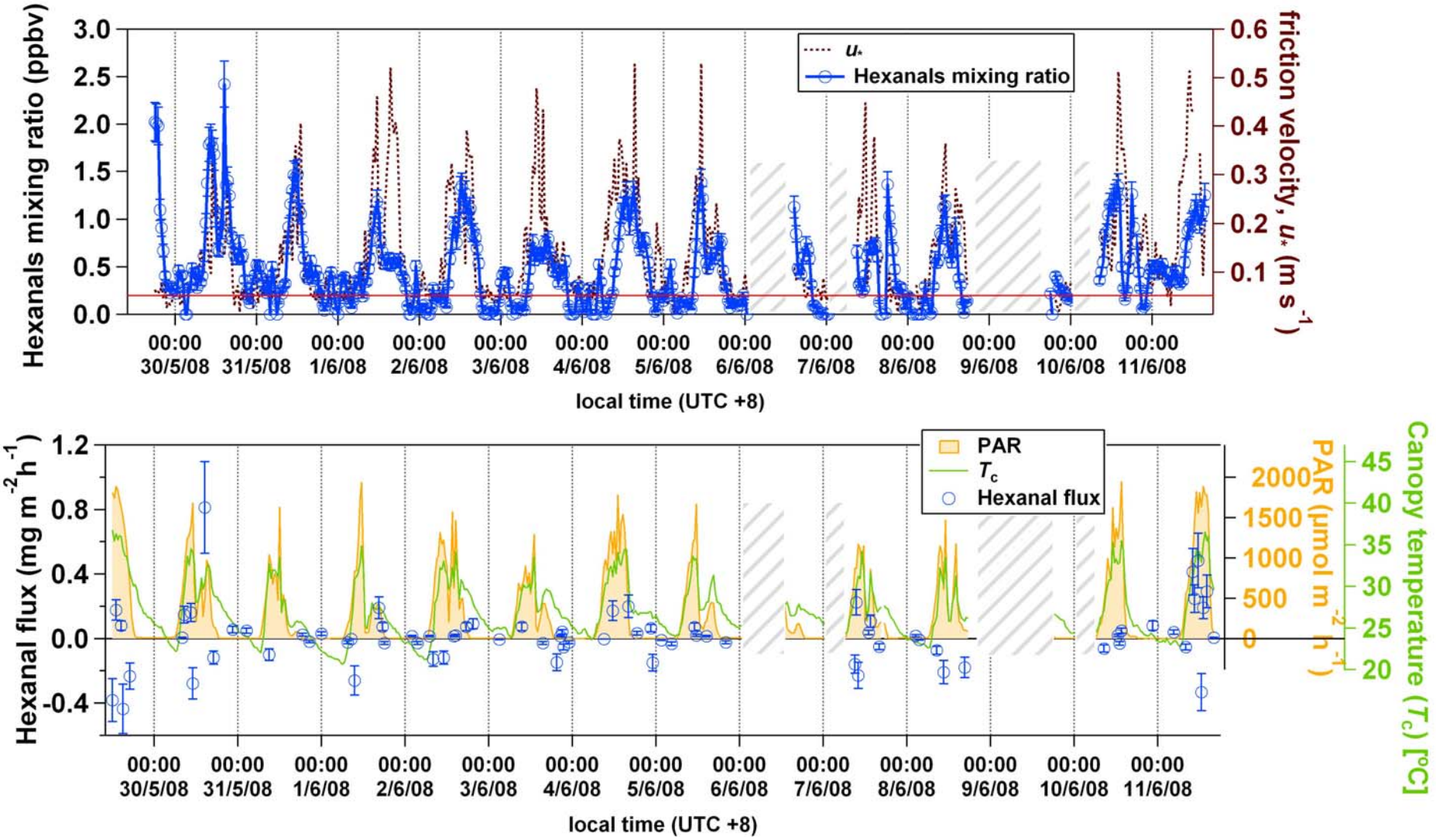

Figure 2.3-24 Hexanals (*m/z* 83) volume mixing ratios (top graph) in relation to u_*, and validated flux (bottom graph) in relation to T_c and PAR. Crosshatch zones correspond to power interruptions and a red line to the detection limit.

2.3.4.6.11 Sesquiterpenes (m/z^+ 205)

Sesquiterpene quantification is of great interest to atmospheric chemistry due to their high reactivity and large aerosol formation potentials, and because of limited data due to analytical challenges faced in their reliable measurement. Despite the inclusion of *m/z* 205 in the vDEC flux mode with the hope of capturing emission episodes, the proportion of VMR data points above the detection limit (LOD [graphical] = 0.2 ppbv) was relatively small (33%). Measurement of low mixing ratios of sesquiterpenes is difficult because of humidity effects, detection limits, and decreasing sensitivity at the higher end of the *m/z* spectrum (Kim et al., 2009). Using the statistical method (Sect. 2.3.4.2) an average value for the mixing ratios was estimated at 0.13 ppbv which is approximately 3 times less than the value for monoterpenes and 33 times less than the value for isoprene. Small emission of sesquiterpenes from fronds was also detected in the leaf cuvettes (Owen et al., 2010). Due to flux quality assessment criteria the number of flux rejections was too high to include the fluxes in this work with just a few validated points for emission (e.g., 0.154 mg m^{-2} h^{-1} on 30/05/2008 15:00 LT, 0.111 mg m^{-2} h^{-1} on 02/06/2010 10:00 LT; 0.159 mg m^{-2} h^{-1} on 4/06/2010 16:00; 0.124 mg m^{-2} h^{-1} on 07/06/2010 9:30, and 0.096 mg m^{-1} h^{-1} on 08/06/2010 11:00) and deposition (e.g. -0.098 mg m^{-2} h^{-1} on 01/06/2010 17:30). If the criteria were lowered to permit the fluxes of the lower quality (rank 4 – rank 6) the resulting flux would be a small emission (0.007 mg m^{-1} h^{-1}). Although these data suggest that sesquiterpenes could be definitely present and that their relative proportion was likely to be small it is not possible to give a more precise flux estimate. The uncertainty bandwidth for sesquiterpenes in relation to mixing ratios was ±150% related to the uncertainty in the reaction rate constant and transmission plus estimated at ±50% due to sensitivity variation as a function of relative humidity (Kim et al., 2009).

2.3.4.7 Carbon loss

Despite the fact that the total reported concentrations and fluxes of the total VOCs exceed many times those encountered at the rainforest (Langford et al., 2010), oil

palms appear to be a much higher CO_2 sink than the rainforest.. The net photosynthetic carbon loss (Figure 2.3-25) integrated over a day amounted to 0.8% due to the total VOC emission. This was derived by dividing the total VOC flux of 128 mg C m^{-2} d^{-1} by the total CO_2 downward flux of 17100 mg C m^{-2} d^{-1}. The value of 0.8% is double that found for the SE Asian rainforest (Langford et al., 2010) but still lower than the values reported for the Amazon rainforest (Karl et al., 2004; Kuhn et al., 2007). Although this value may seem relatively small, the implications of this portion of the carbon for atmospheric chemistry are huge due to its reactivity, aerosol formation potential, and influence on the oxidative capacity of the atmosphere.

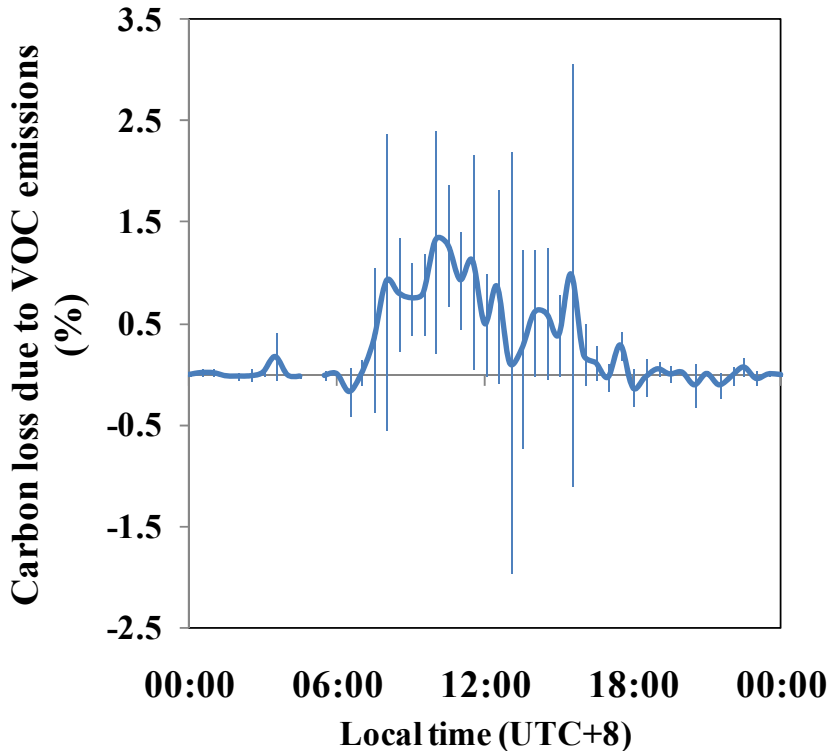

Figure 2.3-25 Net canopy carbon loss due to BVOC emissions at oil palm.

The data, which were used to derive the diurnal trend in the carbon loss, are presented separately in Figure 2.3-26. It is interesting that the peak associated with regular noon rain episodes which is reflected in both the total VOC flux and the CO_2 flux data occurred slightly later in the previous graph (Figure 2.3-25). This could be due to the fact that the ratio was obtained for each half hour and the variability in this

ratio was very high in the afternoon as seen from the standard deviations of the individual fluxes in Figure 2.3-26.

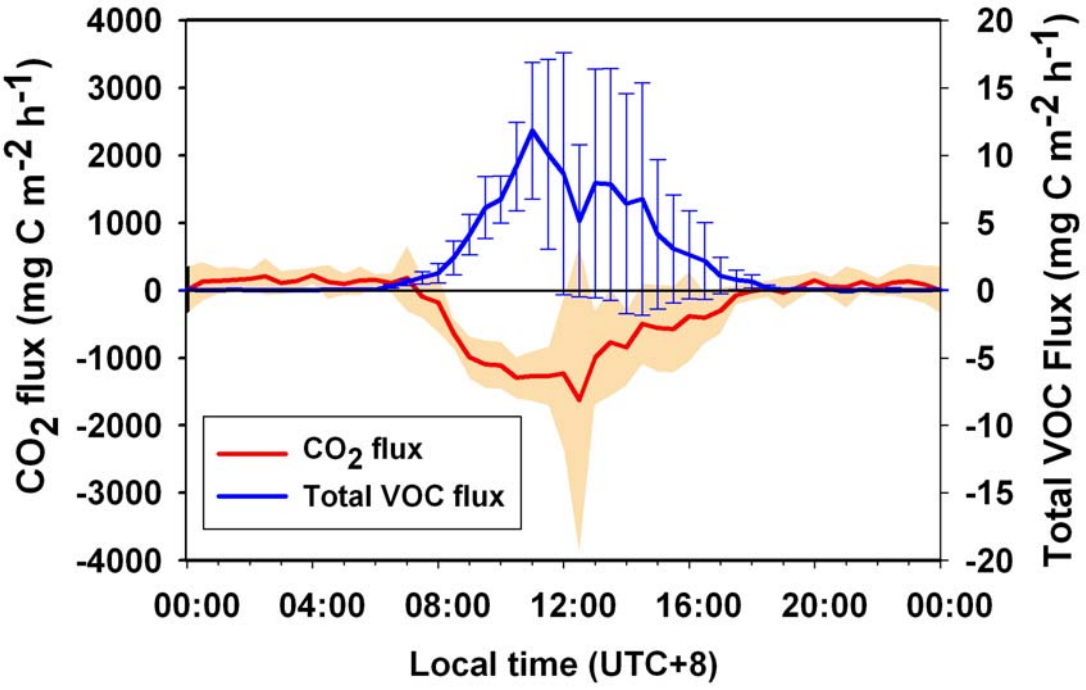

Figure 2.3-26 Diurnal trend of total VOC flux in comparison with CO_2 flux. The data for CO_2 flux are courtesy of Mhairi Coyle (CEH). The data sets correspond to the same 2 week period.

2.3.4.8 Use and parameterisations of flux algorithms

2.3.4.8.1 Isoprene emission (empirical G06)

The program used to fit ten empirical variables in the G06 algorithm was performed using the solver feature of Microsoft Excel software, which employs the Newton-Raphson iteration method. This method could change the parameters freely until the best possible fit of the algorithm and the measured canopy flux data was obtained. It is shown in Table 2.3-5, that the parameterisation can change some of the parameter values remarkably while not altering others. Also a sign of a parameter may be reversed. These changes lead to improvement in the overall fits with the measurement data even when the ambient temperature $T_a(z)$ is used, which can be up

to two degrees lower than the actual leaf temperature and therefore cause estimation of a smaller BER from the measurement. The C_{T1} and C_{T2} temperature response parameters and the maximal isoprene synthase temperature (T_b) have been previously measured in the lab by Wilkinson (2005). Comparison between the original G06 model using T_a(15 m), 3 meters above the canopy, and the measurement is presented in Figure 2.3-27a, and the analogous comparison but using the canopy temperature (T_c) in the G06 model in Figure 2.3-27b. Clearly the use of canopy temperature improves the fit. Which temperature is used impacts on the absolute value of BER that is required to achieve a 1:1 slope of the fit. It is therefore obvious that modellers who use leaf-level estimates of BERs may not use the available ambient temperature (e.g. from a weather station) without a conversion to the canopy temperature (see Sect. 2.3.3.5). There is currently no BER value for oil palm plant functional type (PFT) present in the MEGAN model (Guenther et al., 2006) and the value for crops is just 1 mg m^{-2} h^{-1}, so 8 times smaller than the BER value required to make the slope of the original G06 (T_c) and oil palm canopy scale measurement equal to 1. However, even despite the fact that the BER value of 8 mg m^{-2} h^{-1} would be sufficient for the model to achieve a quantitative agreement in the average flux, this value would not be a true BER because the original algorithm does not deal with species which are under strong circadian control of emissions (i.e. which have a diurnal pattern in BERs) and thus the response function parameters need adjustment. The measured leaf-level values of BER (at 1000 µmol m^{-2} s^{-1} PAR and 30 ºC) are much higher, e.g. 14.5 mg m^{-2} h^{-1} in 2003 (Wilkinson et al., 2006) or 19.25 mg m^{-2} h^{-1} (Owen et al., 2010). However, the leaf level BER can be variable depending on the time of a day it is taken despite setting PAR and temperature to the constant values. The parameterisation on the measured canopy flux using a constant basal emission rate (BER) and T_a(15 m) improves significantly the linear fit of the G06 (r^2 = 0.91). Replacing T_a(15 m) for T_c in the parameterised model increases the coefficient of determination to 0.93 (Figure 2.3-27c). The corresponding time series are presented in Figure 2.3-28 and are almost identical. The modelled timeseries are used afterwards to gap-fill the data used in providing the global estimates (Sect. 2.3.5.1).

Table 2.3-5 Empirical parameters from G06 for isoprene.

G06 parameters	G06 original (T_c)	Oil palm optimised $T_a(z_m)$	Oil palm optimised (T_c)
C_{T1}	95	130	174
C_{T2}	230	235	2750
b_1	0.004	-0.00005	0.0007
b_2	0.0005	-0.00003	0.00002
b_3	0.0468	0.0977	0.116
b_4	0.6	3.7	0.58
b_5	2.034	2.608	3.790
b_6	0.05	0.042	-0.01
T_a	313	313	317
P_0	200 (sun leaves) 50 (shaded leaves)	204	200
BER (mg m^{-2} hr^{-1})	12.8*	18.8	22.8
R^2 vs measured	0.75	0.91	0.93

*derived from mean mid-day flux value (11:00 LT) over 12 days.

derived from M. Wilkinson's thesis (Wilkinson, 2005)

An important feature of oil palms is that they exhibit a circadian rhythm for isoprene emission (Wilkinson et al., 2006) which is expected to influence the modelling of emissions from this ecosystem type (Hewitt et al., 2009b). The comparison of the original and the parameterised G06 model outputs for oil palms has a quadratic relationship (Figure 2.3-27d), which can be due to the parameterisation

compensating for the circadian character of the oil palm emissions despite a constant BER used in these algorithms. For the adjusted BER to 1:1 slope with measurement the original G06 has a tendency to overestimate the small flux region (morning, afternoon) while underestimating the high fluxes (noon). As a result of the circadian rhythm of isoprene emission, the daily peaks of the measured isoprene flux and the parameterised G06 are narrower than that of the original G06.. This comparison is presented in Figure 2.3-29 where an 11:00LT mean BER is used in the original G06.

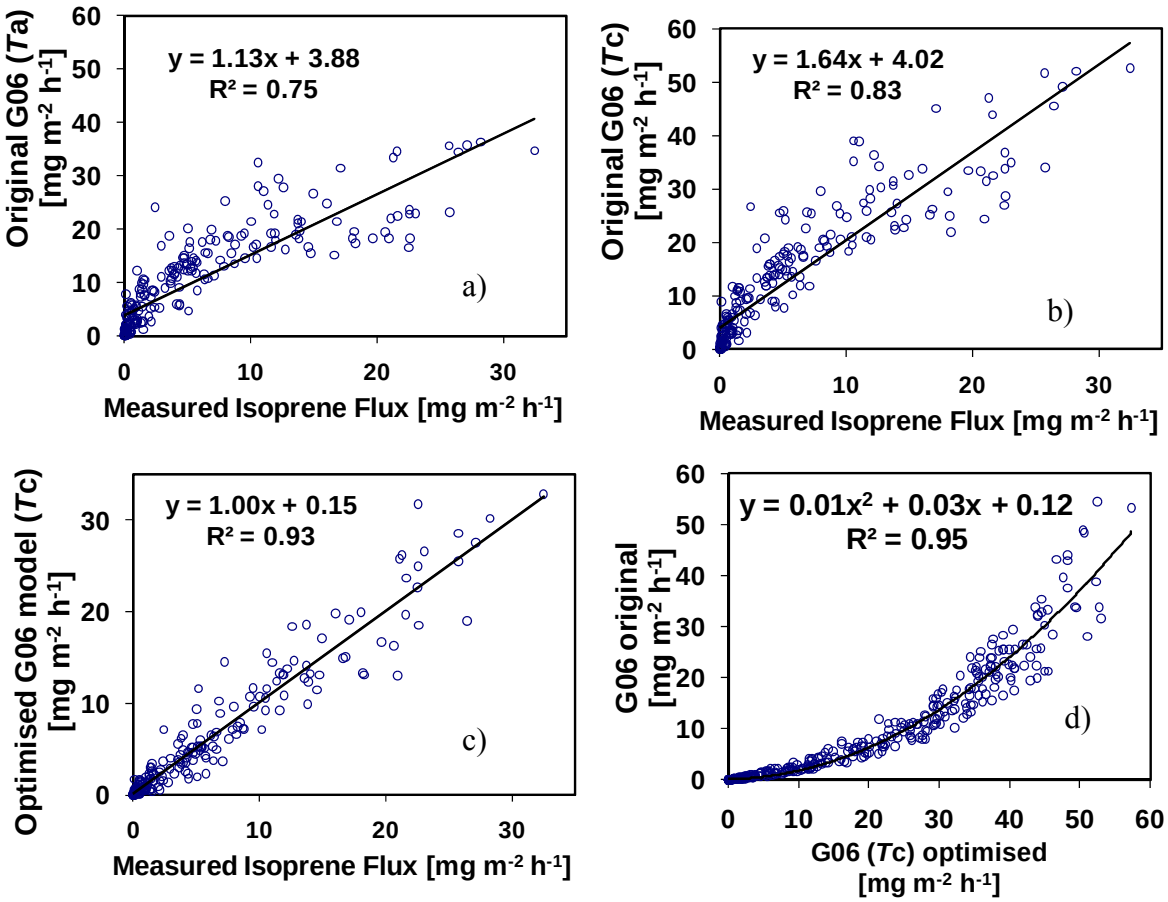

Figure 2.3-27 Comparison of measured fluxes with the original G06 using ambient temperature at a constant BER of 12.8 mg m^{-2} h^{-1} (a), with the original G06 using canopy temperature at a constant BER of 12.8 mg m^{-2} h^{-1} (b), and the parameterised G06 optimised for oil palm plantation using canopy temperature at a constant BER of 22.8 mg m^{-2} h^{-1} (c). The relationship between original and optimised G06 model is shown in (d).

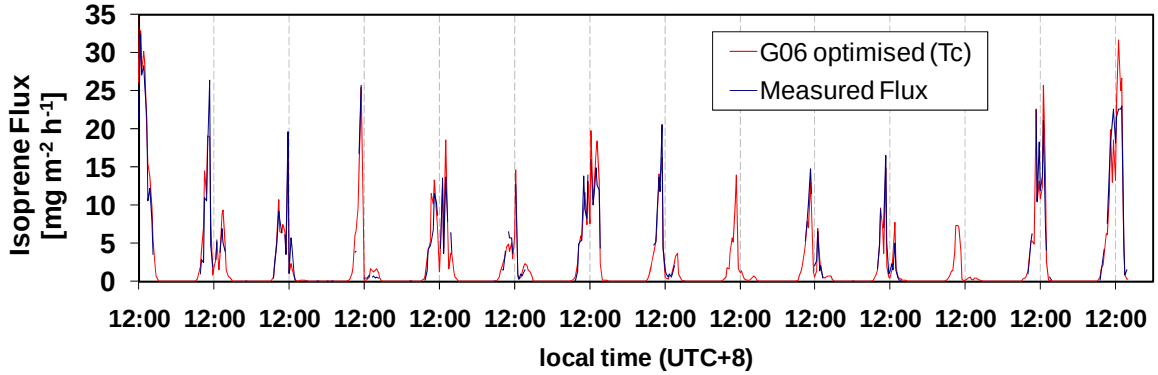

Figure 2.3-28 The timeseries of measured isoprene fluxes and the parameterised G06 algorithm.

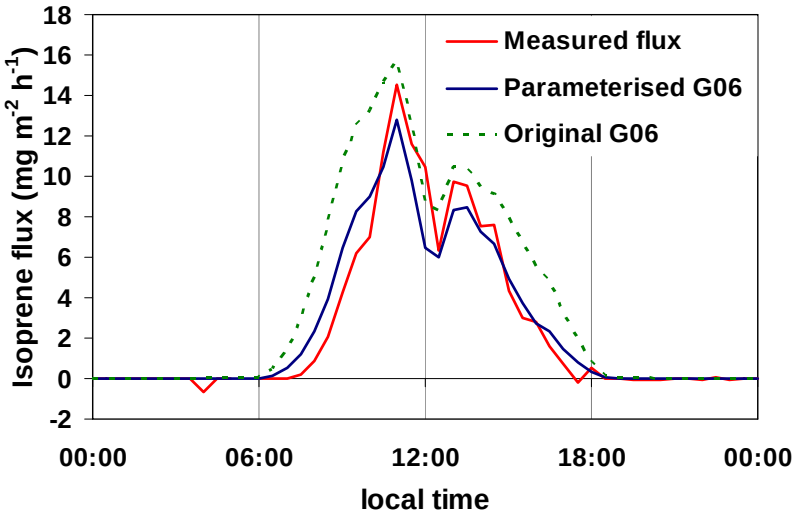

Figure 2.3-29 Comparison of the daily patterns of measured flux, and fluxes from the original and the parameterised G06 algorithm.

The best agreement can be achieved by using a dynamic BER for oil palm emissions (Sect. 2.3.4.9), when the goodness of fit between measured and modelled fluxes increases even further (i.e., from r^2 of 0.93 to 0.95). By introducing hourly BERs (Wilkinson et al., 2006) the daily peak can be made slightly narrower, closer to measured values. However, as demonstrated earlier, the agreement for the parameterised algorithm with a fixed BER was already very good since the circadian effect could be embedded in the parameterisation. The consistency of BER definition

may seem enigmatic in the modelling practice, as it could be just a value from a leaf-level measurement under the normalised PAR (1000 μmol m^{-2} h^{-1}) and temperature (30 ºC) conditions, a range of those values, or an average of the values (Niinemets et al., 2010a; Niinemets et al., 2010b; Guenther, 2010; Niinemets, 2010).

There is also a question whether those normalised values for PAR and temperature are optimal for all the plants, since there might be a saturation in some of them or a too high value leading to a stress for a plant (Possell et al., 2010). Apart from that, when considering the circadian rhythm in BERs there may be a problem with which BER value is best to use, what time of day is the most appropriate, or whether an average of measurements spanned over a day would be better. For the circadian species, taking the noon BER would probably lead to significant overestimations while taking a morning or an afternoon BER would underestimate the fluxes. Another possibility could be parameterisation of the algorithm for the use of the average BER from a day (10:00 - 14:00 LT).

Finally, the parameterisation for oil palm reveals several significant differences from that for the rainforest reported by Langford et al. (2010), where most of the parameters did not change as a result of the parameterisation, which suggests that only the BERs required updating for the MEGAN model. The fit of the model to measurement was much better at the oil palm plantation than at the rainforest mainly because of the lower sensor height, higher concentrations, minimal dilution effect, and a higher sensitivity of the PTR-MS for isoprene at the oil palm site. However, estimating the canopy temperature at the rainforest from the ambient temperature at 75 m and the heat fluxes improved the agreement significantly, although factors such as advection, transport delays, chemical reactions, etc. could be more pronounced than over the oil palms.

One of the conclusions could be that the original G06 cannot be used for oil palm without parameterisation or appropriately collected hourly BERs or at least updating the BER used in MEGAN for oil palms with an adjusted BER of 8 mg m^{-2} h^{-1}. For precise modelling, a combination of an appropriate diurnal function of BERs (Sect.

2.3.4.9) and optimised empirical parameters in G06 is essential for simulating correct oil palm isoprene emission with MEGAN.

2.3.4.8.2 Isoprene emission (process based models (N99, A07)

Despite an excellent agreement of a semi-empirical algorithm such as G06 after parameterisation for the oil palm isoprene emission, process-based emission modelling may become more important if one would like to investigate the influences of the past or future climates at significantly different CO_2 levels (Possell et al., 2005), assuming that the potential future increase in CO_2 will not be compensated by a related increase in the CO_2 sinks such as the soil respiration rate (Heath et al., 2005). Briefly, in the Niinemets et al. (1999) model (N99) isoprene production is primarily dependent on dimethylallyl pyrophosphate (DMAPP) and isoprene synthase activity. The model assumes that there is only a certain fraction of electrons available to reduce CO_2 to isoprene and that metabolic pathway strength is proportional to the total isoprene synthase activity in leaves. The model of Arneth et al. (2007) (A07) is an extension of the N99 model, which takes into account the CO_2 concentrations, which may impact on the induction of the inhibition of the emissions, through accounting for the limitation of a substrate for isoprene synthesis. The intercomparison between the models and measurements is shown on a diurnal graph (Figure 2.3-30).

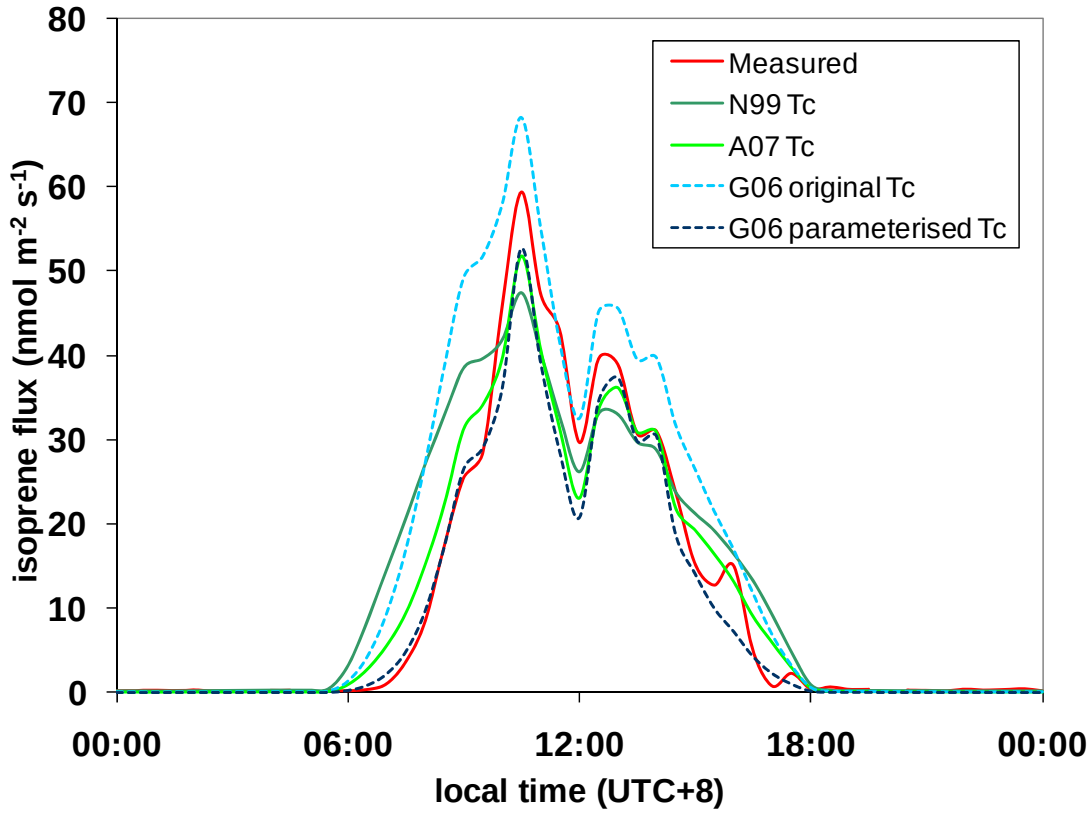

Figure 2.3-30 Diurnal profile of the measured flux in comparison with different models.

By using the parameterised G06 model for oil palm it is possible to achieve the best fit to the measurement. The process-based A07 model has almost an identical course as the parameterised G06 model but there is a small overestimation in the morning (6:00 to 10:00 LT) and in the afternoon (14:00 to 18:00) which might be because the process-based model is a leaf-level model in comparison and G06 is the canopy model. However, the process-based models seem the right ones to use at leaf-level scale, since the photosynthesis is directly linked to the circadian effect. The old N99 model has a significantly worse performance especially in the morning and afternoon. As explained above, the original G06 does not account for the circadian rhythm and therefore it is unable to fit the measurements very well.

2.3.4.8.3 MVK/MACR deposition

As was shown earlier in Figure 2.3-16 the $V_d(z_m)$ of MVK and MACR was often close in value to V_{max}, the maximum adsorption capacity of leaf surfaces. However, the deposition rates were not always close to V_{max} so it would be interesting to find out whether leaves could actually take up MVK or MACR for returning back a portion of the lost carbon. Some VOCs such as acetaldehyde are known to be taken up by stomata (Rottenberger et al., 2004), although they can also adsorb to cuticular waxes. The deposition fluxes were parameterised similarly to Nemitz et al. (2009a) (N09) except that instead of taking the average value of V_d, the fitting of a diurnal function to the available R_c timeseries was made, and the modelling of flux timeseries relied on the available measured mixing ratio data ($\chi(z_m)$) and V_d derived as in Equation 2.3-6.

Equation 2.3-8

$$F_{MVK+MACR} = -\frac{\chi(z_m)}{R_a(z-d)+R_b+R_c}$$

The fluxes modelled in this way were used for gap-filling and the resulting timeseries combining measured and modelled fluxes are presented in Figure 2.3-31.

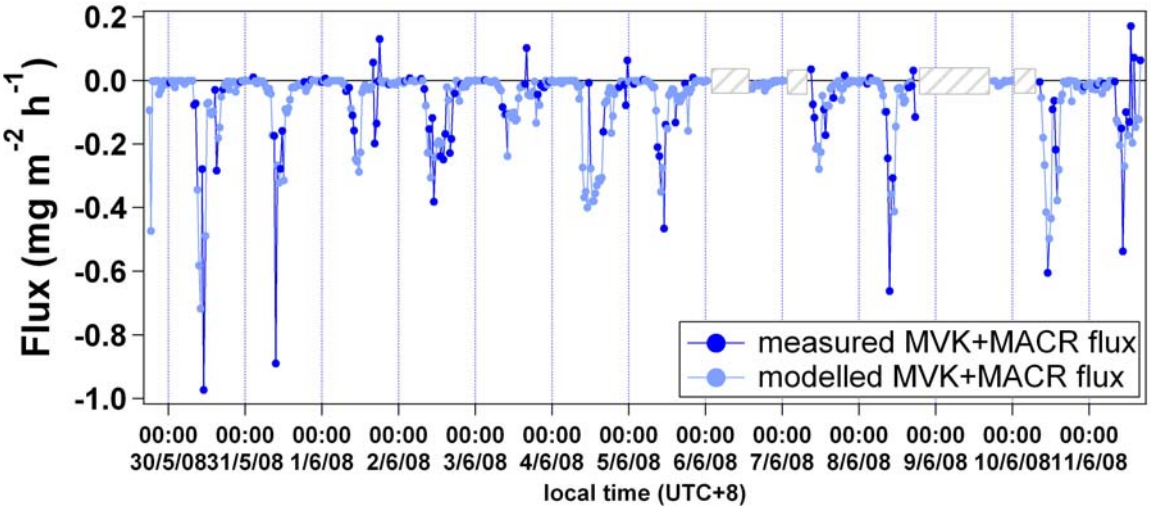

Figure 2.3-31 Measured MVK+MACR flux gapfilled by modelled flux (resistance analogy, N09)

2.3.4.8.4 Parameterisations for other VOCs

The success of the model depends, among other things, on the dependence of emissions on environmental driving variables. For the temperature and PAR-dependent emission G06 seems to be an ideal model, which is relatively easy to parameterise. The individual parameters in that model may have a biological meaning, since many of them were derived in leaf-level measurement. Here, the parameterisation is applied freely with a goal to investigate how well the model can be made simulate the measurement and the application for gap-filling of the fluxes to achieve a higher representativeness of the reported fluxes. If the driving parameters are not associated with light and temperature responses then parameterisation would not succeed in producing a good fit. Therefore only isoprene, estragole and toluene were found to be strongly temperature dependent, although the last two had a delayed response with temperature and PAR, most probably because the floral biochemistry and release are different from those of the leaves but also because of the longer atmospheric lifetimes compared with isoprene. It is also possible that toluene emissions might be mainly temperature dependent, but the relationship with temperature was not exponential as is typically the case for isoprene and monoterpene emissions. In Table 2.3-6 are listed the default parameters of G06 in comparison with the optimised parameters for each of the 3 emitting VOCs. Surprisingly the C_{T1} and C_{T2} for toluene did not change in the parameterisation compared to the original parameters in MEGAN for isoprene. The b_1 and b_2 components of the activity factor associated with PAR response decreased by orders of magnitude to very small values but b_3 increased by a few factors. The empirical components of temperature-related activity factors rose relatively weakly, 2.5 times in b_4, and by a tiny fraction in b_5 and b_6. The maximal enzyme temperature decreased by 1 degree. The modelled data were used for gap-filling, as shown in Figure 2.3-32.

Table 2.3-6 Comparison of G06 optimised parameters for isoprene, estragole, and toluene. Canopy temperature was used in all cases. Values for estragole were taken from Misztal et al. (2010c).

G06 parameters	G06 original	Oil palm optimised	Oil palm optimised	Oil palm optimised
compound	isoprene	isoprene	estragole	toluene
C_{T1}	95	174	131	95
C_{T2}	230	2750	542	230
b_1	0.004	0.0007	0.031	0.0002
b_2	0.0005	0.00002	0.0030	$-6 \cdot 10^{-6}$
b_3	0.0468	0.116	0.0453	0.174
b_4	0.6	0.58	-0.32	1.5
b_5	2.034	3.790	1.812	2.161
b_6	0.05	-0.01	-0.21	0.06
T_b	313 K	317 K	307 K	312 K
P_0	200 (sun leaves) 50 (shaded leaves)	200	200	200
BER (mg m^{-2} hr^{-1})	7.8	22.8	0.80	0.53
R^2 vs measured	0.75	0.93	0.64	0.71

*derived from 1:1 slope of the fit with the measurement. derived from M. Wilkinson's thesis (Wilkinson, 2005)

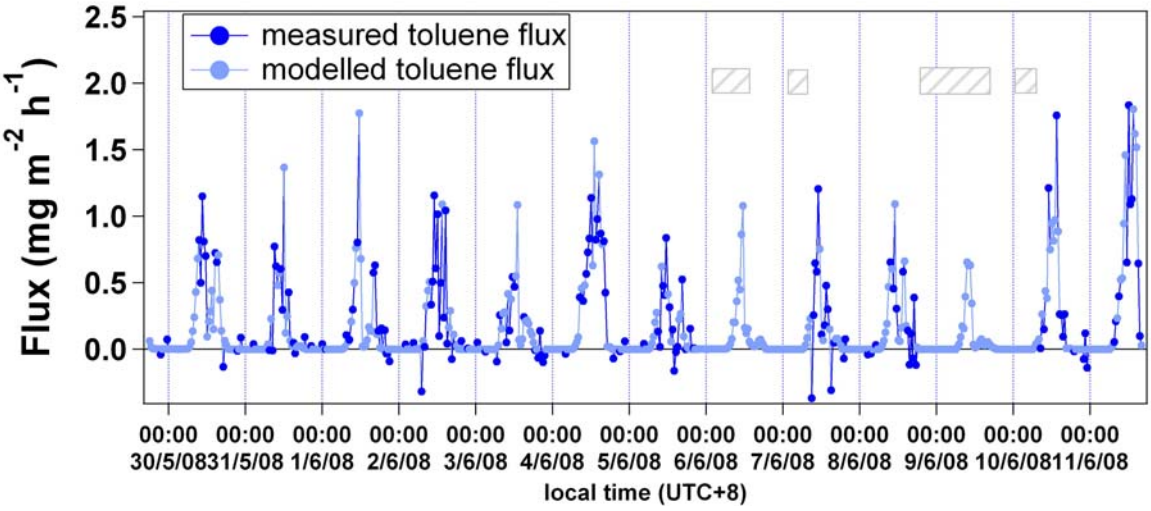

Figure 2.3-32 Toluene flux timeseries gap-filled with modified G06 for oil palm toluene.

2.3.4.9 Circadian control of isoprene emissions

Some of the data in this chapter contributed to a paper in preparation led by N. Hewitt (Nature, under review)

As demonstrated earlier, the optimisation of G06 parameters could provide a good fit to the measured data and thus optimise the algorithm for the response compensate to the circadian rhythm. Since MEGAN is the global model the optimal situation would be to leave the parameters as they are in the original model but adjust only the BER value for oil palm (currently 1 mg m^{-2} h^{-1} for crops) so that the average of an output value is the same as the average of the measurement. This could be achieved by using as the BER for isoprene the 7.8 mg m^{-2} h^{-1} value (reduced compared to the measurement). However, for precise modelling, especially of oil palm isoprene emissions, whose BERs are strongly circadian, it is necessary to update also the G06 parameters because of the following reasons: firstly, the enzyme optimal temperatures are different for oil palms than for other species; secondly, the temperature and PAR responses obtained from leaf-level studies are different than for the non-circadian species (Wilkinson, 2005; Wilkinson et al., 2006); and thirdly, it is not possible to match the diurnal profile of the flux by only adjusting a constant

BER. Another solution could be the use of variable BERs, which can be obtained by dividing the measured canopy flux by the activity factor in the original G06. Figure 2.3-33a shows that the variable BERs collected that way were similar in pattern to BERs obtained in leaf-level measurements by Wilkinson et al. (2006), although in the former case the absolute BER values derived were smaller, which was an analogous situation to a constant BER, also reduced, obtained from the fit with G06. Consequently, the use of variable BERs does not totally relax the need for the parameterisation, mostly because of the different optimal enzyme temperatures and responses of oil palm with regard to other species. A perfect agreement both in patterns and absolute values can only be achieved if variable BERs are used, for example, as a function (Figure 2.3-33b) fitted to the average diurnal data of measured canopy BERs. The best function to describe canopy BERs at the oil palm was the 6th order polynomial, which was applied instead of constant BER in the G06 model. In order for both the pattern and the absolute values to agree well with leaf level measurements (Owen et al., 2010) the variable BERs would require the division of canopy flux by the parameterised G06 activity factor. The comparison of the diurnal flux outputs of the G06 model with the variable BERs and the constant BER with the measured flux is shown in Figure 2.3-34a.

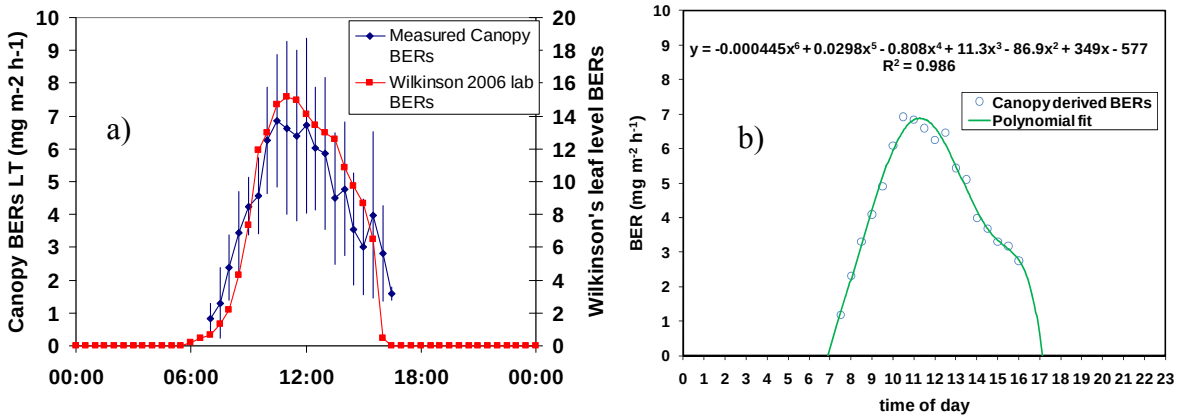

Figure 2.3-33 a) Comparison of BERs derived from canopy measurement in blue (this work) in comparison with BERs obtained at leaf level in the lab (Wilkinson et al., 2006); b) Polynomial fitting of the canopy BERs for use in the variable-BER G06 algorithm.

Previously the author suggested that an appropriately scaled (reduced) constant BER in the original G06 could minimise the discrepancy in terms of daily mean (overestimating morning and afternoon; underestimating middle of a day). This claim could be justified by scaling the BER using the direct canopy flux. However, leaf-level BERs are commonly measured during the middle of a day, and should they be introduced as such to the G06 model the discrepancy in the overall flux could be up to a factor of ten in the morning and a factor of 2 in the evening (Figure 2.3-34b).

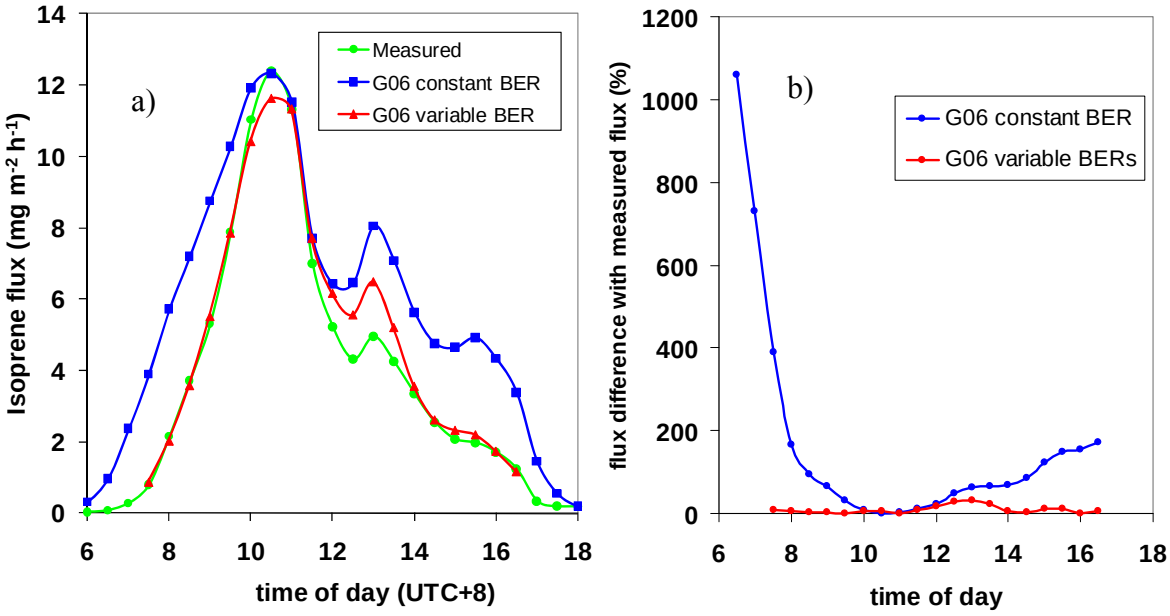

Figure 2.3-34 (a) Comparison of the G06 models depending on the type of BER used (constant or variable), and the measurement; (b) the percentage difference between these models flux outputs.

There may be other circadian species aside from oil palm where variable BER would be applicable. Another issue could be with seasonality in BERs (Barkley et al., 2009), and therefore more atmospheric eddy covariance BER measurements are required.

2.3.5 Discussion

2.3.5.1 Estimation of regional and global emissions from oil palm plantations

According to the latest estimates, in 2008 oil palm plantation area extended globally over 14.586 MHa (FAO, 2010) with 5.000 MHa in Indonesia and 3.900 MHa in Malaysia, which corresponded to approximately a 5% global increase with reference to the values for the previous year 2007 (FAO, 2009). Therefore, a global flux could be estimated simply by taking the representative average over the entire period (incl. night times and gap filling) and converting to an annual flux per hectare. Such a simplified approach assumes no seasonality, which is, to first approximation, true for the oil palm which yields fruits all year round, although there might be mild season-related differences. Another assumption which must be made is that the palm tree density at the measurement location is representative for other plantations, since the average global density of oil palms is not known.

For the compounds which can be well modelled using the approaches presented earlier (2.3.3.5) the flux integration period could be extended for a 2 week longer period when temperature and PAR had been recorded before the PTR-MS measurements started. This may increase the representativeness, since the temperatures were higher in the preceding period. As an example an extended time series of isoprene flux is shown in Figure 2.3-35. The inclusion of the additional modelled series for isoprene flux increases the mean isoprene flux value from 2.121 mg m^{-2} h^{-1} (N = 633) to 3.962 mg m^{-2} h^{-1} (N = 1251). This almost doubling is due to the emissions being very sensitive to the temperature (exponential dependence). An analogous increase was noted for toluene flux from 0.186 mg m^{-2} h^{-1} (N = 633) to 0.328 mg m^{-2} h^{-1} (N = 1251), but less so for estragole, i.e. from 0.398 (N = 633) to 0.452 mg m^{-2} h^{-1} (N = 1251) because of the weaker responses of estragole emissions to temperature and PAR. The summary of the global estimates of net BVOC emissions from oil palms is shown in Table 2.3-7.

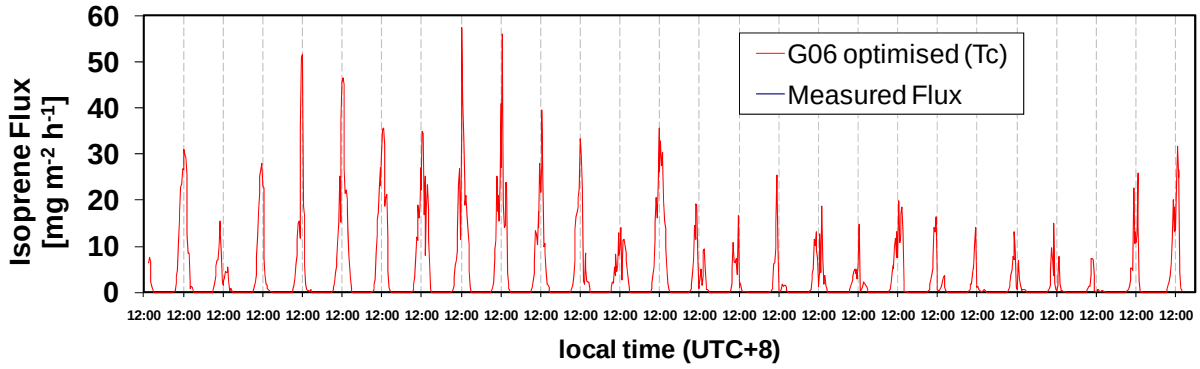

Figure 2.3-35 Extended time series for isoprene flux. The temperatures in the period preceding the measurements were higher which had a strong effect on the higher flux due to an exponential increase.

Table 2.3-7 Global and regional estimates of BVOC oil palm emissions (Gg a^{-1}). Isoprene, estragole and toluene timeseries were gapfilled and extended through modelling.

	Methanol	Acetal-dehyde	Acetone	Isoprene	MVK+ MACR	MT	Hexanals	Toluene	Estragole
Global		12.8	15.3	5070			15.3	419	578
Malaysia		3.42	4.10	1400			4.10	112	155
Indonesia	sink	4.38	5.26	1700	sink	sink	5.26	144	198

Even despite such high isoprene emissions from oil palm, this type of ecosystem delivers only 5 Tg annually, which is approximately 1% of estimated global isoprene emissions from vegetation. However, the regional impact is expected to be very high for the Malaysia and Indonesia region where most global oil palm plantations are concentrated. The sum of global estragole and toluene emissions is approximately 1 Tg which might be important contribution to aerosol chemistry (Sect. 2.3.5.2). Other compounds, due to their low flux or deposition, do not seem to have a high global contribution from this ecosystem but the finding of deposition for isoprene products and for species with high Henry's law constants are important since yields of these species obtained from chambers may be effectively overestimated if the deposition is not considered.

2.3.5.2 BVOC effects on BSOA – land-use change implications

It is well established that BVOCs are large contributors to organic aerosols although the exact mechanisms of gas/aerosol chemistry and partitioning are not entirely explored (e.g. Camredon et al., 2007). The majority of studies have been conducted in photooxidation chambers (e.g. Barley and McFiggans, 2010; Fuentes et al., 2010; McFiggans et al., 2006; Meyer et al., 2009; Alfarra et al., 2006) which are very useful for defining the aerosol yields, properties and mechanisms. These studies, in combination with in situ measurements of the atmospheric aerosol composition and fluxes (e.g. Allan et al., 2003; Beddows et al., 2004; Coe et al., 2006; DeCarlo et al., 2008; Dall'Osto et al., 2004; Dall'Osto et al., 2006; Dorsey et al., 2002; Gallagher et al., 2002; Huffman et al., 2009; Nemitz et al., 2009b; Nemitz et al., 2008; Rollins et al., 2010; Zorn et al., 2008) and atmospheric measurements of their precursors (Davison et al., 2009; de Gouw, 2007; Goldstein et al., 2004; Grabmer et al., 2004; Karl, 2004; Karl and Guenther, 2004; Karl et al., 2004; Kim et al., 2010; Langford et al., 2009a; Langford et al., 2009b; Rinne et al., 2007b; Rizzo et al., 2010), can help in better understanding of atmospheric chemistry, physics, and the biosphere-climate interactions.

Large BVOC emissions from oil palm may have a high impact on BSOA formation. In Table 2.3-8 are listed SOA mass yields for the most dominant expected aerosol precursors which were used in Figure 2.3-36 to derive equivalent aerosol fluxes for the oil palm and rainforest. It seems that isoprene, due to its relatively small aerosol yield, is not as important as other compounds such as monoterpenes, estragole and toluene, although the significance of isoprene from oil palm may be considerable because of the very high emissions, although it is possible that these emissions may paradoxically lead to the inhibition of the aerosol formation due to OH scavenging (Kiendler-Scharr et al., 2009). Furthermore, the yield of isoprene takes into account its oxygenated products, which exhibited strong deposition at the site. Therefore the effect of isoprene on BSOA formation is quite uncertain but the parallel eddy covariance aerosol flux measurements at the site (Nemitz et al., 2010) show elevated

nitrate fraction coinciding in time with isoprene flux, which might be due to isoprene nitrate formation, which has recently been reported to have different isomeric forms with different lifetimes (Lockwood et al., 2010). On the other hand the most abundant organic fraction is shifted to later in the day, coinciding with floral estragole and probably also toluene. The total equivalent aerosol flux derived from VOC fluxes is in agreement to an order of magnitude with the total measured flux by the ToF-AMS. Perfect agreement would not be expected due to different reaction timescales within the measurement footprint. Therefore, this comparison cannot be used for making statements about the validity of the yields obtained in the chambers.

Table 2.3-8 Comparison of mass yields and mean values of fluxes at oil palm plantation and rainforest

Compound	SOA mass YIELD (%)	OIL PALM mid-day Flux (mg m^{-2} h^{-1})	RAINFOREST mid-day Flux (mg m^{-2} h^{-1})
Isoprene	2 (Lee et al., 2006b)	8.6	2.1
Monoterpenes	31-58 (Lee et al., 2006b)	deposition	0.31
Estragole	40 (Lee et al., 2006b)	0.5	ND
Toluene	30 (Ng et al., 2007)	1.2	0.0
MVK/MACR	15-18 (Ruppert and Heinz Becker, 2000)	deposition	0.0
Acetone	small	0.2	0.2

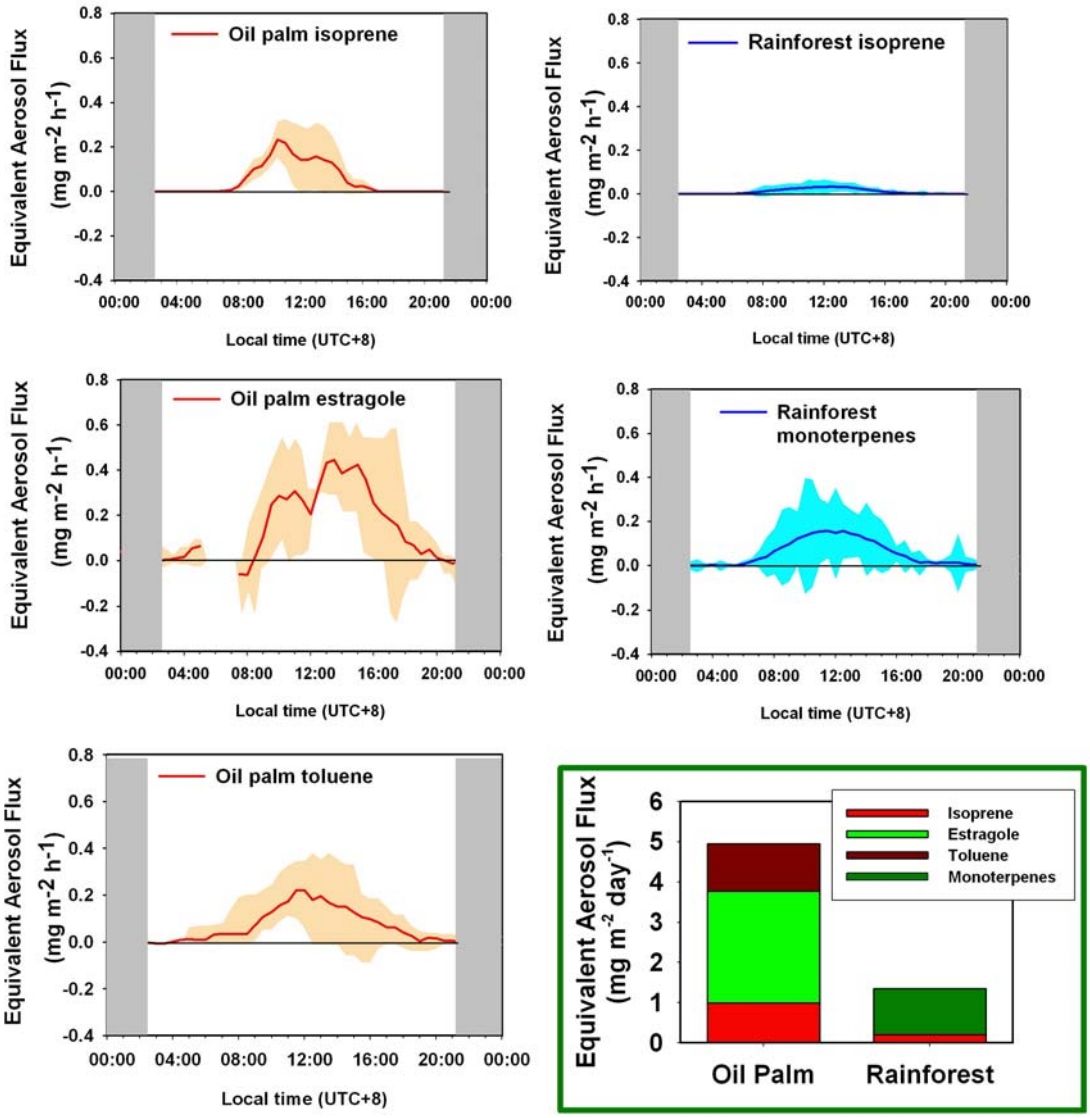

Figure 2.3-36 Comparison of equivalent aerosol fluxes from dominant VOCs at the oil palm plantation (left, red) and the nearby rainforest site (right, blue).

From the comparison of the two land uses it is clear that monoterpenes are the largest aerosol contributors at the rainforest whereas at the oil palm plantation monoterpenes were not primarily emitted but were net deposited. However, the absence of net monoterpene emission from oil palm is offset by the large estragole fluxes which have a similar SOA yield to monoterepenes. Considering only isoprene and estragole then clearly aerosol production from oil palm emissions exceeds that from rainforest emissions by approximately a factor of 2. Including the emissions of what has been identified most probably as toluene increases this domination of oil palms to SOA

formation to a factor of 3, as was shown in the bar chart of Figure 2.3-36. More comparisons are discussed in the next section (2.3.5.3).

2.3.5.3 Major differences with rainforest

The VOC concentrations and fluxes for rainforest can be found in Langford et al. (2010). The general difference was a different mix and total quantity of VOC over these types of ecosystem. The most striking difference was in isoprene fluxes and concentrations at the oil palm site which exceeded by 4 to 8 times the values at the rainforest. The other major feature of oil palms was a relatively high level of the floral pollinator attractant estragole which was not detected at the rainforest. On the other hand the fluxes of monoterpenes at the plantation were either very small or deposited, whereas they were very high at the rainforest with total monoterpene to isoprene ratio of 0.24 – 0.27 which is the second highest value reported so far from tropical regions. The impact of these main dissimilarities on aerosol formation was discussed in Sect. 2.3.5.2. A different ecosystem is likely to differ in various aspects such as biodiversity of plant and animal species. In this respect, oil palm is a very homogenous monoculture whereas rainforest is extremely diverse and heterogenic. Measurements were conducted at different heights at the two sites (i.e. 15 m at the plantation, and 75 m at the rainforest), which could have an influence on the mixing ratio values but the flux of non-divergent compounds was assumed to be independent of the height in this range. Therefore the comparison of the mass spectra relative fractions of the total ranges of VOC compositions at the two sites were compared in Figure 2.3-37. One can see that some compounds are dominant at one site while others can be more important at the other site, which can be better visualised in the bottom graph of this figure, where differences in the mixing ratios of the sites are divided by the sum of these mixing ratios, i.e. $(c_{m/zOP}-c_{m/zRF})/(c_{m/zOP}+c_{m/zRF})$. For example isoprene (*m/z* 69), MVK+MACR (*m/z* 71), HA (*m/z* 75), toluene (*m/z* 93), and estragole (*m/z* 149) are dominant at the oil palm, whereas acetic acid (*m/z* 61), monoterpenes (*m/z* 81, 137) and, possibly, methyl salicylate (MeSa) (*m/z* 153) are dominant at the rainforest. It has been reported that MeSa can be used as a stress tracer at an ecosystem scale (Karl et al., 2008).

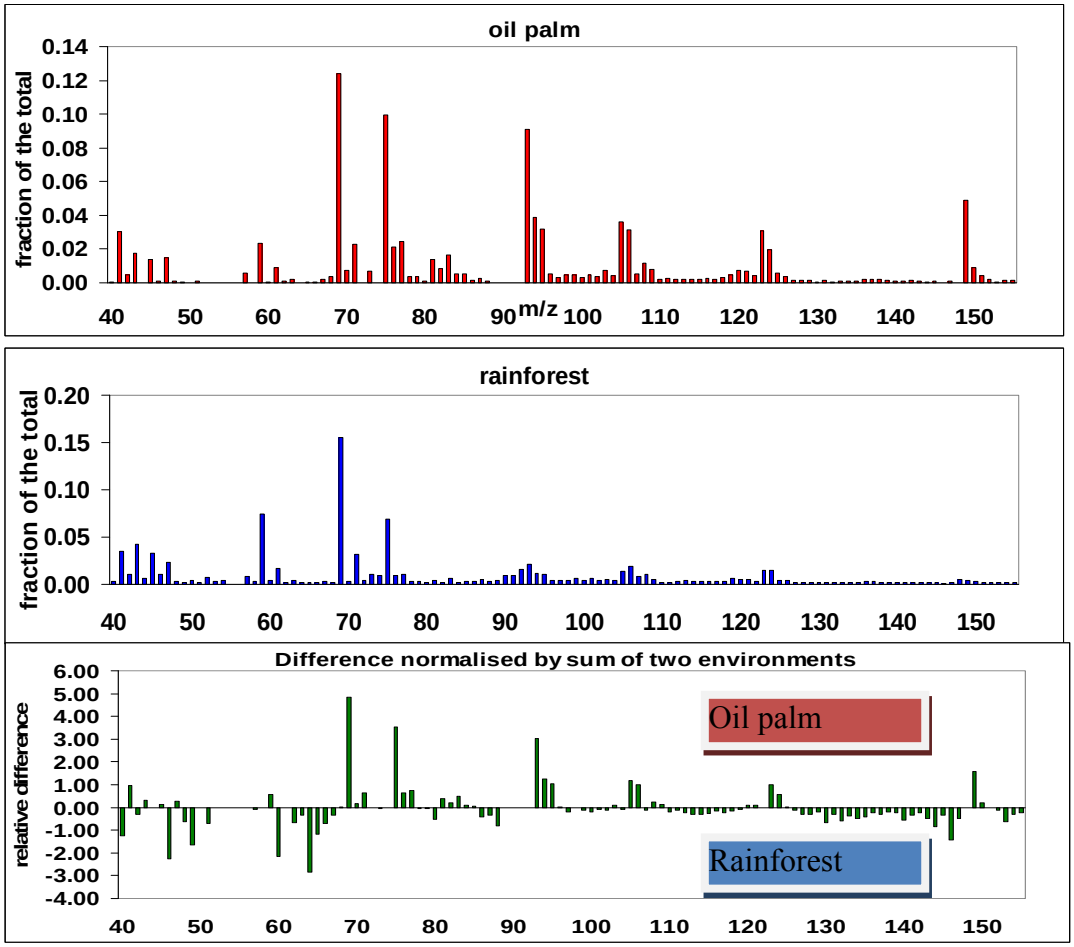

Figure 2.3-37 Qualitative comparison of VOC compositions at an oil palm and a rainforest

2.3.5.4 A future scenario

Predictions from global climate models (IPCC, 2007) are for an increase in mean global temperature in the 21st century in the range 1.1 ºC to 6.4 ºC. The uncertainties in these predictions are high and variable depending on the model and related to the estimates in greenhouse gas emissions. The El Niño-Southern Oscillation has an inter-annual variability which may have a strong influence on the temperature rise although there may be large regional variations. A hypothetical scenario presented here assumes an annual increase of 0.02 ºC in temperature, 0.5% rise in [CO_2], and a 5% increase in oil palm plantation area. Taking these into a simulation for the year 2058 (in 50 years time) an increase in temperature by 1 ºC, in [CO_2] by 25% and a

250% increase in the plantation area is projected with reference to the measurement period in 2008. Using the A07 model for such a scenario the increase of temperature of 1 ºC at unchanged [CO_2] would increase the emission of isoprene by approximately 20%. This increase would drop to 10% if the increase in [CO_2] by 25% was considered. However, these are minor increases compared with the effect of area expansion. Overall, for this 2058 scenario predicted global emissions of isoprene from oil palm plantations would rise from 5 Tg a^{-1} to 14 Tg a^{-1}, which is almost a 3-fold increase, and would correspond to 3% of current global isoprene emissions from vegetation. However, if biodiesel requirements rise dramatically due to exhaustion of fossil fuels the rate of oil palm plantation expansion may be much higher than the current 5% p.a.

2.3.5.5 Levels of uncertainty

Although much effort was expended on optimisation of the quality and precision of the measurements presented, uncertainty nevertheless remains. The main sources of uncertainty are likely to result from the relatively short measurement period of 12 days. As was shown using the temperature and PAR values recorded prior to the PTR-MS measurements, the emissions could be almost twice higher for isoprene. However, using the combination of measurement and optimised modelling approaches the data for the 3 weeks could be reconstructed, which should form a representative picture of the fluxes during the May/June period. The variations in temperature in different months should be considered although they are not significantly different since the climate in Sabah has only weak seasonality compared, for example, with the Amazon. The absolute humidity in Sabah was very high, which is not typically encountered elsewhere. This could have an effect on somewhat elevated detection limits for compounds such as methanol or acetaldehyde, although both the sensitivity and the detection limit were in the typical range for isoprene.

The errors from the derivation of mixing ratios were different for compounds present in the calibration standard, derived using a relative transmission approach and were assumed higher for large *m/*z (Sect. 2.3.3.3). The errors deriving from disjunct sampling and the number of masses in a cycle and dwell time used were typical for

other vDEC setups. Most of these and other significant errors were discussed in Sect. 2.3.3.4. The modelling approaches and parameterisations were performed with the main aim to use the optimised model for gap-filling. The fitted G06 coefficients should form a comparative basis with other studies, but the biological function of these parameters requires more lab studies on the circadian control.

2.3.6 Conclusions

These were the first direct canopy scale measurements of VOC mixing ratios and fluxes from an oil palm plantation.

In the varied VOC mix, isoprene constituted almost half of the mixing ratios during the mid-day (10:00 – 14:00 LT) with an average 13.1 ppbv. In the mid-day fluxes isoprene dominated 84% of the emitted compounds at 9.7 mg m^{-2} h^{-1}. The BER obtained from the fit of Guenther et al. (2006) activity factor and measurement was 7.8 mg m^{-2} h^{-1}, which is almost 8 times higher than the default value used in MEGAN for crops. However, the values of BER obtained in the leaf level measurements and from the parameterised G06 algorithm were much higher due to the circadian control of emissions from oil palm.
The oxidation products of isoprene MVK+MACR exhibited clear deposition with the maximal deposition velocities reaching 1.5 cm s^{-1}. This may have an effect on the atmospheric modelling since deposition of MVK and MACR is typically not observed in the photo-oxidation chambers.

Oil palm has not been found to be a clear monoterpene emitter, and although small amounts were detected, more precise studies are required to understand the mechanism of the small monoterpene emissions from oil palms. From the available data it appears that they might not be typically temperature and light dependent but might be of more stress related in reference to fronds and also could be floral or from outside of the footprint.
Floral emissions from oil palms can be the highest sources of BVOCs after isoprene from fronds since oil palm inflorescences contain thousands of flowers which emit

anise-like odour of estragole, whose canopy fluxes were the second highest during the mid-day at 0.81 mg m^{-2} h^{-1} although its emission maximum was shifted towards later in the day. Our findings suggest that probably the flowers may also be a source of toluene, which was emitted at a similar rate of 0.76 mg m^{-2} h^{-1} but had a quadratic relationship with temperature, which made it to be well described by a parameterised G06 algorithm. Toluene was earlier found emitted from vegetation but the emissions reported here are the highest biogenic source of toluene.

Both estragole and toluene have a high BSOA formation potential. Their sum of equivalent aerosol fluxes including isoprene was estimated at approximately 1 mg of SOA m^{-2} h^{-1}. This is approximately 3 times higher potential than that at the rainforest.

The expansion of oil palm areas may lead to tripling of these VOC emissions globally in the next 50 years. The findings suggest that much higher emissions of VOCs from oil palms than from a rainforest may have implications for land-use change, regional chemistry and in the long term also globally. More studies over this ecosystem are required to measure the impact of these emissions on oxidative capacity of the atmosphere, peroxyradical mediated OH recycling and other climatological impacts.

2.3.7 References

Alfarra, M. R., Paulsen, D., Gysel, M., Garforth, A. A., Dommen, J., Prevot, A. S. H., Worsnop, D. R., Baltensperger, U., and Coe, H.: A mass spectrometric study of secondary organic aerosols formed from the photooxidation of anthropogenic and biogenic precursors in a reaction chamber, Atmospheric Chemistry and Physics, 6, 5279-5293, 2006.

Allan, J. D., Alfarra, M. R., Bower, K. N., Williams, P. I., Gallagher, M. W., Jimenez, J. L., McDonald, A. G., Nemitz, E., Canagaratna, M. R., Jayne, J. T., Coe, H., and Worsnop, D. R.: Quantitative sampling using an Aerodyne aerosol mass spectrometer: 2. Measurements of fine particulate chemical composition in two UK cities (vol 108, art no 4091, 2003), J. Geophys. Res.-Atmos., 108, 10.1029/2003jd001608, 2003.

Apel, E. C., Brauers, T., Koppmann, R., Bandowe, B., Bossmeyer, J., Holzke, C., Tillmann, R., Wahner, A., Wegener, R., Brunner, A., Jocher, M., Ruuskanen, T., Spirig, C., Steigner, D., Steinbrecher, R., Alvarez, E. G., Muller, K., Burrows, J.

P., Schade, G., Solomon, S. J., Ladstatter-Weissenmayer, A., Simmonds, P., Young, D., Hopkins, J. R., Lewis, A. C., Legreid, G., Reimann, S., Hansel, A., Wisthaler, A., Blake, R. S., Ellis, A. M., Monks, P. S., and Wyche, K. P.: Intercomparison of oxygenated volatile organic compound measurements at the SAPHIR atmosphere simulation chamber, J. Geophys. Res.-Atmos., 113, 24, D20307
10.1029/2008jd009865, 2008.

Arneth, A., Niinemets, U., Pressley, S., Back, J., Hari, P., Karl, T., Noe, S., Prentice, I. C., Serca, D., Hickler, T., Wolf, A., and Smith, B.: Process-based estimates of terrestrial ecosystem isoprene emissions: incorporating the effects of a direct CO2-isoprene interaction, Atmospheric Chemistry and Physics, 7, 31-53, 2007.

Atkinson, R., Baulch, D. L., Cox, R. A., Crowley, J. N., Hampson, R. F., Hynes, R. G., Jenkin, M. E., Rossi, M. J., and Troe, J.: Evaluated kinetic and photochemical data for atmospheric chemistry: Volume II - gas phase reactions of organic species, Atmospheric Chemistry and Physics, 6, 3625-4055, 2006.

Baraldi, R., Rapparini, F., Rossi, F., Latella, A., and Ciccioli, P.: Volatile organic compound emissions from flowers of the most occurring and economically important species of fruit trees, Phys. Chem. Earth Pt B-Hydrol. Oceans Atmos., 24, 729-732, 1999.

Barkley, M. P., Palmer, P. I., De Smedt, I., Karl, T., Guenther, A., and Van Roozendael, M.: Regulated large-scale annual shutdown of Amazonian isoprene emissions?, Geophys. Res. Lett., 36, L04803, 10.1029/2008gl036843, 2009.

Barley, M. H., and McFiggans, G.: The critical assessment of vapour pressure estimation methods for use in modelling the formation of atmospheric organic aerosol, Atmospheric Chemistry and Physics, 10, 749-767, 2010.

Beddows, D. C. S., Donovan, R. J., Harrison, R. M., Heal, M. R., Kinnersley, R. P., King, M. D., Nicholson, D. H., and Thompson, K. C.: Correlations in the chemical composition of rural background atmospheric aerosol in the UK determined in real time using time-of-flight mass spectrometry, J. Environ. Monit., 6, 124-133, 10.1039/b311209h, 2004.

Borgkarlson, A. K., Bergstrom, G., and Groth, I.: Chemical basis for the relationship between Ophrys orchids and their pollinators .1. Volatile compounds of Ophrys-lutea and O-fusca as insect mimetic attractants excitants, Chemica Scripta, 25, 283-&, 1985.

Borgkarlson, A. K., Bergstrom, G., and Kullenberg, B.: Chemical basis for the relationship between Ophrys orchids and their pollinators .2. Volatile compounds of O-insectifera and O-speculum as insect mimetic attractants excitants, Chemica Scripta, 27, 303-&, 1987.

Brunner, A., Ammann, C., Neftel, A., and Spirig, C.: Methanol exchange between grassland and the atmosphere, Biogeosciences, 4, 395-410, 2007.

Bubenheim, D., Potter, C., Schlick, G., and Klooster, S.: Biogenic Emision Sources of Acetone, 35th COSPAR Scientific Assembly, Paris, France, 18 - 24 July 2004, 3183, 2004.

Camredon, M., Aumont, B., Lee-Taylor, J., and Madronich, S.: The SOA/VOC/NOx system: an explicit model of secondary organic aerosol formation, Atmospheric Chemistry and Physics, 7, 5599-5610, 2007.

Carter, W. P. L., and Atkinson, R.: Development and evaluation of a detailed mechanism for the atmospheric reactions of isoprene and NOx, Int. J. Chem. Kinet., 28, 497-530, 1996.

Caudill, S. P., Wong, L. Y., Turner, W. E., Lee, R., Henderson, A., and Patterson, D. G.: Percentile estimation using variable censored data, Chemosphere, 68, 169-180, 10.1016/j.chemosphere.2006.12.013, 2007.

Christian, T. J., Kleiss, B., Yokelson, R. J., Holzinger, R., Crutzen, P. J., Hao, W. M., Shirai, T., and Blake, D. R.: Comprehensive laboratory measurements of biomass-burning emissions: 2. First intercomparison of open-path FTIR, PTR-MS, and GC- MS/FID/ECD, J. Geophys. Res.-Atmos., 109, 12, D02311 10.1029/2003jd003874, 2004.

Clarke, J. U.: Evaluation of censored data methods to allow statistical comparisons among very small samples with below detection limit observations, Environ. Sci. Technol., 32, 177-183, 1998.

Clement, R. J., Burba, G. G., Grelle, A., Anderson, D. J., and Moncrieff, J. B.: Improved trace gas flux estimation through IRGA sampling optimization, Agric. For. Meteorol., 149, 623-638, 10.1016/j.agrformet.2008.10.008, 2009.

Coe, H., Allan, J. D., Alfarra, M. R., Bower, K. N., Flynn, M. J., McFiggans, G. B., Topping, D. O., Williams, P. I., O'Dowd, C. D., Dall'Osto, M., Beddows, D. C. S., and Harrison, R. M.: Chemical and physical characteristics of aerosol particles at a remote coastal location, Mace Head, Ireland, during NAMBLEX, Atmospheric Chemistry and Physics, 6, 3289-3301, 2006.

Coyle, M.: in preparation, 2010.

Custer, T., and Schade, G.: Methanol and acetaldehyde fluxes over ryegrass, Tellus B, 59, 673-684, doi:10.1111/j.1600-0889.2007.00294.x, 2007.

Dall'Osto, M., Beddows, D. C. S., Kinnersley, R. P., Harrison, R. M., Donovan, R. J., and Heal, M. R.: Characterization of individual airborne particles by using aerosol time-of-flight mass spectrometry at Mace Head, Ireland, J. Geophys. Res.-Atmos., 109, 10.1029/2004jd004747, 2004.

Dall'Osto, M., Harrison, R. M., Beddows, D. C. S., Freney, E. J., Heal, M. R., and Donovan, R. J.: Single-particle detection efficiencies of aerosol time-of-flight mass spectrometry during the North Atlantic marine boundary layer experiment, Environ. Sci. Technol., 40, 5029-5035, 10.1021/es050951i, 2006.

Davison, B., Brunner, A., Ammann, C., Spirig, C., Jocher, M., and Neftel, A.: Cut-induced VOC emissions from agricultural grasslands, Plant Biology, 10, 76-85, doi:10.1055/s-2007-965043, 2008.

Davison, B., Taipale, R., Langford, B., Misztal, P., Fares, S., Matteucci, G., Loreto, F., Cape, J. N., Rinne, J., and Hewitt, C. N.: Concentrations and fluxes of biogenic volatile organic compounds above a Mediterranean macchia ecosystem in western Italy, Biogeosciences, 6, 1655-1670, 2009.

de Gouw, J., Warneke, C., Karl, T., Eerdekens, G., van der Veen, C., and Fall, R.: Sensitivity and specificity of atmospheric trace gas detection by proton-transfer-reaction mass spectrometry, International Journal of Mass Spectrometry, 223-224, 365-382, 2003a.

de Gouw, J. A., Goldan, P. D., Warneke, C., Kuster, W. C., Roberts, J. M., Marchewka, M., Bertman, S. B., Pszenny, A. A. P., and Keene, W. C.: Validation of proton transfer reaction-mass spectrometry (PTR-MS) measurements of gas-phase organic compounds in the atmosphere during the

New England Air Quality Study (NEAQS) in 2002, J. Geophys. Res.-Atmos., 108, 2003b.

de Gouw, J. A., Warneke, C., Kuster, W. C., Goldan, P. D., and Fall, R.: Validation of Atmospheric VOC Measurements by Proton-Transfer- Reaction Mass Spectrometry Using a Gas-Chromatographic Preseparation Method, Environ. Sci. Technol., 37, 2494-2501, 2003c.

de Gouw, J. W., Carsten: Measurements of Volatile Organic Compounds in the Earth's Atmosphere using Proton-Transfer-Reaction Mass Spectrometry, Mass Spectrometry Reviews, 26, 223-257, 2007.

DeCarlo, P. F., Dunlea, E. J., Kimmel, J. R., Aiken, A. C., Sueper, D., Crounse, J., Wennberg, P. O., Emmons, L., Shinozuka, Y., Clarke, A., Zhou, J., Tomlinson, J., Collins, D. R., Knapp, D., Weinheimer, A. J., Montzka, D. D., Campos, T., and Jimenez, J. L.: Fast airborne aerosol size and chemistry measurements above Mexico City and Central Mexico during the MILAGRO campaign, Atmospheric Chemistry and Physics, 8, 4027-4048, 2008.

Dorsey, J. R., Nemitz, E., Gallagher, M. W., Fowler, D., Williams, P. I., Bower, K. N., and Beswick, K. M.: Direct measurements and parameterisation of aerosol flux, concentration and emission velocity above a city, Atmospheric Environment, 36, 791-800, 2002.

Eerdekens, G., Ganzeveld, L., Vilà -Guerau de Arellano, J., Klüpfel, T., Sinha, V., Yassaa, N., Williams, J., Harder, H., Kubistin, D., Martinez, M., and Lelieveld, J.: Flux estimates of isoprene, methanol and acetone from airborne PTR-MS measurements over the tropical rainforest during the GABRIEL 2005 campaign, Atmos. Chem. Phys., 9, 4207-4227, 10.5194/acp-9-4207-2009, 2009.

EPA On-line Tools for Site Assessment Calculation: http://www.epa.gov/athens/learn2model/part-two/onsite/estdiffusion-ext.htm, access: 15 Aug 2009, 2007.

Fall, R.: Abundant Oxygenates in the Atmosphere: A Biochemical Perspective, Chemical Reviews, 103, 4941-4952, 10.1021/cr0206521, 2003.

FAOSTAT Online Statistical Service. Item: Oil palm fruit; element: area harvested; year: 2007; country: World, South East Asia, Malaysia, Indonesia. http://faostat.fao.org (Accessed April 2009) http://faostat.fao.org, 2009.

FAOSTAT Online Statistical Service. Item: Oil palm fruit; element: area harvested; year: 2008; country: World, South East Asia, Malaysia, Indonesia. http://faostat.fao.org (Accessed June 2010) http://faostat.fao.org, 2010.

Fares, S., Oksanen, E., Lannenpaa, M., Julkunen-Tiitto, R., and Loreto, F.: Volatile emissions and phenolic compound concentrations along a vertical profile of Populus nigra leaves exposed to realistic ozone concentrations, Photosynth. Res., 104, 61-74, 10.1007/s11120-010-9549-5, 2010.

Filella, I., Wilkinson, M. J., Llusia, J., Hewitt, C. N., and Penuelas, J.: Volatile organic compounds emissions in Norway spruce (Picea abies) in response to temperature changes, Physiologia Plantarum, 130, 58-66, doi:10.1111/j.1399-3054.2007.00881.x, 2007.

Foken, T., and Wichura, B.: Tools for quality assessment of surface-based flux measurements, Agric. For. Meteorol., 78, 83-105, 1996.

Foken, T., Göckede, M., Mauder, M., Mahrt, L., Amiro, B., and Munger, W.: Post-field data quality control, in: Handbook of Micrometeorology: A guide for

surface flux measurement and analysis., edited by: Lee, W. M. X., and Law, B., Kluwer Academic Publishers, Dordrecht, 181-203, 2004.

Folkers, A., Huve, K., Ammann, C., Dindorf, T., Kesselmeier, J., Kleist, E., Kuhn, U., Uerlings, R., and Wildt, J.: Methanol emissions from deciduous tree species: dependence on temperature and light intensity, Plant Biology, 10, 65-75, doi:10.1111/j.1438-8677.2007.00012.x, 2008.

Fuentes, E., Coe, H., Green, D., de Leeuw, G., and McFiggans, G.: Laboratory-generated primary marine aerosol via bubble-bursting and atomization, Atmospheric Measurement Techniques, 3, 141-162, 2010.

Gallagher, M. W., Nemitz, E., Dorsey, J. R., Fowler, D., Sutton, M. A., Flynn, M., and Duyzer, J.: Measurements and parameterizations of small aerosol deposition velocities to grassland, arable crops, and forest: Influence of surface roughness length on deposition, J. Geophys. Res.-Atmos., 107, 10.1029/2001jd000817, 2002.

Geron, C., Guenther, A., Sharkey, T., and Arnts, R. R.: Temporal variability in basal isoprene emission factor, Tree Physiol., 20, 799-805, 2000.

Goldstein, A. H., McKay, M., Kurpius, M. R., Schade, G. W., Lee, A., Holzinger, R., and Rasmussen, R. A.: Forest thinning experiment confirms ozone deposition to forest canopy is dominated by reaction with biogenic VOCs, Geophys. Res. Lett., 31, 10.1029/2004gl021259, 2004.

Grabmer, W., Graus, M., Lindinger, C., Wisthaler, A., Rappengluck, B., Steinbrecher, R., and Hansel, A.: Disjunct eddy covariance measurements of monoterpene fluxes from a Norway spruce forest using PTR-MS, International Journal of Mass Spectrometry, 239, 111-115, 2004.

Guenther, A., Hewitt, C. N., Erickson, D., Fall, R., Geron, C., Graedel, T., Harley, P., Klinger, L., Lerdau, M., McKay, W. A., Pierce, T., Scholes, B., Steinbrecher, R., Tallamraju, R., Taylor, J., and Zimmerman, P.: A global-model o fnatural volatile organic-compound emissions, J. Geophys. Res.-Atmos., 100, 8873-8892, 1995.

Guenther, A., Baugh, B., Brasseur, G., Greenberg, J., Harley, P., Klinger, L., Serça, D., and Vierling, L.: Isoprene emission estimates and uncertainties for the Central African EXPRESSO study domain, J. Geophys. Res., 104, 30625-30639, 10.1029/1999jd900391, 1999.

Guenther, A., Karl, T., Harley, P., Wiedinmyer, C., Palmer, P. I., and Geron, C.: Estimates of global terrestrial isoprene emissions using MEGAN (Model of Emissions of Gases and Aerosols from Nature), Atmos. Chem. Phys. Discuss., 6, 107-173, 2006.

Guenther, A.: Interactive comment on "The emission factor of volatile isoprenoids: caveats, model algorithms, response shapes and scaling" by Ü. Niinemets et al., Biogeosciences Discuss., 7, C531–C533, 2010.

Guenther, A. B., Zimmerman, P. R., Harley, P. C., Monson, R. K., and Fall, R.: Isoprene and monoterpene emission rate variability - model evaluations and sensitivity analyses, J. Geophys. Res.-Atmos., 98, 12609-12617, 1993.

Hadacek, F., and Weber, M.: Club-Shaped Organs as Additional Osmophores within the Sauromatum Inflorescence: Odour Analysis, Ultrastructural Changes and Pollination Aspects⁴, Plant Biology, 4, 367-383, 2002.

Hanson, D. T., and Sharkey, T. D.: Rate of acclimation of the capacity for isoprene emission in response to light and temperature, Plant Cell Environ., 24, 937-946, 2001.

Heath, J., Ayres, E., Possell, M., Bardgett, R. D., Black, H. I. J., Grant, H., Ineson, P., and Kerstiens, G.: Rising atmospheric CO2 reduces sequestration of root-derived soil carbon, Science, 309, 1711-1713, 10.1126/science.1110700, 2005.

Heiden, A. C., Kobel, K., Komenda, M., Koppmann, R., Shao, M., and Wildt, J.: Toluene Emissions from Plants, Geophys. Res. Lett., 26, 1283-1286, 1999.

Hellén, H., Dommen, J., Metzger, A., Gascho, A., Duplissy, J., Tritscher, T., Prevot, A. S. H., and Baltensperger, U.: Using Proton Transfer Reaction Mass Spectrometry for Online Analysis of Secondary Organic Aerosols, Environ. Sci. Technol., 42, 7347-7353, 10.1021/es801279m, 2008.

Helsel, D. R.: Less than obvious - statistical treatment of data below the detection limit, Environ. Sci. Technol., 24, 1766-1774, 1990.

Henderson, J., Davies, H. A., Heyes, S. J., and Osborne, D. J.: The study of a monocotyledon abscission zone using microscopic, chemical, enzymatic and solid state 13C CP/MAS NMR analyses, Phytochemistry, 56, 131-139, 2001.

Hewitt, C. N., MacKenzie, A. R., Di Carlo, P., Di Marco, C. F., Dorsey, J. R., Evans, M., Fowler, D., Gallagher, M. W., Hopkins, J. R., Jones, C. E., Langford, B., Lee, J. D., Lewis, A. C., Lim, S. F., McQuaid, J., Misztal, P., Moller, S. J., Monks, P. S., Nemitz, E., Oram, D. E., Owen, S. M., Phillips, G. J., Pugh, T. A. M., Pyle, J. A., Reeves, C. E., Ryder, J., Siong, J., Skiba, U., and Stewart, D. J.: Nitrogen management is essential to prevent tropical oil palm plantations from causing ground-level ozone pollution, Proceedings of the National Academy of Sciences, 106, 18447-18451, 10.1073/pnas.0907541106, 2009.

Hewitt, C. N., Lee, J. D., MacKenzie, A. R., Barkley, M. P., Carslaw, N., Carver, G. D., Chappell, N. A., Coe, H., Collier, C., Commane, R., Davies, F., Davison, B., DiCarlo, P., Di Marco, C. F., Dorsey, J. R., Edwards, P. M., Evans, M. J., Fowler, D., Furneaux, K. L., Gallagher, M., Guenther, A., Heard, D. E., Helfter, C., Hopkins, J., Ingham, T., Irwin, M., Jones, C., Karunaharan, A., Langford, B., Lewis, A. C., Lim, S. F., MacDonald, S. M., Mahajan, A. S., Malpass, S., McFiggans, G., Mills, G., Misztal, P., Moller, S., Monks, P. S., Nemitz, E., Nicolas-Perea, V., Oetjen, H., Oram, D. E., Palmer, P. I., Phillips, G. J., Pike, R., Plane, J. M. C., Pugh, T., Pyle, J. A., Reeves, C. E., Robinson, N. H., Stewart, D., Stone, D., Whalley, L. K., and Yin, X.: Overview: oxidant and particle photochemical processes above a south-east Asian tropical rainforest (the OP3 project): introduction, rationale, location characteristics and tools, Atmos. Chem. Phys., 10, 169-199, 2010.

Holzinger, R., Lee, A., Paw, K. T., and Goldstein, A. H.: Observations of oxidation products above a forest imply biogenic emissions of very reactive compounds, Atmospheric Chemistry and Physics, 5, 67-75, 2005.

Huffman, J. A., Docherty, K. S., Aiken, A. C., Cubison, M. J., Ulbrich, I. M., DeCarlo, P. F., Sueper, D., Jayne, J. T., Worsnop, D. R., Ziemann, P. J., and Jimenez, J. L.: Chemically-resolved aerosol volatility measurements from two megacity field studies, Atmospheric Chemistry and Physics, 9, 7161-7182, 2009.

IPCC: "Summary for Policymakers" (PDF). Climate Change 2007: The Physical Science Basis. Contribution of Working Group I to the Fourth Assessment Report of the Intergovernmental Panel on Climate Change.

http://www.ipcc.ch/pdf/assessment-report/ar4/wg1/ar4-wg1-spm.pdf. Access date 02 June 2010., 2007.

Jardine, K., Harley, P., Karl, T., Guenther, A., Lerdau, M., and Mak, J. E.: Plant physiological and environmental controls over the exchange of acetaldehyde between forest canopies and the atmosphere, Biogeosciences, 5, 1559-1572, 2008.

Jardine, K., Karl, T., Lerdau, M., Harley, P., Guenther, A., and Mak, J. E.: Carbon isotope analysis of acetaldehyde emitted from leaves following mechanical stress and anoxia, Plant Biology, 11, 591-597, 10.1111/j.1438-8677.2008.00155.x, 2009.

Karl, T., Guenther, A., Lindinger, C., Jordan, A., Fall, R., and Lindinger, W.: Eddy covariance measurements of oxygenated volatile organic compound fluxes from crop harvesting using a redesigned proton-transfer-reaction mass spectrometer, J. Geophys. Res.-Atmos., 106, 24157-24167, 2001.

Karl, T., and Guenther, A.: Atmospheric variability of biogenic VOCs in the surface layer measured by proton-transfer-reaction mass spectrometry, International Journal of Mass Spectrometry, 239, 77-86, 2004.

Karl, T., Potosnak, M., Guenther, A., Clark, D., Walker, J., Herrick, J. D., and Geron, C.: Exchange processes of volatile organic compounds above a tropical rain forest: Implications for modeling tropospheric chemistry above dense vegetation, J. Geophys. Res.-Atmos., 109, 24, D18306
10.1029/2004jd004738, 2004.

Karl, T., Harley, P., Guenther, A., Rasmussen, R., Baker, B., Jardine, K., and Nemitz, E.: The bi-directional exchange of oxygenated VOCs between a loblolly pine (Pinus taeda) plantation and the atmosphere, Atmospheric Chemistry and Physics, 5, 3015-3031, 2005.

Karl, T., Guenther, A., Yokelson, R. J., Greenberg, J., Potosnak, M., Blake, D. R., and Artaxo, P.: The tropical forest and fire emissions experiment: Emission, chemistry, and transport of biogenic volatile organic compounds in the lower atmosphere over Amazonia, J. Geophys. Res.-Atmos., 112, 17, D18302
10.1029/2007jd008539, 2007.

Karl, T., Guenther, A., Turnipseed, A., Patton, E. G., and Jardine, K.: Chemical sensing of plant stress at the ecosystem scale, Biogeosciences, 5, 1287-1294, 2008.

Karl, T., Guenther, A., Turnipseed, A., Tyndall, G., Artaxo, P., and Martin, S.: Rapid formation of isoprene photo-oxidation products observed in Amazonia, Atmos. Chem. Phys., 9, 7753-7767, 2009.

Karl, T., M. Potosnak, et al.: Exchange processes of volatile organic compounds above a tropical rain forest: Implications for modeling tropospheric chemistry above dense vegetation, J. Geophys. Res.-Atmos., 109, 2004.

Karl, T. G., C. Spirig, et al.: Virtual disjunct eddy covariance measurements of organic compound fluxes from a subalpine forest using proton transfer reaction mass spectrometry, Atmospheric Chemistry and Physics, 2, 279-291, 2002.

Kiendler-Scharr, A., Wildt, J., Maso, M. D., Hohaus, T., Kleist, E., Mentel, T. F., Tillmann, R., Uerlings, R., Schurr, U., and Wahner, A.: New particle formation in forests inhibited by isoprene emissions, Nature, 461, 381-384, 2009.

Kim, S., Karl, T., Helmig, D., Daly, R., Rasmussen, R., and Guenther, A.: Measurement of atmospheric sesquiterpenes by proton transfer reaction-mass spectrometry (PTR-MS), Atmos. Meas. Tech., 2, 99-112, 2009.

Kim, S., Karl, T., Guenther, A., Tyndall, G., Orlando, J., Harley, P., Rasmussen, R., and Apel, E.: Emissions and ambient distributions of Biogenic Volatile Organic Compounds (BVOC) in a ponderosa pine ecosystem: interpretation of PTR-MS mass spectra, Atmos. Chem. Phys., 10, 1759-1771, 10.5194/acp-10-1759-2010, 2010.

Kleindienst, T. E.: Epoxying Isoprene Chemistry, Science, 325, 687-688, 10.1126/science.1178324, 2009.

Knudsen, J., Eriksson, R., Gershenzon, J., and Ståhl, B.: Diversity and distribution of floral scent, The Botanical Review, 72, 1-120, 2006.

Kuanprasert, N., Kuehnle, A. R., and Tang, C. S.: Floral fragrance compounds of some Anthurium (araceae) species and hybrids, Phytochemistry, 49, 521-+, 1998.

Kuhn, U., Andreae, M. O., Ammann, C., Araujo, A. C., Brancaleoni, E., Ciccioli, P., Dindorf, T., Frattoni, M., Gatti, L. V., Ganzeveld, L., Kruijt, B., Lelieveld, J., Lloyd, J., Meixner, F. X., Nobre, A. D., Poschl, U., Spirig, C., Stefani, P., Thielmann, A., Valentini, R., and Kesselmeier, J.: Isoprene and monoterpene fluxes from Central Amazonian rainforest inferred from tower-based and airborne measurements, and implications on the atmospheric chemistry and the local carbon budget, Atmospheric Chemistry and Physics, 7, 2855-2879, 2007.

Kuster, W. C., Jobson, B. T., Karl, T., Riemer, D., Apel, E., Goldan, P. D., and Fehsenfeld, F. C.: Intercomparison of volatile organic carbon measurement techniques and data at la porte during the TexAQS2000 Air Quality Study, Environ. Sci. Technol., 38, 221-228, 10.1021/es034710r, 2004.

Langford, B., Davison, B., Nemitz, E., and Hewitt, C. N.: Mixing ratios and eddy covariance flux measurements of volatile organic compounds from an urban canopy (Manchester, UK), Atmos. Chem. Phys., 9, 1971-1987, 2009a.

Langford, B., Nemitz, E., House, E., Phillips, G. J., Famulari, D., Davison, B., Hopkins, J. R., Lewis, A. C., and Hewitt, C. N.: Fluxes and concentrations of volatile organic compounds above central London, UK, Atmos. Chem. Phys. Discuss., 9, 17297-17333, 2009b.

Langford, B., Misztal, P. K., Nemitz, E., Davison, B., Helfter, C., Pugh, T. A. M., MacKenzie, A. R., Lim, S. F., and Hewitt, C. N.: Fluxes and concentrations of volatile organic compounds from a South-East Asian tropical rainforest, Atmos. Chem. Phys. Discuss., 10, 11975-12021, 10.5194/acpd-10-11975-2010, 2010.

Laothawornkitkul, J., Paul, N. D., Vickers, C. E., Possell, M., Taylor, J. E., Mullineaux, P. M., and Hewitt, C. N.: Isoprene emissions influence herbivore feeding decisions, Plant, Cell & Environment, 31, 1410-1415, 2008.

Lee, A., Goldstein, A. H., Kroll, J. H., Ng, N. L., Varutbangkul, V., Flagan, R. C., and Seinfeld, J. H.: Gas-phase products and secondary aerosol yields from the photooxidation of 16 different terpenes, J. Geophys. Res.-Atmos., 111, 10.1029/2006jd007050, 2006.

Legros, S., Mialet-Serra, I., Clement-Vidal, A., Caliman, J. P., Siregar, F. A., Fabre, D., and Dingkuhn, M.: Role of transitory carbon reserves during adjustment to climate variability and source-sink imbalances in oil palm (Elaeis guineensis), Tree Physiol, tpp057, 10.1093/treephys/tpp057, 2009.

Lockwood, A. L., Shepson, P. B., Fiddler, M. N., and Alaghmand, M.: Isoprene nitrates: preparation, separation, identification, yields, and atmospheric chemistry, Atmos. Chem. Phys. Discuss., 10, 10625-10651, 10.5194/acpd-10-10625-2010, 2010.

Loreto, F., Mannozzi, M., Maris, C., Nascetti, P., Ferranti, F., and Pasqualini, S.: Ozone Quenching Properties of Isoprene and Its Antioxidant Role in Leaves, Plant Physiol., 126, 993-1000, 10.1104/pp.126.3.993, 2001.

Maleknia, S. D., Bell, T. L., and Adams, M. A.: PTR-MS analysis of reference and plant-emitted volatile organic compounds, International Journal of Mass Spectrometry, 262, 203-210, 2007.

McFiggans, G., Artaxo, P., Baltensperger, U., Coe, H., Facchini, M. C., Feingold, G., Fuzzi, S., Gysel, M., Laaksonen, A., Lohmann, U., Mentel, T. F., Murphy, D. M., O'Dowd, C. D., Snider, J. R., and Weingartner, E.: The effect of physical and chemical aerosol properties on warm cloud droplet activation, Atmospheric Chemistry and Physics, 6, 2593-2649, 2006.

Meyer, N. K., Duplissy, J., Gysel, M., Metzger, A., Dommen, J., Weingartner, E., Alfarra, M. R., Prevot, A. S. H., Fletcher, C., Good, N., McFiggans, G., Jonsson, A. M., Hallquist, M., Baltensperger, U., and Ristovski, Z. D.: Analysis of the hygroscopic and volatile properties of ammonium sulphate seeded and unseeded SOA particles, Atmospheric Chemistry and Physics, 9, 721-732, 2009.

Millet, D. B., Guenther, A., Siegel, D. A., Nelson, N. B., Singh, H. B., de Gouw, J. A., Warneke, C., Williams, J., Eerdekens, G., Sinha, V., Karl, T., Flocke, F., Apel, E., Riemer, D. D., Palmer, P. I., and Barkley, M.: Global atmospheric budget of acetaldehyde: 3-D model analysis and constraints from in-situ and satellite observations, Atmos. Chem. Phys., 10, 3405-3425, 10.5194/acp-10-3405-2010, 2010.

Misztal, P. K., Owen, S. M., Guenther, A. B., Rasmussen, R., Geron, C., Harley, P., Phillips, G. J., Ryan, A., Edwards, D. P., Hewitt, C. N., Nemitz, E., Siong, J., Heal, M. R., and Cape, J. N.: Large estragole fluxes from oil palms in Borneo, Atmos. Chem. Phys., 10, 4343-4358, 10.5194/acp-10-4343-2010, 2010.

Moncrieff, J., Valentini, R., Greco, S., Guenther, S., and Ciccioli, P.: Trace gas exchange over terrestrial ecosystems: methods and perspectives in micrometeorology, J. Exp. Bot., 48, 1133-1142, 10.1093/jxb/48.5.1133, 1997.

Monson, R. K., Harley, P. C., Litvak, M. E., Wildermuth, M., Guenther, A. B., Zimmerman, P. R., and Fall, R.: Environmental and developmental controls over the seasonal pattern of isoprene emission from aspen leaves, Oecologia, 99, 260-270, 1994.

Murphy, J. G., Oram, D. E., and Reeves, C. E.: Measurements of volatile organic compounds over West Africa, Atmos. Chem. Phys. Discuss., 10, 3861-3892, 10.5194/acpd-10-3861-2010, 2010.

Nemitz, E., Jimenez, J. L., Huffman, J. A., Ulbrich, I. M., Canagaratna, M. R., Worsnop, D. R., and Guenther, A. B.: An eddy-covariance system for the measurement of surface/atmosphere exchange fluxes of submicron aerosol chemical species - First application above an urban area, Aerosol Science and Technology, 42, 636-657, 10.1080/02786820802227352, 2008.

Nemitz, E., Dorsey, J. R., Flynn, M. J., Gallagher, M. W., Hensen, A., Erisman, J. W., Owen, S. M., DÃ¤mmgen, U., and Sutton, M. A.: Aerosol fluxes and

particle growth above managed grassland, Biogeosciences, 6, 1627-1645, 10.5194/bg-6-1627-2009, 2009a.

Nemitz, E., Dorsey, J. R., Flynn, M. J., Gallagher, M. W., Hensen, A., Erisman, J. W., Owen, S. M., Dammgen, U., and Sutton, M. A.: Aerosol fluxes and particle growth above managed grassland, Biogeosciences, 6, 1627-1645, 2009b.

Nemitz, E., Hargreaves, K. J., Neftel, A., Loubet, B., Cellier, P., Dorsey, J. R., Flynn, M., Hensen, A., Weidinger, T., Meszaros, R., Horvath, L., Dämmgen, U., Frühauf, C., Löpmeier, F. J., Gallagher, M. W., and Sutton, M. A.: Intercomparison and assessment of turbulent and physiological exchange parameters of grassland, Biogeosciences, 6, 1445-1466, 2009c.

Nemitz, E., Loubet, B., Lehmann, B. E., Cellier, P., Neftel, A., Jones, S. K., Hensen, A., Ihly, B., Tarakanov, S. V., and Sutton, M. A.: Turbulence characteristics in grassland canopies and implications for tracer transport, Biogeosciences, 6, 1519-1537, 2009d.

Nemitz, E., Phillips, G. J., Di Marco, C. F., Siong, J., Farmer, D., Kimmel, J. R., Jimenez, J. L., and Fowler, D.: Concentrations and fluxes of of submicron aerosol components above an oil palm plantation in Sabah, Malaysia, in preparation, 2010.

Ng, N. L., Kroll, J. H., Chan, A. W. H., Chhabra, P. S., Flagan, R. C., and Seinfeld, J. H.: Secondary organic aerosol formation from m-xylene, toluene, and benzene, Atmos. Chem. Phys., 7, 3909-3922, 10.5194/acp-7-3909-2007, 2007.

Niinemets, U., Tenhunen, J. D., Harley, P. C., and Steinbrecher, R.: A model of isoprene emission based on energetic requirements for isoprene synthesis and leaf photosynthetic properties for Liquidambar and Quercus, Plant Cell Environ., 22, 1319-1335, 1999.

Niinemets, Ü.: Interactive comment on "The emission factor of volatile isoprenoids: caveats, model algorithms, response shapes and scaling" by Ü. Niinemets et al., Biogeosciences Discuss., 7, C509–C512, 2010.

Niinemets, Ü., Arneth, A., Kuhn, U., Monson, R. K., Peñuelas, J., and Staudt, M.: The emission factor of volatile isoprenoids: stress, acclimation, and developmental responses, Biogeosciences Discuss., 7, 1529-1574, 10.5194/bgd-7-1529-2010, 2010a.

Niinemets, Ü., Monson, R. K., Arneth, A., Ciccioli, P., Kesselmeier, J., Kuhn, U., Noe, S. M., Peñuelas, J., and Staudt, M.: The emission factor of volatile isoprenoids: caveats, model algorithms, response shapes and scaling, Biogeosciences Discuss., 7, 1233-1293, 10.5194/bgd-7-1233-2010, 2010b.

Oram, D.: Aircraft PTR measurements of VOC, OP3 Science Meeting, University of Leeds, 27-29 November 2008, 2008.

Orlando, J. J., Tyndall, G. S., Fracheboud, J.-M., Estupiñan, E. G., Haberkorn, S., and Zimmer, A.: The rate and mechanism of the gas-phase oxidation of hydroxyacetone, Atmospheric Environment, 33, 1621-1629, 1999.

Owen, S. M., Wilkinson, M. J., Ryan, A., Linatoc, A., and Hewitt, C. N.: Variability in leaf level isoprene emission rate from oil palm, in preparation, 2010.

Paulot, F., Crounse, J. D., Kjaergaard, H. G., Kurten, A., St. Clair, J. M., Seinfeld, J. H., and Wennberg, P. O.: Unexpected Epoxide Formation in the Gas-Phase Photooxidation of Isoprene, Science, 325, 730-733, 10.1126/science.1172910, 2009.

Petron, G., Harley, P., Greenberg, J., and Guenther, A.: Seasonal temperature variations influence isoprene emission, Geophys. Res. Lett., 28, 1707-1710, 2001.

Porter, P. S., Ward, R. C., and Bell, H. F.: The detection limit, Environ. Sci. Technol., 22, 856-861, 1988.

Pöschl, U., Williams, J., Hoor, P., Fischer, H., Crutzen, P. J., Warneke, C., Holzinger, R., Hansel, A., Jordan, A., Lindinger, W., Scheeren, H. A., Peters, W., and Lelieveld, J.: High Acetone Concentrations throughout the 0–12 km Altitude Range over the Tropical Rainforest in Surinam, Journal of Atmospheric Chemistry, 38, 115-132, 2001.

Possell, M., Hewitt, C. N., and Beerling, D. J.: The effects of glacial atmospheric CO2 concentrations and climate on isoprene emissions by vascular plants, Glob. Change Biol., 11, 60-69, 10.1111/j.1365-2486.2004.00889.x, 2005.

Possell, M., Ryan, A., Vickers, C. E., Mullineaux, P. M., and Hewitt, C. N.: Effects of fosmidomycin on plant photosynthesis as measured by gas exchange and chlorophyll fluorescence, Photosynth. Res., 104, 49-59, 10.1007/s11120-009-9504-5, 2010.

Pugh, T. A. M., MacKenzie, A. R., Hewitt, C. N., Langford, B., Edwards, P. M., Furneaux, K. L., Heard, D. E., Hopkins, J. R., Jones, C. E., Karunaharan, A., Lee, J., Mills, G., Misztal, P., Moller, S., Monks, P. S., and Whalley, L. K.: Simulating atmospheric composition over a South-East Asian tropical rainforest: performance of a chemistry box model, Atmos. Chem. Phys., 10, 279-298, 2010.

Rinne, J., Durand, P., and Guenther, A.: An airborne disjunct eddy covariance system: Sampling strategy and instrument design, 15th Symposium on Boundary Layers and Turbulence, 151-154, 2002.

Rinne, J., Taipale, R., Markkanen, T., Ruuskanen, T. M., Hellén, H., Kajos, M. K., Vesala, T., and Kulmala, M.: Hydrocarbon fluxes above a Scots pine forest canopy: measurements and modeling, Atmos. Chem. Phys., 7, 3361-3372, 2007.

Rinne, J., Douffet, T., Prigent, Y., and Durand, P.: Field comparison of disjunct and conventional eddy covariance techniques for trace gas flux measurements, Environmental Pollution, 152, 630-635, 2008.

Rizzo, L. V., Artaxo, P., Karl, T., Guenther, A. B., and Greenberg, J.: Aerosol properties, in-canopy gradients, turbulent fluxes and VOC concentrations at a pristine forest site in Amazonia, Atmospheric Environment, 44, 503-511, 10.1016/j.atmosenv.2009.11.002, 2010.

Rollins, A. W., Fry, J. L., Hunter, J. F., Kroll, J. H., Worsnop, D. R., Singaram, S. W., and Cohen, R. C.: Elemental analysis of aerosol organic nitrates with electron ionization high-resolution mass spectrometry, Atmospheric Measurement Techniques, 3, 301-310, 2010.

Rottenberger, S., Kuhn, U., Wolf, A., Schebeske, G., Oliva, S. T., Tavares, T. M., and Kesselmeier, J.: Exchange of short-chain aldehydes between Amazonian vegetation and the atmosphere, Ecol. Appl., 14, S247-S262, 2004.

Ruppert, L., and Heinz Becker, K.: A product study of the OH radical-initiated oxidation of isoprene: formation of C5-unsaturated diols, Atmospheric Environment, 34, 1529-1542, 2000.

Ryder, J., Langford, B., Oram, D., Coyle, M., Phillips, G. J., Helfter, C., Misztal, P. K., Cape, J. N., and Nemitz, E.: Sources and sinks of biogenic volatile organic

compounds inside a South-East Asian rainforest canopy, Atmos. Chem. Phys. Discuss., in preparation for submission, 2010.

Sander, R.: Compilation of Henry's Law Constants for Inorganic and Organic Species of Potential Importance in Environmental Chemistry (Version 3), available online at: http://www.henrys-law.org 1999.

Seco, R., Penuelas, J., and Filella, I.: Short-chain oxygenated VOCs: Emission and uptake by plants and atmospheric sources, sinks, and concentrations, Atmospheric Environment, 41, 2477-2499, 2007.

Sharkey, T., and Schrader, S.: High temperature stress, in: Physiology and Molecular Biology of Stress Tolerance in Plants, 101-129, 2006.

Sharkey, T. D., Singsaas, E. L., Lerdau, M. T., and Geron, C. D.: Weather effects on isoprene emission capacity and applications in emissions algorithms, Ecol. Appl., 9, 1132-1137, 1999.

Sharkey, T. D., Wiberley, A. E., and Donohue, A. R.: Isoprene Emission from Plants: Why and How, Ann Bot, 101, 5-18, 10.1093/aob/mcm240, 2008.

Singh, H. B., Ohara, D., Herlth, D., Sachse, W., Blake, D. R., Bradshaw, J. D., Kanakidou, M., and Crutzen, P. J.: Acetone in the atmosphere - distribution, sources and sinks, J. Geophys. Res.-Atmos., 99, 1805-1819, 1994.

Singles, R., Sutton, M. A., and Weston, K. J.: A multi-layer model to describe the atmospheric transport and deposition of ammonia in Great Britain, Atmospheric Environment, 32, 393-399, 1998.

Sinha, V., Williams, J., MeyerhÃ¶fer, M., Riebesell, U., Paulino, A. I., and Larsen, A.: Air-sea fluxes of methanol, acetone, acetaldehyde, isoprene and DMS from a Norwegian fjord following a phytoplankton bloom in a mesocosm experiment, Atmos. Chem. Phys., 7, 739-755, 2007.

Siong, J., Helfter, C., DiMarco, C., Linatoc, A., Nemitz, E., Fowler, D., and Skiba, U. M.: Green-house gas (N2O, CH4 and CO2) exchange with contrasting land uses in SE Asia, Atmos. Chem. Phys. Discuss., in preparation, 2010.

Spirig, C., Neftel, A., Ammann, C., Dommen, J., Grabmer, W., Thielmann, A., Schaub, A., Beauchamp, J., Wisthaler, A., and Hansel, A.: Eddy covariance flux measurements of biogenic VOCs during ECHO 2003 using proton transfer reaction mass spectrometry, Atmospheric Chemistry and Physics, 5, 465-481, 2005.

Steinbacher, M., Dommen, J., Ammann, C., Spirig, C., Neftel, A., and Prevot, A. S. H.: Performance characteristics of a proton-transfer-reaction mass spectrometer (PTR-MS) derived from laboratory and field measurements, International Journal of Mass Spectrometry, 239, 117-128, 2004.

Sutton, M. A., Burkhardt, J. K., Guerin, D., Nemitz, E., and Fowler, D.: Development of resistance models to describe measurements of bi-directional ammonia surface-atmosphere exchange, International Conference on Atmospheric Ammonia - Emissions, Deposition and Environmental Impacts, Culham, England, 1995, ISI:000072633600029, 473-480,

Taipale, R., Ruuskanen, T. M., Rinne, J., Kajos, M. K., Hakola, H., Pohja, T., and Kulmala, M.: Technical Note: Quantitative long-term measurements of VOC concentrations by PTR-MS - measurement, calibration, and volume mixing ratio calculation methods, Atmospheric Chemistry and Physics, 8, 6681-6698, 2008.

Tani, A., Hayward, S., and Hewitt, C. N.: Measurement of monoterpenes and related compounds by proton transfer reaction-mass spectrometry (PTR-MS), International Journal of Mass Spectrometry, 223, 561-578, 2003.

Tani, A., Hayward, S., Hansel, A., and Hewitt, C. N.: Effect of water vapour pressure on monoterpene measurements using proton transfer reaction-mass spectrometry (PTR-MS), International Journal of Mass Spectrometry, 239, 161-169, 2004.

Taraborrelli, D., Lawrence, M. G., Butler, T. M., Sander, R., and Lelieveld, J.: Mainz Isoprene Mechanism 2 (MIM2): an isoprene oxidation mechanism for regional and global atmospheric modelling, Atmos. Chem. Phys., 9, 2751-2777, 10.5194/acp-9-2751-2009, 2009.

Tatsuka, K., Suekane, S., Sakai, Y., and Sumitani, H.: Volatile constituents of kiwi fruit flowers - simultaneous distillation and extraction versus headspace sampling, J. Agric. Food Chem., 38, 2176-2180, 1990.

Terry, G. M., Stokes, N. J., Hewitt, C. N., and Mansfield, T. A.: Exposure to isoprene promotes flowering in plants, J. Exp. Bot., 46, 1629-1631, 10.1093/jxb/46.10.1629, 1995.

Tie, X., Guenther, A., and Holland, E.: Biogenic methanol and its impacts on tropospheric oxidants, Geophys. Res. Lett., 30, 10.1029/2003gl017167, 2003.

Warneke, C., van der Veen, C., Luxembourg, S., de Gouw, J. A., and Kok, A.: Measurements of benzene and toluene in ambient air using proton-transfer-reaction mass spectrometry: calibration, humidity dependence, and field intercomparison, International Journal of Mass Spectrometry, 207, 167-182, 2001.

Warneke, C., S. L. Luxembourg, et al.: Disjunct eddy covariance measurements of oxygenated volatile organic compounds fluxes from an alfalfa field before and after cutting, J. Geophys. Res.-Atmos., 107, 2002.

White, M. L., Russo, R. S., Zhou, Y., Ambrose, J. L., Haase, K., Frinak, E. K., Varner, R. K., Wingenter, O. W., Mao, H., Talbot, R., and Sive, B. C.: Are biogenic emissions a significant source of summertime atmospheric toluene in the rural Northeastern United States?, Atmos. Chem. Phys., 9, 81-92, 2009.

Wilkinson, M.: PhD thesis, University of Lancaster, 2005.

Wilkinson, M. J., Owen, S. M., Possell, M., Hartwell, J., Gould, P., Hall, A., Vickers, C., and Hewitt, C. N.: Circadian control of isoprene emissions from oil palm (Elaeis guineensis), Plant Journal, 47, 960-968, 10.1111/j.1365-313X.2006.02847.x, 2006.

Winters, A. J., Adams, M. A., Bleby, T. M., Rennenberg, H., Steigner, D., Steinbrecher, R., and Kreuzwieser, J.: Emissions of isoprene, monoterpene and short-chained carbonyl compounds from Eucalyptus spp. in southern Australia, Atmospheric Environment, 43, 3035-3043, 10.1016/j.atmosenv.2009.03.026, 2009.

Zhao, J., and Zhang, R.: Proton transfer reaction rate constants between hydronium ion (H3O+) and volatile organic compounds, Atmospheric Environment, 38, 2177-2185, 2004.

Zorn, S. R., Drewnick, F., Schott, M., Hoffmann, T., and Borrmann, S.: Characterization of the South Atlantic marine boundary layer aerosol using an aerodyne aerosol mass spectrometer, Atmospheric Chemistry and Physics, 8, 4711-4728, 2008.

2.4 Floral estragole from oil palms – specific case

This chapter corresponds to the article led by me in a collaboration which was publish in Atmospheric Chemistry and Physics (Misztal et al., 2010; Appendix II-H). Here is only my contribution presented and therefore based mostly on PTR-MS measurement and analysis.

Others involved in the study:
CEH: Neil Cape, Sue Owen, Jambery Siong
Univerisity of Lancaster: Nick Hewitt, Annette Ryan
University of Edinburgh: Mat Heal
NCAR: Alex Guenther, Peter Harley
Oregon Institute: Rei Rasmussen
EPA USA: Chris Geron
University of Leeds: David Edwards

Table of contents

2.4.1 Abstract

During two field campaigns (OP3 and ACES), which ran in Borneo in 2008, we measured large emissions of estragole (methyl chavicol; IUPAC systematic name 1-allyl-4-methoxybenzene; CAS number 140-67-0) in ambient air above oil palm canopies (0.81 mg m^{-2} h^{-1} and 3.2 ppbv for mean midday fluxes and mixing ratios respectively) and subsequently from flower enclosures. However, we did not detect this compound at a nearby rainforest. Estragole is a known attractant of the African oil palm weevil (*Elaeidobius kamerunicus*), which pollinates oil palms (*Elaeis guineensis*). There has been recent interest in the biogenic emissions of estragole but it is normally not included in atmospheric models of biogenic emissions and atmospheric chemistry despite its relatively high potential for secondary organic aerosol formation from photooxidation and high reactivity with OH radical. We report the first direct canopy-scale measurements of estragole fluxes from tropical oil palms by the virtual disjunct eddy covariance technique and compare them with previously reported data for estragole emissions from Ponderosa pine. Flowers, rather than leaves, appear to be the main source of estragole from oil palms; we derive a global estimate of estragole emissions from oil palm plantations of ~ 0.5 Tg y^{-1}. The observed ecosystem mean fluxes (0.44 mg m^{-2} h^{-1}) and mean ambient volume mixing ratios (3.0 ppbv) of estragole are the highest reported so far. The value for midday mixing ratios is not much different from the total average as, unlike other VOCs (e.g. isoprene), the main peak occurred in the evening rather than in the middle of the day. Despite this, we show that the estragole flux can be parameterised using a combination of a modified G06 algorithm for emission and a canopy resistance approach for deposition. However, the model underestimates the afternoon peak even though a similar approach works well for isoprene. Our measurements suggest that this biogenic compound may have an impact on regional atmospheric chemistry that previously has not been accounted for in models and could become more important in the future due to expansion of the areas of oil palm plantation.

2.4.2 Introduction

Estragole or 1-allyl-4-methoxybenzene (AMOB) is an oxygenated volatile organic compound (OVOC) with molecular weight of 148 and a boiling point of 216 ºC at

atmospheric pressure, and therefore should be regarded as a semi-volatile organic compound. Although it is a C-10 compound ($C_{10}H_{12}O$) it is not classified as terpenoid because it is produced by the phenylpropanoid pathway rather than a terpenoid pathway. It has many synonyms, of which the most commonly used after estragole are methyl chavicol, p-allylanisole, isoanethole, chavicyl methyl ether or 1-methoxy-4-prop-2-enylbenzene. Estragole is the original name attributed to the compound and it is used throughout this article. It derives from "estragon", the French and German word for tarragon (*Artemesia dracunculus*), a herb to which it gives its anis-like odour.

Even though estragole was reported to be a major component of ponderosa pine emissions almost 30 years ago (Altshuller, 1983), the growing interest in this compound in the atmospheric science community has been relatively recent. The interest follows analytical improvements over the last decade which have extended biogenic emission studies to a wider variety of compounds, including estragole. Bouvier-Brown et al. (2009a) recently reported measurements of estragole emissions and ambient concentrations from ponderosa pine trees and highlighted the importance this compound might have for atmospheric chemistry. Lee et al. (2006b) found that the secondary organic aerosol (SOA) yield from full photochemical oxidation of this compound was the highest of all oxygenated terpenes (40%) and also that it was significantly higher than the SOA yield from its ozonolysis (6%) (Lee et al., 2006a). Emissions of estragole from oil palms have not yet been quantified even though, as shown later, they exceed many times those reported from other species, and thus their contribution to regional photochemistry is likely to be considerable. Estragole, like many other BVOCs, is suspected to be harmful to human health at high concentrations (EPA, 2002).

The area of oil palm (Arecaceae *Elaeis*) plantations is rapidly expanding in South East Asia, in order to meet the global demand for palm oil. Globally the land area of oil palm plantations is estimated at 13.9 million hectares, where the majority (60%) is concentrated in Malaysia (3.8 Mha) and Indonesia (4.6 Mha) (FAO, 2009). The oil palm cultivated there is usually a high yielding cross between dura and pisifera forms of *Elaeis guineensis* Jacq., which is native to tropical Africa, or hybrids of *E. guineensis* with *E. oleifera*, which is native to Latin America. Plantation area has

increased in Malaysia from 55,000 hectares in 1960, to half a million in 1975, and a million hectares were under cultivation in 1980 (Hartley, 1988). Nowadays the area is nearly 4 million ha.

It was originally thought that the oil palm is mainly wind pollinated, until Syed (1979) showed experimentally that the oil palm is mainly insect pollinated. Estragole is the known attractant for the weevil (*Elaeidobius kamerunicus* Faust) which is the specific pollinator of *Elaeis guineensis* flowers. *E. guineensis* is monoecious containing both female and male flowers on one tree which open at different times and which are pollinated all year round (Henderson, 1986; Syed, 1979; Tandon et al., 2001).This weevil responds specifically to estragole and not its derivatives, as was experimentally shown by Hussein et al. (Henderson, 1986; Syed, 1979; Tandon et al., 2001). It is not native to Borneo but was introduced from Cameroon in 1981 for the purpose of improving pollination and increasing crop yields (1989). The specificity of the pollinator and lack of predators led to a great success for the palm oil industry, saving tens of million pounds on hand pollination (Hartley, 1988). Estragole emissions are therefore of great importance to the oil palm industry.

The lifetime of estragole in the atmosphere has been estimated for temperate latitudes by Bouvier-Brown et al. (Hussein et al., 1991) as 55 min and 18 h for reaction with OH and O_3, respectively, suggesting that this compound can have an impact on regional photochemistry. Estragole oxidation is not included in the Master Chemical Mechanism (MCM)[2], nor are any other aromatic species with methoxy or 2-propenyl substituents. The reactivity of estragole to OH might be expected to be similar to that of methoxybenzene, or the methoxy-substituted aromatic ring (~3×10^{-11} cm^3 $molecule^{-1}$ s^{-1}), with the side chain reacting similarly to a terminal alkene (M.E. Jenkin, personal communication). Recently, Bouvier-Brown et al. (2009a) reported two consistent estimates for k_{OH} of 5.7×10^{-11} cm^3 $molecule^{-1}$ s^{-1} from ozonolysis studies performed by Lee et al. (2006a) and 5.4×10^{-11} cm^3 $molecule^{-1}$ s^{-1} derived using the Environmental Protection Agency's Estimation Program Interface Suite (2006a; 2006b). These are similar to the k_{OH} value for 2-methyl-3-buten-2-ol

[2] http://mcm.leeds.ac.uk/MCM/

(MBO). The same authors also estimated rate coefficients for the reaction of estragole with ozone (k_{O3}) of 1.4×10^{-17} cm^3 $molecule^{-1}$ s^{-1} and 1.2×10^{-17} cm^3 $molecule^{-1}$ s^{-1} the same experimental and modelling approaches, respectively. It would be anticipated that the initial stages of estragole degradation are efficient at generating ozone, since 1-alkenes typically have photochemical ozone creation potentials (POCP) of around 100. On the other hand, if degradation leads to compounds of structures similar to benzaldehyde or nitrophenols, then the impact on ozone formation will be near zero or negative since these compounds lead to near-irreversible sequestration of NOx and organic material into species which deposit efficiently or are incorporated into aerosol. But in that case, estragole would be expected to act as an efficient SOA precursor. In both instances estragole oxidation will likely have an impact on regional photochemistry.

In May and June 2008 measurements of VOC fluxes by virtual disjunct eddy covariance (continuous flow disjunct) were made using proton transfer reaction mass spectroscopy (PTR-MS), and were supplemented by GC-MS study (leaf level and ambient) at an oil palm plantation in Sabah, Borneo[3]. Estragole was the second most abundant BVOC (after isoprene) at the plantation and the observed concentration and fluxes are the highest reported so far from vegetation.

2.4.3 Methods

2.4.3.1 Site and setup

The experiment site was a flat 33 ha commercial oil palm plantation located at 5°14'52.67 (N) latitude and 118°27'14.96 (E) longitude within a much larger oil palm area belonging to the Sabahmas Oil Palm Plantation owned by Wilmar International Ltd. (Figure 2.4-1). This location is 28 km NE of Lahad Datu in the Malaysian province of Sabah in NE Borneo. The palms were 12 year old *E. guineensis* × *E.*

[3] Misztal, P. K., Nemitz, E., Langford, B., Coyle, M., Ryder, J., DiMarco, C., Phillips, G., Oram, D., Owen, S., Heal, M. R. and Cape, J. N.: First direct ecosystem fluxes of VOCs from oil palms in SE Asia, Atmos. Chem. Phys. Discuss., in preparation for submission, 2010

oleifera hybrids of the progeny "Gutherie", with an average height of 12 m and a single-sided leaf area index (LAI) of about 6, planted at a commercial density of 124 trees per ha. The suite of atmospheric measurements at this site and a rainforest site during OP3 and ACES measurement campaigns is summarised in the introductory paper of this issue (EPA, 2000)

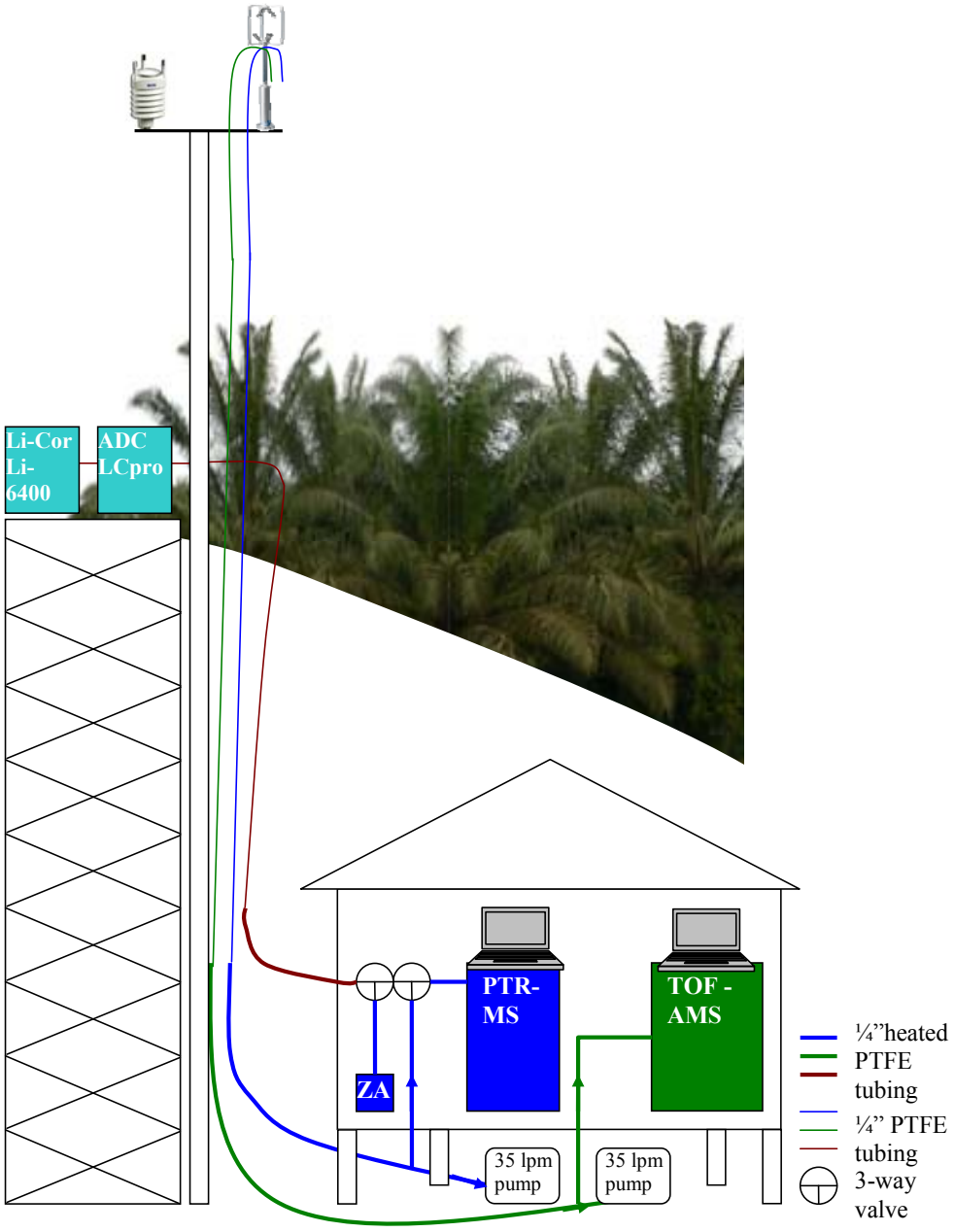

Figure 2.4-1. Schematic of the sampling setup at the Sabahmas Oil Palm plantation, Borneo. Measurements of estragole (and other VOCs) were made at canopy and leaf

level using proton-transfer-reaction mass spectrometry (PTR-MS) and leaf cuvettes (Li-COR Li-6400 and ADC LCpro). ZA refers to the zero-air (pure air) generator, and TOF-AMS refers to a time-of-flight aerosol mass spectrometer deployed at the site. In addition, a portable gas chromatograph with a mass spectrometer (Hapsite Smart, Inficon, East Syracuse NY) was used (not presented here) for ambient air and enclosure *in-situ* analysis.

2.4.3.2 Proton Transfer Reaction Mass Spectrometer (PTR-MS)

A Proton Transfer Reaction Mass Spectrometer (PTR-MS) was employed to monitor the VOC concentrations and eddy fluxes of various compounds including estragole. The PTR-MS instrument was a high sensitivity model (Ionicon Innsbruck, Austria, s/n: 04-03) incorporating an additional turbopump for the detection chamber and Teflon instead of Viton rings in the drift tube. In addition in our instrument the Pfeiffer turbopumps have been replaced by their Varian analogues. Operational details have been described elsewhere (Hewitt et al., 2009), and very recently the PTR-MS technique has been reviewed by Blake et al.(e.g. de Gouw et al., 2003; Lindinger et al., 1998), hence only a brief description is presented here. The VOCs under study, whose proton affinities exceed that of water, are soft-ionised in a drift tube by collision with hydronium ions, formed in the hollow cathode of the ion source. The products of the proton transfer reactions are either protonated compounds or their protonated fragments or clusters. The magnitude of fragmentation/clustering can be optimised by adjusting the electric field (E) and the buffer gas number density (N) in the drift tube, so that the E/N ratio is most commonly in the range of 120-140 Td (1 Td = 10^{-17} V cm^2). The relative abundance of the product cations, separated by the quadrupole mass filter, can be derived from the number of pulses counted by the Secondary Electron Multiplier (SEM) during a given dwell time. During the PTR-MS measurements at the plantation the E/N ratio was kept constant at 140 Td by adjusting drift tube parameters of pressure to 160 Pa, temperature to 45 °C and the drift voltage to 485 V. The sampling inlet and the 20 Hz sonic anemometer (Solent R3, Gill Instruments) were placed above the canopy at about 15 m. A 20 m PTFE sampling line (1/4'' OD, 3/16'' ID) was used to draw a

flow rate of 35 L min^{-1} past the instrument, which sub-sampled at a flow rate of 400 mL min^{-1}. The instrument and PTFE tubing were protected against water condensation by heating above the ambient temperature (approx. 50 ºC) using a heating tape. In order to get absolute volume mixing ratios, either calibration with an external standard is required, or less precise calculation can be made based on the calibrated transmission of the instrument and the proton transfer reaction rate of estragole. As no estragole calibration standard was available for PTR-MS at the site, the instrument was calibrated against several other VOCs (i.e. methanol, acetonitrile, acetone, acetaldehyde, isoprene, a monoterpene: d-limonene) and then the relative transmission curve was obtained to yield an empirical calibration coefficient for estragole (method described by Taipale et al., (2009)).

The biggest advantage of PTR-MS is the high frequency of data acquisition, which makes it suitable for use in micrometeorological flux measurement techniques such as eddy covariance (EC). Here, data were processed according to the virtual disjunct eddy covariance concept (2008), where for each *m/z* of interest the PTR-MS makes a measurement which is sufficiently fast (as determined by the dwell and instrument response time), but discontinuous (while the PTR-MS scans the other *m/z* of interest), thus providing fewer data points than continuous EC. For the flux mode the instrument was running in the multiple ion detection (MID) for 25 minutes every half hour cycling through 13 m/z channels including estragole and remaining 10 VOC-related protonated masses analysed at 0.5-s dwell time each, whereas a shorter 0.2 s dwell time was used for the hydronium ($H_3{}^{18}O^+$) ions measured at m/z 21 and water clusters $(H_2O)H_3O^+$ measured at m/z 37. This corresponded to a cycle length of 7 s with 210 PTR-MS and 30 000 wind rows in 25 min. The effective time lag associated with the residence time in the tubing was calculated from the cross-correlation between vertical wind speed and the VOC mixing ratio as a function of lag time (Karl et al., 2002; Rinne et al., 2001). If no true peak was present in the covariance function, or if it was smaller than the detection limit derived by multiplying the standard deviation of the noise over 180 s by 1.5, or if the lag time was not stable during an averaging period (25 min), then the flux data point was discarded. In addition, the data were filtered for stationarity using the criterion of Foken and Wichura (Davison et al., 2009; Langford et al., 2009; Rinne et al., 2007;

Spirig et al., 2005) , for low friction velocity (u_* < 0.15 m s^{-1}), and for rain events. More than one fifth of the data for estragole flux passed all these validation criteria. In order to assess the likely impact on the representativeness of the timeseries which followed the rejections, the volume mixing ratio (VMR) data corresponding to rejected flux periods was compared with the full VMR timeseries. Although their diurnal average pattern became noisier as a result of those rejections (as later shown in Fig. 2.4-3), the total average VMR did not change by more than 0.1%.

Estragole is detected at *m/z* 149 in PTR-MS as the protonated molecular ion. It was measured for the first time with PTR-MS in ambient air by Holzinger et al. (1996). This compound is relatively resistant to fragmentation at typical working conditions, with only small fragmentation to *m/z* 121, and thus PTR-MS can be used reliably for monitoring its concentrations and fluxes. There are only a few known minor contributions to *m/z* 149 from other compounds that have been reported so far, of which the most significant are from sesquiterpenes (2005). When the volume mixing ratio of sesquiterpenes relative to estragole is very low, one can assume these contributions to be insignificant. In addition, a GC-MS was used to check the ambient air for any interference with the *m/z* 149 signal. Fluxes of other compounds measured with the PTR-MS at the oil palm plantation included isoprene, total monoterpenes and methanol. These results are presented in a separate paper (Misztal et al., 2010)[4] and chapter 2.3 of this thesis.

2.4.3.3 Parameterisations for Estragole emission and deposition

There are many algorithms for modelling foliar emissions of BVOCs, some of which have been incorporated into models such as MEGAN (Bouvier-Brown et al., 2007; Bouvier-Brown et al., 2009b; Helmig et al., 2006; Kim et al., 2008). The potential importance of floral emissions for atmospheric chemistry was recognized by Arey et al. (1991) who report linalool concentrations in an orange tree plantation that are of a

[4] Misztal, P. K., Nemitz, E., Langford, B., Coyle, M., Ryder, J., DiMarco, C., Phillips, G., Oram, D., Owen, S., Heal, M. R. and Cape, J. N.: First direct ecosystem fluxes of VOCs from oil palms in SE Asia. Atmos. Chem. Phys. Discuss., in preparation for submission 2010

similar magnitude to the estragole concentrations observed in this study. However, floral emissions have not been included as a component of regional biogenic emission models due to both the limited quantitative emission rate data and the lack of suitable driving parameters. As a result, it is not known what contribution they make to canopy emission. However, oil palms occupy a large land area, and as we show, the contribution of estragole emissions to total BVOCs can be very high. The actual estragole release and its magnitude are likely to be constrained by biological factors related to the pollination cycle. Temperature of vegetative surfaces can be different from ambient temperature above the canopy, and therefore it is important to use the former in the parameterisations.

Canopy temperature (T_c), as estimated from the resistance approach (Equation 2.4-1), was generally higher by approximately 2 °C during midday and lower by 0.2 °C during the night than T_a (the ambient temperature at the 15 m sensor height).

$$T_c = T(z'_0) = T_a(z_m) + \frac{H(R_a(z_m) + R_b)}{\rho c_p}$$

Equation 2.4-1

Here H is the sensible heat flux, $R_a(z_m)$ is the aerodynamic resistance, R_b is the laminar boundary layer resistance close to the surface of the leaves, ρ is air density, and c_p is the specific heat of air.

Since estragole may also exhibit occasional deposition, for the highest accuracy atmospheric models would either need to consider this as a loss of part of the emission flux or by including this compound in deposition models. The available data for validated measured deposition are insufficient for the implementation of the canopy resistance analogy (Guenther et al., 2006), in which the overall modelled flux is represented as:

$$F_{net} = F^{+} - V_d(z)\,\chi(z_m)$$

Equation 2.4-2

where F_{net} is the net flux above the canopy, F^{+} is the parameterised emission from the vegetation, $V_d(z)$ is the parameterised deposition velocity, and $\chi(z_m)$ is the concentration measured. For this modelling exercise we limit the investigation only to modelling emission flux (F^{+}) (Equation 2.4-3) and we neglect deposition ($- V_d(z)\,\chi(z_m)$), which is likely to be minor in relation to the emission of estragole.

$$F^{+} = \mathrm{BER_c} \cdot \gamma_T \cdot \gamma_P$$

Equation 2.4-3

$\mathrm{BER_c}$ is the canopy-derived basal emission rate (for standard conditions) which can be obtained from Eq. (2.4-3) by substituting F^{+} with the eddy covariance flux above the canopy (filtered to exclude deposition periods), γ_T and γ_P are the temperature and PAR activity factors, respectively, compensating for changes in emission due to deviations from standard conditions:

$$\gamma_P = C_P\left[\left(\alpha \cdot \mathrm{PAR}\right)/\left(\sqrt{1+\alpha^2 \cdot \mathrm{PAR}^2}\right)\right]$$

Equation 2.4-4

$$\gamma_T = E_{\mathrm{opt}} \cdot \frac{\mathrm{C}_{T2} \cdot \exp\left[\mathrm{C}_{T1} \cdot \left(\frac{1}{T_{\mathrm{opt}}} - \frac{1}{T}\right) \cdot \frac{1}{0.00831}\right]}{\mathrm{C}_{T2} - \mathrm{C}_{T1} \cdot \left[1 - \exp\left(\mathrm{C}_{T2} \cdot \left(\frac{1}{T_{\mathrm{opt}}} - \frac{1}{T}\right) \cdot \frac{1}{0.00831}\right)\right]}$$

Equation 2.4-5

where C_P, α, E_{opt}, and T_{opt} can be expanded further:

$$\alpha = \mathrm{b}_1 - \mathrm{b}_2 \ln(P_{240})$$

Equation 2.4-6

$$C_P = \mathrm{b}_3 \cdot \exp\left[\mathrm{b}_2 \cdot \left(P_{24} - P_0\right) \cdot \left(P_{240}\right)^{0.6}\right]$$

Equation 2.4-7

$$T_{\mathrm{opt}} = \mathrm{T_b} + \left[\mathrm{b}_4 \cdot \left(T_{240} - 297\right)\right]$$

Equation 2.4-8

$$E_{\mathrm{opt}} = \mathrm{b}_5 \cdot \exp\left[\mathrm{b}_6 \cdot \left(T_{24} - 297\right)\right] \cdot \exp\left[\mathrm{b}_6 \cdot \left(T_{240} - 297\right)\right]$$

Equation 2.4-9

In the above equations PAR and T are photosynthetically active radiation (μmol m^{-2} h^{-1}) and leaf temperature (K), respectively. The latter was approximated by deriving T_c (Equation 2.4-1). The 24 and 240 subscripts correspond to 24-hour and 240-hour averages, respectively. CT1, CT2, T_b and $b_1 \ldots b_6$ are the empirical constants.

In the formalism of the G06 algorithm (Nemitz et al., 2009; Sutton et al., 1995), F^+ (Equation 2.4-3) is a function of the lag-adjusted ambient temperature (T) and photosynthetically active radiation (PAR). The G06 algorithm is an advanced emission model simulating direct canopy scale emission (mg m^{-2} h^{-1}) rather than the emission per dry leaf mass, as it has an integrated canopy environmental model. The G06 algorithm for isoprene is essentially similar to the earlier Guenther algorithms (Guenther et al., 2006), except that many empirical parameters, which used to have prescribed constant values (e.g. C_P, α, E_{opt} and T_{opt}) have been expanded to contain more parameters specific to the simulation of variations in isoprene emission in response to previous PAR and temperature history, which is related to the changes in enzyme-driven substrate synthesis for isoprene and phosphorylation dependent on ATP availability. The actual parameters in the original model derive from a number of measurements, where isoprene light and temperature responses as affected by many factors (PAR and temperature history, response to CO_2 or ozone, and enzymatic kinetics) were studied (Guenther et al., 1999; Guenther et al., 1995; Guenther et al., 1993). Because of such diversity in empirical parameters this algorithm has many degrees of freedom, which was one of the reasons for its choice for fitting the measured estragole canopy flux. Since no light and temperature responses to estragole floral emissions are available, the parameters were constrained to a restricted range, so the fitted values of these parameters should be treated with caution in inferring any physiological significance.

Although the formalism of the Guenther et al. (2006) approach has been adopted, the fitted empirical constants were derived from the measurement data for estragole eddy covariance fluxes at the site. The Equations. (2.4-3 – 2.4-9) were merged into one large equation and overall 10 empirical constants were optimised using the estragole flux data in order to achieve the best fit. The comparison between original and modified parameters is given in Table 2.4-3.

2.4.4 Results and discussion

2.4.4.1 Estragole mixing ratios

2.4.4.1.1 Specificity for oil palm and screening for anisoles

Estragole, being p-allyl-anisole, belongs to the family of anisole compounds whose structure includes a methoxy group attached to a benzene ring. Emission of aromatic compounds from vegetation, although very interesting biochemically, is still not well represented in published data, but includes reports of biogenic emissions of typical anthropogenic compounds like toluene (e.g. Geron et al., 2000; Hanson and Sharkey, 2001; Monson et al., 1994; Petron et al., 2001; Sharkey et al., 1999). During measurements in Borneo, estragole was only found at the oil palm plantation, and it was not detected either above a rainforest canopy or in the screening of individual tree foliage in a jungle. In fact, in the rainforest, anisole and many of its derivatives (e.g. p-vinyl-anisole, p-ethyl-anisole, p-ethylene-anisole) were detected lower in the canopy by PTR-MS, but not p-allyl-anisole (estragole), neither below nor above canopy.

By comparison, in the oil palm ambient air, estragole, but none of its derivatives, was the second most abundant measured VOC after isoprene. It is worth noting that the high abundance of estragole in the ambient air above the oil palm canopy was recorded by both PTR-MS and GC-MS, while the leaf-cuvette study detected only very small concentrations of estragole and in only a few percent of the samples. This clearly indicates that estragole is not primarily emitted by the fronds, but almost certainly is released by the flowers, which is not surprising, given its role in pollination. As leaf surfaces can adsorb and store significant amounts of deposited gases (Heiden et al., 1999) it is likely that small emissions from fronds are secondary to previous deposition, which was quite frequent for this semi-volatile compound. Due to the fact that sampling was not directly from the flowers, one might argue about possibly different sources (e.g. fruit, stems, etc.). Nevertheless, estragole has an intense aniseed scent and from observation of the weevil's role in pollination it seems apparent that it is attracted to the flower (Binnie et al., 2002). Neither fruit nor leaves had an obvious smell of aniseed.

2.4.4.1.2 Diurnal cycles

The time series for estragole mixing ratios recorded by PTR-MS is shown in Figure 2.4-2 and the diurnal average is presented in Figure 2.4-3a in comparison with temperature and PAR. In addition, the box-and-whisker plot in Figure 2.4-3b illustrates its day-to-day variability. As most insects avoid tropical heat, the synergy of estragole maximum release with the likely feeding/pollinating time of the insect can be seen in the estragole diurnal cycles, which moderately correlate with temperature corrected by a lag of ~3.5 h, suggesting a short-term storage pool in the plant before release a few hours later. It is possible that estragole accumulates later in the evening in the collapsing boundary layer, but its flux is not picked up by the eddy covariance flux due to insufficient turbulence at those times.

The estragole mixing ratio from PTR-MS was moderately correlated with the 3.5 h lag-adjusted temperature (r^2 = 0.4) and the 4.5 h lag-adjusted PAR (r^2 = 0.34), but without a lag correction no correlations were found. This is different for the case of other VOCs (e.g. isoprene), whose responses to temperature (or PAR) were almost instantaneous. Based on the mass scan (*m*/*z* 21-205) performed on the PTR-MS every hour the highest correlations between estragole normalised signal at *m*/*z* 149 were found with *m*/*z* 95 (r^2 = 0.38), *m*/*z* 75 (r^2 = 0.33), *m*/*z* 47 (r^2 = 30) and *m*/*z* 121 (r^2 = 0.24), which could be due to internal fragmentation. There were also weak correlations with some other *m/z* representing biogenic compounds (r^2 < 0.2). The latter would be higher after applying the time lag of 3.5 h.

It is common for some fragmenting compounds (e.g. isoprene) to deviate from the relative transmission curve but it was assumed that fragmentation of estragole was not significant. The uncertainty of such empirical sensitivity approach lies between the error of calibration with a standard (typically 5-10%) and the error of deriving the mixing ratios from drift tube reaction kinetics and proton transfer reaction rate constants (up to 100%) (Mahbob, 2008) and was estimated at 30% by Taipale et al. (2008).

Table 2.4-1. Intercomparison of estragole volume mixing ratios.

Site/ date / source	PTR-MS (ambient 15 m)	GC-MS (flower enclosure) *enclosures done by Dave Edwards GC-MS analysis by Sue Owen and the author*	GC-MS (ambient) *data from Alex Guenther*	GC-MS (leaf) *data from Sue Owen*	PTR-MS/GC-MS/TAG (9.3 m above the ground)
Borneo (Oil palm) / 29-05-2008 – 11/06/2008 (e.g. Steinbacher et al., 2004)	3.0[a] ppbv (3.0[b] ppbv)				
Borneo (Oil palm) / 25-05-2008 (Misztal et al., 2010; Appendix II-H)			1.2 ppb (morning 9:00 to 10:00) 3.0 ppb (early afternoon 12:00 to 14:00) 3.8 ppb (late afternoon 14:00 to 16:00)	< 0.2 ppbv	
Blodget Forest (ponderosa pine)/ (Bouvier-Brown et al., 2009a; Bouvier-Brown et al., 2009b)					few pptv – 0.5 ppbv
Borneo (Oil palm)/ 15/5/2009 – 17/5/2009 / (Misztal et al., 2010; Appendix II-H)		Female flowers ~0.26–1.39 ppm[c] (60 ppm[c]) Male flowers ~ 150 ppb			

[a]mean over the measurement period (N=537) [b]if only the VMR points corresponding to periods of validated flux were taken into account (N=109), [c]accumulated in the enclosure (~40L headspace); [c]it might be possible that the tube touched the flower;

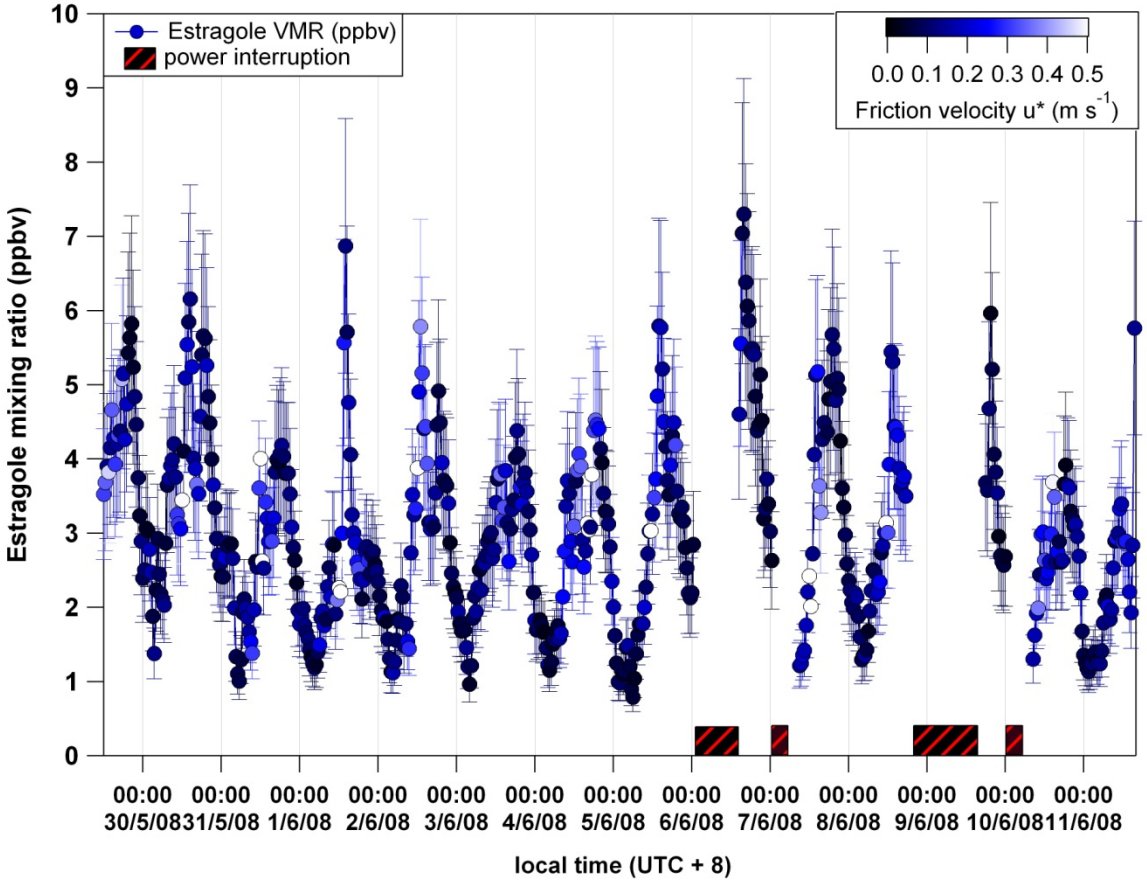

Figure 2.4-2 Time-series of volume mixing ratios (ppbv) of estragole measured by PTR-MS above the oil palm canopy (local time [UTC + 8]). The dots are coloured by friction velocity (u^*) to show that potentially large fluxes likely occurring later in the day could be missed out in eddy covariance because of low values of u^* (corresponding to black - dark blue). Error bars denote an estimated 30% error in obtaining VMRs using an empirical sensitivity derived from relative transmission (see chapter 2.4.3 above).

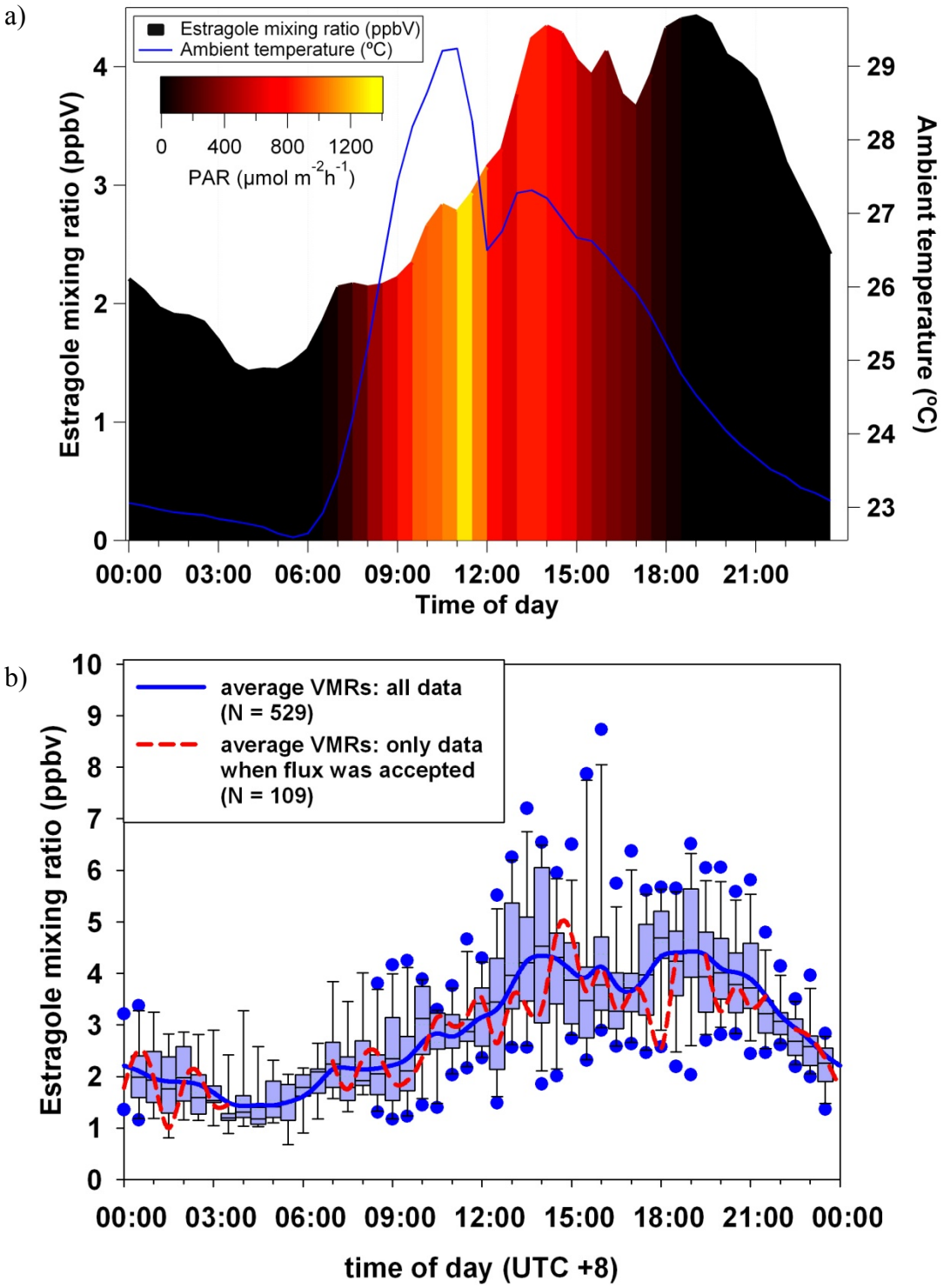

Figure 2.4-3 Average diurnal cycles of estragole mixing ratios (left axis): a) average in relation to temperature (right axis) and PAR (colour scale); b) Box-and-Whisker plot of day-to-day variability, showing averages (blue line), median with 25th and 75th percentile (box), 5th and 95th percentiles (whiskers) and outliers (dots).

2.4.4.2 Estragole fluxes

Previous PTR-MS measurements over Ponderosa pines (*Pinus ponderosa)* showed concentrations of extragole to correlate closely with 2-methyl-3-butenol (MBO) (Misztal et al., 2010). However, MBO was not observed at the oil palm plantation, implying different biochemistries of conifer leaf and oil palm floral emissions. Therefore the method suggested by Bouvier-Brown et al. (Bouvier-Brown et al., 2009a; Bouvier-Brown et al., 2009b; Holzinger et al., 2005) for inferring estragole emissions from correlations with MBO is not applicable for oil palm. A comparison of fluxes reported from other environments is shown in Table 2.4-2. The observed fluxes above oil palms are the highest reported so far, and for the first time reported from tropical oil palms. The flux time series is presented in Figure 2.4-4 in relation to canopy temperature (T_c), which is the most likely driver for estragole emission (or deposition). Estragole net emission can be decreased by periods of estragole deposition, which can be affected by delayed temperature response, and local gradients caused by possibly slightly different release times of particular inflorescences. Night time emission and deposition are uncertain as the flux was generally below the detection limit and the turbulence was insufficient (small u_*). However, the small estragole concentrations observed in the shallow night-time boundary layer confirm that night-time emissions are very small. The highest fluxes were normally observed during the middle of the day, peaking at approximately 2 mg m^{-2} h^{-1}. There were also periods of apparent deposition for estragole, which is, however, less certain being often at the edge of the rejection thresholds and could be driven by varying gradients caused by different opening times of male and female flowers. On the averaged diurnal graph (Figure 2.4-5a) one can see the estragole flux in comparison with T_c and PAR (on the colour scale). Although in the mixing ratios there was a delayed correlation observed with temperature, it seems that there is not a large shift in the flux compared with the T_c but the afternoon peak is disproportionally higher in relation to T_c and PAR This is because most of the flux is transported by turbulent eddies, and thus as soon as mixing within the PBL decreases it appears that there is an accumulation of estragole, which slowly decays overnight.

.

Table 2.4-2 Comparison of estragole fluxes

Site/ date / source	PTR-MS vDEC (ambient 15 m)	GC-MS (flowers) *enclosure by David Edwards; analysis by Sue Owen and the author*	GC-MS (fronds) *data from Alex Guenther*	GC-FID and PTR-MS (branch level)
Borneo (Oil palm) / 29-05-2008 – 11/06/2008 (Misztal et al., 2010; Appendix II-H)	0.81[a] mg m^{-2} h^{-1} 0.44[b] mg m^{-2} h^{-1}			
Borneo (Oil palm) / 25-05-2008 (Misztal et al., 2010; Appendix II-H)			~ 1 µg g^{-1} h^{-1}	
Blodget Forest (ponderosa pine)/ (2009a)				0.20[c] mg m^{-2} h^{-1}
Borneo (Oil palm)/ 15/52009 – 17/5/2009 (Misztal et al., 2010; Appendix II-H)		Female flowers ~ 0.2 mg m^{-2} h^{-1} [d]		

[a]mid-day mean 10:00 – 14:00 (N = 26); [b]24-h average of 12 days of validated flux (N =109) [c]converted from basal rate of 1.37 µmol m^{-2} hr^{-1} (Bouvier-Brown et al., 2009b); [d]expected to be underestimated; the value was estimated assuming 150 trees ha^{-1} average global density although the actual density at the site was smaller (124 trees ha^{-1})

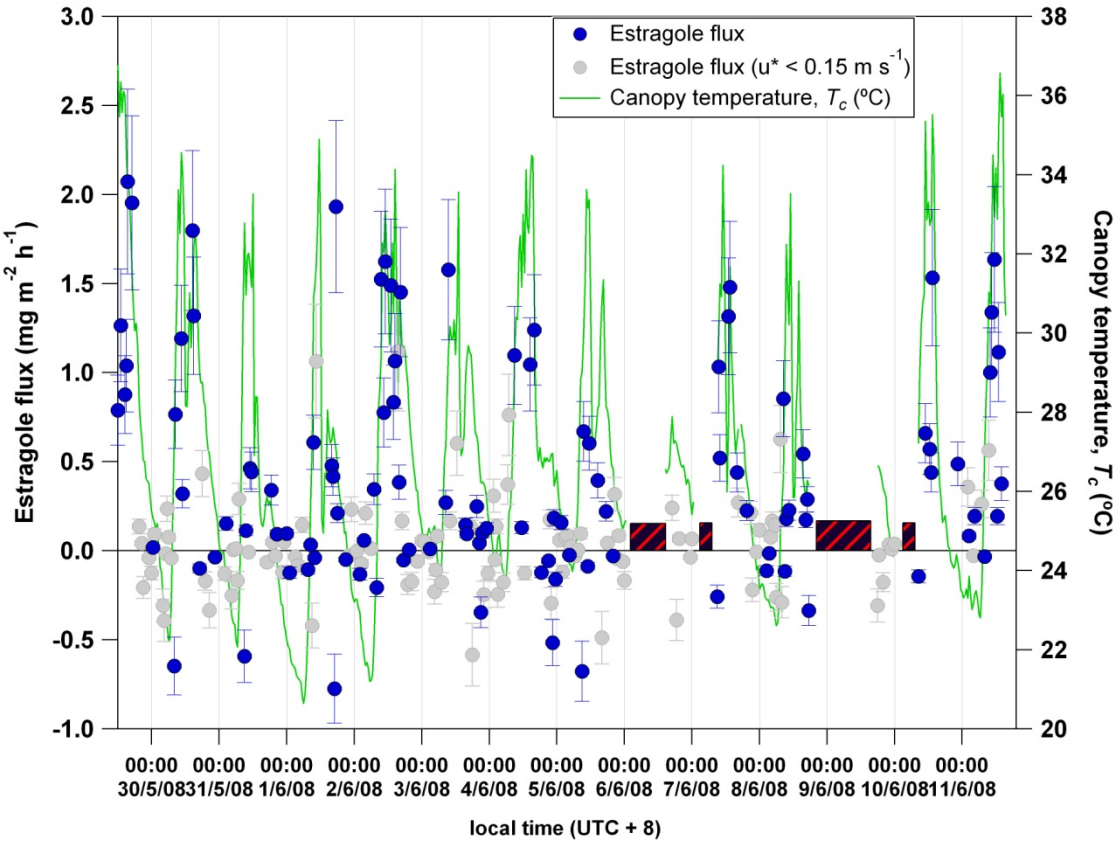

Figure 2.4-4. Estragole flux with uncertainty bars, and Canopy temperature.

However, also because of the laminar conditions it is possible that the true flux at night time might not be captured by eddy covariance. It would be interesting to study if estragole can be taken up by palms during the night, whether it can penetrate into the soil, and to better understand its ventilation and chemistry at night. The Box-and-Whisker plot in Figure 2.4-5b shows high day-to-day variability, probably due to periods of deposition but also because the strength of the particular flower sources operating in a 5 day pollination cycle (Bouvier-Brown et al., 2009a) can be varied as more flowers, on the spikelets /inflorescences, are becoming active/inactive.

a)

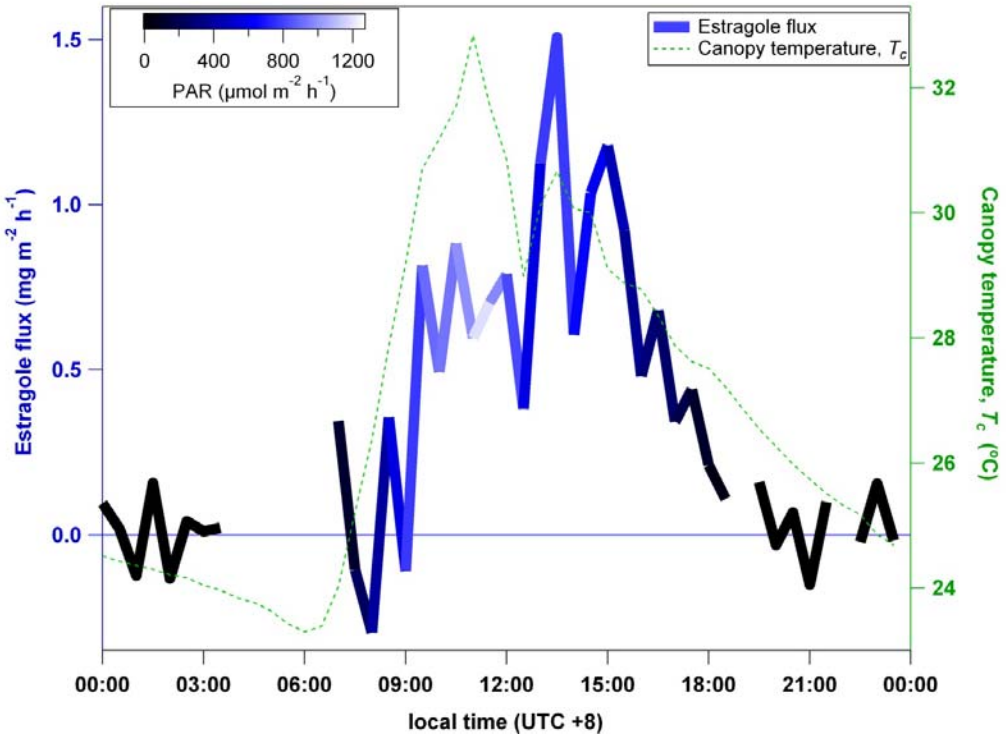

b)

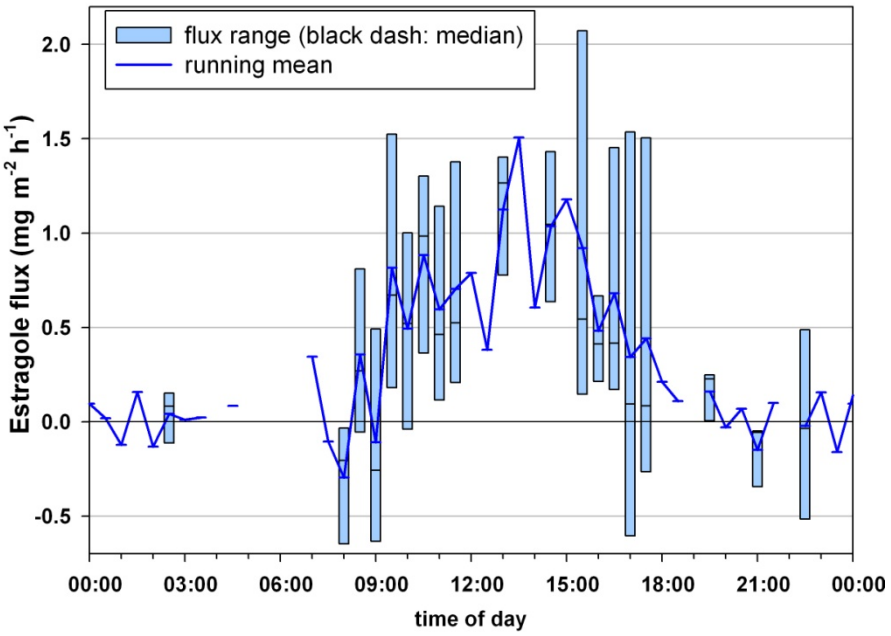

Figure 2.4-5. Average diurnal cycles of the estragole flux: a) in comparison with canopy temperature (right axis), and shaded by PAR; b) Box-and-Whisker plots showing day-to-day variability.

2.4.4.2.1 Contribution of estragole from oil palms to global emissions

The 24-hour average canopy flux of estragole for the period 29/05 – 11/06/2008 (12 days of measurement) including both emission and deposition was 0.44 mg m^{-2} h^{-1}. Given the total area of oil palm plantations worldwide of 13.9 million hectares (Syed, 1979) and assuming that this net flux is representative for the annual average (oil palms produce flowers and fruit all year) this average flux would yield 535 Gg (10^9 g) of globally emitted estragole per year, with the regional 60% contribution for Indonesia and Malaysia of 321 Gg y^{-1}. This is a very large flux in terms of regional contribution, and probably the highest global floral emission source, which is however three orders of magnitudes lower than estimates of global isoprene emission.

2.4.4.2.2 Parameterisations for estragole flux

It is worth noting the uniqueness of estragole emissions, for example in comparison with isoprene, which was the most abundant BVOC at the plantation and whose response to temperature and PAR was instantaneous rather than delayed. In Figure 2.4-6 the ratio of estragole to isoprene flux is presented on a diurnal graph, which shows the dominance of isoprene emissions during midday, whereas estragole flux takes over after about 15:30 LT.

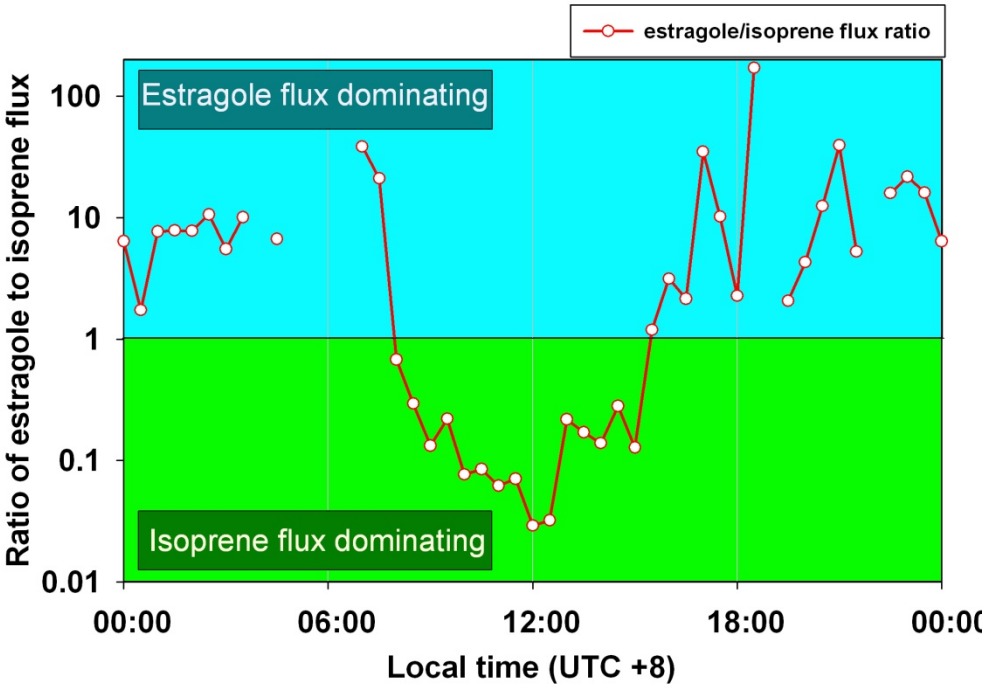

Figure 2.4-6. Diurnal trend of the ratios of estragole to isoprene flux, showing the morning and afternoon times when estragole flux dominated over the isoprene flux, which was very high during the day. The fluxes of these two compounds had similar values at around 0800 and 1530 h local time (UTC + 8)

This skewness of estragole emission response to PAR and temperature towards later in the day placed severe constraints on the parameterisation using empirical method such as the G06 algorithm. The modelled emission and total flux are compared with measured flux in Fig. 9. The modelled flux was derived as described in Sect. 2.5 with the fitted parameters given in Table 3. The overall average of modelled total flux amounted to 0.48 mg m^{-2} h^{-1} which is only smaller by 0.04 mg m^{-2} h^{-1} than the actual measurement. Although the parameterised emission for isoprene gave an almost identical fit with measurements above the canopy[5], the same parameterisation for estragole was unable to fully resolve the late peak of emissions, which is underestimated. Nevertheless, bearing in mind that flowers are governed by different,

[5]Misztal, P. K., Nemitz, E., Langford, B., Coyle, M., Ryder, J., DiMarco, C., Phillips, G., Oram, D., Owen, S., Heal, M. R. and Cape, J. N.: First direct ecosystem fluxes of VOCs from oil palms in SE Asia, Atmos. Chem. Phys. Discuss., in preparation for submission, 2010

often complex, mechanisms from leaves with stomata (e.g., different production, mechanical release), the overall agreement is rather impressive. This could be further improved if the model was adjusted to contain other factors such as thermogenesis.

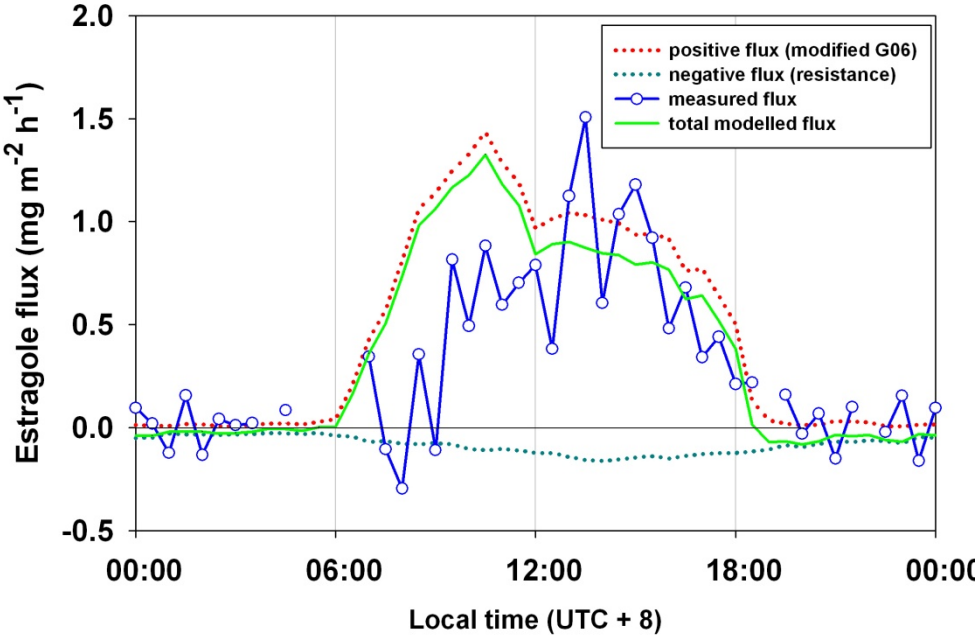

Figure 2.4-7. Diurnal patterns for measured estragole flux (solid blue) in relation to modelled emission by modified G06 (dotted red), modelled deposition using the resistance approach (dotted cyan) and total modelled flux (solid green). The current G06 algorithm is unable to accurately represent the second peak of estragole (occurring at 1300-1800 h), which could be due to possible thermogenesis and/or specific circadian control of emission.

Table 2.4-3Comparison of empirical constants between G06 for isoprene and modified G06 for estragole.

Parameter	Type of activity factor	Original G06 for isoprene	Modified G06 for estragole
C_{T1} (eq. 5)	γ_T	95	131
C_{T2} (eq. 5)	γ_T	230	542
b_1 (eq. 6)	γ_P	0.004	0.031
b_2 (eq. 6,7)	γ_P	0.0005	0.0030
b_3 (eq. 7)	γ_P	0.0468	0.0453
b_4 (eq. 8)	γ_T	0.6	-0.32
b_5 (eq. 9)	γ_T	2.034	1.812
b_6 (eq. 9)	γ_T	0.05	-0.21
T_b (eq. 8)	γ_T	313 K	307 K
P_0 (eq. 7)	γ_P	200 µmol m^{-2} s^{-1} (sun leaves) 50 µmol m^{-2} s^{-1} (shade leaves)	200 µmol m^{-2} s^{-1}

It is possible that inflorescences of *E. guineensis* are thermogenic as has been reported for other oil palm species (FAO, 2009). Thermogenesis presumably helps to volatilise floral scents (in this case estragole) and serves as a cue for pollinators (Knudsen et al., 2001). However, although not explicitly tested during this study, thermogenic volatilisation after the decrease in ambient temperature could explain the delayed peak of estragole concentrations with temperature (Ervik et al., 1999).

2.4.5 Conclusions

Using data from this study it is estimated that approximately 500 Gg of estragole are emitted from oil palm plantations annually. Although three orders of magnitude less than global isoprene emissions from vegetation, these estragole emissions are probably the highest single floral contribution of reactive carbon to global atmospheric chemistry. Estragole is probably present also in the particle phase as

well as the gas phase and is also subject to deposition as well as emission. Since estragole emissions are likely to make a regionally-important contribution to BSOA, whether by directly partitioning into the aerosol phase or after reacting to more condensable oxidation products, it is possible that estragole emissions may have an important influence on regional climate. Although the processes driving floral emissions are less well understood than for foliar emissions, we have shown that the former can also be described by a Guenther-type algorithm.

A number of uncertainties accompany the above conclusions, including: a comparatively short measurement period; not always the same period of measurement for the different techniques; seasonal variations in emissions; calibration precision; flux errors; and influence of high humidity on measurement sensitivity. Despite these caveats, it is estimated that the overall measurement error should be within a factor of 2 for the PTR-MS concentrations and fluxes, smaller for the *in situ* GC-MS results, but much larger for data from the enclosures. Clearly, more research is required to understand the mechanisms of estragole formation, its biotic and abiotic controls, and to quantify its emission rates from other tropical species.

2.4.6 Acknowledgements

This work was funded by the UK Natural Environment Research Council (NERC) through the ACES (Aerosol Coupling in the Earth System) project of the APPRAISE (Aerosol Properties PRocesses and InfluenceS on the Earth's climate) research programme. Pawel Misztal thanks his supervisors J. Neil Cape and Mathew R. Heal, and the Centre for Ecology & Hydrology and the School of Chemistry, University of Edinburgh, for funding his PhD. We are grateful to the Sabahmas Plantation of PPB Oil Palms Bhd., and in particular to Mr. Foo Koh Kei (senior manager) and Mr. Chang Sip Woon (group manager) for the provision of lodging, transport and site infrastructure. This is paper number 505 of the Royal Society's South East Asian Rainforest Research Programme.

2.4.7 References

Altshuller, A. P.: Review - Natural volatile organic-substances and their effect on air-quality in the United-States, Atmospheric Environment, 17, 2131-2165, 1983.

Binnie, J., Cape, J. N., Mackie, N., and Leith, I. D.: Exchange of organic solvents between the atmosphere and grass - the use of open top chambers, Science of the Total Environment, 285, 53-67, 2002.

Blake, R. S., Monks, P. S., and Ellis, A. M.: Proton-Transfer Reaction Mass Spectrometry, Chemical Reviews, 109, 861-896, doi:10.1021/cr800364q, 2009.

Bouvier-Brown, N. C., Holzinger, R., Palitzsch, K., and Goldstein, A. H.: Quantifying sesquiterpene and oxygenated terpene emissions from live vegetation using solid-phase microextraction fibers, Journal of Chromatography A, 1161, 113-120, 2007.

Bouvier-Brown, N. C., Goldstein, A. H., Worton, D. R., Matross, D. M., Gilman, J. B., Kuster, W. C., Welsh-Bon, D., Warneke, C., de Gouw, J. A., Cahill, T. M., and Holzinger, R.: Methyl chavicol: characterization of its biogenic emission rate, abundance, and oxidation products in the atmosphere, Atmos. Chem. Phys., 9, 2061-2074, 2009a.

Bouvier-Brown, N. C., Holzinger, R., Palitzsch, K., and Goldstein, A. H.: Large emissions of sesquiterpenes and methyl chavicol quantified from branch enclosure measurements, Atmospheric Environment, 43, 389-401, 10.1016/j.atmosenv.2008.08.039, 2009b.

Davison, B., Taipale, R., Langford, B., Misztal, P., Fares, S., Matteucci, G., Loreto, F., Cape, J. N., Rinne, J., and Hewitt, C. N.: Concentrations and fluxes of biogenic volatile organic compounds above a Mediterranean macchia ecosystem in western Italy, Biogeosciences, 6, 1655-1670, 2009.

de Gouw, J., Warneke, C., Karl, T., Eerdekens, G., van der Veen, C., and Fall, R.: Sensitivity and specificity of atmospheric trace gas detection by proton-transfer-reaction mass spectrometry, International Journal of Mass Spectrometry, 223-224, 365-382, 2003.

Test Plan for Estragole: http://www.epa.gov/HPV/pubs/summaries/estragole/c14022tp.pdf, access: 21/04/2009, 2002.

Ervik, F., Tollsten, L., and Knudsen, J. T.: Floral scent chemistry and pollination ecology in phytelephantoid palms (Arecaceae), Plant Syst. Evol., 217, 279-297, 1999.

FAOSTAT Online Statistical Service. Item: Oil palm fruit; element: area harvested; year: 2007; country: World, South East Asia, Malaysia, Indonesia. http://faostat.fao.org (Accessed April 2009) http://faostat.fao.org, 2009.

Foken, T., and Wichura, B.: Tools for quality assessment of surface-based flux measurements, Agric. For. Meteorol., 78, 83-105, 1996.

Geron, C., Guenther, A., Sharkey, T., and Arnts, R. R.: Temporal variability in basal isoprene emission factor, Tree Physiol., 20, 799-805, 2000.

Guenther, A., Hewitt, C. N., Erickson, D., Fall, R., Geron, C., Graedel, T., Harley, P., Klinger, L., Lerdau, M., McKay, W. A., Pierce, T., Scholes, B., Steinbrecher, R., Tallamraju, R., Taylor, J., and Zimmerman, P.: A global-model o fnatural

volatile organic-compound emissions, J. Geophys. Res.-Atmos., 100, 8873-8892, 1995.

Guenther, A., Baugh, B., Brasseur, G., Greenberg, J., Harley, P., Klinger, L., Serça, D., and Vierling, L.: Isoprene emission estimates and uncertainties for the Central African EXPRESSO study domain, J. Geophys. Res., 104, 30625-30639, 10.1029/1999jd900391, 1999.

Guenther, A., Karl, T., Harley, P., Wiedinmyer, C., Palmer, P. I., and Geron, C.: Estimates of global terrestrial isoprene emissions using MEGAN (Model of Emissions of Gases and Aerosols from Nature), Atmos. Chem. Phys. Discuss., 6, 107-173, 2006.

Guenther, A. B., Zimmerman, P. R., Harley, P. C., Monson, R. K., and Fall, R.: Isoprene and monoterpene emission rate variability - model evaluations and sensitivity analyses, J. Geophys. Res.-Atmos., 98, 12609-12617, 1993.

Hanson, D. T., and Sharkey, T. D.: Rate of acclimation of the capacity for isoprene emission in response to light and temperature, Plant Cell Environ., 24, 937-946, 2001.

Hartley, C. W. S.: The oil palm (*Elaeis guineensis* Jacq.), 3rd ed., Tropical Agriculture Series, Longman Scientific & Technical, Harlow, 1988.

Heiden, A. C., Kobel, K., Komenda, M., Koppmann, R., Shao, M., and Wildt, J.: Toluene Emissions from Plants, Geophys. Res. Lett., 26, 1283-1286, 1999.

Helmig, D., Ortega, J., Guenther, A., Herrick, J. D., and Geron, C.: Sesquiterpene emissions from loblolly pine and their potential contribution to biogenic aerosol formation in the Southeastern US, Atmospheric Environment, 40, 4150-4157, 2006.

Henderson, A.: A Review of Pollination Studies in the Palmae, Botanical Review, 52, 221-259, 1986.

Hewitt, C. N., Lee, J., Barkley, M. P., Carslaw, N., Chappell, N. A., Coe, H., Collier, C., Commane, R., Davies, F., DiCarlo, P., Di Marco, C. F., Edwards, P. M., Evans, M. J., Fowler, D., Furneaux, K. L., Gallagher, M., Guenther, A., Heard, D. E., Helfter, C., Hopkins, J., Ingham, T., Irwin, M., Jones, C., Karunaharan, A., Langford, B., Lewis, A. C., Lim, S. F., MacDonald, S. M., MacKenzie, A. R., Mahajan, A. S., Malpass, S., McFiggans, G., Mills, G., Misztal, P., Moller, S., Monks, P. S., Nemitz, E., Nicolas-Perea, V., Oetjen, H., Oram, D., Palmer, P. I., Phillips, G. J., Plane, J. M. C., Pugh, T., Pyle, J. A., Reeves, C. E., Robinson, N. H., Stewart, D., Stone, D., and Whalley, L. K.: Oxidant and particle photochemical processes above a south-east Asian tropical rain forest (the OP3 project): introduction, rationale, location characteristics and tools, Atmos. Chem. Phys. Discuss., 9, 18899-18963, 2009.

Holzinger, R., Lee, A., Paw, K. T., and Goldstein, A. H.: Observations of oxidation products above a forest imply biogenic emissions of very reactive compounds, Atmospheric Chemistry and Physics, 5, 67-75, 2005.

Hussein, M. Y., Lajis, N. H., Kinson, A., and Teo, C. B.: Laboratory and field evaluation on the attractancy of *Elaeidobius kamerunicus* Faust to 4-allylanisole, Porim Bull. , 18, 20-26, 1989.

Hussein, M. Y., Lajis, N. H., and Ali, J. H.: Biological and chemical factors associated with the successful introduction of *Elaeidobius kamerunicus* Faust, the oil palm pollinator in Malaysia, Acta Hort. (ISHS) 288, 81-87, 1991.

Karl, T. G., Spirig, C., Rinne, J., Stroud, C., Prevost, P., Greenberg, J., Fall, R., and Guenther, A.: Virtual disjunct eddy covariance measurements of organic compound fluxes from a subalpine forest using proton transfer reaction mass spectrometry, Atmospheric Chemistry and Physics, 2, 279-291, 2002.

Kim, S., Karl, T., Helmig, D., Daly, R., Rasmussen, R., and Guenther, A.: Measurement of atmospheric sesquiterpenes by proton transfer reaction-mass spectrometry (PTR-MS), Atmos. Meas. Tech. Discuss., 1, 401-433, 2008.

Knudsen, J. T., Tollsten, L., and Ervik, F.: Flower scent and pollination in selected neotropical palms, Plant Biology, 3, 642-653, 2001.

Langford, B., Davison, B., Nemitz, E., and Hewitt, C. N.: Mixing ratios and eddy covariance flux measurements of volatile organic compounds from an urban canopy (Manchester, UK), Atmos. Chem. Phys., 9, 1971-1987, 2009.

Lee, A., Goldstein, A. H., Keywood, M. D., Gao, S., Varutbangkul, V., Bahreini, R., Ng, N. L., Flagan, R. C., and Seinfeld, J. H.: Gas-phase products and secondary aerosol yields from the ozonolysis of ten different terpenes, J. Geophys. Res.-Atmos., 111, 10.1029/2005jd006437, 2006a.

Lee, A., Goldstein, A. H., Kroll, J. H., Ng, N. L., Varutbangkul, V., Flagan, R. C., and Seinfeld, J. H.: Gas-phase products and secondary aerosol yields from the photooxidation of 16 different terpenes, J. Geophys. Res.-Atmos., 111, 10.1029/2006jd007050, 2006b.

Lindinger, W., Hansel, A., and Jordan, A.: On-line monitoring of volatile organic compounds at pptv levels by means of proton-transfer-reaction mass spectrometry (PTR-MS) - Medical applications, food control and environmental research, International Journal of Mass Spectrometry, 173, 191-241, 1998.

Mahbob, A.: The Pollinator *E. Camerunicus* is Nature's little helper, Global Oil & Fats Business Magazine, 5, 58-59, 2008.

Misztal, P. K., Owen, S. M., Guenther, A. B., Rasmussen, R., Geron, C., Harley, P., Phillips, G. J., Ryan, A., Edwards, D. P., Hewitt, C. N., Nemitz, E., Siong, J., Heal, M. R., and Cape, J. N.: Large estragole fluxes from oil palms in Borneo, Atmos. Chem. Phys., 10, 4343-4358, 10.5194/acp-10-4343-2010, 2010.

Monson, R. K., Harley, P. C., Litvak, M. E., Wildermuth, M., Guenther, A. B., Zimmerman, P. R., and Fall, R.: Environmental and developmental controls over the seasonal pattern of isoprene emission from aspen leaves, Oecologia, 99, 260-270, 1994.

Nemitz, E., Loubet, B., Lehmann, B. E., Cellier, P., Neftel, A., Jones, S. K., Hensen, A., Ihly, B., Tarakanov, S. V., and Sutton, M. A.: Turbulence characteristics in grassland canopies and implications for tracer transport, Biogeosciences, 6, 1519-1537, 2009.

Petron, G., Harley, P., Greenberg, J., and Guenther, A.: Seasonal temperature variations influence isoprene emission, Geophys. Res. Lett., 28, 1707-1710, 2001.

Rinne, H. J. I., Guenther, A. B., Warneke, C., de Gouw, J. A., and Luxembourg, S. L.: Disjunct eddy covariance technique for trace gas flux measurements, Geophys. Res. Lett., 28, 3139-3142, 2001.

Rinne, J., Taipale, R., Markkanen, T., Ruuskanen, T. M., Hellén, H., Kajos, M. K., Vesala, T., and Kulmala, M.: Hydrocarbon fluxes above a Scots pine forest canopy: measurements and modeling, Atmos. Chem. Phys., 7, 3361-3372, 2007.

Sharkey, T. D., Singsaas, E. L., Lerdau, M. T., and Geron, C. D.: Weather effects on isoprene emission capacity and applications in emissions algorithms, Ecol. Appl., 9, 1132-1137, 1999.

Spirig, C., Neftel, A., Ammann, C., Dommen, J., Grabmer, W., Thielmann, A., Schaub, A., Beauchamp, J., Wisthaler, A., and Hansel, A.: Eddy covariance flux measurements of biogenic VOCs during ECHO 2003 using proton transfer reaction mass spectrometry, Atmospheric Chemistry and Physics, 5, 465-481, 2005.

Steinbacher, M., Dommen, J., Ammann, C., Spirig, C., Neftel, A., and Prevot, A. S. H.: Performance characteristics of a proton-transfer-reaction mass spectrometer (PTR-MS) derived from laboratory and field measurements, International Journal of Mass Spectrometry, 239, 117-128, 2004.

Sutton, M. A., Burkhardt, J. K., Guerin, D., Nemitz, E., and Fowler, D.: Development of resistance models to describe measurements of bi-directional ammonia surface-atmosphere exchange, International Conference on Atmospheric Ammonia - Emissions, Deposition and Environmental Impacts, Culham, England, 1995, ISI:000072633600029, 473-480,

Syed, R. A.: Studies on oil palm pollination by insects, Bull. ent. Rev., 69, 1979.

Taipale, R., Ruuskanen, T. M., Rinne, J., Kajos, M. K., Hakola, H., Pohja, T., and Kulmala, M.: Technical Note: Quantitative long-term measurements of VOC concentrations by PTR-MS - measurement, calibration, and volume mixing ratio calculation methods, Atmospheric Chemistry and Physics, 8, 6681-6698, 2008.

Tandon, R., Manohara, T. N., Nijalingappa, B. H. M., and Shivanna, K. R.: Pollination and Pollen-pistil Interaction in Oil Palm, Elaeis guineensis, Ann Bot, 87, 831-838, 10.1006/anbo.2001.1421, 2001.

2.5 Development of a new lag-time validation method for eddy covariance

Table of contents

2.5.1 Abstract

Precise determination of the lag time between measurements of vertical wind speed and chemical component in eddy correlation methods can be a challenging task because of the lack of lag-time validation tools. Errors derived from using the wrong or imprecise lag times can be very high but are generally underplayed in flux papers as it is commonly assumed without reservations that a valid lag-time determination has been made. The main focus of the eddy covariance flux community has been on flux validation and corrections, but these may be meaningful only when the lag time is correct. Recently it has been suggested that the widely used maximum-in-the-covariance method is prone to overestimations (Taipale et al., 2010). This is consistent with the findings reported here. Although most of the currently-used approaches to finding the lag time have been described recently in the literature (Hörtnagl et al., 2010; Taipale et al., 2010; Turnipseed et al., 2009; Wolfe et al., 2009), finding the true lag time is still a challenge especially for noisy covariance

functions, which are typical for disjunct time-series obtained in PTR-MS and in particular for the low concentration compounds. It is suspected that the currently-used approaches may be the cause of large uncertainties propagating into flux models, if the lag time is not validated. Another problem is the great number of data rejections due only to inability to find the lag time, which may impact on the representativeness of the dataset. In addition, automation of the selection and validation of lag times is needed in order to reduce data processing time, which is very long for low-concentration compounds where visual assessment of the covariance function has been the only possible way. However, the visual method could be subject to human errors and can be controversial. This chapter introduces a new non-arbitrary "lag-validity" technique in an analogy to the Foken and Wichura (1996) stationarity test, which identifies only true non-variable lag times and therefore provides a means for automatic lag validation. Subsequently a new automated method is proposed based on the internal median of non-variable lag times within an integration period. This method was tested and contrasted with one of the most common methods in which lag time is derived from the maximum point in the covariance function. The new automated method worked well also for low-concentration species and could be validated. Although there has been recent interest in methods for the determination of lag times for disjunct systems as those studied here the means of automatic lag-time validation and quality control has not been done. Therefore, this new "lag-time validity" method could be added to the Fluxnet flux quality assessment criteria (Foken et al., 2004). Combination of the internal-median method and validation of lag times by the proposed approach can exclude erroneous lag times derived from the covariance function, erroneous sign of the flux, reduce statistical error of the flux and prevent overestimation of emission and deposition. Finally, this approach can increase the confidence in reported fluxes by introducing quality control of the lag times in an automated manner, where the quality of the lag-time precision can be used as a label for marking individual flux data.

2.5.2 Introduction

Identification of the lag time (LT) between the measurements of the vertical wind speed and the scalar of interest (e.g. concentration) is essential for correct flux derivation (Clement et al., 2009; Davison et al., 2009; Langford et al., 2009a). Although there are different ways of estimating the LT such as volumetric calculation, cross-correlation, balloon test etc, the LT can be the biggest source of flux underestimation or which can lead to the uncertainty in the sign of the covariance. The most commonly used methods and associated errors were recently described by Taipale et al. (2010).

Particularly challenging in typical flux processing is to obtain the true flux for low signal-to-noise ratio data, which is often the case with low concentration species present in the atmosphere. Therefore validation approaches are necessary but which have so far been unavailable. Following the routine flux validation procedures (e.g. Moncrieff et al., 1997) for some compounds may lead to a very high number of rejections of the data and it might happen that the remaining flux is no longer representative. Frequently, a large percentage of rejections can be due to the inability of finding the true peak in the covariance function even when all other criteria are fulfilled, or if the LT peak is erroneously identified in the noisy covariance function. Therefore, an improvement in finding the correct lag time is critical for avoiding unnecessary data rejections.

Moreover, the current rejection protocols practically exclude the night times and deposition events frequently occurring in the morning. One could argue that if the night turbulence is low then there will be no flux anyway due to decoupling of the ground. However, if the turbulence is sufficient at night it might still be difficult to find the true peak in the covariance function as a result of small concentrations of many species. What is frequently the case in such circumstances is that there might be short periods of acceptable conditions (shorter than the integration time), which become unacceptable after longer averaging. Or the conditions satisfy the quality criteria, but a clear peak in the covariance can only be obtained in the shorter

integration periods. If such short high quality periods can be elucidated from the generally low-flux data then they might be applied to the lag-time determination, if other criteria are fulfilled.

One of the methods to help visualise the LT is to average the covariance function before selecting the maximum in the covariance – the AVG method (Taipale et al., 2010). This method had a lower error than the typical method where the lag-time is derived from the maximal point in the covariance function (the MAX method). The authors proposed that the MAX method is prone to overestimation because of the noise superimposed on the covariance in disjunct eddy covariance (DEC). A similar method to AVG has been used here, but instead of subjecting the covariance function to the averaging filter, the peak-detector function of the LabVIEW program was used which disregarded the discrete spikes of the covariance function. Such a method is referred to as the PF method, which was independently found similar to the MAX method in the flux pattern but was free from overestimations.

However, validation approaches for the LT are needed and one method is demonstrated here which can be easily implemented for any eddy covariance setup, although the processing of PTR-MS data is used here as an example. The main specificity of using PTR-MS as a chemical sensor is that it must be used in the disjunct mode, unless only one *m/z* is monitored, because the quadrupole filter analyses one *m/z* after another creating high frequency data for each of them separated by relatively long gaps. Inter-comparisons of the disjunct (DEC) and the conventional (continuous) eddy-covariance methods (EC) (e.g. Rinne et al., 2008) show good agreement provided that the averaging time was sufficiently long in relation to the gaps. However, the covariance function is generally much noisier in DEC and therefore finding the lag-time in the covariance is more challenging. PTR-MS does not require a sampler, which was initially combined with PTR-MS (Rinne et al., 2001), because the mass filter itself serves as a disjunct sampler and hence the name of the method is virtual disjunct eddy covariance (vDEC) (Karl et al., 2002) or the continuous flow disjunct eddy covariance (Rinne et al., 2002), both names signifying the same method. However, early models of a standard PTR-MS

instrument could still benefit from using an external sampler because of longer response time (>0.2 s) of those instruments compared to the high sensitivity models introduced later. Langford et al. (2009a) demonstrated good agreement between DEC (with external disjunct sampler) and vDEC. For generalisation the name disjunct eddy covariance (DEC) will be used here with reference to all disjunct eddy covariance methods, even though the approach presented here has been tested on the vDEC method. A similar approach can be applied to all conventional eddy-covariance systems, such as Li-COR CO_2 and H_2O EC fluxes.

Even in a continuous eddy covariance setup, but particularly in the disjunct mode offered by PTR-MS, it is likely too optimistic to expect a constant LT in the whole measurement period. The TYP approach, which uses the constant LT obtained from the average of several representative LTs, was found by Taipale et al. (2010) to have the second largest error in flux underestimation after the CALC method where the constant time lag is obtained from the flowrate. The sources of the variable LT are numerous and they include pump fluctuation and changes in the ambient temperature, pressure and humidity. For the PTR-MS variable LT is especially evident as additional sources can derive from quadrupole delays (generally very small ~fractions of seconds) and cycle length – as the cycle must be completed before the next *m/z* is analysed. Obviously if one uses mediating software (e.g. the DDE server) for data acquisition, or the wind and tracer data are logged on separate computers/files, then additional delays might be introduced.

Therefore, the method presented here adopts the notion that at least each averaging period (e.g. half-hour) should be assessed individually for its effective LT. The major assumption for the method is that the LT is constant for the relatively short period of time (e.g. 5 min) for the given compound but still can be different for different compounds, depending on their position in the cycle and the affinity to the tube surface. This time should not differ by more than the cycle length. This is only the case if no other delays are present, as mentioned above.

Finally the higher certainty of the LT makes the overall flux closer to correct. It is actually not known how much the global estimates derived from eddy covariance methods differ from the real values as a result of imprecise lag approaches. On one hand, if small fluxes are not reported due to the lack of precise LT, this would lead to overestimation as high flux values only would be averaged. On the other hand constant lag approaches lead to flux underestimation, and in contrast the MAX method to overestimation. However, the highest error is likely to derive from wrong flux signs, which can be the case for not validated lag-times (see Sect. 2.5.6).
The Lag Time Validity (LTV) method for validation and the internal median (IMED) method for lag-time determination are proposed here to be used with eddy covariance techniques.

2.5.3 Current methods of LT determination

2.5.3.1 Volumetric method (theoretical)

The volumetric method is purely empirical and assumes that the LT is equal to the time taken by the volume of gas contained in the tubing to travel the distance of the tubing (outside and inside the instrument) to the detector. The result obtained by this method can deviate substantially from the real lag because the terminal distance to the analyser is often the slowest segment but is often neglected, and many compounds exhibit chromatographic effects or are ‘sticky’. Nevertheless, it is good practice to use this LT calculation as a first approximate guideline.

2.5.3.2 Balloon test (practical)

The ballon test is a very popular method and commonly used (e.g. Davison et al., 2009; Karl et al., 2007; Lee et al., 2005). The principle is to spike a high concentration of a compound at the sampling inlet while simultaneously blocking the transducer of the sonic anemometer so that the LT is determined from the difference

in time between the concentration spike and the disturbance in the sonic data. Again the shortcoming of this method is that for highest precision it would require each individual compound to be tested. In addition, since LT typically varies in practice (see introduction) one would need to balloon-test frequently, which would be at the cost of measurement interruption. With PTR-MS the effective lag-time can differ from the balloon test by the time of the cycle for a given measurement period.

2.5.3.3 Cross-correlation methods (empirical)

Cross-correlations methods are the most common group of methods used with PTR-MS and other systems, and are particularly useful for variable LTs since each averaging period is individually assessed for LT. The covariance function is a cross-correlation (CC) of the covariance between the w and the χ as a function of LT t_{LT}. The time window used for the CC function should be longer than the theoretical lag-time plus the cycle length. Generally, if the peak in the covariance function is not clear then the data are discarded (Taipale et al., 2008). A subvariant of this method involves a fast Fourier transform to the frequency domain for the LT determination and then a back transformation to the time domain (Spirig et al., 2005). It is necessary that the gaps are not variable, but this is not always the case. Again, these methods are not free from weaknesses, the major one of which is the difficulty in assessing noisy covariance functions. Not only is the careful visual investigation of each half-hour period (or different period) time-consuming but it can also be difficult for the assessor to distinguish the peaks, which can be on the limit of noise or just pseudopeaks (from coincidental covariance of noise fluctuation). The visual assessment method, referred to as the VIS method by Taipale et al. (2010), is typically employed when the MAX and AVG methods are unsuccessful or if the lag-time needs to be verified (e.g. uncertain deposition). The VIS method is controversial as it can be prone to human error, but may have been the only possible method before the IMED method introduced later in this chapter. Using VIS one should permit only the obviously evident peaks.

Before the covariance function is derived it is necessary to bring the timeseries of w and χ to the same frequency. As PTR-MS uses dwell times typically ranging from 0.2 s – 1 s in the flux mode, the concentration data are characterised by a lower frequency than the wind data. In addition, the size of the gap between each measurement is equal to the cycle length, dependent on the number of *m/z* in the cycle multiplied by their mean dwell time. For the case of 10 *m/z* at 0.5 s dwell-time each (2 Hz), the PTR-MS cycle data row would be 0.2 Hz while the sonic data are typically at 10 – 40 Hz. In order to adapt the data to the same frequency one can either delete w datapoints when the PTR-MS data are unavailable or as shown by Spirig et al. (2005) fill those gaps with the previous PTR-MS data until the next one is available. The first method can largely attenuate the high frequency region while the other is acting as a low-pass filter. Although corrections for such attenuation are possible, a third method is used, which is a compromise which relies on filling the gaps with not-a-number symbols (NaN) and then shifting the w and χ time series against each other for producing the covariance function.

2.5.4 Design of the new lag-time validity test

The idea for the LT treatment comes by analogy with the stationarity check according to Foken and Wichura (1996), where it is assumed that the flux for the averaging period (e.g. Δt = 30 min) should not differ more than 30% from the average of fluxes derived from the 5-min subperiods of Δt. If the difference lies between 30% and 60% then the flux is of lower quality, and if it is above 60% then the data are non-stationary and need to be omitted from the analysis.

Here the new variable V_{LT} is introduced, which is termed the lag time validity (LTV). The V_{LT} can be defined as the percentage difference of the LT value found from cross-correlation for the half hour (or at least 25 min) averaging period t_{lag0} and the mean lag-time (t_{lag1}, t_{lag2}, …, t_{lag6}) found in the individual cross-correlations of the 5 min subperiods of that half hour (Equation 2.5-1).

Equation 2.5-1

$$V_{LT} = \left| \frac{6t_{LT0} - \left(t_{LT1} + t_{LT2} + t_{LT3} + t_{LT4} + t_{LT5} + t_{LT6}\right)}{6t_{LT0}} \right| \times 100\%$$

If V_{LT} is within 30% then the highest precision of the LT determination is achieved (high LT precision). If the V_{LT} spans between 30% - 60% such data could be conditionally accepted but tagged as low LT precision. This might be typical in the processing of low concentration fluxes when only some of the 5-min subperiods of the averaging period have clear peaks in the covariance function. The additional condition must be made that at least three lag times of the 5-min subperiods must be clear and have a similar value in order to determine their internal median lag time (see Sect. 2.5.5). Finally, if the difference is more than 60% then the lag time is classified as not validated and such data would need to be discarded or the methods of mean constant lag (such as CALC or TYP) could be potentially applied (but then the quality of such a data point would need to be marked as very low).

Some vDEC flux users use the first 5 minutes of the half hour, for example, for sampling the zero air or performing a full *m/z* scan. In this instance only 25 min would be used as an averaging period and the LT validity can be modified as in Equation 2.5-2:

Equation 2.5-2

$$V_{LT} = \left| \frac{5t_{LT0} - \left(t_{LT1} + t_{LT2} + t_{LT3} + t_{LT4} + t_{LT5}\right)}{5t_{LT0}} \right| \times 100\%$$

Five consecutive days of a dataset from a measurement campaign in Borneo were taken and the new lag-time validity (LTV) method was tested. For this lag time experiment no standard rejection protocols were applied. The only rejections were if the LTV was greater than 30%, and the remaining data were compared with corresponding points derived by the MAX method or PF method (analogous to Taipale et al 2010 AVG method). The following criteria have been selected for assessing the goodness of lag-time validation: percentage of necessary rejections,

root mean square (RMS) error of the regression of the fit of the IMED and the MAX method, number of flux sign errors, and lag time variability. Three compounds, which differed in the type of flux (emission, deposition, mixed) and in signal-to-noise ratio, were selected for comparison.

2.5.5 Internal-median lag-time method (Lag IMED)

This is the new method, which has been introduced to provide an unbiased lag-time based only on the non-varying subperiods of integration time. Although the lag-validity test could identify the magnitude of internal variation between the lag times within the half hour, the IMED method derives the lag from the median value of lag times found on those subperiods. In other words, if the lag time did not vary during the half hour then the internal median will be the same as the lag-time value derived on the full integration time. In contrast, if the lag time was partly variable, i.e. constant in at least 3 subperiods and LTV was less than 30 % then the full integration time would be the effect of the superposition of the covariances with two or more maxima. In this case, the standard methods such as the MAX method are likely to select the wrong peak which may result in the calculated flux being of the wrong sign. Therefore the IMED method was selected particularly for performing well on challenging data, where the flow to the pump was not strictly controlled (i.e. no mass-flow control was used) or when applied to compounds at low concentration. Such compounds may make finding a clear peak difficult on the full integration time on which any temporal increases in concentration could be averaged out. Finally for such compounds a peak in the covariance function can be very small, so very difficult to detect, even using the visual method (VIS) where it sometimes can be hard to judge if the peak is not noise-related even if it exceeds the limit of detection derived from the noise sampled much further from the lag-time. If the peak is not real then the internal lag times would be variable (LTV > 60%).

The software applied to processing the fluxes was written in LabVIEW ver.8.5 (National Instruments Corp.). The raw files contained both the sonic and the PTR-

MS data. The details of data acquisition made in the campaign from which the data are drawn for this lag-time development have been described elsewhere (Misztal et al., 2010a; Misztal et al., 2010c). The directory containing such half-hourly files was filtered for short files and files with known disturbances checked against the log book. After such a segregation each of the files was sequentially opened and processed. The array was split into PTR-MS array and sonic array, and then the micromet data (e.g. u^*, L, z_0, etc.) were obtained from the sonic data which had been adjusted using the planar fit rotation in order to correct for the sonic tilt (Wilczak et al., 2001). The process of flux validation, identification of low-turbulence and non-stationary periods is performed independently and the appropriate information is saved to the general comma-delimited output file, which additionally contains the quality tags for each output data row. Normally these tags are used to filter the data according to Fluxnet criteria. However, for the validity method, and in particular the new IMED method, no filtration was made in order to test the sensitivity of the method also on the low quality data.

The LT identification is made by the program subroutines in the following way. First, the whole 30 min (or 25-min) array of vertical wind velocity w data is shifted by one 20-Hz step (for the 20 Hz sonic data) against the concentration data, with gaps filled by "NaN", for the selected m/z, and the cov(w, χ) is calculated for each step. This process is repeated until the LT window of the specified maximal LT is reached. For example, if the LT window is calculated to be 15 s and the sonic frequency is 20 Hz then the process is stopped after the 300th step and the values of the covariances vs time lag (with 0.05 s step) are plotted, thereby generating the covariance function for the 30 min (or 25 min) averaging period. The peak is detected either as the absolute maximum in the covariance (Lag MAX) or by the peak-detector feature (PF) implemented in LabVIEW, where the threshold is the limit of detection (LOD) as 3 standard deviations of the 20 s covariance noise periods sampled at 3 min and -3 min relative to the lag-time. The location of the peak is recorded as lag time t_{LT0}. Using the peak detector resembles the AVG method proposed by Taipale et al. (2010) since the peak must be wider than 0.5 s and the centre of the peak is considered as a valid lag time rather than the absolute maximum

of the discrete spike on that peak. Therefore the PF lags were always smaller than the maximum point in the covariance but were thought to be real. The reason for the MAX method overestimating the covariance function is because in DEC the greater noise is added to the covariance function, and the discrete spikes in this noise at the peak lead to overestimation. Therefore in the IMED method the peak was always detected as PF.

Subsequently in the IMED method, after calculating t_{LT0} for the full 30 min (or 25 min) period, the w and χ data arrays were divided into six (or five if 25-min averaging period) 5 min arrays, which were subjected to the same process for selecting the peak in the covariance function. If no peak could be found then NaN was entered as a result. If more than one peak were present then the largest peak found by PF was selected. The lag time validity was then calculated and the validity tag (high precision, low precision, invalid) was added to the data based on criteria set out in the previous section. If there were no more than 2 NaNs, the median value of the t_{LT1}….t_{LT6} was calculated with the following additional constraints: at least two of the 5 min LTs could not be different by more than 5%; at least three 5 min LTs had to exceed 3 standard deviations of the noise (as defined above); and the V_{LT} had to be either high or low precision, in the valid region.

In ideal situations, all the components of t_{LTx} are more or less similar, but the median was the correct method to use in order to reject any outliers which could make the calculation on the full integration time invalid. This occurred more frequently at low concentrations or low turbulence. Therefore this method could increase the number of valid lag-time points. This median lag-time was subsequently saved to the output file and further applied to the calculation of the flux for that given *m/z*. The entire process was repeated for the next *m/z* as the lag times may not be the same for each compound but may depend on the position of their *m/z* in a cycle and the character of the compound.

2.5.6 Results and discussion

Lag validity test results showed that not all lag-times found in typical integration periods were constant within these periods. By selecting these periods the method delivers a validation tool to the lag time derivation. In Figure 2.5-1, for the isoprene example, the time series of lag-time values (Lag 0 PF) calculated for 25-min integration times are plotted against timeseries of the IMED lag times, i.e. medians of lag-times derived on the 5-min integration times. The ellipse encompasses the IMED data which both passed the LTV test (LTV < 30%) and also agreed with the PF method (full integration) within a half of the cycle-length period (3.5 s). Over half of the data had lag times which agreed well with both the methods. However, half of the remaining points (i.e., from outside the ellipse) had passed the validity test but the Lag 0 PF (i.e. the lag time found by PF in the whole integration period) was significantly different, probably due to inability of the PF to select the right peak if outliers were present. This means that the values of t_{lag0} for these points could have had an erroneous lag, which could result in underestimation and also the wrong sign, although the latter effect would be more typical for compounds which can also be deposited. Finally, approximately one quarter of all data points did not pass the validity test when the lag time could either be missed or vary excessively. Most of the variable lags were common for night times when the turbulence and temperature were low as can be seen from the size of the marker. However, it seems that even some of the smallest markers could have been valid but the conventional method (Lag 0 PF) would be likely to capture less of them reliably as seen from the comparison of the scatter of the two axes.

When lag times for acetone example data are plotted together as the time series (Figure 2.5-2) it is immediately evident that the most variable lag time was the Lag 0 MAX (dashed blue), which was the lag time derived from the full integration period using the maximum in the covariance method. In contrast, the Lag 0 IMED (solid red) was the most stable and was well within the cycle length during the entire period. This type of lag time was very similar or the same as the Lag 0 PF (derived by the peak detector on the peak of the covariance function for the full period). The

difference between Lag 0 IMED and Lag 0 PF can be attributed to the presence of outliers in the underlying lag times of 5 min periods (Lag 1, …, Lag 5) which were denoted by thinner lines. However, all the lag times were in a reasonable agreement during the middle of the day (10:00-14:00). The timeseries of lag validity was plotted in reference to the right vertical axis with the 30% threshold represented by a green line. It seems that during a day the majority of the data were well below the validity threshold but at night or during heavy rain episodes the validity value above the threshold which could be linked to low turbulence and low concentrations. However, even at night there were periods of valid points and stable IMED lag times despite much higher variability in the MAX lag.

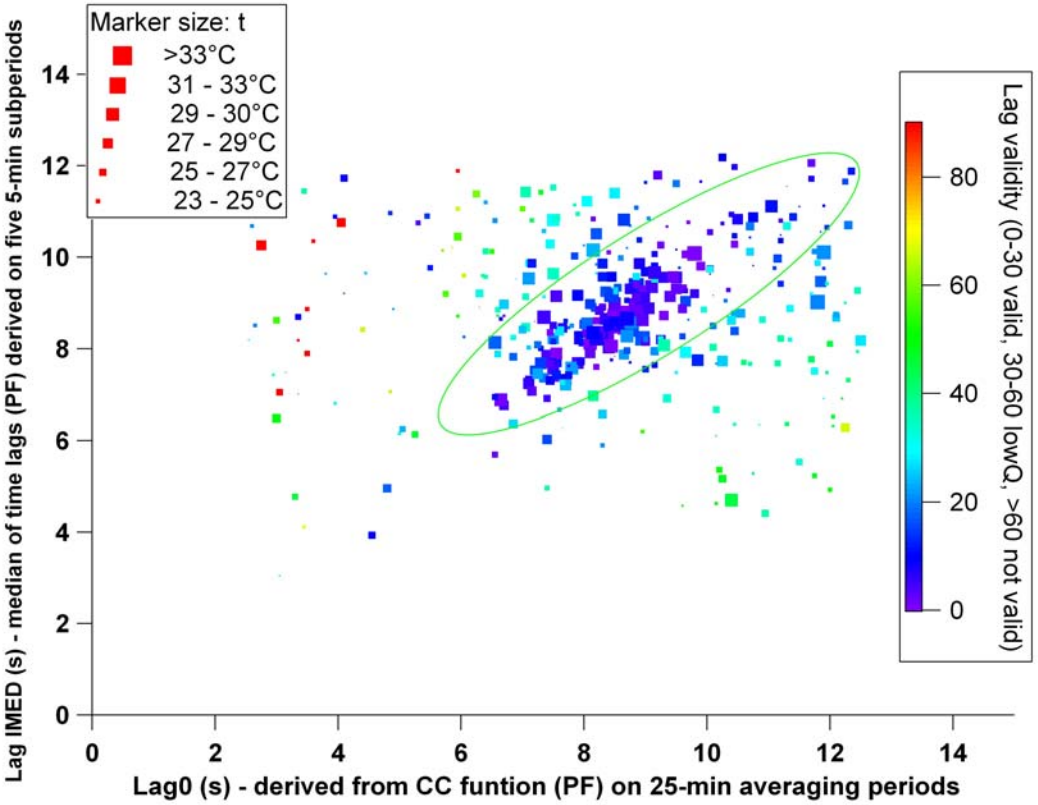

Figure 2.5-1 Median of lag-times derived on 5 minute integration times vs lag time derived classically on the full integration period (here 25 min), using measurements for isoprene. The data points were coloured according to the LTV test and the size of a marker corresponds to the ambient temperature, which was high during day and low at night.

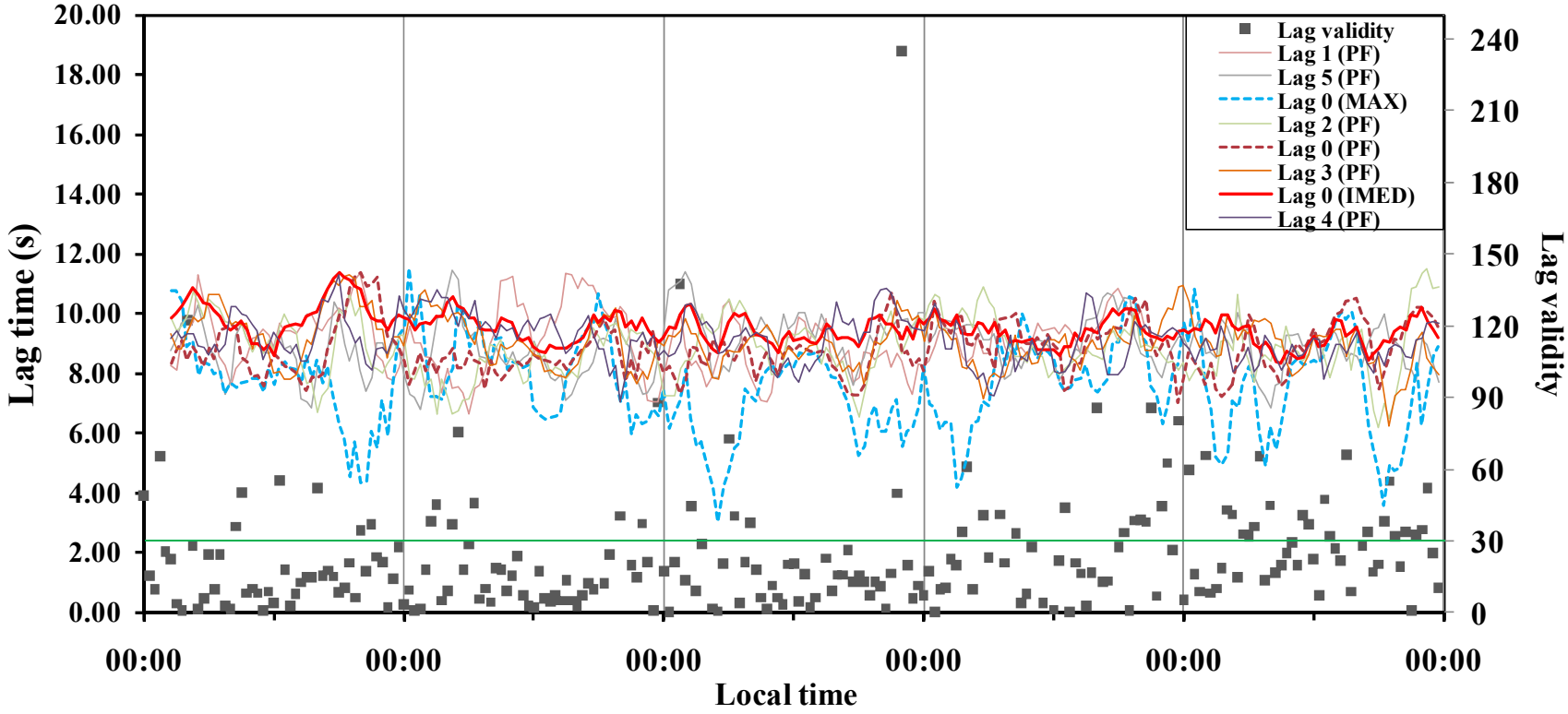

Figure 2.5-2. Lag-time variation time series for *m/z* 59 (acetone, glyoxal, propanal). The horizontal green line represents the validity threshold. Outliers (e.g., caused by spiky covariance) can impact the instability of Lag 0 MAX derived on a full integration period (25 min) although during the mid day it is similar to other lag time types. The lags derived by using peak finder (PF) seem to be less variable. The internal median lag 0 (IMED) derived by a median of lags 1-5 of shorter integration periods is the way of dealing with small concentrations where lag MAX cannot perform well. Lag 0 (IMED) disregards the outliers and can be further validated by the LTV threshold of 30. Therefore the median of validated lag times (derived on 5-min periods) can be the solution to finding the true lag time. All lag-time series were smoothed by a 6-period running average.

As different compounds can have different lag times and different clarity of their covariance functions, the lag time MAX method (most commonly used) and the IMED method were compared in terms of their lag time values and their effect on the fluxes for three different compounds, i.e. isoprene, MVK+MACR, and acetone. Isoprene is an example of a pure emitter, whose flux was very high in the studied data set. MVK and MACR, detected on the same ion channel (*m/z* 71), were predominantly depositing and their concentrations were also very high, although lower than those of isoprene. The distance from the source must have been high in the atmosphere, which could be longer than the distance from the isoprene source (3 m from the top of the canopy). In addition *m/z* 71 picks up two compounds MVK and MACR, which despite being isomers could have slightly different properties (e.g. affinities for tube surfaces) and therefore lag times. Finally, acetone is an example of a low concentration compound, which could have two different sources (one biogenic or leaf litter and another from the VOC oxidation chain higher in the troposphere). Thus, this compound was expected to have a mixed character for flux and generally be difficult to detect lag time from the covariance function because of the low concentrations.

Isoprene was so abundant during the day that its peaks in the covariance function were generally very clear. Figure 2.5-3 shows the comparison of the isoprene fluxes derived by the IMED and MAX methods. The IMED lag time values are presented in this figure relative to the right axis. It seems that the MAX method overestimated only slightly the emission but the general agreement was very good (Figure 2.5-4). However, there were three points in the flux which were causing a scatter on the fit, as they correspond to Lag MAX selecting the highest point in the covariance which could be wrong and suggested a deposition. In fact two of these points would not be stationary so would be rejected anyway, but the IMED method did not show deposition although the two points would be rejected by the lag-time validity test. The third point of those mentioned occurred during a rain episode on the second day. The MAX method identified that point as a small deposition which was outside the 95% prediction interval, the LTV was less than 30% and the IMED lag method identified the same point as a small emission.

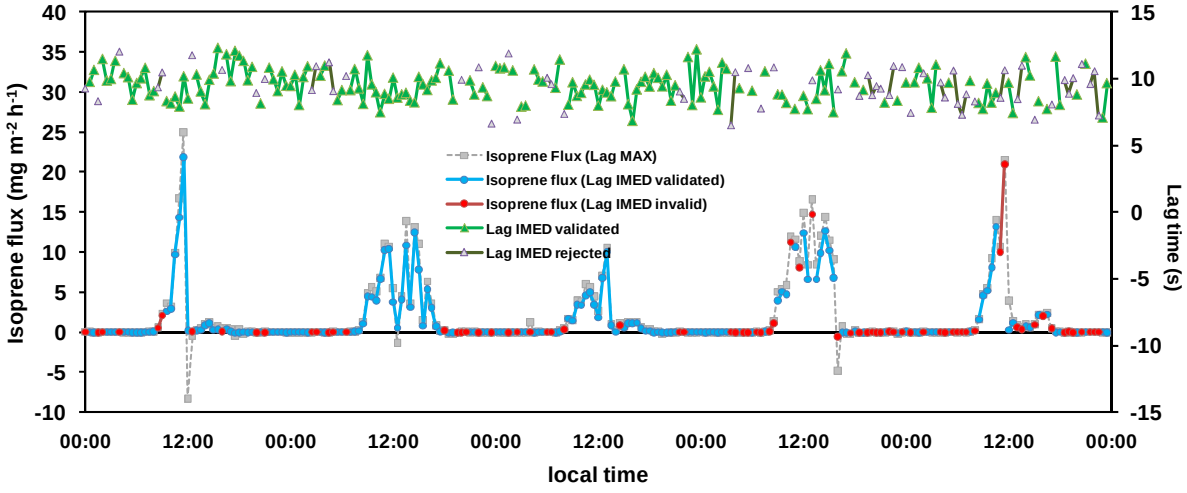

Figure 2.5-3 Comparison of isoprene fluxes derived with Lag MAX (grey), with Lag IMED validated (blue) and with invalid Lag IMED (LTV>30) (red). Series of IMED lag-time values are plotted in reference to the right axis.

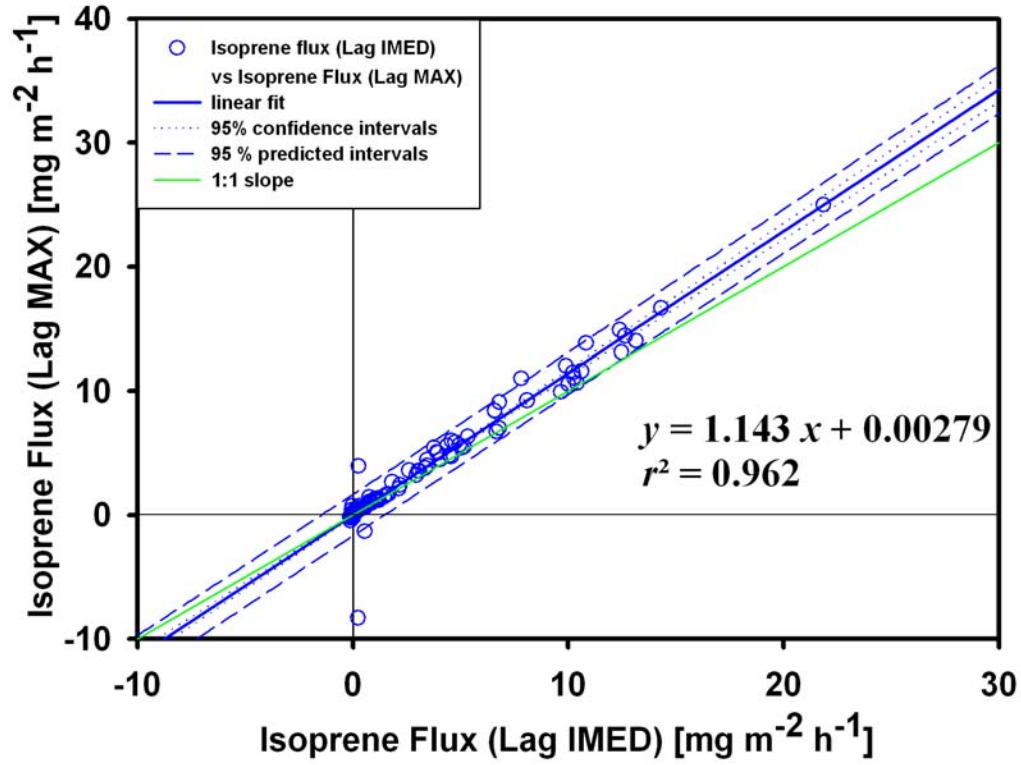

Figure 2.5-4 Regression of isoprene fluxes derived with IMED LT versus isoprene fluxes derived with MAX LT. Since isoprene flux had high signal-to-noise ratio, both methods agree well, although the Lag MAX method overestimates the flux by 14%. One can see an outlier where the Lag MAX predicts deposition, which is not confirmed by the Lag IMED.

Although the type of lag method applied could cause only a relatively minor difference in the fluxes derived for isoprene (14%), the use of the best method seems much more critical for other less abundant or depositing compounds. Figure 2.5-5 presents the comparison of the flux time series of MVK+MACR with lag method used. This time the agreement was not so good but clearly the IMED method provided less noisy fluxes. In contrast the MAX method resulted in the presence of several flux points suggestive of emission which were not observed when the flux calculation was made using the IMED method. It would be rather surprising to observe frequent flux sign changes in the middle of the day so in this respect the IMED method does much better. The flux sign error can be visualised more clearly from the regression of the fluxes derived in the two methods (Figure 2.5-6), which are denoted as outliers in red. The fit of the regression is not as good as in the case of isoprene fluxes even after excluding the outliers. Furthermore the MAX method overestimated fluxes by approximately 50%, which means that finding the lag time on the highest point in the covariance function is particularly not recommended for compounds whose fluxes are low. This is because the noise can have potentially much higher contribution to the absolute value which is added over the true peak by the value of the spike. Alternatively, if there are two or more peaks in the covariance function which have superimposed noise on them, it may happen that the MAX method selects the highest point on the virtually smaller peak but where contribution of noise was higher than the noise contribution to the true peak. This could result in the wrong sign of the flux. The IMED method would not be prone to the same error as the noise is random so it would be unlikely that the noise would give the same contribution to the same portion of the covariance functions in each of the 5 min segments. Using a peak detector ignores the discrete spikes on the peaks so it may de facto resemble the AVG method but this can be even more effective when applied to shorter segments. The IMED method is therefore recommended for use with more difficult fluxes but should always be combined with the LTV test.

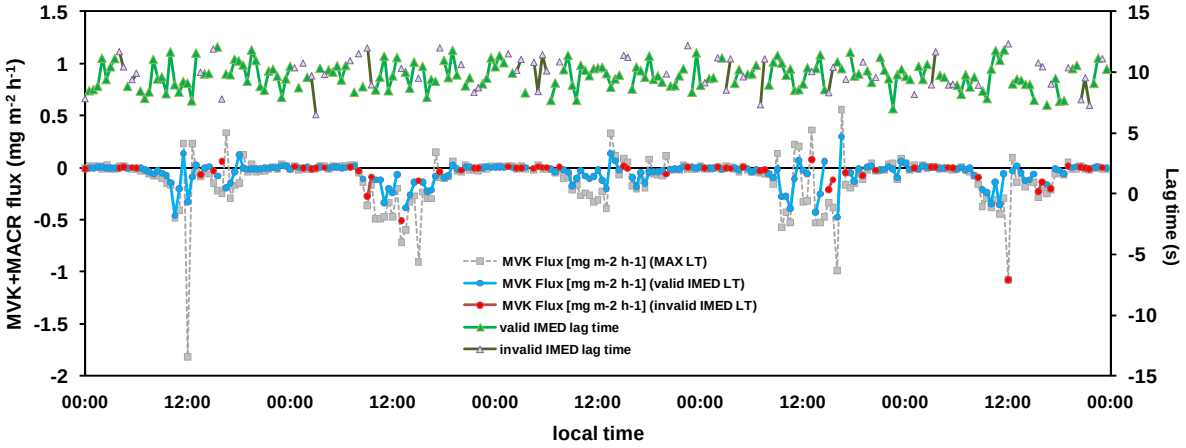

Figure 2.5-5 Comparison of MVK+MACR fluxes derived with Lag MAX (grey), with Lag IMED validated (blue) and with invalid Lag IMED (LTV>30) (red). Series of IMED lag-time values are plotted in reference to the right axis.

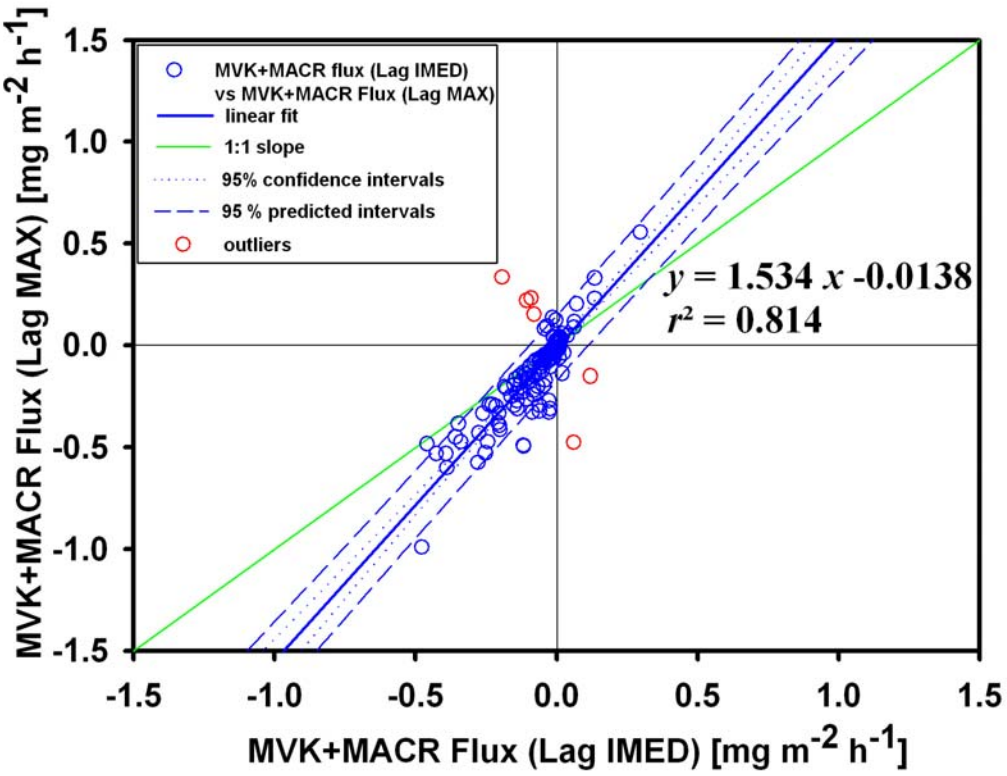

Figure 2.5-6 Regression of MVK+MACR fluxes derived with IMED LT versus MVK+MACR fluxes derived with MAX LT. This compound is an example of depositing VOC. Using Lag MAX without validations has a probability of producing an erroneous sign of the flux resulting in the false emission or deposition. These points are denoted as outliers, and were excluded from regression. Furthermore it seems that the Lag MAX method overestimates emission and deposition by approximately 50% compared to the IMED Lag method.

Processing small fluxes can be the most challenging for a flux investigator, some of which may be made even more complex by their bi-directional character. The example of such a compound was acetone whose fluxes obtained with the two methods are plotted as a timeseries in Figure 2.5-7 and as a regression in Figure 2.5-8. The degree of flux overestimation by the MAX method is slightly lower than in case of MVK + MACR, probably because the bi-directional character of the fluxes compensates the overestimated emission by overestimated deposition (i.e., underestimated negative flux). This is at the cost of the goodness of the fit. The MAX method provided a noisier pattern than was seen in the previously-discussed example compounds. The potential for overestimation can be seen clearly in the amplitude of the grey points at night. In the night time between the first and second days almost all points lacked a lag time within the LTV of 30%. However, the small-flux points derived by IMED and which had a valid lag time (different nights) do not oscillate as much as those found by the MAX method. In addition, during the middle of the first day the absolute flux obtained from the MAX method had almost the same absolute value but its sign alternated excessively, which does not convince the author that the MAX method was correct there. From experience the author noticed in various VOC flux patterns that if the flux sign changes it does so during a rather gradual process, such that normally at least a few integration periods are needed for the value to decrease/increase to the same value of the inverse sign. The exception can be the times when the turbulence starts off quickly (morning) or suddenly fades out (evening) or during a heavy rain episode. However, such a fast change in the flux would often be associated with non-stationary conditions, so the flux would be rarely acceptable anyway. However, the IMED performed much better even during non-stationary periods, most of which coincided with the low LTV. It seems that non-stationary periods with a stable lag time, due to a rapidly changing flux, are particularly prone to flux outlier using the MAX method but the internal median approach does not seem to derive a lag time which would cause the same outlier. So far the comparison suggests that the LTV test is able to identify the variable lag times most of which can be the case for non-stationary periods. The mechanism is not entirely clear,

since one could expect that a non-stationary flux still producing in 5-min covariance functions the same maxima differing in an absolute magnitude rather than a location.

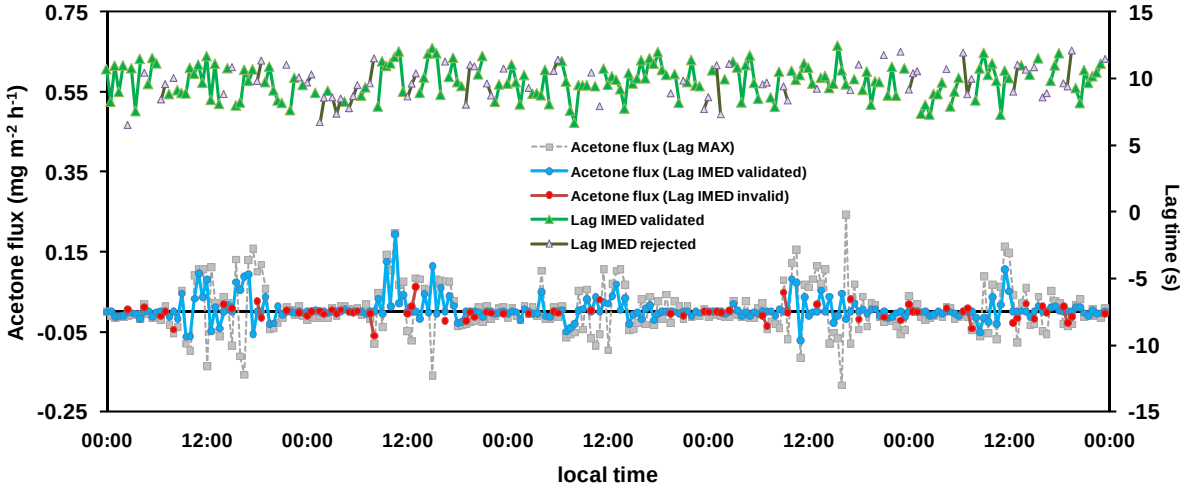

Figure 2.5-7 Comparison of acetone fluxes derived with Lag MAX (grey), with Lag IMED validated (blue) and with invalid Lag IMED (LTV>30) (red). Series of IMED lag-time values are plotted in reference to the right axis.

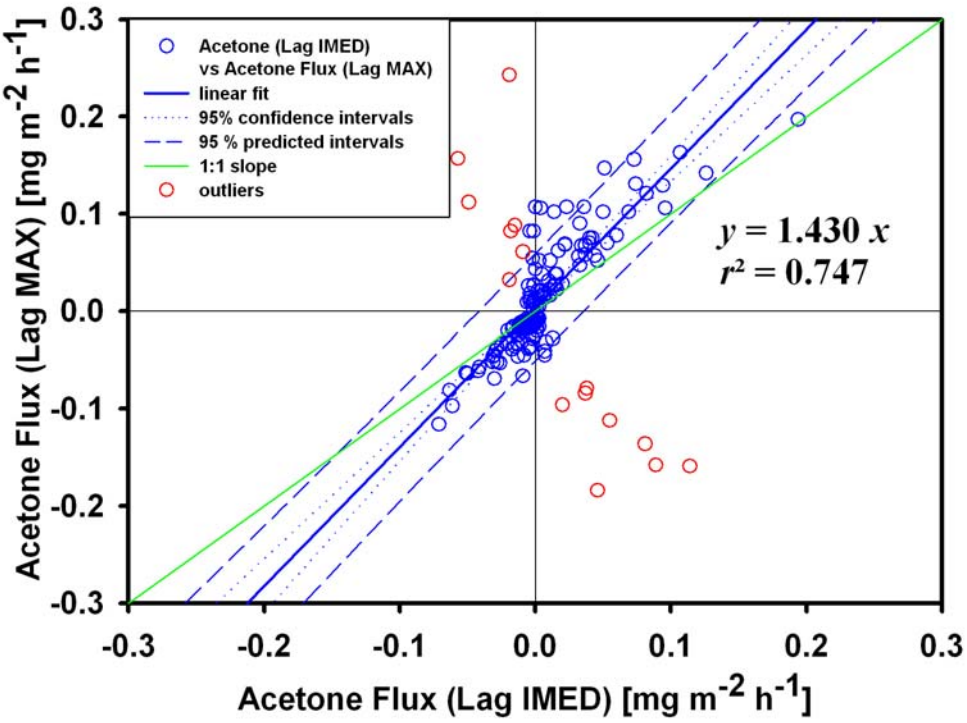

Figure 2.5-8 Regression of acetone fluxes derived with IMED LT versus acetone fluxes derived with MAX LT. This compound is an example of a small flux VOCs, whose lag time can be challenging to find using the classical approaches and which could be both emitted and deposited due to different sources. The use of Lag MAX may result in the flux of

erroneous and thus either false emission or false deposition. These points are denoted as outliers, identified as flux-sign errors and outside the 95% prediction intervals, and were excluded from regression. Furthermore it seems that the Lag MAX method overestimates emission and deposition by approximately 40% compared to the IMED Lag method.

However, during non-stationary periods temperature or humidity can change rapidly and this may affect pump efficiency or alter the affinity of a compound to the surfaces and therefore could lead to a different lag time.

Finally, a general set of criteria was selected to compare the performance of the IMED and the MAX lag times. The comparison is presented in Table 2.5-1. The MAX method had the highest variability in the lag times increasing with the compound of decreasing signal-to-noise ratio. However, the lag times found by the IMED method were much less variable and were not sensitive to the type of compound. This suggests that the IMED method finds only the true lag times, whereas the MAX method simply finds the maximal point in the covariance which does not have to correspond to the true flux, particularly if the covariance function is noisy which happens more frequently in the small-flux compounds. Therefore, the MAX method cannot be simply applied in an automated manner as the majority of data of the low-signal-to-noise compounds would not be clear on the full integration time. In contrast, the IMED method, by decomposing the covariance function on the smaller segments, is promising as an automated method since it has clearly defined lag validation criteria and is not biased by taking the absolute maximum but it takes the maximal point of the peak centre found by the peak detector of set criteria. Such an approach produced 14% more valid lag times in the case of isoprene. However, the particular usefulness of this method is for less abundant species such as MVK+MACR and acetone for which 35% and 52% more valid lag times, respectively were identified using the IMED method rather than the MAX method in this example dataset. The MAX method has been used widely by the flux community and also by the author, which when combined with rigorous rejection criteria did not yield widely differing absolutely flux values for highly abundant compounds. However, the overestimation can be very high for trace compounds or even compounds whose

concentrations are elevated but where mixed character of flux is present. Therefore it is not only the matter of overestimation but also the bias of the flux sign (mirror effect), which leads to a systematic error. The flux is not going to oscillate around zero if the lag-time was found correctly. However, if outliers are excluded (many of which coincide with non-stationary, non-turbulent or rainy periods) the overall agreement of the two methods is reasonable. However the statistical error of the fit is much higher for the MAX method, which even for isoprene was 60% higher in the MAX method. For MVK+MACR and acetone this error was 2.5 and 4.3 times higher, respectively, than in the IMED method. This clearly shows that the IMED method is much better to use, while the MAX method is only suitable for compounds with high abundance and uni-directional fluxes.

Table 2.5-1 Comparison of the IMED LT method with the commonly-used MAX LT method in relation to 3 compounds with different flux characteristics. The IMED data were filtered by the LTV test (LTV<30%) and the same data points were removed from the MAX time series. The number of points left in each data set was 176.

		Isoprene (*m/z* 69)	MVK+MACR (*m/z* 71)	Acetone (*m/z* 59)
Main features	Character of flux	emission	deposition	mixed
	Signal to noise ratio	high	medium	low
LT IMED	Mean LT (s)	9.51	9.79	9.83
	σ_{LT} (s)	1.24	1.16	1.23
	Mean Flux (mg m^{-2} h^{-1})	1.95	-0.060	0.007
	RMS error (mg m^{-2} h^{-1})	0.53	0.059	0.015
	Sign error	impossible	impossible	impossible
	Valid points (% LV<30)	69%	74%	71%
LT MAX	Mean LT	7.67	7.83	7.28
	σ_{LT}	3.85	4.51	4.61
	Mean Flux	2.24	-0.108	0.009
	RMS error	0.84	0.15	0.065
	Sign error	rare (<1%)	moderate (4%)	frequent (10%)
	% clear peak in the covariance	55%	39%	28%

2.5.7 Conclusions

This chapter introduced the first flux lag-time validation technique that can be performed in an automated way. In addition, a new method of lag-time determination was developed based on the internal median of the average maxima of the covariance functions obtained using short subperiod integration times. These methods were tested on a portion of a real dataset from the field using compounds which differed in their flux characteristics. The author's findings that the Lag MAX method can greatly overestimate the fluxes are consistent with the similar finding by Taipale et al., 2010, who compared Lag MAX with other methods on large water vapour fluxes with reference to LiCOR water flux data where DEC was simulated by the addition of artificial noise. However, the comparison for low concentration compounds has not been made before and the MAX method can lead to particularly high flux overestimation of such compounds. In addition for these situations the bias caused erroneous sign can be important. Therefore conventional methods have had to limit the reports of small-flux compounds to periods when their flux was sufficiently high. This could lead to so many rejections that low representativeness of data could affect model precision or could not be applied to modelling at all. Lag-time variability was explored and it was found that only the least variable lag-times within an integration time can guarantee high quality flux derivations.

Therefore it is proposed that the LTV method is included in the Fluxnet criteria, following tests by independent groups to examine if the LTV threshold of 30% produces the same confidence intervals for other PTR-MS systems and set-ups or other eddy covariance variants. The automation of the LTV test and the IMED lag method can substantially reduce the time needed to process difficult fluxes, especially where MAX and AVG methods can no longer perform well.

2.5.8 References

Clement, R. J., Burba, G. G., Grelle, A., Anderson, D. J., and Moncrieff, J. B.: Improved trace gas flux estimation through IRGA sampling optimization, Agric. For. Meteorol., 149, 623-638, 10.1016/j.agrformet.2008.10.008, 2009.

Davison, B., Taipale, R., Langford, B., Misztal, P., Fares, S., Matteucci, G., Loreto, F., Cape, J. N., Rinne, J., and Hewitt, C. N.: Concentrations and fluxes of biogenic volatile organic compounds above a Mediterranean macchia ecosystem in western Italy, Biogeosciences, 6, 1655-1670, 2009.

Foken, T., and Wichura, B.: Tools for quality assessment of surface-based flux measurements, Agric. For. Meteorol., 78, 83-105, 1996.

Foken, T., Göckede, M., Mauder, M., Mahrt, L., Amiro, B., and Munger, W.: Post-field data quality control, in: Handbook of Micrometeorology: A guide for surface flux measurement and analysis., edited by: Lee, W. M. X., and Law, B., Kluwer Academic Publishers, Dordrecht, 181-203, 2004.

Hörtnagl, L., Clement, R., Graus, M., Hammerle, A., Hansel, A., and Wohlfahrt, G.: Dealing with disjunct concentration measurements in eddy covariance applications: A comparison of available approaches, Atmospheric Environment, 44, 2024-2032, 2010.

Karl, T., Guenther, A., Yokelson, R. J., Greenberg, J., Potosnak, M., Blake, D. R., and Artaxo, P.: The tropical forest and fire emissions experiment: Emission, chemistry, and transport of biogenic volatile organic compounds in the lower atmosphere over Amazonia, J. Geophys. Res.-Atmos., 112, 17, D18302
10.1029/2007jd008539, 2007.

Karl, T. G., Spirig, C., Rinne, J., Stroud, C., Prevost, P., Greenberg, J., Fall, R., and Guenther, A.: Virtual disjunct eddy covariance measurements of organic compound fluxes from a subalpine forest using proton transfer reaction mass spectrometry, Atmospheric Chemistry and Physics, 2, 279-291, 2002.

Langford, B., Davison, B., Nemitz, E., and Hewitt, C. N.: Mixing ratios and eddy covariance flux measurements of volatile organic compounds from an urban canopy (Manchester, UK), Atmos. Chem. Phys., 9, 1971-1987, 2009.

Lee, A., Schade, G. W., Holzinger, R., and Goldstein, A. H.: A comparison of new measurements of total monoterpene flux with improved measurements of speciated monoterpene flux, Atmos. Chem. Phys., 5, 505-513, 10.5194/acp-5-505-2005, 2005.

Misztal, P. K., Nemitz, E., Langford, B., Coyle, M., Ryder, J., DiMarco, C., Phillips, G., Oram, D., Owen, S., Siong, J., Heal, M. R., Fowler, D., and Cape, J. N.: First direct ecosystem fluxes of VOCs from oil palms in SE Asia, Atmos. Chem. Phys. Discuss., in preparation for submission, 2010a.

Misztal, P. K., Owen, S. M., Guenther, A. B., Rasmussen, R., Geron, C., Harley, P., Phillips, G. J., Ryan, A., Edwards, D. P., Hewitt, C. N., Nemitz, E., Siong, J., Heal, M. R., and Cape, J. N.: Large estragole fluxes from oil palms in Borneo, Atmos. Chem. Phys., 10, 4343-4358, 10.5194/acp-10-4343-2010, 2010b.

Moncrieff, J., Valentini, R., Greco, S., Guenther, S., and Ciccioli, P.: Trace gas exchange over terrestrial ecosystems: methods and perspectives in micrometeorology, J. Exp. Bot., 48, 1133-1142, 10.1093/jxb/48.5.1133, 1997.

Rinne, H. J. I., Guenther, A. B., Warneke, C., de Gouw, J. A., and Luxembourg, S. L.: Disjunct eddy covariance technique for trace gas flux measurements, Geophys. Res. Lett., 28, 3139-3142, 2001.

Rinne, J., Durand, P., and Guenther, A.: An airborne disjunct eddy covariance system: Sampling strategy and instrument design, 15th Symposium on Boundary Layers and Turbulence, 151-154, 2002.

Rinne, J., Douffet, T., Prigent, Y., and Durand, P.: Field comparison of disjunct and conventional eddy covariance techniques for trace gas flux measurements, Environmental Pollution, 152, 630-635, 2008.

Spirig, C., Neftel, A., Ammann, C., Dommen, J., Grabmer, W., Thielmann, A., Schaub, A., Beauchamp, J., Wisthaler, A., and Hansel, A.: Eddy covariance flux measurements of biogenic VOCs during ECHO 2003 using proton transfer reaction mass spectrometry, Atmospheric Chemistry and Physics, 5, 465-481, 2005.

Taipale, R., Ruuskanen, T. M., Rinne, J., Kajos, M. K., Hakola, H., Pohja, T., and Kulmala, M.: Technical Note: Quantitative long-term measurements of VOC concentrations by PTR-MS - measurement, calibration, and volume mixing ratio calculation methods, Atmospheric Chemistry and Physics, 8, 6681-6698, 2008.

Taipale, R., Ruuskanen, T. M., and Rinne, J.: Lag time determination in DEC measurements with PTR-MS, Atmos. Meas. Tech. Discuss., 3, 405-429, 10.5194/amtd-3-405-2010, 2010.

Turnipseed, A. A., Pressley, S. N., Karl, T., Lamb, B., Nemitz, E., Allwine, E., Cooper, W. A., Shertz, S., and Guenther, A. B.: The use of disjunct eddy sampling methods for the determination of ecosystem level fluxes of trace gases, Atmos. Chem. Phys., 9, 981-994, 10.5194/acp-9-981-2009, 2009.

Wilczak, J. M., Oncley, S. P., and Stage, S. A.: Sonic anemometer tilt correction algorithms, Bound.-Layer Meteorol., 99, 127-150, 2001.

Wolfe, G. M., Thornton, J. A., Yatavelli, R. L. N., McKay, M., Goldstein, A. H., LaFranchi, B., Min, K. E., and Cohen, R. C.: Eddy covariance fluxes of acyl peroxy nitrates (PAN, PPN and MPAN) above a Ponderosa pine forest, Atmos. Chem. Phys., 9, 615-634, 10.5194/acp-9-615-2009, 2009.

2.6 Development of PTR-MS selectivity for monoterpenes

Table of contents

2.6.1 Abstract

Proton-Transfer-Reaction Mass Spectrometry (PTR-MS) is a very useful tool for high frequency detection and quantitation of gas-phase volatile organic compounds (VOCs). To date it has only been possible to measure the sum of monoterpenes which have been monitored most commonly at *m/z* 81 and 137 at a constant drift voltage and a constant drift pressure. Here it is demonstrated for the first time that PTR-MS is capable of discriminating individual monoterpenes when operating in the alternating drift voltage (AD mode). The approach is based on the principle that slightly different energies are required for the fragmentation/clustering of a given monoterpene; or, in other words, in an alternating drift voltage mode each monoterpene has a different time point for detaching a common or uncommon fragment. Therefore from a fragmentation analysis of background-subtracted standards it is possible to calculate the relative percentage of each monoterpene in an absolute concentration of their sum. Although monoterpenes have been chosen as an example in this experiment, this method is likely to be effective for other structural isomeric species such as the sesquiterpenes or MVK/MACR.

2.6.2 Monoterpene fragmentation regimes in PTR-MS

Monoterpenes as a total sum of isomers have been shown to be measurable reliably by PTR-MS (Grabmer et al., 2004; Hayward et al., 2004; Noe et al., 2008; Penuelas et al., 2007). The sensitivity of the technique is dependent on the ambient humidity (Tani et al., 2004; Tani et al., 2003) and drift tube conditions which regulate the proportion of signal at *m/z* 81 and *m/z* 137. This proportion can even have diurnal variations but generally the sum of these ions should be more or less constant. There have been attempts to try to unravel the information behind monoterpene fragmentation but with only small progress to improving PTR-MS specificity in this respect. For example, Maleknia et al. (2007) showed different abundances of monoterpenes and related compounds depending on the drift voltage used, and tested at *m/z* channels 155, 137, 135, 121, 119, 109, 107, 95, 93,

and 81. Although practically all the monoterpenes tested, including related compounds such as oxygenated monoterpenes (linalool, 1,8-cineole), gave high abundance signals at *m/z* 81 (except for p-cymene), not all the species had equally abundant signals at 137. Interestingly, other *m/z* channels in addition to 81 and 137 showed a big variability in abundance with particular monoterpenes. Although the U_d used was 580 V the same authors repeated the study at 480 V and 380 V but only for p-cymene and 1,8-cineole. The case for fragmentation of p-cymene is interesting because its protonated molecular ion detected at *m/z* 135 had the highest abundance at low U_d value (380 V) with only 2% of this abundance for the main fragment ion at *m/z* 93. However, increasing U_d by 100 V caused a shift in the fragmentation such that the main peak was detected at *m/z* 93 and only 55.2% of that abundance was for the parent ion. This was consistent with the study of Tani et al. (2003) who measured 50% of abundance occurring at *m/z* 93 at similar *E/N* conditions (120 Td). However, increasing further the drift voltage by 100 V (i.e., to 580 V) resulted in only 4.3% abundance of the parent ion relative to 100% abundance for *m/z* 93. It is therefore clear that manipulating the drift voltage in this case could potentially distinguish between p-cymene and toluene, which would interfere at *m/z* 93. Steeghs et al. (2007a) reported the possibility of partial monoterpene differentiation by means of Collision Induced Dissociation (CID) in the Proton-Transfer-Reaction Ion Trap Mass Spectrometer (PIT-MS). The authors provided some information on monoterpene fragmentation and focused on the *m/z* 95 fragment in that study, but the method has not been finalised other than to point out the possibility of discrimination by PIT-MS.

As part of this thesis a totally new method, employing a standard PTR-MS without any modifications, is shown to have great potential for discrimination of monoterpenes and other isomers under alternating drift-tube voltage. In the designed experiment (AD mode) the drift voltage was made to alternate by a certain time step per cycle in the range 400 V to 600 V. For the p_d of 200 Pa and T_d of 318 K this range corresponds to 93 – 139 Td. Such a range offers a sufficient energy span to force all parent monoterpene ions to fragment at the higher end of the Td range, but with prevalence of molecular ions at the lower end of the Td range. In between, at smooth

increases in drift energy, different monoterpenes would be likely to release fragments at different points with different efficacy. Therefore from the relative differences of the fragments to the main parent and main fragmented ions the relative proportions of each monoterpene can be deduced. It should be noted that the dependence of monoterpene signals on humidity increases with lowering the drift energies because of second order reactions and a very high number of clusters. This can actually be an advantage for distinguishing individual monoterpenes as the water clusters with monoterpenes could form adducts constituting more or less specific patterns.

2.6.3 Design of an Alternating-Drift PTR-MS (AD-PTR-MS)

In the first trials, initially the author tested a drift voltage (U_d) alternating from 400 V to 600 V with a 2 V time step (dU_d). Once the value of U_d reached its maximum value of 600 V the cycle repeated from 400 V again. Such a design was not optimal because the sudden drop in U_d caused a downward spike in primary ions which manifested as an upward spike in the normalised count for the compound Figure 2.6-1 .

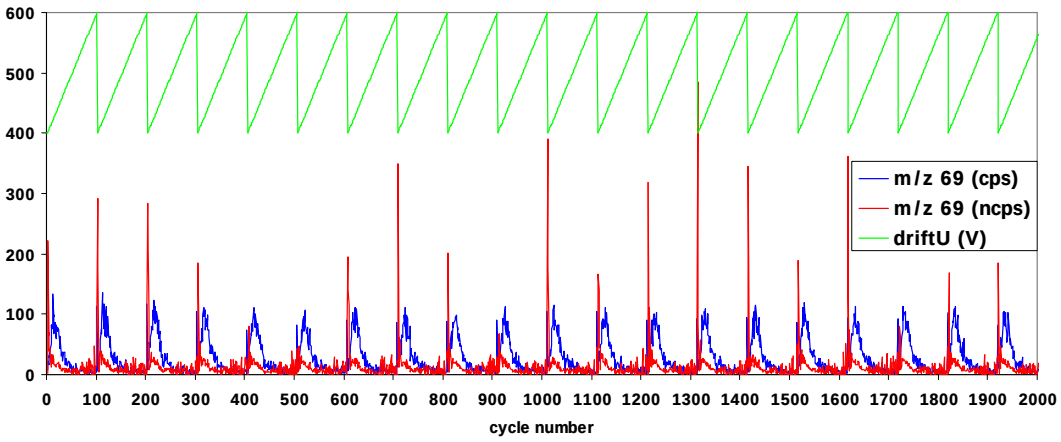

Figure 2.6-1 The impact of alternating U_d on an example time series for background isoprene. The sudden drop in the voltage causes a spike due to temporary destabilisation of the ion source.

Consequently, the change in voltage over time was redesigned so that $U_d = U_d + dU_d$ as before, but after reaching the threshold value of 600 V, $U_d = U_d - \mathrm{d}U_d$. On reaching the minimum voltage again the cycle restarted. As capturing the *m/z* spectrum from 21 to 206 amu requires a relatively long acquisition time, for example, ~ 1.5 min per scan at 0.5 s dwell time, the *dU* step was adjusted to 25 V, providing 18 data points per AD cycle and therefore two replicates for each voltage (i.e. 9 ascending voltages and 9 descending voltages). Such an approach gives approximately 25 min for the full AD mode, where the rest of the hour could be devoted for instance to eddy covariance flux measurement, and zero-air sampling. In addition, at least one zero air AD scan is required for the subtraction from the ambient AD spectra.

The section of the Balzer's code managing the changes of the drift voltage is presented below as extracted from driftad.seq (see electronic version in 'drift software' folder):

```
 //driftad.seq Pawel Misztal CEH, The University of Edinburgh

// i[0] main loop counter
// i[1] year
// i[2] month
// i[3] day
// i[4] hours of current time
// i[5] minutes of current time



SetPar( BarWidth=15, ColorMode=single, Cycles=500, DispOpt=last, LineType=solid,
Marker=on, YRaster=on )

Loop( i[0]=0;0 )
Begin
```

```
GetDate( Day=i[3], Month=i[2], Year=i[1] )
GetTime( Hour=i[4], Min=i[5] )
SetString( gs[0] = "@@@@" )
SetString( gs[0] = gs[0];i[2] )
SetString( gs[0] = gs[0];i[3] )
SetString( gs[0] = gs[0];i[4] )
SetString( gs[0] = gs[0];i[5] )

//changes drift voltage from 400-600 V with 25 V step


Loop( i[9]=400;600;25 )
Begin
    GetDate( Day=i[3], Month=i[2], Year=i[1] )
    GetTime( Hour=i[4], Min=i[5] )
    SetString( gs[0] = "@@@@" )
    SetString( gs[0] = gs[0];i[2] )
    SetString( gs[0] = gs[0];i[3] )
    SetString( gs[0] = gs[0];i[4] )
    SetString( gs[0] = gs[0];i[5] )
    SetString( gs[1] = "A" )
    SetString( gs[1] = gs[0];gs[1] )
    Message( Text="currently Udrift:";i[9] )
    SetAO( 3=i[9] )
    ScanBar( Par="drift.sbp", Disp=on, SaveCyc=gs[1] )

End
// changes voltage back from 600 to 400 with the 25 V step
Loop( i[9]=600;400;-25 )
Begin
```

```
        GetDate( Day=i[3], Month=i[2], Year=i[1] )
        GetTime( Hour=i[4], Min=i[5] )
        SetString( gs[0] = "@@@@" )
        SetString( gs[0] = gs[0];i[2] )
        SetString( gs[0] = gs[0];i[3] )
        SetString( gs[0] = gs[0];i[4] )
        SetString( gs[0] = gs[0];i[5] )
        SetString( gs[1] = "D" )
        SetString( gs[1] = gs[0];gs[1] )
        Message( Text="currently Udrift:";i[9] )
        SetAO( 3=i[9] )
        ScanBar( Par="drift.sbp", Disp=on, SaveCyc=gs[1] )

    End
```

The changes of U_d resulted in characteristic profiles of the first water cluster signal (*m/z* 37); it also affected primary ions and other *m/z* intensities. Examples are provided in **Figure 2.6-2**.

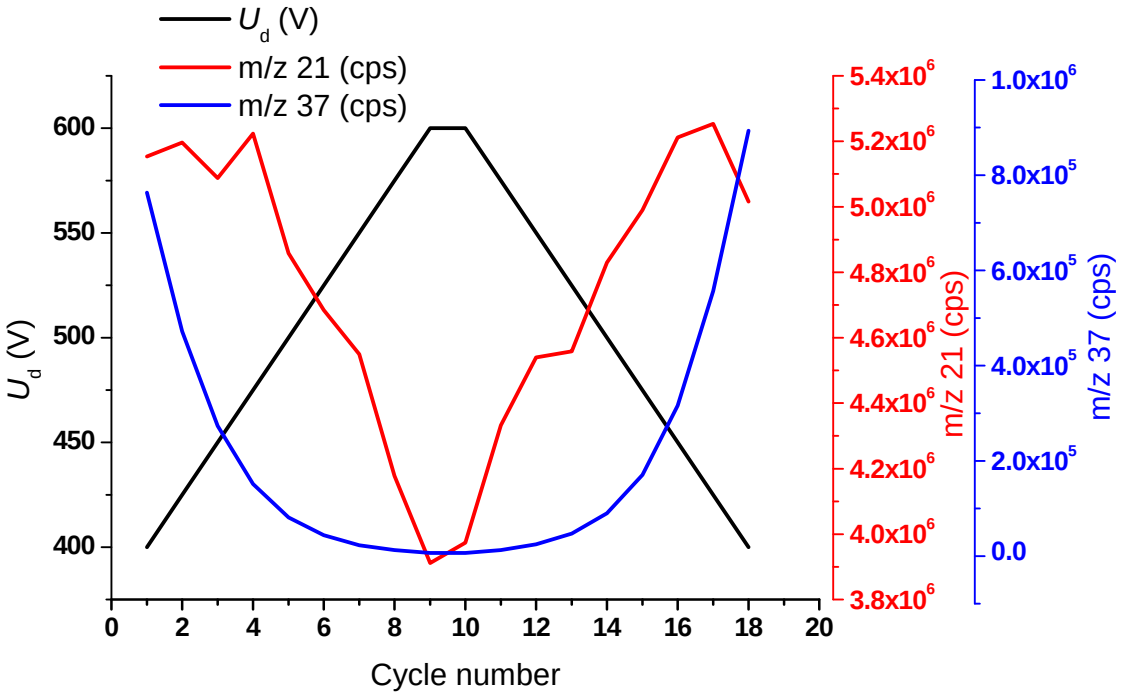

Figure 2.6-2. A typical AD cycle showing changes in primary ions (*m/z* 21 x 500 cps) and water cluster (*m/z* 37) as a result of alternating U_d.

As has been mentioned earlier, varying U_d varies the *E/N* ratio, and hence varies the collisional energies, which in turn impact on the distribution of the fragments. Even though the fragmentation can be regarded as soft, isomeric structures can still degrade at slightly different energies. Clearly, there is also an associated impact on the varying sensitivities, which, since recently, have been known to vary between individual isomers. For this reason using a single monoterpene for calibration of the monoterpene sum is not optimal but is acceptable at typical constant drift voltages, after normalisation for *m/z* 21 and *m/z* 37, and after including the sum of at least the most significant fragments. In the AD-PTR-MS mode water clusters vary greatly from below 1% of the primary ions at U_d = 600 V to as much as 20% at U_d = 400 V. These changes are beneficial for elucidations of specific features since collisions with water clusters provide additional opportunity for specific fragmentation and also for the creation of

molecular clusters, which is likely to occur at different drift voltages for different structures of the same isomer. Under certain conditions a dimerisation of fragments can be facilitated. As is shown later, the simple analysis of the main fragments selected from the scan can already be sufficient in many cases to discriminate between isomers measured in AD-PTR-MS. However, application of multivariate factor analysis such as positive matrix factorisation (PMF) is ideal for the recognition of the AD-PTR-MS scans and is described in detail below.

2.6.4 Methods

2.6.4.1 AD Calibration

For the AD-PTR-MS calibration the drift pressure was maintained constant at 200 Pa, drift temperature at 40 ºC, and the water vapour flow to the hollow cathode at 6.5 sccm. The U_d was alternated between 400 V and 600 V as described in the previous section. Samples of individual monoterpenes were vaporised in clean Tedlar ® bags filled with 3 L VOC-free air by injecting 2 µL of an ultrapure liquid standard (Sigma Aldrich, UK). The resulting concentration (~ 700 ppb) was expected to be high enough to ensure the domination of the *m/z* spectrum by a given monoterpene but not high enough to cause a decline in primary ions. The air flow in the PTR-MS inlet was reduced from 300 ml min^{-1} to 50 ml min^{-1} which was sufficient to perform the full AD course (1 ascending and 1 descending voltage ramp) withdrawing less than half the gas from a bag. Altogether six monoterpenes (α-pinene, β-pinene, d-limonene, 3-carene, γ-terpinene, and α-phellandrene) and one monoterpene-related compound (p-cymene) were prepared, each in separate identical bags (7 bags in total + 1 bag with zero air).
A zero air generator (Sonimix 3052B), which is a self regenerating system operating on the principle of the pressure difference and the inverse flow, was used as dilution gas for the bags. This generator was able to strip all VOCs from the ambient (lab) air except for

methanol whose counts constituted 0.05% of the primary ions. In fact only a small portion of the counts at *m/z* 33 corresponded to true ambient methanol as the background at this ion channel is typically high (as compared with the other Pt/Al_2O_3–based zero air filter removing methanol). The amount of methanol that could be in the bags was insignificant with reference to the concentrations of the monoterpenes used in the study and it was about the same level for all bags. The reason for the use of the Sonimix 3052B generator for this study was slightly better removal efficiency towards the compounds above 45 amu and substantially higher flow rate. All bags were analysed on one day starting from the bag containing only the zero air.

Each full course of the AD-mode, automated from the Quadstar platform for a given compound, contained 18 cycles of the scans between *m/z* 21 and 206. Starting from U_d of 400 V the voltage was kept constant during a scan cycle and increased by 25 V between each cycle until 600 V was reached (ascending mode). Subsequently, starting from 600 V the voltage was reduced by 25 V between each cycle finishing at 400 V (descending mode). Then the bag was detached from the instrument and the PTR-MS was flushed with zero air sampled directly for at least 15 minutes before another bag was connected. The AD-course for β-pinene was repeated a second time on the next day from the same bag (stored in the dark) in order to check for the amount of variability between the replicates. The actual AD patterns for main fragments were almost identical although the whole spectrum contained somewhat more small peaks than earlier and the normalised absolute values of main fragments were very slightly smaller, which could be due to internal degradation of the standard.

2.6.4.2 Postprocessing

A LabVIEW program was written for the post analysis (ADProcess_tested_LV8.5.llb, Misztal, PK, CEH, UoE; available in electronic version in ‘drift software’ folder). The program automatically reads the scan files, and normalises the counts at each cycle to 1×10^6 cps of the primary ions and water cluster at *m/z* 37. In addition each cycle had a corresponding cycle of the zero air bag subtracted and returned three spreadsheets: with

absolute counts (_cps suffix), normalised only for primary ions (ncps), and normalised for both the primary ions and water clusters (ncps_w). Normalised counts (ncps) were derived as in Equation 2.6-1, whereas normalised counts for both the primary and water-cluster ions (ncps_w) as in Equation 2.6-2.

Equation 2.6-1

$$I_{\mathrm{ncps}} = \mathrm{d}_{\mathrm{norm}} \cdot \frac{I_{\mathrm{cps}} \cdot I_{\mathrm{ZAm/z21}} - I_{\mathrm{ZAcps}} \cdot I_{\mathrm{m/z21}}}{I_{\mathrm{m/z21}} \cdot I_{\mathrm{ZAm/z21}}}$$

Equation 2.6-2

$$I_{\mathrm{ncps}} = \mathrm{d}_{\mathrm{norm}} \cdot \frac{I_{\mathrm{cps}} \cdot \left(I_{\mathrm{ZAm/z21}} + I_{\mathrm{ZAm/z37}}\right) - I_{\mathrm{ZAcps}} \cdot \left(I_{\mathrm{m/z21}} + I_{\mathrm{m/z37}}\right)}{\left(I_{\mathrm{m/z21}} + I_{\mathrm{m/z37}}\right) \cdot \left(I_{\mathrm{ZAm/z21}} + I_{\mathrm{ZAm/z37}}\right)}$$

In these equations, I_{cps} and I_{ZAcps} are the signals in counts s^{-1} of a monoterpene and corresponding zero-air, respectively, while $I_{m/z21}$ and $I_{\mathrm{ZA}m/z21}$ are the corresponding signals at *m/z* 21 of a monoterpene and the zero air, respectively. The normalisation constant $\mathrm{d}_{\mathrm{norm}}$ is equal to 2000 ncps accounting for the 1×10^6 ncps normalisation level of primary ions divided by an approximate *m/z* 19 to 21 isotopic ratio of 500 corresponding to the abundance ratio between $H_3{}^{16}O^+$ and $H_3{}^{18}O^+$. The parameters $I_{m/z37}$ and $I_{\mathrm{ZA}m/z37}$ denote water-cluster [$H_3{}^{16}O^+(H_2{}^{16}O)$] counts at *m/z* 37 ion channels of a sample and the zero air, respectively.

The analysis of the fragmentation patterns had two stages: analysis of the selected fragments and the covariate analysis of the whole patterns.

The first stage consisted of the selection of the prevailing ions at the cumulative mass spectra (neglecting *m/z* ratios which had less than 0.05% abundance), then the derivation of their dependence on the U_{d}, and the extraction of the critical (in the most cases stationary) U_{d} points with the potential for their use as specific features of a particular monoterpene. The selected protonated ions were 137, 121, 93, 81, 79, 67, 57, 41, and 39.

All these ions have been deduced to be specific to a monoterpene from the highest abundance and later it was confirmed in the PMF analysis (see section 2.6.5.2) that these ions indeed had the highest coefficient of determination (r^2) of the observed and predicted values in the PMF model. However, *m/z* 95 and *m/z* 88, despite their elevated abundance, were regarded as pollution from the material of Tedlar® bags (Steeghs et al., 2007b), where the latter is most likely N,N-dimethylacetamide used in their production. Tani et al. (2003), using a thermal diffusion approach of the pure standards, identified ions at *m/z* 71, 93, 97, 109 and 119 as impurities and used ions at *m/z* 67, 68, 81, 82, 95, 96, 137 and 138 in the analysis for monoterpenes. On the other hand, Maleknia et al. (2007) used protonated masses 93, 95, 107, 109, 119, 121 and 137 in referring to terpenes.

In the AD approach presented here the selection of the protonated masses was done independently. The ion $C_9H_{13}^+$ at *m/z* 121 might be potentially important as it can form presumably from the abstraction of CH_4 from a parent monoterpene ion $C_{10}H_{17}^+$ (*m/z* 137). For p-cymene $C_{10}H_{15}^+$ (*m/z* 135) the similar abstraction would lead to $C_9H_{11}^+$ at *m/z* 119, so 135 and 119 ion were added in p-cymene analysis. Clearly, many of the fragments might coincide with either impurities or other common masses like higher-order water clusters. This can be easily picked up on the AD graphs of U_d dependence and factor analysis, which can extract common features of many fragments together. However, for calibration purposes it is sensible to use sufficiently high concentrations. For example *m/z* 39 receives an input from $H_3{}^{18}O(H_2O)^+$, which is typically 0.5% of the *m/z* 37 signal for $H_3{}^{16}O(H_2O)^+$, but on the other hand it could be the protonated cyclopropenylidene (c-$C_3H_3^+$), which can potentially further attract (H_2O) to cluster at *m/z* 57, although *m/z* 57 could be regarded also as butyl fragment, depending on the monoterpene structure and *m/z*. Assuming *m/z* 37 constitutes 1% of the primary ions, the contribution from water clusters to *m/z* 39 would be around 0.005% of primary ions so approximately 50 cps normalised to $1 \cdot 10^6$ cps. If 1% of monoterpenes fragments onto *m/z* 39 and assuming 5 times higher sensitivity for monoterpenes at this *m/z* than at *m/z* 137, then approximately 5 ppb level of monoterpenes would be needed to exceed the contribution from the water cluster signal. As a matter of fact the signal related to water

clusters at *m/z* 37 could be converted using the isotopic ratio and subtracted from the *m/z* 39 signal in the AD spectra. Typically the *m/z* 41 (C_3H_4) fragment is elevated, which could represent propadiene or cyclopropene, in monoterpene-rich atmospheres. Another interesting fragment which dominates monoterpene spectra occurs at *m/z* 67 ($C_5H_7^+$), which could be either cyclopentadiene or [1.1.1]propellane. It was rather surprising to observe *m/z* 79 for some monoterpenes (e.g. > 1% in α-phellandrene). Previously it has only been reported as contributing to 14% of fragments of adamantane ($C_{10}H_{16}$) (Steeghs et al., 2007a) but has not yet been described as a monoterpene fragment, possibly because of an assumption that it might be benzene present as an impurity in the standard. However, the relationship of the *m/z* 79 signal in response to the change in U_d suggests that it could be benzene or less likely a fragment isomeric to benzene (e.g. bicyclopropenyl), formed when the C_4H_{10} (butane, isobutane) moiety is lost from a monoterpene. Given the theoretical stability of bicyclopropenyl (Dinadayalane et al., 2004), it is possible that it fragments further in order to form a very short lived cyclopropenylidene or other isomeric C_3H_2-H^+ ion at (*m/z* 39). The dependence on U_d suggests this *m/z* to be the fragmentation product (increasing with U_d) whereas fragmentation of benzene is not favoured in the soft ionisation offered by PTR-MS (Ammann et al., 2004; Warneke et al., 2001), but highly probably it may be formed easily via the dehyhydrogenation of the cyclohexadienyl fragment.

The data were normalised and expressed as the relative percentage of the sum of the ions selected but the normalised counts were not transmission corrected. Normally, transmission is derived by a measurement at a constant *E/N* condition, so for this study no transmission correction has been made but, in general, derivation of a transmission in the AD-mode might be useful. However, the relative differences of the voltage-dependent changes should be the same in all cases despite different absolute differences. Because normally the transmission starts to decline rapidly after 100 amu due to the fringing field effect (Kim et al., 2009), the corrected signal would be higher at the larger *m/z*; for example at *m/z* 137 it should be around 2.5 times higher than without the correction (as used here). As a matter of fact, different monoterpenes may be likely to

have a similar transmission measurement, but the uncertainty in the proton transfer reaction rates for each of them could introduce a bias. So the method presented here is principally qualitative. If the method can produce the relative proportions of isomers, then the absolute concentration could be derived from the comparison with the classical calibration approach for the sum of monoterpenes.

2.6.4.3 Double-blind trial

The analysis of unknown samples was done under the same conditions as those during the AD calibration but the concentrations were much lower in order to bring the challenge of discrimination to be closer to ambient levels. All 6 bags previously used in calibration, containing approx. 700 ppb of each monoterpenes (p-cymene bag excluded) were selected for randomisation. Opaque labels were used to cover the old labels with names of a monoterpene. Then the bags were shuffled and 4 of them were randomly picked by a person not involved in the experiment, who marked their labels A1, A2, A3 and A4. Four brand new bags flushed 5 times with zero air were filled with approximately 3 L of zero air. Subsequently, 50 mL of A3 monoterpene was injected to the first bag, 50 mL of A1 to the second, and the third bag was prepared to contain a mixture of A2 and A4 monoterpenes (25 mL each). The last bag was left to serve as the first zero air run. Therefore bags contained approximately 10 ppb of a monoterpene/monoterpenes, so just on the limit of detection for some small fragments.

2.6.4.4 Positive Matrix Factorisation

Positive Matrix Factorisation (PMF) has been recently employed successfully for the interpretation of organic components of aerosol mass spectrometric data (Ulbrich et al., 2009). Even more recently it has been applied for the first time to PTR-MS fragmentation patterns (Slowik et al., 2010). Here for the first time PMF is used for the analysis of the AD-PTR-MS fragmentation patterns.

The PMF model belongs to algorithms used in multivariate receptor modelling. Other matrix factorisation techniques include Principal Component Analysis (PCA) or Singular Value Decomposition (SVD). These methods differ in the types of constraint used in the data analysis, for example, in PMF the factor matrices must not be negative, so another name for this method is Non-Negative Matrix Factorisation (NNMF). The original PMF model (Paatero, 1997; Paatero and Tapper, 1994) assumes that a measured dataset fulfils mass balance conservation of a number of constant source profiles of the concentration of species variable in time, so that:

Equation 2.6-3

$$x_{ij} = \sum_{h=1}^{p} g_{ih} f_{hj} + e_{ij}$$

where i and j refer to the dimensions of matrix **X** with j being the *m/z* in the dataset and i the individual *m/z* scans. The number of factors p, the elements of the species' factor profile f_{hj} for each source (rows of matrix **F**) and the elements of the amount of factor contribution g_{hj} in the factor time series expressed as columns in the matrix **G** are desired to be produced by the model with e_{ij} being the elements of the residual matrix **E** which do not fit the model for each experimental data point (**E** = **X** – **GF**). Finally, **G** and **F** are fitted to the data by minimising the quality of fit parameter Q by using a least-squares method:

$$Q = \sum_{i=1}^{n} \sum_{j=1}^{m} \left(\frac{e_{ij}}{u_{ij}} \right)^2$$

where u_{ij} is the uncertainty.

Application of PMF to AD-PTR-MS mass spectra requires making slightly different assumptions from those used normally in the mass spectral analyses. The major

difference is that in classical approaches the concentrations of species are thought to vary over time according to the constant reaction chamber parameters (sensitivity, fragmentation), whereas in AD-PTR-MS the concentration is assumed to be constant during an AD course, which is relatively short, but the *E/N* ratio is variable as affected by alternating U_d. For this part of the experiment, the additional hypotheses were assumed: 1) the factors and their profiles found by PMF in AD-PTR-MS can be related to the structure of an isomer, and 2) the common factors have different relationships with the drift voltage.

For the initial PMF analysis the program EPA PMF 3.0 (EPA, 2010), designed for receptor modelling of air quality data, was used. The AD-PTR-MS normalised for *m/z* 19 and 37 and zero-air subtracted data output from the AD_Process program was used as a matrix **X** input. The negative values resulting from zero-air subtraction were replaced by zeros. The EPA PMF 3.0 program also requires a file with uncertainties and detection limits. For consistency and simplicity, the universal 10 ncps was set for all *m/z* as the detection limit, while the error of determination was set for all to 1%. Also as previously, the data were not corrected for transmission, in order to limit the amount of data manipulation only to the minimum necessary, and to avoid bias arising from uncertainty in the reaction rate constants for given isomer species and their fragments. Although the sensitivities vary substantially in the AD mode, the relative transmission is thought to be generally constant if all the contributing fragments/clusters can be taken into account.

For different PTR-MS instruments, either an AD calibration would be needed or a derivation of the relationship to the transmission measured at a constant *E/N* ratio. It is possible that different structures can have slightly different proton-transfer reaction rate constants independent of the *E/N* ratio whereas the transmission for each monoterpene is likely to be similar but can be slightly varied with *E/N* ratio, not because of the change in the drift energies *per se* (as these would be compensated), but possibly because of the different ion extraction efficiency (identical for all the monoterpenes) through the aperture to the detection chamber.

2.6.5 Results

2.6.5.1 AD patterns – differences in fragmentation.

Even general inspection of the AD patterns presented in Figure 2.6-3 makes it clear that reliance only on the usual *m/z* values for monoterpenes (81 and 137) under a constant U_d might be insufficient to draw conclusion about the specificity of a monoterpene compound. On the other hand, the curves of 81 and 137 versus U_d in the AD mode do look different for different monoterpenes (e.g., more or less pronounced curvature, straight line or a line with inflexion point). However, a limitation to just 81 and 137 prevents us from obtaining additional specific features from the many other fragments which can be used in the discrimination. The immediate differences are in the range of a percentage of a given mass, and a drift-voltage dependent abundance. The characteristic can also be seen in stationary points of U_d which can be visualised on individual graphs for the most important fragments (see next sections), and in the factors derived from PMF analysis and their behaviour versus U_d (Sect. 2.6.5.2). Differences in fragmentation patterns of the monoterpenes themselves (Figure 2.6-3) may not be as obvious as the difference with a monoterpene-like compound such as p-cymene (Figure 2.6-4), which differs in the presence of the aromatic ring. One can see that the colour-coded drift voltage affects the variability of *m/z* ratios impacting their relative abundances. From the vast information that these AD spectra provide, it can be seen, for example, that variability in the relative abundance of m/z 81 in α-pinene (or β-pinene) is significantly lower than the corresponding variability in d-limonene. Another example difference concerns *m/z* 121 which differs both in the range and the values although some isomers are similar in this respect (e.g. α-phellandrene and β-pinene have a higher spread in abundance whereas 3-carene and d-limonene have a clustered appearance). There seem to be slightly different *m/z* 137 patterns although more evident differences might be sought in the isotopic *m/z* 138 and *m/z* 139. Interestingly there is significantly elevated *m/z* 153 ion in γ-terpinene, also present but at lower level in α-phellandrene and d-limonene, and reaching highest abundances at the lower *E/N* ratio regions. These

monoterpenes have an atmospheric lifetime of the order of tens of minutes while for example pinenes or carenes in the order of hours (Atkinson and Arey, 2003) so *m/z* 153 (137+16) could indicate an oxygenated molecule, which could form in a tedlar bag or following exposure to the drift-tube temperature. Impurity of a standard must also be considered as a possibility. Another interesting feature was manifested by 3-carene which produced two specific signals, at *m/z* 135 (middle range at 400 V as in *m/z* 121) and *m/z* 151, which might be 3-caron aldehyde fragments, while small *m/z* 151 in α-pinene could be a fragment from pinon aldehyde. Behaviour in AD suggests that these were not clusters, so must have formed a priori. However, *m/z* 81 and 137 together take up typically more than 95% and therefore reliance on other fragments puts additional strain on the sensitivity, so might not be effective at low mixing ratios. It is shown later (Sect. 2.6.5.3) that actually m/z 81 and m/z 137 alone can be sufficient in an alternating *E/N* mode, although better confidence can be achieved with conjunction with PMF, which take into account the whole fragmentation profiles.

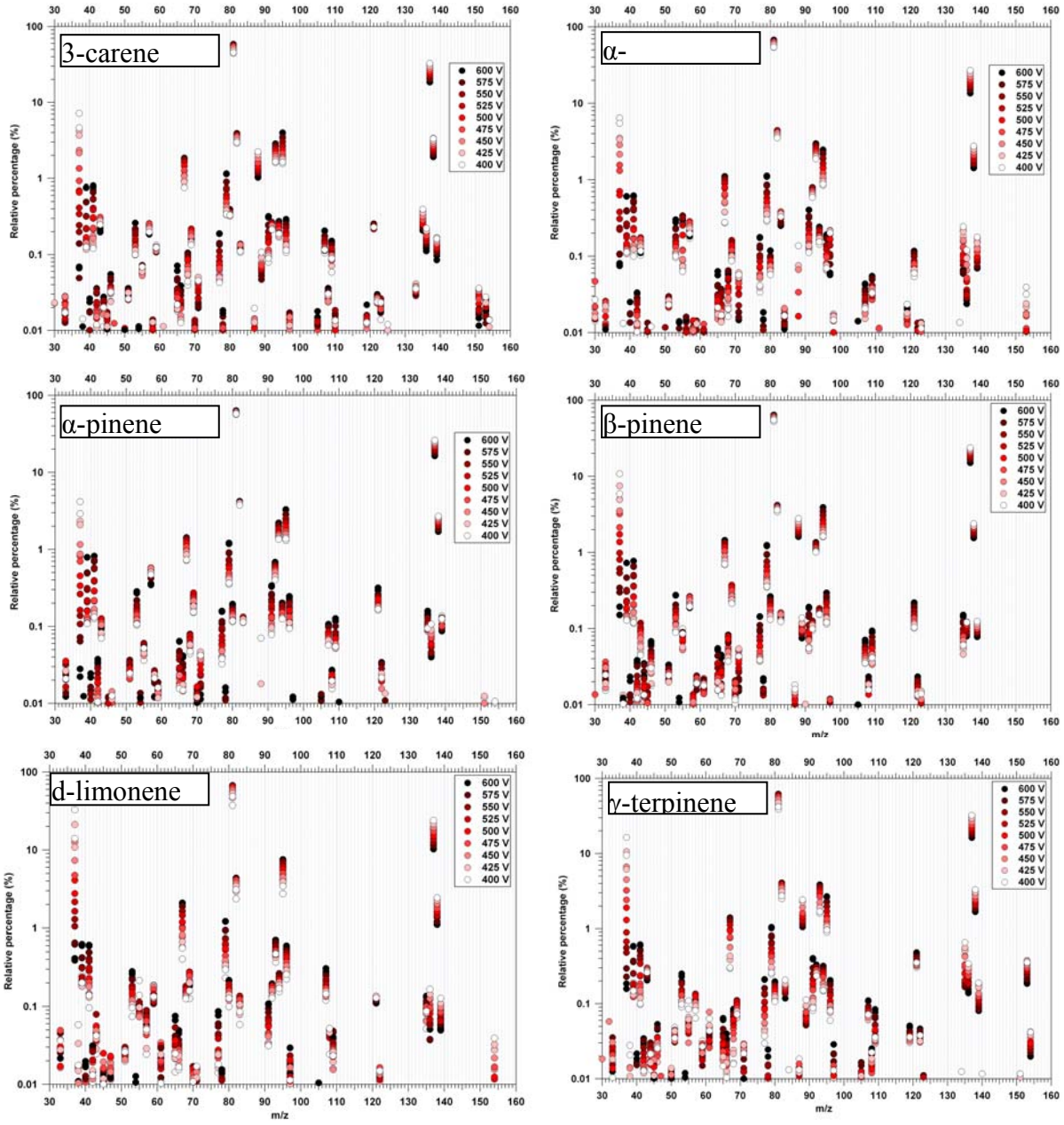

Figure 2.6-3. Patterns for six structurally different monoterpenes ($C_{10}H_{16}$) in relation to drift voltage (colour scale).

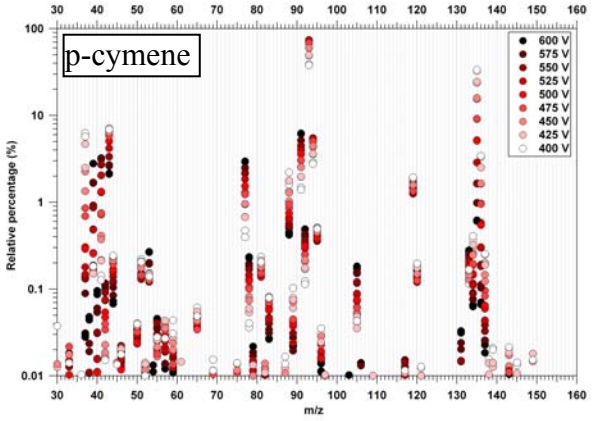

Figure 2.6-4. Fragmentation pattern for p-cymene ($C_{10}H_{14}$). Note analogous fragments to those of monoterpenes but – 2 (*m/z* 119 for *m/z* 121, *m/z* 93 for *m/z* 95, and many common fragments (e.g. butyl at *m/z* 57, or carbenium ion at *m/z* 41, cyclopropenylidene ion at *m/z* 39). The parent ion at *m/z* 135 seems to be much more variable than *m/z* 137 for any monoterpene.

2.6.5.1.1 α-phellandrene

IUPAC name: 2-methyl-5-(1-methylethyl)-1,3-cyclohexadiene

One of the main features of this monoterpene is that it has a hexadienyl ring but does not have any double bonds in its alkyl radicals. The principal fragmentation with characteristic critical voltages ($U_{dc\_m/z}$) is presented in Figure 2.6-5.

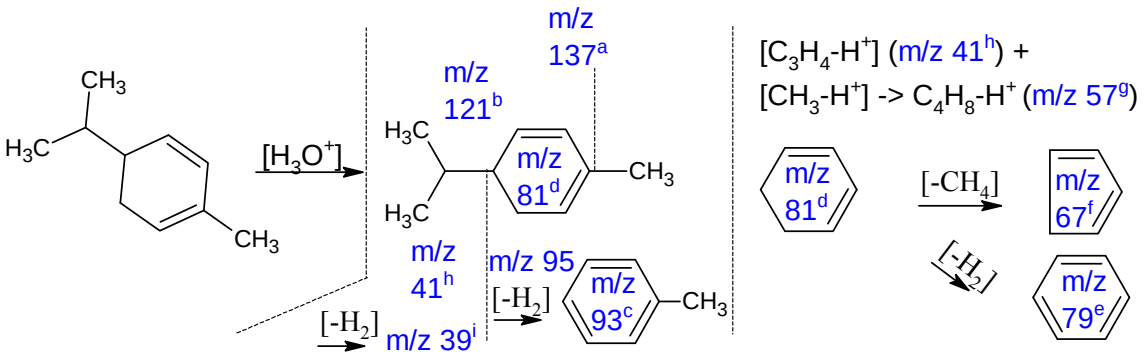

Figure 2.6-5. Schematic for the fragmentation of α-phellandrene with the attribution of the fragments to their corresponding protonated *m/z* channels. The superscripts at each *m/z* (except for 95 in order to avoid possible interference with Tedlar™ bag material) refer to characteristic $U_{dc\_m/z}$, which are further explained in the text.

The critical voltages $U_{dc\_m/z}$ denoted as superscripts to the *m/z* values (Figure 2.6-5) are as follows: a) $U_{dc\_137} = 475$ V; b) U_{dc_121} = N/A; c) $U_{dc\_93a} = 463$ V, $U_{dc\_93b} = 563$ V; d) $U_{dc\_81} = 475$ V; e) $U_{dc\_79} = 550$ V; f) $U_{dc\_67} = 525$; g) $U_{dc\_57} = 500$ V; h) $U_{dc\_41} = 588$ V; $U_{dc\_39} = 550$ V. These voltages were derived by analysing the dependence of the relative proportion of the fragment versus U_d (Figure 2.6-6) either by calculating the intersection of the lines tangential to the curve or by extrapolating the U_d value if the curve has an evident peak or trough (e.g., as in *m/z* 57 in Figure 2.6-6). In the same figure the normal distributions are presented for observing the cumulative spread in relative values.

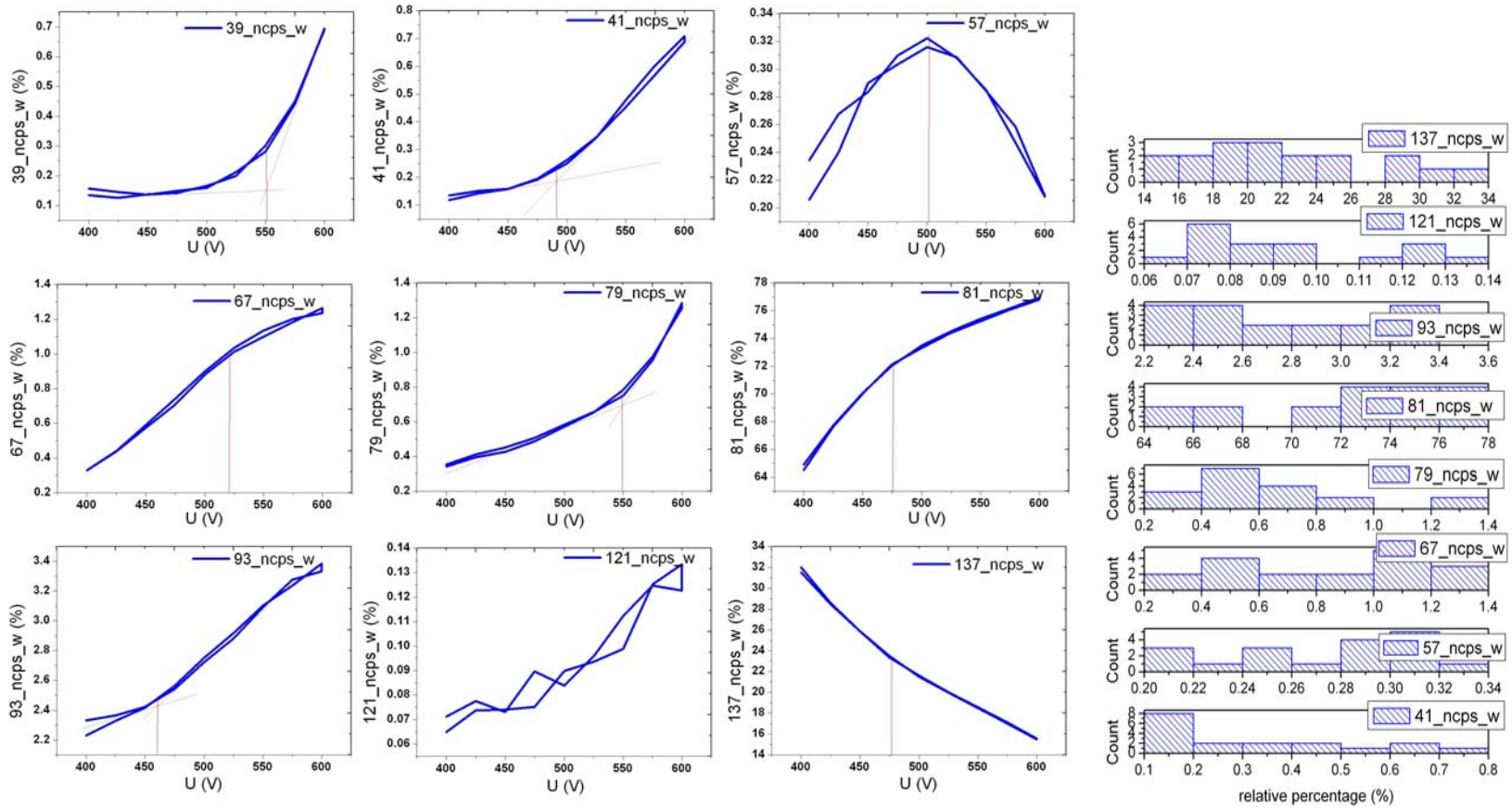

Figure 2.6-6 Variability with U_d and distributions of the key ions (as relative abundance) in AD-PTR-MS of an α-phellandrene rich atmosphere. The distributions serve to aid in recognising the frequency of ion occurrence at a given percentage abundance.

2.6.5.1.2 α-pinene

IUPAC name: (1S,5S)-2,6,6-trimethylbicyclo[3.1.1]hept-2-ene

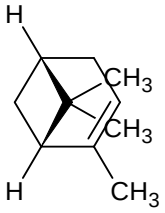

The fragmentation is not presented for this species, since the major fragments will be the same as presented for α-phellandrene. The only difference will be in the critical voltages or the shape of the dependence of the abundance of a given fragment on U_d. The α-pinene molecule has only one double bond in the cyclohexenyl ring, a tertiary carbon and a similar conformation of the methyl substituent to that of α-phellandrene. Therefore the differences would be expected in *m/z* 57, which is probably a product of the two substituents (C1+C3) detached from the ring. As shown in Figure 2.6-7 the formation of this adduct at *m/z* 57 increases until approximately 450 V and then it becomes stabilised, as shown by the plateau, before the ionisation energy at about 550 V further fragments this molecule. At the same voltage (i.e., 550 V) one can notice a simultaneous sharp increase in *m/z* 79 and *m/z* 39, which is probably an effect of dehydrogenation [$-H_2$] leading to formation of stable benzene from cyclohexadienyl fragment (*m/z* 81) and cyclopropenylidene from the carbenium ion (*m/z* 41). In the light of this, it is unlikely that *m/z* 79 is bicyclopropenyl since it is extremely unstable so would lead to a decrease in *m/z* 79 due to dissociation. It might be possible that the high *E/N* conditions enable certain fragmented moieties to undergo cyclisation and/or proton-bound dimerisation (typical for low *E/N*), but which will not dissociate even at so high energy because of the exceptional stability of the proton-bound adduct (Audier et al., 1996). However, the most important can be highly abundant ions at *m/z* 137 which showed almost linear relationship with U_d. This is a unique feature shared with only one other monoterpene (β-pinene).

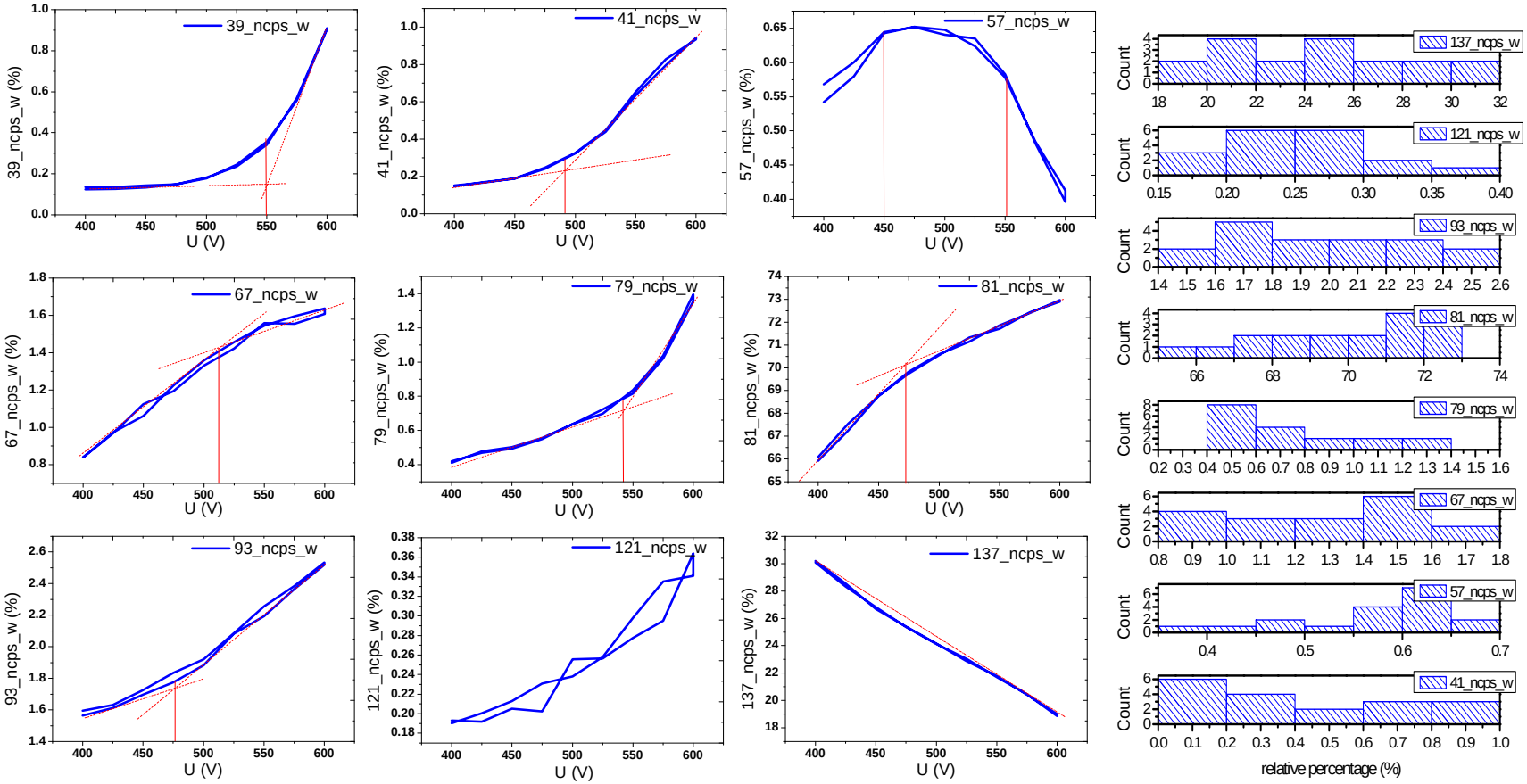

Figure 2.6-7. Variability with U_d and distributions of the key ions (as relative abundance) in AD-PTR-MS for α-pinene.

2.6.5.1.3 β-pinene

IUPAC name: 6,6-dimethyl-2-methylenebicyclo [3.1.1] heptane

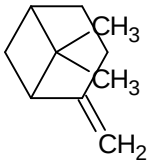

An analysis of *m/z* intensities as a function of U_d for β-pinene, shown in Figure 2.6-8, indicates many similar features to those of α-pinene such as the near linearity for *m/z* 137 and the increase in likely phenyl ion at *m/z* 79 and C_3H_2-H^+ at *m/z* 39 sharply increasing after 550 V. However, compared with α-pinene there is more than a factor of two lower abundance at *m/z* 57 giving a slightly noisier shape, whereas *m/z* 121 exhibits a much clearer signal. These changes are very likely due to the presence of the double bond in the methylene group attached to the 6,6-dimethylbicyclo [3.1.1] heptane structure. The noisy appearance of *m/z* 57 may be related to substrate unavailability, whereas the clearer signal at *m/z* 121 is likely the result of the detachment of the methylene substituent. Possibly the toluene fragment (*m/z* 93) cannot be formed as efficiently during the loss of the C_3H_4-H^+ fragment (*m/z* 41), if the methylene group has been detached first, not favouring the excess of methylcyclohexadiene ions. Since this is also the only monoterpene without double bonds in the ring, one could regard the formation of toluene less favourable, which can be seen in a noisy pattern of *m/z* 93 at a low relative abundance (< 1.6 %). However, it is not clear why no differences can be seen for *m/z* 79 ions, which are similar in pattern in all monoterpenes with only small variations in the characteristic voltages, but can possibly be formed from always highly abundant m/z 81, whereas the benzyl ion (*m/z* 93) requires the availability of a stable methyl group in the ring. Quite remarkable difference is in the pattern of *m/z* 137, which is almost linear. This feature is very similar to α-pinene but not to other monoterpenes whose parent ion exhibited a pronounced curvature (less pronounced in α-phellandrene).

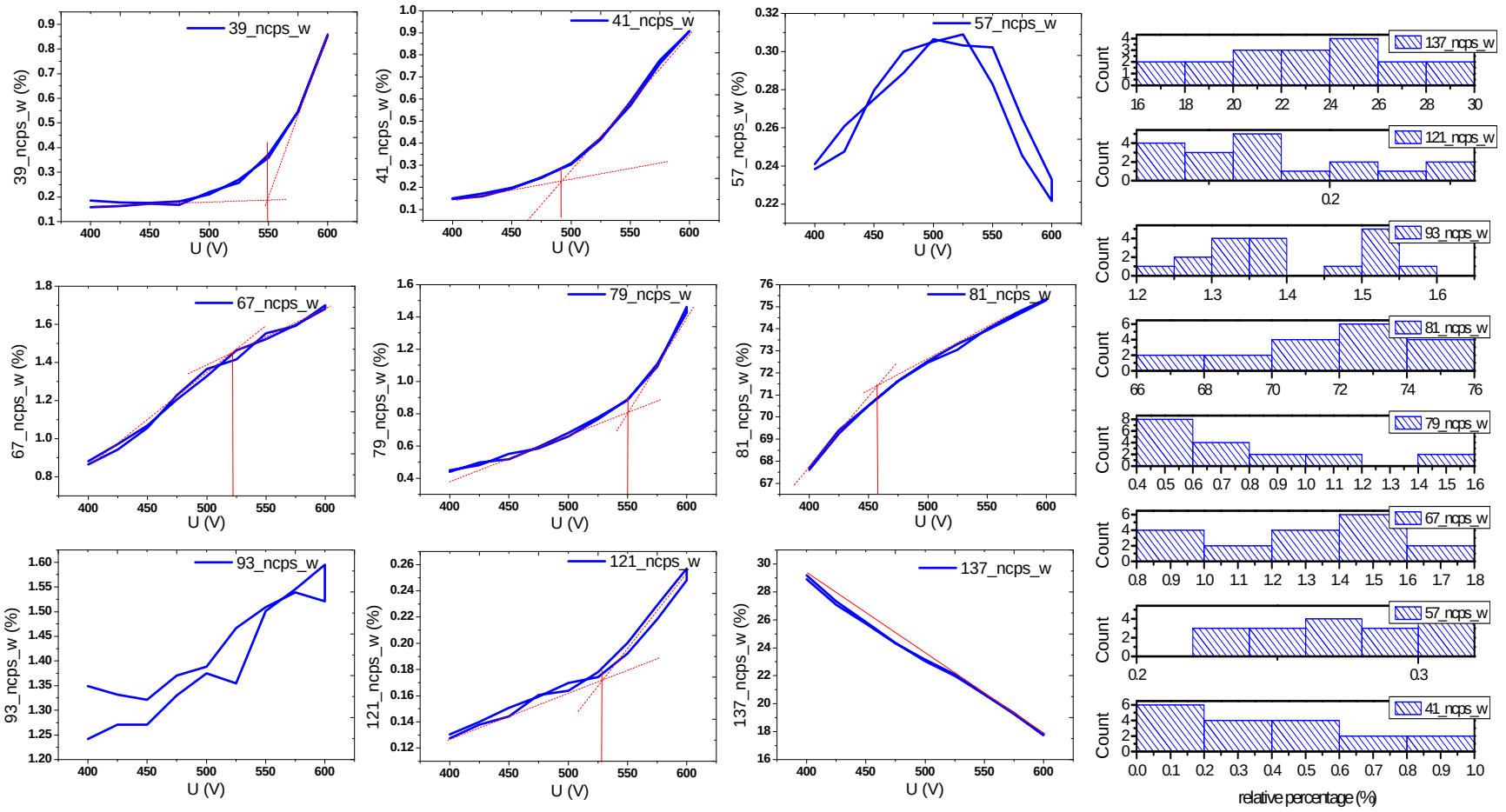

Figure 2.6-8. Variability of main fragments with U_d and their distributions (as relative abundance) in AD-PTR-MS for β-pinene.

2.6.5.1.4 d-limonene

IUPAC name: 4-isopropenyl-1-methylcyclohexene

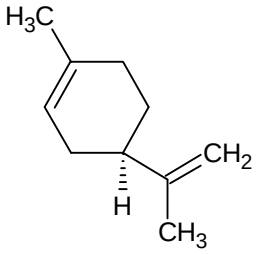

A unique feature of this monoterpene molecule is the presence of the isopropenyl connected to the cyclohexenyl ring. Only one double bond in the ring is also common to α-pinene (also next to methyl substituent) and 3-carene (different position in the ring). The general observation from the AD patterns is that a strong signal at *m/z* 93 (benzyl ion) is associated with a weak signal for m/z 121 which can be related to the tendency to form either an isopropyl-deficient or methyl-deficient ion, respectively. However, this monoterpene, as seen in Figure 2.6-9, has low and noisy patterns for both of the ions, so it might be that the isopropyl is not detached completely from the ring but forms either p-methyl or p-methylethyl or p-methylethenyl ring structures. One piece of supporting evidence for this can be the highest *m/z* 107 signal as observed earlier from fragmentation patterns (Figure 2.6-3). The only other monoterpene with almost as elevated xylene *m/z* was 3-carene, whose structure may also permit formation of this in addition to formation of toluene. The distribution of the parent ion *m/z* 137 is the most skewed to the left in comparison with all other monoterpenes, so it is highly probable that the isopropenyl substituent makes this structure the least resistant to fragmentation.

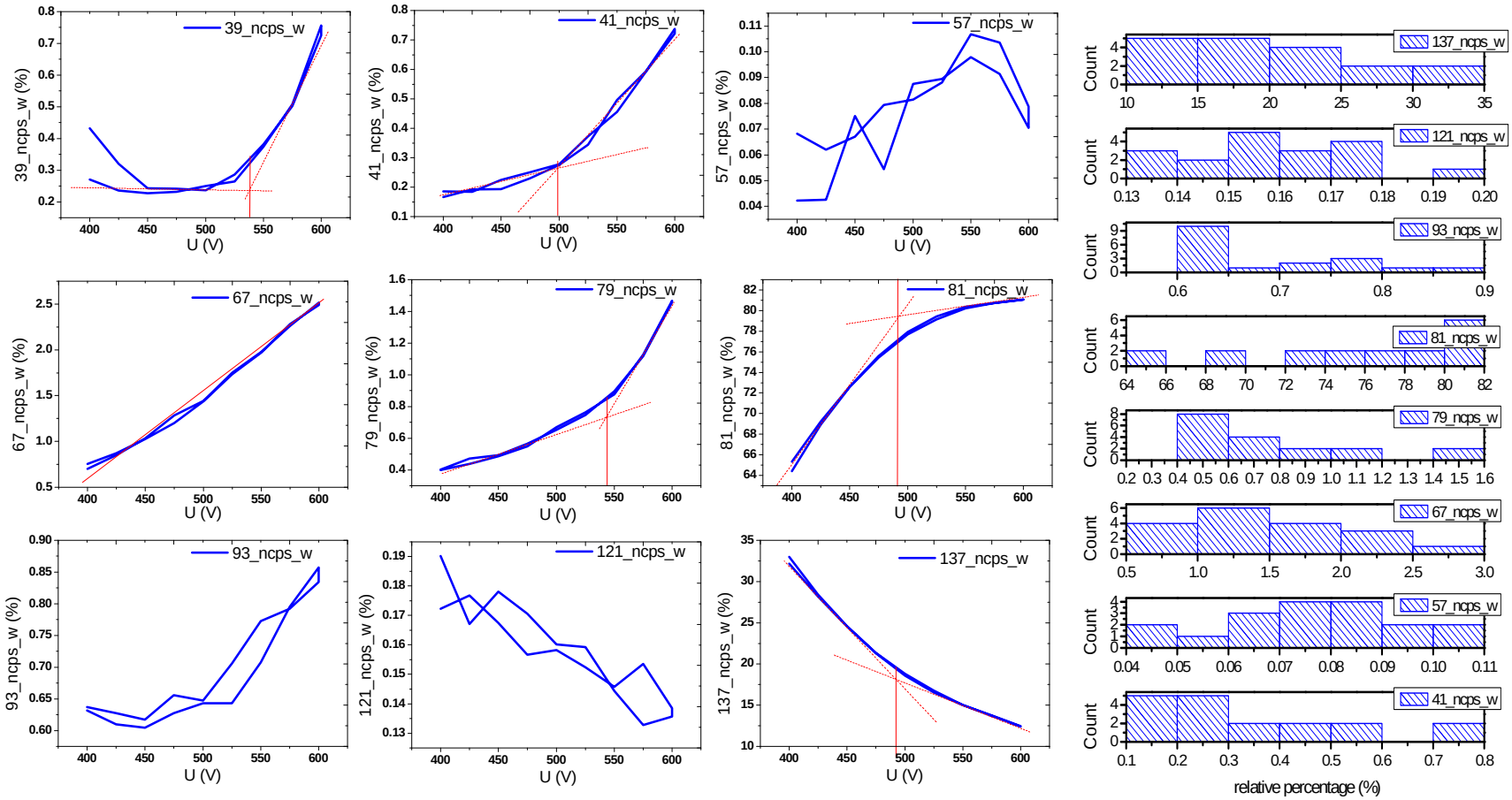

Figure 2.6-9. Variability of main fragments with U_d and their distributions (as relative abundance) in AD-PTR-MS for d-limonene.

2.6.5.1.5 γ-terpinene

IUPAC name: 4-methyl-1-(1-methylethyl)-1,4-cyclohexadiene)

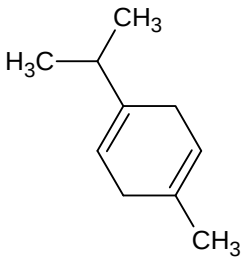

The structure of γ-terpinene at first glance might seem almost identical to that of α-phellandrene differing only in the position of one of the two double bonds in the ring, i.e. this monoterpene has a differing double bond next to the isopropyl substituent. This relatively minor difference in the structure can be highly important for the γ-terpinene fragmentation in the AD mode assuming different facilities for the isopropyl fragment detachment (*m/z* 41) which in turn affects the rate of isopropylbenzene (*m/z* 121) and benzyl (*m/*z 93) formation. In the patterns of targeted ions for γ-terpinene (Figure 2.6-10) one can observe approximately 5 times higher relative proportion of *m/z* 121 than encountered for α-phellandrene (Figure 2.6-6) which might suggest that the presence of the double bond next to isopropyl makes this substituent more resistant to the detachment in the collisions with hydronium ions. Zooming in on the pattern of the benzyl fragment one can notice a moderate upward-curved deviation from a straight line with a centre around 500 V and the opposite but more pronounced pattern in *m/*z 121. The detached isopropyl seems to cluster with abundant methyl ions which can be seen from the pattern in *m/z* 57 which gives a different unique pattern compared with α-phelandrene and other monoterpenes.

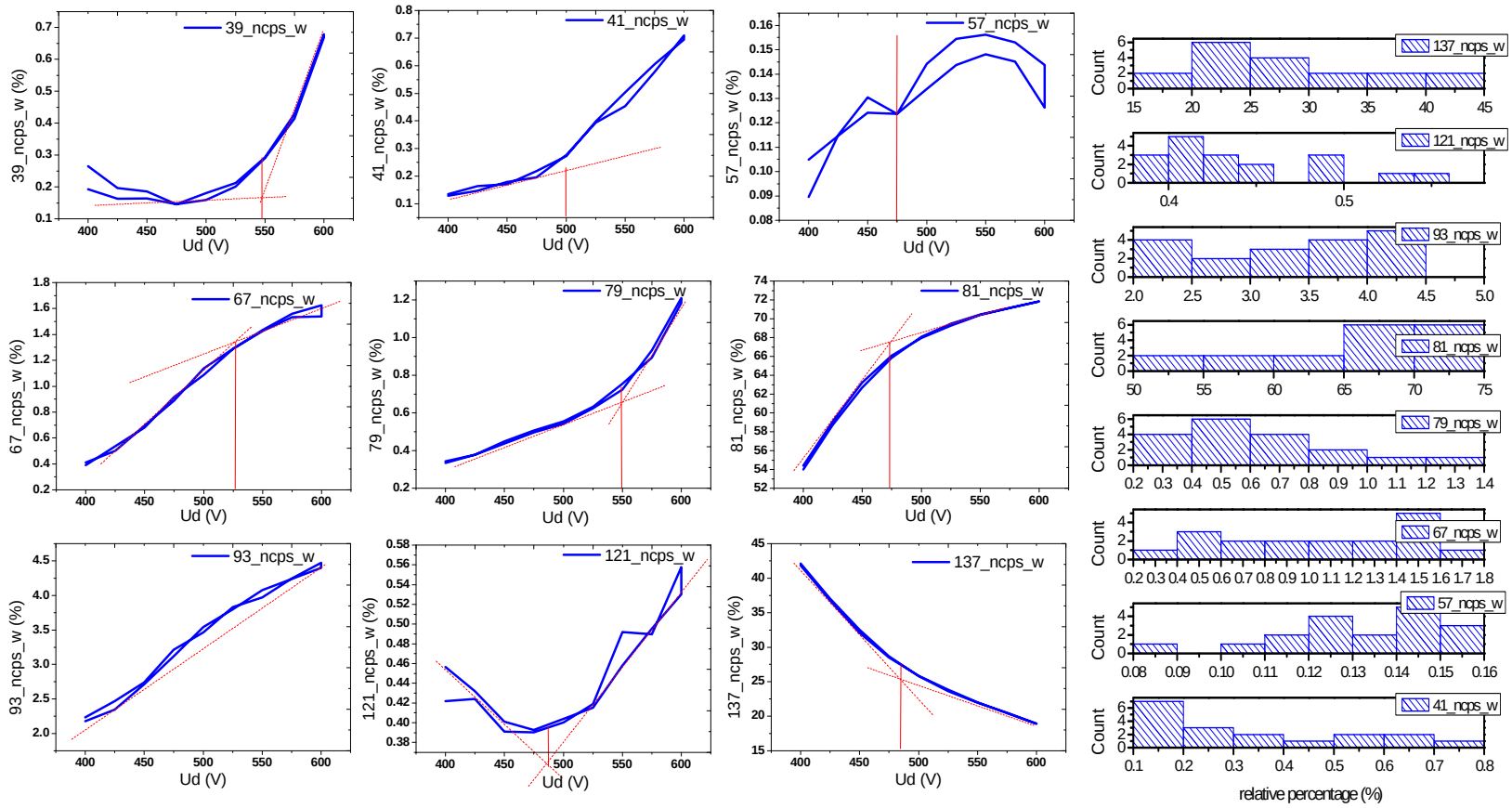

Figure 2.6-10. Variability of main fragments with U_d and their distributions (as relative abundance) in AD-PTR-MS for γ-terpinene.

2.6.5.1.6 3-carene

IUPAC name: 3,7,7-trimethylbicyclo[4.1.0]hept-3-ene

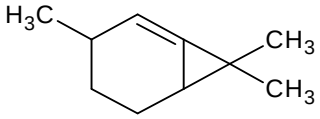

The structure of the molecule of 3-carene lacks double bonds in the substituents, which is a similar feature to that of α-phellandrene, α-pinene, and γ-terpinene. The hexenyl ring is also only present in d-limonene and α-pinene, with the latter also having only one double bond per whole molecule. The analysis of the AD-patterns for this monoterpene (Figure 2.6-11) suggests that the toluene (*m/z* 93) is easily formed with almost ideally linear proportionality with U_d. There is also a noisy but remarkable pattern in *m/z* 121, which resembles that of γ-terpinene. It seems that *m/z* 67 which results from ring fragmentation has a very clear plateau starting from about 550 V, which is also more or less the case in other monoterpenes except for d-limonene, where *m/z* 67 was linear in the whole range. Generally all the targeted *m/z* channels exhibited some signal indicating that all types of fragmentation are possible for 3-carene although their different rates in respect to U_d can provide clues regarding the discrimination. Furthermore, differences in characteristic voltages provide additional information. However, not all fragmentation types were present with respect to d-limonene or β-pinene as gathered from the noisy *m/z* 121, *m/z* 93, and *m/z* 67, which might be further useful in the discrimination approaches.

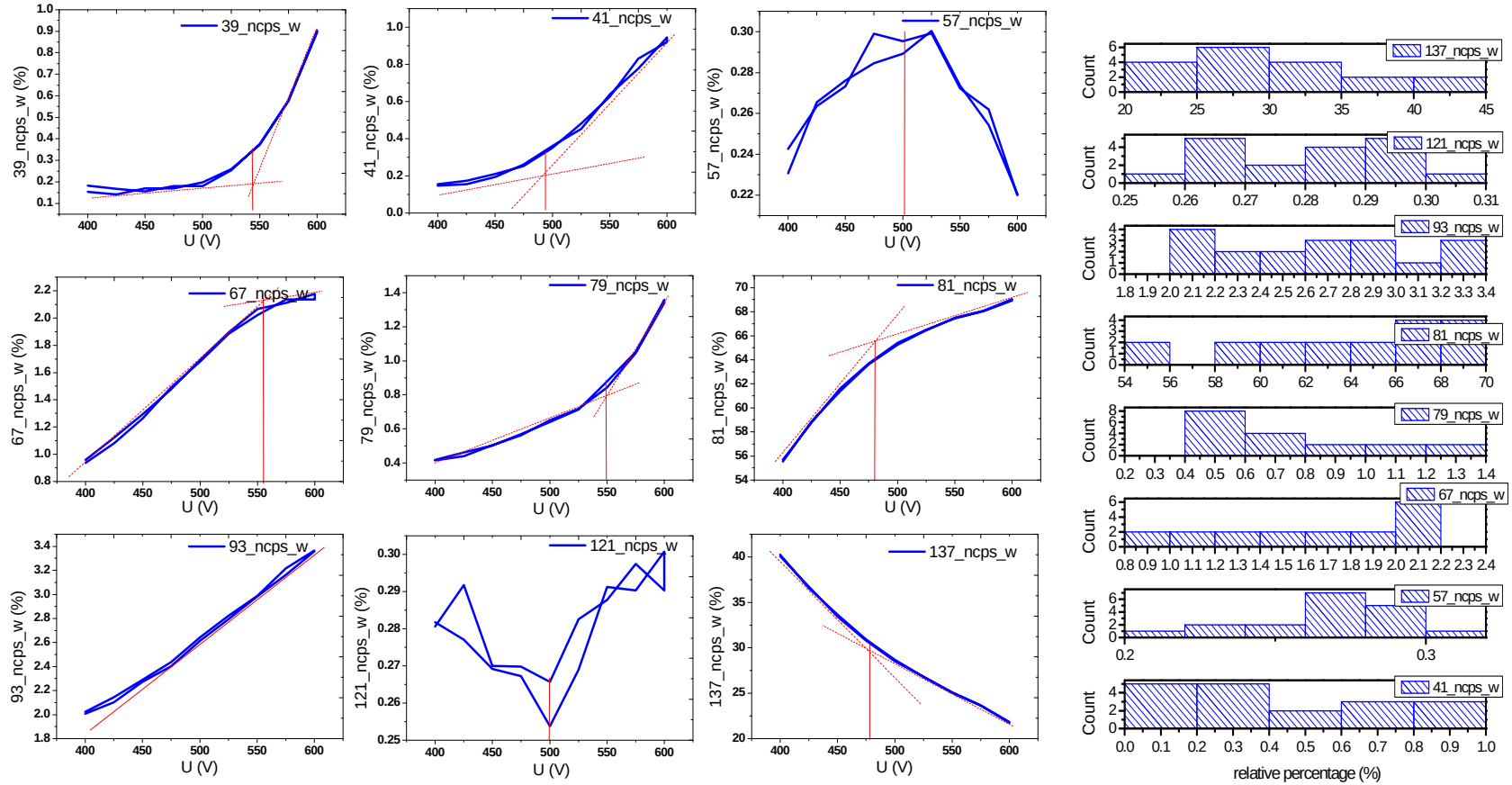

Figure 2.6-11. Variability of main fragments with U_d and their distributions (as relative abundance) in AD-PTR-MS for 3-carene.

2.6.5.1.7 p-cymene

IUPAC name: 1-methyl-4-(1-methylethyl)benzene

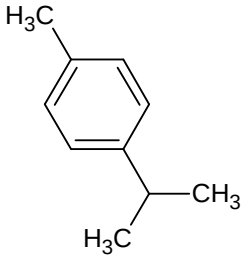

The compound p-cymene is not a monoterpene but it is only different in the presence of the aromatic ring, which is responsible for the shift in the fragmentation giving high abundances on different *m/z* ion channels, and therefore AD mode is not necessary to distinguish this compound from monoterpenes. However, it is interesting to observe analogies in fragmentation in the AD mode for this compound (Figure 2.6-12), as many ions are encountered at *m/z* – 2 compared with monoterpenes. For example, the parent ion is now detected at *m/z* 135 (so 2 amu less than for monoterpenes), and the second most abundant fragment is toluene at *m/z* 93, and not benzene (*m/z* 79) as one could expect from the analogies to *m/z* 81 in monoterpenes. This must be because of the exceptional stability of toluene formed after collisional dissociation resulting in the loss of isopropyl fragment. The detachment of the methyl substituent is also possible although the abundance at *m/z* 119 (analogous to *m/z* 121 in monoterpenes) is not high. Another evident difference is that the fragmentation of the parent ion of monoterpenes was never complete although different for different monoterpenes in the AD mode, whereas for p-cymene *m/z* 135 reaches almost zero level after exceeding U_d value of 550 V. The *m/z* 93 ion ranges from about 50% to 85% of the relative abundance in reference to the sum of the selected most abundant ions. The formation of toluene seems to reach saturation after exhausting the main substrate at about 550 V and then tends to start declining. It is possible that the abundance of *m/z* 137 in monoterpenes would have also decreased to zero analogously, if *E/N* ratios could be increased much higher (e.g. >200 Td), but which would require decreasing the drift pressure.

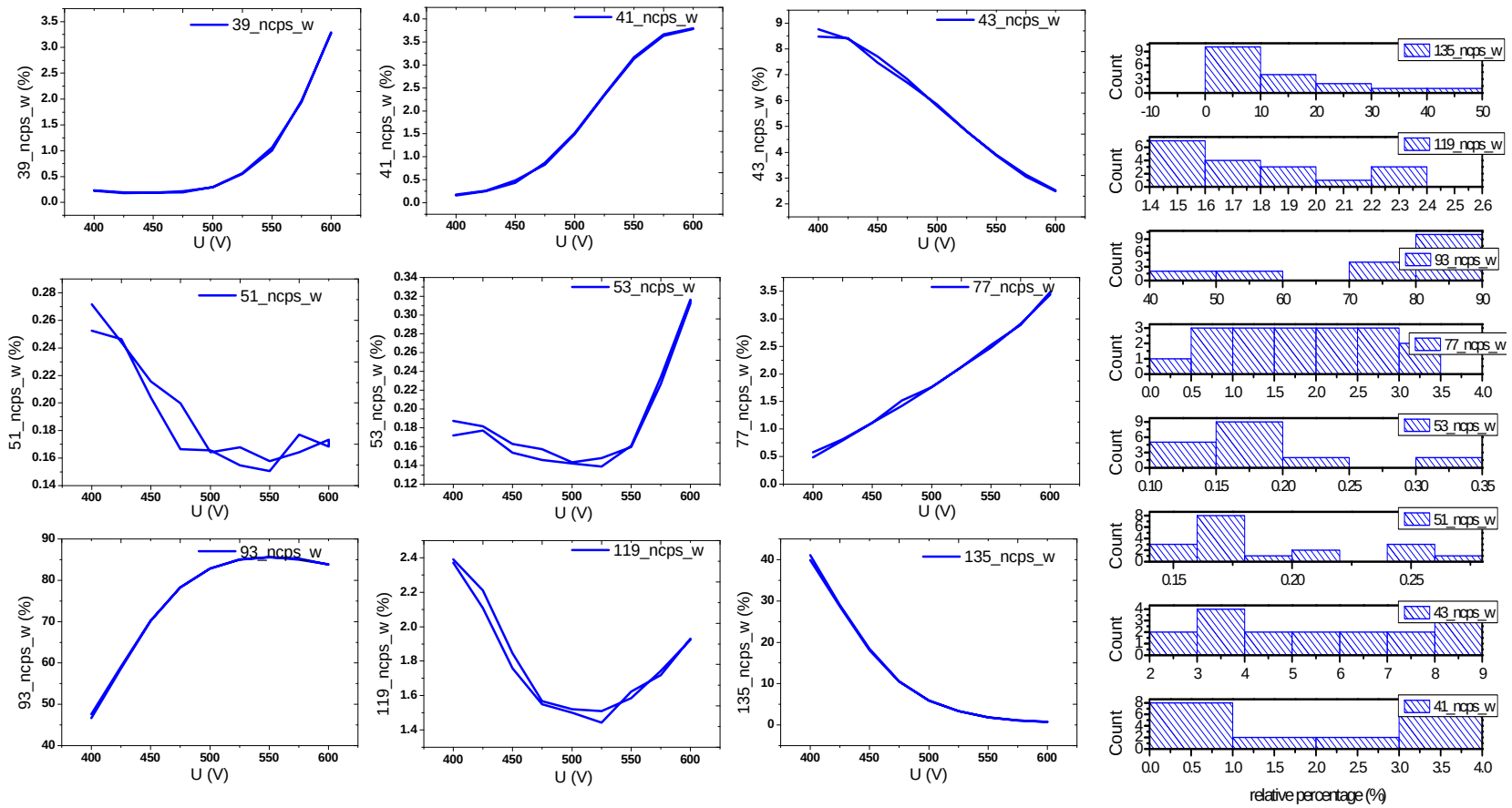

Figure 2.6-12. Variability of main fragments with U_d and their distributions (as relative abundance) in AD-PTR-MS for p-cymene.

2.6.5.2 PMF results

One of the most important tasks with PMF is to identify the number of factors (p) in the dataset, which is unknown. One method to derive the true number of factors is to compare the quantities Q_{robust}, Q_{true} *and* $Q_{theoretical}$. Q_{robust} is the quality of fit parameter which does not take into account the outliers, which are the data points below their detection limits or highly uncertain columns, while Q_{true} is considering all the data points in the analysis. Both these parameters can be calculated in the EPA PMF program. The program, however, does not derive the theoretical Q_{theor}, yet this can be approximated by the following equation:

$$Q_{theor} = nm - p(n+m) \qquad \textbf{Equation 2.6-4}$$

where n is the number of m/z in the scan and m is the number of measurements. Selecting too small a number of factors may lead to merging of factors and inaccurate representation of the data by the PMF model. On the other hand selecting too high a number of factors, i.e. higher than the true number, can also impact detrimentally on the analysis and lead to factor splitting or non-converged solutions. A sudden rise in Q_{theor}/Q_{true} can signify that the addition of the next factor helps in obtaining a better fit with the data. In contrast, if performing PMF with an increased number of factors changes the Q_{theor}/Q_{true} only very slightly, then it might be that the factor is not absolutely necessary for the explanation of the data series. The optimal p number has been selected from the dependence of Q_{theor}/Q_{true} on the number of factors (p) for the AD-PTR-MS scan course (Figure 2.6-13) which suggested the use of 7 factors. Although it is probable that such a number of factors would sufficiently describe the fragmentation it is not certain whether this number would work best for monoterpene discrimination as some of the factors could become less specific or less sensitive with possible attribution derived from noise. Consequently, using a trial-and-error approach it

was decided to limit the analysis just to 4 factors, which ensured best visual representation of factor dynamics in relation to the drift voltage, without any evident factor splitting. Since datasets for different monoterpenes may have different true total numbers of factors, by using higher *p* values one could risk factor splitting for some of them, which would make the comparison invalid. Low *p* values may lead to different values of ratios of Q_{theor}/Q_{true} for the particular monoterpene, but at least the first 4 factors are likely to occur in each isomer, so the relation of these 4 factors to the drift voltage can serve as a base for the discrimination.

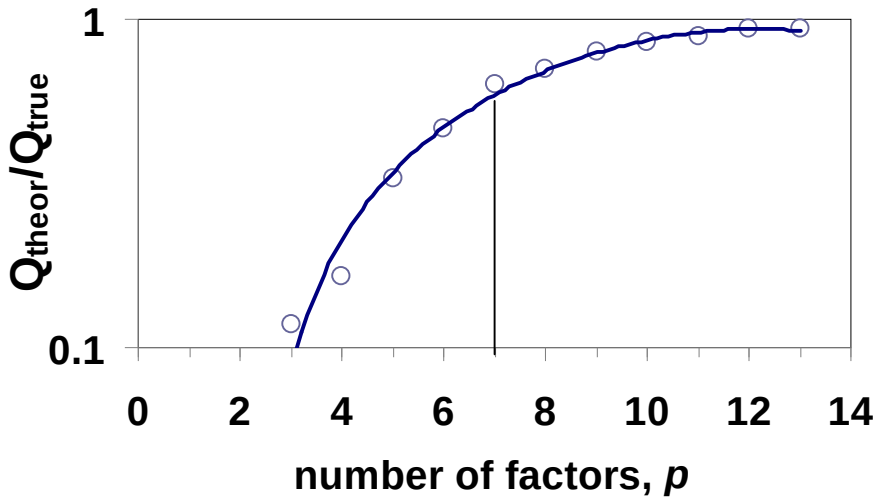

Figure 2.6-13. Estimation of the number of factors in the AD-PTR-MS dataset (α-phellandrene as an example).

Since the same number of factors was used in the treatment of all samples, the Q_{theor}/Q_{true} values for each of the compounds will be slightly different depending on how well the PMF model can simulate the spectra. The assumption has been made that all or any of the first four factors are commonly present in all monoterpene data and the specific information can be obtained from the total factor contribution profile (Figure 2.6-14 as an example) and the individual contributions of factors to a given *m/z* (Figure 2.6-15 as an example). Some *m/z* channels will contain a contribution from one factor,

some from two or more, but most monoterpene fragments contain all 4 factors although not always in the same proportion.

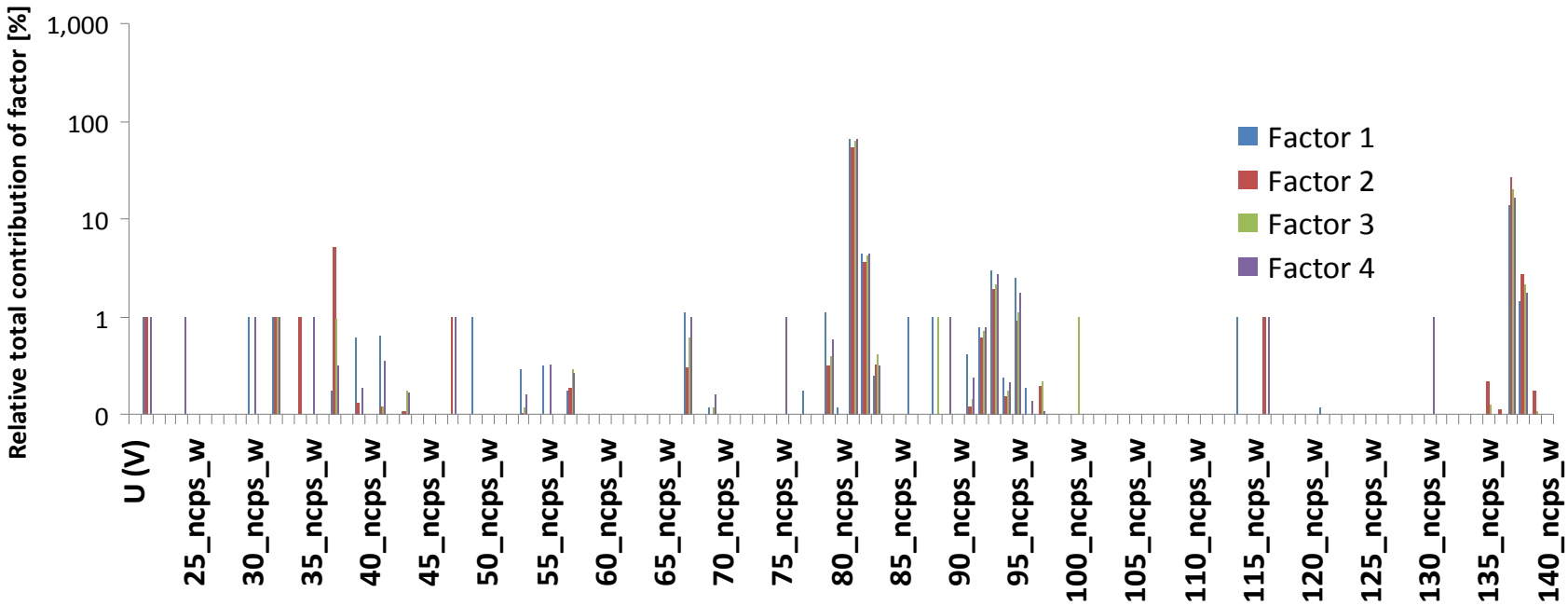

Figure 2.6-14. Factor profiles of the relative total contribution as a percentage of the whole *m/z* spectrum (α-phellandrene example).

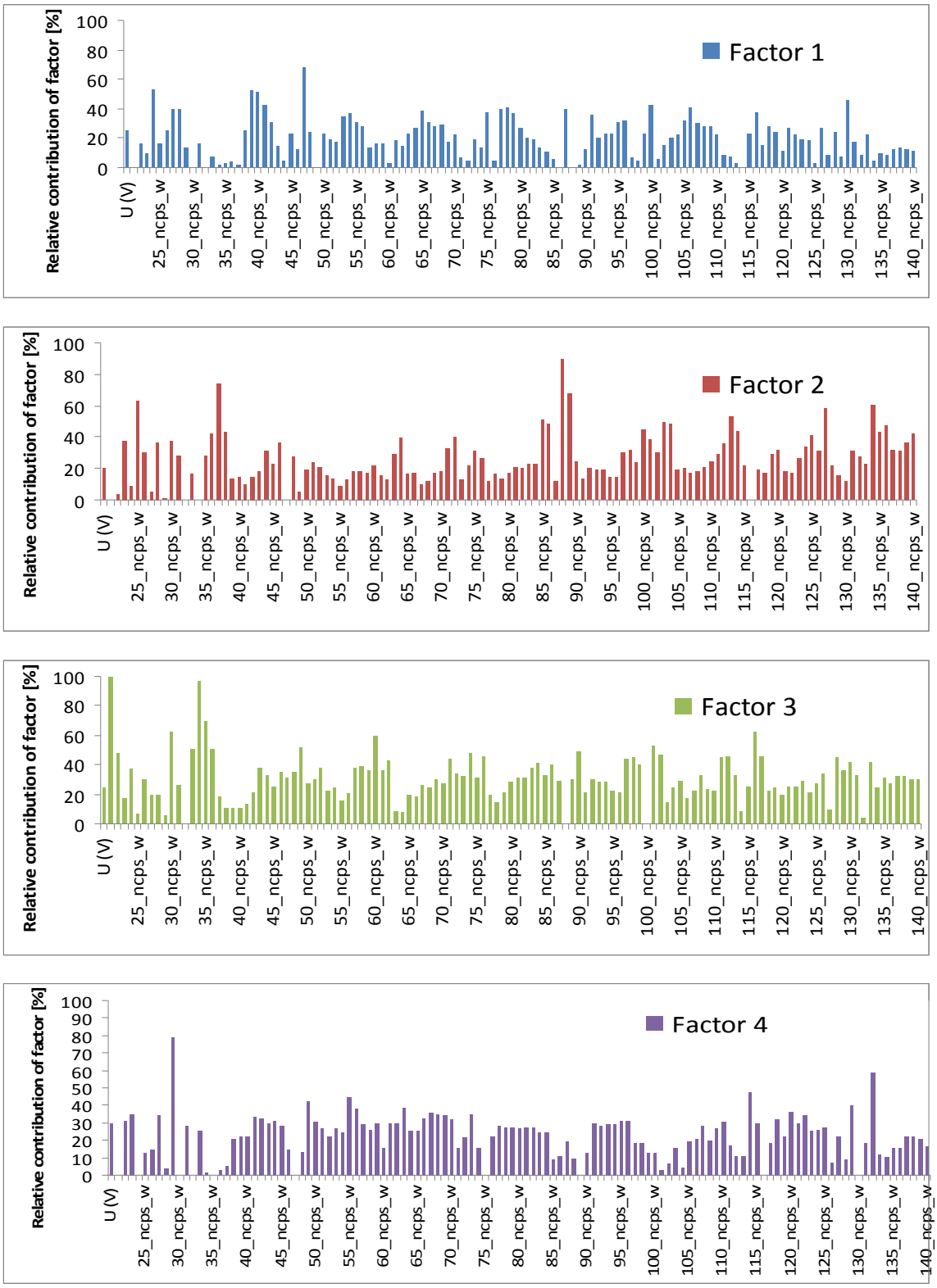

Figure 2.6-15. Relative individual contributions of 4 main factors for α-phellandrene.

Identification of the significance of a factor may not be always obvious, but the relationships between those factors and U_d (Figure 2.6-16) suggest the occurrence of similar four factors in each monoterpene which differ in characteristic U_d, noisiness and relative proportions. Most probably the factor 1 can be related to the degree of fragmentation or in other words to the m/z species which are the result of fragmentation. This factor can be specific for a given monoterpene structure, which seems to fragment with different abundance at different U_d. Factor 2 may denote clustering and/or dependence on humidity. Anticipating from Section. 2.6.5.3, this factor might not be specific to monoterpenes, probably because of interferences from water or other clusters, or second order reactions which might explain the splitting of the factor 2 curve in the lower U_d range, i.e. different for ascending and descending part of the AD cycle. Factors 3 and 4 might refer to specific features related to the structure or other characteristic of one of the isomers. It appears that these factors do not only occur in monoterpenes but a quite similar representation can be observed for p-cymene (Figure 2.6-17).

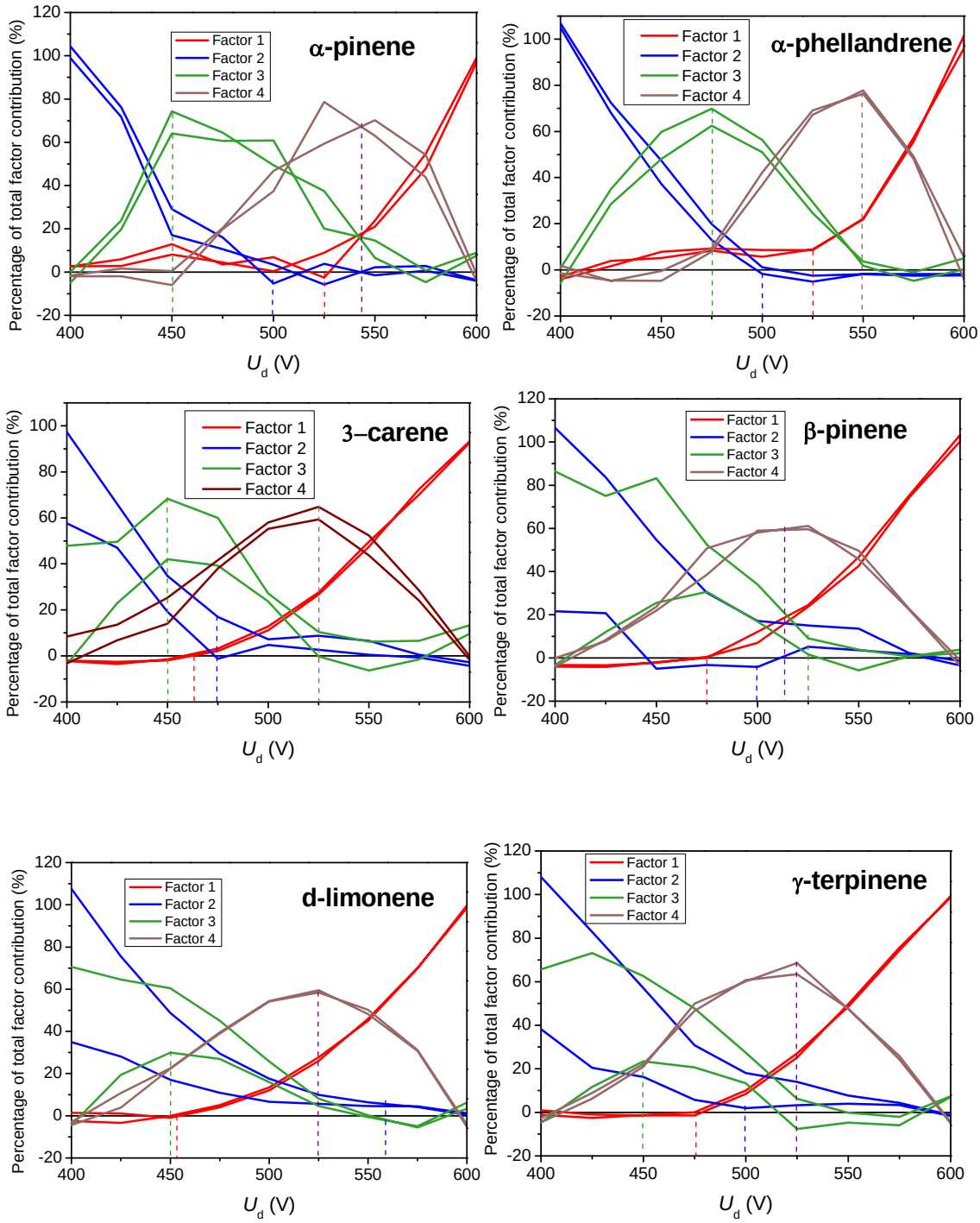

Figure 2.6-16 Comparison between factor contributions for each monoterpene in relation to U_d

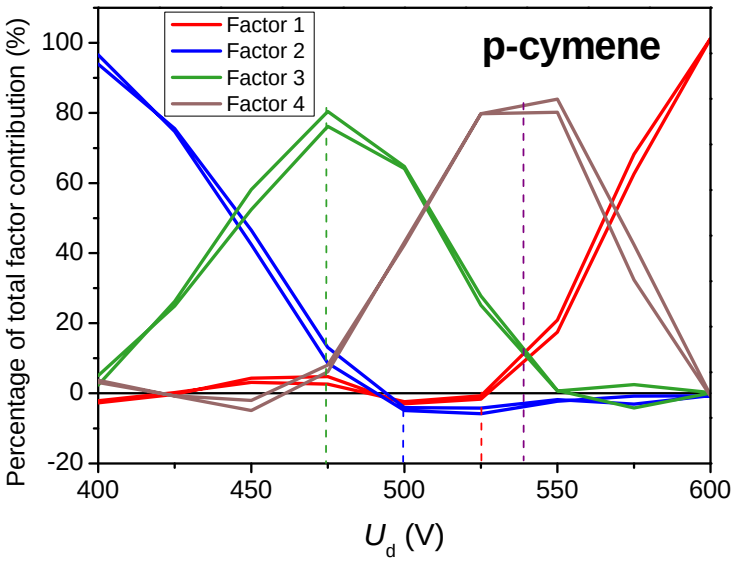

Figure 2.6-17 Factor contribution for p-cymene in relation to U_d.

Factor 1 can be presented as a fragmentation profile (Figure 2.6-18) which clearly shows the power of its discrimination capabilities, elucidating large differences in *m/z* 81, 137, 95, 67, 79 and 39 and others. Obviously the factor "fragmentation" is completely different for p-cymene despite similarities found in Figure 2.6-17. These differences can be high for the factor 2 (Figure 2.6-19) but as mentioned previously this can be interfered by differences in *m/z* 37, so is probably not specific to the structure. Although the true significance of factors 3 (Figure 2.6-20) and 4 (Figure 2.6-21) is unknown, its potential for discrimination might be quite high. Generally, all factor profiles show differences in the channels of highest abundance, i.e. *m/z* 137 and *m/z* 81, which may be the key to the higher sensitivity of the method. In addition *m/z* 95 may be important and many other discrete features but which are not clearly visible in the factor profiles.

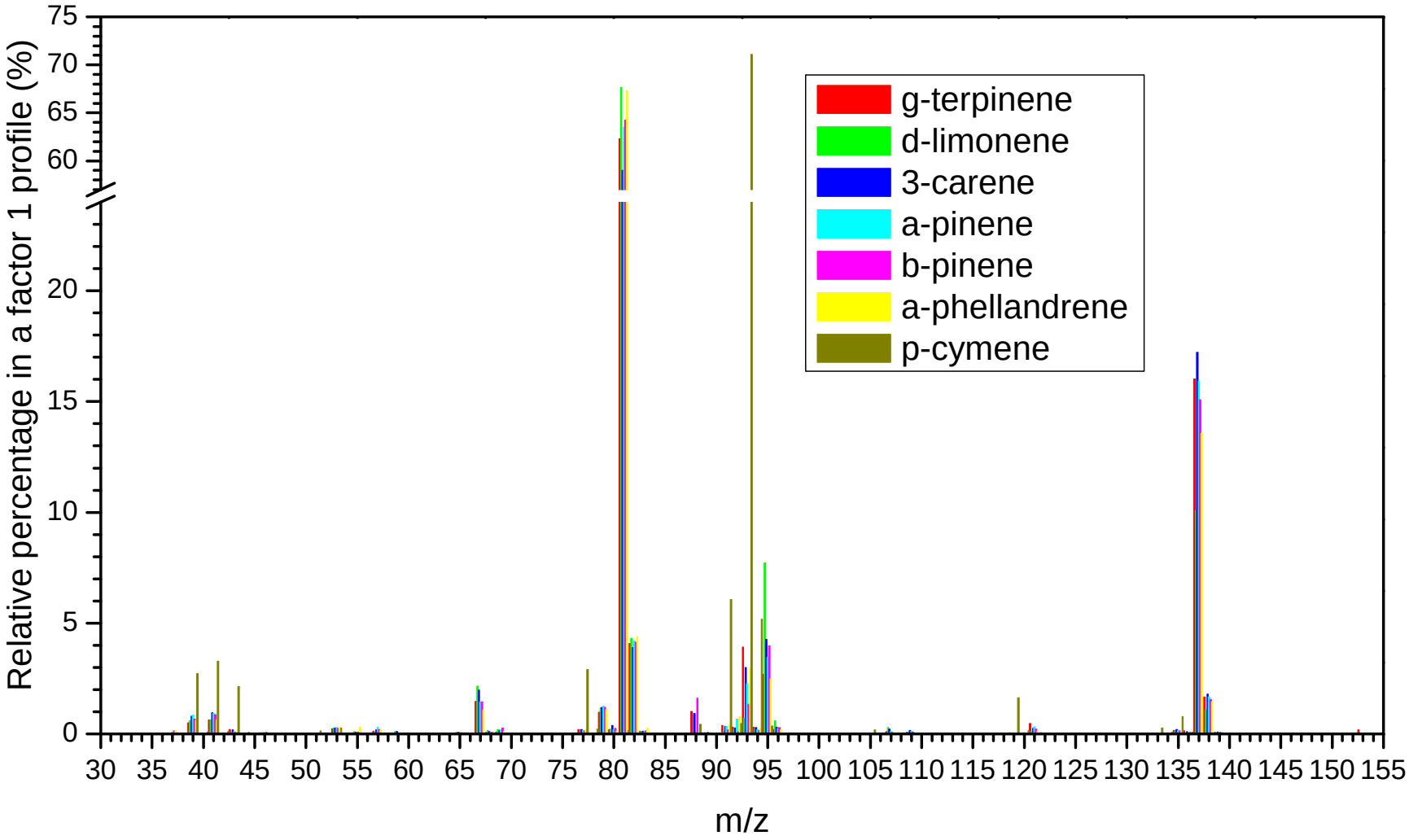

Figure 2.6-18 Profile of the PMF factor 1 for the six monoterpenes tested and p-cymene.

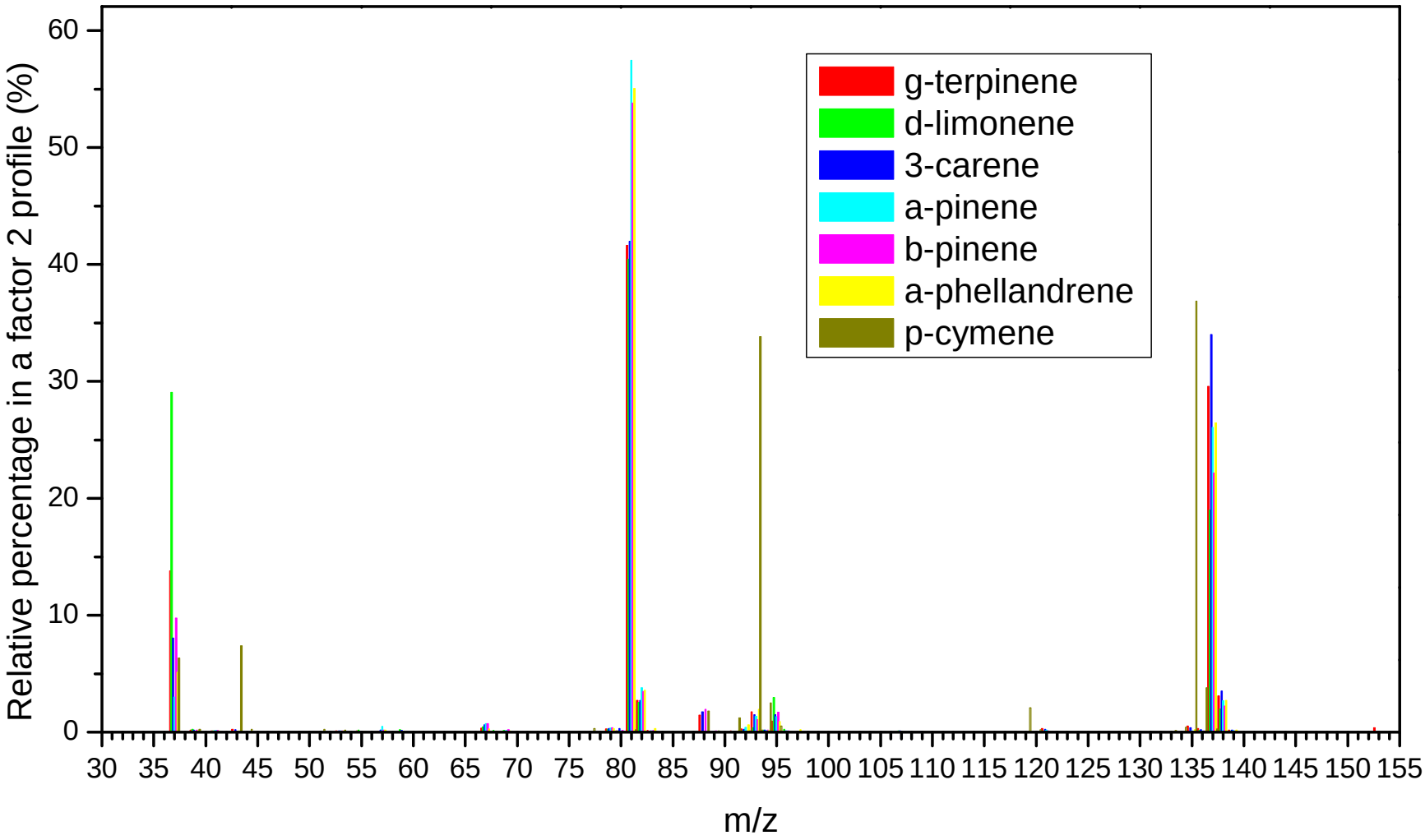

Figure 2.6-19 Profile of the PMF factor 2 for the six monoterpenes tested and p-cymene.

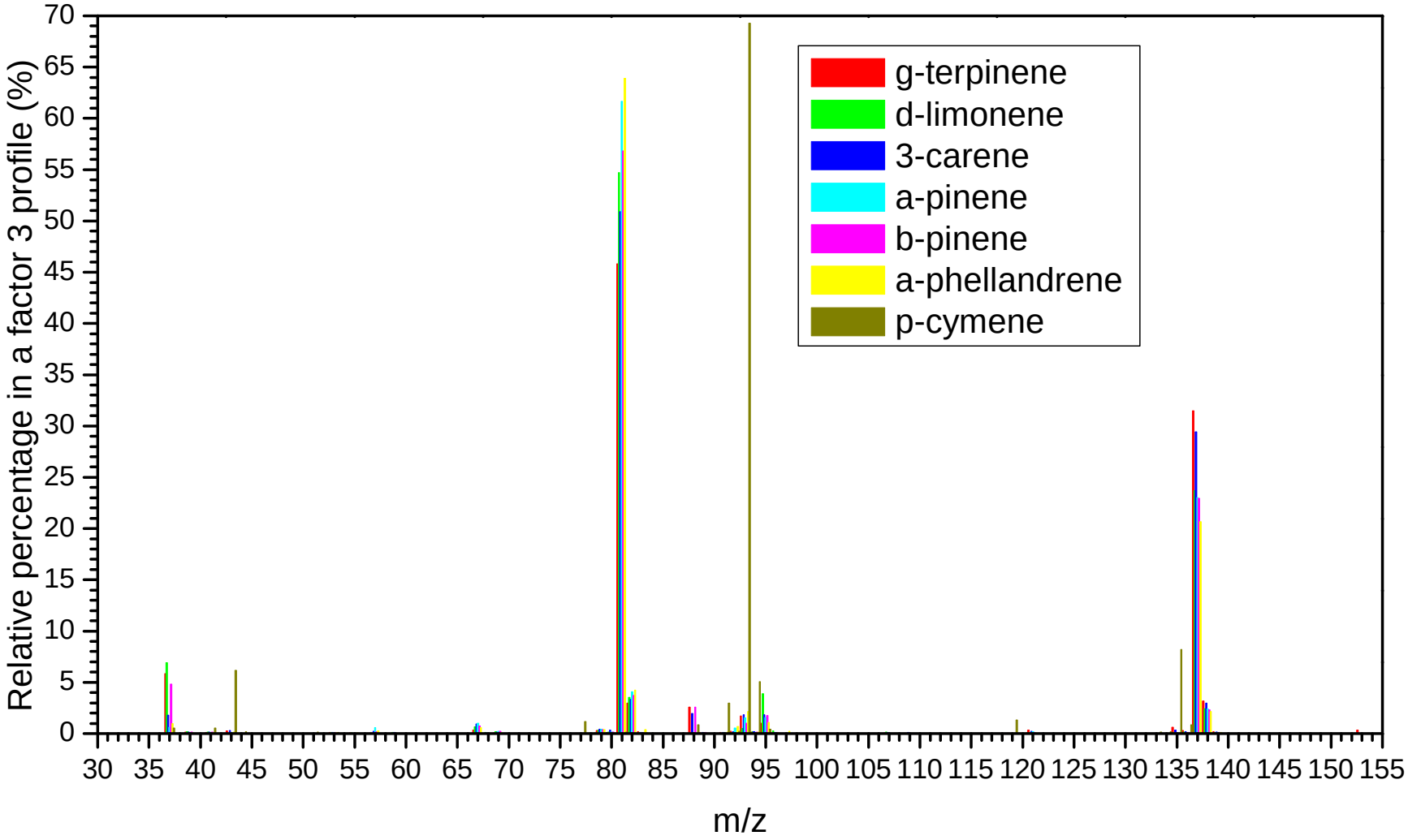

Figure 2.6-20 Profile of the PMF factor 3 for the six monoterpenes tested and p-cymene.

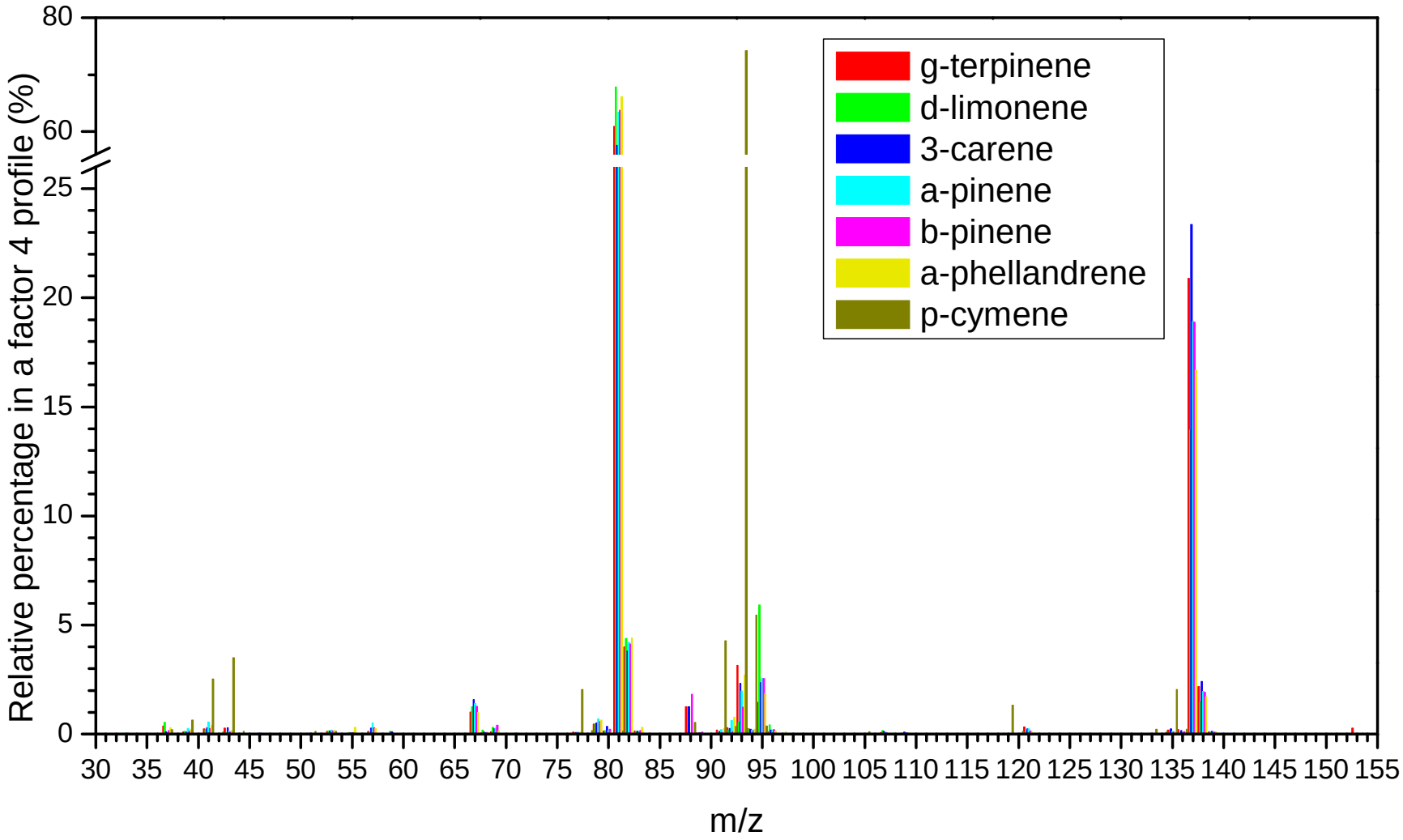

Figure 2.6-21 Profile of the PMF factor 4 for the six monoterpenes tested and p-cymene.

2.6.5.3 Identification experiment (double blind trial)

As shown in the previous sections, discriminating features can be found in relatively small fragments of the spectra which may not be practically useful when the level of monoterpenes becomes generally low. The identification experiment was dealing with approximately 10 ppb levels, so still quite high in relation to concentrations typically encountered in the environment. As can be seen from Figure 2.6-22, Figure 2.6-23, and Figure 2.6-24 for abundance and Figure 2.6-25 for PMF factors, the AD patterns became noisier. In addition, on the bar graphs for each factor (Figure 2.6-26) one can notice fewer peaks than were shown for the high concentration calibration compounds in the previous section. Nevertheless, one can see that many characteristic features and differences have been retained but how they could help in the discrimination is not immediately obvious.

The ideal situation would be that the AD approach could deal with the separation of monoterpenes at low concentrations. This would only be possible if the most abundant *m/z* (i.e., 81 and 137) or their ratio could be used. This can be justified as there are remarkable differences in relative abundances of those ions derived in the AD mode. Consequently, the analysis based on the ratios of *m/z* 81 and *m/z* 137 was attempted with the assumption that a full AD cycle would yield different absolute ratios of those ions. It has been known that the relative proportion between *m/z* 81 and *m/z* 137 changes with the *E/N* ratio, but the absolute values of those proportions for a range of *E/N* ratios for each monoterpene isomer have not been tested, so it has not been known whether they could serve as a discrimination tool. The normalised data for the full AD cycle were summed, and the ratios of *m/z* 81 to *m/*z 137 ($K_{AD81/137}$) are presented in Table 2.6-1 for the 6 monoterpenes tested. These data can be compared with the data for unknown monoterpenes (Table 2.6-2) for the purpose of identification of 'unknowns'.

Table 2.6-1 Values of the ratios of m/z 81 and m/z 137 ($K_{AD81/137}$) for monoterpenes used in AD calibration (integrated U_d range of 400 V to 600V). The (a) to (f) labels in the column headers are used for attributing the unknown monoterpenes.

Isomer	γ-terpinene (a)	d-limonene (b)	3-carene (c)	α-pinene (d)	β-pinene (e)	α-phellandrene (f)
$K_{AD81/137}$	2.42	3.80	2.13	2.84	3.05	3.20

Table 2.6-2 Values of the ratios of m/z 81 and m/z 137 ($K_{AD81/137}$) for unknown monoterpenes. The superscripts refer to the monoterpenes which were identified using the scoring system (explanation in the text below).

Isomer(s)	A1	A3	A2+A4
$K_{AD81/137}$	3.48^{f}	$3.04^{e,(d,f)}$	$2.34^{a,(b)}$

It appears that ratios of *m/z* 81 to *m/*z 137 of the first four PMF factors ($F_{1\text{-}AD81/137}$ … $F_{4\text{-}AD81/137}$) are different for a given monoterpene. The data for the calibration and unknown compounds are listed in Table 2.6-3 and Table 2.6-4, respectively. However, it might be that not all the factors are specific for the discrimination. Factor 2 in particular is not useful since all $F_{2\text{-}AD81/137}$ values for unknown monoterpenes were much lower than those derived in calibration, so possibly they could be related to quantitative relationships with *m/z* 37.

Table 2.6-3 Values of the ratios of *m/z* 81 and *m/z* 137 from the factor 1-4 spectra ($F_{n\text{-}AD81/137}$) for monoterpenes used in AD calibration. The (a) to (f) labels in the column headers are used for attributing the unknown monoterpenes.

Isomer	γ-terpinene (a)	d-limonene (b)	3-carene (c)	α-pinene (d)	β-pinene (e)	α-phellandrene (f)
$F_{1\text{-}AD81/137}$	3.89	6.71	3.43	3.99	4.26	4.96
$F_{2\text{-}AD81/137}$	1.41	2.13	1.24	2.20	2.43	2.08
$F_{3\text{-}AD81/137}$	1.46	2.31	1.73	2.68	2.48	3.09
$F_{4\text{-}AD81/137}$	2.92	4.87	2.47	3.35	3.38	3.96

Table 2.6-4 Values of the ratios of *m/z* 81 and *m/z* 137 from the factor 1-4 spectra ($F_{n\text{-}AD81/137}$) for unknown monoterpenes. The superscripts refer to the monoterpenes which were identified using the scoring system (explanation in the text below).

Isomer(s)	A1	A3	A2+A4
$F_{1\text{-}AD81/137}$	4.95^{f}	$4.14^{e,(d)}$	3.34^{c}
$F_{2\text{-}AD81/137}$	0.12	0.95	0.94
$F_{3\text{-}AD81/137}$	$2.74^{d,(e)}$	$2.82^{d,(f)}$	$1.55^{a,(c)}$
$F_{4\text{-}AD81/137}$	3.84^{f}	$2.68^{c,(a)}$	1.92

Excluding the analysis of characteristic voltages (as this could work only on high concentration data) a scoring system was applied to identify the compounds from the double-blind trial based solely on the $K_{AD81/137}$ and $F_{n\text{-}81/137}$ values. The closest match was denoted by a superscript corresponding to the letter of the monoterpene (a-f), and the second closest match(es) were placed in parentheses, provided that no value was falling beyond a ±0.3 window. If all values exceeded the window then no score was

awarded and an attempt to associate a monoterpene was not superscripted. Two points were credited for any superscript without bracket in Table 2.6-2 and Table 2.6-4 whereas only one point for a second superscript(s) in bracket. In total A1 received 6 points towards being α-phellandrene, 2 points towards α-pinene, and only 1 point towards β-pinene, identifying A1 as α-phellandrene with the highest probability. A3 obtained 4 points towards β-pinene, and also 4 points towards α-pinene, then 2 points towards 3-carene, 2 points for α-phellandrene, and 1 point for γ-terpinene. This gives an equally high probability towards either α-pinene or β-pinene. Finally the mixture of two monoterpenes (A2+A4) was rated 4 points of probability that it contains γ-terpinene, 3 points that it comprises 3-carene and 1 point for having d-limonene.

Since at low concentrations fragments which are of the order of a percent of the *m/z* 81 abundance may get lost in the noise, the ratio method seems reasonable. For example, when looking at the AD patterns of the monoterpenes to be identified, i.e. A1 (Figure 2.6-22), A3 (Figure 2.6-23), and A2+A4 (Figure 2.6-24), it is clear that predominantly *m/z* 137 and *m/z* 81 retained a clear relationship, while the characteristics of other ion channels was affected by contribution from noise, or water clusters in case of *m/z* 39. Consequently, the pattern for *m/z* 137 looks linear in the A1 and A3 cases and curvy in the case of A2+A4. Thus one could expect A1 and A3 to possibly be pinenes. The ratio method also identified A3 as either of the pinenes but A1 was identified as α-phellandrene with a high probability. However, looking back at Figure 2.6-6 it seems that *m/z* 137 in α-phellandrene deviated only slightly from linearity, whereas d-limonene or γ-terpinene had evident curvature. On the other hand, a curvature of *m/*z 137 observed in A2+A4 mixture excludes the possibility of it containing only pinenes. However, it is clear that for low concentration samples the ratio method and PMF can be more useful.

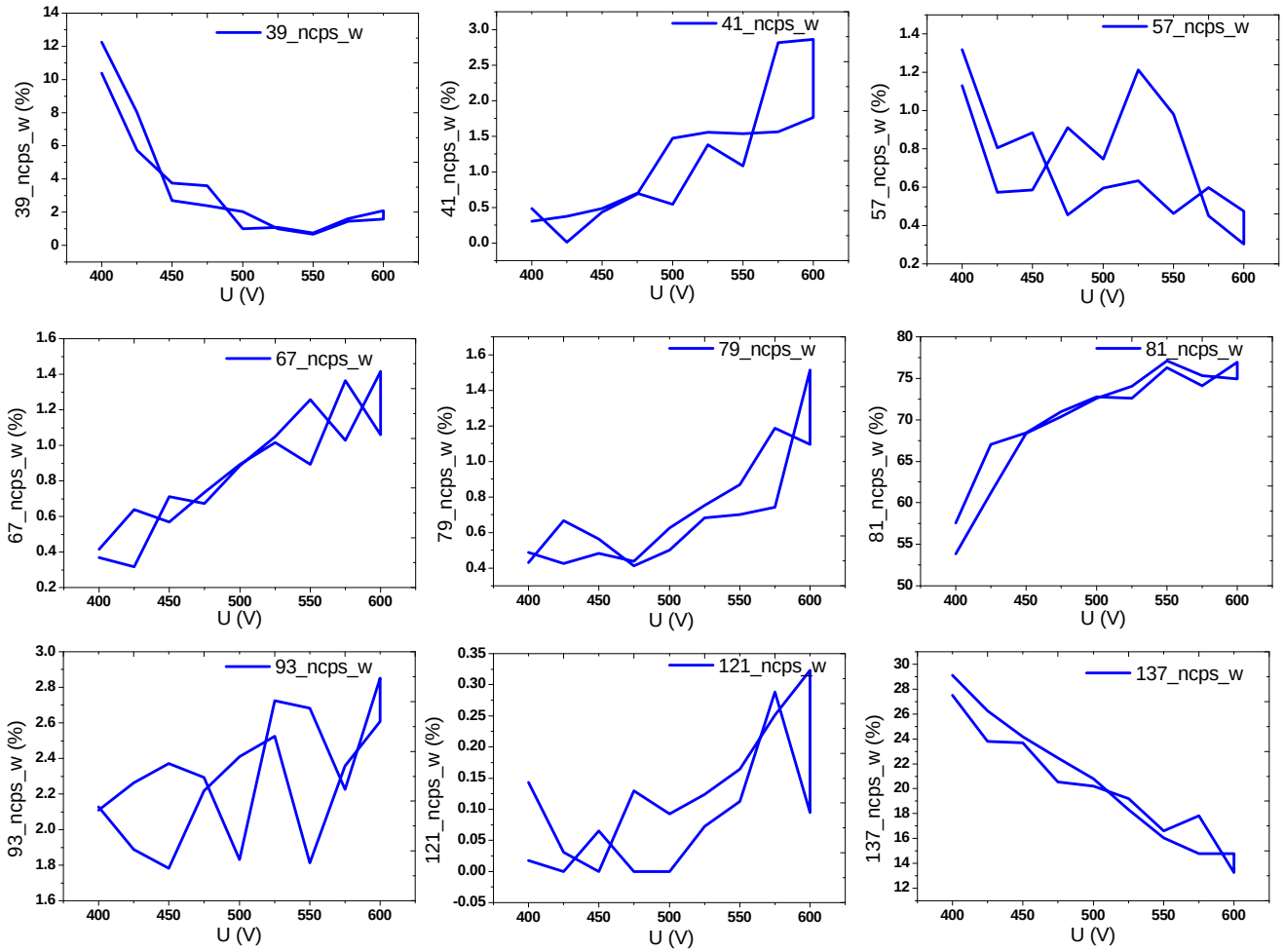

Figure 2.6-22 AD patterns for A1 monoterpene (10 ppb)

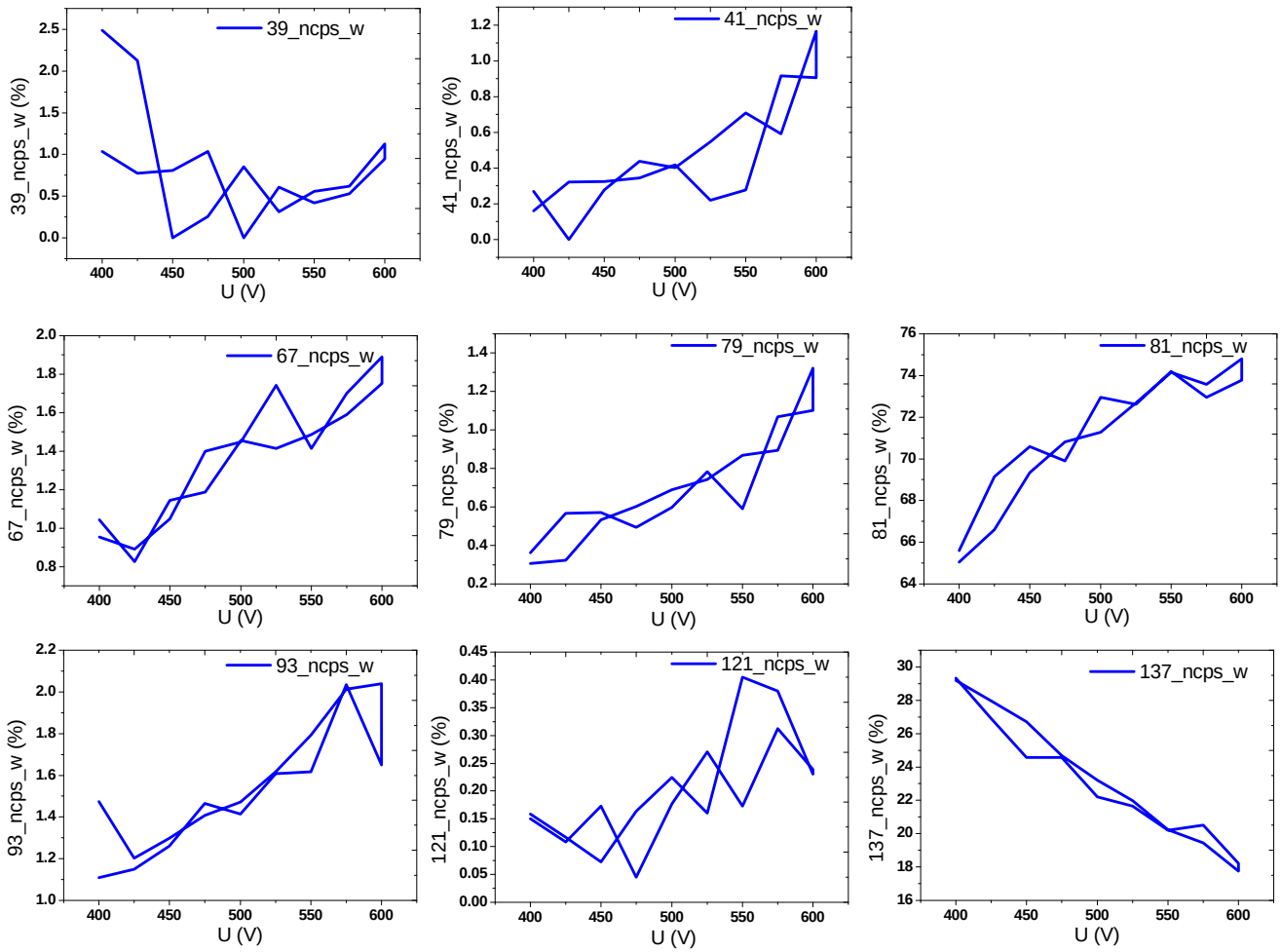

Figure 2.6-23 AD patterns for A3 monoterpene (10 ppb)

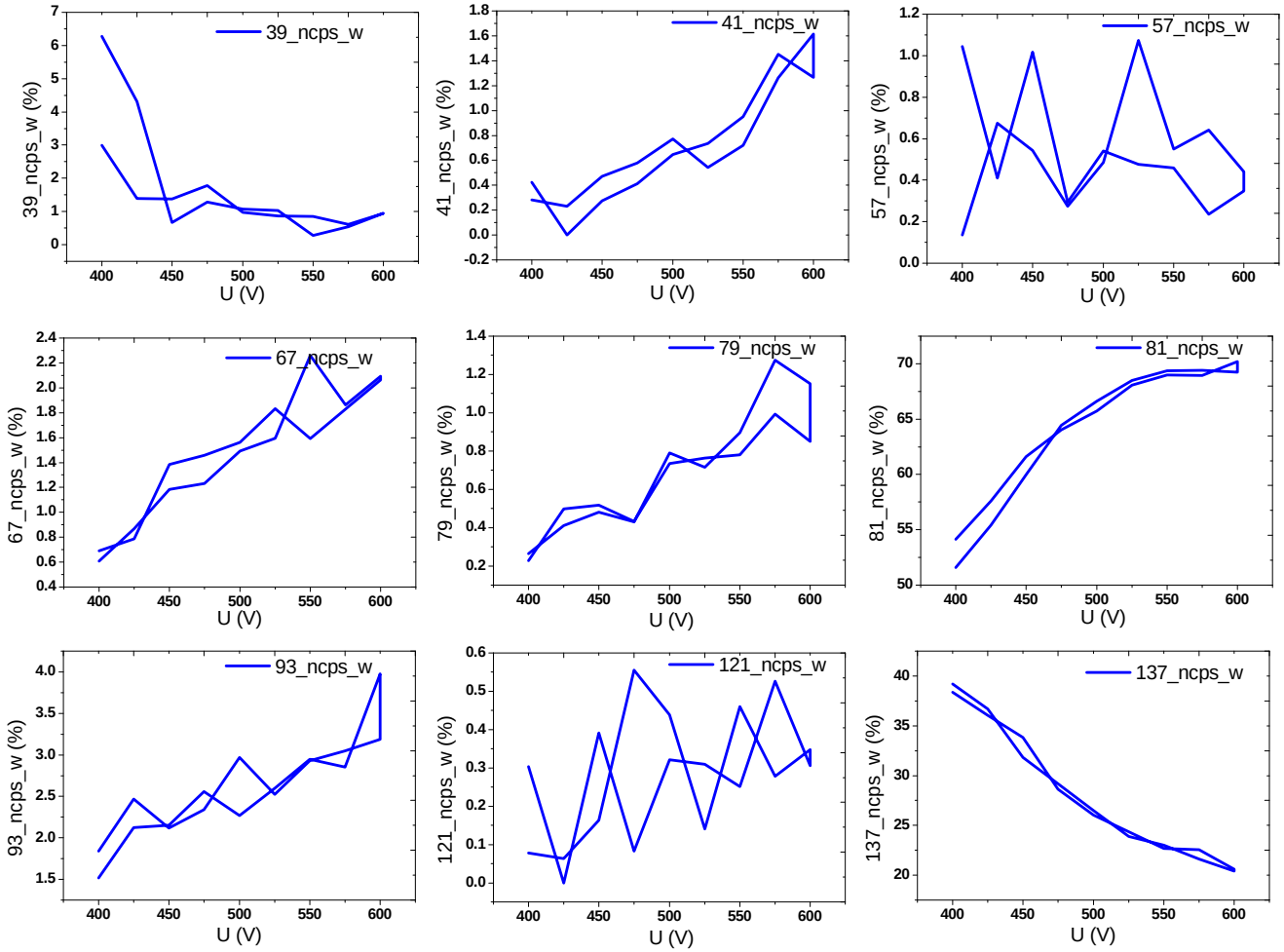

Figure 2.6-24 AD patterns for A2+A4 monoterpene mixture (10 ppb)

Although the factor contributions became noisier, as seen in Figure 2.6-25, the general characteristics is retained the most clearly for Factor 1, slightly less clearly for Factor 2 and much less clearly for Factor 3 and Factor 4. This information is unlikely to be decisive for the discrimination, but their profile spectra, and specifically the ratios of cumulative values of *m/z* 81 and *m/z* 137, seem to have the highest potential usefulness in this respect.

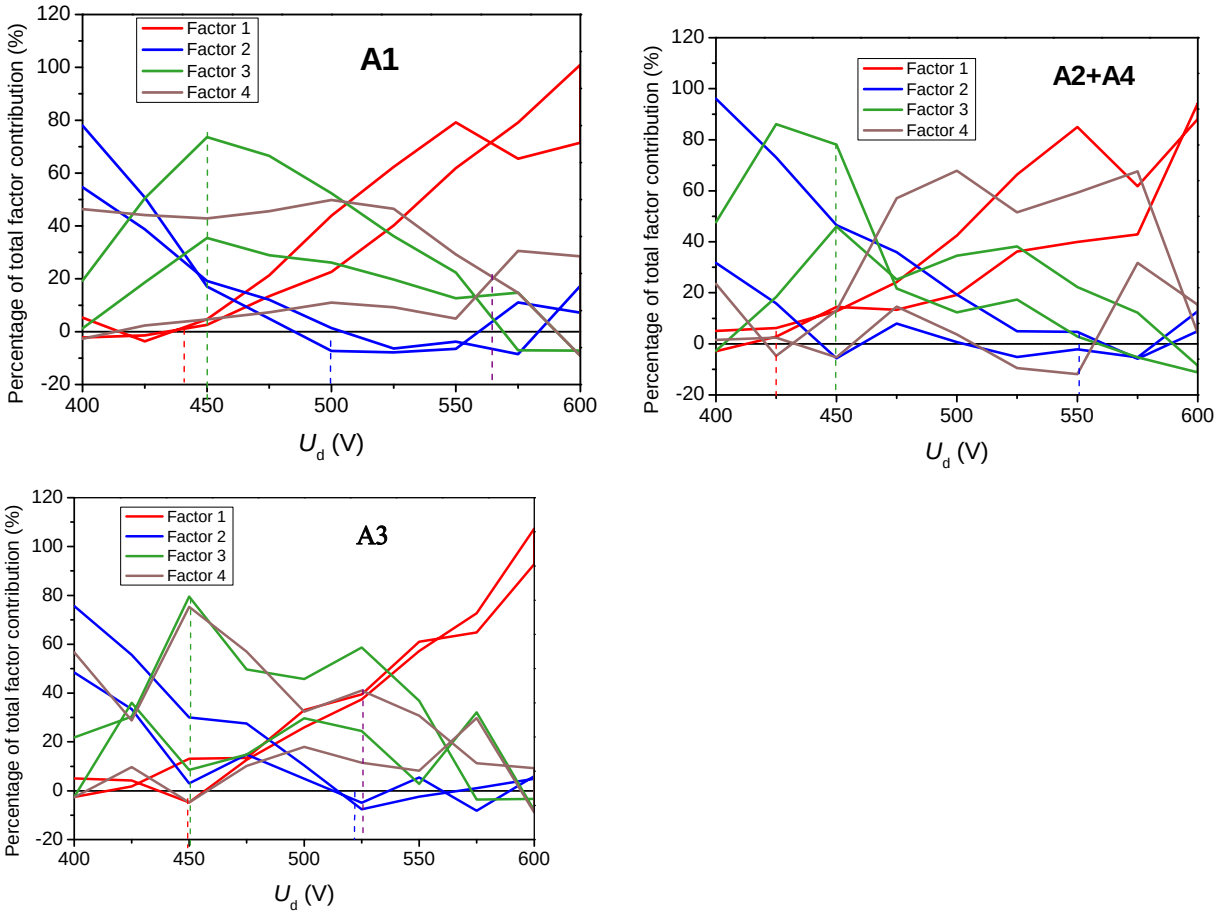

Figure 2.6-25 Factor contributions in relation to U_d for unknown monoterpenes (low concentration).

The individual factor profiles for monoterpenes from the double-blind trial are presented in (Figure 2.6-26) showing differences in the values for *m/z* 81 and *m/z* 137. It can be noticed that their ratios can also differ. These ratios, as shown earlier in Table 2.6-3 and in Table 2.6-4, seemed very specific to a given monoterpene although the significance of all the factors is not entirely recognised and neither is the usefulness of other ion channels such as *m/z* 95 in these profiles.

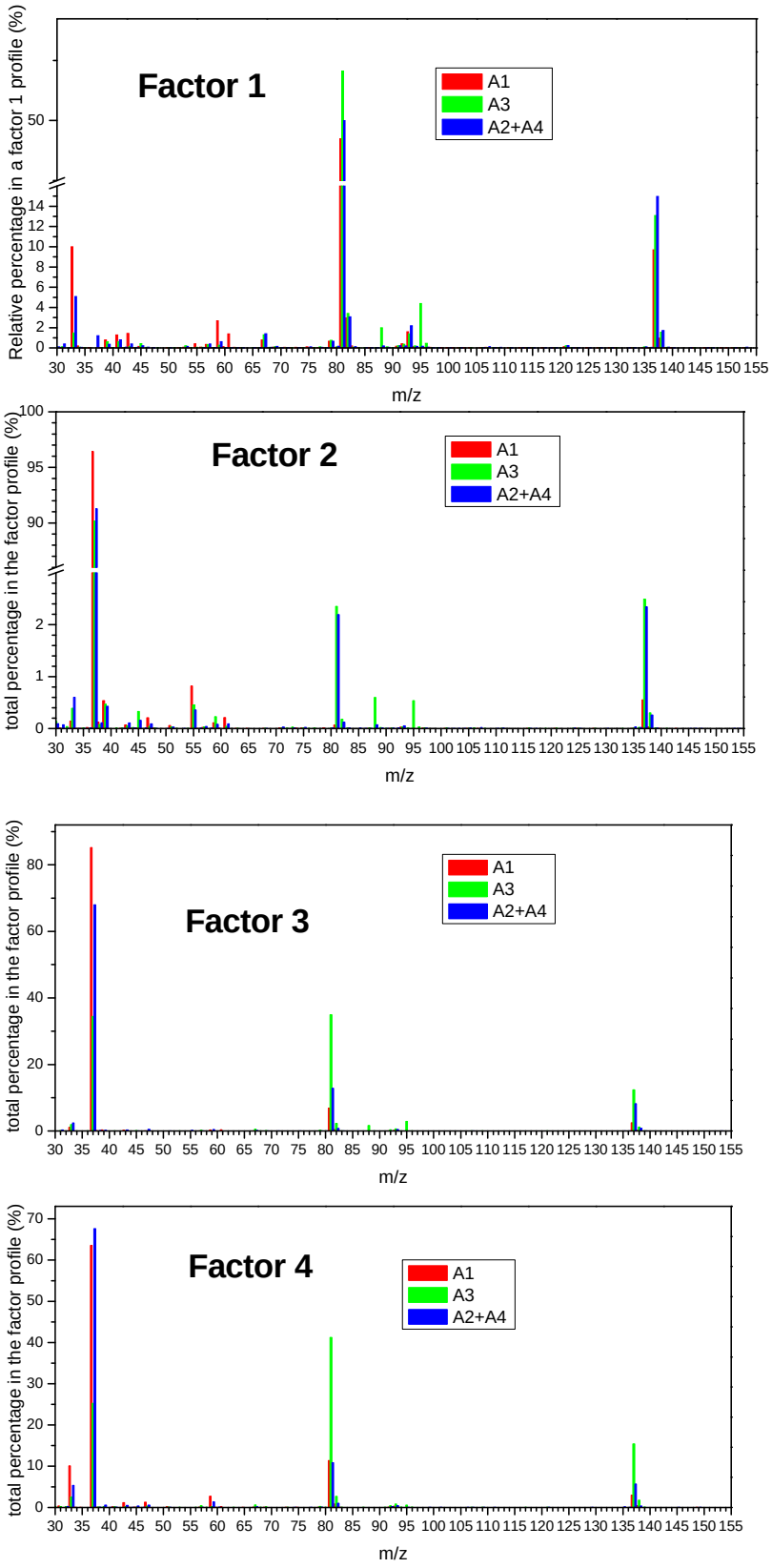

Figure 2.6-26 Profiles of the PMF factors for unknown monoterpenes

2.6.6 Discussion

The results shed light on the behaviour of monoterpenes in the AD mode, which supplements the current knowledge on their measurement with PTR-MS. The identification of monoterpene isomers by AD-PTR-MS looks very encouraging because of the following findings:

both the summed normalised spectra and the PMF profile spectra provide differences between each isomer tested, which may be more or less specific but which deliver additional qualitative information that is otherwise lacking in the commonly-used constant *E/N* PTR-MS mode;
characteristic voltages for each *m/z* fragment are the clue to differences in the spectra, although many specific features can be lost in the noise if the monoterpene concentration is small;
the ratio of *m/z* 81 and *m/z* 137 in AD-PTR-MS has a promising potential for discrimination, even based on just normalised counts of the summed AD cycle values. This finding could warrant shortening the AD cycle to scan through the few *m/z* of interest, leaving more time for fluxes and quantitative measurements. However, PMF requires the full spectra for elucidating the factors of which relative ratios of contributions from *m/z* 81 and *m/z* 137 can further aid identification.

At the end of the identification analysis, the true contents of unknown monoterpenes used in the double blind trial were revealed to be A1 – α-phellandrene, A2 – 3-carene, A3 – α-pinene, A4 - γ-terpinene. This means that the identification was successful except for not being able to distinguish between pinenes. In fact, if no PMF data was used β-pinene could have been mistaken for α-pinene. Therefore, the method can be regarded successful but only in predicting the probabilities at this stage, since AD-PTR-MS has not yet been tested in field experiments in conjunction with GC-MS to validate the uniqueness of the identification and of the scoring system proposed here. There are numerous shortcomings of this approach. For example: difficulty in the discrimination of α-pinene and β-pinene, although this might be possible using additional information warranted by a different position of

the double bond such as differences in characteristic voltages; purity of the standards can be an issue; complication with identification of multi-component mixtures can be high; and relatively low sensitivity. However, this looks like a good starting point for more studies, which could tune the scoring system presented here to the attribution of a minimal number of scoring points for the certainty of the identification; and which could derive algorithms based on correlations of measured PMF spectra with calibrated spectra.

Despite a range of characteristic voltages found for different *m/z* as well as characteristic voltages for the factors of PMF spectra for given monoterpenes, it did not provide as simple an identification clue as had been initially thought. However, these data can be useful for studying the relationships between the structure and the fragmentation and can serve as a supplement to the method based on $K_{AD81/137}$ and $F_{AD81/137}$ in unobvious cases. The purpose of the experiment described in this chapter was to show that although it has not been recognised to date, the unequivocal identification of monoterpenes using just a PTR-MS is possible.

2.6.7 Conclusions

Differences in monoterpene structures make it possible to distinguish monoterpenes in the alternating *E/N* ratio mode (AD-PTR-MS), which has been demonstrated on cumulative mass spectra, relationships of *m/z* species in the alternating drift voltage, and PMF analysis. However, the limit of detection can be an issue if minor fragments are lost in the interferences with other fragments or noise. Therefore the solution is to use the cumulative ratios of *m/z* 81 and 137 as a primary step of discrimination. The experiment suggested that reliance on $K_{AD81/137}$ and $F_{AD81/137}$ should work well even on relatively small concentrations. Another solution could be accumulation of monoterpenes on an adsorbent so as to achieve higher concentrations. The study presented the first successful attempt to distinguish monoterpenes using a standard PTR-MS. More studies are necessary and the use of different standards (different

isotopic ratios) are needed to verify the uniqueness of $K_{AD81/137}$ and $F_{AD81/137}$ for all monoterpenes, not just those studied here. Although the method extends the selectivity of a PTR-MS instrument it cannot compete with GC-MS identification which is regarded as the gold standard.

2.6.8 References

Ammann, C., Spirig, C., Neftel, A., Steinbacher, M., Komenda, M., and Schaub, A.: Application of PTR-MS for measurements of biogenic VOC in a deciduous forest, International Journal of Mass Spectrometry, 239, 87-101, 2004.

Atkinson, R., and Arey, J.: Gas-phase tropospheric chemistry of biogenic volatile organic compounds: a review, Atmospheric Environment, 37, S197-S219, 10.1016/s1352-2310(03)00391-1, 2003.

Audier, H. E., Fossey, J., Mourgues, P., McMahon, T. B., and Hammerum, S.: Formation of Proton-Bound Dimers as the Driving Force for Alkyl Radical Loss in the Gas Phase Reactions of Radical Cations, The Journal of Physical Chemistry, 100, 18380-18386, 10.1021/jp960114q, 1996.

Dinadayalane, T. C., Priyakumar, U. D., and Sastry, G. N.: Exploration of C6H6 Potential Energy Surface: A Computational Effort to Unravel the Relative Stabilities and Synthetic Feasibility of New Benzene Isomers, The Journal of Physical Chemistry A, 108, 11433-11448, 10.1021/jp0467696, 2004.

EPA PMF 3.0 Software, v. 3.0.2.2: http://www.epa.gov/heasd/products/pmf/pmf.html, access: 15 April 2010, 2010.

Grabmer, W., Graus, M., Lindinger, C., Wisthaler, A., Rappengluck, B., Steinbrecher, R., and Hansel, A.: Disjunct eddy covariance measurements of monoterpene fluxes from a Norway spruce forest using PTR-MS, International Journal of Mass Spectrometry, 239, 111-115, 2004.

Hayward, S., Tani, A., Owen, S. M., and Hewitt, C. N.: Online analysis of volatile organic compound emissions from Sitka spruce (Picea sitchensis), 24, 721-728, 2004.

Kim, S., Karl, T., Helmig, D., Daly, R., Rasmussen, R., and Guenther, A.: Measurement of atmospheric sesquiterpenes by proton transfer reaction-mass spectrometry (PTR-MS), Atmos. Meas. Tech., 2, 99-112, 2009.

Maleknia, S. D., Bell, T. L., and Adams, M. A.: PTR-MS analysis of reference and plant-emitted volatile organic compounds, International Journal of Mass Spectrometry, 262, 203-210, 2007.

Noe, S. M., Penuelas, J., and Niinemets, U.: Monoterpene emissions from ornamental trees in urban areas: a case study of Barcelona, Spain, Plant Biology, 10, 163-169, doi:10.1111/j.1438-8677.2007.00014.x, 2008.

Paatero, P., and Tapper, U.: POSITIVE MATRIX FACTORIZATION - A NONNEGATIVE FACTOR MODEL WITH OPTIMAL UTILIZATION OF ERROR-ESTIMATES OF DATA VALUES, Environmetrics, 5, 111-126, 1994.

Paatero, P.: Least squares formulation of robust non-negative factor analysis, Chemometrics and Intelligent Laboratory Systems, 37, 23-35, 1997.

Penuelas, J., Llusia, J., and Filella, I.: Methyl salicylate fumigation increases monoterpene emission rates, Biologia Plantarum, 51, 372-376, 10.1007/s10535-007-0078-9, 2007.

Slowik, J. G., Vlasenko, A., McGuire, M., Evans, G. J., and Abbatt, J. P. D.: Simultaneous factor analysis of organic particle and gas mass spectra: AMS and PTR-MS measurements at an urban site, Atmospheric Chemistry and Physics, 10, 1969-1988, 2010.

Steeghs, M. M. L., Crespo, E., and Harren, F. J. M.: Collision induced dissociation study of 10 monoterpenes for identification in trace gas measurements using the newly developed proton-transfer reaction ion trap mass spectrometer, International Journal of Mass Spectrometry, 263, 204-212, 2007a.

Steeghs, M. M. L., Cristescu, S. M., and Harren, F. J. M.: The suitability of Tedlar bags for breath sampling in medical diagnostic research, Physiol. Meas., 28, 73-84, 10.1088/0967-3334/28/1/007, 2007b.

Tani, A., Hayward, S., and Hewitt, C. N.: Measurement of monoterpenes and related compounds by proton transfer reaction-mass spectrometry (PTR-MS), International Journal of Mass Spectrometry, 223, 561-578, 2003.

Tani, A., Hayward, S., Hansel, A., and Hewitt, C. N.: Effect of water vapour pressure on monoterpene measurements using proton transfer reaction-mass spectrometry (PTR-MS), International Journal of Mass Spectrometry, 239, 161-169, 2004.

Ulbrich, I. M., Canagaratna, M. R., Zhang, Q., Worsnop, D. R., and Jimenez, J. L.: Interpretation of organic components from Positive Matrix Factorization of aerosol mass spectrometric data, Atmos. Chem. Phys., 9, 2891-2918, 2009.

Warneke, C., van der Veen, C., Luxembourg, S., de Gouw, J. A., and Kok, A.: Measurements of benzene and toluene in ambient air using proton-transfer-reaction mass spectrometry: calibration, humidity dependence, and field intercomparison, International Journal of Mass Spectrometry, 207, 167-182, 2001.

2.7 Conclusions and future work

Concentrations and fluxes of BVOCs were measured above different ecosystems by PTR-MS coupled to the vDEC technique. The data are useful as they serve to facilitate the recognition of atmospheric processes and feedbacks, and provide a basis for modelling. Discussions of the implications of BVOC emissions were made in the particular chapters.

However, all measurements are associated with an uncertainty, which is the general problem even in state-of-the-art analytical approaches such as those presented here. The author has identified sources of uncertainty such as lag-time imprecision, which is particularly important for the vDEC technique. Errors attributed to lag-time identification had been downplayed in prior reports, probably because in conventional eddy covariance the lag time is typically constant and relatively easy to derive. Some researchers may not have been aware that, as shown here, the lag-time in PTR-MS may not be the same for each integration time, because of the nature of the quadrupole MS used as a detector. Therefore, using approximated constant lag times without an insight into the covariance function may not provide an acceptable estimate of the likely uncertainty. Since the correct lag-time is so crucial for the calculation of the precise flux, and in particular of the flux associated with small concentration or depositing compounds, the need for lag-time validation was evident and for this reason the author derived the IMED and LTV methods. They are potentially valuable for all the community making flux measurements using the vDEC approach, and possiblyalso for other eddy covariance variants. More data are waiting to be validated using these methods. The lag-time validity test, or a similar approach, should be included in the FLUXNET criteria.

Obviously the flux cannot be certain if the mixing ratio is imprecise. Therefore, the need for precise external calibrations and transmission measurements was highlighted at various points of this thesis. It is true that sometimes an external standard is not available, but then the uncertainty should be made clear. Progress has been made as the empirical approaches which combine the standard calibration with

transmission could greatly decrease the uncertainty. However, the fact that the higher end of the mass spectrum has the higher uncertainty, if the calibration standard does not include heavy *m/z,* is still not widely perceived. Despite these uncertainties, the vDEC method combined with a PTR-MS sensor is currently the most valuable technique to date, as it offers a direct real-time measurement of VOC behaviour in the atmosphere. A ToF-PTR-MS is still not widely available but has a promising future in providing better qualitative information because of its much greater resolution of *m/z*. The atmospheric modelling community is waiting to feed global dynamic models with more data of the true net flux or to constrain the much more uncertain estimates from leaf level measurements which are, however, valuable for understanding biochemical and mechanical processes governing the production and release of BVOCs to the atmosphere.

More large-scale measurements such as aircraft PTR-MS vDEC measurements are particularly needed and obviously this is a direction for the future. However, the interface between scientists and politicians needs to be improved, as more funding is requireded for undertaking airborne measurements, which are necessary for understanding atmospheric chemistry, processes and climate feedbacks.

The impacts on aerosols could be huge from VOCs in the tropics, but the role of large oil palm isoprene (and other BVOC) emissions is still not entirely clear. Isoprene could inhibit the formation of aerosol through scavenging of OH but the reaction rate for isoprene photo-oxidation at oil palm could be different from over other vegetation, as suggested by the narrow isoprene peak of emission.. However, the basal emissions rates from oil palms are under circadian control , so the solar radiation and temperature are less effective in producing isoprene in the mornings and afternoon than for other vegetation types. However isoprene could produce hydrogen hydroperoxides and epoxides, which can play an important role insustaining the oxidative capacity of the atmosphere. Clearly, measurements above oil palms showed distinct deposition of isoprene oxidation products, so the small aerosol yield obtained in chamber studies is likely to be even smaller in the field. Nevertheless, floral compounds are particularly important in the case of oil palms,

which bear fruit all year and constantly release estragole to attract pollinators. Estragole may even be more important than the more abundant isoprene, since estragole has a high SOA potential yield. However, estragole which seems to be still emitted during the evening, after the boundary layer collapses, may not be so easily transported as the mid-day isoprene. The cause of floral toluene emissions, and their physiological and ecological role is still unknown. Could it be that they attract flies as is the case for other Arecaceae species; could it be a herbivore deterrent or maybe is it simply a byproduct of a biochemical cycle? Regardless, toluene is also a very high SOA contributor, so the flowers do seem responsible for the majority of BVOC-derived aerosols. The preliminary findings from ToF-AMS studies are consistent with the results reported here. The story needs to be further developed by conducting more measurements over oil palms.

In nature, it is often the case that one or two monoterpenes dominate emissions to and concentrations in the atmosphere. The PTR-MS cannot distinguish between them but can measure the total sum. In the last decade various teams have tried to extend the selectivity of the PTR-MS instrument. As these were not successful, attempts have been made to combine PTR-MS with other expensive approaches, such as a triple quadrupole MS. The author has proved that monoterpene discrimination is possible with a standard PTR-MS by using alternating collision energies without modification of the instrument, but by changing the data acquisition routine to alternate the drift voltage. This approach, although promising, should still be tested in the field and validated on more monoterpene isomers.

Finally, atmospheric chemistry is not the whole story. The broader picture is to understand the true role of VOCs in ecosystems. The algorithms for BVOC emissions are based on environmental parameters but in isolation from, for example, their role in plant-plant and plant-animal communication. It is not obvious how to include stress, which can be sensed from the canopy (Karl et al, 2008), to the models or how to predict the increase in monoterpene emission rates by a factor of ten caused by an infestation of bark beetle (Alex Guenther, p.c.). Although this PhD effort has uncovered many known unknowns it has also added more other known

unknowns to the puzzle, but most importantly has reduced the feeling of unknown unknowns which are definitely present. The collaborative achievements to which the author has and is contributing could not be mentioned in detail, but the reader is referred to Appendix 2. Instead, only a portion of the author's original work has been presented here. The continuation of the paths and enthusiasm marked during this PhD will be an endeavour of the author.

Photographs from the Borneo fieldwork

SEM change (rainforest site)

View from the GAW tower 75 m (5:00 LT)

Closed canopy (oil palm site)

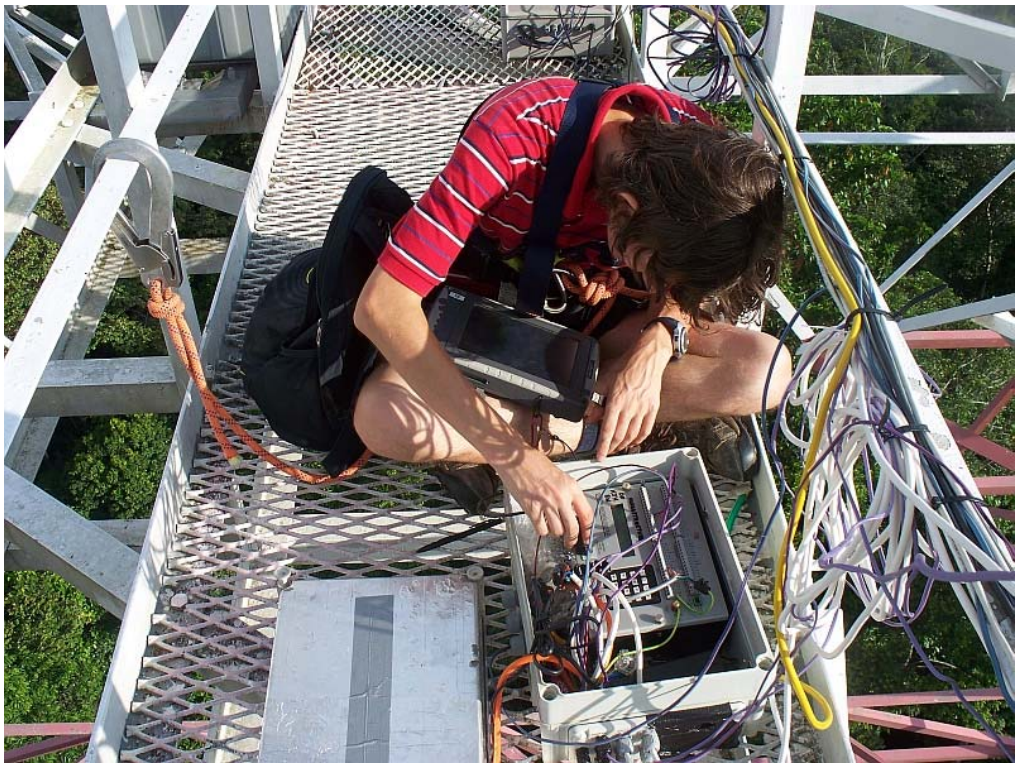

Transferring data from loggers (GAW tower)

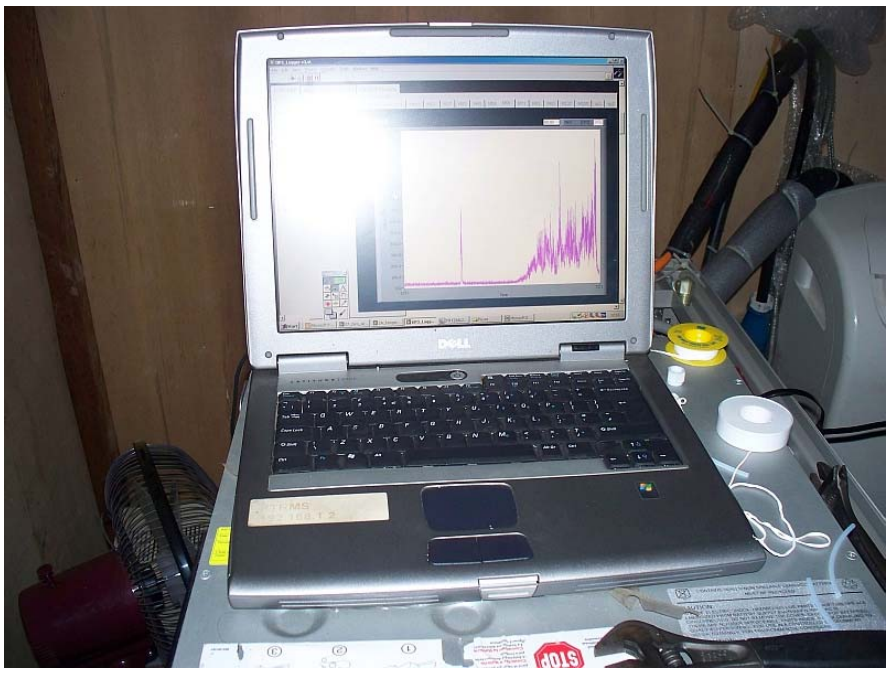

Logging PTR-MS data at the oil palm plantation.

Appendix I Software developments

I-A Data analysis software

PawEddy (Pawel Misztal)

The program PawEddy has been designated to processing the vDEC fluxes from PTR-MS and mixing ratios, which can be derived from the normalised sensitivities or from the transmission coeficients. PawEddy is a postprocessing program for PTR-MS but could be adjusted to any vDEC systems whose data look similarly to those presented in Figure I-1. The major features of the program include outputting concentrations and fluxes,using a range of lag time methods (MAX, IMED, PF, VIS); deriving micrometeorological parameters from the sonic data, quality control: stationarity, LODs, u* threshold, lag time validation (LTV) test. The program is fully automated and has a user interface with setup of validation critera, number of compounds and lag-time method, and calibration mode. The latest version of the program is attached in the electronic supplement (‘Analysis Software\PawEddy’)

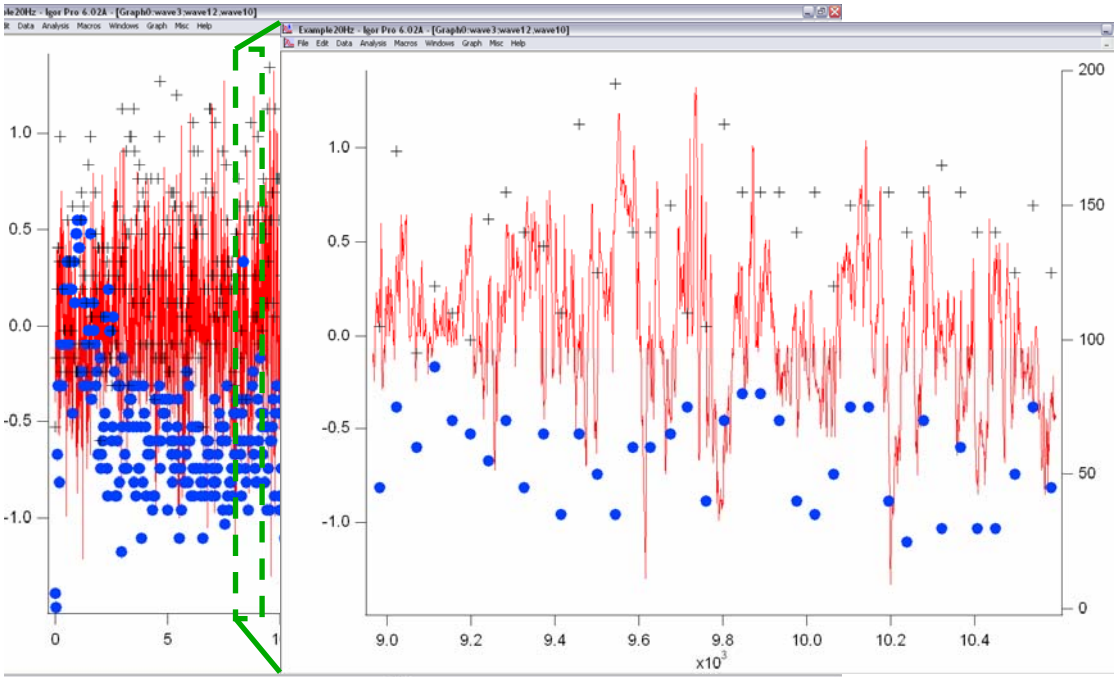

Figure I-1 Disjunct time series of the wind (continuous) and PTR-MS data (gaps due to disjunct sampling).

PawSB (Pawel Misztal, CEH)

The program is dedicated to processing the full scans from PTR-MS and delivering normalised counts. The latest version can be found in Analysis Software/PawSB folder of the electronic supplement. Previously, the Quadstar scanbar files had to be processed manually one by one.

I-B Field software

GriffinLog (Eiko Nemitz, Pawel Misztal, Ben Langford)

This program was used to log the fluxes from PTR-MS into one file during the measurements in the Griffin Forest in Scotland (data not presented in this thesis).

OilPalmLog (Ben Langford, Pawel Misztal, Eiko Nemitz)

This program was used to log vDEC fluxes at oil palm. The program was not new, it has been earlier used within CEH and Lancaster groups, but was amended by the author to enable loggin the desired suite of compounds and acquisition of a different sonic routine.

I-C Drift software

PawSBdrift (Pawel Misztal)

This is a similar program to PawSB, but is specifically designed for processing AD-PTR-MS data (see chapter 2.6). The program can be found in electronic supplement in the 'Drift software/PawSBdrift' folder.

driftad.seq (Pawel Misztal)

This is a sequence file that enables measurement in the AD-PTR-MS mode ('Drift software/driftad.seq').

I-D Other software

PawCal (Pawel Misztal)

This program has been written for the purpose of optimising sensitivity. The user has a preview of normalised counts (rather than the raw counts as in other software), which can enable tuning voltages upon connecting the standard to ensure the highest sensitivity. This program can be found in 'Other software/PawCal' of the electronic supplement.

Various files

They include Quadstar sequences for SEM optimisation, and transmission, and other small programs. The electronic version contains these files in the 'Other software/various files' folder Although the files in this folder were derived by the author, similar programs could have been written by others due to their relative simplicity.

Appendix II Publications

This appendix contains articles to which the author has contributed in collaboration

II-A Cieslik, …, and Misztal, P.: Turbulence in a coastal Mediterranean area: surface fluxes and related parameters at Castel Porziano, Italy, Biogeosciences Discuss., 6, 3355-3372, 2009.

II-B Davison, B., …., Misztal, P., et al.: Concentrations and fluxes of biogenic volatile organic compounds above a Mediterranean macchia ecosystem in western Italy, Biogeosciences, 6, 1655-1670, 2009.

II-C Fowler, D., …, Misztal, P., et al.: Atmospheric composition change: Ecosystems-Atmosphere interactions, Atmospheric Environment, 43, 5193-5267, 10.1016/j.atmosenv.2009.07.068, 2009.

II-D Hewitt, C. N., …, Misztal, P., et al.: Nitrogen management is essential to prevent tropical oil palm plantations from causing ground-level ozone pollution, Proceedings of the National Academy of Sciences, 106, 18447-18451, 10.1073/pnas.0907541106, 2009.

II-E Hewitt, C. N., … , Misztal, P., et al.: Overview: oxidant and particle photochemical processes above a south-east Asian tropical rainforest (the OP3 project): introduction, rationale, location characteristics and tools, Atmos. Chem. Phys., 10, 169-199, 2010.

II-F Langford, B., Misztal, P. K., et al.: Fluxes and concentrations of volatile organic compounds from a South-East Asian tropical rainforest, Atmos. Chem. Phys. Discuss., 10, 11975-12021, 10.5194/acpd-10-11975-2010, 2010.

II-G Misztal, P., Fares, S., and Taraborrelli, D.: Report on an e-working module on biogenic emissions, in:Report on Surface Emissions and Prediction of Atmospheric Composition Changes – GEIA Summer School Ile d'Oleron, France, 44-48, 2007.

II-H Misztal, P. K., et al.: Large estragole fluxes from oil palms in Borneo, Atmos. Chem. Phys., 10, 4343-4358, 2010.

II-I Pike, R. C., … , Misztal, P.,et al.: Can a global model chemical mechanism reproduce NO, NO2, and O3 measurements above a tropical rainforest?, Atmos. Chem. Phys. Discuss., 9, 27611-27648, 2009

II-J Pugh, T. A. M., … , Misztal, P., et al. : Simulating atmospheric composition over a South-East Asian tropical rainforest: performance of a chemistry box model, Atmos. Chem. Phys., 10, 279-298, 2010.

II-A Cieslik, …, and Misztal, P.: Turbulence in a coastal Mediterranean area: surface fluxes and related parameters at Castel Porziano, Italy, Biogeosciences Discuss., 6, 3355-3372, 2009.

Open access at: http://www.biogeosciences-discuss.net/6/3355/2009/bgd-6-3355-2009.html

Biogeosciences Discuss., 6, 3355–3372, 2009
www.biogeosciences-discuss.net/6/3355/2009/

Biogeosciences Discussions

Biogeosciences Discussions is the access reviewed discussion forum of *Biogeosciences*

Turbulence in a coastal Mediterranean area: surface fluxes and related parameters at Castel Porziano, Italy

S. A. Cieslik[1], G. Gerosa[2], A. Finco[2], G. Matteucci[3], N. Cape[4], and P. Misztal[4]

[1]Institute for Environment and Sustainability, JRC, Ispra, Italy
[2]Dipartimento di Matematica e Fisica, Università Cattolica del S.C., Brescia, Italy
[3]Istituto di Biologia Agro-ambientale e Forestale, CNR, Porano, Italy
[4]Centre for Ecology and Hydrology, Penicuik, UK

Received: 29 December 2008 – Accepted: 25 January 2009 – Published: 30 March 2009

Correspondence to: S. A. Cieslik (stanislaw.cieslik@jrc.it)

Published by Copernicus Publications on behalf of the European Geosciences Union.

Abstract

During the ACCENT/VOCBAS measuring campaign conducted at Castel Porziano, Italy over a Mediterranean macchia ecosystem located near the coastline, a series of micrometeorological observations were made. Sensible and latent heat fluxes, as well as ozone fluxes, are presented. The behaviour of the main meteorological variables such as temperature, humidity, wind speed and direction, is analysed.

1 Introduction

The main goal of the measuring campaign described in this issue is a study of the chemical exchange between biosphere and atmosphere at a coastal site near Rome, covered by sand dunes and dry Mediterranean vegetation. The determination of exchange fluxes of chemical species (volatile organic compounds, nitrogen oxides, ozone, water vapour, carbon dioxide) largely made use of micrometeorological methods like eddy-covariance. The chemical fluxes are generated by the properties of the air/vegetation interface and driven by turbulence. For example, the emission flux of a given biogenic volatile organic compound (BVOC) is due to the production of the substance inside the cells followed by its release through the stomata or other leaf surface elements, but, once the emitted molecules are present in the air, they are transported aloft by turbulence. So, a study of turbulence is essential if we wish to describe the air/vegetation chemical exchange processes. Several participating groups operated micrometeorological instrumentation, whose working principles are based on the properties of turbulent motion. Turbulent atmospheric variables were thus recorded and used throughout this issue. Further, this campaign constituted a good occasion to study phenomena related with turbulence in a coastal area covered by sclerophyllic vegetation. Important features characterizing turbulent air motion at the measuring site are land-sea breezes, thermal inversions, small-scale phenomena due to the presence of dunes and low, non-homogeneously distributed vegetation. Very few studies (see

e.g. Valentini et al., 1990) have been carried out previously over an ecosystem similar to the Castel Porziano seashore.

In the present article we deal with physical variables such as temperature, humidity, and wind vector, the chemical and biological aspects being addressed in other contributions of this issue. The characteristics of turbulence presented here have been used in other contributions of this special issue.

2 Site and instrumentation

The observation site was located near the Mediterranean seashore in the Castel Porziano estate near Rome. For a more general description, see Fares et al. (2009). The micrometeorological measurements were located in a dune area covered by non-homogeneously distributed macchia-type vegetation. A description of the instrumental set-up installed by the different groups is outlined below.

1. The group "Università Cattolica del Sacro Cuore", Brescia, Italy (hereafter referred to as UCSC), operated, on a small tower, a METEK USA-1 sonic anemometer and a LI-7500 LI-COR open path infrared absorption sensor for water vapour and CO_2 concentrations placed at a height of 3.8 m above ground level (a.g.l.) to measure turbulent vertical fluxes of sensible and latent heat, as well as related micrometeorological variables such as friction velocitites and fluxes of chemical substances.

A net radiometer (NR lite, Kipp&Zonen, Holland), a sensor for the measurement of the photosynthetically active radiation (PAR; LI-COR, mod. 190SA, Lincoln, Neb., USA) and a temperature and relative humidity probe (50Y, Campbell Scientific, Shepshed, United Kingdom) were placed at 3.8 m a.g.l.

This measuring site was also equipped with additional instrumentation to describe the vertical temperature and humidity profiles, the soil water content, the non-turbulent energy fluxes and the microclimate of the area: two additional temperature and

relative humidity probes (50Y, Campbell Scientific, Shepshed, United Kingdom) at 1 m and 0.1 m; three soil heat flux plates, (HFP01SC, Hukseflux, Delft, Holland); three TDR reflectometers (C616, Campbell Scientific, Shepshed, United Kingdom); three leaf temperature probes (Pt100, DeltaT, United Kingdom); two surrogate leaves (237, Campbell Scientific, United Kingdom) to measure leaf wetness, one rain gauge (52202, Young/Campbell Scientific, Cambridge, United Kingdom) and one barometer (PTB101B, Vaisala, Finland).

2. The "Istituto di biologia agro-ambientale e forestale", Porano, Italy (IBAF), operated a Young 81000 sonic anemometer and a LI-COR 7500 open path infrared absorption sensor for water vapour and CO_2 concentrations at 6.0 m a.g.l. on the same tower.

3. The Joint Research Centre, Ispra, Italy (JRC) operated a METEK USA-1 sonic anemometer and a Campbell Sci. KH20 krypton hygrometer at a height of 9.5 m on a tower located at a distance of about 30 m westwards respect to the UCSC-IBAF tower. The JRC tower was erected on a small dune, and the height reported here is expressed respect to the base of the UCSC-IBAF tower.

The general layout of the observation facilities is represented on Fig. 1.

The fluxes and other micrometeorological variables were measured using the eddy covariance technique (see e.g. Swinbank, 1951; Hicks and Matt, 1988). The data recorded by the fast sensors were sampled at 20 Hz (UCSC, IBAF) and 10 Hz (JRC) with home-made software packages written in Delphi 5.0 (UCSC) and Labview 6 (JRC). Slow sensors were sampled every 15 s and data were collected by a data logger (CR10x, Campbell Scientific, Shepshed, United Kingdom) equipped with a signal multiplexer device (AM16/32, Campbell Sci., United Kingdom), and data were averaged every 30 min.

3 Results and observations

Observations during the major part of one month, May 2007, such that the meteorological variables recorded could be averaged. Mean vertical profiles of temperature, absolute and relative humidity, and wind speed and direction, were calculated in order to identify the main features of the daily behaviour of these parameters (Fig. 2a, b, c).

During daytime the vertical temperature profile, averaged over the whole month (Fig. 2a), was strongly superadiabatic near the surface, with a temperature difference of 3 degrees between 0.1 and 3.5 m a.g.l. The solar radiation very efficiently heats up the sandy soil of the dunes, which in turn heats the air aloft. From 06:00 p.m. onwards this strong negative temperature gradient becomes weaker and around 07:30 p.m. the vegetation (canopy) becomes colder than both the soil and the air above, resulting in a complex vertical profile. The full inversion including all levels is established only at 11:00 p.m., and persists during the whole night until 08:30 a.m. At that time, the canopy becomes warmer that both the soil and the above air layer. This transition period is short and at 09:00 a.m. the inversion is completely destroyed.

The night time formation of inversion layers near the soil is regular and the inversions are strong. As a consequence, dew formation is frequent, as indicated by the daily course of the dew point temperature, shown on Fig. 3, together with the surrogate leaf resistance. This latter variable is very close to zero during nigh time, indicating a wet, dew covered surface. The dew may be used by the sclerophyllic vegetation present on the macchia as a way of limiting water shortage, since a part of the water condensed ends up in the soil and is subsequently pumped by the plant roots. It is also possible that a small portion of the dew penetrates directly into the plant tissues. The formation of dew is an element of the coupling between the atmosphere and the surface, as it modifies the hydrological balance.

The behaviour of the vertical profile of absolute humidity χ, as expressed in g/m^3 (Fig. 2b), is similar to the temperature profile in the lower layers. At highest level (9.5 m) the role of advection appears clearly as the air is rather dry during night time, due to

advection of dryer air from inland, whereas it is much wetter during daytime hours due to the wet air advected from the sea and transported by the breeze.

The behaviour of the absolute humidity in the upper layers appears decoupled from that observed in the lower layers, with a stronger difference during night time. This is probably due to the advection effect in which wet air is transported from the sea during daytime and dryer air comes from inland during night time.

The wind velocity (Fig. 2c) appears systematically higher in the upper levels, as expected, the difference being weaker in the night time hours. The prevailing night time wind direction (Fig. 4a) is from north. After sunrise and in the upper levels the wind direction becomes more variable between NW and NE. From 09:00 a.m. onwards, the wind rotates to E, and later to S. The daytime, southerly, sea-breeze regime, is reached at 01:00 p.m. The wind direction rotation process is more rapid in the lower layers, where the prevailing daytime wind direction is reached around 10:00 a.m. It is to be noted that, between 09:00 a.m. and 01:00 p.m., the wind directions near ground and at the highest level may differ considerably from each other, with a maximum difference of about 90° clockwise. From 09:00 p.m. onwards the near-ground wind rotates to north, briefly followed by the wind at higher levels. The breeze circulation is also illustrated on Fig. 4b with the wind recorded at 9.5 m a.g.l.

Figure 5 shows the evolution of the main micrometeorological variables during the whole month of May 2007: friction velocity (Fig. 5a), sensible heat flux (Fig. 5b), latent heat flux (Fig. 5c) and total ozone flux (Fig. 5d) during May 2007 at the measuring site.

An important feature in micrometeorology is the constant flux hypothesis, which states that, in a horizontally homogeneous surface layer, the fluxes of turbulent variables (enthalpy or sensible heat, momentum, chemical concentrations) are almost constant with height. Fulfillment of this assumption permits the description of the atmospheric boundary layer in terms of characteristic quantities such as the friction velocity and scaling temperature (see e.g. Stull, 1988) which in turn permit the calculation of vertical profiles of various quantities like concentrations. The presence of three levels of measurement (3.8 m, 6 m and 9.5 m) permitted to check the fulfilment of the constant

flux hypothesis and to decide whether these measurements could be used for further studies at the observation site, such as the derivation of vertical profiles. Examination of the fluxes of sensible and latent heat, as well as the ozone fluxes and the friction velocities (which are an alternative expression of the momentum fluxes) measured at the different levels showed the following characteristics: the differences between fluxes where very low between the upper two levels (6 m and 9.5 m) for all variables (see Fig. 6), whereas there is less agreement between the upper two levels and the lowest level (3.8 m), respectively. This is due to the fact that the lowest level is sensitive to the irregularities in the topography due to the presence of dunes (the mean height of the dunes was about 5 m) and the non-homogeneously distributed vegetation with portions of bare sandy soil exposed to strong solar radiation. The upper levels have a wider footprint, and do not "see" the details of the surface elements. As a consequence, it can be stated that the constant flux hypothesis is fulfilled for the levels above 6 m and that the corresponding measurements can be used for further investigations. This was made e.g. to calculated vertical ozone fluxes from ozone concentration profile measurements by using the gradient method (see Mereu et al., 2009), through the derivation of the vertical turbulent diffusion coefficient,

$$K(z)=k\cdot u^{*}z/\Phi(u^{*},H) \quad (1)$$

where z is the height a.g.l., k is the von Karman's constant (~0.4), u^{*} is the friction velocity, L is the Monin-Obukhov length, and Φ is the Monin-Obukhov stability function of friction velocity and H, the sensible heat flux. The $K(z)$ coefficient were thus calculated from the measured friction velocities and sensible heat fluxes, shown on Fig. 5a and b.

The different terms of the surface *energy* balance: net radiation, soil heat flux, turbulent sensible and latent heat fluxes, during May 2007, showed a very regular diurnal course, except for the few days in which synoptic perturbations were passing over the area. The Bowen ratio $\beta=H/\lambda E$ was very high during most of the campaign (Fig. 7, upper frame), ranging between 3 and 4 in the central part of the day (11:00 a.m. to 07:00 p.m.), indicating that water availability was very limited, characterising an environment where sclerophyllic, drought-adapted vegetation is dominant. The mean evap-

orative efficiency, $\lambda E/(H+\lambda E)$ was about 20%. These features show that the coupling between the physical conditions prevailing in the atmosphere and the characteristics of vegetation is strong. This coupling can also be expressed by a decoupling coefficient Ω introduced by McNaughton and Jarvis (1983) and expressed by

$$\Omega=\frac{\frac{s}{\gamma}+1}{\frac{s}{\gamma}+1+\frac{R_c}{R_a}} \quad (2)$$

where s ist he slope of the saturation curve of water vapour pressure against temperature, γ is the psychrometric constant, R_c and R_a are the canopy and aerodynamic resistances, respectively. Figure 7 (middle frame) shows the mean daily course of the coupling coefficient 1-Ω, which is ranges between 0.6 and 0.7 in the central hours of the day.

The hourly averages of the terms of the surface energy balance are represented on Fig. 7b. Three values of the measured soil heat flux are represented, corresponding to different locations of the flux sensors. One sensor was located in bare sandy soil, where the strongest heating is observed during the central hours of the day, whereas the maximum heating of the soil occurs in the afternoon for the sensors placed beneath plants. Figure 8 illustrates the closure of the surface energy balance, showing the sum of turbulent heat fluxes ($H+\lambda E$) against the available energy at the surface (Rn-G). It appears that, notwithstanding problems which may arise from advection effects or surface non-homogeneities (see e.g. Foken et al., 2006), the closure of the balance is reasonably good.

4 Conclusions

Turbulent fluxes of scalar quantities such as energy and ozone concentration, as well as various micrometeorological variables, were measured during May 2007 by the eddy covariance method in the coastal dune area of the Castel Porziano estate near Rome,

Italy. The measurements were carried out in support of the air/vegetation chemical exchange observation campaign conducted in the frame of the ACCENT/VOCBAS project. The observations showed some characteristics of the coastal meteorology in a dry climate, such as land-sea breezes, strong nocturnal inversions, water use schemes used by sclerophyllic plants to save water. The importance of advection was revealed by the different behaviour of some meteorological parameters at higher and lower levels, as the higher levels appeared more influenced by the wet air advected from the sea during day time than the lower levels. The local non-homogeneity of both hypsometry and distribution of vegetation, also plays a role and causes deviations from the theoretically predicted vertical distribution of fluxes.

References

Fares, S., Mereu, S., Scarascia Mugnozza, G., Vitale, M., Manes, F., Frattoni, M., Ciccioli, P., and Loreto, F.: The ACCENT-VOCBAS field campaign on biosphere-atmosphere interactions in a Mediterranean ecosystem of Castelporziano (Rome): site characteristics, climatic and meteorological conditions, and eco-physiology of vegetation, Biogeosciences Discuss., 6, 1185–1227, 2009, http://www.biogeosciences-discuss.net/6/1185/2009/.

Foken, T., Wimmer, F., Mauder, M., Thomas, C., and Liebethal, C.: Some aspects of the energy balance closure problem, Atmos. Chem. Phys., 6, 4395–4402, 2006, http://www.atmos-chem-phys.net/6/4395/2006/.

Hicks, B. B. and Matt, D. R.: Combining biology, chemistry and meteorology in modeling and measuring dry deposition, J. Atmos. Chem., 6, 117–131, 1988.

NcNaughton, K. G. and Jarvis, P. G.: Predicting effects of vegetation changes on transpiration and evaporation, in: Water deficit and plant growth, edited by: Koslowski, T. T., Academic Press, New York, USA, 7, 1–47, 1983.

Mereu, S., Salvatori, E., Fusaro, L., Gerosa, G., Muys, B., and Manes, F.: A whole plant approach to evaluate the water use of mediterranean maquis species in a coastal dune ecosystem, Biogeosciences Discuss., 6, 1713–1746, 2009, http://www.biogeosciences-discuss.net/6/1713/2009/.

Swinbank, W. C.: The Measurement of Vertical Transfer of Heat and Water Vapor by Eddies in the Lower Atmosphere, J. Meteorol., 8, 135–145, 1951.

Valentini, R., Scarascia-Mugnozza, G. E., De Angelis, P., and Bimbi, R.: An experimental test of the eddy correlation technique over a Mediterranean macchia canopy, Plant Cell Environ., 14, 987–994, 1991.

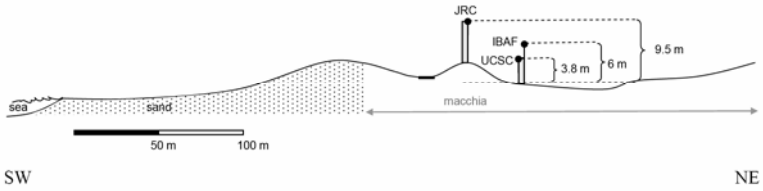

Fig. 1. Topographic profile of the measuring site, showing the location of the three eddy covariance systems (back dots).

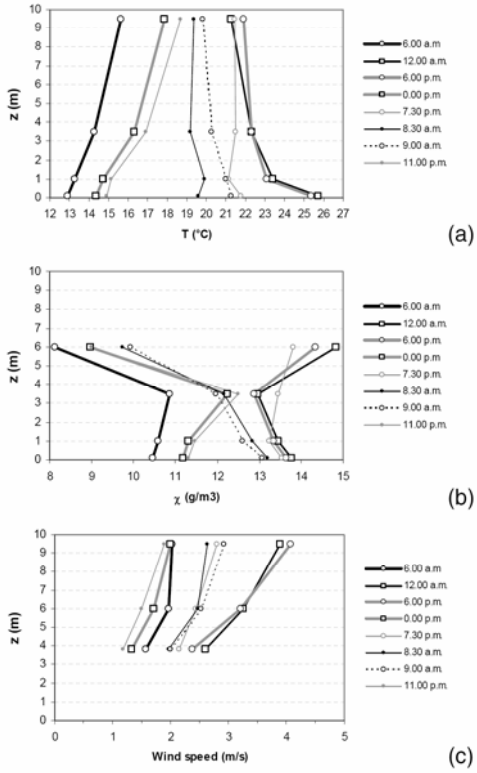

Fig. 2. Vertical profiles of different meteorological variables at synoptic hours (00:00, 06:00, 12:00, 18:00) and at other selected hours (08:30, 09:00, 19:30, 21:00) when inversions occur. **(a)** Mean air temperature; **(b)** Mean absolute humidity; **(c)** mean wind speed.

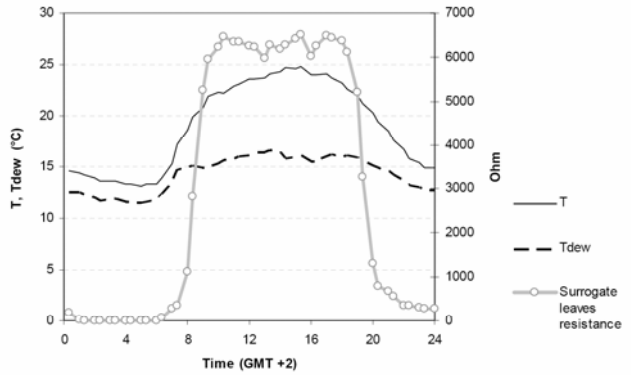

Fig. 3. Mean air temperature and dew temperature at canopy level compared with the surface resistance of the surrogate leaves (values close to 0 Ohm indicate wet surfaces while values around 6999 Ohm, the maximum value, indicate completely dry surfaces).

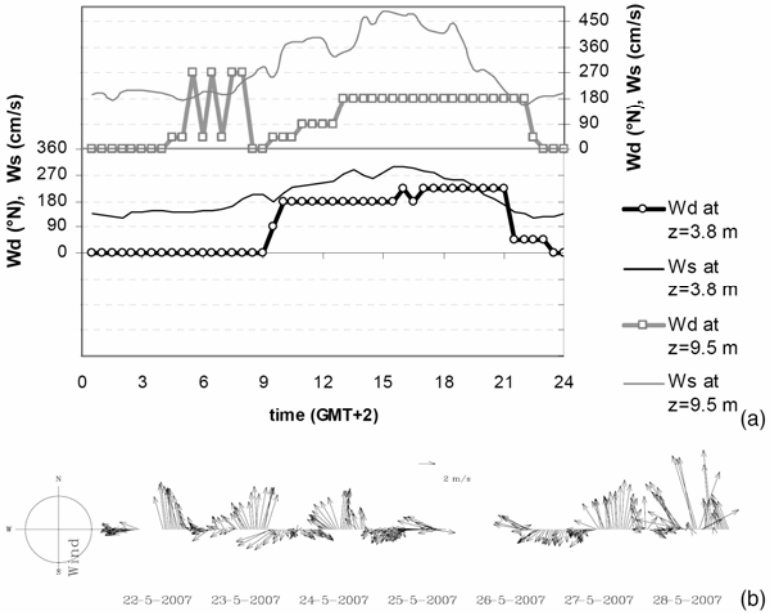

Fig. 4. **(a)** Prevailing wind direction (Wd) and mean wind speed (Ws) during daytime (note than the wind speed is expressed in cm/s) **(b)** Representation of the horizontal wind vector measured at 9.5 m a.g.l., from 22 to 28 May, which illustrates the breeze circulation.

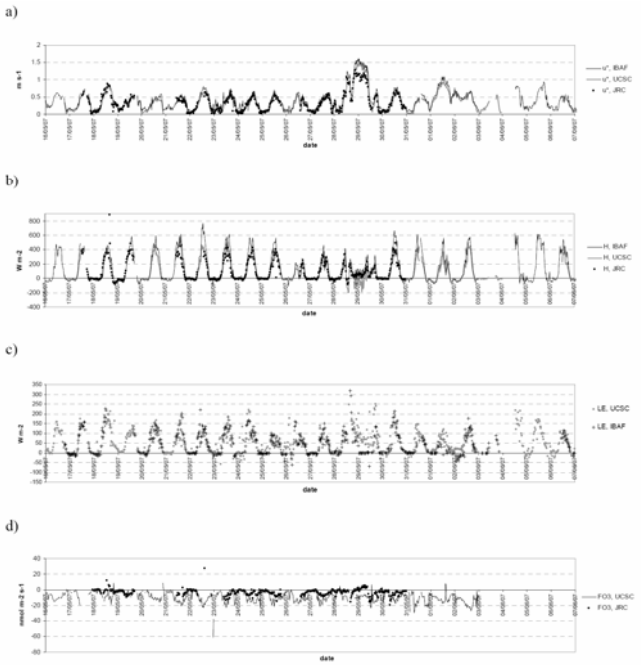

Fig. 5. Turbulent sensible heat flux and ozone flux at different heights: JRC=9.5 m, IBAF=5.5 m, UCSC=3.8 m. **(a)** friction velocity; **(b)** sensible heat flux; **(c)** latent heat flux; **(d)** total ozone flux.

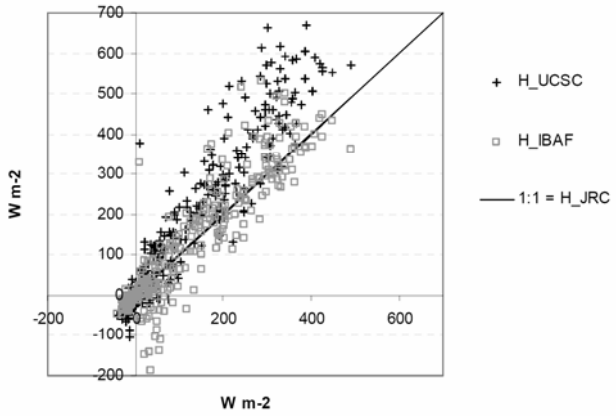

Fig. 6. Comparison between sensible heat fluxes obtained at different levels. Crosses: 3.8 m (UCSC) against 9.5 m (JRC). Squares: 5.5 m (IBAF) against 9.5 m (JRC). The constant flux hypothesis is fully respected between the 5.5 m and 9.5 m levels.

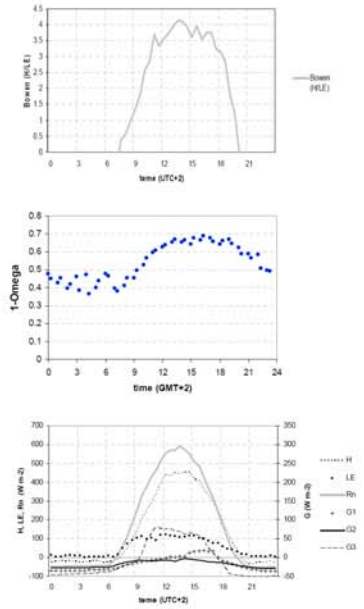

Fig. 7. Mean daily course of the following variables: Upper: bowen ratio, showing rather dry conditions prevailing during the campaign; Middle: coupling coefficient 1-Ω; Lower: the different terms of the surface energy balance: *H* is the sensible heat flux; *LE* is the latent heat flux; *Rn* is the net radiation; *G*1, *G*2 and *G*3 are ground heat fluxes. *G*1 was measured under a juniper, phyllirea and rosemary bush; *G*2 under an Erica bush; *G*3 was recorded in the bare sand. Positive *G* values are in-ground fluxes, negative values are outward fluxes.

3371

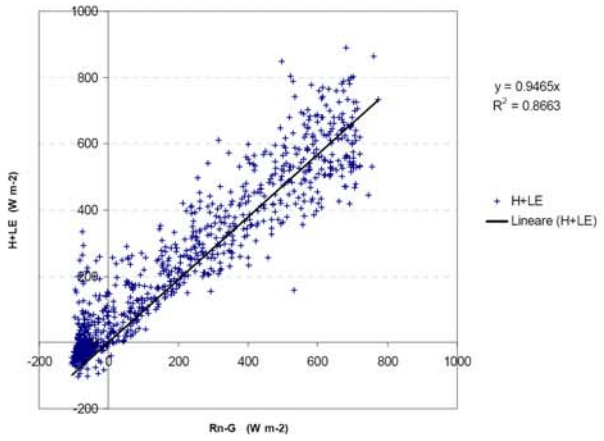

Fig. 8. Energy balance closure, represented as the sum of turbulent fluxes (sensible and latent heat fluxes) against the available energy at the surface (net radiation minus ground heat flux).

3372

II-B Davison, B., …., Misztal, P., et al.: Concentrations and fluxes of biogenic volatile organic compounds above a Mediterranean macchia ecosystem in western Italy, Biogeosciences, 6, 1655-1670, 2009.

Open access at: http://www.biogeosciences.net/6/1655/2009/bg-6-1655-2009.html

Biogeosciences, 6, 1655–1670, 2009
www.biogeosciences.net/6/1655/2009/

Biogeosciences

Concentrations and fluxes of biogenic volatile organic compounds above a Mediterranean macchia ecosystem in western Italy

B. Davison[1], R. Taipale[2], B. Langford[1], P. Misztal[3,4], S. Fares[5,*], G. Matteucci[5], F. Loreto[5], J. N. Cape[3], J. Rinne[2], and C. N. Hewitt[1]

[1]Lancaster Environment Centre, Lancaster University, Lancaster LA1 4YQ, UK
[2]University of Helsinki, Department of Physics, P.O. Box 64, 00014 University of Helsinki, Finland
[3]Centre for Ecology & Hydrology, Bush Estate, Penicuik, Midlothian EH26 0QB, UK
[4]School of Chemistry, University of Edinburgh, Edinburgh EH9 3JJ, UK
[5]National Research Council, Institute of Agro-environmental and Forest Biology, Via Salaria km. 29300, 00016 Monterotondo Scalo, Rome, Italy
[*]now at: University of California, Department of Environmental Science, Policy, and Management, 137 Mulford Hall, Berkeley, CA 94720, USA

Received: 21 November 2008 – Published in Biogeosciences Discuss.: 23 February 2009
Revised: 24 June 2009 – Accepted: 26 June 2009 – Published: 14 August 2009

Abstract. Emission rates and concentrations of biogenic volatile organic compounds (BVOCs) were measured at a Mediterranean coastal site at Castelporziano, approximately 25 km south-west of Rome, between 7 May and 3 June 2007, as part of the ACCENT-VOCBAS field campaign on biosphere–atmosphere interactions. Concentrations and emission rates were measured using the disjunct eddy covariance (DEC) method utilizing three different proton transfer reaction mass spectrometers (PTR-MS) so allowing a comparison between the instruments. The high resolution data from the PTR-MS instruments considerably enhances the original BEMA measurements of the mid 1990s.

Depending on the measurement period, the volume mixing ratios were in the range 1.6–3.5 ppbv for methanol, 0.44–1.3 ppbv for acetaldehyde, 0.96–2.1 ppbv for acetone, 0.10–0.14 ppbv for isoprene, and 0.13–0.30 ppbv for monoterpenes. A diurnal cycle in mixing ratios was apparent with daytime maxima for methanol, acetaldehyde, acetone, and isoprene. The fluxes ranged from 370–440 $\mu g\,m^{-2}\,h^{-1}$ for methanol, 180–360 $\mu g\,m^{-2}\,h^{-1}$ for acetaldehyde, 180–450 $\mu g\,m^{-2}\,h^{-1}$ for acetone, 71–290 $\mu g\,m^{-2}\,h^{-1}$ for isoprene, and 240–860 $\mu g\,m^{-2}\,h^{-1}$ for monoterpenes. From the measured flux data (7 May–3 June) an average basal emission rate for the Macchia vegetation was calculated of 430 $\mu g\,m^{-2}\,h^{-1}$ for isoprene and 1100 $\mu g\,m^{-2}\,h^{-1}$ for monoterpenes.

Correspondence to: B. Davison
(b.davison@lancaster.ac.uk)

1 Introduction

Emissions of biogenic volatile organic compounds (BVOCs) play an important role in atmospheric chemistry. Oxidation of VOCs (both biogenic and anthropogenic) in a NO_x-rich atmosphere may lead to the production of tropospheric ozone, which has impacts on human health and can cause damage to crops, forest ecosystems, and buildings (e.g. Sillman et al., 1999; Fowler et al., 2008).

In Mediterranean areas, where both emission and oxidation rates of BVOCs are high, production of ozone and particles from BVOC precursors represent a significant air quality challenge. Previous measurements have shown that isoprene and monoterpenes form the bulk of the total BVOC emissions from Mediterranean type ecosystems (Helmig et al., 1999). However, little is known about emissions of oxygenated compounds, such as methanol and acetone, from these ecosystems. Emissions of isoprene and monoterpenes are strongly regulated by variations in light and temperature (e.g., Guenther et al., 1993). Nonetheless, the light and temperature dependent emission algorithms are still limited by uncertainties, particularly of the basal emission rates on which they depend.

Published by Copernicus Publications on behalf of the European Geosciences Union.

To better understand the processes controlling photochemical pollution episodes, regional and global scale BVOC emission models have been developed. Until recently, many model estimates for biogenic emissions from Mediterranean type ecosystems (Guenther et al., 1995; Simpson et al., 1999), which could include regions of Chile, California, South Africa, Australia, and Europe, were calculated using basal emission rates determined for Californian Mediterranean type ecosystems only (Owen et al., 1997). However isoprene and monoterpene emissions both tend to be very species specific, which generates considerable uncertainty in the model.

In recent years, efforts have been made to determine emission rates for a number of Mediterranean type ecosystems. In Europe, BVOC emissions in the Mediterranean area were extensively studied as part of the Biogenic Emissions in the Mediterranean Area (BEMA) project (Bertin et al., 1997; Ciccioli et al., 1997; Kesselmeier et al., 1997; Owen et al., 1997, 2001, 2002; Seufert et al., 1997; Street et al., 1997; Valentini et al., 1997). The BEMA project focused on emissions from the Castelporziano nature reserve near Rome, Italy. As the site comprised a number of vegetation types, both species specific and averaged ecosystem (forest, pseudosteppe, or macchia) emission rates could be calculated, which allowed improved modelled BVOC emission estimates within this region.

Since the BEMA campaigns there have been improvements in analytical techniques for VOCs. The advent of proton transfer reaction mass spectrometry (PTR-MS) has allowed online VOC measurements at ambient mixing ratio levels (e.g., Hansel et al., 1995; Lindinger et al., 1998; de Gouw and Warneke, 2007; Hayward et al., 2004; Tani et al., 2003; Hewitt et al., 2003). The ability of the PTR-MS to measure VOC mixing ratios at the pptv (parts per trillion by volume) level with a response time of a second or less has enabled the use of the PTR-MS instrument in micrometeorological flux measurement methods such as disjunct eddy covariance (DEC) (Rinne et al., 2001; Karl et al., 2002).

This paper presents the results of the mixing ratio and flux measurements made at Castelporziano within the frame of the ACCENT-VOCBAS campaign on biosphere–atmosphere interactions (for an overview, see Fares et al., 2009).

The determination of ecosystem scale emission potentials for terpenoids from species diverse ecosystems, such as Macchia, using species specific leaf level measurements is challenging. Thus micrometeorological flux measurement techniques can be very useful as ecosystem scale emission potentials can be derived directly using these measurements (e.g. Rinne et al., 2001). One specific aim of this study is to derive the terpenoid emission potentials for the Macchia and compare them with the ones derived by leaf level measurements.

The measurements conducted in many ecosystems have shown considerable emissions of non-terpenoid VOCs, such as methanol and acetone. However, our knowledge on the emission of these compounds from many ecosystems and regions is still far from complete. The second major aim of this study is to quantify the emissions of non-terpenoid VOC emissions in relation to terpenoid emissions.

2 Methods

2.1 Measurement site

The Presidential Estate of Castelporziano (41° 40′ 49″ N, 12° 23′ 31″ E) is located about 25 km to the south-west from the city centre of Rome, Italy. It covers an area of 60 km^2 and has a coastline of 5 km (for a detailed description of the site and the reason for its choice see Fares et al., 2009). Due to restricted public access, a number of Mediterranean ecosystem types have been preserved (e.g., macchia and pseudosteppe). The estate has few roads and low traffic but is bounded on its north-west by the busy Ostia-Rome commuter road. The smaller SS601 public road transects the southern edge creating a boundary between the high and low macchia. The low macchia was chosen as the site for this study.

A measurement tower was erected in a slight valley depression separated from the sea by two lines of sand dunes. The vegetation in the vicinity of the tower consisted mainly of *Arbutus unedo*, *Rosmarinus officinalis*, *Quercus ilex*, *Phillyrea angustifolia*, and *Erica multiflora* (Fares et al., 2009). The average canopy height, 1.2 m, was estimated by calculating the weighted average of the average heights of these main species, which covered 80% of the total area of 1070 m^2 around the tower. The weight factor was the proportion of the total area covered by a particular species. A forest of 23 km^2 dominated by Holm oak (*Quercus ilex*) was located approximately 1 km to the north-east (Seufert et al., 1997).

2.2 Measurement setup and procedure

Commercial PTR-MS instruments (Ionicon Analytik GmbH) were used in the measurements. Lancaster University (LU) and the National Research Council and University of Helsinki (CNR-UH) used two instruments which both featured two turbomolecular pumps, a heated silica steel inlet system, and a 9.6 cm long stainless steel drift tube. According to the manufacturer, the response time was about 1 s for these instruments. The PTR-MS used by the Centre for Ecology & Hydrology (CEH) contained a third turbomolecular pump and its response time was about 0.2 s.

Each group used its own measurements regime so allowing the opportunity to compare these. The measurement setup used by LU and CEH during the first measurement period consisted of a three-dimensional ultrasonic anemometer (Gill Instruments Ltd., Solent R2), and two PTR-MS instruments. LU also used a humidity sensor (Honeywell International, Inc., HIH-4000-001) and an ozone monitor (2B Technologies, Inc., 205 dual beam). The anemometer was mounted

Table 1. PTR-MS measurement cycles, the compounds contributing to the measured masses, and the PTR-MS integration, or dwell, times. For LU and CEH the cycle length was 1.4 s in the micrometeorological flux measurements **(A)** and 7.1 s in the ambient mixing ratio measurements **(B)**. For CNR-UH the cycle lengths were 13.3 and 37.5 s, respectively.

Protonated mass [amu] and contributing compound(s)		*Formula*	*Dwell time [s]*			
			LU and CEH		CNR-UH	
			A	B	A	B
21	water isotope	$H_2^{18}O$	0.1	0.1	0.1	0.1
33	methanol	CH_4O	0.2	–	1.0	2.0
37	water cluster	$(H_2O)_2$	–	–	0.1	–
39	water cluster isotope	$H_2OH_2^{18}O$	0.1	–	–	0.1
42	acetonitrile	C_2H_3N	–	–	–	2.0
45	acetaldehyde	C_2H_4O	0.2	–	1.0	2.0
55	water cluster	$(H_2O)_3$	–	–	0.1	0.1
59	acetone	C_3H_6O	0.2	–	1.0	2.0
63	dimethylsulfide	C_2H_6S	–	1.0	–	2.0
69	isoprene	C_5H_8	0.2	–	1.0	2.0
	methylbutenol fragment					
71	methacrolein	C_4H_6O	–	–	1.0	2.0
	methyl vinyl ketone	C_4H_6O				
73	methyl ethyl ketone	C_4H8O	–	1.0	–	–
77	peroxyacetyl nitrate fragment	$C_2H_3NO_5$	–	1.0	–	–
79	benzene	C_6H_6	–	1.0	–	2.0
81	monoterpene fragments		0.2	–	1.0	2.0
	hexenal fragment					
83	*cis*-3-hexenol fragment		–	–	1.0	2.0
	hexanal fragment					
87	methylbutenol	$C_5H_{10}O$	–	–	1.0	2.0
93	toluene	C_7H_8	–	1.0	–	2.0
99	hexenal	$C_6H_{10}O$	–	–	1.0	2.0
101	*cis*-3-hexenol	$C_6H_{12}O$	–	–	1.0	2.0
	hexanal	$C_6H_{12}O$				
107	xylenes	C_8H_{10}	–	1.0	–	2.0
113			–	–	1.0	2.0
121	C_9 aromatics		–	1.0	–	–
137	monoterpenes	$C_{10}H_{16}$	0.2	–	1.0	2.0
157			–	–	–	2.0

at 5 m above ground on the south-west corner of the measurement tower. This position gave a fetch of approximately 300 m to the north-west, more than 500 m to the south-east, but less than 60 m in the two major wind directions (south-west and north-east). The analytical instrumentation was housed in an air-conditioned cabin 10 m to the south-east of the tower. A 20 m length of 3/8 inch Teflon tube, heated to avoid condensation was used as the main sampling line taking air at 18 l min^{-1} from a position 30 cm below the anemometer.

The PTR-MS instruments sampled from the main sampling line at 0.25 l min^{-1}. They were optimised to an E/N ratio of 128 Td using a drift tube pressure, temperature, and voltage of 2.02 hPa, 45°C, and 500 V, respectively. The reaction time was 100 μs and the count rate of $H_3O^+H_2O$ ions was 1.2–2.6% of the count rate of H_3O^+ ions, which was (1.6–3.1)$\times 10^6$ counts s^{-1}. The data from the ultrasonic anemometer and PTR-MS were logged into the same computer using a programme written in LabView (National Instruments Corp.). The humidity sensor and ozone monitor sampled from the main line at a rate of 0.5 Hz and ancillary measurements of air pressure, temperature, photosynthetically active radiation, and CO_2 and H_2O mixing ratios were recorded by an environmental gas analyser (PP Systems, EGM-4) with a time resolution of 20 s.

Both PTR-MS instruments measured in three modes: flux, ambient mixing ratio, and zero air. Each instrument measured zero air for a 5-min period each hour followed by a 25-min flux measurement period and then a 5-min mixing ratio measurement period before a second 25-min flux measurement period. Zero air was generated by passing ambient air through a glass tube containing a platinum catalyst powder at 0.5 l min^{-1}. In the flux measurements, the PTR-MS measurement cycle contained eight masses, of which six were related to BVOCs (Table 1). The PTR-MS integration, or dwell, time was 0.2 s for each BVOC-related mass and the total measurement cycle length was 1.4 s. This corresponded to approximately 1070 measurements over the 25-min flux averaging period. In the ambient mixing ratio measurements, seven BVOC-related masses were measured within a PTR-MS measurements cycle of 7.1 s (Table 1) with an integration time of 1 s for each VOC-related mass.

The measurement setup of CNR-UH during the second measurement period consisted of a three-dimensional ultrasonic anemometer (R. M. Young Company, model 81000) and a PTR-MS. As in the setup of LU and CEH, the anemometer and the inlet of the main sampling line were attached to the measurement tower at 5 m above ground and the PTR-MS was housed in the air-conditioned cabin. The main sampling line, unheated was 25 m long, its inner diameter was 8 mm, and it was made of Teflon (PTFE). Previous test had shown line losses to be minimal provided no condensation was in the line. As the building housing the PTR-MS was warmer than outside, despite air conditioning condensation was considered unlikely. A continuous flow of 25 l min^{-1} was used in the main line and a side flow of 0.12 l min^{-1} was taken into the PTR-MS via a 1.5 m long PTFE tube, which had an inner diameter of 1.6 mm. A PTFE filter (1 μm pore size, LI-COR, Inc., part number 9967-008) was installed in front of the PTR-MS inlet to prevent particles from entering the instrument.

The operating parameters of the PTR-MS were held constant during the measurement period (20 May–3 June), except for the secondary electron multiplier voltage, which was optimized before every calibration. The drift tube pressure, temperature, and voltage were 2.2 hPa, 55°C, and 600 V, respectively. The parameter E/N was about 130 Td and the reaction time was about 97 μs. The count rate of $H_3O^+H_2O$ ions was 1–9% of the count rate of H_3O^+ ions, which was (2.9–5.5)$\times 10^6$ counts s^{-1}.

The wind measurements were conducted continuously at a sampling frequency of 20 Hz and the data were recorded on a different computer than the BVOC data. The BVOC measurement procedure was controlled with the Balzers Quadstar 422 software of the PTR-MS and it contained two hour-long sequences. Every second hour was allocated to the flux measurements. The PTR-MS measurement cycle consisted of 15 masses of which 12 were related to BVOCs (Table 1). The measurement cycle length was 13.3 s and the cycle was repeated 264 times an hour. The PTR-MS integration time was 1 s for each BVOC-related mass. The other hour-long sequence consisted of zero air measurements and ambient mixing ratio measurements. In the zero air measurements, VOC-free air produced from ambient air with a zero air generator (catalytic converter, Parker Hannifin Corp., ChromGas Zero Air Generator 1001) was fed into the PTR-MS to determine BVOC background signals of the instrument. Zero air was measured for about 12.5 min (20 cycles) and then the PTR-MS was set to measure ambient air for about 37.5 min (60 cycles). In both measurements, the PTR-MS measurement cycle contained 21 masses, 18 of which were related to BVOCs (Table 1). The measurement cycle length was 37.5 s and the integration time was 2 s for each VOC-related mass. The last 10 min of the sequence were allocated to mass scan measurements of ambient air. The scan range was 40–250 amu and the integration time was 2 s for each mass.

2.3 Calculation of BVOC volume mixing ratios

The PTR-MS instruments of LU and CEH were calibrated against the same gas standard, which contained methanol, acetaldehyde and acetone at a mixing ratio of 1 ppmv. The gas standard was prepared by diluting known volumes of the gas standard with zero hydrocarbon free air in Tedlar bags. These were then used to calibrate the PTR-MS over the range of 2–700 ppbv. In the first period, BVOC calibrations were done on 6 and 13 May.

LU and CEH calculated the normalized sensitivities for isoprene and monoterpenes (Table 2) using the proton transfer reaction rate coefficients of Zhao and Zhang (2004) and the instrument specific transmission coefficients which were calculated following the procedure described by Wilkinson (2006).

The PTR-MS of CNR-UH was calibrated three times during the measurement period: on 20, 25, and 31 May. These calibrations were performed with gas standards prepared by diluting pure liquid standards in nitrogen and analysed with a gas chromatograph-mass spectrometer at CNR. The monoterpene mixing ratio in the standard gas was 2.35 ppmv and the mixing ratios of methanol, acetaldehyde, acetone, and isoprene were 1 ppmv. The monoterpenes used in the calibrations were α-pinene (1 ppmv), limonene (1 ppmv), and ocimene (350 ppbv). The standard gas was diluted with zero air so that the mixing ratios fed into the PTR-MS were 225 ppbv for monoterpenes and 96 ppbv for the other compounds. The measured normalized sensitivities (Table 2) were determined for all three instruments using similar methods as described by Taipale et al. (2008). The range of normalised sensitivities measured during the second period is shown in Table 2.

VOC volume mixing ratios (VMR) were calculated using a similar approach by all groups as described by Taipale et al. (2008):

$$\mathrm{VMR}=\frac{I\left(\mathrm{RH}^+\right)_{\mathrm{norm}}}{S_{\mathrm{norm}}} \quad (1)$$

Table 2. Normalized sensitivities for the BVOCs presented in this paper. The PTR-MS instruments of LU and CEH were calibrated twice (on 6 and 13 May 2007) and the PTR-MS of CNR-UH was calibrated three times during the second part of the campaign (on 20, 25, and 31 May).

BVOC and its protonated mass [amu]	Normalized sensitivity [ncps ppbv^{-1}]			
		LU	CEH	CNR-UH
33	methanol	5.7	5.8	8.5–10.3
45	acetaldehyde	6.3	6.9	10.0–11.4
59	acetone	7.8	8.6	13.0–15.4
69	isoprene	8.3*	9.4*	6.2–7.6
81	monoterpenes	8.4*	10.0*	3.7–4.4
137	monoterpenes	5.7*	10.7*	1.1–1.5

* These values were not measured but calculated using proton transfer reaction rate coefficients and transmission coefficients.
$\alpha-$pinene, limonene, and ocimene were used in the calibrations by CNR-UH.

where S_{norm} is the normalized sensitivity in units of normalized counts s^{-1} ppbv^{-1} (ncps ppbv^{-1}). The normalized count rate of RH^+ ions is

$$I\left(RH^+\right)_{\mathrm{norm}} = I\left(RH^+\right)\left(\frac{I\left(H_3O^+\right)+I\left(H_3O^+H_2O\right)}{I_{\mathrm{norm}}}\right)^{-1}\left(\frac{p_{\mathrm{drift}}}{p_{\mathrm{norm}}}\right)^{-1} - \frac{1}{n}\sum_{i=1}^{n} I\left(RH^+\right)_{\mathrm{zero},i} \left(\frac{I\left(H_3O^+\right)_{\mathrm{zero},i}+I\left(H_3O^+H_2O\right)_{\mathrm{zero},i}}{I_{\mathrm{norm}}}\right)^{-1}\left(\frac{p_{\mathrm{drift,zero},i}}{p_{\mathrm{norm}}}\right)^{-1} \quad (2)$$

where $I(RH^+)$, $I(H_3O^+)$, and $I(H_3O^+H_2O)$ are the count rates of RH^+, H_3O^+, and $H_3O^+H_2O$ ions, p_{drift} is the drift tube pressure, and n is the number of zero air measurement cycles. The sum of the primary and water cluster ion count rate is normalized to a count rate of $I_{\mathrm{norm}} = 10^6$ cps and the drift tube pressure is normalized to a pressure of $p_{\mathrm{norm}} = 2$ hPa. The primary ion count rate was determined using the signal of the primary ion isotopes detected at 21 amu (M21). During the ambient concentration mode the water cluster ions were measured indirectly by recording the isotopes at M39 and multiplying by 250 to infer the total water cluster count observed at M37, thus minimising the exposure of the SEM to high count rates. In contrast, during the flux measurement mode, the water cluster ion count rate was measured directly at M37 to minimise propagation of errors when calculating fluxes. The contribution of the oxygen isotope, $^{16}O^{17}O$, was not subtracted from the signal detected at M33 when calculating the methanol mixing ratios since the oxygen count rate (M32) was not measured.

2.4 Calculation of BVOC fluxes

VOC fluxes were measured with the continuous flow disjunct eddy covariance method (DEC_{cf}). To determine the measured fluxes, F_m, a covariance function was calculated for each compound:

$$F_{\mathrm{m}}(\Delta t) = \frac{1}{N}\sum_{i=1}^{N} w'\left(i - \Delta t/\Delta t_w\right)c'(i). \quad (3)$$

In this equation, $w'=w-\bar{w}$ is the momentary deviation of the vertical wind speed, w, from its average, $c'=c-\bar{c}$ is that of the BVOC mass concentration, Δt is the lag time between the wind and concentration measurements, Δt_w is the sampling interval in the wind measurements, and N is the number of PTR-MS measurement cycles during the flux averaging time. LU and CEH used a flux averaging time of 25 min which corresponded to $N = 1070$. The averaging time of CNR-UH was 30 min, corresponding to $N = 132$. The sampling interval was 0.05 s in the wind measurements of both LU-CEH and CNR-UH.

When no clear maximum was apparent in the PTR-MS signal LU used the data from the humidity sensor connected to the main sampling line at the same point as the PTR-MS to aid identification of the lag time. The humidity data were combined with the vertical wind speed data, allowing a correlation function to be applied and the lag time to be estimated. A six-second time window was used to refine the lag time. A BVOC flux measurement was rejected if no clear peak was detected above the general noise of the covariance function within the time window.

The CEH group adopted a variable lag time approach, assuming there were several sources of delays. A procedure for estimating the lag time by performing the cross-correlation between the vertical wind speed component and the BVOC signal on all individual half-hour periods for each compound separately was used. Visual assessments of both the position and the quality of the peak in the covariance function were made for all the compounds measured in the flux mode within a 10 s window. The rejection criteria were similar to the ones described by Spirig et al. (2005). For example the lag times for a given m/z should not differ by more than a cycle length. Normally, variability of 2 s deviation from expected mean lag time was considered acceptable.

In the flux measurements by CNR-UH, the wind data were recorded on a different computer than the PTR-MS data. This means that there was an uncertainty in the timing of the wind and concentration time series in addition to the lag time due to the residence time of the sample air in the sampling lines. Therefore, the covariance functions were calculated for a rather wide lag time interval of ±3 min, using a time step of 0.05 s. To facilitate the identification of the lag time, the covariance function was calculated also for $H_3O^+H_2O$ ions detected at M37 (Rinne et al., 2007). Since the signal of these water cluster ions is high and depends on the ambient

water vapour mixing ratio (Ammann et al., 2006), there usually is a clear maximum in a covariance function related to daytime measurements. If a clear maximum could be identified from the covariance function of M37, a lag time window of ±13.3 s around the maximum was chosen. Finally, the BVOC fluxes were determined by finding the maxima of the respective covariance functions within the lag time window. Normally, CNR-UH could calculate the fluxes from the measurements conducted between 08:00 and 21:00 LT.

Two micrometeorological quality criteria were employed in the post-processing of the flux data of LU, CEH, and CNR-UH. A flux measurement was discarded if it was obtained in stable conditions or if the friction velocity was below 0.2 m s^{-1}. The high-frequency attenuation of the measured flux caused by the response time of the PTR-MS was estimated from the equation.

$$\frac{F_m}{F} = \frac{1}{1 + \left(2\pi n_m \tau \bar{u}/(z-d)\right)^{\alpha}} \quad (4)$$

where F is the non-attenuated flux, τ is the response time, and $\bar{u}$ is the average wind speed at the measurement height, z (Horst, 1997). For neutral and unstable stratification, the dimensionless frequency at the cospectral maximum is $n_m = 0.085$ and the exponent is $\alpha = 7/8$. The displacement height was calculated using the relation $d = 2h/3 = 0.80$ m (e.g., Garratt, 1994) and the average canopy height of $h = 1.2$ m. The response time was 1 s for the LU and CNR-UH instruments and 0.2 s for the CEH instrument. The range of the high-frequency attenuation was 0.62–0.98 for the LU data, 0.87–0.99 for the CEH data, and 0.45–0.97 for CNR-UH data. The median values were 0.78, 0.93, and 0.71, respectively.

2.5 Identification of BVOCs

To assist identification of the compounds contributing to the masses measured by PTR-MS, occasional measurements with gas-chromatographic methods were performed during the first measurement period 7–13 May. The technique has been described in more detail by Davison et al. (2008). At a flow rate of 200 ml min^{-1} a total volume of 41 air was sampled through stainless steel sampling tubes packed with Tenax and Carbopack B to pre-concentrate VOCs. These samples were analysed by thermal desorption (Perkin Elmer Turbomatrix thermal desorption system) and GC-MS (Perkin Elmer Turbomass Gold GC-MS). The compounds were separated on an Ultra 2 column (50 m×0.2 mm, I.D., 0.11 μm P/N 19091-005 Agilent Technologies). Compound identification was by standards whenever possible and Wiley and NIST spectral libraries. Light compounds, usually below C_4, are readily lost in the pre-concentration step on the Tenax tubes and so are not reliably detected by this method. Measurements using Tenax tubes were also made during the second measurement period and are reported in the companion paper (Fares et al., 2009).

3 Results and discussion

3.1 Weather during the campaign

Figure 1 shows meteorological parameters measured at the Castelporziano site during the campaign and longer term measurements at the CarboEurope tower about 500 m northeast from the site. A comparison of temperature and PAR measurements from the two sites shows a good agreement vindicating the use of measurements from the CarboEurope data set whenever meteorology data at the flux site was unavailable. During the first part of the campaign (7–14 May), the site experienced a diurnal sea breeze with winds from the sea, 180° to 270° during the day from around 11:00 to 19:00 LT and a land breeze from a northerly direction dominating from 03:00 or 04:00 until 11:00. The wind speed was between 0.1 and 4.3 m s^{-1}, averaging 1.8 m s^{-1}. The highest wind speed was observed around 13:00 with the lowest coinciding with the sea-land breeze reversal during the evening. Prior to the start of the campaign the region experienced heavy rain and flash flooding. From 1 to 7 May the site experienced 18.5 mm of rain of which 11.7 mm fell overnight on 4 May. This unsettled weather gradually gave way to clear skies and warmer conditions. The ambient temperature ranged from 13 to 24°C which gradually increased between 7 and 14 May. During the second part of the campaign 20 May–3 June, the sea breeze pattern was slightly more irregular. Wind direction varied typically from 180° to 280° between 09:00 and 21:00 and from 50° to 150° during the night. The wind speed ranged from 0.1 to 5 m s^{-1} with the exception of 29 May when winds up to 10 m s^{-1} were observed. The highest values were observed between 14:00 and 19:00 and the lowest between 21:00 and 02:00. The air temperature ranged from 10 to 31°C and the typical values were 19–23°C in the daytime and 15–19°C at night. The daily maximum values of photosynthetically active radiation were around 1400–1900 μmol m^{-2} s^{-1}. The cumulative rainfall during 20 May–3 June was 22 mm. The most intensive showers took place on 28 and 29 May and there was a period of continuous rain on 3 June.

3.2 BVOC mixing ratios

Figure 2 shows the half-hour averages of the mixing ratios of methanol, acetaldehyde, acetone, isoprene, and monoterpenes during the measurement campaign. In general, the agreement between the simultaneous measurements with the LU and CEH instruments was good, particularly for methanol with a correlation coefficient (R^2) of over 0.98. The correlation coefficients for the other compounds ranged from 0.89 for acetaldehyde to 0.94 for monoterpenes. The LU and CEH isoprene and monoterpene concentrations were calculated using PTR-MS transmission factors as gas standards were not available for these compounds. The results from the two periods in early and late May exhibit similar

Table 3. Medians of BVOC mixing ratios and fluxes calculated from all, daytime (12:00–17:00), and night-time (00:00–05:00) measurements. The measurement period was 7–14 May 2007 for LU and CEH and 20 May–3 June 2007 for CNR-UH. The number of measurements contributing to the median is given in parentheses.

	LU			CEH			CNR-UH		
	Volume mixing ratio [ppbv]								
	all (339–340)	day (63–64)	night (76)	all (245)	day (57)	night (46)	all (441–480)	day (91–102)	night (98–107)
methanol	3.51	4.07	2.73	3.44	4.32	2.56	1.64	1.72	1.58
acetaldehyde	0.980	1.32	0.674	1.29	1.74	0.641	0.441	0.519	0.404
acetone	1.58	2.36	0.962	2.07	2.84	1.24	0.964	1.15	0.889
isoprene	0.103	0.160	0.0760	0.135	0.253	0.062	0.130	0.166	0.108
monoterpenes	0.303	0.208	0.577	0.132	0.102	0.264	0.181	0.161	0.357
	Flux [μg m^{-2} h^{-1}]								
	all (54–69)	day (22–27)	night (1–3)	all (81–97)	day (32–41)	night (2–3)	all (106–112)	day (62–66)	night (0)
methanol	421	579	−125	439	597	−205	368	424	
acetaldehyde	301	391	−132	363	422	−188	180	185	
acetone	299	411	11.7	448	543	−146	182	212	
isoprene	70.5	96.6	−36.0	125	160	−47.5	290	317	
monoterpenes	240	325	183	254	320	−102	857	963	

overall trends though the average mixing ratios of methanol, acetaldehyde, and acetone were slightly lower during the second period.

Table 3 shows a summary of the concentration results from the two measurement periods. During the first measurement period (7–14 May 2007) concentrations of all species were highest during the first few days. Methanol emissions are known to be influenced by abiotic stress factors such as elevated ozone levels, drought, flooding and mechanical leaf wounding (Fukui and Doskey, 1998; Holzinger et al., 2000; Beauchamp et al., 2005; Karl et al., 2005; Loreto et al. 2006; Brunner et al., 2007; Penuelas et al., 2005) as well as leaf age, with higher emissions typical of young developing leaves (Nemecek-Marshall et al., 1995). BVOC emissions, in particular of methanol are strongly dependent on water soil content and photosynthesis. Whether the elevated concentration levels observed over the first few days of the campaign were due to the heavy rain encountered during this period or disturbance of the site during setting up is unclear but there were also notably higher concentrations during the early part of the second period of the campaign (20 May to 3 June 2007).

An analysis of various meteorological factors such as temperature, RH and light did not show any clear correlation across the data set. While there was some agreement between temperature and oxygenated VOC concentrations for part of the data during the beginning of the second sampling period this was not consistent across the whole data set. The leaf level measurements performed throughout the campaign indicated the plants were not showing any signs of stress due to the heavy rainfall during the first period or the higher temperatures of the second period. Damaged plant can emit considerable amounts of VOC. As no other reason for the elevated concentrations can be definitely identified mechanical plant damage during set up must also be considered as a possible source of the elevated VOC concentrations observed at the beginning of both sampling periods.

Measurements over crop fields have shown methanol to be one of the most abundant biogenically emitted VOCs (Warneke et al., 2002; Fall, 2003; Schade and Custer, 2004; Davison et al., 2008). Our data confirms that methanol is also a prominent BVOC in natural ecosystems. Along with acetaldehyde, acetone and isoprene, methanol showed a similar trend with a clear diurnal cycle with a daytime maximum. Monoterpenes showed a diurnal trend but with a night time maximum. Measurements during the original BEMA campaigns observed oxygenated compounds emitted from pine and oak species. Acetic and formic acid, and acetaldehyde and formaldehyde were collected by a cartridge trap technique which was less sensitive, less compound-specific and with poorer resolution, than the PTR-MS available during this campaign (Kesselmeier et al., 1997). The results did however show broadly similar diurnal trends to those observed during this campaign with ambient concentrations varying from 0 to 7 ppbv with a daytime maximum. This has proved to be in keeping with the measurements from this campaign where a 4 ppbv daytime maximum concentrations was measured using PTR-MS.

On a daily basis, concentrations of methanol, acetaldehyde, acetone and isoprene typically began to increase at around 07:00 local time (05:00 UTC). Methanol and

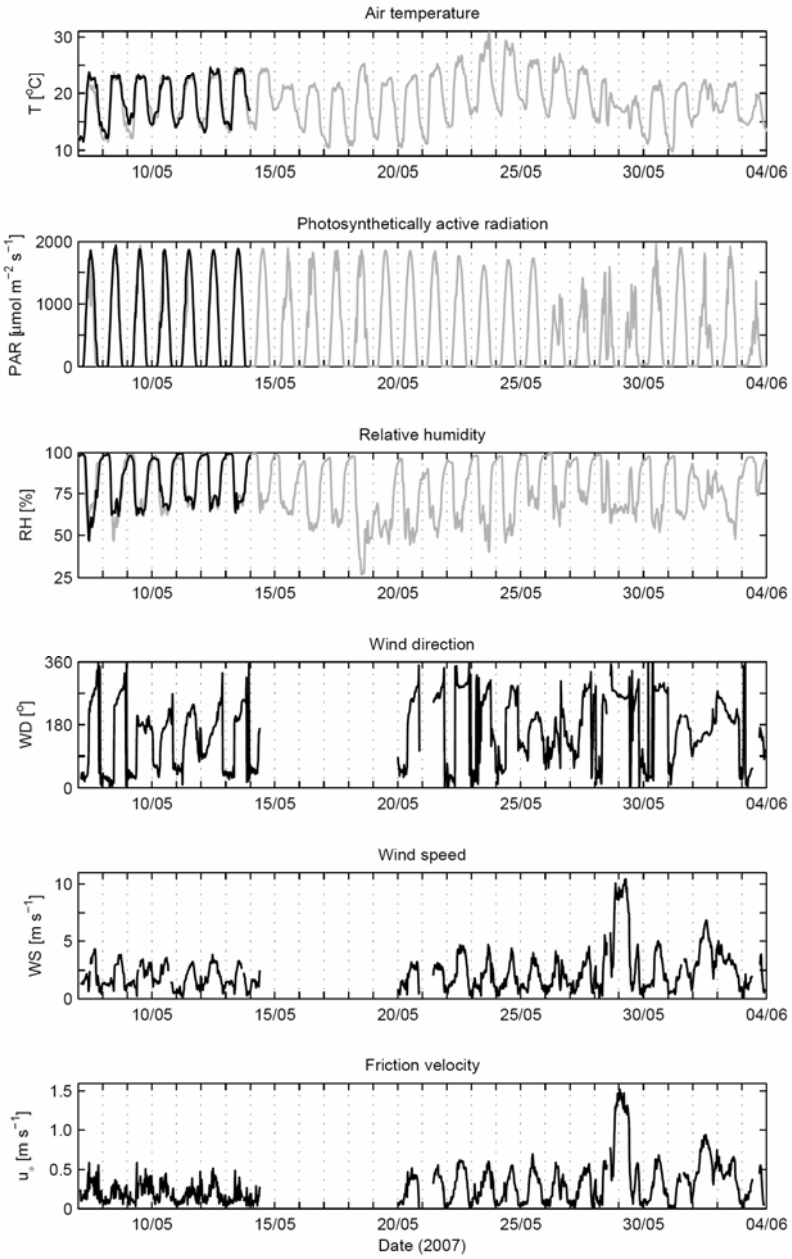

Fig. 1. Meteorological variables measured at the Castelporziano site (black lines) and the CarboEurope tower (grey lines).

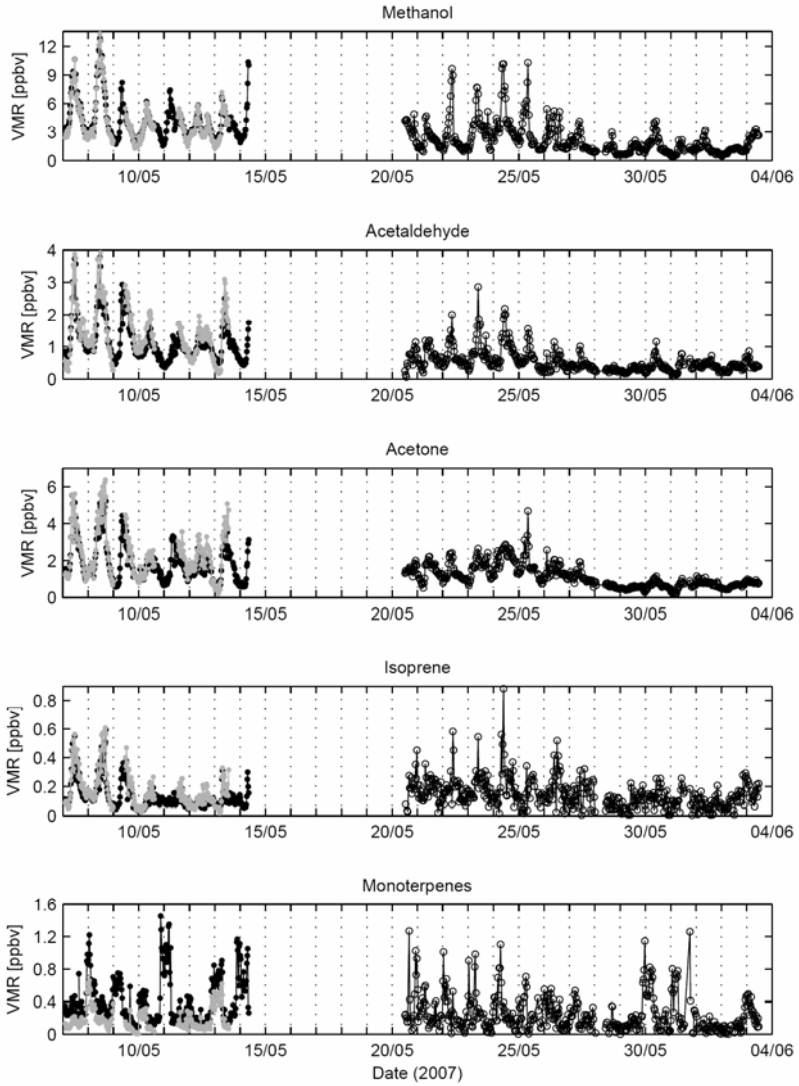

Fig. 2. Half-hour averages of BVOC mixing ratios measured by LU (black circles, 7–14 May), CEH (grey circles), and CNR-UH (open circles, 20 May–3 June).

acetaldehyde both peaked in the early morning (10:00) with a secondary afternoon peak followed by a gradual decrease throughout the rest of the day. Plant physiology controls the emissions of methanol from vegetation through relationships to plant growth (Fall and Benson, 1996; Schade and Goldstein, 2006; Folkers et al., 2008), cell expansion and protein repair reactions (Mudgett and Clarke, 1993). The emission of methanol is controlled via the transpiration stream, which is itself governed by light and leaf temperature (which explains the close agreement with temperature), as well as stomatal conductance (Niinemets et al., 2004). Methanol is associated with cell wall degradation during leaf expansion, which happen especially during night time. Huve et al. (2007) described a strong dependence of methanol on

stomatal conductance because methanol can accumulate in the intercellular spaces and be released when stomata open. This is consistent with the observed measurements of concentration in the early morning, coincident with stomatal opening.

Similar trends were observed by Kesselmeier et al. (1997) for acetic and formic acid released from oak and related to transpiration patterns. The strong stomatal dependency of the emission of soluble compounds, such as methanol has been highlighted previously (Niinemets et al., 2004; Huve et al., 2007).

Measurements of acetone, although similar to those of methanol and acetaldehyde, showed some differences, such as a sharp decline in concentration at around 19:00. Isoprene concentrations increased throughout the afternoon after an initial peak at 08:00, to reach a maximum at 14:00, before decreasing sharply, similar to acetone. Ozone measurements at the site showed a diurnal trend with a daytime maximum occurring a few hours after the maximum in BVOC concentrations. This maximum probably relates more to the change in direction of the sea-land breeze than to any reaction with VOCs emitted from the vegetation.

The low molecular weight compounds (methanol, acetaldehyde, acetone and isoprene), as well as showing similar trends, had good correlation between each compound when all measurements are plotted together. The correlation coefficients ranged from an $R^2 = 0.52$ between methanol and isoprene to a $R^2 = 0.78$ for acetone and acetaldehyde. While VOC concentrations show general agreement with meteorological parameters, such as light and temperature, the correlation was generally not as pronounced as for isoprene or monoterpene and no clear drivers could be identified from the field data to explain the variations observed. These compounds are known to have different biosynthetic pathways and any close correlation may suggest similar meteorological controls (e.g. light and temperature) on the precursors or on the enzymes that catalyze the limiting biosynthetic steps. For example, the metabolic production of isoprenoid precursor (predominantly photosynthetates) and the demethylation of pectins in the cell walls for methanol production may be similarly controlled by the environmental factors. It is also possible that the control of all emitted compounds also includes a physico-chemical component, mainly attributable to stomatal conductance, although Niinemets et al. (2004) mainly assign such a physical control to oxygenated hydrocarbons only.

A wind rose of BVOC concentrations and fluxes (Fig. 3) shows a scatter of concentrations around the site with predominance of daytime concentrations coming from the seaward side and night time concentrations from the landward side of the sampling footprint due to the sea-land breeze effect. Unlike the other BVOCs measured, the highest monoterpene concentrations originate from the north-east. This trend was more pronounced during the first part of the campaign, which experienced a more noticeable breeze effect than during the second measurement period. A natural forest of Holm oak, a known monoterpene emitter, and a plantation of stone pine are located in this direction.

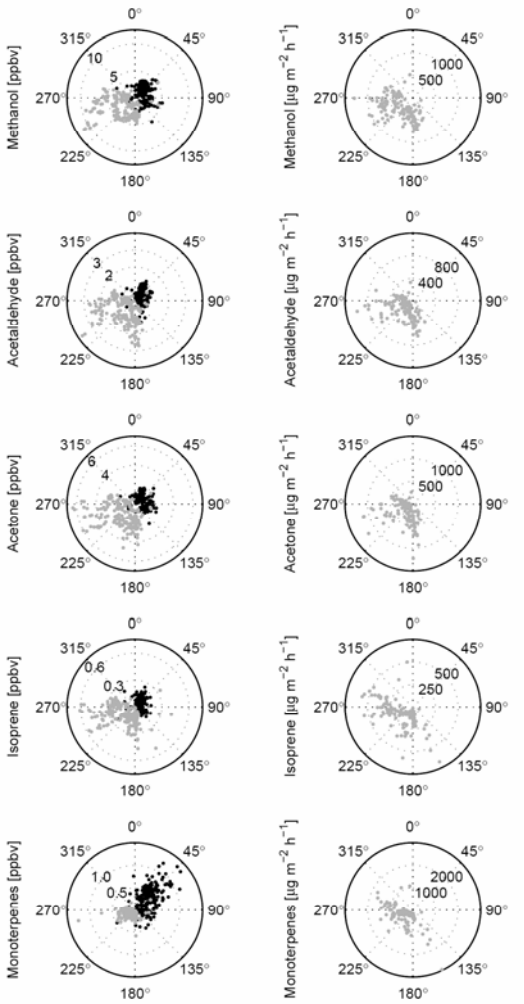

Fig. 3. Wind roses of BVOC mixing ratios and fluxes measured by LU, CEH, and CNR-UH. The grey circles represent the measurements made between 12:00 and 17:00 (day) and the black circles show the measurements between 00:00 and 05:00 (night).

The highest monoterpene concentrations during both campaign periods were observed at night once the wind had switched direction and the land breeze dominated, bringing air from the Holm oak and stone pine forest to the measurement site. While monoterpene emissions from Holm oaks is mainly controlled by light they continue to emit

monoterpenes at night although at much lower rates than during the day (Street et al., 1997; Staudt and Bertin, 1998; Grote et al., 2006). A considerable fraction of the monoterpene emission from pines originates from large storage structures and as such they continue to emit at night at a higher relative level than Holm oaks provided nocturnal temperatures remain sufficiently high (Owen et al., 1997; Staudt et al., 1997). While the emissions from this species are lower at night the rapid removal of compounds by reaction with light induced hydroxyl radicals ceases and the vertical mixing is strongly suppressed, leading to high surface layer concentrations. This, in conjunction with the wind direction change, leads to higher night time monoterpene concentrations being observed. A similar directional trend is not apparent in the monoterpene flux (Fig. 3), though most night time fluxes failed the flux acceptance criteria due to the stable boundary layer conditions.

Monoterpene emissions were higher during the second period of the campaign, both as measured by PTR-MS over the sampling site and from leaf cuvette measurements of specific plant species. This may be related to the temperature, which was approximately 3°C higher during the second part of the campaign (Fares et al., 2009), and the more advanced phenological state of the plants in the flux footprint area. Isoprene emission is known to be dependent on leaf development (Wiberley et al., 2005) and monoterpene emission from deciduous broad leafed trees exhibit the same developmental behaviour (Hakola et al., 1998; Kuhn et al., 2004).

The concentrations measured simultaneously by the CEH and LU PTR-MS instruments were almost identical in patterns. The absolute values for the compounds for which external calibration was available was very good, but worse for monoterpenes and isoprene, whose sensitivities were calculated during the first part of the campaign using the instrumental transmission rather than calibration with gas standards. This indicates that external standards are required for the highest accuracy of results, as the differences between calculated and measured sensitivities have been reported to be up to a factor of 2 (Warneke et al., 2002; de Gouw and Warneke, 2007).

3.3 BVOC fluxes

Figure 4 shows the fluxes of the five BVOCs emitted by the macchia as measured during the first and second period of the campaign. Emission rates were highest during mid to late afternoon and lowest during the night. This reflects the diurnal cycle of the biological and physical processes affecting the emissions. Most of the night time flux data were rejected due to quality criteria, as the stably stratified conditions, low wind speeds and weak mixing often encountered at night time leads to a decoupling of measured fluxes from surface exchange, so cases of low friction velocity (below $0.2\,m\,s^{-1}$) are routinely excluded from flux calculations (Goulden et al., 1996; Göckede et al., 2004).

Methanol fluxes closely followed the diurnal profile of light and temperature with emissions peaking at around midday. The concentration measurements showed a slight difference peaking in early morning, before declining steadily throughout the afternoon.

The fluxes derived by the two groups in the first period agree reasonably well, showing the scale of uncertainty caused by individual lag time determination, which was done separately by each group, leading to a slight difference in the amount of data rejected due to an unclear lag time. The negative fluxes may be the result of flux divergence, with considerable uncertainties from advection and general low turbulence conditions. The fluxes of monoterpenes were derived differently by both groups in the first period. For example, in the processing of CEH data, the lag times for m/z 81 and m/z 137 were derived independently, while in the LU analysis the lag times were derived for the sum of the fragments. This led to coincidental good agreement in values, but in fact the LU flux should be higher, considering the higher concentrations that were reported.

The canopy flux measurements were used to calculate an ecosystem scale basal emission rate for the footprint area of the Macchia vegetation by fitting the flux data to the light and temperature dependent G97 algorithm of Guenther (1997). As the basal emission rates are expected to change with leaf development, we divided the measured time series into three sections: 7 to 14 May, 20 to 27 May, and 28 May to 3 June. The measured fluxes were fitted to the emission activity factors separately for these periods.

For the first period of the campaign the isoprene basal emission rate calculated from the flux measurements was $315\,\mu g\,m^{-2}\,h^{-1}$ with a monoterpene emission rate of $710\,\mu g\,m^{-2}\,h^{-1}$. During the second sampling period meterological conditions changed just prior to a small storm on 28 May and activity factors were noted to have been affected. This point has therefore been used as a cut off when calculating basal emission rates. Basal emission rates calculated between 20 to 27 May showed isoprene rates of $511\,\mu g\,m^{-2}\,h^{-1}$ a and monoterpene rates of $1490\,\mu g\,m^{-2}\,h^{-1}$ while the period after the storm, from 28 May to 3 June had emission rates of $1010\,\mu g\,m^{-2}\,h^{-1}$ for isoprene and $3290\,\mu g\,m^{-2}\,h^{-1}$for monoterpenes. This increase in the basal emission rate throughout the measurements period may reflect the physiological state of the plants as they developed over the months (Kuhn et al., 2004).

Fares et al. (2009) from leaf and plant emission measurements made during the second part of this study calculated an isoprene emissioin rate of $79\,\mu g\,m^{-2}\,h^{-1}$ and a monoterpene emission rate of $1199\,\mu g\,m^{-2}\,h^{-1}$ while Owen et al. (1997) calculated a rate of $563\,\mu g\,m^{-2}\,h^{-1}$ for isoprene and $918\,\mu g\,m^{-2}\,h^{-1}$ for monoterpene from the Macchia area during May.

The basal emission rates show a reasonable agreement, only the isoprene value of Fares et al. (2009) at $79\,\mu g\,m^{-2}\,h^{-1}$ is significantly below other estimates. Using

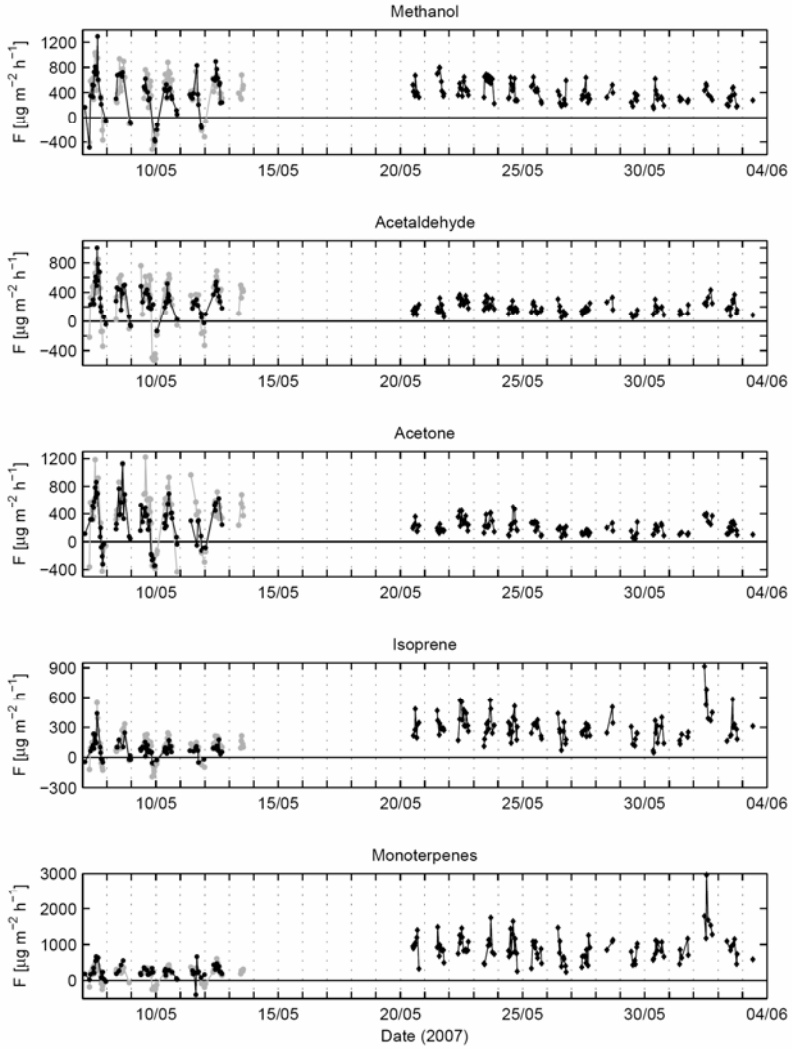

Fig. 4. BVOC fluxes measured by LU (black circles, 7–12 May), CEH (grey circles), and CNR-UH (black diamonds, 20 May–3 June).

a bottom up approach for calculating an area basal emission rate is highly dependent upon the plant species selected and the estimation of coverage over the area which may explain the large difference between the isoprene emission potential of Fares et al. (2009) and that calculated from our flux rate approach.

Isoprene and monoterpene fluxes were calculated using the algorithm from Guenther (1997; G97) which assumes light and temperature dependent isoprene and monoterpene emitters. These model results were compared with the measured fluxes obtained using the DEC_{cf} technique. As can be seen from Fig. 5 the G97 isoprene emission algorithm describes the ecosystem scale emissions of both isoprene and monoterpenes reasonably well when fitted to the available measured data. We can see the general increase of emission potentials during the campaign. This is likely due to the effect of the leaf phenology in the emission of terpenoids, as at the same time the methanol emission is decreasing, but the

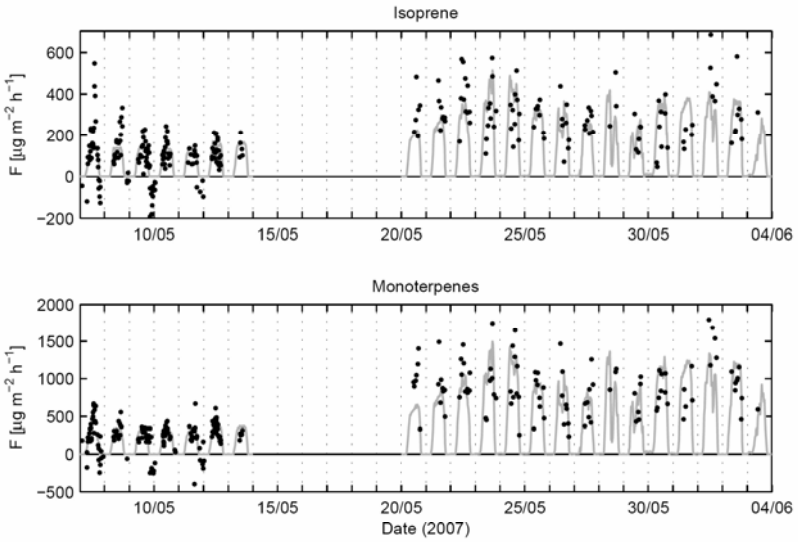

Fig. 5. Comparison of the measured (black circles) and modelled isoprene and monoterpene emissions from the G97 algorithm.

direct effect of rising temperatures during the season cannot be ruled out altogether. Leaf development changes leaf scale emissions, the amount of emitting biomass, and microclimate of the canopy. Since the emission factors used in this work depend only on light and temperature, the ecosystem scale basal rates can include effects of other variables as well.

4 Conclusions

High resolution atmospheric measurements of the oxygenated biogenic VOCs, methanol, acetaldehyde and acetone, along with isoprene and monoterpenes, were conducted at a site among macchia vegetation at Castelporziano, Italy during two periods 7 to 14 May and 20 May to 3 June 2007. These data allowed for the first set of direct, canopy-scale VOC flux measurements above Mediterranean Macchia vegetation which considerably enhances the leaf-level emission estimates made during the original BEMA campaign.

Monoterpene basal emission rates calculated using our direct flux measurements for the Macchia site show reasonable agreement with emission rates calculated from leaf measurements. Yet, there is considerable difference between the basal emission rates for isoprene which may be due to unrepresentative sampling of species in the measurement area.

The VOC concentrations showed a clear diurnal cycle with a daytime maximum for methanol, acetaldehyde, acetone and isoprene and a night time maximum in monoterpene concentrations. In contrast a daytime maximum was observed in monoterpene fluxes. During the campaign the monoterpenes measured at night time were advected horizontally into the flux footprint area from a nearby Holm oak and pine forest once the wind direction had switched to a land breeze. This explains the night time maximum in concentrations and daytime maximum in monoterpene fluxes from the vegetation within the flux footprint area.

The campaign offered the opportunity to compare results from three PTR-MS instruments with slightly differing sampling protocols. The results obtained show good instrumental agreement, and confirm the reliability of this instrument for field research.

Acknowledgements. We thank the European Network of Excellence of Atmospheric Composition Change (ACCENT) and the Volatile Organic Compounds in the Biosphere-Atmosphere System (VOCBAS) project of the European Science Foundation for financial support. We acknowledge Riccardo Valentini for use of meteorology data and Annette Ryan and Malcolm Possell for plant phenology information and advice. We thank the Academy of Finland, (projects 120 434, 125 238, and 209 216), Helsinki University Centre for Environment and the Kone Foundation for additional financial support. We would also like to express our gratitude to the Scientific Committee of the Presidential Estate of Castelporziano and in particular to Giantommaso Scarascia Mugnozza and to Aleandro Tinelli.

Edited by: A. Arneth

References

Ammann, C., Brunner, A., Spirig, C., and Neftel, A.: Technical note: Water vapour concentration and flux measurements with PTR-MS, Atmos. Chem. Phys., 6, 4643–4651, 2006, http://www.atmos-chem-phys.net/6/4643/2006/.

Beauchamp, J., Wisthaler, A., Hansel, A., Kleist, E., Miebach, M., Niinemets, U., Schurr, U., and Wildt, J.: Ozone induced emissions of biogenic VOC from tobacco: Relationships between ozone uptake and emission of LOX products, Plant Cell Environ., 28, 1334–1343, 2005.

Bertin, N., Staudt, M., Hansen, U., Seufert, G., Ciccioli, P., Foster, P., Fugit, J. L., and Torres, L.: Diurnal and seasonal course of monoterpene emissions from *Quercus ilex* (L.) under natural conditions – application of light and temperature algorithms, Atmos. Environ., 31(SI), 135–144, 1997.

Brunner, A., Ammann, C., Neftel, A., and Spirig, C.: Methanol exchange between grassland and the atmosphere. Biogeosciences, 4, 395–410, 2007

Ciccioli, P., Fabozzi, C., Brancaleoni, E., Cecinato, A., Frattoni, M., Cieslik, S., Kotzias, D., Seufert, G., Foster, P., and Steinbrecher, R.: Biogenic emission from the Mediterranean pseudosteppe ecosystem present in Castelporziano, Atmos. Environ., 31(SI), 167–175, 1997.

Davison, B., Brunner, A., Ammann, C., Spirig, C., Jocher, M., and Neftel, A.: Cut induced VOC emissions from agricultural grasslands. Plant Biol., 10, 76–85, doi:10.1055/s-2007-965043, 2008.

de Gouw, J. and Warneke, C.: Measurements of volatile organic compounds in the Earth's atmosphere using proton-transfer-reaction mass spectrometry, Mass Spectrom. Rev., 26, 223–257, 2007.

Fall, R. and Benson, A. A.: Leaf methanol – the simplest natural product from plants, Trends Plant Sci., 1, 296–301, 1996.

Fall, R.: Abundant oxygenates in the atmosphere: A biochemical perspective, Chem. Rev., 103, 4941–4951, 2003.

Fares, S., Mereu, S., Scarascia-Mugnozza, G., Vitale, M., Frattoni, M., Ciccioli, P., and Loreto, F.: The ACCENT-VOCBAS field campaign on biosphere-atmosphere interactions in a Mediterranean ecosystem of Castelporziano (Rome): site characteristics, climatic and meteorological conditions, and eco-physiology of vegetation, Biogeosciences, 6, 1043–1058, 2009 2009.

Folkers, A., Huve, K., Ammann, C., Dindorf, T., Kesselmeier, J., Kleist, E., Kuhn, U., Uerlings, R., and Wildt, J.: Methanol emissions from deciduous tree species: Dependence on temperature and light intensity, Plant Biol., 10, 65–75, 2008.

Fowler, D.: Ground-level ozone in the 21st century: future trends, impacts and policy implications, Royal Society, London, UK, 2008.

Fukui, Y. and Doskey, P. V.: Air-surface exchange of non-methane organic compounds at a grassland site: Seasonal variations and stressed emissions, J. Geophys. Res.-Atmos., 103, 13153–13168, 1998.

Garratt, J. R.: The atmospheric boundary layer, Cambridge University Press, Cambridge, UK, pp. 316, 1994.

Göckede, M., Rebmann, C., and Foken, T.: A combination of quality assessment tools for eddy covariance measurements with footprint modelling for the characterisation of complex sites, Agr. For. Meteorol., 127, 175–188, 2004.

Goulden, M. L., Munger, J. W., Fan, S.-M., Daube, B. C., and Wofsy, S. C.: Measurements of carbon sequestration by long-term eddy covariance: methods and a critical evaluation of accuracy, Global Change Biol., 2, 169–182, 1996.

Grote, R., Mayrhofer, S., Fischbach, R. J., Steinbrecher, R., Staudt, M., and Schnitzler, J. P.: Process-based modelling of isoprenoid emissions from evergreen leaves of *quercus ilex* (l.), Atmos. Environ., 40, S152–S165, 2006.

Guenther, A. B., Zimmerman, P. R., Harley, P. C., Monson, R. K., and Fall, R.: Isoprene and monoterpene emission rate variability: model evaluations and sensitivity analyses, J. Geophys. Res., 98(D7), 12609–12617, 1993.

Guenther, A., Hewitt, C. N., Erickson, D., Fall, R., Geron, C., Graedel, T., Harley, P., Klinger, L., Lerdau, M., McKay, W. A., Pierce, T., Scholes, B., Steinbrecher, R., Tallamraju, R., Taylor, J., and Zimmerman, P.: A global model of natural volatile organic compound emissions, J. Geophys. Res., 100(D5), 8873–8892, 1995.

Guenther, A.: Seasonal and spatial variations in natural volatile organic compound emissions. Ecol. Appl., 7, 34–45, 1997.

Hakola, H., Rinne, J., and Laurila, T.: Hydrocarbon emission rates of tea-leafed willow (Salix phylicifolia), Silver birch (Betula pendula) and European aspen (Populus tremula), Atmos. Environ., 32, 1825–1833, 1998.

Hansel, A., Jordan, A., Holzinger, R., Prazeller, P., Vogel, W., and Lindinger, W.: Proton transfer reaction mass spectrometry: online trace gas analysis at the ppb level, Int. J. Mass Spectrom., 149–150, 609–619, 1995.

Hayward, S., Tani, A., Owen, S. M., and Hewitt, C. N.: Online analysis of volatile organic compound emissions from Sitka spuce (*Picea sitchensis*). Tree Physiology, 24, 721–728, 2004.

Helmig, D., Klinger, L.F., Guenther, A., Vierling, L., Geron, C., and Zimmerman, P.: Biogenic volatile organic compound emission (BVOCs): II. Landscape flux potentials from three continental sites in the US, Chemosphere, 38(9), 2189–2204, 1999.

Hewitt, C. N., Hayward, S., and Tani, A. Application of proton transfer reaction mass spectrometry for the monitoring and measurement of volatile organic compounds in the atmosphere, Environ. Monitor., 5, 1–7, 2003.

Holzinger, R., Sandoval-Soto, L., Rottenberger, S., Crutzen, P. J., and Kesselmeier, J.: Emissions of volatile organic compounds from quercus ilex l. Measured by proton transfer reaction mass spectrometry under different environmental conditions, J. Geophys. Res.-Atmos., 105, 20573–20579, 2000.

Horst, T. W.: A simple formula for attenuation of eddy fluxes measured with first-order-response scalar sensors, Bound.-Layer Meteorol., 82, 219–233, 1997.

Huve, K., Christ, M. M., Kleist, E., Uerlings, R., Niinemets, U., Walter, A., and Wildt, J.: Simultaneous growth and emission measurements demonstrate an interactive control of methanol release by leaf expansion and stomata, J. Exp. Bot., 58(7), 1783–1793, 2007.

Karl, T. G., Spirig, C., Rinne, J., Stroud, C., Prevost, P., Greenberg, J., Fall, R., and Guenther, A.: Virtual disjunct eddy covariance measurements of organic compound fluxes from a subalpine forest using proton transfer reaction mass spectrometry, Atmos. Chem. Phys., 2, 279–291, 2002, http://www.atmos-chem-phys.net/2/279/2002/.

Karl, T., Harley, P., Guenther, A., Rasmussen, R., Baker, B., Jardine, K., and Nemitz, E.: The bi-directional exchange of oxy-

genated vocs between a Loblolly pine (*Pinus Taeda*) plantation and the atmosphere, Atmospheric Chemistry And Physics, 5, 3015–3031, 2005.

Kesselmeier, J., Bode, K., Hofmann, U., Müller, H., Schäfer, L., Wolf, A., Ciccioli, P., Brancaleoni, E., Cecinato, A., Frattoni, M., Foster, P., Ferrari, C., Jacob, V., Fugit, J. L., Dutaur, L., Simon, V., and Torres, L.: Emission of short chained organic acids, aldehydes and monoterpenes from *Quercus ilex* L. and *Pinus pinea* L. in relation to physiological activities, carbon budget and emission algorithms, Atmos. Environ., 31(SI), 119–133, 1997.

Kuhn, U., Rottenberger, S., Biesenthal, T., Wolf, A., Schebeske, G., Ciccioli, P., and Kesselmeier, J.,: Strong correlation between isoprene emission and gross photosynthetic capacity during leaf phenology of the tropical tree species Hymenaea courbaril with fundamental changes in volatile organic compounds emission composition during early leaf development, Plant Cell Environ., 27(12), 1469–1485, 2004.

Lindinger, W., Hansel, A., and Jordan, A.: On-line monitoring of volatile organic compounds at pptv levels by means of Proton-Transfer-Reaction Mass Spectrometry (PTR-MS) – Medical applications, food control and environmental research, Int. J. Mass Spectrom., 173, 191–241, 1998.

Loreto, F., Barta, C., Brilli, F., and Nogues, I.: On the induction of volatile organic compound emissions by plants as consequence of wounding or fluctuations of light and temperature, Plant Cell Environ., 29, 1820–1828, 2006.

Mudgett, M. B., and Clarke, S.: Characterization of plant l-isoaspartyl methyltransferases that may be involved in seed survival – purification, cloning, and sequence-analysis of the wheat-germ enzyme, Biochemistry, 32, 11100–11111, 1993.

Nemecek-Marshall, M., MacDonald, R. C., Franzen, J. J., Wojciechowski, C. L. and Fall, R.: Methanol Emission from Leaves (Enzymatic Detection of Gas-Phase Methanol and Relation of Methanol Fluxes to Stomatal Conductance and Leaf Development), Plant Physiol., 108, 4, 1359–1368. 1995

Niinemets, U., Loreto, F., and Reichstein, M.: Physiological and physicochemical controls on foliar volatile organic compund emissions. Trends in plant science, 4, 180–186, 2004.

Owen, S. M., Boissard, C., Street, R. A., Duckham, S. C., Csiky, O., and Hewitt, C. N.: Screening of 18 Mediterranean plant species for volatile organic compound emissions, Atmos. Environ., 31(SI), 101–117, 1997.

Owen, S. M., Boissard, C., and Hewitt, C. N.: Volatile organic compounds (vocs) emitted from 40 mediterranean plant species: Voc speciation and extrapolation to habitat scale, Atmos. Environ., 35, 5393–5409, 2001.

Owen, S. M., Harley, P., Guenther, A., and Hewitt, C. N.: Light dependency of VOC emissions from selected Mediterranean plant species, Atmos. Environ., 36, 3147–3159, 2002.

Penuelas, J., Filella, I., Stefanescu, C., and Llusia, J.: Caterpillars of Euphydryas aurinia (Lepidoptera: Nymphalidae) feeding on Succisa pratensis leaves induce large foliar emissions of methanol, New Phytol., 167, 851–857, 2005.

Rinne, H. J. I., Guenther, A. B., Warneke, C., de Gouw, J. A., and Luxembourg, S. L.: Disjunct eddy covariance technique for trace gas flux measurements, Geophys. Res. Lett., 28(16), 3139–3142, 2001.

Rinne, J., Taipale, R., Markkanen, T., Ruuskanen, T. M., Hellén, H., Kajos, M. K., Vesala, T., and Kulmala, M.: Hydrocarbon fluxes above a Scots pine forest canopy: measurements and modeling, Atmos. Chem. Phys., 7, 3361–3372, 2007, http://www.atmos-chem-phys.net/7/3361/2007/.

Schade, G. W. and Custer, T. G.: OVOC emissions from agricultural soil in northern Germany during the 2003 European heat wave, Atmos. Environ., 38, 6105–6114, 2004.

Schade, G. W. and Goldstein, A. H.: Seasonal measurements of acetone and methanol: Abundances and implications for atmospheric budgets, Global Biogeochem. Cy., 20, 2006.

Seufert, G., Bartzis, J., Bomboi, T., Ciccioli, P., Cieslik, S., Dlugi, R., Foster, P., Hewitt, C. N., Kesselmeier, J., Kotzias, D., Lenz, R., Manes, F., Perez Pastor, R., Steinbrecher, R., Torres, L., Valentini, R., and Versino, B.: An overview of the Castelporziano experiments, Atmos. Environ., 31(SI), 5–17, 1997.

Sillman, S.: The relation between ozone, NO_X and hydrocarbons in urban and polluted rural environments, Atmos. Environ., 33, 1821–1845, 1999.

Simpson, D., Winiwarter, W., Borjesson, G.,Cinderby, S., Ferreiro, A. Guenther, A., Hewitt, C. N., Janson, R., Khalil, A., Owen, S., Pierce, T. E., Puxbaum, H., Shearer, M., Skiba, U., Steinbrecher, R., Tarrason, L., and Oquist, M. G.: Inventorying emissions from Nature in Europe, J. Geophys. Res., 104, 8113–8152, 1999.

Spirig, C., Neftel, A., Ammann, C., Dommen, J., Grabmer, W., Thielmann, A., Schaub, A., Beauchamp, J., Wisthaler, A., and Hansel, A.: Eddy covariance flux measurements of biogenic VOCS during echo 2003 using proton transfer reaction mass spectrometry, Atmos. Chem. Phys., 5, 465–481, 2005, http://www.atmos-chem-phys.net/5/465/2005/.

Staudt, M., Bertin, N., Hansen, U., Seufert, G., Ciccioli, P., Foster, P., Frenzel, B., and Fugit, J. L.: Seasonal and diurnal patterns of monoterpene emissions from *Pinus Pinea* (L) under field conditions, Atmos. Environ. 31(SI), 145–156, 1997.

Staudt, M. and Bertin, N.: Light and temperature dependence of the emission of cyclic and acyclic monoterpenes from Holm Oak (*Quercus ilex* l.) leaves, Plant Cell Environ., 21, 385–395, 1998.

Street, R. A., Owen, S., Duckham, S. C., Boissard, C., and Hewitt, C. N.: Effect of habitat and age on variations in volatile organic compound (VOC) emissions from *Quercus ilex* and *Pinus pinea*, Atmos. Environ., 31(SI), 89–100, 1997.

Taipale, R., Ruuskanen, T. M., Rinne, J., Kajos, M. K., Hakola, H., Pohja, T., and Kulmala, M.: Technical Note: Quantitative long-term measurements of VOC concentrations by PTR-MS – measurement, calibration, and volume mixing ratio calculation methods, Atmos. Chem. Phys., 8, 6681–6698, 2008, http://www.atmos-chem-phys.net/8/6681/2008/.

Tani, A., Hayward, S., and Hewitt, C. N.: Measurement of monoterpenes and related compounds by proton transfer reaction mass spectrometry, Int. J. Mass Spectrom., 223–224, 561–578, 2003.

Valentini, R., Greco, S., Seufert, G., Bertin, N., Ciccioli, P., Cecinato, A., Brancaleoni, E., and Frattoni, M.: Fluxes of biogenic VOC from Mediterranean vegetation by trap enrichment relaxed eddy accumulation, Atmos. Environ., 31(SI), 229–238, 1997.

Warneke, C., Luxembourg, S. L., de Gouw, J. A., Rinne, H. J. I., Guenther, A. B., and Fall, R.: Disjunct eddy covariance measurements of oxygenated volatile organic compounds fluxes from an alfalfa field before and after cutting, J. Geophys. Res., 107(D8), 4067, doi:10.1029/2001JD000594, 2002.

Wiberley, A. E., Linskey, A. R., Falbel, T. G., and Sharkey, T. D.: Development of the capacity for isoprene emission in kudzu,

Plant Cell Environ., 28(7), 898–905, 2005.
Wilkinson, M. J.: Circadian control of isoprene emissions from oil palm. Ph.D. Thesis, Lancaster University, UK, 2006.
Zhao, J. and Zhang, R.: Proton transfer reaction rate constants between hydronium ion (H_3O^+) and volatile organic compounds, Atmos. Environ., 38, 2177–2185, 2004.

II-C Fowler, D., …, Misztal, P., et al.: Atmospheric composition change: Ecosystems-Atmosphere interactions, Atmospheric Environment, 43, 5193-5267, 10.1016/j.atmosenv.2009.07.068, 2009.

Access via ScienceDirect: http://dx.doi.org/**10.1016/j.atmosenv.2009.07.068**

II-D Hewitt, C. N., …, Misztal, P., et al.: Nitrogen management is essential to prevent tropical oil palm plantations from causing ground-level ozone pollution, Proceedings of the National Academy of Sciences, 106, 18447-18451, 10.1073/pnas.0907541106, 2009.

Open access: http://www.pnas.org/content/106/44/18447

PNAS

Nitrogen management is essential to prevent tropical oil palm plantations from causing ground-level ozone pollution

C. N. Hewitt[a,1], A. R. MacKenzie[a], P. Di Carlo[b], C. F. Di Marco[c], J. R. Dorsey[d], M. Evans[e], D. Fowler[c], M. W. Gallagher[d], J. R. Hopkins[f], C. E. Jones[f], B. Langford[a], J. D. Lee[f], A. C. Lewis[f], S. F. Lim[g,2], J. McQuaid[e], P. Misztal[c], S. J. Moller[f], P. S. Monks[h], E. Nemitz[c], D. E. Oram[i], S. M. Owen[c], G. J. Phillips[c], T. A. M. Pugh[a], J. A. Pyle[i], C. E. Reeves[i], J. Ryder[c], J. Siong[c], U. Skiba[c], and D. J. Stewart[i,3]

[a]Lancaster Environment Centre, Lancaster University, Lancaster, LA1 4YQ, United Kingdom; [b]Dipartimento di Fisica, University of L'Aquila, 67010 L'Aquila, Italy; [c]Centre for Ecology and Hydrology, Penicuik, Edinburgh EH26 0QB, United Kingdom; [d]School of Earth, Atmospheric and Environmental Sciences, University of Manchester Manchester, M13 9PL, United Kingdom; [e]School of Earth and Environment, University of Leeds, Leeds LS2 9JT, United Kingdom; [f]Department of Chemistry, University of York, York YO10 5DD, United Kingdom; [g]Malaysian Meteorological Department, Jalan Sultan, Petaling Jaya, Selangor Darul Ehsan, Malaysia; [h]Department of Chemistry, University of Leicester, Leicester LE1 7RH, United Kingdom; [i]School of Environmental Sciences, University of East Anglia, Norwich NR4 7TJ, United Kingdom; and [j]Department of Chemistry, University of Cambridge, Cambridge CB2 1EW, United Kingdom

Edited by Mario J. Molina, University of California at San Diego, La Jolla, CA, and approved September 3, 2009 (received for review July 8, 2009)

More than half the world's rainforest has been lost to agriculture since the Industrial Revolution. Among the most widespread tropical crops is oil palm (*Elaeis guineensis*): global production now exceeds 35 million tonnes per year. In Malaysia, for example, 13% of land area is now oil palm plantation, compared with 1% in 1974. There are enormous pressures to increase palm oil production for food, domestic products, and, especially, biofuels. Greater use of palm oil for biofuel production is predicated on the assumption that palm oil is an "environmentally friendly" fuel feedstock. Here we show, using measurements and models, that oil palm plantations in Malaysia directly emit more oxides of nitrogen and volatile organic compounds than rainforest. These compounds lead to the production of ground-level ozone (O_3), an air pollutant that damages human health, plants, and materials, reduces crop productivity, and has effects on the Earth's climate. Our measurements show that, at present, O_3 concentrations do not differ significantly over rainforest and adjacent oil palm plantation landscapes. However, our model calculations predict that if concentrations of oxides of nitrogen in Borneo are allowed to reach those currently seen over rural North America and Europe, ground-level O_3 concentrations will reach 100 parts per billion (10^9) volume (ppbv) and exceed levels known to be harmful to human health. Our study provides an early warning of the urgent need to develop policies that manage nitrogen emissions if the detrimental effects of palm oil production on air quality and climate are to be avoided.

air quality | land use change | sustainable development | biofuel

Ground-level ozone (O_3) is a priority air pollutant that damages human health, plants, and materials, reduces crop productivity, and has direct and indirect effects on the Earth's climate system (1). It is formed in the atmosphere by reactions involving oxides of nitrogen (NO_x) and volatile organic compounds (VOCs) in the presence of sunlight. The terrestrial biosphere is a major source of both these families of trace gases; in fact, the great majority of reactive VOCs globally are of biogenic origin (2). Here we show, using integrated and fully comprehensive measurements of biosphere-to-atmosphere trace gas fluxes and atmospheric composition, together with atmospheric chemistry modeling, that conversion of tropical rainforest to oil palm plantations results in much greater emissions of these reactive trace gases that lead to O_3 formation. Increased NO_x emissions will cause severe ground-level O_3 pollution (> 100 ppbv), but this pollution could be prevented by strict control of emissions of reactive nitrogen species to the atmosphere. Our study shows the importance of quantifying the current and future effects of land use change on air quality when assessing the "environmental friendliness" of palm oil and other biofuel crops. Of course, air quality is only a single consideration; in assessing the consequences of biofuel production, effects on greenhouse gas emissions and climate change, deforestation, biodiversity, water pollution and freshwater availability, and food prices and food security are all important (3); these factors are not considered here. Specifically, our study provides an early warning of the urgent need to develop policies that manage nitrogen emissions to the atmosphere from the tropics if the detrimental effects of palm oil production on air quality and climate are to be avoided.

Results

Our study comprises a truly integrated and fully comprehensive set of biosphere-to-atmosphere flux measurements, atmospheric composition measurements, and atmospheric chemistry modeling in the tropics for 2 distinct but contiguous land use types. The project was based in Sabah, Malaysian Borneo, during April through July 2008. Our measurements (Table 1) show that emissions of VOCs from the rainforest and oil palm plantation landscapes are dominated by emissions of isoprene (2-methyl-1,3-butadiene). On a land area basis, isoprene emissions from the plantation (27 tonnes of isoprene per km^2 per year) are 5 times greater than from the rainforest. Isoprene and other VOC emission rates depend, in part, on leaf temperature (4). Temperatures were higher at the oil palm site than at the rainforest site (campaign averages 27.9 °C and 25.7 °C, respectively), but this difference in temperature explains only 7% of the observed difference in isoprene emission rates; the remainder is the result of the higher biogenic VOC emission rates from oil palm (*Elaeis guineensis*) trees (5) compared with rainforest tree

Author contributions: C.N.H., A.R.M.K., M.E., D.F., A.C.L., P.S.M., J.A.P., and C.E.R. designed research; C.N.H., A.R.M.K., M.E., D.F., J.D.L., E.N., and C.E.R. analyzed data; P.D.C., C.F.D.M., J.R.D., M.W.G., J.R.H., C.E.J., B.L., J.D.L., A.C.L., S.F.L., J.M., P.M., S.J.M., E.N., D.E.O., S.M.O., G.J.P., T.A.M.P., J.R., J.S., U.S., and D.J.S. performed research; and C.N.H., A.R.M.K., D.F., and J.A.P. wrote the paper.

Conflict of interest: The authors declare no conflict of interest.

This article is a PNAS Direct Submission.

Freely available online through the PNAS open access option.

[1]To whom correspondence should be addressed. E-mail: n.hewitt@lancaster.ac.uk.

[2]Retired.

[3]Present address: Department of Chemistry, University of Reading, Reading, RG6 6AH, United Kingdom.

This article contains supporting information online at www.pnas.org/cgi/content/full/0907541106/DCSupplemental.

SUSTAINABILITY SCIENCE

Table 1. Fluxes of isoprene, monoterpenes, reactive oxides of nitrogen, and nitrous oxide

Site		Isoprene: flux at the canopy scale (10.00–16.00 h) (mg/m²/h)	Monoterpenes: flux at the canopy scale (10.00–16.00 h) (mg/m²/h)	Reactive oxides of nitrogen: flux from soils (00.00–24.00 h) (mg N/m²/h)	Reactive oxides of nitrogen: flux at the landscape scale, inferred from model (00.00–24.00 h) (mg N/m²/h)	Nitrous oxide: flux from soils (00.00–24.00 h) (mg N_2O–N/m²/h)
Rainforest	Mean	1.55 ± 0.39	0.38 ± 0.20	0.14 ± 0.115	0.009	0.036 ± 0.041
	Variability	1.22	0.34	0.035		N/A
	n	619	619	5509		89
Oil palm plantation	Mean	7.77 ± 1.94	0.09 ± 0.20	N/A	0.019	0.051 ± 0.040
	Variability	7.68	0.35			N/A
	n	164	37			101

Fluxes of isoprene, monoterpenes, reactive oxides of nitrogen, and nitrous oxide from the Bukit Atur rainforest site and the Sabahmas oil palm plantation site, with an estimate of their uncertainty, their temporal variability (calculated as the standard deviation of the 30-min or hourly measurements) and the number of observations (n) on which they are based.

species. Isoprene has a 5 times greater potential for photochemical ozone creation than the weighted average of VOC compounds emitted by urban anthropogenic activity (6). After normalizing for this difference in VOC reactivity, the effective emissions of VOCs from the oil palm canopy per unit land area exceed those of a typical European city, such as London (7).

Our observations show that the plantation landscape and associated agro-industrial activities give rise to NO_x emissions several (≈2.5) times greater than from the rainforest on a land area basis (Table 1). The 3 major NO_x sources responsible for this increase are all linked to agro-industrial activity—vehicle exhaust, combustion at the palm oil processing plant, and substantial soil nitrogen fertilization in the plantations (≈0.5 tonnes of nitrogen per hectare per year). Aircraft measurements of acetylene, a well-established combustion tracer (8), show no significant enhancement in the boundary layer over the plantation landscape compared with the rainforest landscape. This finding is a strong indication that non-combustion sources make the major contribution to the elevated NO_x concentrations observed over the plantation landscape. Further corroboration of enhanced denitrification of oil palm plantation soils is given by the N_2O emissions from these soils, which are ≈50% larger than those from the rainforest soils (Table 1).

As well as dominating VOC emission flux rates, isoprene is the dominant (> 80%) reactive VOC by atmospheric mixing ratio in both landscapes. The concentrations of isoprene were 2 to 5 times higher over the plantation landscape than over the rainforest (Fig. 1), consistent with the observations of fluxes. The C_{10} monoter-

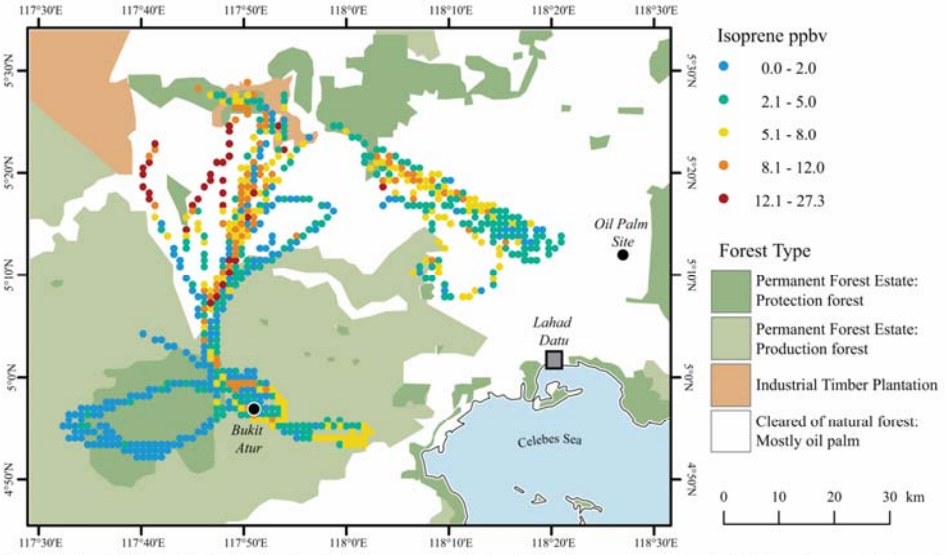

Fig. 1. The aircraft flight tracks in the boundary layer for the data averaged in Fig. 2, colored by isoprene concentrations (ppbv). The markers are at 10-s intervals with the 15-s isoprene data merged onto this time stamp. Each marker represents a single measurement, and there are only a small number of instances, mostly around 5.05° North, 117.8° East, where several points overlay each other.

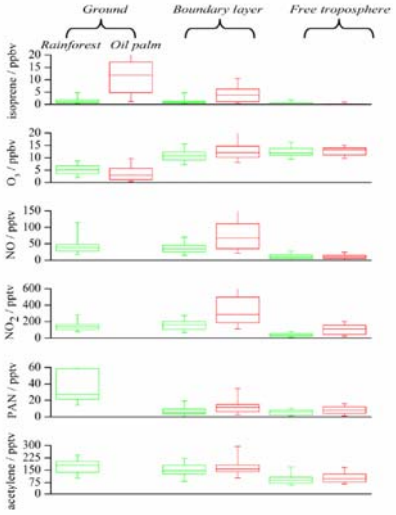

Fig. 2. Isoprene, ozone, nitric oxide, nitrogen dioxide, peroxyacetyl nitrate, and acetylene measured between 10.00 and 16.00 hours local time at ground sites (2 left columns), from the aircraft flying within the boundary layer (500–800 m above ground level) (2 middle columns), and from the aircraft flying in the free troposphere (3,000–6,000 m above ground level) (2 right columns). The green symbols show data from the rainforest landscape, and the red symbols show data from the oil palm plantation landscape. Symbol boxes show median and quartile values, with the whiskers showing 95th and 5th percentiles. Measurements of NO, NO_2, PAN, and acetylene were not made on the ground at the Sabahmas oil palm plantation and therefore do not appear in the figure. Information on sampling frequency and averaging is given in the SI.

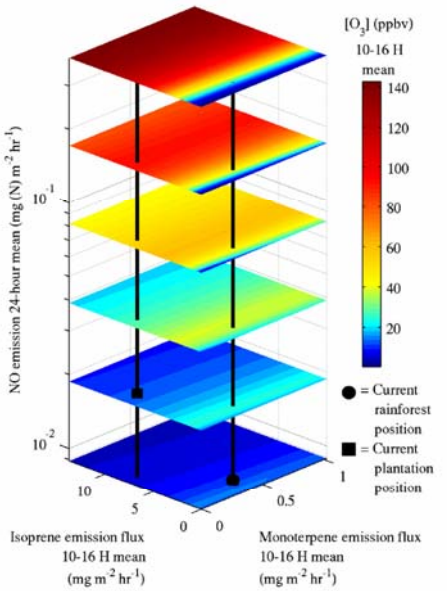

Fig. 3. Sensitivity of mean mixed boundary layer ozone concentrations (from 10.00–16.00 hours) to fluxes of isoprene, monoterpenes, and NO, as computed by CiTTyCAT. VOC fluxes are the mean over 10.00–16.00 hours; NO fluxes are the mean over a 24-hour period. The black lines show the rainforest and plantation VOC emission scenarios. The current rainforest and plantation positions are determined by observed VOC emission rates and ozone concentrations.

penes are the second most important group of biogenic VOCs. At both the rainforest and the plantation sites, γ-terpinene, α-pinene, and limonene dominate the emissions and concentrations of the C_{10} compounds, giving an approximately equal split between more and less reactive monoterpenes (9).

Fig. 2 shows that the differences in emission rates in NO_x and isoprene between the rainforest and the oil palm plantations give rise to differences in concentrations throughout the boundary layer and into the free troposphere. Over the rainforest, median boundary layer mixing ratios of NO, NO_2, and isoprene were 35, 161, and 767 parts per trillion (10^{12}) by volume (pptv), respectively, and over the plantation the median mixing ratios were 67, 288, and 3870 pptv, respectively. Surprisingly, ozone concentrations were similar over both landscapes in the boundary layer (rainforest: 11 ppbv; oil palm plantation: 12 ppbv). The ozone measurements at the Bukit Atur Global Atmosphere Watch station confirm that our measurement period is typical of the long-term record at this site. However, the concentrations of peroxyacetyl nitrate (PAN) increased from 6 pptv in the boundary layer over the rainforest to 12 pptv over the plantation landscape, demonstrating enhanced photochemical processing of the increased NO_x and VOC emissions and concentrations over the plantations.

To understand current and future ozone levels over these 2 landscapes, we have used the CiTTyCAT box model of atmospheric photochemistry (10–12). These computations explore the sensitivity of atmospheric composition in the boundary layer to VOC and NO_x emission rates for the calm, nonprecipitating, atmosphere, consistent with conditions during the measurement period.

Fig. 3 shows the model-calculated average boundary-layer ozone concentrations between 10:00 and 16:00 hours as a function of isoprene, monoterpene, and NO_x emission rates. The model has been enhanced by the inclusion of monoterpene oxidation to capture the rainforest chemistry. Monoterpenes are not yet generally included in atmospheric chemistry models such as those used in the Fourth Assessment Report of the Intergovernmental Panel on Climate Change (13).

Although the 2 landscapes currently have different NO_x and VOC concentrations, the model predicts similar ozone concentrations, as confirmed by our measurements. The ozone concentrations are similar because ozone production, although driven by increased NO and VOC emissions and oxidation, is moderated here by the rapid sequestering of reactive nitrogen to form organic nitrates that deposit to the surface and by ozone destruction resulting from its direct reaction with monoterpenes.

Fig. 3 also suggests that ozone concentrations at the 2 locations respond quite differently to increasing NO_x emissions and concentrations. In both landscapes, NO_x concentrations will increase with increasing fossil fuel consumption, associated with industrialization, across the region. Additionally, NO_x concentrations will increase in the plantation landscape with increased mechanization, fossil fuel use, and fertilizer application. Total VOC emissions in these landscapes will not be so sensitive to

SUSTAINABILITY SCIENCE

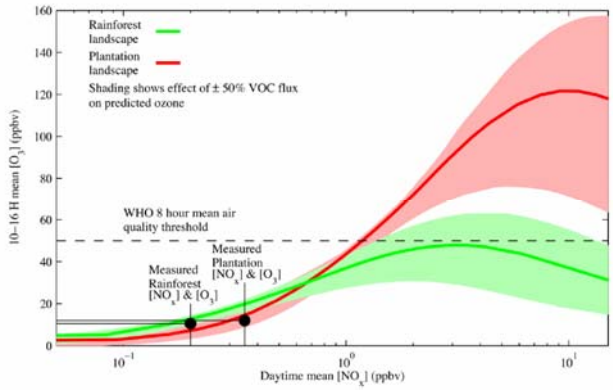

Fig. 4. Sensitivity of daytime (10.00–16.00 hours) average ozone concentration to concentrations of NO_x in the boundary layer, for the isoprene and monoterpene emission rates measured at the rainforest and oil palm landscapes, as computed by CiTTyCAT. Each model run has a similar shape but with a different point of inflection, so the solid lines are not always in the centre of the shaded region. Current measured concentrations of NO_x and O_3 in the rainforest and plantation are marked.

industrialization because of the current large biogenic VOC emission rates (Table 1).

Fig. 4 shows the sensitivity of ozone to NO_x concentrations for the VOC emission rates specific to the 2 locations. The nonlinearity in the chemistry becomes more apparent when the model results are presented this way. Our model predicts that ozone concentrations in the rainforest most probably will not exceed 50 ppbv (except by advection of ozone and its precursors from outside the rainforest landscape), irrespective of NO_x concentration, whereas in the oil palm landscape ozone concentrations will exceed 100 ppbv when NO_x concentrations reach 3–5 ppbv. Such NO_x concentrations are currently widely observed in rural areas of Western Europe (14), North America, and Asia (15). Ozone at 100 ppbv has significant detrimental effects on human health and crop yields and enhances global warming through its strong radiative forcing (1).

Discussion

Our measurements show that the conversion of rainforest to oil palm plantation substantially increases VOC and NO_x emissions and concentrations. The increase in VOC emission rates comes directly from the oil palm plants. The increase in NO_x emission rates comes from agro-industrialization, especially from fertilized soils. These differences in emission rate have increased the concentrations of some photochemical pollutants, notably PAN. Fortunately, they have not, to date, increased the ground-level concentrations of the most hazardous photochemical air pollutant, ozone. However, ozone will increase substantially in this region as NO_x emissions rise with industrialization and economic development.

The degree to which oil palm production will contribute to poor air quality in the future will depend almost entirely on the emission rates of nitrogen oxides. Although ozone concentrations in the rainforest are predicted to remain below 50 ppbv, regardless of the development path taken with respect to emissions of NO_x, there is the potential for ozone concentrations in the plantation landscape to greatly exceed the current World Health Organization 8-hour mean air quality threshold of 50 ppbv. Only stringent controls on emissions to maintain NO_x concentrations below those currently observed in rural parts of Western Europe and North America will prevent this increase from occurring. Controlling nitrogen emissions at both the local (plantation) and regional scales is necessary to prevent large-scale palm oil production from having very serious effects on regional air quality. Genetic modification of the oil palm cultivar to extinguish isoprene emissions (as already demonstrated for poplar [ref. 16]) would also avoid ozone air quality exceedances at any NO_x concentration (see Fig. 3). Without NO_x emissions controls or genetic modification, palm oil production for biofuel and other uses will incur significant future costs in terms of human health effects and crop yield reductions that have yet to be included in sustainability criteria for the industry. The utility of palm oil as an environmentally friendly crop may be therefore severely time-limited.

Methods

The project was based in Sabah, Malaysia, April through July, 2008. Ground-based measurements were performed at the 100-m-high Global Atmosphere Watch tower at Bukit Atur (4° 58′ 49.33″ North, 117° 50′ 39.05″ East, 426 m above sea level) and at the Sabahmas oil palm plantation (5.2° North, 118.45° East), 70 km east-northeast of Bukit Atur. Airborne measurements were made from the Natural Environment Research Council/U.K. Meteorological Office's BAe 146–301 large atmospheric research aircraft, which was based at Kota Kinabalu International Airport. Kota Kinabalu (population 580,000) is the largest city in Sabah and is 250 km northwest of Bukit Atur. Sandakan (population 430,000) and Tawau (population 370,000) are about 100 km north and south of Bukit Atur, respectively. The southern part of Sabah and the adjoining region of Indonesia are largely pristine, and selectively logged, rainforest and local anthropogenic emissions are insignificant. The lowland parts of northern and coastal Sabah are largely oil palm plantations. These plantations are serviced by processing mills, mainly powered by biomass (oil palm husks). No attempt was made to avoid or preferentially to sample the visible mill plumes from the aircraft. The boundary layer was sampled from the aircraft using low-level runs following the terrain, originating above the plantations and terminating above the pristine rain forest. Flying time totaled 68 hours. Measurements included trace gas concentrations and fluxes. Modeling was carried out using the CiTTyCAT box model of atmospheric chemistry. Full details of the measurement and modeling methods used are given in the supporting information (SI).

ACKNOWLEDGMENTS. We dedicate this paper to the memory of Kate Furneaux, a core member of the OP3 project team, who was killed in a traffic accident while cycling in Leeds on 28 July 2009. We thank the Malaysian and Sabah Governments for their permission to conduct research in Malaysia; the Malaysian Meteorological Department for access to the Bukit Atur Global

Atmosphere Watch station and its long-term ozone record; Wilmar International Ltd for access to and logistical support at their PPB Oil Palms Bhd Sabahmas Estate; Waidi Sinun of Yayasan Sabah and his staff, Glen Reynolds of the Royal Society's South East Asian Rainforest Research Programme and his staff, and Nick Chappell and Brian Davison of Lancaster University for logistical support at the Danum Valley Field Centre; the ground staff, engineers, scientists, and pilots of the Natural Environment Research Council/U.K. Meteorological Office's BAe 146–301 large atmospheric research aircraft; Nick Chappell, Gemma Davies, Virginia Nicolas-Perea, and M.H. Phua for drawing and validating Fig. 1; and all the members of the OP3 project team for their support and individual and collective efforts. The work was funded by the Natural Environment Research Council Grants NE/D002117/1 and NE/E011179/1.

1. The Royal Society, London (2008) Science Policy Report 15/08. Ground-level ozone in the 21st century: Future trends, impacts and policy implications (The Royal Society, London).
2. Guenther AB, et al. (1995) A global model of natural volatile organic compound emissions. *J Geophys Res-Atmos* 100:8873–8892.
3. Howarth RW, Bringezu S, eds (2008) *Biofuels: Environmental Consequences and Interactions with Changing Land Use*. Proceedings of the Scientific Committee on Problems of the Environment (SCOPE) International Biofuels Project Rapid Assessment, September 22–25 2008, Gummersbach, Germany (Ithaca, NY, Cornell U Press). Available at http://cip.cornell.edu/biofuels/. Accessed 07/01/09.
4. Laothawornkitkul J., Taylor JE, Paul ND, Hewitt CN (2009) Biogenic volatile organic compounds in the Earth system: A Tansley review. *New Phytol* 183:27–51.
5. Wilkinson MJ, et al. (2006) Circadian control of isoprene emissions from oil palm (*Elaeis guineensis*). *Plant J* 47:960–968.
6. Derwent RG, Jenkin ME, Passant NR, Pilling MJ (2007) Photochemical ozone creation potentials (POCPs) for different emission sources of organic compounds under European conditions estimated with a Master Chemical Mechanism. *Atmospheric Environment* 41:2570–2579.
7. Emissions of air pollutants in the UK, National Atmospheric Emissions Inventory (2009). Available at http://www.naei.org.uk/. Accessed 04/01/09.
8. Whitby RA, Altwicker ER (1978) Acetylene in the atmosphere: Sources, representative ambient concentrations and ratios to other hydrocarbons. *Atmospheric Environment* 12:1289–1296.
9. Atkinson R, Arey J (2003) Gas-phase tropospheric chemistry of biogenic volatile organic compounds: A review. *Atmospheric Environment* 37(52):197–219.
10. Wild O, et al. (1996) Photochemical trajectory modeling studies of the North Atlantic region during August 1993. *J Geophys Res* 10(1):29269–29288.
11. Evans MJ, et al. (2000) Evaluation of a Lagrangian box model using field measurements from EASE (Eastern Atlantic Summer Experiment) 1996. *Atmospheric Environment* 34:3843–3863.
12. Donovan RG, Hope ES, Owen SM, Mackenzie AR, Hewitt CN (2005) Development and application of an urban tree air quality score for photochemical pollution episodes using the Birmingham, United Kingdom, area as a case study. *Environ Sci Technol* 39:6730–6738.
13. Denman KL, et al. (2007) Couplings between changes in the climate system and biogeochemistry. Solomon S. et al., eds *Climate Change 2007: The Physical Science Basis. Contribution of Working Group I to the Fourth Assessment Report of the Intergovernmental Panel on Climate Change* (Cambridge Univ Press, Cambridge, UK), pp 500–587.
14. Tarrason L, Nyiri A, eds (2008) *Transboundary Acidification, Eutrophication and Ground Level Ozone in Europe in 2006* (European Monitoring and Evaluation Programme Status Report 1, Oslo).
15. Collins WJ, Stevenson DS, Johnson CE, Derwent RG (1997) Tropospheric ozone in a global-scale 3-dimensional Lagrangian model and its response to NO_X emission controls. *Journal of Atmospheric Chemistry* 26:223–274.
16. Behnke K, et al. (2007) Transgenic, non-isoprene emitting poplars don't like it hot. *Plant J* 51:485–499.

II-E Hewitt, C. N., … , Misztal, P., et al.: Overview: oxidant and particle photochemical processes above a south-east Asian tropical rainforest (the OP3 project): introduction, rationale, location characteristics and tools, Atmos. Chem. Phys., 10, 169-199, 2010.

Open access: http://www.atmos-chem-phys.net/10/169/2010/acp-10-169-2010.html

Atmos. Chem. Phys., 10, 169–199, 2010
www.atmos-chem-phys.net/10/169/2010/

Atmospheric Chemistry and Physics

Overview: oxidant and particle photochemical processes above a south-east Asian tropical rainforest (the OP3 project): introduction, rationale, location characteristics and tools

C. N. Hewitt[1], J. D. Lee[2], A. R. MacKenzie[1], M. P. Barkley[3], N. Carslaw[4], G. D. Carver[5], N. A. Chappell[1], H. Coe[6], C. Collier[7], R. Commane[8,*], F. Davies[7], B. Davison[1], P. DiCarlo[9], C. F. Di Marco[10], J. R. Dorsey[6], P. M. Edwards[8], M. J. Evans[11], D. Fowler[10], K. L. Furneaux[,†], M. Gallagher[6], A. Guenther[12], D. E. Heard[8], C. Helfter[10], J. Hopkins[13], T. Ingham[8], M. Irwin[6], C. Jones[13], A. Karunaharan[14], B. Langford[1], A. C. Lewis[13], S. F. Lim[15], S. M. MacDonald[8], A. S. Mahajan[8], S. Malpass[4], G. McFiggans[6], G. Mills[16], P. Misztal[10,17], S. Moller[13], P. S. Monks[14], E. Nemitz[10], V. Nicolas-Perea[14], H. Oetjen[8], D. E. Oram[16], P. I. Palmer[3], G. J. Phillips[10], R. Pike[5], J. M. C. Plane[8], T. Pugh[1], J. A. Pyle[5], C. E. Reeves[16], N. H. Robinson[6], D. Stewart[16,***], D. Stone[8,11], L. K. Whalley[8], and X. Yin[5]**

[1]Lancaster Environment Centre, Lancaster University, Lancaster LA1 4YQ, UK
[2]National Centre for Atmospheric Science, University of York, York YO10 5DD, UK
[3]School of GeoSciences, University of Edinburgh, Edinburgh EH9 3JW, UK
[4]Environment Department, University of York, York YO10 5DD, UK
[5]Centre for Atmospheric Science, Department of Chemistry, Cambridge University, Cambridge, CB2 1EW, UK
[6]School of Earth, Atmospheric and Environmental Sciences, University of Manchester, Manchester M13 3PL, UK
[7]Centre for Environmental Systems Research, University of Salford, Salford M5 4WT, UK
[8]School of Chemistry, University of Leeds, Leeds LS2 9JT, UK
[9]CETEMPS – Dipartimento di Fisica, Università di L'Aquila, 67010 Coppito, L'Aquila, Italy
[10]Biogeochemistry Programme, Centre for Ecology and Hydrology, Penicuik, EH26 0QB, UK
[11]School of the Environment, University of Leeds, Leeds, LS2 9JT, UK
[12]National Center for Atmospheric Research, Boulder CO 80301, USA
[13]Department of Chemistry, University of York, York YO10 5DD, UK
[14]Department of Chemistry, University of Leicester, Leicester LE1 7RH, UK
[15]Retired, formerly at Malaysian Meteorological Department, Jalan Sultan, Petaling Jaya, Selangor Darul Ehsan, Malaysia
[16]School of Environmental Sciences, University of East Anglia, Norwich NR4 7TJ, UK
[17]Department of Chemistry, University of Edinburgh, Edinburgh EH9 3JW, UK
[*]now at: School of Engineering and Applied Sciences, Harvard University, MA, USA
[**]formerly at: School of Chemistry, University of Leeds, Leeds LS2 9JT, UK
[***]now at: Department of Chemistry, University of Reading, Reading RG6 6AH, UK
[†]deceased

Received: 8 July 2009 – Published in Atmos. Chem. Phys. Discuss.: 11 September 2009
Revised: 4 December 2009 – Accepted: 9 December 2009 – Published: 12 January 2010

Abstract. In April–July 2008, intensive measurements were made of atmospheric composition and chemistry in Sabah, Malaysia, as part of the "Oxidant and particle photochemical processes above a South-East Asian tropical rainforest" (OP3) project. Fluxes and concentrations of trace gases and particles were made from and above the rainforest canopy at the Bukit Atur Global Atmosphere Watch station and at the nearby Sabahmas oil palm plantation, using both ground-based and airborne measurements. Here, the measurement and modelling strategies used, the characteristics of the sites and an overview of data obtained are described. Composition measurements show that the rainforest

Correspondence to: C. N. Hewitt
(n.hewitt@lancaster.ac.uk)

Published by Copernicus Publications on behalf of the European Geosciences Union.

site was not significantly impacted by anthropogenic pollution, and this is confirmed by satellite retrievals of NO_2 and HCHO. The dominant modulators of atmospheric chemistry at the rainforest site were therefore emissions of BVOCs and soil emissions of reactive nitrogen oxides. At the observed BVOC:NO_x volume mixing ratio (~100 pptv/pptv), current chemical models suggest that daytime maximum OH concentrations should be ca. 10^5 radicals cm^{-3}, but observed OH concentrations were an order of magnitude greater than this. We confirm, therefore, previous measurements that suggest that an unexplained source of OH must exist above tropical rainforest and we continue to interrogate the data to find explanations for this.

1 Introduction

Tropical and equatorial forests account for over half of the World's forests (1.8 billion ha) and act as a massive source of matter and energy to the lower atmosphere. They exhibit some of the most dynamic yet poorly understood biogeochemical behaviour on Earth. This behaviour is driven by solar radiation and is largely mediated by its transformation into latent and sensible heat, with the concomitant uptake of carbon by photosynthesis and the associated emission of reactive, less-reactive and un-reactive trace gases, water vapour and energy into the atmosphere. Simultaneously, ozone and other trace gases, aerosol particles, and momentum, are lost to the forest surface. A further important consequence of the large solar radiation flux in the tropics is the very vigorous convective uplift that occurs, which results in the rapid movement of chemical species emitted at or near ground level into the free troposphere, as shown, for example, in Surinam (Andreae et al., 2001). Hence reactive trace gas emissions from the surface in the tropics may take part in chemical processes at greater distances and at higher altitudes from their sources than might otherwise occur.

Globally, tropical and equatorial forests are estimated to account for almost half of all biogenic reactive volatile organic compound (VOC) emissions into the atmosphere (Guenther et al., 1995, 2006: global total 1150 Tg C/y, estimate for tropical forests ~500 Tg C/y). These compounds are believed to play a major role in mediating the chemistry of the atmosphere, yet their roles in controlling chemical budgets and processes in the atmosphere on the local, regional and global scales are poorly understood, with considerable and surprising gaps and uncertainties in knowledge remaining (e.g. Lelieveld et al., 2008). In addition, it is possible that biological primary and secondary organic particles play a pivotal role in the formation of cloud condensation nuclei (CNN) and thus control precipitation patterns in forested regions (Barth et al., 2005).

Most previous work on the interactions between tropical forests and atmospheric composition has been carried out in Amazonia (e.g. the LBA project: Andreae et al., 2002; Avissar et al., 2002), with less in Africa (e.g. the AMMA project: Redelsperger et al., 2006) and very little in SE Asia. Unlike the LBA and AMMA domains, which are contiguous continental regions, the complex mosaic of tropical seas and islands that exists in SE Asia makes the likely atmospheric chemistry occurring there somewhat different to that elsewhere. Structurally and floristically, the lowland dipterocarp forest of SE Asia is very different to the rainforest of Amazonia, and it is not known what differences this may cause in the speciation and rates of emission of VOCs and hence in atmospheric composition and chemistry. Furthermore, there is strong evidence that transport from the boundary layer in this "maritime continent" region into the upper troposphere, and possibly subsequently into the stratosphere, is particularly efficient (Fueglistaler and Haynes, 2005), so that the region's importance to global atmospheric processes may be disproportionately large.

In common with the other tropical forest regions, SE Asia is undergoing very rapid, and in some cases catastrophic, rates of land use change. For example, in Malaysia, the area of total land cover dedicated to oil palm plantations has increased from ~1% in 1974 to ~13% (FAO, 2005; MPOC, 2008). In spite of attempts to implement policies to conserve rainforest, logging of this dwindling resource continues at a rapid rate, and natural forests are being replaced by crop monocultures.

The multi-national OP3 ("Oxidant and particle photochemical processes above a south-east Asian tropical rainforest") project had the goal of better understanding the interactions that exist between natural forests, atmospheric composition and the Earth's climate system. The project had the specific objectives of (a) understanding how emissions of reactive trace gases from a tropical rainforest mediate the regional scale production and processing of oxidants and particles, and (b) better understanding the impacts of these processes on local, regional and global scale atmospheric composition, chemistry and climate. By very closely coupling ground-based and airborne measurements of surface fluxes and atmospheric composition of reactive trace gases and particles with modelling studies of chemical processes, the project aimed to address the following questions:

1. What are the rates of transfer of organic compounds emitted from the tropical forest?
2. How are these organic compounds chemically processed immediately after release?
3. To what extent do the regional organic emissions contribute to the atmospheric aerosol in the region, and what are the effects of the aerosol? What is the composition of the organic fraction of the aerosol?
4. What are the effects of these biogenic emissions on global chemistry and climate?

The OH radical initiates the oxidative degradation of biogenically emitted VOCs, and its concentration defines the rate of production of secondary products. A consistent and important finding from field studies conducted in forested environments, characterised by high emissions of isoprene and low levels of NO_X, is the significant underestimation of OH by models (Lelieveld et al., 2008; Ren et al., 2008; Butler et al., 2008; Carslaw et al., 2001; Martinez et al., 2008; Tan et al., 2001; Kubistin et al., 2009). These model underestimations scale with isoprene concentration and indicate a current inability to correctly describe isoprene oxidation. The OP3 project provided an excellent opportunity to confirm these findings and to seek an explanation. Atmospheric chemistry models, constrained to measured isoprene emission rates, predict dramatic reductions in ambient OH concentrations in forested areas, in contrast to observations and, as a consequence, predict unrealistically high concentrations of other trace gas constituents (Guenther et al., 2008). Simultaneous measurements of the OH concentration, isoprene concentration and fluxes and isoprene oxidation products were made during OP3, together with many species that control the rate of production and destruction of OH, providing a stringent set of model constraints to investigate in detail any modelled/measured discrepancies for OH.

Similarly, current models suggest that secondary organic aerosol (SOA) in the tropics is dominated by biogenic aerosol (e.g. Kanakidou et al., 2005), but the measurement database is sparse. Emerging first measurements by aerosol mass spectrometry indicate that sub-micrometre organic aerosol concentrations are at the lower end of the model estimates, with median concentrations of around 1 $\mu g\,m^{-3}$ observed in subtropical West Africa and Amazonia (Capes et al., 2009). Despite recent progress, our picture of the formation processes of biogenic SOA (BSOA) is still far from complete (Hallquist et al., 2009). Again, the suite of measurements during OP3 was designed to improve our understanding of the levels, composition and formation processes of BSOA in the SE Asian domain.

As described below, the focus of activity was the Global Atmosphere Watch (GAW) station at Bukit Atur, Sabah, Malaysia, on the island of Borneo (4°58′49.33″ N, 117°50′39.05″ E, 426 m a.s.l.) (http://gaw.empa.ch/gawsis/). Two field campaigns were held during the periods 7 April–4 May 2008 (OP3-I) and 23 June–23 July 2008 (OP3-III). During OP3-III, the UK's largest atmospheric science research aircraft, a converted BAe 146–301, was based at Kota Kinabalu International Airport during the period 8–23 July 2008 and operated for over 60 h over northern Borneo. Between these two forest campaigns, a sub-set of instruments were deployed in an oil palm plantation, where measurements were made during the period 11 May–20 June 2008 (OP3-II).

In this paper, the land use, vegetation and climate characteristics of the ground-based measurement sites are described, together with an overview of the chemical climatology of the region. The measurement and modelling tools used in the project are also described, as are some preliminary conclusions.

2 Climate, weather, land use and vegetation of Sabah

2.1 Equatorial climate and forest formations

The equatorial tropics are characterised by rain throughout the year, i.e., an absence of marked seasonal droughts. This climatic regime covers: (i) Malaysia, Papua New Guinea and much of Indonesia within tropical monsoon Asia, (ii) coastal regions of Liberia, Nigeria and Cameroon, and central Congo in Africa, and (iii) western Amazonia and a belt extending from the western Caribbean coast to the Pacific coast in Ecuador in tropical America (McGregor and Nieuwolt, 1998; Walsh, 1996). The equatorial tropics can be further classified into tropical superwet, tropical wet and tropical wet seasonal, using a perhumidity index, based on a cumulative annual score of the number of months with >200 mm (+2 index value), 100–199 mm (+1), 50–99 mm (−1) and <50 mm (−2) of rainfall (Walsh, 1996). The extent of tropical superwet and wet climates (with a perhumidity index >10) shown in Walsh (1996) is similar to the extent of tropical climates of Asia and America lacking marked dry seasons shown in McGregor and Nieuwolt (1998).

With the exception of the central Congo and the western Caribbean, there is a good correspondence of regions with a tropical wet or superwet climate and the extent of tropical lowland evergreen broadleaf rainforest. This forest formation dominates within the majority of the Asian, West African and American wet/superwet zone of the equatorial tropics (Whitmore, 1998), and is the most common forest formation in the tropics as a whole (Schmitt et al., 2008). However, in areas locally above 750–1200 m altitude, lowland evergreen broadleaf rainforest grades into lower montane and then upper montane forest. Such areas of mountain forests are noted particularly in the wet/superwet zones of the Asian tropics. Within low-lying areas of the wet and superwet zone, peat swamp, freshwater swamp and heath forest are also present. In areas of podzolic sands, limestone or ultrabasic rocks other forest formations are developed locally.

The key exception to the link between climate and the extent of lowland evergreen rainforest is found within central Congo and the western Caribbean, where tropical semi-evergreen rainforest dominates in areas classified as tropical wet. This semi-evergreen forest formation is important throughout the surrounding seasonal tropics of continental tropical Asia, north-east Australia, and eastern and southern Amazonia (Whitmore, 1998).

Within the equatorial tropics, the dominant lowland evergreen broadleaf rainforest is characterised by a lofty (45 m or taller) and dense canopy with a large number of different tree species occurring together. Usually over two thirds of the upper canopy comprises tree species not contributing

more than 1% to the total number (Whitmore, 1998). The soils typically associated with the occurrence of this forest formation in tropical Asia are the Ultisol group, and within western Amazonia the Oxisol group (Baillie, 1996; Chappell et al., 2007).

2.2 Local climate and forest formations

The majority of the island of Borneo (total area 743 330 km^2) has a superwet climate (Walsh, 1996) and the most extensive forest formation is lowland evergreen broadleaf rainforest, occupying some 257 000 km^2 (Schmitt et al., 2008). A similar situation is observed at the 76 115 km^2 regional scale of the state of Sabah, Malaysian Borneo. Within Borneo Island, and elsewhere within equatorial Asia, the lowland evergreen rainforest typically has a tree family dominance of *Dipterocarpaceae* (Whitmore, 1984). Most of the state of Sabah was once covered with rainforest (Schmitt et al., 2008), particularly such mixed dipterocarp forest. Currently, some 47% (36 049 km^2) of the state lies within Permanent Forest Estate (PFE: Fig. 1a). Most of this PFE (74%) is maintained under a selective harvesting system (PFE Production Forest), while the remaining 26% is classified as PFE Protection Forest. Within eastern Sabah, most of the cleared lands are now used for the cultivation of oil palm trees (Fig. 1b). Some commercial timber plantations are also present within Sabah.

The Bukit Atur GAW tower used for OP3 sampling is located within the PFE Production Forest of the Ulu Segama – Malua Forest Reserve, but is less than 5 km east of the 438 km^2 area of PFE Protection Forest known as the Danum Valley Conservation Area (DVCA). The Ulu Segama – Malua Forest Reserve is 2411 km^2 in area and is divided into annual timber harvesting coupes. The GAW tower lies at the centre of the 22.6 km^2 "Coupe 88" which was subjected to selective timber harvesting in 1988. An average of 96 m^3 of timber ha^{-1} was cut by both tractor and high-lead harvesting (Tangki and Chappell, 2008). The central area of this coupe was subsequently rehabilitated by enrichment planting (Moura-Costa, 1996). As part of a study covering a 225 km^2 area Tangki and Chappell (2008) calculated an average tree biomass of 172 t ha^{-1} for Coupe 88, (using five inventory plots surveyed in March 1997), and demonstrated a strong correlation (r^2=0.76) between such coupe-averaged values and Landsat-5 TM band 4 (near-infra red) radiance. Tangki (2008) demonstrated that *Dipterocarpaceae* were the most abundant tree family recorded for the 225 km^2 area as a whole (comprising of only lowland evergreen broadleaf rainforest), but *Euphobiaceae* had become more abundant in Coupe 88 following timber harvesting.

Within the immediate vicinity of the Bukit Atur GAW tower, we calculate the average perhumidity index to be 22 (using the daily rainfall data for the period 1996–2008 from the Danum Valley Field Centre (DVFC), located 8 km from Bukit Atur at 4°58′ N, 117°48″ E, 100 m a.s.l.). Hence Bukit Atur is classified as having a superwet climate. The index

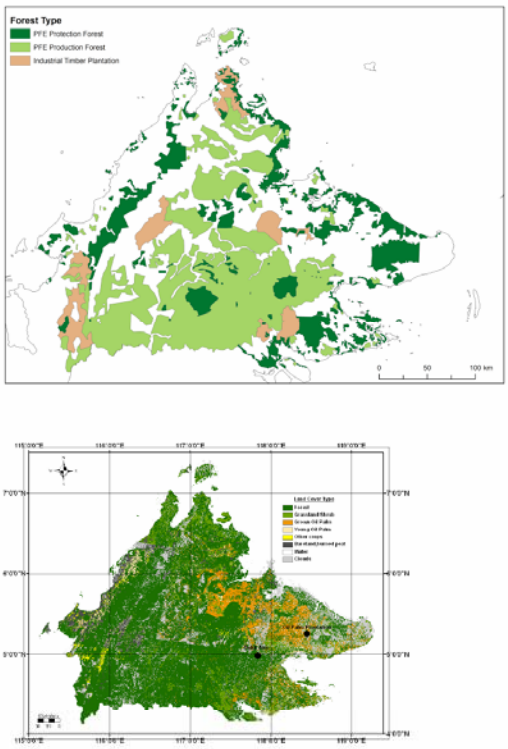

Fig. 1. Land cover maps of Sabah showing **(a)** the extent of Permanent Forest Estate (PFE) based on Sabah Forest Department (1998) data, where dark green shows PFE Protection Forest, and light green PFE Production Forest; non-PFE commercial timber plantation is also shown in light brown, and **(b)** extent of oil palm (orange) and other land covers based on a preliminary classification of remote sensing imagery. The satellite data used to produce this map was medium resolution data from Landsat7-ETM+. Eight images from 2005 to 2008 were used. All the images were first geo-referenced using 1:50 000 topographic maps of Sabah. After refinements of the training area collection, the data were reclassified into the eight land cover classes, excluding cloud and shadow.

did however range from 9 (1997) to 23 (1999) as a result of the 4–5 year cycle in the rainfall caused by El Niño South Oscillation phenomena (Chappell et al., 2001). During the OP3 campaign year of 2008, the perhumidity index was 22, and therefore identical to the longer-term average.

The 23-year mean rainfall (1986–2008 inclusive) for the DVFC rain gauge is 2840 mm (±438 mm standard deviation). The wettest month is typically January with 310 mm precipitation. April is typically the driest month with 155 mm on average, but it also has the most variable rainfall total with a coefficient of variation (CV) of 69% against

a mean monthly CV of 46%. Indeed, the three-month period from February to April has the least predictable rainfall totals, with CV values all over 57%. This variability in rainfall totals may relate to the period being at the change from the northeast monsoon (approximately November–April) to the southwest monsoon (approximately May–October: Bidin and Chappell, 2006).

Rainfall in 2008 totalled 3220 mm, the fifth wettest year in the 23-year record with 113% of normal rainfall. The magnitude of the seasonal variations in rainfall was the smallest on record with a CV of 23%, against the long-term average monthly CV of 47%. This lack of marked seasonality was also shown in the number of days with rainfall. A total of 257 rain-days, the largest number in the 23-year record, were observed in 2008 against an average of 226 rain-days.

2.3 Campaign meteorology

Most of the OP3 measurements were undertaken within the four-month period of April to July 2008. This period was 124% more wet than normal, with 1045 mm of rainfall. Notably, the driest month according to the longer-term record, April, received 170% of the normal rainfall at 263 mm. The April–July 2008 period was also cooler, with a mean temperature of 27.1 °C, which was 99% of the norm for April–July 2001–2008.

A clear diurnal cycle in the rainfall is observed, even within the records of the relatively short OP3 campaign period of April–July (Fig. 2a). The presence of a late afternoon peak in rainfall at DVFC, which is more pronounced when several years of data are summarised, as in Bidin and Chappell (2006), results from the diurnal development of convective rainfall cells, which is consistent with LIDAR observations (peak rainfall typically observed around 15:00 LT) and measurements of radiation and heat fluxes at the site (Pearson et al., 2010; Helfter et al., 2010). The predominance of rainfall delivery by convective events also results in an extreme localisation of the rainfall field. Within a 5 km^2 region encompassing the summit of Bukit Atur, Bidin and Chappell (2003) demonstrated that inter-gauge correlation in annual rainfall totals fell to 0.90 over distances of only 1.1 km, which is short even by comparison with other convective systems.

Figure 2 also shows median temperatures at various heights at Bukit Atur for the combined periods of OP3-I and OP3-III, measured with aspirated thermocouples. The overall median temperature at 30 m was 25.1±1.6 °C. This is similar to the long-term surface temperature data from DVFC, taking into account a typical temperature gradient with altitude. During the campaign, the atmospheric stability varied from strongly stable at night to strongly unstable during the middle of the day, as would be expected for a convective region with low wind speeds.

When the boundary layer was stable, the rainforest canopy was decoupled from the overlying atmosphere, resulting very frequently in nocturnal radiation fogs. LIDAR data (not shown) demonstrate this, and also suggest a day-time (10:00–18:00 LT) mixing height of ~800 m. The strong

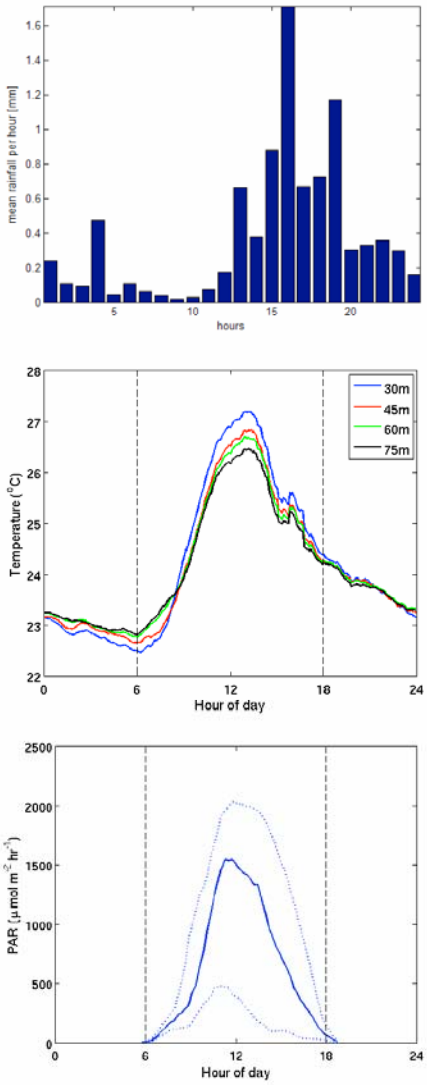

Fig. 2. Local-time diurnal cycles in (top panel) mean rainfall, (middle panel) median temperature at various heights on the Bukit Atur GAW tower, and (bottom) median canopy-top photosynthetically active radiation (PAR), over the OP3 campaign months of April–July 2008. Dashed lines on temperature and PAR graphs show approximate sunrise and sunset times. Dotted lines on the PAR graph show 5th and 95th percentiles.

daytime turbulence, along with weak winds, makes chemical box-modelling a reasonable strategy for interpretation of daytime atmospheric composition (Sect. 5, below), but understanding measurements made at night, when the atmosphere near the surface is strongly stratified, requires more careful consideration of vertical mixing (Pugh et al., 2010a).

The bottom panel of Fig. 2 shows the diurnal cycle in photosynthetically active radiation (PAR), measured at canopy-top height. There is a tail of dull days (shown by the 5th percentile) but, on the whole, the period of the campaign was bright. The warm temperatures and bright sunshine produced substantial emissions of biogenic volatile organic compounds (BVOCs) from the forest (Sect. 4.2.2, below).

Turning from vertical mixing/convective effects, to take a more horizontal/advective view, backwards air mass trajectories were analysed in order to characterise the origins of chemical species measured at Bukit Atur during the measurement campaigns. They were calculated by the British Atmospheric Data Centre (BADC) Web Trajectory Service using European Centre for Medium-Range Weather Forecasts (ECMWF) wind fields. A series of trajectories was calculated, with one trajectory for every hour during OP3-I and OP3-III. These were then analysed to give an ensemble representation of air mass residency time as a function of location for the whole of each campaign (Ashbaugh et al., 1985). Back trajectories are calculated for the 24 h before arrival at Bukit Atur, with a time resolution of 30 min, and a final pressure altitude of 950 hPa. Back trajectories that touch the ground have been removed. Figure 3a and b show air mass residency time on a $0.1° \times 0.1°$ grid for all back trajectories from the first and third campaign periods, respectively.

The first campaign period (OP3-I) was influenced by air masses from most directions, in contrast to OP3-III when the air was predominantly from the south. The southern air in the third period can be split into two main areas of origin: the SE air from the sea with a minimal fetch over land, and the SW air which is exclusively over land. This can be used to identify and compare periods of marine and terrain influenced air. It is possible to extend this analysis by using only trajectories from periods when a certain measurement is elevated, giving a coloured probability distribution of the source of the measured quantity. A subsequent paper will use these techniques to present a more in-depth analysis of chemical origins in the future.

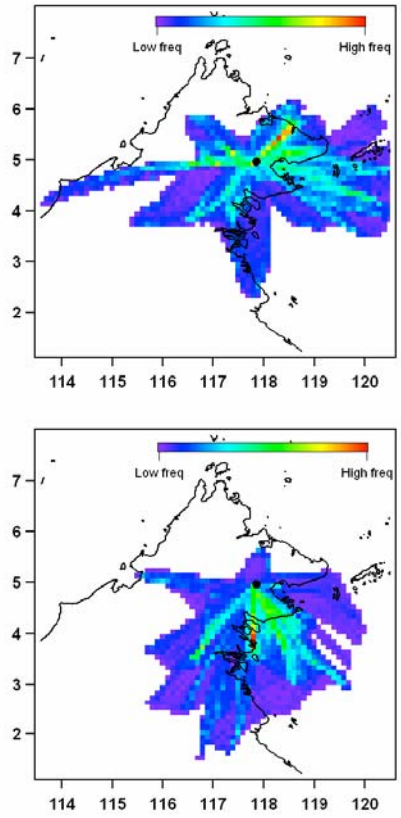

Fig. 3. Air mass residency times for air reaching Bukit Atur (black circle) during (top panel) OP3-I and (bottom panel) OP3-III. No colour means no trajectories passed over that area in the last 24 h.

2.4 Land-cover classification and VOC emissions modelling

Biogenic VOC emissions are highly sensitive to land-cover characteristics and can vary over several orders of magnitude across different landscapes. This is partly due to variability in total biomass density but is greatly enhanced by variability among different plant species, especially for compounds such as isoprene that are emitted by less than a third of all plant species. This presents a daunting challenge for attempts to characterize regional BVOC emissions, especially in highly diverse tropical forests.

Guenther et al. (1995) estimated global biogenic VOC emissions using the highest resolution (0.5°) and most detailed global map of land-cover and land-use (Olson, 1992) available at that time. Figure 4 (top left panel) illustrates the Olson (1992) classification of Borneo landscapes, which include six unmanaged land-cover types, dominated by tropical rainforest (50%), marsh/swamp (14%) and tropical montane (7%) and three managed land-cover types dominated by re-growing woods (9%) and paddy rice (7%). The associated isoprene emission factor map shown in Fig. 4 (top right panel) characterizes the gross features of Borneo but does not represent the full diversity of landscapes in this region. A major limitation of the Olson global ecosystem approach is that, for example, all re-growing woods are lumped together and observations from North American and European forests

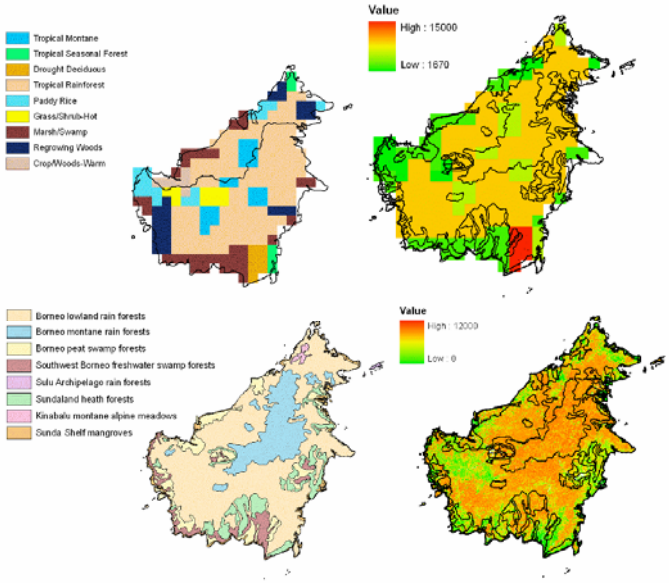

Fig. 4. Land cover distributions for Borneo used by the global biogenic VOC emissions inventory of Guenther et al., 1995) (top left) and by MEGAN (Guenther et al., 2006) (bottom left) and associated isoprene emission factor ($\mu g\, m^{-2}\, h^{-1}$) map used by Guenther et al. (1995) (top right) and by MEGAN (Guenther et al., 2006) (bottom right).

were used to assign a single isoprene emission factor to all occurrences of this land-cover type across the globe. The Guenther et al. (1995) estimate of annual isoprene emission from Borneo is about 10 Tg of carbon, which is 2% of the estimated global total.

The availability of satellite observations has greatly improved quantitative estimates of eco-region distributions and other land-cover variables, including leaf area indices (LAI) and plant functional type (PFT) cover fractions. In addition, the development of a global geo-referenced eco-region map by Olson et al. (2001) represents an additional major advance for biogenic emission modeling. This high resolution digital map is the product of over 1000 biogeographers, taxonomists, conservation biologists and ecologists from around the world. Each of the 867 eco-regions represented on this map has relatively uniform species composition and is accompanied by an online database (http://www.nationalgeographic.com/wildworld/) that includes a description of the dominant plant species. Figure 4 (lower left) shows that this database divides Borneo into seven eco-regions with Borneo lowland rainforests covering just over half of the total land area, Borneo montane rainforests and Sundaland heath forests together comprise about 25%, and the remaining four ecoregions (Kinabalu montane alpine meadows, Borneo peat swamp forests, Borneo freshwater swamp forests, Sunda Shelf mangroves) each make up 1 to 8% of the total. While the total area associated with broad types (e.g. tropical forest, montane forest) agree reasonably well with the Olson (1992) database, the details differ considerably. Figure 4 (bottom right) shows that land-cover results in considerable differences between the isoprene emission factor distribution of Guenther et al. (1995) and the MEGAN model (Guenther et al., 2006) which uses the Olson et al. (2001) eco-region map and satellite derived PFT (e.g. crop, broadleaf tree, shrub) cover fractions. In addition, MEGAN uses plant species composition estimates from the Olson et al. (2001) global terrestrial eco-region database and the Leff et al. (2004) crop species distribution database. Although the spatial pattern is quite different, the annual isoprene emission for Borneo differs by less than 5% when the MEGAN land-cover is used in place of Guenther et al. (1995) land-cover data. This good agreement, however, is the result of major offsetting differences between these two land-cover databases. The Guenther et al. (1995) foliar density and LAI estimates are about 50% higher, resulting in about 25% more isoprene, but the emission factors are about 25% lower. The result is a very similar annual isoprene emission but for different reasons.

The MEGAN framework can be used to estimate regional to global biogenic VOC emissions but the accuracy of the results is dependent on the availability of representative measurements of individual ecoregions. A lack of BVOC

measurements from Borneo resulted in the assignment of MEGAN version 2.1 emission factors to the ecoregions of Borneo that were based on observations from other tropical regions. Improved estimates for future versions of MEGAN and other models are highly dependent on the availability of observations characterizing the dominant plant functional types within major global ecoregions. In fact, our initial analysis of emissions from Bukit Atur show that the default base emission rates in MEGAN prior to the OP3 observations are a factor of four too high for this forest ecoregion. We also confirm that, unusually for a species classified as crop in MEGAN, oil palm is an intense isoprene emitter.

3 Measurement strategy and methods

The overall measurement strategy for OP3 was to perform integrated measurements from the forest-floor, through the forest canopy, above the canopy and then up-scaled to the regional scale using airborne measurements, with clear linkages between measurements made at the different sites at the different scales.

3.1 Ground based measurements

Ground based measurements were centred on the 100 m tower at the Bukit Atur GAW station (4°58′49.33″ N, 117°50′39.05″ E, 426 m a.s.l.) (http://gaw.empa.ch/gawsis/). An "in-canopy" sampling site was established 2 km E of the Bukit Atur tower (4°58′49.10″ N, 117°51′19.12″ E) and a further "oil palm plantation" sampling site was established at the Sabahmas oil palm estate, 70 km NE of Bukit Atur (5°14′58.69″ N, 118°27′15.76″ E).

3.1.1 Forest floor (soil) NO_x flux measurements

The fluxes of NO_x from forest soil were measured using a continuous automated dynamic chamber system at the "in-canopy site". Seven spatially distributed chambers were used in order to represent the spatial variation inherent in soil NO_x emissions at each site. The chamber construction and operation is described in Pilegaard (2001) while the flux calculation method was modified from Conrad (1994), with further details available in Dorsey and Gallagher (2010). In addition, fluxes of nitrous oxide (N_2O) and methane (CH_4) were made at the "in-canopy site", at a near-by undisturbed primary forest site, at a heavily disturbed road-side site and from the soils at the oil palm plantation (see below), using static soil chambers (Siong et al., 2009; Ryder et al., 2010).

3.1.2 Within-canopy concentration profiles

At the "in-canopy site", measurements were made of the vertical gradients (from the ground to 32 m height) of the concentrations of ozone, NO_x, volatile organic compounds, particle size distribution and composition, as well as temperature, relative humidity, radiation and turbulence. Four platforms were strapped against an emergent tree (*Canarium decumanum*), at 8, 16, 24, 32 m. Each platform supported sonic anemometers, inlets to a gradient system for O_3/NO/NO_2 and fine thermocouples. In addition, an automated winch system continuously raised and lowered a temperature/humidity probe, a PAR sensor, an optical particle spectrometer (GRIMM 1.08) and an inlet leading to a PTR-MS. This gave vertical gradient measurements between 2 and 28 m (Ryder et al., 2010). In a clearing near the in-canopy site, LIDAR measurements were made of wind speed and direction and of aerosol backscatter throughout the boundary layer.

3.1.3 Concentration and flux measurements at Bukit Atur

The largest number of ground-based measurements were made at the Bukit Atur GAW station, which routinely records CO_2 and O_3 mixing ratios, and various aerosol parameters. The station consists of a main building with four air-conditioned laboratories at the base of a 100 m tower, all located in a large (~150×50 m) clearing on the top of a hill and surrounded by forest. The surrounding forest canopy extends ~10 m above the base of the tower. Four mobile sea-container laboratories were deployed around the base of the tower to provide extra instrument accommodation. Electrical power was provided by generators, located 2 km E of the station. Pollution events, attributable to individual vehicles arriving on site, the generators, or to small leaks of reactive compounds on site, were identified by elevated concentrations of the oxides of nitrogen and by wind direction analysis, and are excluded from subsequent data analysis. Table 1 summarises the measurements made at Bukit Atur: the critical measurements included:

- eddy covariance and gradient flux measurements of trace gases and particles;
- speciated concentration measurements of trace gases and particles;
- measurements of aerosol size-dependent hygroscopicity and critical supersaturations for cloud growth;
- concentration measurements of OH, HO_2, and the sum of hydroperoxy and organic peroxy radicals;
- OH reactivity measurements (the rate at which OH is removed from the atmosphere);
- characteristics of boundary layer turbulence and mixing.

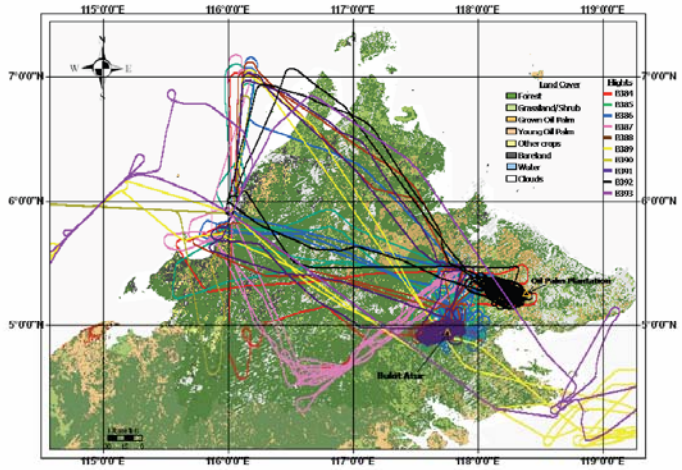

Fig. 5. Flight tracks of the BAe 146 research aircraft over Sabah during OP3-III. The underlying map is as shown in Fig. 1b.

3.1.4 Concentration and flux measurements at the Sabamas oil palm plantation

The Sabahmas oil palm plantation measurement site used during OP3-II was located in a 33 ha flat area of oil palm (*Elaeis guineensis* × *Elaeis oleifera* hybrid, progeny "Guthrie") trees. The trees were of uniform age (12 years) and height (12 m). The site comprised a 15 m tower and an 8 m canopy access platform. Instruments were housed in a hut at the base of the platform. The analytical methods used were the same as at Bukit Atur, including the measurements of aerosol sub-micrometre composition, fluxes of aerosol, BVOCs, ozone and CO_2, although the suite of measurements made was not as comprehensive. In particular, measurements of OH and other radicals and of the oxides of nitrogen were not made.

3.1.5 Airborne measurements

Airborne measurements (see Table 1) were made during OP3-III using the Natural Environment Research Council/UK Meteorological Office's BAe 146–301 Facility for Airborne Atmospheric Measurements (FAAM) aircraft (Lewis et al., 2007), deployed to Kota Kinabalu airport, less than 30 min flying time from Bukit Atur. In general, the same type of flight plan was executed on each flight, with one profile up and one down, interrupted by straight and level runs at altitudes of 100–250, 1500, 3000 and 6000 m above ground over the rainforest (centred on Bukit Atur), over an extensive and homogeneous agro-industrial oil palm landscape surrounding and including the Sabahmas oil palm plantation estate, and in transects between the two sites. Flights were made morning and afternoon giving typically four stacked profiles, allowing a picture to be built up of the concentrations of trace gases and particles during the daytime. Two flights were also made over the ocean up- and down-wind of Sabah.

In order to link the ground-based and airborne measurements, the aircraft flew past the Bukit Atur measurement station on more than ten occasions, at the same height above sea-level as the base of the GAW tower and at approximately 500 m horizontal separation. Table 2 summarises the flights made during the OP3 deployment and Fig. 5 shows the geographical extent of the flights over Sabah.

4 The chemical climatology of Sabah and Bukit Atur

4.1 Satellite observations

Satellite observations of key tropospheric trace gases allow the surface and aircraft trace gas measurements above the rainforest surrounding Bukit Atur to be put in a wider context relative to Borneo and the larger south-east Asian region. We focus on formaldehyde (HCHO) and nitrogen dioxide (NO_2), which are good indicators of emissions and photochemical activity, to examine the atmospheric chemistry over Borneo during the OP3 campaigns in 2008. Global background concentrations of HCHO are determined by the balance between the source (from the oxidation of methane) and the OH sink. Concentrations are typically much larger over continents due to additional sources from the oxidation of biogenic and anthropogenic VOCs, and from biomass burning (either directly released or from the oxidation of co-emitted VOCs) (Palmer et al., 2003; Fu et al., 2007). Anthropogenic activities, biomass burning and soil emissions are the main source

Table 1. Overview of the measurements made in OP3.

Species	Method/ Analytical Technique	Ground†	Air	Temporal Resolution	Detection Limit	Measurement Uncertainty	Reference
NMHC, including isoprene and oxygenates	Disjunct eddy covariance flux measurement with continuous flow and analysis by PTR-MS	√BA, OP		Fluxes: 30 min Mixing ratios: ~7 s	Fluxes: < 0.05 mg m^{-2} h^{-1} Mixing ratios: 10–100 pptv	Fluxes: Precision = ~±30% Mixing ratios ~±10%	(Langford et al., 2009)
NMHC, including isoprene and oxygenates	Automated PTR-MS gradient	√IC		Gradient every 7 min	10–100 pptv		(Karl et al., 2007)
NMHC, including isoprene, monoterpenes and oxygenates	Dual Channel Gas Chromatograph with Flame ionisation detectors (DC-GC-FID)	√BA	√	1 h ground variable air	1 pptv	variable, typically around 10%	(Lewis et al., 2007; Lewis et al., 2005)
Terpenoids, alcohols, aldehydes	GC-PID, portable mass spectrometer	√BA					
CO_2/H_2O flux	Eddy-covariance flux using infrared gas analyser Li-Cor 7000/7500	√BA, OP		30 min fluxes			(Aubinet et al., 2000)
NO_2 flux	Eddy covariance using laser induced fluorescence	√BA		30 min fluxes			(Farmer et al., 2006)
HNO_3, HCl, HNO_2, NH_3, SO_2, NH_4^+, NO_3^-, Cl^-, SO_4^{2-}	Wet effluent denuder & steam jet aerosol collector, online IC (GRAEGOR)	√BA		1 h			(Thomas et al., 2009)
Turbulence, sensible heat flux	Eddy-covariance using sonic anemometry	√BA		30 min fluxes			
Soil NO flux	Dynamic autochamber using NO analyser	√IC					(Pilegaard et al., 2006)

Table 1. Continued.

Species	Method/ Analytical Technique	Ground†	Air	Temporal Resolution	Detection Limit	Measurement Uncertainty	Reference
Soil N_2O/CH_4 flux	Static soil chamber with off-line GC analysis	√IC, OP		1 h			
OH, HO_2	FAGE (Fluorescence Assay by Gas Expansion) laser-induced fluorescence	√BA		10 s	(OH) 2.4×10^5 molecule cm^{-3} (3 min av.) (HO_2) 3.8×10^6 molecule cm^{-3} (3 min av.)	44 % (OH) 50 % (HO_2) (2σ)	(Whalley et al., 2010a, b)
OH, HO_2	FAGE (Fluorescence Assay by Gas Expansion) laser-induced fluorescence		√	60 s	(OH) 2.3×10^6 molecule cm^{-3} (1 min av.) (HO_2) 2.0×10^6 molecule cm^{-3} (1 min av.)	28 % (OH & HO_2) (2σ)	
OH Reactivity	FAGE	√BA		1 min		22 % (2σ)	(Ingham et al., 2009)
$\Sigma RO_2 + HO_2$, HO_2	PERCA (PEroxy Radical Chemical Amplifier), dual inlet	√BA	√	1 min	0.4 pptv (10 min)	38% (1σ)	(Fleming et al., 2006)
NO_3, CH_2O, NO_2, HONO, O_3, CHOCHO	Differential Optical Absorption Spectroscopy	√BA		10min	2 pptv, 480 pptv, 80 pptv, 150 pptv, 4.6 ppbv, 150 pptv	1.5 pptv, 500 pptv, 60 pptv, 130 pptv, 4 ppbv, 130 pptv	(Plane and Saiz-Lopez, 2006)
NO_2, HCHO, CHOCHO	MAX-DOAS	√BA					(Leigh et al., 2006)
Photolysis frequencies (incl. $j(O^1D)$,$j(NO_2)$)	Calibrated filter (2π and 4π sr) radiometers and spectralradiometer	√BA/IC	√	1s	n/a	14% and 13% 0–90° SZA	(Bohn et al., 2008; Edwards and Monks, 2003; Volz-Thomas, et al., 1996)
O_3	UV absorption	√BA	√	1 s	0.6 ppbv	10%±3.4 ppbv ($\pm1\sigma$)	(Heard et al., 2006)

Table 1. Continued.

Species	Method/ Analytical Technique	Ground†	Air	Temporal Resolution	Detection Limit	Measurement Uncertainty	Reference
O_3 flux eddy correlation	Dry chemiluminescence	√BA, OP		30 min fluxes from 0.05 s	0.1 ppbv		(Güsten et al., 1990; Gusten and Heinrich, 1996)
O_3/NO/NO_2 gradient	Chemiluminescence (O_3), thermal converter	√BA/IC		15 min			
NO NO_2 ΣNO_y, ΣNO_y-HNO_3	NO/O_3 chemiluminescence detectors Photochemical convertor + above Gold tube/CO converter + above Gold tube convertor and denuder	√BA		10 min	3 pptv for NO, 7 pptv for NO_2	15% for NO and 20% for NO_2 at 50 pptv	Pike et al., 2009
NO NO_2 ΣNO_y, ΣNO_y-HNO_3	NO/O_3 chemiluminescence detectors Photochemical convertor + above Gold tube/CO converter + above Gold tube convertor and denuder		√	10 s	3 pptv for NO and 15 pptv for NO_2	8% for NO at 1 ppbv and 9% for NO_2 at 1 ppbv	(Brough et al., 2003; Stewart, et al., 2008)
NO_2	Laser-induced fluorescence (LIF)	√BA		1 Hz	3.6 pptv/60 s	20%	(Dari-Salisburgo et al., 2009)
ΣPNs	Thermal-dissociation LIF	√BA		1 Hz	13 pptv/60 s	40%	(Dari-Salisburgo et al., 2010)
ΣANs	Thermal-dissociation LIF	√BA		1 Hz	13 pptv/60 s	40%	(Aruffo et al., 2010)
NO_2 flux	LIF-Eddy covariance	√BA		10 Hz	11 pptv/60s	20%	(Dari-Salisburgo et al., 2010)

Table 1. Continued.

Species	Method/ Analytical Technique	Ground†	Air	Temporal Resolution	Detection Limit	Measurement Uncertainty	Reference
H_2O_2, Σ ROOH	Dual-channel fluorometric detector		√	1 min	50 pptv	14% (1σ)	(Penkett et al., 1995)
H_2O vapour	Dew point hygrometer	√BA	√				
H_2O flux	Eddy-covariance using UV Absorption	√BA		30 min fluxes 100 Hz		8% (q-dependent)	(Coe et al., 1995)
CH_2O	Fluorometric detection (Hantzsh reaction)	√BA		1 min	100 pptv	17% (2σ)	(Still et al., 2006)
Speciated aldehydes, ketones and alcohols NMHC, including isoprene and oxygenates	GC/GC detection, PTR-MS		√	15 s	50–120 pptv	13–16% (1σ)	
>C7 NMHC (e.g. terpenes)	Adsorbent tubes & GC/TOF-MS		√	Variable	50 pptv	±(5%+20 pptv)	(Capes et al., 2009)
CO	Chemiluminesence	√BA	√				(Gerbig et al., 1999)
PAN	GC/ECD (electron capture detection)		√	90 s	5 pptv	5%	(Whalley et al., 2004)
PAN	GC/ECD (electron capture detection)	√BA		10 min	PAN:15 pptv, PPAN, MPAN:25 pptv	20% (2σ)	(Harrison et al., 2006)
Alkyl nitrates, organic N	GC and negative ion CI GC/MS	√BA	√	G: 1 h A: variable	0.005 pptv	13% (2σ)	(Reeves et al., 2007; Worton et al., 2008)
Reactive halocarbons	GC/MS	√BA	√	G: 1 h A: variable	0.005 pptv	15% (2σ)	(Worton et al., 2008)
Halocarbons	GC/ECD	√BA		~ 15 min	~ 0.5 pptv	5–10%	(Gostlow et al., 2009)

Table 1. Continued.

Species	Method/ Analytical Technique	Ground†	Air	Temporal Resolution	Detection Limit	Measurement Uncertainty	Reference
Aerosol number concentration	CPCs total particle number concentration (>3 nm);	√BA	√	30 min (ground) 1 s (aircraft)	N/A	N/A	
Aerosol size distribution	SMPS ground: 3< D_{md} <700 nm Air: 3< D_{md} <350 nm	√BA/IC	√	30 min (ground) 1 min (aircraft)	N/A	N/A	
	Optical and aerodynamic particle counters (0.3/0.1–20/3µm)	√BA/IC	√	30 min (ground) 1 s (aircraft) in-canopy gradients (2–32 m)	N/A	N/A	
Ultra-fine particle fluxes	Eddy Correlation D_p >3 nm, >10 nm, independent CPCs	√BA		Fluxes 30 min. Raw 0.3 s.	< 0.01 particle/cm^3	±10% @ 3×10^5 particles/cm^3.	(Buzorius et al., 1998)
Aerosol size segregated chemical composition	Aerodyne Aerosol Mass Spectrometer (40 nm< D_{vad} < 0.8 µm), non-refractory SO_4^{2-}, NO_3^-, NH_4^+, organic species	√BA, OP	√	30 min (ground) 10 s (profile) 30 s (SLR)	Ground: 3 ng m^{-3} (NO_3^-, SO_4^{2-}) and 11 ng m^{-3} (NH_4^+), 10 min average, high res mode Air: 3 ng m^{-3} (NO_3^-, SO_4^{2-}) and 30 ng m^3 (NH_4^+) 30 s average	15%	Ground: (Aiken et al., 2008; Canagaratna et al., 2007) Aircraft: (Crosier et al., 2007)
Size segregated chemically speciated aerosol mass fluxes	Eddy-covariance using Aerodyne Aerosol Mass Spectrometer. (40 < D_{vad} <800 nm), non-refractory SO_4^{2-}, NO_3^-, NH_4^+, organic species	√BA, OP		30-min fluxes	10 ng m^{-2} s^{-1}	±10 ng m^{-2} s^{-1}	(Nemitz et al., 2008)

Table 1. Continued.

Species	Method/ Analytical Technique	Ground†	Air	Temporal Resolution	Detection Limit	Measurement Uncertainty	Reference
Size-segregated bioaerosol	WIBS	√BA, IC					(Kaye et al., 2005)
Genetic bioaerosol	Genetic analysis of filters	√BA, IC, OP		12-h			
Cloud liquid water	Gerber PVM-100		√	0.1 s	0.005 g m^{-3}		(Gerber, 1991)
Aerosol Scattering properties	3 wavelength nephelometer		√		2 mm^{-1}	5%	(Osborne et al., 2008)
Cloud Condensation Nuclei Activity	CCN spectrometer	√BA (single)	√ (two)	1 h (ground)			(Roberts and Nenes, 2005)
Aerosol hygroscopicity	Hygroscopic Tandem Differential Mobility Analyser	√BA		1 h			(Gysel et al., 2007)
Meteorological parameters (Wind speed & direction, solar radiation, PAR, precipitation, wetness, pressure, temperature, RH, turbulence, sensible heat flux)	Standard meteorological sensors (aspirated thermocouples, Vaisala WXT)	√BA, IC, OP		30 min temperature gradients			
Boundary Layer Height	LIDAR	√BA		1 s	20–60 m		(Pearson et al., 2009)

† – BA=Bukti Atur site; IC=In-canopy site; OP=oil-palm site (OP3-II).

of variability in the tropospheric NO_2 columns (Martin et al., 2002, 2003).

Figure 6a and b shows HCHO and NO_2 column distributions over Borneo during April–July 2008, quantified using UV spectroscopic measurements taken by the nadir-viewing data from SCIAMACHY (HCHO; De Smedt et al., 2008) and OMI (NO_2; ATBD-OMI-02) instruments respectively. NO_2 is a strong absorber at UV wavelengths and, because the OMI instrument provides daily coverage, the NO_2 column data can be averaged onto a fine resolution grid of 1.0°×1.0° (longitude × latitude). In contrast, we average the HCHO columns onto a coarser 2.5°×2.0° grid (to improve the signal-to-noise ratio), since it is a much weaker absorber and because global coverage is only achieved by SCIAMACHY at the Equator every 6 days. Scenes with fractional cloud coverage >40% are excluded from our analysis.

Figure 6b shows that NO_2 measurements from OMI identify anthropogenic NO_x signals from Bangkok, Jakarta, Surabaya and Singapore. Enhanced HCHO also seen over these cities indicates intense photochemical activity, likely associated with polluted conditions. Over Indochina in April, elevated HCHO and NO_2 columns are loosely correlated

Table 2. Overview of aircraft flights made in OP3.

Flight	Flight description	Date in 2008	Take off-Landing Times (UTC)
B384	Survey flight (Bukit Atur, oil palm, SW of Kota Kinabalu)	9 July	02:13–05:32
B385	Bukit Atur (ground sampling site) and SW of Kota Kinabalu	10 July	01:10–05:04 07:04–10:41
B386	Bukit Atur	12 July	01:02–04:48 06:10–9:59
B387	Maliau Basin, S of Sabah. N of Bukit Atur and W of oil palm plantation	13 July	00:54–06:01 06:30–10:10
B388	Bukit Atur and oil palm	15 July	00:54–04:43 06:01–09:33
B389	Ocean flight SE of Sabah	16 July	00:49–04:31 05:39–09:40
B390	CASCADE (Marine flight, W and NW of Sabah)	18 July	22:57–03:14
B391	SW of Bukit Atur, oil palm	19 July	00:54–05:06 06:15–09:48
B392	Mainly oil palm plantation	21 July	00:48–04:46 05:53–09:46
B393	Ocean flight (NW and SE of Sabah)	22 July	00:43–05:10

Local Time is (UTC+8).

with AATSR fire-counts (not shown) (Arino et al., 2005) and hence are probably due to fire emissions (Fu et al., 2007). During May, enhanced HCHO columns over the Gulf of Thailand may reflect outflow from fires occurring in Sumatra and from the Sibu area of eastern Borneo. However, during the OP3 campaigns, fire activity over Malaysian Borneo was minimal and the levels of HCHO and NO_2 were generally low, with their column amounts typically approaching their background values of $\sim 5 \times 10^{15}$ molecules cm^{-2} and $\sim 5 \times 10^{14}$ molecules cm^{-2}, respectively. These low values also suggest that during the OP3 measurement period the HCHO source from biogenic VOC oxidation was weak. We observe a slight HCHO enhancement during April over Danum Valley (Fig. 6a), but it is difficult to assign source attribution.

In Fig. 6c we show the monthly-mean 12-year time series of (continuous) HCHO and (non-continuous) NO_2 columns, retrieved from the GOME and SCIAMACHY instruments (De Smedt et al., 2008; Martin et al., 2002, 2003), together with the total number of fire-counts detected by the ATSR/AATSR instruments (Arino et al., 2001, 2005). High correlations between HCHO and NO_2 columns and the fire-count data suggest that biomass burning over Borneo drives observed variability of these trace gases. We find that anomalously high HCHO and NO_2 columns were due to intense burning periods associated with strong El Nino conditions, indicated here by the Multivariate El Nino Southern Oscillation (ENSO) Index (Wolter and Timlin, 1998), as expected. For example, during 1997/98 an increased number of forest and peat fires during the warmer and drier El Nino conditions (Levine, 1999) led to extremely high trace gas column concentrations.

Our recent analysis shows that spatial correlations between the 12-year HCHO and NO_2 data, and the associated assimilated meteorological data, vegetation activity and fire-counts were strongest in southernmost Borneo and not over the Bukit Atur (Danum Valley) region (Barkley et al., 2009). The low trace gas columns observed over this region during 2008 are consistent with our understanding of past variability.

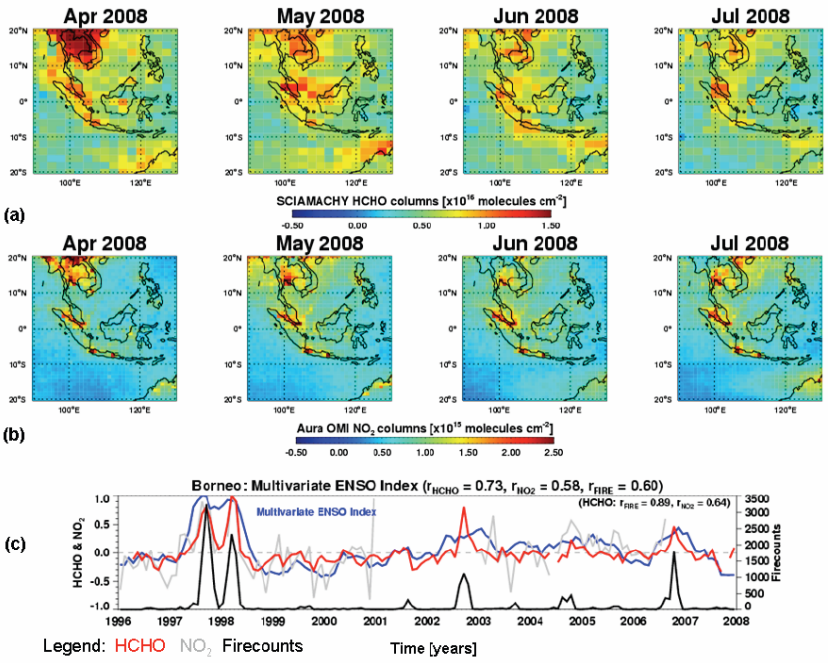

Fig. 6. (a). Monthly averaged SCIAMACHY HCHO columns on a 2.5°×2.0° (longitude × latitude) grid, with cloud coverage ≤40%. **(b)** Monthly averaged OMI NO_2 columns on a 1.0°×1.0° grid, with cloud coverage ≤40%. **(c)** The (deseasonalized and normalized) monthly-mean time series anomalies over Borneo of HCHO (red) and NO_2 (grey) columns retrieved by the GOME and SCIAMACHY instruments (De Smedt et al., 2008; Martin et al., 2002). The total number of firecounts detected by the ATSR/AATSR instruments (Arino et al., 2001, 2005) (black) and the Multivariate El Nino Southern Oscillation Index (MEI) (Wolter and Timlin, 1998) (blue) are also shown. The correlation of the MEI with the HCHO, NO_2 and firecount timeseries is given in the plot-title; the correlation of the HCHO timeseries with NO_2 and firecounts are shown inset.

4.2 In-situ observations

4.2.1 Airborne measurements

The in-situ observations made during the OP3 project were centred on sites representative of natural rainforest and oil palm plantations (see above), with aircraft flights over each landscape and over the up- and down-wind oceans (see above). Figure 7 shows aircraft measurements of six species taken on flights near to the Bukit Atur GAW station and the adjacent oil palm plantations. Data are shown from flights (a) below 500 m above ground level, representative of the boundary layer and (b) above 2500 m, representative of the free troposphere. Also indicated on the plots is the approximate boundary between the natural rainforest and the palm oil plantations.

Within the boundary layer (Fig. 7a), the most striking concentration difference between the rainforest and plantation is for isoprene. Concentrations over the rainforest were typically 1000–3000 pptv, with concentrations over the plantation significantly higher (2–5 times higher; 5000–10 000 pptv). This is consistent with the higher emission rate of isoprene from oil palm trees (*Elaeis guineensis*) compared to most rainforest tree species (Wilkinson et al., 2006). The plantation landscape also contains associated agro-industrial activities (e.g. road traffic, oil palm processing plants and nitrogenous fertiliser application) and as a result, NO_x concentrations were also higher compared to the rainforest. However, whereas the higher isoprene concentrations observed tended to be in the west of the oil palm plantation area, higher NO_x levels were concentrated in the north and east of the plantation area, where the majority of plantation processing plants were observed to be situated. In this area, typical NO_x levels were 1000–1500 pptv, with up to >2000 pptv observed when flying through or close to the plume of a processing plant. Further south in the plantation area, closer to the boundary with the rainforest, NO_x was much lower, with levels typically <300 pptv, which is similar to levels that are observed over the rainforest.

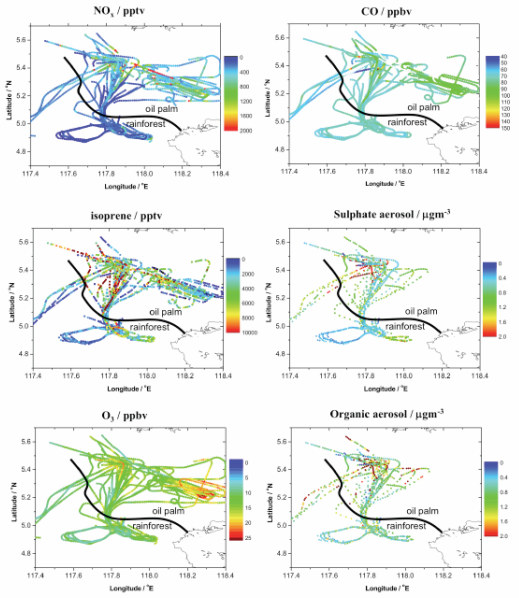

Fig. 7a. Flight track of all data collected from the aircraft below 500 m (above ground level), coloured by NO_x, isoprene, ozone and organic/sulphate aerosol concentrations.

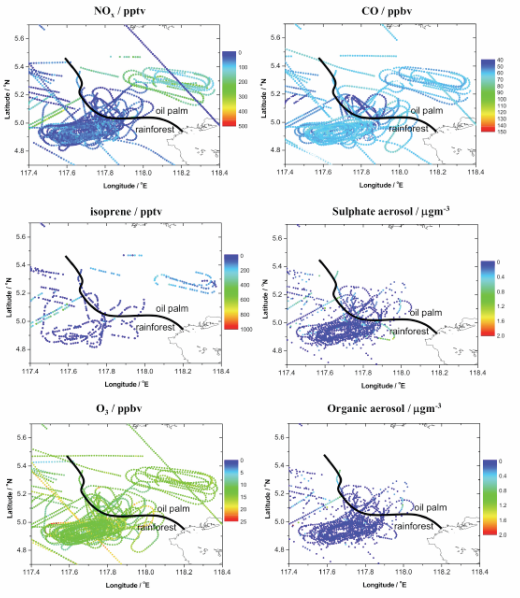

Fig. 7b. Flight track of all data collected from the aircraft above 2500 m (in the free troposphere), coloured by NO_x, isoprene, ozone and organic/sulphate aerosol content.

CO shows a similar behaviour to NO_x, with higher levels (100–110 ppbv) observed over the northern and eastern plantation area compared to further south and over the rainforest (70–90 ppbv). Levels of sulphate aerosol show little difference between the two land use areas, with both exhibiting aerosol loading of 0.25–1 $\mu g\,m^{-3}$.

The result of the increased levels of primary pollutants over the oil palm plantation compared to the rainforest can be seen in the observed ozone, a species that is not directly emitted into the atmosphere but produced photochemically. Ozone was significantly higher (20–25 ppbv) over the eastern area of oil palm plantation, corresponding to the area where NO_x was generally higher. Over the western area of oil palm plantation, where NO_x levels are lower but isoprene levels are still high, and over the natural rainforest, where both NO_x and isoprene are lower, ozone is observed to be 8–15 ppbv. This demonstrates the need for increased NO_x emissions, as well as isoprene, in order for significant extra ozone production to occur (Hewitt et al., 2009). More organic particulate was observed over the oil palm plantation than the rainforest, with average loadings of 0.67 $\mu g\,m^{-3}$ and 0.48 $\mu g\,m^{-3}$ respectively, which is consistent with our ground based measurements (see below) and could be due to enhanced production of secondary organic material, although primary emissions from the processing plants and human settlements may also be contributing.

In the free troposphere (Fig. 7b), very little isoprene or sulphate aerosol was observed over either the rainforest or plantation and levels of CO were similar over both areas (~50–60 ppbv). NO_x levels were higher in the eastern plantation region (200–300 pptv) compared to the rainforest (<50 pptv); however this did not lead to increased ozone in the free troposphere over the plantation. This is likely to be due to the very low levels of isoprene and other biogenic VOCs, which do not have a long enough lifetime to escape the boundary layer. Organic aerosol was also very low over both plantation and rainforest in the free troposphere, with an average organic loading of 0.03 $\mu g\,m^{-3}$.

As described above, some flights were also undertaken over the ocean, both upwind and downwind of Sabah. Levels of isoprene and NO_x were very low in both cases and there was no obvious enhancement in ozone in the upwind flights. These data were collected on only two days; however our initial interpretation of this is that Sabah is not a large exporter of primary or processed pollutants to the wider region.

4.2.2 Bukit Atur measurements

Data were taken within the rainforest at the Bukit Atur GAW station during two four-week intensive measurement periods (OP3-I and OP3-III). The GAW station has made ozone measurements since January 2007 and these data are shown in

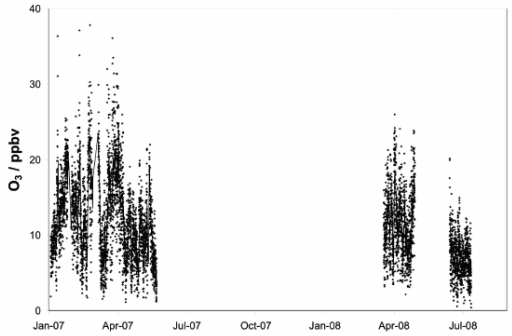

Fig. 8. Ground level ozone concentrations measured at the Bukit Atur GAW site 2007–2008. Data are shown as hourly points with a 24 h running average.

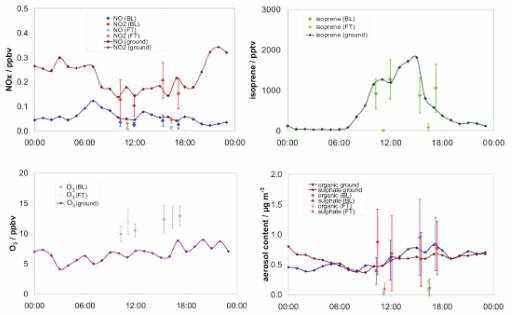

Fig. 9a. Average diurnal concentration profiles for NO_x, isoprene, ozone and organic/sulphate aerosol content for the Bukit Atur ground site and aircraft data taken over surrounding rainforest below 500 ms above ground level (BL) and in the free troposphere above 2500 m (FT). The error bars on the aircraft data indicate 1σ standard deviations for data taken on the four flights.

Fig. 8. Gaps in the data are due to lightning strikes rendering the instrument inoperable. However the plot shows that the levels of ozone observed during the OP3 intensive periods in 2008 are typical for the site.

Campaign daytime (10:00–14:00) average isoprene and total monoterpene fluxes measured at 75 m on the GAW tower were 1.2 and 0.3 mg m^{-2} h^{-1} respectively during OP3-I and 2.1 and 0.49 mg m^{-2} h^{-1} during OP3-III (Langford et al., 2010). These values were comparable to measurements made above regions of the Congo during the EXPRESSO field campaigns (Greenberg et al., 1999; Klinger et al., 1998; Serca et al., 2001) and are somewhat smaller than values reported above regions of the Amazon (Karl et al., 2007; Kuhn et al., 2007). The typical monoterpene to isoprene ratio was between 0.2–0.25, which is within the upper range of ratios reported in other tropical regions (Guenther et al., 2008). The fluxes of other biogenic VOCs, including methanol, acetone and acetaldehyde, were very much smaller, accounting for just 2% of the total measured VOC emissions.

Figure 9a shows hourly averaged median diurnal cycles for NO, NO_2, O_3, isoprene and sulphate and organic aerosol mass concentration, taken at Bukit Atur during June and July 2008. Only data from the six days when flights took place over the station were used in the averaging for a direct comparison between the ground-based and aircraft data in the boundary layer and free troposphere over the rainforest. Note that since Bukit Atur is on a ridge, some of the boundary layer data collected by the aircraft over the surrounding forest were at the same or lower altitude (above sea level) as the GAW tower.

For NO, a peak of ~100 pptv was observed between 07:00 and 08:00 local time, which corresponds to the onset of NO_2 photolysis. This was followed by a drop to ~40 pptv by 11:00, with NO then remaining fairly constant throughout the day, until a further drop to ~20 pptv occurred at around 17:00. NO then remained constant throughout the night. NO_2 exhibits a clear diurnal cycle peaking at around midnight at 300 pptv, with a minimum of ~150 pptv in mid-afternoon. These values are comparable to NO_x measurements made in Amazonia (e.g. Ganzeveld et al., 2008) and over West Africa during the AMMA experiments (e.g. Saunois et al., 2009).

Boundary layer aircraft measurements of NO and NO_2 were in reasonable agreement with the ground based measurements, although airborne NO levels were consistently lower. This, along with the non-zero night-time levels, suggests a local NO source that was diluted throughout the boundary layer. NO and NO_2 levels in the free troposphere were much lower, being <10 pptv and ~20 pptv, respectively. A full description of ground level NO_x data and discussion of the chemistry is given by Pike et al. (2009) and Pugh et al. (2010b).

Isoprene was the most abundant terpenoid compound observed and showed a clear diurnal cycle with very low (<40 pptv) levels at night and a peak of ~2000 pptv in mid afternoon. This was caused by the dependence of isoprene emission from trees on temperature and light (Guenther et al., 1993). Boundary layer isoprene measurements from the aircraft were in good agreement with the ground-based Bukit Atur measurements, and free tropospheric isoprene levels were, as expected, very low. Limonene, alpha-pinene and beta-pinene were the most abundant monoterpene compounds observed. Relatively high concentrations of 2-ethyl hexanol and some aldehydes were also seen in samples taken from within the forest canopy in the vicinity of Bukit Atur.

The concentrations of NO_2, peroxy nitrate (RO_2NO_2) and alkyl nitrate ($RONO_2$) were measured at Bukit Atur with a laser induced fluorescence system (Aruffo et al., 2009). The diurnal cycle of RO_2NO_2 followed the isoprene diurnal cycle, with maximum concentrations in the afternoon. Since

RO_2NO_2 compounds are produced in the oxidation of isoprene and other terpenoids, this result provides evidence for the oxidation of BVOC in the vicinity of the forest canopy. Additional evidence for the active photochemical processing of isoprene is provided by the increase in concentrations of its oxidation products, methyl vinyl ketone and methacrolein, observed in the afternoons.

The concentrations of HO_2+RO_2 were measured at Bukit Atur using PEroxy Radical Chemical Amplification (PERCA) technology (Karunaharan et al., 2009) over 20 days in OP3-I and 29 days in OP3-III. Mean midday mixing ratio of 33.5±3.3 and 35.5±3.5 parts per trillion (pptv) were calculated from the continuous measurements of the sum of the inorganic and organic peroxy radicals from OP3-I and OP3-III respectively. The mean net ozone production rate may then be calculated using:

$$N(O_3) = k_p[NO][HO_2 + RO_2] - \{f \cdot j(O_1D) + k_1[OH] + k_2[HO_2]\}[O_3]$$

where k_p is a combined rate coefficient for the oxidation of NO to NO_2 by all peroxy radicals and $f \cdot j(O_1D)[O_3]$ represents the fraction of ozone photolysed to yield $O(_1D)$ atoms and then OH (with f being the proportion of $O(_1D)$ atoms which react with H_2O to give OH rather than being collisionally deactivated). The rate constants k_1 and k_2 are from the ozone loss reactions:

$$OH + O_3 = HO_2 + O_2 \quad (R1)$$

$$HO_2 + O_3 = OH + 2O_2 \quad (R2)$$

The net formation of ozone was found to be strongly dependent on the concentration of isoprene, having a linear sensitivity (e.g. $d\ln(P(O_3))/d\ln(\text{isoprene})=1$). Since HO_2+RO_2 are produced during the oxidation of isoprene and other terpenoids, taken together with the observations of MVK and methacrolein formation, this result provides evidence for the oxidation of BVOC in the vicinity of the forest canopy and of the role of isoprene in the formation of ozone in the near-canopy environment during the daytime.

Evidence of BVOC reactivity also comes from differential optical absorption spectroscopy (DOAS) measurements. DOAS was used at Bukit Atur to make the first measurements in a tropical rainforest of glyoxal (CHOCHO), one of the major products of isoprene oxidation by OH. Mixing ratios much higher than in other rural locations were observed, with a maximum of 1.6 ppbv and average around 600 pptv. HCHO was also measured, peaking at 4.5 ppbv and with an average around 3 ppbv. Both species were closely correlated to isoprene (which should be their major source in this environment), and peaked in the early afternoon. A box model indicates that the production efficiency of glyoxal from isoprene is ∼10%. Although glyoxal was significantly scavenged during rain showers, it is mostly removed by reaction with OH and photolysis (lifetime at midday ∼2.3 h) rather than uptake on background aerosol in this environment, because, as discussed earlier, aerosol mass loadings were low.

There was a slight diurnal trend in ground-based O_3 measurements, with levels of ∼5 ppbv at 06:00, rising to ∼8 ppbv in mid afternoon. Note that the very small amplitude in the diurnal pattern is typical of a hill-top site (Fowler et al., 2008) and contrasts with that observed at the in-canopy site and over the low-lying palm plantations (see below). These values are comparable to above canopy measurements made above regions of Amazonia (Karl et al., 2007). Boundary layer O_3 levels also show an increase throughout the day, but at higher levels (10–13 ppbv), probably because the boundary layer O_3 is less depleted by deposition to the canopy (Matsuda et al., 2006; Cros et al., 2000). These boundary layer values are slightly less than those measured over Amazonia and West Africa during the GABRIEL and AMMA campaigns (Ganzveld et al., 2008; Saunois et al., 2009). There is little vertical structure in the O_3 mixing ratio at higher heights above the rainforest, with levels in the free troposphere being very similar to those in the boundary layer. Ozone vertical profiles were therefore more like those observed during the monsoon over northern Australia, than those observed during monsoon break periods (Heyes et al., 2009).

Concentrations of OH display a clear diurnal cycle, peaking at solar noon, with significant concentrations observed: up to 8.7×10^6 molecules cm^{-3} (60 min average) was recorded on one day. During the GABRIEL campaign above Amazonia, average midday boundary layer OH concentrations were 5.75×10^6 molecules cm^{-3} (Martinez et al., 2008). Although $j(O^1D)$ levels and humidity were high, the relatively low O_3 concentrations limit primary OH production. The measured OH reactivity was very high, up to 87 s^{-1} (corresponding to a lifetime for OH approaching 10 ms). According to the measurements of reactive hydrocarbons (above), this reactivity is dominated by reaction with isoprene, indicating that significant OH sources must be present – in addition to primary production following ozone photolysis – in order to maintain the elevated levels of OH levels recorded (Whalley et al., 2010b). The OH diurnal profile was asymmetric (i.e., lower post-noon than the equivalent time pre-noon). This may be due to its main measured sink, isoprene, being present at higher concentrations in the afternoon, but the asymmetric profile could also result from other factors that have yet to be identified. OH concentrations up to 6×10^5 molecule cm^{-3} (60 min average) were also recorded on several nights, consistent with measurements by other groups in forested environments (Tan et al., 2001), with some residual OH observed after $j(O^1D)$ had dropped to zero. Measured concentrations of HO_2 and the sum of HO_2+RO_2 displayed similar profiles.

Boundary layer OH concentrations recorded on the aircraft over Bukit Atur were similar to those measured at ground level, whereas aircraft HO_2 concentrations were higher than measured at the ground, a reflection of the elevated NO levels

at the surface. A full description of the OH, HO_2 and OH reactivity measurements is given in Whalley et al. (2009, 2010a) and Edwards et al. (2009, 2010).

The non-refractory sub-micrometre aerosol as measured by aerosol mass spectrometry at the Bukit Atur ground site was mostly composed of organics, sulphate, and ammonium, with low levels of nitrate and chloride. Average loadings were 0.74, 0.61, 0.21, 0.04 and 0.01 $\mu g\,m^{-3}$, respectively, giving a total aerosol loading of 1.61 $\mu g\,m^{-3}$. The sulphate was observed to be largely neutralised to ammonium sulphate. Organics showed a diurnal profile peaking around 21:00. The ensemble organic spectrum had a m/z=44 to total organics ratio of 0.15%, with prominent peaks at m/z=55 and 53, features which would be considered typical of a partially oxygenated organic aerosol (e.g., Hallquist et al., 2009). The sulphate showed no distinct diurnal profile, suggesting it was regional in nature, potentially from the anthropogenic background, volcanoes or oxidised dimethyl sulphate originating from marine phytoplankton (Dacey and Wakeham, 1986). Of all the gas and aerosol species measured at Bukit Atur, sulphate aerosol most clearly showed the influence of regional-scale transport rather than local sources and sinks. Both nitrate and chloride showed strong nocturnal peaks that could be caused by partitioning from the gas phase as the temperature falls and humidity increases at night.

Slightly larger aerosol concentrations were measured from the aircraft than the ground, both over the rainforest and oil palm, with mean total loadings in the boundary layer of 1.66 and 1.78 $\mu g\,m^{-3}$, respectively. Aerosol loadings were much lower in the free troposphere, with an average total of 0.22 $\mu g\,m^{-3}$. Free-tropospheric aerosol showed a larger sulphate contribution of 69%, compared with 43% in the boundary layer.

The water uptake ability of the atmospheric aerosol at Bukit Atur was probed in both the sub- and super-saturated regimes with the use of a Hygroscopicity Tandem Differential Mobility Analyser (HTDMA; Cubison et al., 2005; Gysel et al., 2007) and Cloud Condensation Nucleus counter (CCNc; Roberts et al., 2005), respectively. Aerosol hygroscopic growth factors (GF) at 90% relative humidity (RH) for particles of dry diameter (D_0) from 27 to 217 nm showed the aerosol to be externally mixed, with a mean growth factor ($GF_{D0,90\%}$) ranging between 1.3 and 1.6 with increasing dry diameter and multiple growth factor modes at each dry size evident. A Scanning Mobility Particle Analyser (SMPS; TSI 3080) was operated upstream of the CCNc, to supply quasi-monodisperse aerosol in the size range 30 to 220 nm. Critical supersaturations (S_c) derived from fraction activated CCN spectra, showed a diurnal variation in supersaturation between 0.2 and 0.8% required to activate particles of a given D_0, primarily in the dry diameter range 50 to 120 nm.

4.2.3 Oil palm plantation measurements

Campaign daytime average (10:00–14:00) isoprene fluxes measured at 15 m at the Sabahmas oil palm plantation site were 8.6 $mg\,m^{-2}\,h^{-1}$ during OP3-II (Misztal et al., 2010a). This is four to seven times greater than the isoprene flux measured at Bukit Atur (see above). The fluxes of other biogenic VOCs, including oxygenated species and more exotic compounds (e.g. estragole: Misztal et al., 2010b), were smaller, contributing ~15% of the total measured VOC emissions. Net fluxes of monoterpenes were very small (<1% of total VOC flux).

Figure 9b shows diurnal cycles of data taken at the ground-based site within the Sabahmas oil palm plantation. Species plotted are the same as for the Bukit Atur rainforest ground site, with the exception of NO and NO_2 which were not measured at ground level at Sabahmas. Boundary layer NO and NO_2 levels show slightly higher levels compared to the rainforest but the scatter on the data (indicated by the 1σ error bars) is much larger. This is indicative of the high NO_x concentrations observed in certain areas of the plantation landscape, as described above. Free troposphere NO and NO_2 levels over the plantation were again much lower and very similar to those observed over the rainforest.

Ground based isoprene data show a similar diurnal cycle to the rainforest, with near zero levels at night, but with an earlier peak at around 12:00. Isoprene concentrations are much higher in the plantation, with peak daytime levels of ~16 000 pptv. Isoprene concentrations in the boundary layer over the plantation show a very similar diurnal profile, but with a significantly lower peak of ~5000 pptv. The ground-based measurements were made at the top of the oil palm canopy, and hence this difference may be explained by dilution. Also, since the oil palm plantations are generally situated in low-lying, flat land, the aircraft measurements were always made at a significant height above the ground level measurements, unlike at Bukit Atur where the aircraft was able to fly past the base of the GAW tower, located on a hill.

Measurements of O_3 at the ground in the plantation exhibit a very different diurnal cycle compared to the rainforest, with near zero night-time concentrations and a peak of ~5 ppbv at 11:00–12:00. This is followed by a steady decrease throughout the day until O_3 reaches close to zero at around 23:00. This general pattern is typical of that for a low-lying site, where O_3 lost by reaction with NO emitted from fertilised plantation soils and deposition at night is not replenished by mixing from aloft, due to the more ready establishment of a stable boundary layer compared with elevated, more windy, sites (Fowler et al., 2008). Data taken in the boundary layer above the plantation show a similar diurnal cycle to the rainforest, with an increase throughout the day to a peak of ~15 ppbv. This mean value is 2 to 3 ppbv higher than the rainforest levels, but as indicated by the 1σ error bars there is scatter in this value, which reflects the variability in the NO_x and its impact on O_3 concentrations. Increased

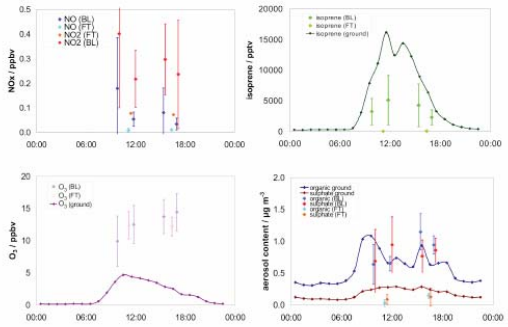

Fig. 9b. Average diurnal profiles for isoprene, ozone and organic/sulphate aerosol content for the oil palm plantation ground site and aircraft data (also with NO_x) taken over surrounding oil palm plantations and below 500 m above ground level (BL) and in the free troposphere above 2500 m (FT). The error bars on the aircraft data indicate 1σ standard deviations for data taken on the four flights.

deposition to the oil palm trees, reaction with NO_x from local sources, and reaction with isoprene, are three possible contributing factors for the low concentrations and earlier peak of day-time O_3 observed on the ground in the plantation.

The total aerosol loading, as measured by the AMS, at the oil palm site was on average 1.6 µg m ^{3}, similar to the aerosol loading measured by AMS at the forest site (Nemitz et al., 2009, 2010). The mass was dominated by organic aerosol, which made up on average 65% of the total mass, with sulphate contributing 20% of the total mass. The organic aerosol exhibits a clear diurnal trend with two maxima, occurring at approximately 08:00 and 15:00 local time. The ensemble mass spectrum measured at the oil palm resembles the classic oxygenated organic aerosol spectrum (e.g. Hallquist et al., 2009), dominated by mass fragment *m/z* 44, resulting from carboxylic acid functionality. An examination of mass fragment-specific diurnal profiles indicates that fragments thought to be associated with less oxygenated organic aerosol make a smaller contribution to the afternoon maximum in the organic mass relative to those masses arising from oxygenated fragments, e.g. *m/z* 44.

Sulphate aerosol shows a slightly different trend in mass to the total organics, with a broader maximum during the daytime, although there was large day-to-day variability. Both the nitrate and chloride fractions showed an obvious maximum, coincident with the morning organic aerosol maximum, but both lacked the increase in mass observed in the organic fraction during the afternoon.

5 Modelling and assessment

As stated in the introduction above, a fundamental aim of the OP3 project was to understand the role played by biogenic emissions from the tropical rainforest: what is the nature of the emissions, how are they transformed and how do these processes then impact local, regional and hemispheric scale atmospheric chemistry; what will be the implications of global change for these processes and their impacts?

To address these questions, the OP3 project employed a range of models, varying in their spatial scale of interest and chemical complexity, as shown in Table 3. Thus, a model of transport and chemistry through and above the forest canopy has been used to address the canopy measurements, to study vertical transport of gas and aerosol species, their emission and deposition, and chemical transformation (Ryder et al., 2009). A range of chemical box models (some run along air parcel trajectories) has been employed to study local chemistry, addressing both the ground based and aircraft measurements. These very detailed models aim to inform the chemical mechanisms used in our regional and global models that, in turn, are used to study the impact of the biogenic emissions at the regional and wider scales. They are also used to investigate transport and variability.

Understanding the fast photochemistry processes (mainly involving HO_x and RO_x) is carried out using constrained box models. These use the observed concentrations of species providing HO_x sources, sinks and inter-conversion pathways, to calculate the concentrations of OH, HO_2 and other short lived species such as the sum of peroxy radicals (RO_2), for comparison with observations. Insight from these calculations allows our understanding of the complex organic chemistry occurring in this region to be evaluated, the level of chemical complexity required to capture these processes to be quantified and the impact of the approximations made in the chemical transport models to be evaluated.

The constrained-box-model focus is split between the ground-based and aircraft data. One investigation has used the Master Chemical Mechanism, a near-explicit mechanism that considers the degradation of a suite of hydrocarbons in the atmosphere (Jenkin et al., 2003; Saunders et al., 2003). For both ground and aircraft data, a zero-dimensional box model is constrained with the observed concentrations of longer-lived species such as hydrocarbons, NO_x, O_3, relevant meteorological data and observed photolysis rates; the models predict radical concentrations which can be compared with those measured. The ground-based model is a continuation of a previous modelling framework (e.g. Emmerson et al., 2007) that has been used extensively for similar comparisons (Heard and Pilling, 2003). The aircraft based model uses the Dynamically Simple Model of Atmospheric Chemical Complexity (DSMACC) (Emmerson and Evans, 2009) model and follows previous aircraft based work (Jaegle et al, 2000; Olson et al., 2006). Preliminary results show that for the first (April–May) ground-based campaign,

Table 3. Modelling tools employed in the OP3 project.

Model name	Brief description	Domain	References
Canopy model	1-D transport and chemistry	Ground to canopy top – six levels	Ryder et al. (2009)
MCM – York	4500 species, >12 500 reactions. Near-explicit chemistry; long lived gases constrained by observations	Ground-based box	Emmerson et al. (2007)
Dynamically Simple Model of Atmospheric Chemical Complexity (DSMACC)	Reduced chemistry; long lived gases constrained by observations	Steady state calculations along aircraft flight track	Emmerson and Evans (2009)
CiTTyCAT	200 species, >800 reactions including MIM2 isoprene scheme, Jenkin alpha-pinene and RACM limonene	Boundary layer: one well-mixed layer in daytime, two at night.	Pugh et al. (2010b)
Cambridge p-TOMCAT chemical transport model	63 species, 177 reactions. Simple organic mechanism, including isoprene. Separate bromocarbon scheme.	Global. Variable resolution, usually $3^{\circ}\times3^{\circ}$ or $0.5^{\circ}\times0.5^{\circ}$	Cook et al. (2007), Voulgarakis et al. (2009)
p-TOMCAT box	As above	Box model	Pike et al. (2009)

there is reasonable agreement between modelled and measured OH on some days, but an under-prediction on others. The OH loss for the OP3 campaigns was dominated by isoprene chemistry, with smaller contributions from γt terpinene and limonene. γ-Terpinene becomes much more important at night-time, when isoprene emissions are effectively zero. Modelling of the aircraft data is in a more preliminary state but shows relatively good agreement between the observed and simulated HO_2 with poorer agreement for the OH. Whether this reflects issues with making OH observations from aircraft or with our understanding of the chemistry of isoprene will require further analysis.

Reduced chemical mechanisms, of the kind traditionally employed in global chemical transport models, have also been used in box model mode, to compare against the measured constituent data and to investigate the significance of processes. Thus, the CiTTyCAT model (Wild et al., 1996; Evans et al., 2000; Emmerson et al., 2004; Donovan et al., 2005) has been used to study the chemical regimes probed by the OP3 measurements, both over the rainforest and over palm oil plantations, and to explore how local air quality could be affected should palm oil (a major isoprene-emitter) become an even more dominant crop, replacing the rainforest. Hewitt et al. (2009) show that under these circumstances, what happens to local and regional-scale emissions of NO_x will be crucial. Without control of NO_x emissions, the levels of ozone could become unacceptably high, damaging both crop and human health.

We find that CiTTyCAT can represent the broad features of atmospheric composition above a tropical rainforest (Pugh et al., 2010a). In particular, the model can fit daytime NO_x and O_3 chemistry. Ambient concentration measurements have been used to estimate a net NO flux of 5 $\mu g\,N\,m^{-2}\,h^{-1}$. Deposition of intermediate VOC oxidation products can have a very significant influence on their concentrations and the chemistry of the boundary layer, highlighting the need for further investigation into deposition processes over tropical forests.

Another box model study with a reduced chemical mechanism has focussed on the ground-based measurements of ozone and NO_x (Pike et al., 2009). This study suggests that the chemical mechanism included in the Cambridge global chemistry transport model, p-TOMCAT (Cook et al., 2007; Voulgarakis et al., 2009a, b) can reproduce the measurements

if a parametrization of mixing out of and into the boundary layer is included.

The Cambridge p-TOMCAT global model has been used to look at regional-scale chemistry. Figure 10 (Pike et al., 2009) shows surface ozone concentrations from two calculations for April 2008, with the model run at two different spatial resolutions (approx $3^{\circ}\times3^{\circ}$ and $0.5^{\circ}\times0.5^{\circ}$, respectively). At the lower resolution (typical of multi-annual integrations), the model significantly overestimates surface ozone over Borneo. Little spatial structure is evident and detailed flight track comparisons (not shown) fail to reproduce much observed structure. In contrast, at the high resolution, the model now captures a significant land – sea difference in surface ozone, driven by deposition over the land. Modelled ozone concentrations are still somewhat higher than observed but are now closer to the observations.

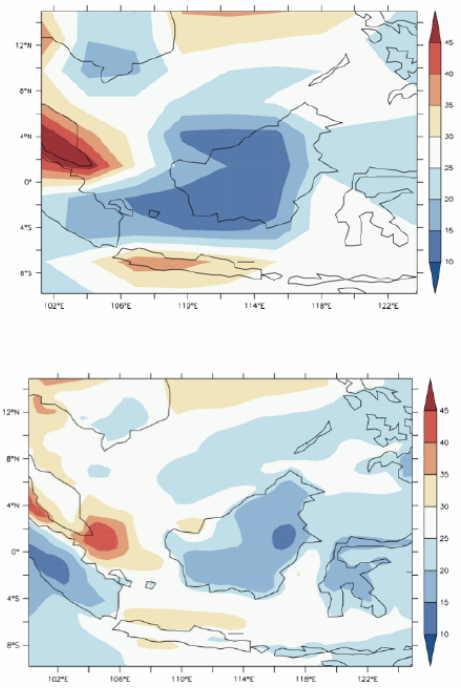

Fig. 10. Mean surface ozone concentrations (ppbv) for April 2008 taken from two integrations of the Cambridge p-TOMCAT chemical transport model. The upper plot shows mean ozone from an integration at 3×3 degrees horizontal resolution. At this resolution, Borneo is poorly represented and ozone is over estimated. The lower plot shows the same result but when the model is run at 0.5×0.5 degree horizontal resolution. Ozone concentrations have improved and there is a noticeable land-sea difference consistent with the shape of the island.

6 Conclusions

The overall aim of the OP3 project was to better understand the interactions that exist between SE Asian rainforests, atmospheric composition and, ultimately, the Earth's climate system. In pursuing this aim, an extensive field deployment was carried out in 2008, supported by satellite data retrievals and modelling studies. The field deployment, from April to the end of July 2008, comprised extensive composition and flux measurements within and above the rainforest canopy, along with a more limited set of measurements in and above an oil palm plantation. Composition measurements across most of the state of Sabah in northern Borneo, and out to sea on both windward and leeward sides of the island, were provided by flights of the FAAM BAe 146. Remote sensing of land cover has shown that the chosen sites were representative of large areas of Borneo and the rest of insular SE Asia; long-term meteorological and ozone data gathered as part of the Global Atmosphere Watch programme show that weather and ozone mixing ratios during the time period of the field deployment were typical of the long term record.

Composition measurements show that the rainforest site was not impacted significantly by anthropogenic pollution, and this is confirmed by satellite retrievals of NO_2 and HCHO. The dominant modulators of atmospheric chemistry at the rainforest site were therefore emissions of BVOCs and soil emissions of reactive nitrogen oxides. At the observed BVOC:NO_x volume mixing ratio (∼100 pptv/pptv), current chemical models suggest that daytime maximum OH concentrations should be ca. 10^5 radicals cm^{-3}, but observed OH concentrations were an order of magnitude greater than this. We confirm, therefore, previous measurements which suggest that an unexplained source of OH must exist above tropical forests (Lelieveld et al., 2008) and continue to interrogate the data to find explanations for this.

Marked differences in BVOC and NO_x concentrations, and in BVOC fluxes, were measured in the rainforest and the oil palm plantation. By an accident of the non-linearity of boundary-layer chemistry, ozone mixing ratios over the two landscapes were similar, although plumes of higher ozone were observed in air impacted by emissions from oil-palm processing plants.

The land-sea mosaic of SE Asia makes it difficult for global atmospheric chemistry-and-transport models run at typical resolution to capture the observed atmospheric composition; runs at higher horizontal resolution provide much better agreement with measurements. A missing OH source notwithstanding, simple chemistry schemes, as currently implemented in most global models, can match observed ozone and NO_x diurnal patterns, if a parametrization of mixing out of and into the boundary layer is included.

Overall, the SE Asian rainforest has shown itself to have significant differences from the more intensively studied

Amazon rainforest – in tree speciation and, hence, in BVOC emission potential, and in the apparent lack of seasonality of emissions. It also exhibits significant differences to the oil palm plantations that are replacing it. A striking similarity, however, is the sustained oxidative capacity of the atmosphere above the rainforest in both SE Asia and Amazonia. Our current inability to adequately explain this limits the confidence we can have in our projections of how atmospheric composition and climate may change in the future.

Acknowledgements. The OP3 project was funded by the UK Natural Environment Research Council (NE/D002117/1). Measurements made during OP3-II were, in part, performed as part of the ACES (Aerosol Coupling in the Earth System; NE/E011179/1) project of the NERC APPRAISE (Aerosol Properties, PRocesses And Influences on the Earth's Climate) programme. We thank the Malaysian and Sabah Governments for their permission to conduct research in Malaysia; the Malaysian Meteorological Department (MMD) for access to the Bukit Atur Global Atmosphere Watch station and their long term ozone record; Leong Chow Peng (formerly of MMD) for her support in the early stages of the project; Wilmar International Ltd (and particularly Simon Siburat and his staff) for access to and considerable logistical support at their PPB Oil Palms Bhd Sabahmas Estate; Waidi Sinun of Yayasan Sabah and his staff and Glen Reynolds of the Royal Society's South East Asian Rainforest Research Programme and his staff for logistical support at the Danum Valley Field Centre; the ground staff, engineers, scientists and pilots of the UK Natural Environment Research Council/UK Meteorological Office's BAe 146-301 large atmospheric research aircraft; the NERC Facility for Ground-based Atmospheric Measurements and Halo Photonics for support with the LIDAR deployment; Phua Mui How of the Universiti Malaysia Sabah for his help with the land cover map; and the rest of the OP3 project team for their individual and collective efforts. Isabelle De Smedt and Michel Van Roozendael (Belgian Institute for Space Aeronomy) provided the GOME and SCIAMACHY HCHO products and the OMI NO_2 product was downloaded from the NASA Data and Information Services Center. This is paper number 501 of the Royal Society's South East Asian Rainforest Research Programme and is dedicated to the memory of Kate Furneaux, a core member of the OP3 project team, who was killed in a traffic accident while cycling in Leeds on 28 July 2009.

Edited by: W. T. Sturges

References

Aiken, A. C., Decarlo, P. F., Kroll, J. H., Worsnop, D. R., Huffman, J. A., Docherty, K. S., Ulbrich, I. M., Mohr, C., Kimmel, J. R., Sueper, D., Sun, Y., Zhang, Q., Trimborn, A., Northway, M., Ziemann, P. J., Canagaratna, M. R., Onasch, T. B., Alfarra, M. R., Prevot, A. S. H., Dommen, J., Duplissy, J., Metzger, A., Baltensperger, U., and Jimenez, J. L.: O/C and OM/OC ratios of primary, secondary, and ambient organic aerosols with high-resolution time-of-flight aerosol mass spectrometry, Environ. Sci. Technol., 42, 4478–4485, 2008.

Andreae, M. O., Artaxo, P., Brandao, C., Carswell, F. E., Ciccioli, P., da Costa, A. L., Culf, A. D., Esteves, J. L., Gash, J. H. C., Grace, J., Kabat, P., Lelieveld, J., Malhi, Y., Manzi, A. O., Meixner, F. X., Nobre, A. D., Nobre, C., Ruivo, M., Silva-Dias, M. A., Stefani, P., Valentini, R., von Jouanne, J., and Waterloo, M. J.: Biogeochemical cycling of carbon, water, energy, trace gases, and aerosols in amazonia: The LBA-EUSTACH experiments, J. Geophys. Res.-Atmos., 107, 8066, doi:10.1029/2001JD000524, 2002.

Andreae, M. O., Artaxo, P., Fischer, H., Freitas, S. R., Gregoire, J. M., Hansel, A., Hoor, P., Kormann, R., Krejci, R., Lange, L., Lelieveld, J., Lindinger, W., Longo, K., Peters, W., de Reus, M., Scheeren, B., Dias, M., Strom, J., van Velthoven, P. F. J., and Williams, J.: Transport of biomass burning smoke to the upper troposphere by deep convection in the equatorial region, Geophys. Res. Lett., 28, 951–954, 2001.

Arino, O., Plummer, S., and Defrenne, D.: Fire disturbance: the ten years time series of the ATSR world fire atlas. Proceedings of the MERIS-AATSR workshop 2005, Frascati, Italy, September 2005.

Arino, O., Simon, M., Piccolini, I., and Rosaz, J. M.: The ERS-2 ATSR-2 World Fire Atlas and the ERS-2 ATSR-2 World Burnt Surface Atlas projects. Proceedings of the 8th ISPRS conference on Physical Measurement and Signatures in Remote Sensing, Aussois, 8–12 January 2001.

Aruffo E., Di Carlo P., Dari Salisburgo C., and Giammaria F.: Thermal-dissociation Laser Induced fluorescence (TD-LIF) instrument for NOy speciation: observations of total peroxy nitrate and total alkyl nitrate, Atmos. Chem. Phys. Discuss., in preparation, 2010.

Ashbaugh, L. L., Malm, W. C., and Sadeh, W. Z.: A residence time probability analysis of sulfur concentrations at Grand Canyon National Park, Atmos. Environ., 19, 1263–1270, 1985.

ATBD-OMI-02: OMI Algorithm Theoretical Basis Document Volume IV OMI Trace Gas Algorithms, edited by: Chance, K., Smithsonian Astrophysical Observatory Cambridge, MA, USA, Version 1.0, September 2001.

Aubinet, M., Grelle, A., Ibrom, A., Rannik, U., Moncrieff, J., Foken, T., Kowalski, A. S., Martin, P. H., Berbigier, P., Bernhofer, C., Clement, R., Elbers, J., Granier, A., Grunwald, T., Morgenstern, K., Pilegaard, K., Rebmann, C., Snijders, W., Valentini, R., and Vesala, T.: Estimates of the annual net carbon and water exchange of forests: The EUROFLUX methodology, in Advances in Ecological Research, Vol 30, Academic Press Inc, San Diego, 113–175, 2000.

Avissar, R., Dias, P. L. S., Dias, M., and Nobre, C.: The large-scale biosphere-atmosphere experiment in Amazonia (LBA): Insights and future research needs, J. Geophys. Res.-Atmos., 107, 8086, doi:10.1029/2002JD002704, 2002.

Baillie, I. C.: Soils of the humid tropics, in: The tropical rainforest (Second edition), edited by: Richards P. W., Cambridge University Press, Cambridge, 256–286, 1996.

Barkley, M. P., Palmer, P. I., De Smedt, I., Karl, T., Guenther, A., and Van Roozendael, M.: Regulated large-scale annual shutdown of amazonian isoprene emissions?, Geophys. Res. Lett., 36, L04803, doi:10.1029/2008GL036843, 2009.

Barth, M., McFadden, J., Sun, J., Wiedinmyer, C., Chuang, P., Collins, D., Griffin, R., Hannigan, M., Karl, T., Kim, S.-W., Lasher-Trapp, S., Levis, S., Litvak, M., Mahowald, N., Moore, K., Nandi, S., Nemitz, E., Nenes, A., Potosnak, M., Raymond, T., Smith, J., Still, C., and Stroud, C.: Coupling between land

ecosystems and the atmospheric hydrologic cycle through biogenic aerosol pathways, B. Am. Meteor. Soc., 86(12), 1738–1742, 2005.

Bidin, K. and Chappell, N. A.: TECHNICAL NOTE: First evidence of a structured and dynamic spatial pattern of rainfall within a small humid tropical catchment, Hydrol. Earth Syst. Sci., 7, 245–253, 2003, http://www.hydrol-earth-syst-sci.net/7/245/2003/.

Bidin, K. and Chappell, N. A.: Characteristics of rain events at an inland locality in northeastern Borneo, Malaysia, Hydrol. Process., 20, 3835–3850, 2006.

Bohn, B., Corlett, G. K., Gillmann, M., Sanghavi, S., Stange, G., Tensing, E., Vrekoussis, M., Bloss, W. J., Clapp, L. J., Kortner, M., Dorn, H.-P., Monks, P. S., Platt, U., Plass-Dülmer, C., Mihalopoulos, N., Heard, D. E., Clemitshaw, K. C., Meixner, F. X., Prevot, A. S. H., and Schmitt, R.: Photolysis frequency measurement techniques: results of a comparison within the ACCENT project, Atmos. Chem. Phys., 8, 5373–5391, 2008, http://www.atmos-chem-phys.net/8/5373/2008/.

Brough, N., Reeves, C. E., Penkett, S. A., Stewart, D. J., Dewey, K., Kent, J., Barjat, H., Monks, P. S., Ziereis, H., Stock, P., Huntrieser, H., and Schlager, H.: Intercomparison of aircraft instruments on board the C-130 and Falcon 20 over southern Germany during EXPORT 2000, Atmos. Chem. Phys., 3, 2127–2138, 2003, http://www.atmos-chem-phys.net/3/2127/2003/.

Buzorius, G., Rannik, Ü., Mäkelä, J. M., Vesala, T., and Kulmala, M.: Vertical aerosol particle fluxes measured by eddy covariance technique using condensational particle counter, J. Aerosol Sci., 29, 157–171, 1998.

Canagaratna, M. R., Jayne, J. T., Jimenez, J. L., Allan, J. D., Alfarra, M. R., Zhang, Q., Onasch, T. B., Drewnick, F., Coe, H., Middlebrook, A., Delia, A., Williams, L. R., Trimborn, A. M., Northway, M. J., DeCarlo, P. F., Kolb, C. E., Davidovits, P., and Worsnop, D. R.: Chemical and microphysical characterization of ambient aerosols with the Aerodyne aerosol mass spectrometer, Mass Spectrom. Rev., 26, 185–222, 2007.

Capes, G., Murphy, J. G., Reeves, C. E., McQuaid, J. B., Hamilton, J. F., Hopkins, J. R., Crosier, J., Williams, P. I., and Coe, H.: Secondary organic aerosol from biogenic VOCs over West Africa during AMMA, Atmos. Chem. Phys., 9, 3841–3850, 2009, http://www.atmos-chem-phys.net/9/3841/2009/.

Carslaw, N., Creasey, D. J., Harrison, D., Heard, D. E., Hunter, M. C., Jacobs, P. J., Jenkin, M. E., Lee, J. D., Lewis, A. C., Pilling, M. J., Saunders, S. M., and Seakins, P. W.: OH and HO_2 radical chemistry in a forested region of north-western Greece, Atmos. Environ., 35, 4725–4737, 2001.

Chappell, N. A., Sherlock, M., Bidin, K., Macdonald, R., Najman, Y., and Davies, G.: Runoff processes in Southeast Asia: role of soil, regolith and rock type, in: Forest Environments in the Mekong River Basin, edited by: Sawada, H., Araki, M., Chappell, N. A., LaFrankie, J. V., and Shimizu ,A., Springer Verlag, Tokyo, 3–23, 2007.

Chappell, N. A., Bidin, K., and Tych, W.: Modelling rainfall and canopy controls on net-precipitation beneath selectively-logged tropical forest, Plant Ecol., 153, 215–229, 2001.

Coe, H., Gallagher, M. W., Choularton, T. W., and Dore, C.: Canopy Scale Measurements of Stomatal and Cuticular O3 Uptake by Sitka Spruce, Atmos. Environ., 29, 1413–1423, 1995.

Conrad, R.: Compensation Concentration as Critical Variable for Regulating the Flux of Trace Gases between Soil and Atmosphere, Biogeochemistry, 27, 155–170, 1994.

Cook, P. A., Savage, N. H., Turquety, S., Carver, G. D., O'Connor, F. M., Heckel, A., Stewart, D., Whalley, L. K., Parker, A. E., Schlager, H., Singh, H. B., Avery, M. A., Sachse, G. W., Brune, W., Richter, A., Burrows, J. P., Purvis, R., Lewis, A. C., Reeves, C. E., Monks, P. S., Levine, J. G., and Pyle, J. A.: Forest fire plumes over the north Atlantic: p-TOMCAT model simulations with aircraft and satellite measurements from the ITOP/ICARTT campaign, J. Geophys. Res.-Atmos., 112, D10S43, doi:10.1029/2006JD007563, 2007.

Cros, B., Delon, C., Affre, C., Marion, T., Druilhet, A., Perros, P. E., and Lopez, A.: Sources and sinks of ozone in savanna and forest areas during EXPRESSO: Airborne turbulent flux measurements, J. Geophys. Res.-Atmos., 105, 29347–29358, 2000.

Crosier, J., Allan, J. D., Coe, H., Bower, K. N., Formenti, P., and Williams, P. I.: Chemical composition of summertime aerosol in the Po Valley (Italy), northern Adriatic and Black Sea, Q. J. Roy. Meteorol. Soc., 133, 61–75, 2007.

Cubison, M. J., Coe, H., and Gysel, M.: A modified hygroscopic tandem DMA and a data retrieval method based on optimal estimation, J. Aerosol Sci., 36, 846–865, 2005.

Dacey, J. W. H. and Wakeham, S. G.: Oceanic dimethylsulfide - production during zooplankton grazing on phytoplankton, Science, 233, 1314–1316, 1986.

Dari-Salisburgo C., Di Carlo P., Aruffo E., Langford B., Dorsey J., and Giammaria F.: Flux measurements of NO_2 in Asian tropical rainforest using laser induced fluorescence and eddy covariance, Atmos. Chem. Phys. Discuss., in preparation 2010.

Dari-Salisburgo, C., Di Carlo, P., Giammaria, F., Kajii, Y., and D'Altorio, A.: Laser induced fluorescence instrument for NO_2 measurements: observations at a central Italy background site, Atmos. Environ., 43, 970–977, 2009.

De Smedt, I., Müller, J.-F., Stavrakou, T., van der A, R., Eskes, H., and Van Roozendael, M.: Twelve years of global observations of formaldehyde in the troposphere using GOME and SCIAMACHY sensors, Atmos. Chem. Phys., 8, 4947–4963, 2008, http://www.atmos-chem-phys.net/8/4947/2008/.

Donovan, R. G., Hope, E. S., Owen, S. M., Mackenzie, A. R., and Hewitt, C. N.: Development and Application of an Urban Tree Air Quality Score for Photochemical Pollution Episodes Using the Birmingham, United Kingdom, Area as a Case Study, Environ. Sci. Technol., 39, 6730–6738, 2005.

Dorsey, J. R and Gallagher, M. W.: NO_x flux measurements from a south east Asian tropical rainforest soil, Atmos. Chem. Phys. Discuss., in preparation, 2010.

Edwards, G. D. and Monks, P. S.: Performance of a single-monochromator diode array spectroradiometer for the determination of actinic flux and atmospheric photolysis frequencies, J. Geophys. Res., 108, 8546, doi:10.1029/2002JD002844, 2003.

Edwards, P. M., Edwards, P., Whalley, L. K., Heard, D. E., et al.: OH reactivity measurements in a South-East Asian tropical Rainforest, Atmos. Chem. Phys. Discuss., in preparation, 2010.

Emmerson, K. M., MacKenzie, A. R., Owen, S. M., Evans, M. J., and Shallcross, D. E.: A Lagrangian model with simple primary and secondary aerosol scheme 1: comparison with UK PM10 data, Atmos. Chem. Phys., 4, 2161–2170, 2004, http://www.atmos-chem-phys.net/4/2161/2004/.

Emmerson, K. M. and Evans, M. J.: Comparison of tropospheric gas-phase chemistry schemes for use within global models, Atmos. Chem. Phys., 9, 1831–1845, 2009, http://www.atmos-chem-phys.net/9/1831/2009/.

Emmerson, K. M., Carslaw, N., Carslaw, D. C., Lee, J. D., McFiggans, G., Bloss, W. J., Gravestock, T., Heard, D. E., Hopkins, J., Ingham, T., Pilling, M. J., Smith, S. C., Jacob, M., and Monks, P. S.: Free radical modelling studies during the UK TORCH Campaign in Summer 2003, Atmos. Chem. Phys., 7, 167–181, 2007, http://www.atmos-chem-phys.net/7/167/2007/.

Emmerson, K. M., Carslaw, N., and Pilling, M. J.: Urban Atmospheric Chemistry during the PUMA Campaign. 2: Radical budgets for OH, HO_2 and RO_2, J. Atmos. Chem., 52(2), 165–183, 2005.

European Centre for Medium-Range Weather Forecasts, ECMWF Trajectories: British Atmospheric Data Centre, 2006–2009, online available at: http://badc.nerc.ac.uk/data/ecmwf-trj/, March 2009.

Evans, M. J., Shallcross, D. E., Law, K. S., Wild, J. O. F., Simmonds, P. G., Spain, T. G., Berrisford, P., Methven, J., Lewis, A. C., McQuaid, J. B., Pilling, M. J., Bandy, B. J., Penkett, S. A., And Pyle, J. A.: Evaluation of a Langrangian box model using field measurements from EASE (Eastern Atlantic Summer Experiment) 1996, Atmos. Environ., 34, 3843–3863, 2000.

Farmer, D. K., Wooldridge, P. J., and Cohen, R. C.: Application of thermal-dissociation laser induced fluorescence (TD-LIF) to measurement of HNO_3, Σalkyl nitrates, Σperoxy nitrates, and NO_2 fluxes using eddy covariance, Atmos. Chem. Phys., 6, 3471–3486, 2006, http://www.atmos-chem-phys.net/6/3471/2006/.

Fleming, Z. L., Monks, P. S., Rickard, A. R., Heard, D. E., Bloss, W. J., Seakins, P. W., Still, T. J., Sommariva, R., Pilling, M. J., Morgan, R., Green, T. J., Brough, N., Mills, G. P., Penkett, S. A., Lewis, A. C., Lee, J. D., Saiz-Lopez, A., and Plane, J. M. C.: Peroxy radical chemistry and the control of ozone photochemistry at Mace Head, Ireland during the summer of 2002, Atmos. Chem. Phys., 6, 2193–2214, 2006, http://www.atmos-chem-phys.net/6/2193/2006/.

Fowler, D.: Ground-level ozone in the 21st century: future trends, impacts and policy implications, Royal Society, London, 2008.

Fu, T.-M., Jacob, D. J., Palmer, P. I., Chance, K., Wang, Y. X., Barletta, B., Blake, D. R., Stanton, J. C., and Pilling, M. J.: Space-based formaldehyde measurements as constraints on volatile organic compound emissions in east and south Asia and implications for ozone, J. Geophys. Res., 112, D06312, doi:10.1029/2006JD007853, 2007.

Fueglistaler, S. and Haynes, P. H.: Control of interannual and longer-term variability of stratospheric water vapor, J. Geophys. Res.-Atmos., 110, D24108, doi:10.1029/2005JD006019, 2005.

Ganzeveld, L., Eerdekens, G., Feig, G., Fischer, H., Harder, H., Königstedt, R., Kubistin, D., Martinez, M., Meixner, F. X., Scheeren, H. A., Sinha, V., Taraborrelli, D., Williams, J., Vilà-Guerau de Arellano, J., and Lelieveld, J.: Surface and boundary layer exchanges of volatile organic compounds, nitrogen oxides and ozone during the GABRIEL campaign, Atmos. Chem. Phys., 8, 6223–6243, 2008, http://www.atmos-chem-phys.net/8/6223/2008/.

Gerber, H.: Direct Measurement of Suspended Particulate Volume Concentration and Far-Infrared Extinction Coefficient with a Laser-Diffraction Instrument, Appl. Optics, 30, 4824–4831, 1991.

Gerbig, C., Schmitgen, S., Kley, D., Volz-Thomas, A., Dewey, K., and Haaks, D.: An improved fast-response vacuum-UV resonance fluorescence CO instrument, J. Geophys. Res., 104, 1699–1704, 1999.

Global Forest Resources: Assessment 2005, FAO, Rome, ISBN-92-5-105481-9, 2006.

Gostlow, B., Robinson, A. D., Harris, N. R. P., O'Brien, L. M., Oram, D. E., Mills, G. P., Newton, H. M., and Pyle, J. A.: μDirac: an autonomous instrument for halocarbon measurements, Atmos. Meas. Tech. Discuss., 2, 2123–2159, 2009, http://www.atmos-meas-tech-discuss.net/2/2123/2009/.

Gostlow, B., Robinson, A. D., Harris, N. R. P., O'Brien, L. M., Oram, D. E., Mills, G. P., Newton, H. M., and Pyle, J. A.: Dirac: an autonomous instrument for halocarbon measurements, Atmos. Meas. Tech. Discuss., 2, 2123-2159, 2009, http://www.atmos-meas-tech-discuss.net/2/2123/2009/.

Greenberg, J. P., Guenther, A. B., Madronich, S., Baugh, W., Ginoux, P., Druilhet, A., Delmas, R., and Delon, C.: Biogenic volatile organic compound emissions in central Africa during the experiment for the regional sources and sinks of oxidants (EXPRESSO) biomass burning season, J. Geophys. Res.-Atmos., 104, 30659–30671, 1999.

Guenther, A., Hewitt, C. N., Erickson, D., Fall, R., Geron, C., Graedel, T., Harley, P., Klinger, L., Lerdau, M., McKay, W. A., Pierce, T., Scholes, B., Steinbrecher, R., Tallamraju, R., Taylor, J., and Zimmerman, P.: A global-model of natural volatile organic-compound emissions, J. Geophys. Res.-Atmos., 100, 8873–8892, 1995.

Guenther, A., Karl, T., Harley, P., Wiedinmyer, C., Palmer, P. I., and Geron, C.: Estimates of global terrestrial isoprene emissions using MEGAN (Model of Emissions of Gases and Aerosols from Nature), Atmos. Chem. Phys., 6, 3181–3210, 2006, http://www.atmos-chem-phys.net/6/3181/2006/.

Guenther, A. B., Zimmerman, P. R., Harley, P. C., Monson, R. K., and Fall, R.: Isoprene and monoterpene emission rate variability - model evaluations and sensitivity analyses, J. Geophys. Res.-Atmos., 98, 12609–12617, 1993.

Guenther, A., Hewitt, C. N., Karl. T., Harley, P., and Reeves. C.: Biogenic VOC emissions from African American and Asian tropical rainforests, Eos Trans. AGU, 89(53), Fall Meet. Suppl., Abstract A14C-04, 2008.

Güsten, H., Heinrich, G., Schmidt, R. W. H., and Schurath, U.: A Novel Ozone Sensor for Direct Eddy Flux Measurements, paper presented at 7th International Symp of the Commission for Atmospheric Chemistry and Global Pollution : the Chemistry of the Global Atmosphere, Kluwer Academic Publ, Chamrousse, France, 5–11 September, 1990.

Gusten, H. and Heinrich, G.: On-line measurements of ozone surface fluxes .1. methodology and instrumentation, Atmos. Environ., 30, 897–909, 1996.

Gysel, M., Crosier, J., Topping, D. O., Whitehead, J. D., Bower, K. N., Cubison, M. J., Williams, P. I., Flynn, M. J., McFiggans, G. B., and Coe, H.: Closure study between chemical composition and hygroscopic growth of aerosol particles during TORCH2, Atmos. Chem. Phys., 7, 6131–6144, 2007, http://www.atmos-chem-phys.net/7/6131/2007/.

Hallquist, M., Wenger, J. C., Baltensperger, U., Rudich, Y., Simp-

son, D., Claeys, M., Dommen, J., Donahue, N. M., George, C., Goldstein, A. H., Hamilton, J. F., Herrmann, H., Hoffmann, T., Iinuma, Y., Jang, M., Jenkin, M. E., Jimenez, J. L., Kiendler-Scharr, A., Maenhaut, W., McFiggans, G., Mentel, Th. F., Monod, A., Prévôt, A. S. H., Seinfeld, J. H., Surratt, J. D., Szmigielski, R., and Wildt, J.: The formation, properties and impact of secondary organic aerosol: current and emerging issues, Atmos. Chem. Phys., 9, 5155–5235, 2009, http://www.atmos-chem-phys.net/9/5155/2009/.

Harrison, R. M., Yin, J., Tilling, R. M., Cai, X., Seakins, P. W., Hopkins, J. R., Lansley, D. L., Lewis, A. C., Hunter, M. C., Heard, D. E., Carpenter, L. J., Creasy, D. J., Lee, J. D., Pilling, M. J., Carslaw, N., Emmerson, K. M., Redington, A., Derwent, R. G., Ryall, D., Mills, G., and Penkett, S. A.: Measurement and modelling of air pollution and atmospheric chemistry in the UK West Midlands conurbation: Overview of the PUMA Consortium project, Sci. Total Environ., 360, 5–25, 2006.

Heard, D. E., Read, K. A., Methven, J., Al-Haider, S., Bloss, W. J., Johnson, G. P., Pilling, M. J., Seakins, P. W., Smith, S. C., Sommariva, R., Stanton, J. C., Still, T. J., Ingham, T., Brooks, B., De Leeuw, G., Jackson, A. V., McQuaid, J. B., Morgan, R., Smith, M. H., Carpenter, L. J., Carslaw, N., Hamilton, J., Hopkins, J. R., Lee, J. D., Lewis, A. C., Purvis, R. M., Wevill, D. J., Brough, N., Green, T., Mills, G., Penkett, S. A., Plane, J. M. C., Saiz-Lopez, A., Worton, D., Monks, P. S., Fleming, Z., Rickard, A. R., Alfarra, M. R., Allan, J. D., Bower, K., Coe, H., Cubison, M., Flynn, M., McFiggans, G., Gallagher, M., Norton, E. G., O'Dowd, C. D., Shillito, J., Topping, D., Vaughan, G., Williams, P., Bitter, M., Ball, S. M., Jones, R. L., Povey, I. M., O'Doherty, S., Simmonds, P. G., Allen, A., Kinnersley, R. P., Beddows, D. C. S., Dall'Osto, M., Harrison, R. M., Donovan, R. J., Heal, M. R., Jennings, S. G., Noone, C., and Spain, G.: The North Atlantic Marine Boundary Layer Experiment (NAMBLEX). Overview of the campaign held at Mace Head, Ireland, in summer 2002, Atmos. Chem. Phys., 6, 2241–2272, 2006, http://www.atmos-chem-phys.net/6/2241/2006/.

Heard, D. E. and Pilling, M. J.: Measurement of OH and HO_2 in the troposphere, Chem. Rev., 103, 5163–5198, 2003.

Helfter, C., Phillips, G. J., Coyle, M., Di Marco, C. F., Langford, B., Whitehead, J., Dorsey, J. R., Gallagher, M. W., Sei, E. Y., Fowler, D., and Nemitz, E.: Momentum and heat exchange above South East Asian rainforest in complex terrain. Atmos. Chem. Phys. Discuss., in preparation, 2010.

Hewitt, C. N., MacKenzie, A. R., Di Carlo, P., Di Marco, C. F., Dorsey, J. R., Evans, M., Fowler, D., Gallagher, M. W., Hopkins, J. R., Jones, C. E., Langford, B., Lee, J. D., Lewis, A. C., Lim, S. F., McQuaid, J., Misztal, P., Moller, S. J., Monks, P. S., Nemitz, E., Oram, D. E., Owen, S. M., Phillips, G. J., Pugh, T. A. M., Pyle, J. A., Reeves, C. E., Ryder, J., Siong, J., Skiba, U., and Stewart, D. J.: Nitrogen management is essential to prevent tropical oil palm plantations from causing ground-level ozone pollution, P. Natl. Acad. Sci. USA, 106, 18447–18451, 2009.

Ingham, T., Goddard, A., Whalley, L. K., Furneaux, K. L., Edwards, P. M., Seal, C. P., Self, D. E., Johnson, G. P., Read, K. A., Lee, J. D., and Heard, D. E.: A flow-tube based laser-induced fluorescence instrument to measure OH reactivity in the troposphere, Atmos. Meas. Tech., 2, 465–477, 2009, http://www.atmos-meas-tech.net/2/465/2009/.

Jaegle, L., Jacob, D. J., Brune, W. H., Faloona, I., Tan, D., Heikes, B. G., Kondo, Y., Sachse, G. W., Anderson, B., Gregory, G. L., Singh, H. B., Pueschel, R., Ferry, G., Blake, D. R., and Shetter, R. E.: Photochemistry of HO_x in the upper troposphere at northern midlatitudes, J. Geophys. Res.-Atmos., 105(D3), 3877–3892, 2000.

Jenkin, M. E., Saunders, S. M., Wagner, V., and Pilling, M. J.: Protocol for the development of the Master Chemical Mechanism, MCM v3 (Part B): tropospheric degradation of aromatic volatile organic compounds, Atmos. Chem. Phys., 3, 181–193, 2003, http://www.atmos-chem-phys.net/3/181/2003/.

Kanakidou, M., Seinfeld, J. H., Pandis, S. N., Barnes, I., Dentener, F. J., Facchini, M. C., Van Dingenen, R., Ervens, B., Nenes, A., Nielsen, C. J., Swietlicki, E., Putaud, J. P., Balkanski, Y., Fuzzi, S., Horth, J., Moortgat, G. K., Winterhalter, R., Myhre, C. E. L., Tsigaridis, K., Vignati, E., Stephanou, E. G., and Wilson, J.: Organic aerosol and global climate modelling: a review, Atmos. Chem. Phys., 5, 1053–1123, 2005, http://www.atmos-chem-phys.net/5/1053/2005/.

Kaye, P. H., Stanley, W. R., Hirst, E., Foot, E. V., Baxter, K. L., and Barrington, S. J.: Single particle multichannel bio-aerosol fluorescence sensor, Optics Express, 13(10), 3583–3593, 2005.

Klinger, L. F., Greenberg, J., Guenther, A., Tyndall, G., Zimmerman, P., M'Bangui, M., and Moutsambote, J. M.: Patterns in volatile organic compound emissions along a savanna-rainforest gradient in central Africa, J. Geophys. Res.-Atmos., 103, 1443–1454, 1998.

Langford, B., Davison, B., Nemitz, E., and Hewitt, C. N.: Mixing ratios and eddy covariance flux measurements of volatile organic compounds from an urban canopy (Manchester, UK), Atmos. Chem. Phys., 9, 1971–1987, 2009, http://www.atmos-chem-phys.net/9/1971/2009/.

Langford, B., Misztal, P. Nemitz, E., Davison, B., Helfter, C., Lee, J., MacKenzie, A. R., and Hewitt, C. N.: Fluxes of volatile organic compounds from a south-east Asian tropical rainforest, Atmos. Chem. Phys. Discuss., in preparation, 2010.

Leff, B., Ramankutty, N., and Foley, J. A.: Geographic distribution of major crops across the world, Global Biogeochem. Cy., 18, GB1009, doi:10.1029/2003GB002108, 2004.

Leigh, R. J., Corlett, G. K., Friess, U., and Monks, P. S.: Concurrent multiaxis differential optical absorption spectroscopy system for the measurement of tropospheric nitrogen dioxide, Appl. Optics, 45, 7504–7518, 2006.

Lelieveld, J., Butler, T. M., Crowley, J. N., Dillon, T. J., Fischer, H., Ganzeveld, L., Harder, H., Lawrence, M. G., Martinez, M., Taraborrelli, D., and Williams, J.: Atmospheric oxidation capacity sustained by a tropical forest, Nature, 452, 737–740, 2008.

Levine, J.: The 1997 Fires in Kalimantan and Sumatra, Indonesia: Gaseous and Particulate Emissions, Geophys. Res. Lett., 26(7), 815–818, 1999.

Lewis, A. C., Evans, M. J., Methven, J., Watson, N., Lee, J. D., Hopkins, J. R., Purvis, R. M., Arnold, S. R., McQuaid, J. B., Whalley, L. K., Pilling, M. J., Heard, D. E., Monks, P. S., Parker, A. E., Reeves, C. E., Oram, D. E., Mills, G., Bandy, B. J., Stewart, D., Coe, H., Williams, P., and Crosier J.: Chemical composition observed over the mid-Atlantic and the detection of pollution signatures far from source regions, J. Geophys. Res.-Atmos., 112, D10S39, doi:10.1029/2006JD007584, 2007.

Lewis, A. C., Hopkins, J. R., Carpenter, L. J., Stanton, J., Read, K. A., and Pilling, M. J.: Sources and sinks of acetone, methanol,

and acetaldehyde in North Atlantic marine air, Atmos. Chem. Phys., 5, 1963–1974, 2005, http://www.atmos-chem-phys.net/5/1963/2005/.

Martin, R. V., Jacob, D. J., Chance, K., Kurosu, T. P., Palmer, P. I., and Evans, M. J.: Global inventory of nitrogen oxide emissions constrained by space-based observations of NO_2 columns, J. Geophys. Res., 108(D17), 4537, doi:10.1029/2003JD003453, 2003.

Martin, R. V., Chance, K., Jacob, D. J., Kurosu, T. P., Spurr, R. J. D., Bucsela, E., Gleason, J. F., Palmer, P. I., Bey, I., Fiore, A. M., Li, Q. B., Yantosca, R. M., and Koelemeijer, R. B. A.: An improved retrieval of tropospheric nitrogen dioxide from gome, J. Geophys. Res.-Atmos., 107, 4437, doi:10.1029/2001JD001027, 2002.

Martinez, M., Harder, H., Kubistin, D., Rudolf, M., Bozem, H., Eerdekens, G., Fischer, H., Gurk, C., Klüpfel, T., Königstedt, R., Parchatka, U., Schiller, C. L., Stickler, A., Williams, J., and Lelieveld, J.: Hydroxyl radicals in the tropical troposphere over the Suriname rainforest: airborne measurements, Atmos. Chem. Phys. Discuss., 8, 15491–15536, 2008, http://www.atmos-chem-phys-discuss.net/8/15491/2008/.

Matsuda, K., Watanabe, I., Wingpud, V., Theramongkol, P., and Ohizumi, T.: Deposition velocity of O_3 and SO_2 in the dry and wet season above a tropical forest in northern Thailand, Atmos. Environ., 40, 7557–7564, 2006.

McGregor, G. R. and Nieuwolt, S.: Tropical climatology: an introduction to the climates of the low latitudes (Second Edition), John Wiley & Sons, Chichester, 339 pp., 1998.

Misztal, P. K., Nemitz, E., Langford, B., Coyle, M., Ryder, J., DiMarco, C., Phillips, G., Oram, D., Owen, S., and Cape, J. N.: First direct ecosystem fluxes of VOCs from oil palms in SE Asia, Atmos. Chem. Phys. Discuss., in preparation, 2010a.

Misztal, P. K., Owen, S., Guenther, A., Geron, C., Rasmussen, C., Phillips, G., Ryan, A., Edwards, D. P., Hewitt, C. N., Nemitz, E., and Cape, J. N.: Large estragole fluxes from oil palms in Borneo, Atmos. Chem. Phys. Discuss., submitted, 2010b.

Moura-Costa, P. H., Yap, S. W., Ong, C. L., Ganing, A., Nussbaum, R., and Mojiun, T.: Large scale enrichment planting with dipterocarps as an alternative for carbon offset – methods and preliminary results, 1996, in: Proceedings of the Fifth Round Table Conference on Dipterocarps, edited by: Appanah, S. and Khoo, K. C., Chiang Mai, Thailand, November 1994.

MPOC.: Fact sheet, Malaysian Palm Oil Council, Brussels, 2008.

Nemitz, E., Jimenez, J. L., Huffman, J. A., Ulbrich, I. M., Canagaratna, M. R., Worsnop, D. R., and Guenther, A. B.: An eddy-covariance system for the measurement of surface/atmosphere exchange fluxes of submicron aerosol chemical species - First application above an urban area, Aerosol Sci. Tech., 42, 636–657, 2008.

Nemitz, E., Phillips, G. J., Di Marco, C. F., Misztal, P. K., Farmer, D., Kimmel, J., and Jimenez, J. L.: Concentrations and surface/atmosphere exchange of aerosol chemical components in PM_1 above an oil palm plantation in Sabah, Malaysia, Atmos. Chem. Phys. Discuss., in preparation, 2010.

Olson, J.: World ecosystems (WE1.4): Digital raster data on a 10 minute geographic 1080 x 2160 grid. Global Ecosytems Database, Version 1.0: Disc A. N. G. D. Center, Boulder CO, Nat. Ocean. Atmos. Admin., 1992.

Olson, D. M., Dinerstein, E., Wikramanayake, E. D., Burgess, N. D., Powell, G. V. N., Underwood, E. C., D'Amico, J. A., Itoua, I., Strand, H. E., Morrison, J. C., Loucks, C. J., Allnutt, T. F., Ricketts, T. H., Kura, Y., Lamoreux, J. F., Wettengel, W. W., Hedao, P., and Kassem, K. R.: Terrestrial Ecoregions of the World: A New Map of Life on Earth, BioScience, 51(11), 933–938. 2001.

Olson, J. R., Crawford, J. H., Chen, G., Brune, W. H., Faloona, I. C., Tan, D., Harder, H., and Martinez, M.: A reevaluation of airborne Hox observations from Nasa field campaigns, J. Geophys. Res.-Atmos., 111, D10301, doi:10.1029/2005JD006617, 2006.

Osborne, S. R., Johnson, B. T., Haywood, J. M., Baran, A. J., Harrison, M. A. J., and McConnell, C. L.: Physical and optical properties of mineral dust aerosol during the Dust and Biomass-burning Experiment, J. Geophys. Res.-Atmos., 113(14), D00C03, doi:10.1029/2007JD009551, 2008.

Palmer, P. I., Jacob, D. J., Fiore, A. M., Martin, R. V., Chance, K., and Kurosu, T. P.: Mapping isoprene emissions over North America using formaldehyde column observations from space, J. Geophys. Res., 108(D6), 4180, doi:10.1029/2002JD002153, 2003.

Pearson, G., Davies, F., and Collier, C. G.: An analysis of the performance of the UFAM pulsed Doppler LIDAR for observing the boundary layer, J. Atmos. Ocean. Tech., 26, 240–250, 2009.

Pearson, G., Davies, F., and Collier, C. G.: Remote sensing of the tropical rainforest boundary layer using pulsed Doppler lidar, Atmos. Chem. Phys., in preparation, 2010.

Penkett, S. A., Bandy, B. J., Reeves, C. E., McKenna, D., and Hignett, P.: Measurements of peroxides in the atmosphere and their relevance to the understanding of global tropospheric chemistry, paper presented at Faraday Discussions on Atmospheric Chemistry – Measurements, Mechanics and Models, Royal Soc Chemistry, E Anglia, England, 19–21 April, 1995.

Pike, R. C., Lee, J. D., Young, P. J., Moller, S., Carver, G. D., Yang, X., Misztal, P., Langford, B., Stewart, D., Reeves, C. E., Hewitt, C. N., and Pyle, J. A.: Can a global model chemical mechanism reproduce NO, NO_2, and O_3 measurements above a tropical rainforest?, Atmos. Chem. Phys. Discuss., 9, 27611–27648, 2009, http://www.atmos-chem-phys-discuss.net/9/27611/2009/.

Pilegaard, K.: Air-soil exchange of NO, NO_2 and O_3 in forests, Water Air Soil Pollut., 1, 79–88, 2001.

Pilegaard, K., Skiba, U., Ambus, P., Beier, C., Brüggemann, N., Butterbach-Bahl, K., Dick, J., Dorsey, J., Duyzer, J., Gallagher, M., Gasche, R., Horvath, L., Kitzler, B., Leip, A., Pihlatie, M. K., Rosenkranz, P., Seufert, G., Vesala, T., Westrate, H., and Zechmeister-Boltenstern, S.: Factors controlling regional differences in forest soil emission of nitrogen oxides (NO and N_2O), Biogeosciences, 3, 651–661, 2006, http://www.biogeosciences.net/3/651/2006/.

Plane, J. M. C. and Saiz-Lopez, A.: Analytical Techniques for Atmospheric Measurement, in: Analytical Techniques for Atmospheric Measurement, edited by: Heard, D. E., Blackwell, Oxford, 2006.

Pugh, T. A. M., MacKenzie, A. R., and Hewitt, C. N.: Modelling of nighttime near-surface chemistry in a South-East Asian tropical rainforest, Atmos. Chem. Phys., in preparation, 2010a.

Pugh, T. A. M., MacKenzie, A. R., Hewitt, C. N., Langford, B., Edwards, P. M., Furneaux, K. L., Heard, D. E., Hopkins, J. R., Jones, C. E., Karunaharan, A., Lee, J., Mills, G., Misztal, P., Moller, S., Monks, P. S., and Whalley, L. K.: Simulating atmospheric composition over a South-East Asian tropical rainforest:

performance of a chemistry box model, Atmos. Chem. Phys. Discuss., accepted, 2010b.

Redelsperger, J.-L., Thorncroft, C. D., Diedhiou, A., Lebel, T., Parker, D. J., and Polcher, J.: African Monsoon Multidisciplinary Analysis: An International Research Project and Field Campaign, B. Am. Meteor. Soc., 87, 1739–1746, 2006.

Reeves, C. E., Slemr, J., Oram, D. E., Worton, D., Penkett, S. A., Stewart, D. J., Purvis, R., Watson, N., Hopkins, J., Lewis, A., Methven, J., Blake, D. R., and Atlas, E.: Alkyl nitrates in outflow from North America over the North Atlantic during Intercontinental Transport of Ozone and Precursors 2004, J. Geophys. Res.-Atmos., 112(21), D10S37, doi:10.1029/2006JD007567, 2007.

Roberts, G. C. and Nenes, A.: A continuous-flow streamwise thermal-gradient CCN chamber for atmospheric measurements, Aerosol Sci. Tech., 39, 206–221, 2005.

Ryder, J., Langford, B., Oram, D., Coyle, M., Phillips, G., Helfter, C., Misztal, P., Cape, N., and Nemitz, E.: Sources and sinks of BVOCs inside a SE Asian rainforest canopy, Atmos. Chem. Phys. Discuss., in preparation, 2010.

Saunders, S. M., Jenkin, M. E., Derwent, R. G., and Pilling, M. J.: Protocol for the development of the Master Chemical Mechanism, MCM v3 (Part A): tropospheric degradation of non-aromatic volatile organic compounds, Atmos. Chem. Phys., 3, 161–180, 2003, http://www.atmos-chem-phys.net/3/161/2003/.

Saunois, M., Reeves, C. E., Mari, C. H., Murphy, J. G., Stewart, D. J., Mills, G. P., Oram, D. E., and Purvis, R. M.: Factors controlling the distribution of ozone in the West African lower troposphere during the AMMA (African Monsoon Multidisciplinary Analysis) wet season campaign, Atmos. Chem. Phys., 9, 6135–6155, 2009, http://www.atmos-chem-phys.net/9/6135/2009/.

Schmitt, C., Belokurov, A., Besançon, C., Boisrobert, L., Burgess, N.D., Campbell, A., Coad, L. Fish, L., Gliddon, D., Humphries, K., Kapos, V., Loucks, C., Lysenko, I., Miles, L., Mills, C., Minnemeyer, S., Pistorius, T., Ravilious, C., and Winkel, G.: Global Ecological Forest Classification and Forest Protected Area Gap Analysis: Analyses and Recommendations in view of the 10% target for forest protection under the Convention on Biological Diversity (CBD). Freiburg University Press, Freiburg, Germany, 2008.

Serca, D., Guenther, A., Klinger, L., Vierling, L., Harley, P., Druilhet, A., Greenberg, J., Baker, B., Baugh, W., Bouka-Biona, C., and Loemba-Ndembi, J.: Expresso flux measurements at upland and lowland Congo tropical forest site, Tellus B, 53, 220–234, 2001.

Stewart, D. J., Taylor, C. M., Reeves, C. E., and McQuaid, J. B.: Biogenic nitrogen oxide emissions from soils: impact on NOx and ozone over west Africa during AMMA (African Monsoon Multidisciplinary Analysis): observational study, Atmos. Chem. Phys., 8, 2285–2297, 2008, http://www.atmos-chem-phys.net/8/2285/2008/.

Still, T. J., Al-Haider, S., Seakins, P. W., Sommariva, R., Stanton, J. C., Mills, G., and Penkett, S. A.: Ambient formaldehyde measurements made at a remote marine boundary layer site during the NAMBLEX campaign – a comparison of data from chromatographic and modified Hantzsch techniques, Atmos. Chem. Phys., 6, 2711–2726, 2006, http://www.atmos-chem-phys.net/6/2711/2006/.

Tan, D., Faloona, I., Simpas, J. B., Brune, W., Shepson, P. B., Couch, T. L., Sumner, A. L., Carroll, M. A., Thronberry, T., Apel, E., Riemer, D., and Stockwell, W.: HOx budgets in a deciduous forest: Results from the PROPHET summer 1998 campaign, J. Geophys. Res.-Atmos., 106(D20), 24407–24427, 2001.

Tangki, H.: Biomass variation across selectively logged forest in Borneo and its prediction by Landsat TM data, Unpublished MPhil thesis, Lancaster University, UK, 2008.

Tangki, H., and Chappell, N. A.: Biomass variation across selectively logged forest within a 225 km^2 region of Borneo and its prediction by Landsat TM, Forest Ecol. Manage., 256, 1960–1970, 2008.

Thomas, R. M., Trebs, I., Otjes, R., Jongejan, P. A. C., Ten Brink, H., Phillips, G., Kortner, M., Meixner, F. X., and Nemitz, E.: An Automated Analyzer to Measure Surface-Atmosphere Exchange Fluxes of Water Soluble Inorganic Aerosol Compounds and Reactive Trace Gases, Environ. Sci. Technol., 43, 1412–1418, 2009.

UNEP-WCMC: Global Distribution of Original and Remaining Forests, United Nations Environment Programme – World Conservation Monitoring Centre (UNEP-WCMC), online available at: http://www.unep-wcmc.org/forest/original.htm, 2000.

Voulgarakis, A., Savage, N. H., Wild, O., Carver, G. D., Clemitshaw, K. C., and Pyle, J. A.: Upgrading photolysis in the p-TOMCAT CTM: model evaluation and assessment of the role of clouds, Geosci. Model Dev., online available at: www.geosci-model-dev.net/2/59/2009/2, 59–72, 2009.

Voulgarakis, A., Savage, N. H., Braesicke, P., Wild, O., Carver, G. D., and Pyle, J. A.: Interannual variability of tropospheric composition: the influence of changes in emissions, meteorology and clouds, Atmos. Chem. Phys. Discuss., 9, 14023–14057, 2009, http://www.atmos-chem-phys-discuss.net/9/14023/2009/.

Volz-Thomas, A., Lerner, A., Patz, H. S., Schultz, M., McKenna, D., Schmitt, R., Madronich, S., and Roth, E.: Airborne Measurements of the Photolysis of NO_2, J. Geophys. Res.-Atmos., 101, 18613–18627, 1996.

Walsh, R. P. D.: Climate. The Tropical Rain Forest, edited by: Richards, P. W., 159–205, Cambridge University Press, Cambridge, 352 pp., 1996.

Whalley, L. K., Furneaux, K. L., Goddard, A., Lee, J. D., Mahajan, A., Oetjen, H., Read, K. A., Carpenter, L. J., Lewis, A. C., Plane, J. M. C., Saltzman, E. S., and Heard, D. E.: The Chemistry of OH and HO_2 in the Boundary Layer over the tropical Atlantic Ocean, Atmos. Chem. Phys. Discuss., in preparation, 2010a.

Whalley, L. K., Furneaux, K. L., Heard, D. E.: Measurements of hydroxyl radicals over a SE Asian tropical rainforest, Atmos. Chem. Phys Discuss., in preparation, 2010b.

Whalley, L. K., Lewis, A. C., McQuaid, J. B., Purvis, R. M., Lee, J. D., Stemmler, K., Zellweger, C. and Ridgeon, P.: Two high-speed, portable GC systems designed for the measurement of non-methane hydrocarbons and PAN: Results from the Jungfraujoch High Altitude Observatory, J. Environ. Monit., 6, 234–241, 2004.

Whitmore, T. C.: Tropical rain forests of the Far East, 2nd edition, Oxford University Press, Oxford, 1984.

Whitmore, T. C.: An introduction to tropical rain forests, 2nd edition, Clarendon, Oxford, 1998.

Wild, O., Law, K. S., McKenna, D. S., Bandy, B. J., Penkett, S. A., and Pyle, J. A.: Photochemical trajectory modeling studies of

the North Atlantic region during August 1993, J. Geophys. Res., 101, 29269–29288, 1996.

Wilkinson, M. J., Owen, S. M., Possell, M., Hartwell, J., Gould, P., Hall, A., Vickers, C., and Hewitt, C. N.: Circadian control of isoprene emissions from oil palm (*Elaeis guineensis*), The Plant Journal, 47, 960–968, doi:10.1111/j.1365-313X.2006.02847.x, 2006.

Wolter, K. and Timlin, M. S.: Measuring the strength of ENSO – how does 1997/98 rank?, Weather, 53, 315–324, 1998.

Worton, D. R., Mills, G. P., Oram, D. E., and Sturges, W. T.: Gas chromatography negative ion chemical ionization mass spectrometry: Application to the detection of alkyl nitrates and halocarbons in the atmosphere, J. Chromatogr. A, 1201, 112–119, 2008.

II-F Langford, B., Misztal, P. K., et al.: Fluxes and concentrations of volatile organic compounds from a South-East Asian tropical rainforest, Atmos. Chem. Phys. Discuss., 10, 11975-12021, 10.5194/acpd-10-11975-2010, 2010.

open access: http://www.atmos-chem-phys-discuss.net/10/11975/2010/acpd-10-11975-2010.html

Atmos. Chem. Phys. Discuss., 10, 11975–12021, 2010
www.atmos-chem-phys-discuss.net/10/11975/2010/
doi:10.5194/acpd-10-11975-2010

Atmospheric Chemistry and Physics Discussions

Fluxes and concentrations of volatile organic compounds from a South-East Asian tropical rainforest

B. Langford[1], P. K. Misztal[2,3], E. Nemitz[2], B. Davison[1], C. Helfter[2], T. A. M. Pugh[1], A. R. MacKenzie[1], S. F. Lim[4], and C. N. Hewitt[1]

[1]Lancaster Environment Centre, Lancaster University, LA1 4YQ, UK
[2]Centre for Ecology & Hydrology, Bush Estate, Penicuik, EH26 0QB, UK
[3]School of Chemistry, Edinburgh University, Edinburgh, EH9 3JJ, UK
[4]Retired, formerly at Malaysian Meteorological Department, Jalan Sultan, Petaling Jaya, Selangor Darul Ehsan, Malaysia

Received: 20 April 2010 – Accepted: 21 April 2010 – Published: 6 May 2010

Correspondence to: B. Langford (b.langford1@lancaster.ac.uk)

Published by Copernicus Publications on behalf of the European Geosciences Union.

Abstract

As part of the OP3 field study of rainforest atmospheric chemistry, above-canopy fluxes of isoprene, monoterpenes and oxygenated volatile organic compounds were made by virtual disjunct eddy covariance from a South-East Asian tropical rainforest in Malaysia. Approximately 500 hours of flux data were collected over 48 days in April–May and June–July 2008. Isoprene was the dominant non-methane hydrocarbon emitted from the forest, accounting for 80% (as carbon) of the measured emission of reactive carbon fluxes. Total monoterpene emissions accounted for 18% of the measured reactive carbon flux. Monoterpenes were not emitted at night, and during the day their flux rate was dependent on both light and temperature. The oxygenated compounds, including methanol, acetone and acetaldehyde, contributed less than 2% of the total measured reactive carbon flux. The sum of the VOC fluxes measured represents a 0.4% loss of daytime assimilated carbon by the canopy, but atmospheric chemistry box modelling suggests that most (90%) of this reactive carbon is returned back to the canopy by wet and dry deposition following chemical transformation. The emission rates of isoprene and monoterpenes, normalised to 30°C and 1000 µmol m^{-2} s^{-1} PAR, were 1.6 mg m^{-2} h^{-1} and 0.46 mg m^{-2} h^{-1} respectively, which was 4 and 1.7 times lower respectively than the default value for tropical forests in the widely-used MEGAN model of biogenic VOC emissions. This highlights the need for more direct canopy-scale flux measurements of VOCs from the world's tropical forests.

1 Introduction

It is currently estimated that tropical forests sequester up to 1.3 Pg of carbon annually (Lewis et al., 2009). Some of this is released back into the atmosphere in the form of reactive volatile organic compounds such as isoprene and monoterpenes (Laothawornkitkul et al., 2009). Emissions of biogenic volatile organic compounds (BVOC) therefore contribute to the global carbon cycle. They can influence both atmospheric

composition and global climate in several key ways. First, due to their high reactivity with respect to the hydroxyl radical (OH), BVOC emissions mediate the oxidative capacity of the Earth's atmosphere, possibly amplifying the persistence of important greenhouse gases such as methane and HCFCs (Granier et al., 2000; Lelieveld et al., 2002). Secondly, monoterpenes and sesquiterpenes are known to be precursors for biogenic secondary organic aerosol (BSOA) (e.g., Hallquist et al., 2009), which are radiatively active and hence important in the global climate system. There is evidence that isoprene also contributes to BSOA formation (Claeys et al., 2004; Paulot et al., 2009). Although the aerosol yield from isoprene is small or negligible in chamber studies (Kroll et al., 2005, 2006; Kleindienst et al., 2006; Ng et al., 2008), the globally high emission rates of isoprene (500–750 $Tg\,yr^{-1}$; Guenther et al., 2006) indicate that its contribution to organic aerosol may be significant (Zhang et al., 2007), perhaps through the formation of water soluble compounds such as hydroxyhydroperoxides and epoxides (Paulot et al., 2009). Finally, VOCs mediate in the formation of photochemical pollutants such as tropospheric ozone and peroxyacetyl nitrate (PAN) (e.g., Sillman, 1999; Hewitt et al., 2009). At high concentrations, ozone can be directly toxic with detrimental impacts on human health, crops and forests (Fowler, 2008).

Despite the important roles played by VOCs in mediating atmospheric composition and climate, relatively little is known about their emission rates from tropical forests. Current estimates suggest that these regions may account for up to half of all global BVOC emissions (Guenther et al., 2006), yet this estimate is based on a limited number of field studies. To date, the majority of these field observations have focused on tropical forests in Amazonia (Zimmerman et al., 1998; Helmig et al., 1998; Stefani et al., 2000; Rinne et al., 2002; Kuhn et al., 2007; Karl et al., 2007, 2009) and, to a lesser extent, regions of Africa (Klinger et al., 1998; Greenberg et al., 1999; Serca et al., 2001).

In current global biogenic VOC emission models such as the Model of Emissions of Gases and Aerosols from Nature (MEGAN G06) (Guenther et al., 2006), emissions of isoprene from the world's tropical forests are, in part, based on standardised emis-

sion rates calculated using measurements conducted in Amazonia. This assumes a degree of uniformity across all tropical forests, which has yet to be confirmed by independent observations and which would be surprising, considering the variety of tree species in rainforests (Pitman et al., 1999), and the very substantial interspecies differences in BVOC emission rates amongst those species that have been measured (Guenther, 1997). The influence of seasonality, which has been shown to be significant in Amazonia (Kuhn et al., 2002; Barkley et al., 2009), but less marked in SE Asia, may also require model emission algorithms to be more region-specific. As well as providing improved estimates of natural BVOC emissions, region-specific measurements alsobenchmark the BVOC chemical climatology from which land-use change is causing deviations (Misztal et al., 2010), with potentially serious implications for regional air quality (Hewitt et al., 2009). There is, therefore, an obvious need for more landscape-scale flux measurements, especially in SE Asia where to date no direct micrometeorological flux observations have been made.

Here we present both direct canopy-scale concentration and flux measurements of a range of BVOCs (but not methane) above a tropical rainforest in SE Asia and compare the results to observations made in Amazonia and Africa (Sect. 3.2.1). Our findings are discussed in relation to the meteorology and then used to optimise the light and temperature algorithms of the MEGAN model for the tropical forests of SE Asia (Sect. 3.2.2). Finally, the measured VOC fluxes are related to co-located measurements of CO_2 exchange and a canopy carbon budget is calculated.

2 Methods

2.1 Site description and setup

Measurements were made as part of the OP3 (Oxidant and Particle Photochemical Processes above a South-East Asian Rainforest) project (Hewitt et al., 2010a) at the Bukit Atur global atmosphere watch (GAW) station in the Danum Valley region of

Sabah, Malaysia (4°C 58′49.33″ N, 117°C 50′39.05″ E, 426 m above mean sea level). The aims and objectives of the OP3 project are summarised by Hewitt et al. (2010a), who also give a detailed site description and overview of the measurements located at the GAW station. The flux footprint of the tower encompassed areas of both primary and selectively logged forest, with regions of both clear-felled-forest and oil palm plantations found some distance beyond, well outside the flux footprint. The selectively logged forest in the flux footprint was logged in 1988 and has since been rehabilitated by enrichment planting. Measurements were carried out over two separate four week periods with phase 1 (OP3-I) taking place during the months of April and May 2008 and phase 2 (OP3-III) occurring between June and July 2008. OP3-II consisted of measurements at a nearby oil palm plantation (Misztal et al., 2010).

For analysis of VOC concentrations and fluxes, a high-sensitivity proton transfer reaction mass spectrometer (PTR-MS) (Ionicon Analytik GmbH: Lindinger et al., 1998) equipped with three Varian turbo molecular pumps and heated Silcosteel inlet was used in conjunction with an ultrasonic anemometer (Windmaster Pro, Gill Instruments, UK). The anemometer and main gas sample line (PTFE 1/2″ OD) were fixed to a 2 m boom mounted on the north east edge of the tower at a height above ground level of 75 m. As the GAW tower is a 100 m tall open pylon-type tower located on a hill, the effective measurement height was estimated to be between 100–150 m above the forest canopy below (Helfter et al., 2010). The PTR-MS was housed inside an air-conditioned laboratory located at the base of the tower and sub-sampled from a low pressure (60 kPa) 1/2″ OD inlet line at a rate of 0.3 l min^{-1} via a short length of PTFE tubing (1/8″ OD). All tubing in the air conditioned room was heated to 40°C to prevent condensation. Visual inspection and good agreement between CO_2 and H_2O fluxes measured with open and closed path sensors (sharing the same line) (Siong et al., 2010) confirmed that no condensation occurred in the main inlet. Data from each sensor were logged onto a single laptop computer in combination with meteorological observations using a program written in LabVIEW 8.5 (National Instruments, Austin, Texas, USA).

Throughout the measurement period the PTR-MS operating conditions were held constant to maintain an *E/N* ratio of approximately 140 Td, which represented the best compromise between the optimal detection limit for VOCs and the minimisation of the impact of high relative humidity (Hayward et al., 2002; Hewitt et al., 2003; Tani et al., 2004). Drift-tube pressure, temperature and voltage were typically maintained at 0.165 kPa, 45°C and 500 V respectively, which gave a primary ion count in the range 6 to 8×10^6 ion counts per second (cps). The sensitivity (S_{norm}) of the PTR-MS for each atomic mass unit (amu, *m/z*) was calculated at regular intervals using a gas standard (Apel-Riemer Environmental Inc.), which contained methanol, acetonitrile, acetaldehyde, acetone and isoprene at a nominal concentration of 1.0 ppmv each as well as limonene at 0.18 ppmv. Volume mixing ratios were calculated adopting the approach of Taipale et al. (2008), where the operating conditions of the PTR-MS are first standardised by normalizing the primary ion count to 1×10^6 cps and accounting for the first water cluster:

$$\mathrm{VMR} = \left(\frac{I(\mathrm{RH}^+)_{norm}}{S_{norm}}\right) \quad (1)$$

In this equation $I(RH^+)_{norm}$ is the normalised count rate (ncps) of an individual *m/z* which is calculated using Eq. (2):

$$I(\mathrm{RH}^+)_{norm} = 10^6\left(\frac{\mathrm{RH}_i}{M21+M37} - \frac{\mathrm{RH}_{zero}}{M21_{zero}+M37_{zero}}\right) \quad (2)$$

Here RH_i represents the ion count signal at mass M_i (cps), RH_{zero} is the signal of the mass measured from the zero air source, *M21* and *M37* are the counts of the primary ($H_3^{18}O^+$) and reagent cluster ions $H_3^{16}O^+$ $H_2^{16}O^+$, respectively, while $M21_{zero}$ and $M37_{zero}$ are the primary and reagent cluster ions when measuring from the zero air source.

For those compounds not contained in the gas mixture, empirical sensitivities were calculated based on the instrument-specific transmission characteristics (Taipale et al.,

2008; Davison et al., 2009). During OP3-I the multi-component gas standard was not available. Consequently only isoprene could be calibrated directly, using a low mixing ratio gas standard (4.52 ppbv±5%) (see Lee et al., 2006, for details). Subsequent analysis of the two isoprene standards by GC-FID showed less than 2% difference. Calibration for all other compounds measured during the first campaign was based on the instrument specific transmission curve, relative to isoprene.

2.2 PTR-MS operation and flux calculations

Fluxes of individual VOC species were calculated using the virtual disjunct eddy covariance technique (vDEC) (Karl et al., 2002) as implemented previously (Langford et al., 2009, 2010; Davison et al., 2009). In order to provide both flux data and information on the full VOC composition, the PTR-MS was programmed to operate in two modes, flux and scan. During the flux mode, 13 protonated masses were targeted with a dwell time of 0.5 s per mass, as well as the primary ion count (quantified indirectly from $H_3^{18}O^+$ at *m/z* 21) and the first water cluster ion count (detected directly as $H_3^{16}O^+$ $H_2^{16}O^+$ at *m/z* 37) which were both measured with a 0.1 s dwell time. This resulted in a total scan cycle time of 6.7 s and the acquisition of ~224 data points (N) per 25-min flux averaging period. The remaining 10 min of each hour were used to obtain basic concentration information across the mass spectrum (21–206 amu, *m/z* resolution=1 amu) (5 min), and to monitor the instrument background (5 minutes), which was subtracted during post processing. The instrument background was monitored by sampling ambient air that had passed through a zero air generator, which comprised a glass tube packed with platinum catalyst powder heated to 2°C. A summary of the masses targeted and their likely contributing compounds, formulas, dwell times, instrument sensitivities and detection limits are all summarised in Table 1.

In order to account for the sampling delay induced by the distance between inlet and instrument, and so synchronise the PTR-MS data with that collected by the ultrasonic anemometer, a cross-correlation function of vertical wind velocity (w') and scalar con-

centration (χ') was used with the peak value over a 25 s time window. Following this synchronisation, each 25-min flux file was then subject to a quality assessment, as described by Langford et al. (2010). Briefly, a two dimensional coordinate rotation was applied. Data were rejected where the friction velocity (u_*) fell below 0.15 m s^{-1} or non-stationary conditions were apparent. Data that passed these criteria were ranked as either high- or low-quality, based on the exact outcome of the stationarity test, and the precision of each individual flux measurement was calculated at the 99.7% confidence interval following the procedure outlined by Spirig et al. (2005). This value was then used as a proxy for the limit of detection of the flux system.

2.3 Validity of flux measurements and potential losses

In order to assess the validity of measurements made, several analyses were undertaken. Firstly, the integral turbulent statistics of the vertical wind velocity were evaluated by comparison of the measured ratio of the standard deviation of vertical wind component to friction velocity (σ_w/u_*) with values obtained using the model of Foken et al. (2004), which predicts σ_w/u_* for a set of ideal conditions.

Following the assessment criteria used in the FLUXNET program (Foken et al., 2004), over 90% of the collected data were rated category 6 or better (i.e., suitable for general use) and less than 1% of the data qualified for rejection with a rank of class 9. This suggests that the turbulence encountered at this site, although light, was sufficiently well developed for the precise and accurate determination of fluxes and that flux measurements at this high measurement height were not adversely influenced by the effects of wake turbulence generated by the tower or surrounding topography Helfter et al. (2010).

The vDEC flux system was evaluated to establish flux losses due to bandwidth limitation. High frequency flux losses encountered due to the response time of the PTR-MS, which cannot resolve fluctuations in the sub ~0.2 s range, were estimated from Horst (1997) and found to be negligible, ranging between 1 and 2%. In contrast, the low frequency flux losses, arising from insufficient averaging periods, were more signifi-

cant, as shown by Fig. 1. For a detailed description of the method, see Langford et al. (2010). Eddies with a time period of between 30 and 90 min increase the flux of sensible heat (H) by ~15%, while eddies with a period of 150 min carried a further 6% of the flux. Assuming similarity and identical frequency behaviour between sensible heat and VOC fluxes, it is probable that VOC fluxes measured at the GAW site using 25-min averaging periods will underestimate the true surface exchange by 15–20%. In contrast, an investigation into the daytime energy budget closure at this site suggests closure within 5% based on 30 min flux values (Helfter et al., 2010). However, since the footprint of the net radiation measurements was not ideal, this closure may be slightly fortuitous.

Additional flux losses may be encountered due to the high relative humidity encountered (60–90%), which can cause condensation in sample lines, attenuating the signal of water soluble compounds such as methanol. In order to evaluate these losses, latent-heat fluxes (λE) were calculated using the PTR-MS, which was first calibrated using data recorded by a closed path infrared gas analyser (IRGA) (LI-COR LI-7000, Biosciences, Nebraska, US.) in a method similar to that of Ammann et al. (2006). The IRGA sub-sampled directly after the PTR-MS from the same sample tube. PTR-MS λE was then compared against the measurement of an open-path IRGA (LI-COR LI-7500, Biosciences, Nebraska, US.) which was mounted directly below the 75 m sonic anemometer during the OP3-III campaign (June–July 2008). As the open-path instrument provides an in situ measurement of water vapour concentrations, fluxes calculated using this sensor are not subject to signal damping and therefore a direct comparison with PTR-MS fluxes can provide an estimate of flux losses along the sample line. For a detailed description of the IRGA setup and results, see Siong et al. (2010).

Figure 2 shows λE measured by PTR-MS and open-path IRGA over an 11-day period. Measured fluxes agree reasonably well (R^2=0.54, p=<0.0001), but on average PTR-MS fluxes are lower, suggesting a typical flux loss of around <30%. This flux loss is much larger than direct comparisons between open and closed path IRGA λE fluxes, which showed just a 1% underestimation, again resulting from the long sample

line (R^2=0.93, p=<0.0001, y=0.9916 x–0.9632). It should be noted that the PTR-MS λE fluxes are in fact sampled disjunctly, which, when coupled with (i) the indirect calibration against the closed-path IRGA and (ii) the greater uncertainty associated with lag time analyses of disjunctly sampled data (Taipale et al., 2010), may account for the larger disparity between the measurement systems.

These analyses suggest that VOC fluxes measured at this site are underestimated due to both insufficient averaging periods and some signal attenuation along the ~75 m sampling line, but the flux loss is unlikely to exceed 30% for any compound. No corrections for these flux losses were applied to the data presented in this study. The estimated losses are small compared to the differences between measured and estimated emissions (Sect. 3.2.2, below).

3 Results and discussion

3.1 Ambient BVOC mixing ratios

Figure 3 shows the average diurnal mixing ratios of the nine VOCs measured during the OP3 campaign and the results are summarised in Table 2a. During the daytime, mixing ratios for each compound were always above the calculated limit of detection, with the exception of methanol and m/z 83 and 85, which we tentatively ascribe to hexanal and/or cis-3-hexenol, and ethyl vinyl ketone (EVK), respectively. For methanol, instrument background counts were unusually high, resulting in a very high detection limit of 1.2 ppbv. Although our measurements of methanol were always close to or below the detection limit, they are of a similar magnitude to measurements made by GC-FID during the campaign (Jones et al., 2010), hence their inclusion here.

Isoprene was the second most abundant compound observed after methanol, accounting for approximately 30% of the total measured species. Mixing ratios ranged between 0.17 and 3.4 ppbv with an average of 1.3 ppbv. Methacrolein (MACR) and methyl vinyl ketone (MVK), which are measured at the same atomic mass unit (amu)

by the PTR-MS and consequently presented as the sum of the two (MACR+MVK), ranged between 0.05 and 0.67 ppbv, with an average value of 0.25 ppbv. Isoprene oxidation is the only known source of MACR and MVK; hence, the ratio of (MACR+MVK) to isoprene can provide an indication of the extent of isoprene oxidation. Average ratios of 0.16 and 0.22 were observed for the first and second campaigns, respectively. These findings are similar to observations by Kesselmeier et al. (2002) who reported above-canopy ratios in Amazonia of 0.23 and 0.3 during the wet and dry seasons respectively. Similarly, Kuhn et al. (2007) reported a ratio of 0.3 for dry season measurements above the Amazon. Following the method of Karl et al. (2004), the time taken between isoprene emission and detection by our system was estimated at 8 min (based on the average [isoprene]/[MVK+MACR] ratio and an assumed atmospheric lifetime for isoprene of 40 min). Accordingly, isoprene mixing ratios were estimated to have originated from within a footprint length of 1.4 km (based on an average wind speed of 3 m s^{-1}). This is consistent with approximate footprint calculations reported by Helfter et al. (2010) for OP3 under unstable daytime conditions.

Over the course of a typical day, the (MVK+MACR)-to-isoprene ratio shows a distinct pattern, with a sharp decline observable at dawn as the nocturnal ratio decreased from 0.36 to 0.1 in the early morning. This relates to the response of the canopy to the increasing light and temperature which drives the isoprene emissions and a decrease in the transport time between canopy and the measurement height. As the isoprene emissions are transported away from the canopy they react to form more MVK+MACR and thus the ratio increases steadily throughout the day before reaching a stable nocturnal maximum, when the isoprene emission and photochemistry shut off.

Monoterpene mixing ratios were relatively low, ranging between 0.02 and 0.47 ppbv with an average of 0.17 ppbv, which is approximately 50% lower than the average of measurements made above Amazonia (Karl et al., 2007). Due to limitations of the PTR-MS approach, the measurement can only measure total monoterpene concentrations as this concentration is derived from a fragment that is common to the different compounds. Gas chromatography measurements reported elsewhere indicate that the

monoterpene emissions at this site were dominated by γ-terpinene and camphene (Jones et al., 2010).

Acetone mixing ratios ranged between 0.46–1.10 ppbv, with an afternoon maximum which typically occurred 1 to 3 h after the maximum in isoprene mixing ratios. Our measured values were similar to those reported above a tropical rainforest in Costa Rica (Karl et al., 2004) and approximately half of those reported above regions of Amazonia (Karl et al., 2007; Williams et al., 2001). Mixing ratios of acetone were slightly higher during OP3-I than OP-III which was also the case for acetic acid. Acetic acid mixing ratios ranged between 0.22–0.5 ppbv, but in contrast to the trend in acetone, peak values occurred in the early afternoon, closely following the diurnal pattern in ambient air temperature. This close relationship with temperature is typical for this compound, particularly in remote locations (Martin et al., 1991; Khare et al., 1999), but the observed values are slightly lower than those reported elsewhere (Kuhn et al., 2002; Karl et al., 2004).

3.2 Surface-layer VOC fluxes

3.2.1 Isoprene and monoterpene surface-layer fluxes

Figures 4 and 4 show measured isoprene and total monoterpene fluxes relative to the meteorological drivers light, temperature, wind speed/direction, frictional velocity and sensible heat flux, for both measurement phases and their statistics are summarised in Table 2B. During these periods, midday (10:00–14:00) temperature (at 30 m above ground) ranged between 23 – 28°C, and photosynthetically active radiation (PAR) between 336–2027 µmol m^{-2} s^{-1}, whereas at night, temperatures fell to 22 – 24°C. Sensible heat fluxes were positive during the day, ranging between 200 and 400 W m^{-2}, with occasional troughs associated with convective cloud cover and rain events, as clearly seen on both 30 June and 5 July. Wind speed and friction velocities varied between 0.6–4.7 m s^{-1} and 0.06–0.52 m s^{-1} (5th–95th percentiles), with particularly low values of both recorded at night. Accordingly, VOC fluxes were generally only observed

between 09:00 and 17:00 and not at night.

During the night the measurement platform became de-coupled from the canopy below, as observed from nocturnal cloud formation at the canopy top, below the measurement height, and validated through LIDAR measurements of the mixed layer height (Pearson et al., 2010). Subsequently, any nocturnal emissions such as nocturnal monoterpene fluxes from temperature-dependent plant emitters could not be captured by our measurement system. In contrast, early morning emissions of both isoprene and monoterpenes that accumulated in the shallow nocturnal boundary layer were occasionally observed as large spikes at around 08:00–09:00 during the break up of this stable air. However, in-canopy gradient measurements of these compounds during OP3-III showed that both compounds did not build up inside the canopy during the night and that dark emissions were negligable (Ryder et al., 2010). The LIDAR measurements confirm that after sunrise the boundary layer quickly expanded. Therefore little of the daytime fluxes were lost due to de-coupling from the canopy.

Emissions of isoprene were the largest of all the measured VOCs, with an average midday flux (10:00–14:00 LT) of 1.85 mg m^{-2} h^{-1} for the entire 48-day period. This value represented approximately 80% (as carbon) of all measured non-methane BVOC emissions from the forest canopy, with the remaining 20% accounted for by emissions of total monoterpenes (18% as carbon) and oxygenated VOCs (OVOC) (2% as carbon), including methanol, acetone and acetaldehyde – see Sect. 3.2.3. The mean integrated daily flux of isoprene was 6.0 mg m^{-2} d^{-1} and 12.9 mg m^{-2} d^{-1} respectively, for the OP3-I and OP3-III campaigns with an average of 10.5 mg m^{-2} d^{-1} for all collected data (approximately 500 hours of data collected over 48 days). Here, missing night-time data were gap-filled with zero fluxes, consistent with the light-sensitivity of the isoprene emissions. The mean integrated daily fluxes for each phase are statistically different at the 95% level (two-tailed t-test). The observed increase in emission rates between the two campaigns was consistent with a difference in integrated ambient air temperature (0.3°C) and PAR (3549 µmol m^{-2} s^{-1} PAR) for the average day, and normalising these emissions to standard conditions (30°C and 1000 µmol m^{-2} s^{-1} PAR), using the algo-

rithms of Guenther et al. (2006) described in the next section, reduced the difference in standard emission rates between the two campaigns to within 6%. A recent study has suggested that isoprene-emitting vegetation in Amazonia experiences a wide-scale leaf flushing which promotes new growth in preparation for the coming dry season, resulting in an annual shutdown of isoprene emissions (Barkley et al., 2009). Seasonality in Borneo is much less marked than in Amazonia; and our measurements showed no evidence of a similar process occurring at this site.

The average daytime ratio of monoterpene to isoprene fluxes was 0.23±0.3 (standard deviation) and remained relatively constant throughout the day, including the early morning when nocturnal emissions were vented from the shallow nocturnal boundary layer. This relative constancy suggests that nocturnal, light-independent emissions of monoterpenes are negligible at this site, which is consistent with Owen et al. (2002) and with the in-canopy profile measurements made by Ryder et al. (2010) who did not detect monoterpene emissions from the darker under storey during the day or night-time build-ups inside the canopy. Guenther et al. (2008) summarise the monoterpene: isoprene emission rates observed in other tropical forests, with values typically found to be ~0.15.

Polar plots of isoprene and monoterpene fluxes shown in Fig. 5 (top two panels), indicate that canopy emissions were spatially very heterogeneous, with observed fluxes strongly skewed towards the south-east. Analysis of polar plots for temperature and PAR shows a similar south-east skew. This direction-dependent temperature effect was accounted for by normalising measured fluxes to give the base emission rate (BER; 30°C (canopy temperature) and 1000 µmol m^{-2} s^{-1} PAR). The resulting polar plots of BER (Fig. 5, bottom two panels) were less pronounced in the south east, but still showed considerable variability in emission rates between wind sectors, with values ranging between 0.8 and 2.9 mg m^{-2} h^{-1} for isoprene and between 0.21 and 0.70 mg m^{-2} h^{-1} for monoterpenes. Average BERs during the OP3 campaigns were 1.6 and 0.46 mg m^{-2} h^{-1} for isoprene and monoterpenes, respectively, which was in close agreement with up-scaled leaf level measurements made by Owen et al. (2010)

for isoprene (2.1 mg m^{-2} h^{-1}) and monoterpenes (0.47 mg m^{-2} h^{-1}) within the flux footprint of the GAW tower.

Although the extrapolated leaf level measurements are on average ~13% larger than measured fluxes they are still well within the range of emission rates observed between wind sectors. The close agreement between canopy-scale fluxes and leaf level measurements suggests that, although the tree species composition of the flux footprint is spatially heterogeneous, up-scaling of leaf level measurements can still yield representative results for this area.

Table 3 summarises the isoprene and monoterpene fluxes measured during the OP3 campaigns relative to previous findings from Amazonia, Africa and South East Asia. Our measurements of isoprene compared very closely to leaf-level estimates made from a dipterocarp forest on mainland Malaysia (Saito et al., 2008) and to observations above regions of the Congo, but were at the extreme lower end of observations from Amazonia. In contrast, our measurements of total monoterpene fluxes are somewhat larger than those previously reported for other tropical forests.

3.2.2 Comparison of isoprene and monoterpene fluxes with modelled fluxes

Emissions of isoprene from the flux footprint were simulated using the light and temperature algorithm from the G06 emission model of Guenther et al. (2006). In the original G06 algorithm the fitting coefficients (Eqs. 5–9 of Guenther et al., 2006) are based on observations reported from five independent studies (Monson et al., 1994; Sharkey et al., 1999; Geron et al., 2000; Hanson and Sharkey, 2001; Petron et al., 2001), all of which report measurements from temperate plant species. In light of this, the coefficients used in the G06 algorithm were optimised for the emissions data reported in this paper by minimising the normalised mean square error (M) between observed and modelled data using a quasi-Newton Raphson iterative method (Microsoft Excel 2003,

Microsoft Corporation, Redmond, WA, USA):

$$M = \frac{\left(\overline{E_0 - E_p}\right)^2}{\overline{E_0} \times \overline{E_p}} \quad (3)$$

Here E_o is the observed emission, E_p is the predicted emission and over bars denote mean values. The performance of the model is rated by the M score, which is a function of bias magnitude, bias variance and intensity of association (Guenther et al., 1993) and decreases with increasing model performance. In order to constrain the optimisation to environmentally realistic conditions, each coefficient was given a tolerance of ±50%, with the exception of the temperature maximum (T_{max}) which was restricted to ±1%. Table 4 lists the standard coefficients presented by Guenther et al. (2006) and the new optimised coefficients based on the results of this study.

Model variables such as PAR and temperature (past and present) were supplied from the in situ measurements made at the GAW station. Before use, the ambient air temperature measurements were first converted to give the canopy leaf temperatures required by the model using the resistance analogy described by Nemitz et al. (2009). Leaf temperatures during the afternoon were up to 2°C higher than air temperature. Base emission rates describing isoprene and monoterpene emissions under constant (standard) conditions of temperature and PAR were inferred from the measured fluxes as described above. Our analysis assumes, as do all previous such analyses, that the BER is constant throughout the day. However, there are indications that BER varies throughout the day and this finding is explored more fully elsewhere (Hewitt et al., 2010b). Figure 6 shows the simulated fluxes of isoprene (panel a) and monoterpenes (panel b) relative to the observed emissions over a 19-day period (2–21 July 2008).

Model estimates using the standard coefficients compare reasonably well with measured values, confirming temperature and light to be the primary drivers of observed emissions. On occasion, peak fluxes do not agree temporally between measured and modelled values. On 9–10 July, measured VOC fluxes peak in the morning, 2–3 h

earlier than the modelled output. This is most likely the result of venting of the nocturnal boundary layer, described in Sect. 3.2.1. On other days (12–13 July), the peaks match temporally but are underestimated by the model. As the measured fluxes are integrated across the whole flux footprint, which covers an area of several square kilometres (Helfter et al., 2010) emissions respond to fluctuations in light and temperature across that footprint, which are not fully captured by our point measurements of PAR and temperature. In addition, the tree species composition in the footprint around the tower is very variable. Lowering the point of flux measurement closer to the canopy and thus reducing the flux footprint might improve model performance and result in a closer fit to the data, as demonstrated by measurements above an oil palm plantation reported by Misztal et al. (2010), but at the cost of spatial representativeness.

Optimisation of the standard G06 coefficients resulted in new light and temperature curves, which are shown in Fig. 7. For isoprene, the temperature response (γ_T), shown in panel A, doubles the normalised emission rates at peak values compared with the standard G06 response. The shape, higher T_{max} and increased emission rate of the fitted response is consistent with laboratory measurements of tropical plant species (*Ficus virgata* and *Ficus microcarpa*) made by Oku et al. (2008). In contrast, optimisation of the temperature response based on monoterpene fluxes showed no deviation from the standard G06 response. This is not unexpected due to the light dependent nature of the monoterpene emissions reported at this site (Ryder et al., 2010). Panel B shows the light response (γ_P) of the fitted coefficients alongside the standard G06 light response. The fitted response of isoprene and monoterpenes are very similar, with emission rates following a steeper gradient at lower PAR values and saturating from 500 µmol m^{-2} s^{-1} of PAR onwards. This light response curve is very similar to those derived from laboratory measurements of oil palm (Wilkinson, 2006), a biofuel crop very common to the region, but not present within the GAW tower flux footprint.

Implementation of the optimised light and temperature response curves described above resulted in only a slight improvement in model performance, which suggests that the standard response curves of the G06 algorithm to perform adequately for both

temperate and tropical vegetation, if the BER is adjusted. The BER appears to be the most important parameter, and failure to accurately characterise this can result in very large under- or over-estimations of canopy emission rates. For example, applying the default isoprene BER for tropical forests contained within MEGAN (6.6 mg m^{-2} h^{-1}; value modified by the appropriate land cover type for the Danum valley region, see Hewitt et al. (2010a), Sect. 2.4), a parameter based on measurements made over the Amazonian rainforest, to regions of Borneo would result in a >4 times overestimation of the emission rate. Similarly, applying the default total monoterpene emission rate (0.8 mg m^{-2} h^{-1}) would result in an overestimation of >70%. This highlights the need for more direct canopy-scale flux measurements of VOCs above the world's tropical forests to allow for further evaluation and constraint of models such as MEGAN.

3.2.3 Fluxes of other BVOCs

Fluxes of seven other BVOCs including methanol, acetone, acetaldehyde and acetic acid were measured during the two phases of the OP3 campaign; their average diurnal profiles are plotted alongside those of isoprene and monoterpenes in Fig. 8 with the results summarised in Table 2b. In addition to the canopy emissions of isoprene and monoterpenes discussed above, positive fluxes of acetaldehyde, acetone, hexanal and/or cis-3-hexenol, and EVK, were also observed. Average emission fluxes of acetaldehyde and acetone were of a similar magnitude and range, but emissions of acetone were larger during June and July relative to April and May, whereas acetaldehyde fluxes were slightly larger during April and May. Fluxes of hexanal and EVK were approximately half that of acetone and acetaldehyde, averaging 20 µg m^{-2} h^{-1}, but mixing ratios of these two compounds were either very close to or below the limit of detection and therefore the fluxes of these compounds are not discussed further.

Previous studies over tropical forests have shown the bidirectional exchange of organic acids between canopy and atmosphere (Kuhn et al., 2002; Karl et al., 2004). Our measurements are consistent with these findings, with deposition fluxes observed for acetic acid during morning and early afternoon as well as small emission fluxes at

certain times. Deposition velocities were in the range of 1–3 mm s^{-1}, which is similar to those reported over the Amazonian rainforest by Kuhn et al. (2002) during the wet season. Correlations between instantaneous measurements of fluxes and ambient mixing ratios did not clearly show a compensation point as has been previously reported in leaf-level studies. However, it is likely that other sinks exist in the canopy (such as adsorption to leaf surfaces), which would affect the relationship between fluxes and concentrations. These findings should be treated with some caution as measurements of acetic acid by PTR-MS can be affected by memory effects in the inlet system and drift tube (de Gouw and Warneke, 2007).

Canopy profile measurements of methanol mixing ratios made by Ryder et al. (2010) showed elevated values close to the forest floor, which is suggestive of methanol emissions from decomposing leaf material (Fall, 2003). However, our canopy scale flux measurements showed periods of both emission and deposition, with small net deposition. Previous studies in Amazonia have also shown both positive and negative fluxes of methanol, but the net exchange has always been reported as positive (Karl et al., 2004). The net deposition of methanol at this site, combined with its small deposition velocity, suggests that photo-oxidation is its primary source.

The net exchange of MACR+MVK was negligible, with both positive and negative fluxes observed during each campaign. Positive fluxes were more common in the morning, whereas negative fluxes tended to be observed in the afternoon. This flux pattern may relate to the interplay between chemical sources/sinks and boundary layer dynamics. The net flux is the balance between the chemical production above and below the measurement height. During the first half of the day the boundary layer is shallower and most of the chemical formation happens below the measurement height, while in the afternoon most of the formation occurs above the canopy. Again, from the analysis of in-canopy gradients, Ryder et al. (2010) derived top-of-the-canopy emissions of MVK+MACR of ~0.2 mg m^{-2} h^{-1} which was on average 15% of the isoprene emissions derived by the same technique. This fraction is consistent with the canopy conversion factors that were derived in other studies (e.g., Makar et al., 1999; Stroud

et al., 2005). There is increasing evidence that MVK/MACR are deposited efficiently to vegetation (e.g., Karl et al., 2004; Misztal et al., 2010).

3.3 Net ecosystem exchange of carbon

Tropical forests currently act as a net carbon sink (Grace and Rayment, 2000). However, the sink strength is offset somewhat by the emission of VOCs from both the forest canopy and forest floor. We estimated this offset by analysing total VOC emissions (all VOC measured during OP3; see table 2B for list) with respect to concurrently measured CO_2 fluxes obtained during the OP3-III campaign (20 June–20 July 2008). Figure 9 shows the average diurnal profile of CO_2 fluxes and total VOC exchange occurring above the forest canopy. Integrated CO_2 fluxes yield a daytime (08:00–18:00) net carbon sink strength of 3120 mg C m^{-2} d^{-1}. Total VOC emissions, which had an integrated flux of 13.2 mg C m^{-2} d^{-1} represented 0.4% of this (as carbon). The carbon offset from VOC fluxes above this SE Asian rainforest is lower than values reported above an Amazonian forest (1.2–3.7 %; Kuhn et al., 2007; Karl et al., 2004), but this may be attributable to the limitations of the measurement system, which was de-coupled from the canopy at night (see above) and unable to resolve nocturnal CO_2 emissions due to respiration. Consequently our estimates of net ecosystem exchange (NEE) are for daytime only and guaranteed to be an overestimate. For a more detailed discussion of CO_2 fluxes recorded during this campaign see Siong et al. (2010).

VOC emissions represent a loss of reactive carbon from the canopy, which after emission, will be photochemically processed and some of this carbon may therefore be deposited back to the canopy and hence the amount of carbon escaping the ecosystem is less than the measured VOC flux. In order to trace the fate of carbon emitted as VOCs we ran the CiTTyCAT box model of atmospheric chemistry (Wild et al., 1996; Evans et al., 2000; Donovan et al., 2005; Hewitt et al., 2009; Pugh et al., 2010), including detailed isoprene chemistry (Taraborrelli et al., 2009), in the boundary layer above the flux footprint. The model also includes detailed monoterpene chemistry (Jenkin, 1996; Stockwell et al., 1997), however the lumping of species within these schemes

leads to a carbon loss of around 10% in the model. Therefore monoterpene emissions were neglected in these calculations to conserve carbon. For details on the CiTTyCAT model set-up see Pugh et al. (2010).

Isoprene was emitted following the diurnal cycle defined by the MEGAN algorithm (Guenther et al., 2006). The 24 h average emission rate was 6.88×10^{10} molecules cm^{-2} s^{-1} (0.28 mg m^{-2} h^{-1}). The only other emitted species was NO, at a constant rate of 6.53×10^{9} molecules cm^{-2} s^{-1} (5.5 µg m^{-2} h^{-1}). A deposition velocity of 1.5 cm s^{-1} for MACR and MVK was adopted, following the findings of Pugh et al. (2010). Wet deposition (after Real et al., 2008, S-WET2 scheme) was also employed. A carbon budget was calculated over the final four days of an eight-day model run, tracing the ultimate destination of the carbon emitted as isoprene. The model run indicated the bulk of the reactive carbon emitted from the canopy that is rapidly returned to the canopy in the near vicinity of the point of emission through both wet (60%) and dry (27%) deposition processes. A small fraction (<4 %) of the aldehydes, acids, nitrates and peroxides formed through photochemical reactions persist to be either further oxidised or deposited on a longer timescale, but ultimately only 9% (0.04% of daytime NEE) of the emitted reactive carbon escapes the landscape in the form of CO_2.

4 Summary and conclusions

Direct canopy-scale measurements of VOC fluxes above a SE Asian tropical rainforest showed that isoprene was the dominant compound emitted, accounting for 80% (as carbon) of the total measured reactive carbon fluxes. Typical daytime fluxes ranged between 0.2 and 4.4 mg m^{-2} h^{-1} (10:00–14:00; 5th and 95th percentiles), which, when normalised to standard conditions (30°C; 1000 µmol m^{-2} s^{-1} PAR), gave an average base emission rate of 1.6 mg m^{-2} h^{-1}. This value was found to be 4.1 times smaller than the default standard emission rate used in the MEGAN model for tropical forests. With the exception of BER, optimisation of the empirical coefficients describing the

temperature and PAR response used within MEGAN did not significantly improve the fit between measured and modelled data, lending confidence to the global application of these coefficients.

Total monoterpenes accounted for 18% of the reactive carbon fluxes, ranging between −0.1 and 1.0 mg m^{-2} h^{-1} (10:00–14:00; 5th and 95th percentiles) with an average base emission rate of 0.46 mg m^{-2} h^{-1}. This value was 70% lower than the standard emission rate for monoterpenes used in the MEGAN model for tropical forests. Combined with the evidence from in-canopy measurements, these data demonstrate that monoterpenes were not emitted at night and during the day they were found to be dependent on both light and temperature.

The fluxes of other VOCs including the OVOCs, methanol, acetaldehyde and acetone, accounted for <2% of the total reactive carbon flux. In total, the sum of the measured reactive carbon fluxes offset the daytime net carbon sink strength of the forest canopy by 0.4%, but atmospheric box modelling suggests that most (90%) of this reactive carbon is returned back to the canopy by wet and dry deposition following chemical transformation.

Acknowledgements. BL sincerely thanks Liew Boon Seng and all those who cared for him at the Sabah Medical Centre. The OP3 project was funded by the UK Natural Environment Research Council (NE/D002117/1). We thank the Malaysian and Sabah Governments for their permission to conduct research in Malaysia; the Malaysian Meteorological Department for access to the Bukit Atur Global Atmosphere Watch station; Waidi Sinun of Yayasan Sabah and Glen Reynolds of the Royal Society's South East Asian Rain Forest Research Programme for logistical support at the Danum Valley Research Station and the Royal Society research assistants Alexander Karolus, Johnny Larenus and Hadam Taman for logistical support; Malcolm Possell and Annette Ryan for helpful discussion and the entire OP3 team for their individual and combined efforts. This is paper 506 of the Royal Society's South-East Asian Rainforest Research Programme.

References

Ammann, C., Brunner, A., Spirig, C., and Neftel, A.: Technical note: Water vapour concentration and flux measurements with PTR-MS, Atmos. Chem. Phys., 6, 4643–4651, 2006, http://www.atmos-chem-phys.net/6/4643/2006/. 11983

Barkley, M. P., Palmer, P. I., De Smedt, I., Karl, T., Guenther, A., and Van Roozendael, M.: Regulated large-scale annual shutdown of Amazonian isoprene emissions?, Geophys. Res. Lett., 36, 2009. 11978, 11988

Claeys, M., Graham, B., Vas, G., Wang, W., Vermeylen, R., Pashynska, V., Cafmeyer, J., Guyon, P., Andreae, M. O., Artaxo, P., and Maenhaut, W.: Formation of secondary organic aerosols through photooxidation of isoprene, Science, 303, 1173–1176, 2004. 11977

Davison, B., Taipale, R., Langford, B., Misztal, P., Fares, S., Matteucci, G., Loreto, F., Cape, J. N., Rinne, J., and Hewitt, C. N.: Concentrations and fluxes of biogenic volatile organic compounds above a Mediterranean macchia ecosystem in western Italy, Biogeosciences, 6, 1655–1670, 2009, http://www.biogeosciences.net/6/1655/2009/. 11981

de Gouw, J. and Warneke, C.: Measurements of volatile organic compounds in the earths atmosphere using proton-transfer-reaction mass spectrometry, Mass Spectrom. Rev., 26, 223–257, 2007. 11993

Donovan, R. G., Hope, E. S., Owen, S. M., Mackenzie, A. R., and Hewitt, C. N.: Development and Application of an Urban Tree Air Quality Score for Photochemical Pollution Episodes Using the Birmingham, United Kingdom, Area as a Case Study, Environ. Sci. Technol., 39, 6730–6738, 2005. 11994

Eerdekens, G., Ganzeveld, L., Vilà-Guerau de Arellano, J., Klpfel, T., Sinha, V., Yassaa, N., Williams, J., Harder, H., Kubistin, D., Martinez, M., and Lelieveld, J.: Flux estimates of isoprene, methanol and acetone from airborne PTR-MS measurements over the tropical rainforest during the GABRIEL 2005 campaign, Atmos. Chem. Phys., 9, 4207–4227, 2009, http://www.atmos-chem-phys.net/9/4207/2009/. 12010

Evans, M. J., Shallcross, D. E., Law, K. S., Wild, J. O. F., Simmonds, P. G., Spain, T. G., Berrisford, P., Methven, J., Lewis, A. C., McQuaid, J. B., Pilling, M. J., Bandy, B. J., Penkett, S. A., and Pyle, J. A.: Evaluation of a Langrangian box model using field measurements from EASE (Eastern Atlantic Summer Experiment) 1996, Atmos. Environ., 34, 3843–3863, 2000. 11994

Fall, R.: Abundent oxygenates in the atmosphere: A biochemical perspective, Chem. Rev., 103(12), 4941–4952, 2003. 11993

Foken, T., Gckede, M., Mauder, M., Mahrt, L., Amiro, B., and Munger. W.: Post-field data quality control, in: Handbook of Micrometeorology: A guide for surface flux measurement and analysis, edited by: Lee, W. M. X. and Law, B., Dordrecht, Kluer Academic Publishers, 29, 181–203, 2004. 11982

Fowler, D.: Ground-level ozone in the 21st century: future trends, impacts and policy implications, Royal Society, London, UK, 2008. 11977

Geron, C., Guenther, A., Sharkey, T., and Arnts, R. R.: Temporal variability in basal isoprene emission factor, Tree Physiology, 20, 799–805, 2000. 11989

Geron, C., Guenther, A., Greenberg, J., Loescher, H. W., Clark, D., and Baker, B.: Biogenic volatile organic compound emissions from a lowland tropical wet forest in costa rica, Atmos. Envir., 36, 3793–3802, 2002. 12010

Grace, J. and Rayment, M.: Respiration in the balance, Nature, 404, 819–820, doi:10.1038/35009170, 2000. 11994

Granier, C., Petron, G., Muller, J. F., and Brasseur, G.: The impact of natural and anthropogenic hydrocarbons on the tropospheric budget of carbon monoxide, Atmos. Environ., 34, 5255–5270, 2000. 11977

Greenberg, J. P., Guenther, A. B., Madronich, S., Baugh, W., Ginoux, P., Druilhet, A., Delmas, R., and Delon, C.: Biogenic volatile organic compound emissions in central Africa during the experiment for the regional sources and sinks of oxidants (EXPRESSO) biomass burning season, J. Geophys. Res.-Atmos., 104, 30659–30671, 1999. 11977, 12010

Greenberg, J. P., Guenther, A. B., Petron, G., Wiedinmyer, C., Vega, O., Gatti, L. V., Tota, J., and Fisch, G.: Biogenic voc emissions from forested amazonian landscapes, Global Change Biol., 10, 651–662, 2004. 12010

Guenther, A.: Seasonal and spatial variations in natural volatile organic compound emissions, Ecol. Appl., 7, 34–45, 1997. 11978

Guenther, A., Karl, T., Harley, P., Wiedinmyer, C., Palmer, P. I., and Geron, C.: Estimates of global terrestrial isoprene emissions using MEGAN (Model of Emissions of Gases and Aerosols from Nature), Atmos. Chem. Phys., 6, 3181–3210, 2006, http://www.atmos-chem-phys.net/6/3181/2006/. 11977, 11988, 11989, 11990, 11995, 12017

Guenther, A. B., Zimmerman, P. R., Harley, P. C., Monson, R. K., and Fall, R.: Isoprene and monoterpene emission rate variability – model evaluations and sensitivity analyses, J. Geo-

phys. Res.-Atmos., 98, 12609–12617, 1993. 11990
Guenther, A., Hewitt, C. N., Karl, T., Harley, P., and Reeves. C.: Biogenic VOC emissions from African, American and Asian tropical rainforests, Eos Trans. AGU, 89(53), Fall Meet. Suppl., Abstract A14C-04, 2008. 11988
Hallquist, M., Wenger, J. C., Baltensperger, U., Rudich, Y., Simpson, D., Claeys, M., Dommen, J., Donahue, N. M., George, C., Goldstein, A. H., Hamilton, J. F., Herrmann, H., Hoffmann, T., Iinuma, Y., Jang, M., Jenkin, M. E., Jimenez, J. L., Kiendler-Scharr, A., Maenhaut, W., McFiggans, G., Mentel, Th. F., Monod, A., Prvt, A. S. H., Seinfeld, J. H., Surratt, J. D., Szmigielski, R., and Wildt, J.: The formation, properties and impact of secondary organic aerosol: current and emerging issues, Atmos. Chem. Phys., 9, 5155–5236, 2009, http://www.atmos-chem-phys.net/9/5155/2009/. 11977
Hanson, D. T. and Sharkey, T. D.: Rate of acclimation of the capacity for isoprene emission in response to light and temperature, Plant Cell Environ., 24, 937–946, 2001. 11989
Hayward, S., Hewitt, C. N., Sartin, J. H., and Owen, S. M.: Performance characteristics and applications of a proton transfer reaction-mass spectrometer for measuring volatile organic compounds in ambient air, Environ. Sci. Technol., 36, 1554–1560, 2002. 11980
Helfter, C., Phillips, G. J., Coyle, M., Di Marco, C. F., Langford, B., Whitehead, J., Dorsey, J. R., Gallagher, M. W., Sei, E. Y., Fowler, D., and Nemitz, E.: Momentum and heat exchange above South East Asian rainforest in complex terrain, Atmos. Chem. Phys. Discuss., in preparation, 2010. 11979, 11982, 11983, 11985, 11991
Helmig, D., Balsley, B., Davis, K., Kuck, L. R., Jensen, M., Bognar, J., Smith, T., Arrieta, R. V., Rodriguez, R., and Birks, J. W.: Vertical profiling and determination of landscape fluxes of biogenic nonmethane hydrocarbons within the planetary boundary layer in the Peruvian Amazon, J. Geophys. Res.-Atmos., 103, 25519–25532, 1998. 11977, 12010
Hewitt, C. N., Hayward, S., and Tani, A.: The application of proton transfer reaction-mass spectrometry (ptr-ms) to the monitoring and analysis of volatile organic compounds in the atmosphere, J. Environ. Monitoring, 5, 1–7, 2003. 11980
Hewitt, C. N., MacKenzie, A. R., Di Carlo, P., Di Marco, C. F., Dorsey, J. R., Evans, M., Fowler, D., Gallagher, M. W., Hopkins, J. R., Jones, C. E., Langford, B., Lee, J. D., Lewis, A. C., Lim, S. F., McQuaid, J., Misztal, P., Moller, S. J., Monks, P. S., Nemitz, E., Oram, D. E., Owen, S. M., Phillips, G. J., Pugh, T. A. M., Pyle, J. A., Reeves, C. E., Ryder, J., Siong, J., Skiba, U., and Stewart, D. J.: Nitrogen management is essential to prevent tropical oil palm plantations from causing ground-level ozone pollution, Proceedings of the National Academy

of Sciences of the United States of America, 106, 18447–18451, 2009. 11977, 11978, 11994
Hewitt, C. N., Lee, J. D., MacKenzie, A. R., Barkley, M. P., Carslaw, N., Carver, G. D., Chappell, N. A., Coe, H., Collier, C., Commane, R., Davies, F., Davison, B., DiCarlo, P., Di Marco, C. F., Dorsey, J. R., Edwards, P. M., Evans, M. J., Fowler, D., Furneaux, K. L., Gallagher, M., Guenther, A., Heard, D. E., Helfter, C., Hopkins, J., Ingham, T., Irwin, M., Jones, C., Karunaharan, A., Langford, B., Lewis, A. C., Lim, S. F., MacDonald, S. M., Mahajan, A. S., Malpass, S., McFiggans, G., Mills, G., Misztal, P., Moller, S., Monks, P. S., Nemitz, E., Nicolas-Perea, V., Oetjen, H., Oram, D. E., Palmer, P. I., Phillips, G. J., Pike, R., Plane, J. M. C., Pugh, T., Pyle, J. A., Reeves, C. E., Robinson, N. H., Stewart, D., Stone, D., Whalley, L. K., and Yin, X.: Overview: oxidant and particle photochemical processes above a south-east Asian tropical rainforest (the OP3 project): introduction, rationale, location characteristics and tools, Atmos. Chem. Phys., 10, 169–199, 2010a, http://www.atmos-chem-phys.net/10/169/2010/. 11978, 11979, 11992
Hewitt, C. N., Ashworth, K., Langford, B., MacKenzie, A. R., Misztal, P. K., Nemitz, E., Owen, S. M., Possell, M., Pugh, T. A. M., Ryan, A. C., and Wild, O.: Circadian control reduces isoprene emissions from forests and moderates ground-level ozone, in preparation, 2010a. 11990
Horst, T. W.: A simple formula for attenuation of eddy fluxes measured with first-order-response scalar sensors, Bound.-Lay. Meteor., 82, 219–233, 1997. 11982
Jenkin, M. E.: Chemical Mechanisms forming condensable material. AEA Technology Report. AEA/RAMP/20010010/002, 1996. 11994
Jones, C. E., Hopkins, J. R., Langford, B., Lewis, A. C.: Measurements of isoprene and speciated monoterpenes by GC-FID within a south-east Asian tropical rainforest, Atmos. Chem. Phys. Discuss., in preparation, 2010. 11984, 11986
Karl, T. G., Spirig, C., Rinne, J., Stroud, C., Prevost, P., Greenberg, J., Fall, R., and Guenther, A.: Virtual disjunct eddy covariance measurements of organic compound fluxes from a subalpine forest using proton transfer reaction mass spectrometry, Atmos. Chem. Phys., 2, 279–291, 2002, http://www.atmos-chem-phys.net/2/279/2002/. 11981
Karl, T., Hansel, A., Mark, T., Lindinger, W., and Hoffmann, D.: Trace gas monitoring at the Mauna Loa baseline observatory using proton transfer reaction mass spectrometry, International Journal of Mass Spectrometry, 223–224, 527–538, 2003.
Karl, T., Potosnak, M., Guenther, A., Clark, D., Walker, J., Herrick, J. D., and Geron, C.: Exchange processes of volatile organic compounds above a tropical rain forest: Implications

for modeling tropospheric chemistry above dense vegetation, J. Geophys. Res.-Atmos., 109, D18306, doi:10.1029/2004JD004738, 2004. 11985, 11986, 11992, 11993, 11994, 12010

Karl, T., Guenther, A., Yokelson, R. J., Greenberg, J., Potosnak, M., Blake, D. R., and Artaxo, P.: The tropical forest and fire emissions experiment: Emission, chemistry, and transport of biogenic volatile organic compounds in the lower atmosphere over Amazonia, J. Geophys. Res.-Atmos., 112, D18302, doi:10.1029/2007JD008539, 2007. 11977, 11985, 11986, 12010

Karl, T., Guenther, A., Turnipseed, A., Tyndall, G., Artaxo, P., and Martin, S.: Rapid formation of isoprene photo-oxidation products observed in Amazonia, Atmos. Chem. Phys., 9, 7753–7767, 2009, http://www.atmos-chem-phys.net/9/7753/2009/. 11977

Kesselmeier, J., Kuhn, U., Rottenberger, S., Biesenthal, T., Wolf, A., Schebeske, G., Andreae, M. O., Ciccioli, P., Brancaleoni, E., Frattoni, M., Oliva, S. T., Botelho, M. L., Silva, C. M. A., and Tavares, T. M.: Concentrations and species composition of atmospheric volatile organic compounds (VOCs) as observed during the wet and dry season in Rondonia (Amazonia), J. Geophys. Res.-Atmos., 107(D20), 8053, doi:10.1029/2000JD000267, 2002. 11985

Khare, P., Kumar, N., Kumari, K. M., and Srivastava, S. S.: Atmospheric formic and acetic acids: An overview, Rev. Geophys., 37(2), 227–248, 1999. 11986

Kleindienst, T. E., Edney, E. O., Lewandowski, M., Offenberg, J. H., and Jaoui, M.: Secondary organic carbon and aerosol yields from the irradiations of isoprene and alpha-pinene in the presence of NO_x and SO_2, Environ. Sci. Technol., 40, 3807–3812, 2006. 11977

Klinger, L. F., Greenberg, J., Guenther, A., Tyndall, G., Zimmerman, P., M'Bangui, M., and Moutsambote, J. M.: Patterns in volatile organic compound emissions along a savanna-rainforest gradient in central Africa, J. Geophys. Res.-Atmos., 103, 1443–1454, 1998. 11977, 12010

Kroll, J. H., Ng, N. L., Murphy, S. M., Flagan, R. C., and Seinfeld, J. H.: Secondary organic aerosol formation from isoprene photooxidation under high-NOx conditions, Geophys. Res. Lett., 32, L18808, doi:10.1029/2005GL023637, 2005. 11977

Kroll, J. H., Ng, N. L., Murphy, S. M., Flagan, R. C., and Seinfeld, J. H.: Secondary organic aerosol formation from isoprene photooxidation, Environ. Sci. Technol., 40, 1869–1877, 2006. 11977

Kuhn, U., Rottenberger, S., Biesenthal, T., Ammann, C., Wolf, A., Schebeske, G., Oliva, S. T., Tavares, T. M., and Kesselmeier, J.: Exchange of short-chain monocarboxylic acids by vegetation at a remote tropical forest site in Amazonia, J. Geophys. Res.-Atmos., 107, 8069,

doi:10.1029/2002JD000303, 2002. 11978, 11986, 11992, 11993

Kuhn, U., Andreae, M. O., Ammann, C., Arajo, A. C., Brancaleoni, E., Ciccioli, P., Dindorf, T., Frattoni, M., Gatti, L. V., Ganzeveld, L., Kruijt, B., Lelieveld, J., Lloyd, J., Meixner, F. X., Nobre, A. D., Pschl, U., Spirig, C., Stefani, P., Thielmann, A., Valentini, R., and Kesselmeier, J.: Isoprene and monoterpene fluxes from Central Amazonian rainforest inferred from tower-based and airborne measurements, and implications on the atmospheric chemistry and the local carbon budget, Atmos. Chem. Phys., 7, 2855–2879, 2007, http://www.atmos-chem-phys.net/7/2855/2007/. 11977, 11985, 11994, 12010

Langford, B., Davison, B., Nemitz, E., and Hewitt, C. N.: Mixing ratios and eddy covariance flux measurements of volatile organic compounds from an urban canopy (Manchester, UK), Atmos. Chem. Phys., 9, 1971–1987, 2009, http://www.atmos-chem-phys.net/9/1971/2009/. 11981

Langford, B., Nemitz, E., House, E., Phillips, G. J., Famulari, D., Davison, B., Hopkins, J. R., Lewis, A. C., and Hewitt, C. N.: Fluxes and concentrations of volatile organic compounds above central London, UK, Atmos. Chem. Phys., 10, 627–645, 2010, http://www.atmos-chem-phys.net/10/627/2010/. 11981, 11982, 11983

Laothawornkitkul, J., Taylor, J. E., Paul, N. D., and Hewitt, C. N.: Biogenic volatile organic compounds in the earth system, New Phytologist, 183, 27–51, 2009. 11976

Lee, J. D., Lewis, A. C., Monks, P. S., Jacob, M., Hamilton, J. F., Hopkins, J. R., Watson, N. M., Saxton, J. E., Ennis, C., Carpenter, L. J., Carslaw, N., Fleming, Z., Bandy, B. J., Oram, D. E., Penkett, S. A., Slemr, J., Norton, E., Rickard, A. R., Whalley, L. K., Heard, D. E., Bloss, W. J., Gravestock, T., Smith, S. C., Stanton, J., Pilling, M. J., and Jenkin, M. E.: Ozone photochemistry and elevated isoprene during the UK heat wave of August 2003, Atmos. Environ., 40, 7598–7613, 2006. 11981

Lelieveld, J., Peters, W., Dentener, F. J., and Krol, M. C.: Stability of tropospheric hydroxyl chemistry, J. Geophys. Res.-Atmos., 107, 4715, doi:10.1029/2002JD002272, 2002. 11977

Lewis, S. L., Lopez-Gonzalez, G., Sonke, B., Affum-Baffoe, K., Baker, T. R., Ojo, L. O., Phillips, O. L., Reitsma, J. M., White, L., Comiskey, J. A., Djuikouo, M. N., Ewango, C. E. N., Feldpausch, T. R., Hamilton, A. C., Gloor, M., Hart, T., Hladik, A., Lloyd, J., Lovett, J. C., Makana, J. R., Malhi, Y., Mbago, F. M., Ndangalasi, H. J., Peacock, J., Peh, K. S. H., Sheil, D., Sunderland, T., Swaine, M. D., Taplin, J., Taylor, D., Thomas, S. C., Votere, R., and Woll, H.: Increasing carbon storage in intact African tropical forests, Nature, 457, 1003–1003, 2009. 11976

Lindinger, W., Hansel, A., and Jordan, A.: Proton-transfer-reaction mass spectrometry (PTR-MS): On-line monitoring of volatile organic compounds at pptv levels, Chem.l Soc. Rev., 27, 347–354, 1998. 11979

Makar, P. A., Fuentes, J. D., Wang, D., Staebler, R. M., and Wiebe, H. A.: Chemical processing of biogenic hydrocarbons within and above a temperate deciduous forest, J. Geophys. Res.-Atmos., 104, 3581–3603, 1999. 11993

Martin, R. S., H. Westberg, E. Allwine, L. Ashman, J. C. Farmer, and B. Lamb.: Measurement of isoprene and its atmospheric oxidation products in a central Pennsylvania deciduous forest, J. Atmos. Chem., 13, 1–32, 1991. 11986

Misztal, P. K., Nemitz, E., Langford, B., Coyle, M., Ryder, J., Di Marco, C., Phillips, G., Oram, D., Owen, S., and Cape, J. N.: First direct ecosystem fluxes of VOCs from oil palms in SE Asia. Atmos. Chem. Phys. Discuss, in preparation, 2010. 11978, 11979, 11991, 11994

Monson, R. K., Harley, P. C., Litvak, M. E., Wildermuth, M., Guenther, A. B., Zimmerman, P. R., and Fall, R.: Environmental and developmental controls over the seasonal pattern of isoprene emission from aspen leaves, Oecologia, 99, 260–270, 1994. 11989

Nemitz, E., Hargreaves, K. J., Neftel, A., Loubet, B., Cellier, P., Dorsey, J. R., Flynn, M., Hensen, A., Weidinger, T., Meszaros, R., Horvath, L., Dmmgen, U., Frhauf, C., Löpmeier, F. J., Gallagher, M. W., and Sutton, M. A.: Intercomparison and assessment of turbulent and physiological exchange parameters of grassland, Biogeosciences, 6, 1445–1466, 2009, http://www.biogeosciences.net/6/1445/2009/. 11990

Ng, N. L., Kwan, A. J., Surratt, J. D., Chan, A. W. H., Chhabra, P. S., Sorooshian, A., Pye, H. O. T., Crounse, J. D., Wennberg, P. O., Flagan, R. C., and Seinfeld, J. H.: Secondary organic aerosol (SOA) formation from reaction of isoprene with nitrate radicals (NO_3), Atmos. Chem. Phys., 8, 4117–4140, 2008, http://www.atmos-chem-phys.net/8/4117/2008/. 11977

Oku, H., Fukuta, M., Iwasaki, H., Tambunan, P., and Baba, S.: Modification of the isoprene emission model G93 for tropical tree ficus virgata, Atmos. Environ., 42, 8747–8754, 2008. 11991

Owen, S. M., Harley, P., Guenther, A., and Hewitt, C. N.: Light dependency of voc emissions from selected mediterranean plant species, Atmos. Environ., 36, 3147–3159, 2002. 11988

Owen, S. M., Ryan, A., Linatoc, A., Geron, C., Harley, P., Rasmussen, R., Guenther, A., Wilkinson, M.J., Llusia, J., Penuelas, J., Yap, S. W., Sinun, W., and Hewitt C. N., Leaf level emissions of volatile organic compounds (VOCs) from tropical rainforest tree species in south

east Asia, Atmos. Chem. Phys. Discuss, in preparation, 2010. 11988

Paulot, F., Crounse, J. D., Kjaergaard, H. G., Kroll, J. H., Seinfeld, J. H., and Wennberg, P. O.: Isoprene photooxidation: new insights into the production of acids and organic nitrates, Atmos. Chem. Phys., 9, 1479–1501, 2009, http://www.atmos-chem-phys.net/9/1479/2009/. 11977

Pearson, G., Davies, F., and Collier, C.: Remote sensing of the tropical rain forest boundary layer using pulsed Doppler lidar, Atmos. Chem. Phys. Discuss., 10, 5021–5049, 2010, http://www.atmos-chem-phys-discuss.net/10/5021/2010/. 11987

Petron, G., Harley, P., Greenberg, J., and Guenther, A.: Seasonal temperature variations influence isoprene emission, Geophys. Res. Lett., 28, 1707–1710, 2001. 11989

Pitman, N. C. A., Terborgh, J., Silman, M. R., and Nuez, P.: Tree species distributions in an upper Amazonian forest, Ecology, 80, 2651–2661, 1999. 11978

Pugh, T. A. M., MacKenzie, A. R., Hewitt, C. N., Langford, B., Edwards, P. M., Furneaux, K. L., Heard, D. E., Hopkins, J. R., Jones, C. E., Karunaharan, A., Lee, J., Mills, G., Misztal, P., Moller, S., Monks, P. S., and Whalley, L. K.: Simulating atmospheric composition over a South-East Asian tropical rainforest: performance of a chemistry box model, Atmos. Chem. Phys., 10, 279–298, 2010, http://www.atmos-chem-phys.net/10/279/2010/. 11994, 11995

Real, E., Law, K. S., Schlager, H., Roiger, A., Huntrieser, H., Methven, J., Cain, M., Holloway, J., Neuman, J. A., Ryerson, T., Flocke, F., de Gouw, J., Atlas, E., Donnelly, S., and Parrish, D.: Lagrangian analysis of low altitude anthropogenic plume processing across the North Atlantic, Atmos. Chem. Phys., 8, 7737–7754, 2008, http://www.atmos-chem-phys.net/8/7737/2008/. 11995

Rinne, H. J. I., Guenther, A. B., Greenberg, J. P., and Harley, P. C.: Isoprene and monoterpene fluxes measured above Amazonian rainforest and their dependence on light and temperature, Atmos. Environ., 36, 2421–2426, 2002. 11977, 12010

Ryder, J., Langford, B., Oram, D., Coyle, M., Phillips, G., Helfter, C., Misztal, P., Cape, N., and Nemitz, E.: Sources and sinks of BVOCs inside a SE Asian rainforest canopy, Atmos. Chem. Phys. Discuss., in preparation, 2010. 11987, 11988, 11991, 11993

Saito, T., Yokouchi, Y., Kosugi, Y., Tani, M., Philip, E., and Okuda, T.: Methyl chloride and isoprene emissions from tropical rain forest in southeast Asia, Geophys. Res. Lett., 35, L19812, doi:10.1029/2008GL035241, 2008. 11989, 12010

Serca, D., Guenther, A., Klinger, L., Vierling, L., Harley, P., Druilhet, A., Greenberg, J., Baker,

B., Baugh, W., Bouka-Biona, C., and Loemba-Ndembi, J.: EXPRESSO flux measurements at upland and lowland Congo tropical forest site, Tellus Series B-Chemical and Physical Meteorology, 53, 220–234, 2001. 11977, 12010

Sharkey, T. D., Singsaas, E. L., Lerdau, M. T., and Geron, C. D.: Weather effects on isoprene emission capacity and applications in emissions algorithms, Ecological Applications, 9, 1132–1137, 1999. 11989

Sillman, S.: The relation between ozone, NO_x and hydrocarbons in urban and polluted rural environments, Atmos. Environ., 33, 1821–1845, 1999. 11977

Siong, J., Helfter, C., Di Marco, C. Linatoc, A., Nemitz, E., Fowler, D., and Skiba, U. M.: Greenhouse gas (N_2O, CH_4 and CO_2) exchange with contrasting land uses in SE Asia, Atmos. Chem. Phys. Discuss., in preparation, 2010. 11979, 11983, 11994

Spirig, C., Neftel, A., Ammann, C., Dommen, J., Grabmer, W., Thielmann, A., Schaub, A., Beauchamp, J., Wisthaler, A., and Hansel, A.: Eddy covariance flux measurements of biogenic VOCs during ECHO 2003 using proton transfer reaction mass spectrometry, Atmos. Chem. Phys., 5, 465–481, 2005, http://www.atmos-chem-phys.net/5/465/2005/. 11982

Stefani, P., Valentini, R., Ciccioli, P., Brancaleoni, E., Frattoni, M., Nobre, A., and De Araujo, A.: Preliminary assessment of VOC fluxes from a primary rain forest performed at the LBA site in Manuas, in Proceedings of the First LBA Scientific Conference, edited by: Artaxo, P. and Keller, M., 106, MCT, Belem, Brazil, 2000. 11977, 12010

Stockwell, W.R., Kirchner, F., Kuhn, M. and Seefeld, S.: A new mechanism for regional atmospheric chemistry modeling, J. Geophys. Res., 102(D22), 25847–25879, 1997. 11994

Stroud, C., Makar, P., Karl, T., Guenther, A., Geron, C., Turnipseed, A., Nemitz, E., Baker, B., Potosnak, M., and Fuentes, J. D.: Role of canopy-scale photochemistry in modifying biogenic-atmosphere exchange of reactive terpene species: Results from the CELTIC field study, J. Geophys. Res.-Atmos., 110, D17303, doi:10.1029/2005JD005775, 2005. 11993

Taipale, R., Ruuskanen, T. M., Rinne, J., Kajos, M. K., Hakola, H., Pohja, T., and Kulmala, M.: Technical Note: Quantitative long-term measurements of VOC concentrations by PTR-MS – measurement, calibration, and volume mixing ratio calculation methods, Atmos. Chem. Phys., 8, 6681–6698, 2008, http://www.atmos-chem-phys.net/8/6681/2008/. 11980

Taipale, R., Ruuskanen, T. M., and Rinne, J.: Lag time determination in DEC measurements with PTR-MS, Atmos. Meas. Tech. Discuss., 3, 405–429, 2010,

http://www.atmos-meas-tech-discuss.net/3/405/2010/. 11984

Tani, A., Hayward, S., Hansel, A., and Hewitt, C. N.: Effect of water vapour pressure on monoterpene measurements using proton transfer reaction-mass spectrometry (ptr-ms), Int. J. Mass Spectrom., 239, 161–169, 2004. 11980

Taraborrelli, D., Lawrence, M. G., Butler, T. M., Sander, R., and Lelieveld, J.: Mainz Isoprene Mechanism 2 (MIM2): an isoprene oxidation mechanism for regional and global atmospheric modelling, Atmos. Chem. Phys., 9, 2751–2777, 2009, http://www.atmos-chem-phys.net/9/2751/2009/. 11994

Wild, O., Law, K. S., McKenna, D. S., Bandy, B. J., Penkett, S. A., and Pyle, J. A.: Photochemical trajectory modeling studies of the North Atlantic region during August 1993, J. Geophys. Res., 101, 29269–29288, 1996. 11994

Wilkinson, M. J.: Circadian control of isoprene emissions from oil plam (*Elaeis guineensis*). PhD theis, Lancaster University, 2006. 11991

Williams, J., Poschl, U., Crutzen, P. J., Hansel, A., Holzinger, R., Warneke, C., Lindinger, W., and Lelieveld, J.: An atmospheric chemistry interpretation of mass scans obtained from a proton transfer mass spectrometer flown over the tropical rainforest of Surinam, J. Atmos. Chem., 38, 133–166, 2001. 11986

Zhang, Y., Huang, J. P., Henze, D. K., and Seinfeld, J. H.: Role of isoprene in secondary organic aerosol formation on a regional scale, J. Geophys. Res.-Atmos., 112, D20207, doi:10.1029/2007JD008675, 2007. 11977

Zimmerman, P. R., Greenberg, J. P., and Westberg, C. E.: Measurements of atmospheric hydrocarbons and biogenic emission fluxes in the Amazon boundary-layer, J. Geophys. Res.-Atmos., 93, 1407–1416, 1988. 11977, 12010

Table 1. List of compounds measured during the OP3 campaigns, including their formula, dwell time, average sensitivity and detection limit. Detection limits were calculated based on the signal to noise ratio of measured ion counts following Karl et al. (2003) ($LOD=2\times\sigma_{background}$/sensitivity).

m/z [amu]	Contributing compound(s)	Formula	Dwell time [s]	Average sensitivity [ncps ppbv^{-1}]	Limit of Detection [ppbv]
21	water isotope	$H_2^{18}O$	0.1 s	–	–
33	methanol	CH_4O	0.5 s	11.6	1.2
37	water cluster	$(H_2O)_2$	0.1 s	–	–
42	acetonitrile	C_2H_3N	0.5 s	19.6	–
45	acetaldehyde	C_2H_4O	0.5 s	22.8	0.1
59	acetone propanal	C_3H_6O	0.5 s	25.2	0.1
61	acetic acid	$C_2H_4O_2$	0.5 s	26.5	0.09
69	isoprene furan methyl butenol fragment	C_5H_8	0.5 s	1.6	0.2
71	methyl vinyl ketone methacrolein	C_4H_6O	0.5 s	27.1	0.07
81	monoterpene fragment	–	0.5 s	4.0	0.04
83	hexanal fragment *cis*–3–hexenol fragment	–	0.5 s	30.3	0.04
85	ethyl vinyl ketone	C_5H_8O	0.5 s	30.3	0.06
137	monoterpenes	$C_{10}H_{16}$	0.5 s	3.7	0.04
149	estragole	$C_{10}H_{12}O$	0.5 s	–	–
205	sesquiterpenes	$C_{15}H_{24}$	0.5 s	–	–

Table 2a. Summary of VOC mixing ratios (ppbv) measured during the two intensive OP3 campaigns.

	Isoprene	Σ Monoterpene	Methanol	Acetaldehyde	Acetone	MVK+MACR	Acetic acid	Hexanal	EVK
OP3 I (Wet)									
Mean	1.14	0.24	1.15	0.36	0.91	0.23	0.40	0.05	0.05
Median	0.95	0.22	1.19	0.34	0.90	0.18	0.38	0.05	0.05
Percentiles									
–95th	2.84	0.55	1.88	0.64	1.29	0.67	0.58	0.09	0.07
–5th	0.28	0.06	0.42	0.16	0.50	0.04	0.28	0.02	0.04
σ	0.80	0.15	0.46	0.14	0.22	0.20	0.09	0.02	0.01
n	746	744	746	751	704	745	755	703	751
OP3 III (Early Dry)									
Mean	1.39	0.14	1.48	0.54	0.70	0.26	0.31	0.06	0.06
Median	1.05	0.10	1.38	0.52	0.68	0.19	0.30	0.06	0.06
Percentiles									
–95th	3.57	0.44	2.67	0.84	0.99	0.67	0.43	0.09	0.10
–5th	0.12	0.05	0.48	0.31	0.45	0.05	0.20	0.03	0.03
σ	1.19	0.15	0.67	0.16	0.16	0.20	0.07	0.02	0.02
n	1269	1290	1252	1369	1364	1374	1372	1382	1378
OP3 All data									
Mean	1.30	0.18	1.36	0.48	0.77	0.25	0.34	0.06	0.06
Median	1.00	0.15	1.28	0.47	0.75	0.19	0.33	0.06	0.05
Percentiles									
–95th	3.36	0.48	2.54	0.78	1.10	0.67	0.50	0.09	0.09
–5th	0.17	0.02	0.46	0.22	0.46	0.05	0.22	0.03	0.03
σ	1.07	0.16	0.62	0.18	0.21	0.20	0.09	0.02	0.02
n	2015	2034	1999	2120	2068	2119	2127	2085	2129

Table 2b. Summary of VOC fluxes (mg $m^{-2} h^{-1}$) measured during the two intensive OP3 campaigns.

	Isoprene	Σ Monoterpene	Methanol	Acetaldehyde	Acetone	MVK+MACR	Acetic acid	Hexanal	EVK
OP3 I (Wet)									
Mean	0.54	0.15	−0.02	0.01	0.007	−0.0024	−0.005	0.004	0.004
Median	0.22	0.11	−0.05	0.02	0.009	−0.005	−0.006	0.006	0.005
Percentiles									
−95th	2.23	0.62	0.30	0.11	0.115	0.079	0.052	0.053	0.047
−5th	−0.12	−0.10	−0.34	−0.08	−0.091	−0.098	−0.061	−0.447	−0.035
σ	0.82	0.22	0.21	0.06	0.065	0.055	0.036	0.032	0.025
n	373	329	421	416	417	461	421	406	406
OP3 III (Early Dry)									
Mean	1.18	0.29	−0.04	0.004	0.002	−0.002	−0.003	0.003	0.002
Median	0.76	0.21	−0.08	0.006	0.019	0.003	−0.010	0.005	0.004
Percentiles									
−95th	4.02	0.92	0.51	0.127	0.119	0.091	0.058	0.034	0.032
−5th	−0.38	−0.10	−0.60	−0.116	−0.081	−0.109	−0.059	−0.027	−0.03
σ	1.42	0.37	0.35	0.084	0.065	0.072	0.004	0.021	0.021
n	578	550	622	667	702	739	672	644	647
OP3 All data									
Mean	0.93	0.241	−0.033	0.007	0.012	−0.002	−0.038	0.003	0.003
Median	0.46	0.164	−0.063	0.014	0.014	−0.002	−0.008	0.005	0.004
Percentiles									
−95th	3.67	0.835	0.457	0.120	0.116	0.083	0.058	0.042	0.04
−5th	−0.28	−0.109	−0.537	−0.108	−0.084	−0.107	−0.06	−0.035	−0.033
σ	1.25	0.329	0.299	0.073	0.065	0.066	0.037	0.026	0.023
n	951	879	1043	1083	1119	1200	1093	1050	1053

Table 3. Isoprene and monoterpene flux measurements from the world's tropical forests and their typical ratios (monoterpene/isoprene). All values are in units of mg C $m^{-2} h^{-1}$. Where available, errors show ±1 standard deviation.

Location	Season	Method	Isoprene	Σ Monoterpene	Ratio	Reference
Borneo, SE Asia	L Wet	EC	0.48 ± 0.72	0.13 ± 0.19	0.27	Langford et al., this study
Borneo, SE Asia	E Dry	EC	1.04 ± 1.25	0.25 ± 0.33	0.24	Langford et al., this study
Malaysia, SE Asia	Dry	LL	1.05	–	–	Saito et al. (2008)
Amazon, Brazil	E Dry	MB	2.73	0.24	0.23	Zimmerman et al. (1998)
Amazon, Peru	E Dry	MLG	7.2	0.45	0.06	Helmig et al. (1998)
Amazon, Brazil	L Wet	EC, REA	2.1	0.23	0.11	Rinne et al. (2002)
Amazon, Brazil	L Dry	EC	7.3 ± 2.7	1.5 ± 1.1	0.21	Karl et al. (2007)
Amazon, Brazil	L Dry	MLG	10.2 ± 3.5	2.2 ± 0.7	0.22	Karl et al. (2007)
Amazon, Brazil	L Dry	MLV	11.0 ± 0.9	3.9 ±1.1	0.35	Karl et al. (2007)
Amazon, Brazil	E Dry	REA	2.1 ± 1.6	0.39 ± 0.43	0.19	Kuhn et al. (2007)
Amazon, Brazil	E Dry	SLG	3.4 ± 3.6	0.38 ± 0.58	0.11	Kuhn et al. (2007)
Amazon, Brazil	–	REA	1.1	0.2	0.18	Stefani et al. (2000)
Amazon, Brazil	–	BM	1.9	0.16	0.08	Greenberg et al. (2004)
Amazon, Brazil	–	BM	4.7	0.20	0.04	Greenberg et al. (2004)
Amazon, Brazil	–	BM	8.6	0.54	0.06	Greenberg et al. (2004)
French Guyana, Suriname	Dry	CBL	6.1	–	–	Eerdekens et al. (2009)
Costa Rica	Wet	REA	2.2	–	–	Geron et al. (2002)
Costa Rica	Dry	DEC	2.2	0.29	0.13	Karl et al. (2004)
Congo, Africa	–	A–REA	0.9	–	–	Greenberg et al. (1999)
Congo, Africa	–	LL	0.8 – 1	–	–	Klinger et al. (1998)
Congo, Africa	–	REA	0.46 – 1.4	–	–	Serca et al. (2001)

EC = Eddy covariance; (A)-REA = (Airborne) Relaxed eddy accumulation; SLG = Surface layer gradient; MB = Mass Budget; MLG = Mixed layer gradient; MLV = Mixed layer variance; LL = leaf level extrapolation; BM box = modelling; CBL = Convective boundary layer budgeting.

Table 4. Summary of the coefficients used to drive the MEGAN model. Standard coefficients are based upon studies of temperate plant species, whereas fitted coefficients relate to the measured flux data obtained during OP3-III over a tropical rainforest.

		G06 Standard Coefficients		G06 Fitted Coefficients	
Coefficients		Isoprene	Σ Monoterpenes	Isoprene	Σ Monoterpenes
CT_1	(Eq. 5)	95	95	142	95
CT_2	(Eq. 5)	230	230	232	230
p_o	(Eq. 7)	200	200	200	200
T_{max}	(Eq. 8)	313	313	316.1	312.9
x^1	(Eq. 6)	0.004	0.004	0.006	0.006
x^2	(Eq. 6)	0.0005	0.0005	0.0004	0.00025
x^3	(Eq. 7)	0.0468	0.0468	0.0702	0.0702
x^4	(Eq. 9)	2.034	2.034	3.051	2.058
x^5	(Eq. 8)	0.6	0.6	0.52	0.47
BER		1.65	0.4	2.5	0.5
R^2		0.47	0.44	0.50	0.45
M		0.56	0.51	0.43	0.37

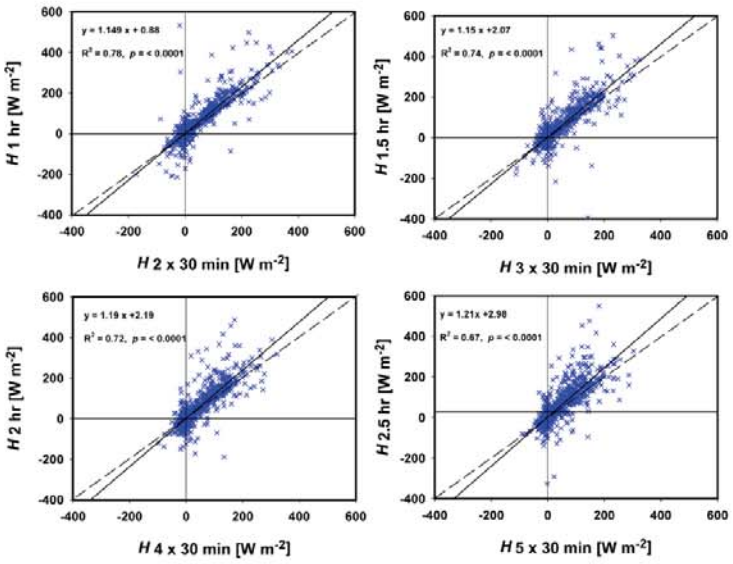

Fig. 1. An analysis of low frequency flux losses for sensible heat flux data *(H)* collected at the GAW site during the OP3 campaign. Solid line shows the best linear fit and dashed line represents the 1:1 line.

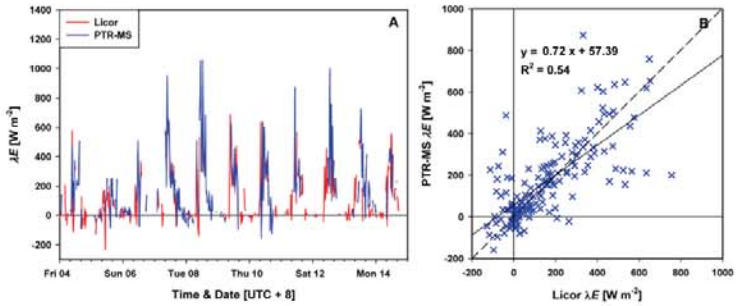

Fig. 2. Latent heat fluxes measured at the GAW site during the period of 4–14 July by open path IRGA (LICOR – 7500) and PTR-MS. PTR-MS water vapour measurements recorded as *m/z* 37 were calibrated against a closed path IRGA (LICOR – 7000) which sampled from the same 70 m sample line as the PTR-MS. **(B)** indicates the amount of flux lost due to dampening of water vapour which can be used to estimate a worst case scenario of VOC flux losses.

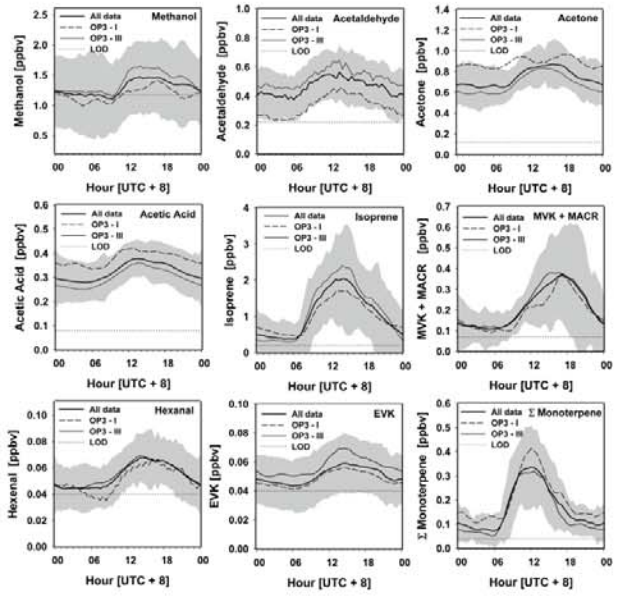

Fig. 3. Average diurnal profiles of VOC mixing ratios measured during the two intensive OP3 field campaigns which took place between 20 April–7 May (OP3-I) and 20 June and 20 July (OP3-III), 2008. Grey error bands show ±1 standard deviation of averaged hourly values and dotted lines show the limit of detection (LOD=2×$\sigma_{background}$/sensitivity).

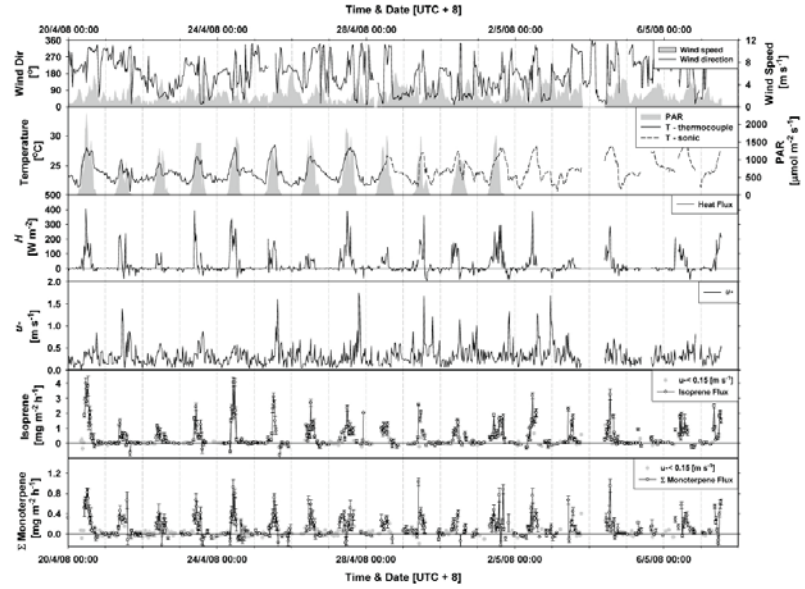

Fig. 4a. Summary of the meteorology and main VOC fluxes during the first intensive OP3 field campaign (OP3 – I) which took place during April and May, 2008. Wind speed and wind direction measurements were recorded by a senor (WXT-510 Weather Transmitter, Vaisala) situated at 75 m on the GAW tower. Temperature was recorded at 30 m by an aspirated thermocouple and sonic anemometer, PAR was measured from the roof of the GAW laboratory and sensible heat, friction velocity and VOC fluxes were all measured from the 75 m platform of the GAW tower. VOC flux data recorded during periods of low turbulence ($u_* < 0.15\,m\,s^{-1}$) were rejected from the final analysis, but are shown here as grey circles.

12015

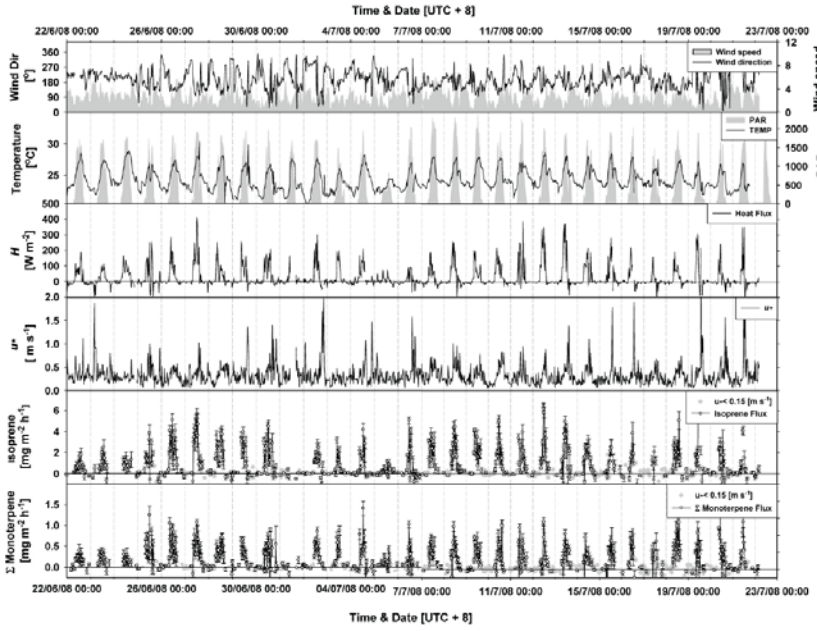

Fig. 4b. Summary of the meteorology and main VOC fluxes during the second intensive OP3 field campaign (OP3 – III) which took place during June and July, 2008. Measurement instrumentation as above. VOC flux data recorded during periods of low turbulence ($u_* < 0.15\,m\,s^{-1}$) were rejected from the final analysis, but are shown here as grey circles.

12016

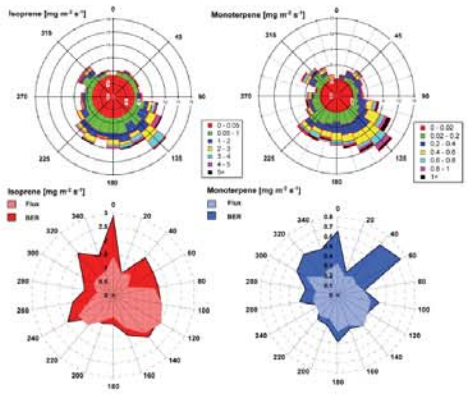

Fig. 5. Wind roses of isoprene and monoterpene fluxes (top) measured during the two OP3 campaigns. The bottom plots show the same flux data normalised to standard conditions (30°C (Canopy temperature), 1000 µmol m^{-2} s^{-1}) using the light and temperature algorithms from the MEGAN model (Guenther et al., 2006).

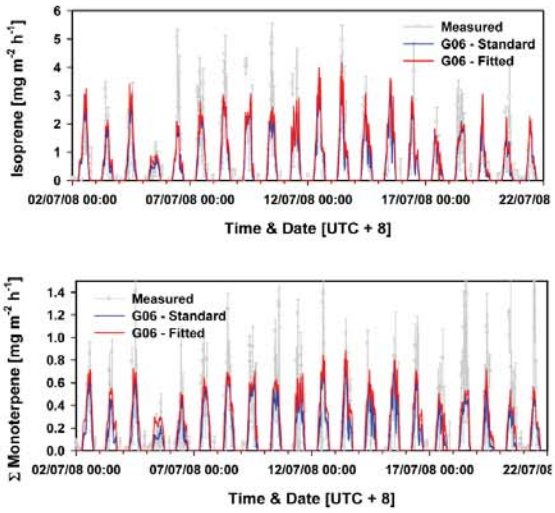

Fig. 6. Isoprene and monoterpene fluxes (grey line) measured by the continuous flow disjunct eddy covariance technique during the OP3-III field campaign. The blue line shows the model output when configured using the standard G06 coefficients and the red line shows the same output generated with empirically fitted parameters. Both sets of parameters, including basal emission rates normalised to 30°C and 1000 µmol m^{-2} s^{-1} are listed in Table 3.

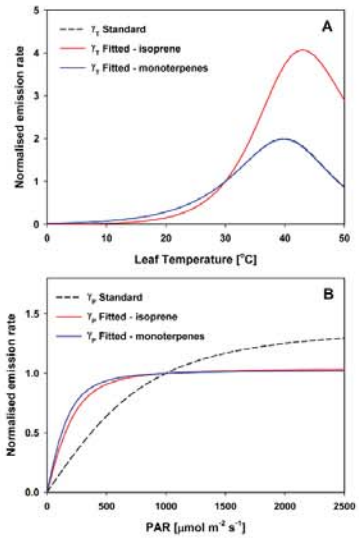

Fig. 7. The temperature **(a)** and light **(b)** response of the G06 algorithm. Dashed lines show the G06 response using standard coefficients which are based on temperate species only (in (a), the dashed line is directly below the blue line). Solid lines show the G06 response for isoprene (red) and monoterpenes (blue) using new coefficients which were obtained by fitting the algorithm response to measured fluxes above a tropical rainforest in Malaysian Borneo. In each response, past light and temperature values were set to: T24=297, T240=297, PAR24=360, PAR 240=375.

12019

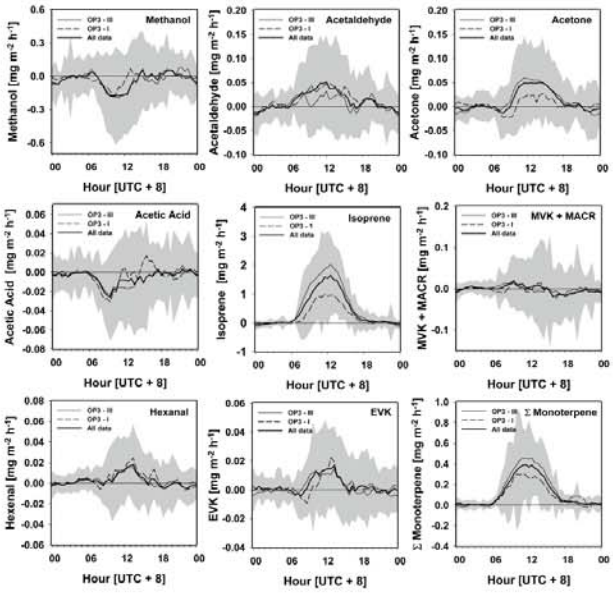

Fig. 8. Average diurnal profiles of VOC fluxes measured during the two intensive OP3 field campaigns which took place between 20 April–7 May (OP3-I) and 20 June and 20 July (OP3-III), 2008. Greyed bands show ±1 standard deviation of averaged hourly values.

12020

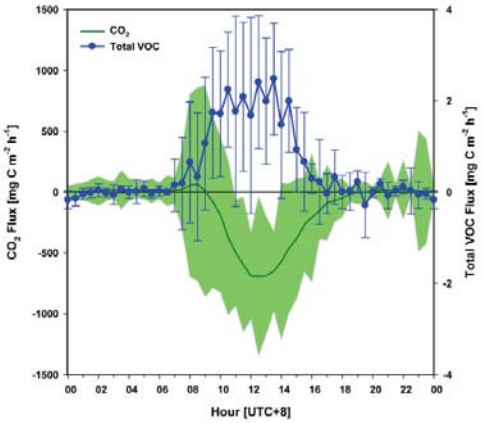

Fig. 9. Averaged diurnal profiles of CO_2 and total VOC (sum of isoprene, monoterpenes, methanol, acetaldehyde, acetone, acetic acid, MVK+MACR, hexanal and EVK fluxes) fluxes measured above a SE Asian tropical rainforest during the period of 20 June–20 July 2008. Error bars and greyed bands show ±1 standard deviation of mean averaged values.

II-G Misztal, P., Fares, S., and Taraborrelli, D.: Report on an e-working module on biogenic emissions, in:Report on Surface Emissions and Prediction of Atmospheric Composition Changes – GEIA Summer School Ile d'Oleron, France, 44-48, 2007.

Open access:
http://www.geiacenter.org/workshops/summerSchool07/presentations/report_school_final.pdf

generation. There should also be sections discussing the production of primary BC and OC, the production and processing of Anthropogenic SOA, sulfate, nitrate and ammonia components of aerosol and the role of photochemical smog. This section should have links with the module on anthropogenic emissions.

Secondary Organic Aerosol (SOA) topics include Biogenic SOA from vegetation and DMS from marine organisms. Both of these topics should link to a discussion of possible feedback couplings involving these natural emissions and climate.

Topic 2: Aerosol effects
This section should include both radiative and health effects. Radiative effects section should describe how aerosols affect the radiative balance of the atmosphere. The health effects of aerosols should include PM10, PM2.5, PM1.0 regulations and discuss the cost of health effects and excess deaths. This could include a link to WHO website.

Topic 3: Aerosol sinks
Aerosol sinks include dry deposition and wet deposition. This section should include information on the relative importance of dry and wet deposition and how this varies for different types of aerosols. The mechanisms controlling wet and dry deposition should be described along with the role of key environmental variables. This could include the ability of particles to be cloud condensation nuclei.

Topic 4: Spatial and Temporal Variability
This topic should describe the magnitude and distribution of aerosol spatial and temporal variability. This should include a discussion of the factors controlling these variations and how they will respond to land-use and climate change. The relative contribution of sources and sinks to this variability should be described.

10. Report on an e-working module on biogenic emissions

Pawel Misztal, Silvano Fares, Domenico Taraborrelli

The e-working module on biogenic VOC emission measurements could describe the reason why hydrocarbons are emitted by plants, which compounds are emitted, as well as the range of approaches and analytical techniques that are used to characterize emissions over different scales (i.e. leaf, canopy, landscape and regional scale). This should include a section on analytical methods and another section on flux techniques.

Which compounds are emitted by plants and why?

These compounds are usually referred with the acronym VOC that stand for **V**olatile **O**rganic **C**ompound. The compounds emitted by vegetations can mostly be classified in terpenes and oxygenated organic compounds (OVOCs). The terpenes homologes compounds that all contain isoprenoid elements, -CH=C(CH_3)CH=CH- .

Plants emit in the atmosphere Biogenic Volatile Organic Compounds (BVOC), and emissions are estimated at 1-1.5 TgC $year^{-1}$ on a global scale. These emissions account no more than 3% of the total carbon exchange between biota and the atmosphere, but they play an important role in the oxidative chemistry of the atmosphere, consuming hydroxyl radicals and consequently the lifetime of radiatively active trace gases like methane. Even more importantly, BVOC may contribute in the presence of anthropogenic pollutants, namely NO_x, to the formation of ozone, photochemical smog, and particulate matter. In non-stressed conditions, Isoprenoids are the main constituent of BVOC, and forest plant species are the most important isoprenoid emitters.

Isoprene (2 mehyl-1,3 butadiene) is an hemiterpene with the formula C_5H_8. It is thought to be the most emitted VOC globally. The estimate of its annual global emission is on average 580 Tg/yr. Its emissions affect substantially the atmospheric composition both near the source area and downwind.

Monoterpenes are 10-carbon atoms very representative emitted by plants, especially oak species in the regions with Mediterranean climate. Their chemical formula is $C_{10}H_{16}$. The estimate of their annual global emission is 127 TgC/yr. Visual association between their chemical formulas and the smells they responsible for. For instance limonene <-> citrus. The most abundant monoterpenes species emitted are Linalool, α,β-pinene, Limonene, Terpinolene, α,β-Phellandrene, c,t-β-Ocimene, also emitted by pines and several tree species belonging to the Fagales group. Moreover, a large group of plants evolved the capacity to store monoterpenes in specialized organs like ducts or glands, and are massively emitted when these organs are broken under mechanical stress. Also if monoterpenes emission is lower then isoprene at a global scale, the role in the atmospheric chemistry for monoterpenes is higher because of the higher reaction time then isoprene with pollutants like ozone and NO_x.

Sesquiterpenes are 15-carbon BVOC and they are synthesized by plants also emitting isoprene or monoterpenes. Their formula is $C_{15}H_{24}$. The most known ones are beta-caryophyllene and alpha-humulene. They turn out to be extracted (and probably emitted) by two plants important for producing beverages. In fact alpha-humulene is extracted from "humulus lupulus" that is commonly used in brewery and beta-caryophyllene from cloves also important to make Gluehwein during Christmas time. (This e-working module would profit from doing the visual association of the chemical structures of these two sesquiterpenes and one glass of bier and one of gluehwein.). Due to their high reactivity often higher than monoterpenes, they are very important in the chemistry of atmosphere, but difficult to measure for their fast reaction with ozone. They have been studied in southern and central Europe.

A second class of BVOC is represented by the oxygenated hydrocarbons. Methanol is one of the most abundant indicator of leaf expansion. Other compounds emitted in response of injury are methyl-jasmonate and ethylene, c-6 compounds from the breakdown of membrane lipids which are giving the "green leaf smell" after cutting the grass. Again a visual association between its formula a person cutting the grass is welcome in this e-working module. Acetaldehyde and methyl-butenol. Acetone, CH_3COCH_3, are emitted in large amounts by the buds of the conifers.

Ethene was found to induce defensive reactions within the plants that produce it. It perhaps more interesting to reader to show that it is also a plant hormone and used to make fruits like lemons and tomatoes ripe.

The role of BVOC emitted in the atmosphere is very important, also because the metabolic cost in terms of fixed carbon re-emitted in the atmosphere is relevant. Normally, the emission of isoprenoids is typical of less evolutionary advanced plants. It was observed that BVOC protect the plants against oxidative drought and ozone stress. It was found that BVOC are involved in a mechanism of thermal protection after observing that isoprene-emitted leaves were more resistant to the stress. The latter hypothesis was confirmed, and the role of antioxidant against all oxidative stress was attributed to the BVOCs. The hypothesis that the lipophylic isoprenoids interact with lipids in membranes strengthening membranes exposed to the stress was proposed. BVOC may also scavenge pollutants in the intercellular spaces with direct and indirect reactions and reducing the potential level of membrane oxidation. It was found that isoprenoids may remove NO_x in the intercellular spaces, thus limiting the signaling cascade which leads to programmed cell death. The emission of isoprenoids was increased after exposure to high ozone levels in plants of transgenic Tobacco and Holm oak although other studies observed a limitation to VOC production probably caused by a biosynthetic limitation of the VOC precursors. Isoprenoids play a defensive role also against biotic stress. They can deter insects and herbivore feedings and block the colonization of wounding by bacteria and fungi.

How are BVOCs emitted?

VOCs that are emitted directly have to be separated from the ones stored in pools. Consequences on the emission dependencies on light and temperature have to be indicated.

A basal emission is usually defined as the emission of a VOC under standard conditions, eg. T= 303 K. It is assumed a constant quantity but unfortunately this turns out to be not case. In fact it changes with the season and the age of the plants (phenology). For instance delay effects have been observed in spring in boreal deciduous forests. The emissions of a certain VOC do not start significantly until a few weeks of warm spring weather is experienced by the plants.

Analytical methods

The most commonly used method for quantifying and identifying biogenic VOC is capillary gas chromatography (GC) with flammable ionisation detection (FID) for quantification and a mass spectrometer (MS) for identification. This approach is relatively slow (~30 minutes) but gives both qualitative and quantitative results. To achieve a detection limit as low as ppt, the sample must be preconcentrated by using preconcentration systems based on cryogenic or sorbent principles. Some recent variants of chromatographic instrumentation with better detection and speciation of biogenic compounds involve gas chromatography-time of flight mass spectrometry (GC-TOF/MS) or comprehensive gas chromatography-time of flight mass spectrometry (GCxGC-TOF/MS)

Another analytical method is Proton Transfer Reaction Mass Spectrometry (PTR-MS), which has been recently widely used for the quantification of many biogenic volatiles. The advantage of this method is that it is very fast with analysis time in the order of seconds and with sensitivity in the ppt range. However, this method often requires combination with other techniques in order to validate what compounds are contributing to which particular masses. On the other hand, the recent development of the Proton Transfer Reaction - Time of Flight - Mass Spectrometer (PTR-TOF-MS) enables much higher mass resolution, thus allowing for the separation and detection of the majority of isobars.

Flux techniques

An estimate of how much of a particular biogenic compound is emitted to the atmosphere or how much is taken up by plants can be made using a variety of methods, which include:
1. Leaf cuvettes. These include systems that are temperature controlled and connected to a data acquisition and control system. When included as a component of a leaf gas exchange measurement system, they can be used for evaluations of photosynthesis, transpiration and stomatal function of a leaf. Cuvettes can be designed for a variety of plant types include conifer species.
2. Branch enclosures. These rely on enclosing individual branches of trees with light transparent Teflon or Tedlar bags. They have the advantage of averaging the measurement over a larger amount of foliage but generally lack environmental control.
3. Flux towers and airborne systems. Canopy scale flux measurements using tower based systems can be used to characterize temporal variations while airborne systems can characterize regional variations. Flux can be determined using the aerodynamic gradient method, where the concentrations are measured at two or more different heights, or by the Eddy Covariance (EC) technique, which is the most direct method for measuring the exchange between the vegetation and atmosphere. The general principle of EC flux is the covariance of the instantaneous deviation of the concentration and the corresponding instantaneous deviation of the vertical wind speed. In order to fulfill the requirements for this method, sensors as fast as 10Hz are normally required. The PTR-MS is suitable for the BVOC flux determination by EC. In addition, a chemiluminescence Fast Isoprene Sensor (FIS) can also be used for eddy covariance flux measurements.

Other ideas to be included in the module

During the discussions about the modules, several ideas were suggested for making the modules more interactive. As a fundamental part of the learning process we find important to make quizzes related to each topics. For instance a multiple choice questionnaire that visualize in a funny way how much of certain VOC is emitted globally by vegetation. Two examples are given below:

Quizzes

1. How much isoprene is emitted every year in term of persons ?
The population of : a. Paris; b. Italy; c. Europe; d. World

Answer: Isoprene is emitted in 580 Tg/yr = 5.8 10^{11} kg/yr (Guenther et al.(2006)). This corresponds to about :
~7.73 billion people(75kg)/year ~ the World + another India

~ 212 million people(75kg)/day > Germany, Italy and France (they could be visualized with the relative maps or with the relative common stereotypes for each of these countries.)
~ 8.8 million people(75kg)/hour ~ the population of a fairly big city

The annual global monoterpene emissions correspond to the population of:
a. Europe + USA; b. China + Europe; c. USA + Africa; d. South America + USA

2. Interactive animation
It is advisable to let the reader interact and play with an animation to fix a few concepts in his/her memory. For instance an animation with the sun rising and setting and the resulting changing emissions of a tree. Another animation would be to let the reader change parameters like basal emission, temperature and light intensity and see the effect on the isoprene emission. Regarding the light intensity, a much more attractive idea would be to let the reader change the level of cloudiness choosing for instance the number of clouds over a tree. The exercise could be repeated with VOC stored in specific pools for which the light intensity does not affect the emissions as strongly as for isoprene. Parameterizations for such variables like temperature and light intensity should be easily derived as simplification of relationships presented in the tutorials.

Looking or making fruits ripe: Ethylene, also known as the 'death' or 'ripening hormone' plays a regulatory role in many processes of plant growth, development and eventually death. There is a nice web page showing the developmental stages of strawberry correlated to the ethene concentration
(http://www.ru.nl/tracegasfacility/life_science_trace/plant_physiology/ethylene_during/)

11. Report on an e-working module on biomass burning emissions

Gaelle Clain, Vijay Kanawade, Lucia Viegas de Barros, Cathy Liousse

Introduction

Human activities – *industrial, agricultural, residential, and transportation* and natural activities – l*ightening induced fires, volcanoes, and extreme temperatures* cause vast quantities of chemical species to be emitted into the Earth's atmosphere, particularly in the troposphere. In turn, atmospheric pollution in the troposphere is becomes a global phenomenon in which local and regional scale emission drive tropospheric chemistry on hemispheric scale and directly impact on the air quality and climate change. Biomass burning is estimated as a major source for the global carbon budgets of many trace gases such as carbon dioxide (CO_2), methane (CH_4), ozone (O_3), carbon monoxide (CO), and non-methane hydrocarbons (NMHCs) and also fine mode particles in the troposphere. Both the CO_2, CH_4 and BC directly influence the global warming on the earth while fine organic particles mostly induce global cooling. Moreover, changes in oxidizing capacity relating to CO variability could perturb the growth rates of many greenhouse gases. Thus, their atmospheric accumulations due to an increase of biomass burning emission will very likely cause future global climate changes. Observation of how the planet system is responding to this perturbation is a key to understanding the consequences of both natural and human induced modifications. On the short term and a local scale, an important

II-H Misztal, P. K., et al.: Large estragole fluxes from oil palms in Borneo, Atmos. Chem. Phys., 10, 4343-4358, 2010.

Open access: http://www.atmos-chem-phys.net/10/4343/2010/acp-10-4343-2010.html

Atmos. Chem. Phys., 10, 4343–4358, 2010
www.atmos-chem-phys.net/10/4343/2010/
doi:10.5194/acp-10-4343-2010

Atmospheric Chemistry and Physics

Large estragole fluxes from oil palms in Borneo

P. K. Misztal[1,2], S. M. Owen[1], A. B. Guenther[4], R. Rasmussen[6], C. Geron[5], P. Harley[4], G. J. Phillips[1], A. Ryan[3], D. P. Edwards[7], C. N. Hewitt[3], E. Nemitz[1], J. Siong[8,1], M. R. Heal[2], and J. N. Cape[1]

[1]Centre for Ecology & Hydrology, Penicuik, EH26 0QB, UK
[2]School of Chemistry, University of Edinburgh, Edinburgh, EH9 3JJ, UK
[3]Lancaster Environment Centre, Lancaster University, Lancaster, LA1 4YQ, UK
[4]Atmospheric Chemistry Division, National Center for Atmospheric Research, 1850 Table Mesa Drive, Boulder, Colorado, 80305, USA
[5]US Environmental Protection Agency, National Risk Management Research Laboratory, Mail Drop E305-02, 109 TW Alexander Dr., Research Triangle Park, NC 27711, USA
[6]Department of Environmental Science and Engineering, Oregon Graduate Institute, P.O. Box 91000, Portland, OR 97291, USA
[7]Institute of Integrative and Comparative Biology, University of Leeds, Leeds, LS2 9JT, UK
[8]School of Science and Technology, Universiti Malaysia Sabah, 88999, Malaysia

Received: 15 December 2009 – Published in Atmos. Chem. Phys. Discuss.: 20 January 2010
Revised: 28 April 2010 – Accepted: 29 April 2010 – Published: 7 May 2010

Abstract. During two field campaigns (OP3 and ACES), which ran in Borneo in 2008, we measured large emissions of estragole (methyl chavicol; IUPAC systematic name 1-allyl-4-methoxybenzene; CAS number 140-67-0) in ambient air above oil palm canopies (0.81 mg m^{-2} h^{-1} and 3.2 ppbv for mean midday fluxes and mixing ratios respectively) and subsequently from flower enclosures. However, we did not detect this compound at a nearby rainforest. Estragole is a known attractant of the African oil palm weevil (*Elaeidobius kamerunicus*), which pollinates oil palms (*Elaeis guineensis*). There has been recent interest in the biogenic emissions of estragole but it is normally not included in atmospheric models of biogenic emissions and atmospheric chemistry despite its relatively high potential for secondary organic aerosol formation from photooxidation and high reactivity with OH radical. We report the first direct canopy-scale measurements of estragole fluxes from tropical oil palms by the virtual disjunct eddy covariance technique and compare them with previously reported data for estragole emissions from Ponderosa pine. Flowers, rather than leaves, appear to be the main source of estragole from oil palms; we derive a global estimate of estragole emissions from oil palm plantations of ~0.5 Tg y^{-1}. The observed ecosystem mean fluxes (0.44 mg m^{-2} h^{-1}) and mean ambient volume mixing ratios (3.0 ppbv) of estragole are the highest reported so far. The value for midday mixing ratios is not much different from the total average as, unlike other VOCs (e.g. isoprene), the main peak occurred in the evening rather than in the middle of the day. Despite this, we show that the estragole flux can be parameterised using a modified G06 algorithm for emission. However, the model underestimates the afternoon peak even though a similar approach works well for isoprene. Our measurements suggest that this biogenic compound may have an impact on regional atmospheric chemistry that previously has not been accounted for in models and could become more important in the future due to expansion of the areas of oil palm plantation.

Correspondence to: P. K. Misztal
(pawel.m@ed.ac.uk)

1 Introduction

Estragole or 1-allyl-4-methoxybenzene (AMOB) is an oxygenated volatile organic compound (OVOC) with molecular weight of 148 and a boiling point of 216 °C at atmospheric pressure, and therefore should be regarded as a semi-volatile organic compound. Although it is a C-10

Published by Copernicus Publications on behalf of the European Geosciences Union.

compound ($C_{10}H_{12}O$) it is not classified as terpenoid because it is produced by the phenylpropanoid pathway rather than a terpenoid pathway. It has many synonyms, of which the most commonly used after estragole are methyl chavicol, p-allylanisole, isoanethole, chavicyl methyl ether or 1-methoxy-4-prop-2-enylbenzene. Estragole is the original name attributed to the compound and it is used throughout this article. It derives from "estragon", the French and German word for tarragon (*Artemesia dracunculus*), a herb to which it gives its anis-like odour.

Even though estragole was reported to be a major component of ponderosa pine emissions almost 30 years ago (Altshuller, 1983), the growing interest in this compound in the atmospheric science community has been relatively recent. The interest follows analytical improvements over the last decade which have extended biogenic emission studies to a wider variety of compounds, including estragole. Bouvier-Brown et al. (2009a) recently reported measurements of estragole emissions and ambient concentrations from ponderosa pine trees and highlighted the importance this compound might have for atmospheric chemistry. Lee et al. (2006b) found that the secondary organic aerosol (SOA) yield from full photochemical oxidation of this compound was the highest of all oxygenated terpenes (40%) and also that it was significantly higher than the SOA yield from its ozonolysis (6%) (Lee et al., 2006a). Emissions of estragole from oil palms have not yet been quantified even though, as shown later, they exceed many times those reported from other species, and thus their contribution to regional photochemistry is likely to be considerable. Estragole, like many other BVOCs, is suspected to be harmful to human health at high concentrations (EPA, 2002).

The area of oil palm (Arecaceae *Elaeis*) plantations is rapidly expanding in South East Asia, in order to meet the global demand for palm oil. Globally the land area of oil palm plantations is estimated at 13.9 million hectares, where the majority (60%) is concentrated in Malaysia (3.8 Mha) and Indonesia (4.6 Mha) (FAO, 2009). The oil palm cultivated there is usually a high yielding cross between dura and pisifera forms of *Elaeis guineensis* Jacq., which is native to tropical Africa, or hybrids of *E. guineensis* with *E. oleifera*, which is native to Latin America. Plantation area has increased in Malaysia from 55 000 hectares in 1960, to half a million in 1975, and a million hectares were under cultivation in 1980 (Hartley, 1988). Nowadays the area is nearly 4 million ha.

It was originally thought that the oil palm is mainly wind pollinated, until Syed (1979) showed experimentally that the oil palm is mainly insect pollinated. Estragole is the known attractant for the weevil (*Elaeidobius kamerunicus* Faust) which is the specific pollinator of *Elaeis guineensis* flowers. *E. guineensis* is monoecious containing both female and male flowers on one tree which open at different times and which are pollinated all year round (Henderson, 1986; Syed, 1979; Tandon et al., 2001). This weevil responds specifically to estragole and not its derivatives, as was experimentally shown by Hussein et al. (1989). It is not native to Borneo but was introduced from Cameroon in 1981 for the purpose of improving pollination and increasing crop yields (Hartley, 1988). The specificity of the pollinator and lack of predators led to a great success for the palm oil industry, saving tens of million pounds on hand pollination (Hussein et al., 1991). Estragole emissions are therefore of great importance to the oil palm industry.

The lifetime of estragole in the atmosphere has been estimated for temperate latitudes by Bouvier-Brown et al. (2009a) as 55 min and 18 h for reaction with OH and O_3, respectively, suggesting that this compound can have an impact on regional photochemistry. Estragole oxidation is not included in the Master Chemical Mechanism (MCM)[1], nor are any other aromatic species with methoxy or 2-propenyl substituents. The reactivity of estragole to OH might be expected to be similar to that of methoxybenzene, or the methoxy-substituted aromatic ring ($\sim 3\times10^{-11}$ cm^3 molecule^{-1} s^{-1}), with the side chain reacting similarly to a terminal alkene (M. E. Jenkin, personal communication, 2009). Recently, Bouvier-Brown et al. (2009a) reported two consistent estimates for k_{OH} of 5.7×10^{-11} cm^3 molecule^{-1} s^{-1} from ozonolysis studies performed by Lee et al. (2006a, b) and 5.4×10^{-11} cm^3 molecule^{-1} s^{-1} derived using the Environmental Protection Agency's Estimation Program Interface Suite (EPA, 2000). These are similar to the k_{OH} value for 2-methyl-3-buten-2-ol (MBO). The same authors also estimated rate coefficients for the reaction of estragole with ozone (k_{O_3}) of 1.4×10^{-17} cm^3 molecule^{-1} s^{-1} and 1.2×10^{-17} cm^3 molecule^{-1} s^{-1}, respectively, using the same experimental and modelling approaches. It would be anticipated that the initial stages of estragole degradation are efficient at generating ozone, since 1-alkenes typically have photochemical ozone creation potentials (POCP) of around 100. On the other hand, if degradation leads to compounds of structures similar to benzaldehyde or nitrophenols, then the impact on ozone formation will be near zero or negative since these compounds lead to near-irreversible sequestration of NO_x and organic material into species which deposit efficiently or are incorporated into aerosol. But in that case, estragole would be expected to act as an efficient SOA precursor. In both instances estragole oxidation will likely have an impact on regional photochemistry.

In May and June 2008 measurements of VOC fluxes by virtual disjunct eddy covariance (continuous flow disjunct) were made using proton transfer reaction mass spectrometry (PTR-MS), and were supplemented by GC-MS study (leaf level and ambient) at an oil palm plantation in Sabah, Borneo (Misztal et al., 2010). Estragole was the second most abundant BVOC (after isoprene) at the plantation and the

[1]http://mcm.leeds.ac.uk/MCM/

observed concentration and fluxes are the highest reported so far from vegetation.

2 Methods

2.1 Site and setup

The experiment site was a flat 33 ha commercial oil palm plantation located at 5°14′52.67 (N) latitude and 118°27′14.96 (E) longitude within a much larger oil palm area belonging to the Sabahmas Oil Palm Plantation owned by Wilmar International Ltd. (Fig. 1). This location is 28 km NE of Lahad Datu in the Malaysian province of Sabah in NE Borneo. The palms were 12 year old *E. guineensis* × *E. oleifera* hybrids of the progeny "Gutherie", with an average height of 12 m and a single-sided leaf area index (LAI) of about 6, planted at a commercial density of 124 trees per ha. The suite of atmospheric measurements at this site and a rainforest site during the OP3 and ACES measurement campaigns is summarised in the introductory paper of this issue (Hewitt et al., 2010).

2.2 Proton Transfer Reaction Mass Spectrometer (PTR-MS)

A Proton Transfer Reaction Mass Spectrometer (PTR-MS) was employed to monitor the VOC concentrations and eddy fluxes of various compounds including estragole. The PTR-MS instrument was a high sensitivity model (Ionicon Innsbruck, Austria, s/n: 04-03) incorporating an additional turbopump for the detection chamber and Teflon instead of Viton rings in the drift tube. In addition in our instrument the Pfeiffer turbopumps have been replaced by their Varian analogues. Operational details have been described elsewhere (e.g. de Gouw et al., 2003; Lindinger et al., 1998), and very recently the PTR-MS technique has been reviewed by Blake et al. (2009), hence only a brief description is presented here. The VOCs under study, whose proton affinities exceed that of water, are soft-ionised in a drift tube by collision with hydronium ions, formed in the hollow cathode of the ion source. The products of the proton transfer reactions are either protonated compounds or their protonated fragments or clusters. The magnitude of fragmentation/clustering can be optimised by adjusting the electric field (E) and the buffer gas number density (N) in the drift tube, so that the E/N ratio is most commonly in the range of 120–140 Td (1 Td=10^{-17} V cm^2). The relative abundance of the product cations, separated by the quadrupole mass filter, can be derived from the number of pulses counted by the Secondary Electron Multiplier (SEM) during a given dwell time. During the PTR-MS measurements at the plantation the E/N ratio was kept constant at 140 Td by adjusting drift tube parameters of pressure to 160 Pa, temperature to 45 °C and the drift voltage to 485 V. The sampling inlet and the 20 Hz sonic anemometer (Solent R3, Gill Instruments) were

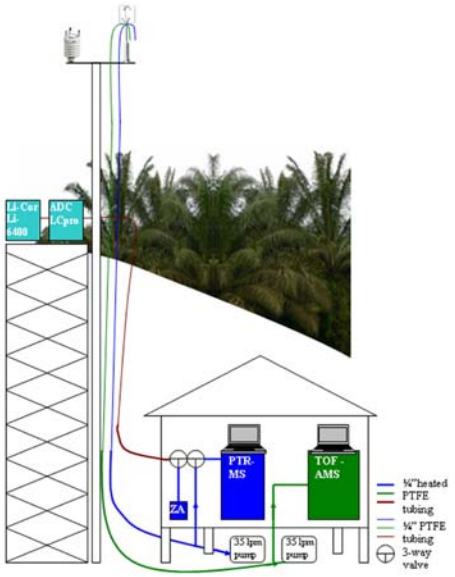

Fig. 1. Schematic of the sampling setup at the Sabahmas Oil Palm plantation, Borneo. Measurements of estragole (and other VOCs) were made at canopy and leaf level using proton-transfer-reaction mass spectrometry (PTR-MS) and leaf cuvettes (Li-COR Li-6400 and ADC LCpro). ZA refers to the zero-air (pure air) generator, and TOF-AMS refers to a time-of-flight aerosol mass spectrometer deployed at the site. In addition, a portable gas chromatograph with a mass spectrometer (Hapsite Smart, Inficon, East Syracuse NY) was used (not presented here) for ambient air and enclosure in-situ analysis.

placed above the canopy at about 15 m. A 20 m PTFE sampling line (1/4″ OD, 3/16″ ID) was used to draw a flow rate of 35 L min^{-1} past the instrument, which sub-sampled at a flow rate of 400 mL min^{-1}. The instrument and PTFE tubing were protected against water condensation by heating above the ambient temperature (approx. 50 °C) using a heating tape (Omega, UK type SRF3-2C self regulating heat cable). In order to get absolute volume mixing ratios, either calibration with an external standard is required, or less precise calculation can be made based on the calibrated transmission of the instrument and the proton transfer reaction rate of estragole. As no estragole calibration standard was available for PTR-MS at the site, the instrument was calibrated against several other VOCs (i.e. methanol, acetonitrile, acetone, acetaldehyde, isoprene, a monoterpene: d-limonene) and then the relative transmission curve was obtained to yield an empirical calibration coefficient for estragole (method described by Taipale et al., 2008). We checked the validity of this approach by comparison with a vapourised estragole standard (98%; Sigma Aldrich) and the results were well within

30% of the values obtained from the relative transmission approach used in the field.

The biggest advantage of PTR-MS is the high frequency of data acquisition, which makes it suitable for use in micrometeorological flux measurement techniques such as eddy covariance (EC). Here, data were processed according to the virtual disjunct eddy covariance concept (Karl et al., 2002; Rinne et al., 2001), where for each *m/z* of interest the PTR-MS makes a measurement which is sufficiently fast (as determined by the dwell and instrument response time), but discontinuous (while the PTR-MS scans the other *m/z* of interest), thus providing fewer data points than continuous EC. For the flux mode the instrument was running in the multiple ion detection (MID) for 25 min every half hour cycling through 13 *m/z* channels including estragole and remaining 10 VOC-related protonated masses analysed at 0.5 s dwell time each, whereas a shorter 0.2 s dwell time was used for the hydronium ($H_3{}^{18}O^+$) ions measured at *m/z* 21 and water clusters $(H_2O)H_3O^+$ measured at *m/z* 37. This corresponded to a cycle length of 7 s with 210 PTR-MS and 30 000 wind rows in 25 min. The effective time lag associated with the residence time in the tubing was calculated from the cross-correlation between vertical wind speed and the VOC mixing ratio as a function of lag time (Davison et al., 2009; Langford et al., 2009; Rinne et al., 2007; Spirig et al., 2005). If no detectable peak was present in the covariance function, or if it was smaller than the detection limit derived by multiplying the standard deviation of the noise over 180 s by 1.5, or if the lag time was not stable during an averaging period (25 min), then the flux data point was discarded. In addition, the data were filtered for stationarity using the criterion of Foken and Wichura (1996), for low friction velocity ($u_* < 0.15\,\mathrm{m\,s^{-1}}$), and for rain events. More than one fifth of the data for estragole flux passed all these validation criteria. In order to assess the likely impact on the representativeness of the time series which followed the rejections, the volume mixing ratio (VMR) data corresponding to rejected flux periods was compared with the full VMR time series. Although their diurnal average pattern became noisier as a result of those rejections (as later shown in Fig. 5), the total average VMR did not change by more than 0.1%.

Estragole is detected at *m/z* 149 in PTR-MS as the protonated molecular ion. It was measured for the first time with PTR-MS in ambient air by Holzinger et al. (2005). This compound is relatively resistant to fragmentation at typical working conditions, with only small fragmentation to *m/z* 121, and thus PTR-MS can be used reliably for monitoring its concentrations and fluxes. There are only a few known minor contributions to *m/z* 149 from other compounds that have been reported so far, of which the most significant are from sesquiterpenes (Bouvier-Brown et al., 2007; Bouvier-Brown et al., 2009b; Helmig et al., 2006; Kim et al., 2009). When the volume mixing ratio of sesquiterpenes relative to estragole is very low, one can assume these contributions to be insignificant. In addition, a GC-MS was used to check the ambient air for any interference with the *m/z* 149 signal. Fluxes of other compounds measured with the PTR-MS at the oil palm plantation included isoprene, total monoterpenes and methanol. These results are presented in a separate paper (Misztal et al., 2010).

2.3 Gas chromatography (GC-MS)

2.3.1 Leaf cuvette sampling method

Two types of leaf cuvette were used for sampling VOC emissions, an ADC LCpro (ADC Bioscientific Ltd. UK), and a Li-Cor Li-6400 (Li-Cor, Inc., Lincoln, Nebraska, USA). Both types of cuvette are portable photosynthesis systems, measuring water vapour (H_2O) and carbon dioxide (CO_2) exchange across the leaf surfaces with infrared gas analyzers (IRGAs) and allowing control of photosynthetic photon flux density (PPFD), leaf and air temperature, humidity, CO_2 concentration, and airflow rate. They were adapted for sampling VOC emissions by introducing a sampling port in the gas line exiting the cuvette.

Before each measurement campaign, the leaf cuvettes had been serviced and checked, and were in optimal working order. A charcoal filter was fitted to the inflow of the leaf cuvettes to remove ambient BVOCs and ozone. This had the effect of elevating the ambient CO_2 concentrations by about 50 ppm on average in the LCpro, but this was fairly consistent for all emission samples. While this is a little higher than the average ambient [CO_2], there are several reports of high [CO_2] between 1 and 5 m from a tropical forest floor during the morning and later in the afternoon (e.g. Buchmann et al., 1997; Culf et al., 1999). Rosenstiel et al. (2003) found that increasing CO_2 concentrations reduces canopy isoprene emission and decouples isoprene emissions from photosynthesis; however, they worked with concentrations of 800 and 1200 ppm, which is far higher than the concentrations the sampled leaves experienced in the investigation reported here (400 ppm). Using a charcoal trap to clean inflowing air would result in upper-limit emission measurements because purified air would lead to a higher concentration gradient of emitted compound than between leaf air space and ambient air.

Inter-comparison experiments performed during previous studies showed that BVOC emissions measured using the ADC LCpro cuvette system were similar to those measured using the Li-COR system (Geron et al., 2006). The leaf cuvettes were installed on a leaf and left to equilibrate for 45 min before VOC samples were taken. Flow rate through the ADC LCpro was $300\,\mathrm{mL\,min^{-1}}$, and $500\,\mathrm{mL\,min^{-1}}$ through the Li-COR. Sampled leaf areas in the ADC LCpro and Li-COR were 6.25 $\mathrm{cm^2}$ and 6 $\mathrm{cm^2}$, respectively. Photosynthetically active radiation (PAR) in the leaf cuvettes was set at an optimum (i.e. $500\,\mu\mathrm{mol\,m^{-2}\,s^{-1}}$ for plants under the canopy; $1000\,\mu\mathrm{mol\,m^{-2}\,s^{-1}}$ for plants that are exposed to sunlight). Carbon dioxide and humidity were both set to

ambient conditions to simulate the plant's actual field condition. Leaf temperature was set at 30 °C or slightly higher to minimise condensation in the cuvettes.

Samples were analyzed by three independent methods including an in-situ portable GC-MS, collection in stainless steel canisters transported to laboratory for analysis, and collection on solid adsorbent cartridges transported to laboratory for analysis. Sample cartridges were filled with 100 mg Carbotrap and 200 mg Tenax and conditioned for 15 min at 300 °C in a flow of helium. Cartridges prepared in this way have been used in our laboratory for many years, and are always very consistent in their adsorbent properties. A cartridge was fitted to the cuvette outlet port, and air from the cuvette drawn through it at 100–120 mL min^{-1} using an SFK mass flow controlled pocket sampling pump. This range of flow rates ensured that only cuvette air was sampled, and was not contaminated with outside air. Samples were taken for 10–20 min, and the cartridges were stored in a refrigerator until returned to CEH, Edinburgh, UK, for analysis using gas chromatography with mass selective detection (GC-MS). In a previous study using the same sampling and analytical system, changes in sample compound content were assessed during storage and transport. Overall, there was between 0.1% and 10.4% more of each compound in the transported standard tubes compared with freshly injected standards, but differences were not significant, due to variability in different batches of diluted standards (Wang et al., 2007). In addition, a sample was taken from an empty leaf cuvette each day to give a blank value which was subtracted from emission samples.

2.3.2 GC-MS analysis

Leaf samples were analysed using a GC-MS system. A thermal desorption autosampler (Perkin-Elmer ATD 400) was connected via a heated (200 °C) transfer line to a Hewlett-Packard 5890 GC with a 5970 mass-selective detector.

Compounds were desorbed at 280 °C for 5 min at 25 mL min^{-1} onto a Tenax-TA cold trap maintained at −30 °C. Secondary desorption was at 300 °C for 6 min onto the GC column. Separation of the compounds was achieved using an Ultra-2 column, Agilent Technologies (50 m × 0.2 mm ID × 0.11 µm film, 5% phenylmethyl silica). The initial oven temperature of 35 °C was maintained for 2 min, then increased at 4 °C min^{-1} to 160 °C followed by an increase of 45 °C min^{-1} to 300 °C which was maintained for 10 min. The carrier gas was helium at ∼1 mL min^{-1}, the injector temperature was 250 °C. For this system, the limit of detection for isoprene and monoterpenes was approximately 0.25 ng on column, whereas for sesquiterpenes it was 2 ng on column. This corresponded to 100 pptv of isoprene, 50 pptv of monoterpenes, and to 400 pptv of sesquiterpenes in a 1 L sample. The level of analytical precision was around 6.5% for isoprene, 5% for monoterpenes and 10% for sesquiterpenes.

Monoterpene and estragole quantification was by comparison with commercially available liquid standards (Aldrich, Fluka and Sigma) appropriately diluted in methanol solution before injecting on column, and isoprene quantification by comparison with a 1 ppmV in N_2 certified gas standard (Air Products UK). Chemstation for Microsoft Windows was used to handle chromatographic data. Identification was achieved by comparison of retention times and mass spectra of authentic standards. Samples were analysed in "scan" mode, but subsequent quantification was achieved by standard calibration and integration of selected ion spectra for isoprene (*m/z* 67) and monoterpenes (*m/z* 93). Ions for identification of estragole were at *m/z* 148, 147, 77, 121, and 117 and the estragole peak appeared at retention time 28.15 min, confirmed by comparison with library spectra.

Ambient air and enclosure samples were also analyzed in-situ with a portable gas chromatograph with a mass spectrometer (Hapsite Smart, Inficon, East Syracuse NY) using a 30 m × 0.32 mm ID × 1 µm film DB-1 column, temperature programmed with an initial 2 min hold at 40 °C followed by a 15 °C min^{-1} ramp to 80 °C followed by a 3 °C min^{-1} ramp to 110 °C followed by a 9 °C min^{-1} ramp to 200 °C with a final 6 min hold. VOCs were quantified with respect to an internal standard referenced to NIST traceable standards.

2.3.3 Flower enclosures

Male and female inflorescences were enclosed using wide transparent Teflon bags (80 L), which were open at both ends. The bags were secured gently around the base of the inflorescence with a cable tie. The other end of the Teflon bag was also closed with a cable tie around the whole inflorescence, leaving enough of a gap to insert a stainless steel sample tube (6 mm OD) filled with Tenax and Carbotrap (as above). The system was static, and after installation, was left for an hour to allow any compounds emitted from the flowers to accumulate inside the Teflon enclosure. A sample tube was then inserted into the small gap left at the closed end. The sample tube was attached to a pump and sampled at a rate of 150 mL min^{-1} for 15 min, giving a total sample volume of 2.25 L. During sampling it was inevitable that air flowed into the Teflon enclosure from outside via the gap around the base of the inflorescence, but the total bag volume was ∼40 L, so the dilution effect would have been at most ∼30%.

2.4 Aerosol mass spectrometer

An Aerodyne high-resolution time-of-flight aerosol mass spectrometer (HR-ToF-AMS) was used to monitor the composition of non-refractory sub-micron PM at the oil palm plantation. The HR-ToF-AMS has been described in detail in DiCarlo et al. (2006) and is a further development of the original Aerodyne quadrupole aerosol mass spectrometer (Jayne et al., 2000; Jimenez et al., 2003). The ambient air was sampled down a 15 m 1/4″ stainless steel inlet tube and

sub-sampled by the AMS via a Nafion drier. The inlet was situated next to the sonic anemometer just above the oil palm canopy co-located with the PTR-MS. The AMS uses an aerodynamic lens in a differentially-pumped vacuum chamber to enhance the aerosol mass over the gas in the sample. The aerosol was vaporised at 600 °C and extracted into the ToF mass spectrometer.

The instrument was operated in the general alternation mode, switching between the MS/PToF mode and the high resolution MS modes every 5 min every other half hour. The remaining half hour was used for eddy-covariance flux measurements not presented in this paper. The data analysis was performed using SQUIRREL, the standard ToF-AMS analysis suite developed by the Universities of Manchester and Colorado and Aerodyne Research and hosted electronically at the University of Colorado at Boulder[2]. Here only parts of the dataset are used, with a more detailed analysis of the aerosol composition and fluxes provided by Nemitz et al. (2010).

2.5 Parameterisations for estragole emission

There are many algorithms for modelling foliar emissions of BVOCs, some of which have been incorporated into models such as MEGAN (Guenther et al., 2006). The potential importance of floral emissions for atmospheric chemistry was recognized by Arey et al. (1991) who report linalool concentrations in an orange tree plantation that are of a similar magnitude to the estragole concentrations observed in this study. However, floral emissions have not been included as a component of regional biogenic emission models due to both the limited quantitative emission rate data and the lack of suitable driving parameters. As a result, it is not known what contribution they make to canopy emission. However, oil palms occupy a large land area, and as we show, the contribution of estragole emissions to total BVOCs can be very high. The actual estragole release and its magnitude are likely to be constrained by biological factors related to the pollination cycle. Temperature of vegetative surfaces can be different from ambient temperature above the canopy, and therefore it is important to use the former in the parameterisations.

Canopy temperature (T_c), as estimated from the resistance approach (Eq. 1), was generally higher by approximately 2 °C during midday and lower by 0.2 °C during the night than T_a (the ambient temperature at the 15 m sensor height).

$$T_c = T\left(z_0'\right) = T_a(z_m) + \frac{H(R_a(z_m) + R_b)}{\rho c_p} \quad (1)$$

Here H is the sensible heat flux, $R_a(z_m)$ is the aerodynamic resistance, R_b is the laminar boundary layer resistance close to the surface of the leaves, ρ is air density, and c_p is the specific heat of air.

[2]http://cires.colorado.edu/jimenez-group/ToFAMSResources/ToFSoftware/index.html

Since estragole may also exhibit occasional deposition, for the highest accuracy atmospheric models would either need to consider this as a loss of part of the emission flux or by including this compound in deposition models. The available data for validated measured deposition are insufficient for the implementation of the canopy resistance analogy (Nemitz et al., 2009; Sutton et al., 1995), in which the overall modelled flux is represented as:

$$F_{net} = F^+ - V_d(z)\chi(z_m) \quad (2)$$

where F_{net} is the net flux above the canopy, F^+ is the parameterised emission from the vegetation, $V_d(z)$ is the parameterised deposition velocity, and $\chi(z_m)$ is the concentration measured. For this modelling exercise we limit the investigation only to modelling emission flux (F^+) (Eq. 3) and we neglect deposition ($-V_d(z)\chi(z_m)$), which is likely to be minor in relation to the emission of estragole.

$$F^+ = \mathrm{BER}_c \cdot \gamma_T \cdot \gamma_P \quad (3)$$

BER_c is the canopy-derived basal emission rate (for standard conditions) which can be obtained from Eq. (3) by substituting F^+ with the eddy covariance flux above the canopy (filtered to exclude deposition periods), γ_T and γ_P are the temperature and PAR activity factors, respectively, compensating for changes in emission due to deviations from standard conditions:

$$\gamma_P = C_P\left[(\alpha \cdot \mathrm{PAR})/(\sqrt{1+\alpha^2 \cdot \mathrm{PAR}^2})\right] \quad (4)$$

$$\gamma_T = E_{opt} \cdot \frac{C_{T2} \cdot \exp\left[C_{T1} \cdot \left(\frac{1}{T_{opt}} - \frac{1}{T}\right) \cdot \frac{1}{0.00831}\right]}{C_{T2} - C_{T1} \cdot \left[1 - \exp\left(C_{T2} \cdot \left(\frac{1}{T_{opt}} - \frac{1}{T}\right) \cdot \frac{1}{0.00831}\right)\right]} \quad (5)$$

where C_P, α, E_{opt}, and T_{opt} can be expanded further:

$$\alpha = b_1 - b_2 \ln(P_{240}) \quad (6)$$

$$C_P = b_3 \cdot \exp\left[b_2 \cdot (P_{24} - P_0) \cdot (P_{240})^{0.6}\right] \quad (7)$$

$$T_{opt} = T_b + [b_4 \cdot (T_{240} - 297)] \quad (8)$$

$$E_{opt} = b_5 \cdot \exp[b_6 \cdot (T_{24} - 297)] \cdot \exp[b_6 \cdot (T_{240} - 297)] \quad (9)$$

In the above equations PAR and T are photosynthetically active radiation (μmol m^{-2} h^{-1}) and leaf temperature (K), respectively. The latter was approximated by deriving T_c (Eq. 1)

In the formalism of the G06 algorithm (Guenther et al., 2006), F^+ (Eq. 3) is a function of the lag-adjusted ambient temperature (T) and photosynthetically active radiation (PAR). The G06 algorithm is an advanced emission model simulating direct canopy scale emission (mg m^{-2} h^{-1}) rather than the emission per dry leaf mass, as it has an integrated canopy environmental model. The G06 algorithm for isoprene is essentially similar to the earlier Guenther algorithms

(Guenther et al., 1993, 1995, 1999), except that many empirical parameters, which used to have prescribed constant values (e.g. C_P, α, E_{opt} and T_{opt}) have been expanded to contain more parameters specific to the simulation of variations in isoprene emission in response to previous PAR and temperature history, which is related to the changes in enzyme-driven substrate synthesis for isoprene and phosphorylation dependent on ATP availability. The actual parameters in the original model derive from a number of measurements, where isoprene light and temperature responses as affected by many factors (PAR and temperature history, response to CO_2 or ozone, and enzymatic kinetics) were studied (e.g. Geron et al., 2000; Hanson and Sharkey, 2001; Monson et al., 1994; Petron et al., 2001; Sharkey et al., 1999). Because of such diversity in empirical parameters this algorithm has many degrees of freedom, which was one of the reasons for its choice for fitting the measured estragole canopy flux. Since no light and temperature responses to estragole floral emissions are available, the parameters were constrained to a restricted range, so the fitted values of these parameters should be treated with caution in inferring any physiological significance.

Although the formalism of the Guenther et al. (2006) approach has been adopted, the fitted empirical constants were derived from the measurement data for estragole eddy covariance fluxes at the site. The Eqs. (3–9) were merged into one large equation and overall 10 empirical constants were optimised using the estragole flux data in order to achieve the best fit. The comparison between original and modified parameters is given in Table 3.

3 Results and discussion

3.1 Estragole mixing ratios

3.1.1 Specificity for oil palm and screening for anisoles

Estragole, being p-allyl-anisole, belongs to the family of anisole compounds whose structure includes a methoxy group attached to a benzene ring. Emission of aromatic compounds, not from anthropogenic sources but from vegetation, is very interesting from a biochemical point of view, but there are very few published data. Toluene is an example of a typical anthropogenic compound which can be emitted by some plants (Heiden et al., 1999; White et al., 2009). During measurements in Borneo, estragole was only found at the oil palm plantation, and it was not detected either above a rainforest canopy or in the screening of individual tree foliage in the rainforest. In fact, in the rainforest, anisole and many of its derivatives (e.g. p-vinyl-anisole, p-ethyl-anisole, p-ethylene-anisole) were detected lower in the canopy by PTR-MS, but not p-allyl-anisole (estragole), neither below nor above canopy.

By comparison, in the oil palm ambient air, estragole, but none of its derivatives, was the second most abundant measured VOC after isoprene. The chromatogram of oil palm ambient air (Fig. 2) reveals that the peak of estragole dominates the signal. The isoprene peak is not shown in this retention-time range. It is worth noting that the high abundance of estragole in the ambient air above the oil palm canopy was recorded by both PTR-MS and GC-MS, while the leaf-cuvette study detected only very small concentrations of estragole and in only a few percent of the samples, even using a measurement system that provides an upper estimate of emission fluxes (see Sect. 2.3.1). This clearly indicates that estragole is not primarily emitted by the fronds, but almost certainly is released by the flowers, which is not surprising, given its role in pollination. As leaf surfaces can adsorb and store significant amounts of deposited gases (Binnie et al., 2002) it is likely that small emissions from fronds are secondary to previous deposition, which was quite frequent for this semi-volatile compound. Due to the fact that sampling was not directly from the flowers, one might argue about possible different sources (e.g. fruit, stems, etc.). Nevertheless, estragole has an intense aniseed scent and from observation of the weevil's role in pollination it seems apparent that it is attracted to the flower (Mahbob, 2008). Neither fruit nor leaves had an obvious smell of aniseed. See Sect. 3.4 (below).

3.1.2 Diurnal cycles

Results from the leaf emission samples and random ambient air samples for analysis by GC-MS are presented in Table 1. The time series for estragole mixing ratios recorded by PTR-MS is shown in Fig. 3 and the diurnal average is presented in Fig. 4a in comparison with temperature and PAR. In addition, the box-and-whisker plot in Fig. 4b illustrates its day-to-day variability. The estragole diurnal cycles may provide information on feeding/pollinating times of the insect. Estragole mixing ratios moderately correlate with temperature corrected by a lag of ~3.5 h, suggesting a short-term storage pool in the plant before release a few hours later. It is possible that estragole accumulates later in the evening in the collapsing boundary layer, but its flux is not picked up by the eddy covariance flux due to insufficient turbulence at those times.

The estragole mixing ratio from PTR-MS was moderately correlated with the 3.5 h lag-adjusted temperature (r^2=0.4) and the 4.5 h lag-adjusted PAR (r^2=0.34), but without a lag correction no correlations were found. This is different for the case of other VOCs (e.g. isoprene), whose responses to temperature (or PAR) were almost instantaneous. Based on the mass scan (*m/z* 21–205) performed on the PTR-MS every hour the highest correlations between estragole normalised signal at *m/z* 149 were found with *m/z* 95 (r^2=0.38), *m/z* 75 (r^2=0.33), *m/z* 47 (r^2=30) and *m/z* 121 (r^2=0.24), which could be due to internal fragmentation. There were also

Table 1. Comparison of estragole volume mixing ratios.

Site/date/source	PTR-MS (ambient 15 m)	GC-MS (flower enclosure)	GC-MS (ambient)	GC-MS (leaf)	PTR-MS/GC-MS/TAG (9.3 m above the ground)
Borneo (Oil palm) / 29-05-2008 – 11/06/ 2008 (this work)	3.0 ppbv[a] (3.0 ppbv[b])				
Borneo (Oil palm) / 25-05-2008 (this work)			1.2 ppb (morning 9:00 to 10:00) 3.0 ppb (early afternoon 12:00 to 14:00) 3.8 ppb (late afternoon 14:00 to 16:00)	< 0.2 ppbv	
Blodget Forest (ponderosa pine)/ (Bouvier-Brown et al., 2009a; Bouvier-Brown et al., 2009b)					few pptv – 0.5 ppbv
Borneo (Oil palm)/ 15/5/2009 – 17/5/2009 / this work		Female flowers ~0.26– 1.39 ppm[c] (60 ppm[d]) Male flowers ~ 150 ppb			

[a] mean over the measurement period (N=537) [b] if only the VMR points corresponding to periods of validated flux were taken into account ($N = 109$), [c] accumulated in the enclosure (~40 L headspace); [d] it might be possible that the tube touched the flower.

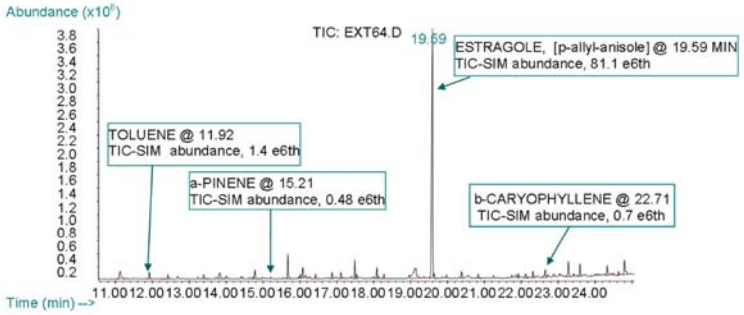

Fig. 2. Chromatogram of ambient air sampled within the oil palm canopy, showing a high abundance of estragole (p-allyl-anisole) but not of any of its derivatives. Oil palm plantation ambient air at ground level sampled on 25 May 2008. 15 *m/z* ions monitored.

weak correlations with some other *m/z* values representing biogenic compounds ($r^2 < 0.2$). The latter would be higher after applying the time lag of 3.5 h.

It is common for some fragmenting compounds (e.g. isoprene) to deviate from the relative transmission curve but it was assumed that fragmentation of estragole was not significant. The uncertainty of such an empirical sensitivity approach lies between the error of calibration with a standard (typically 5–10%) and the error of deriving the mixing ratios

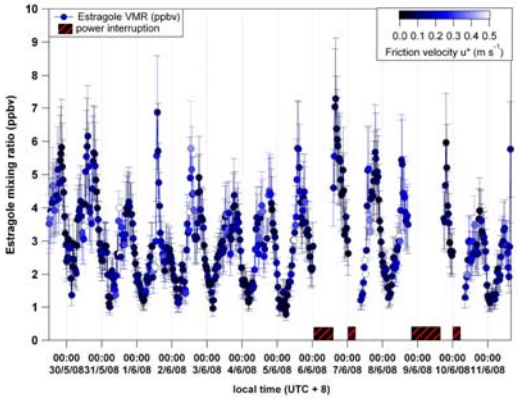

Fig. 3. Time-series of volume mixing ratios (ppbv) of estragole measured by PTR-MS above the oil palm canopy (local time [UTC+8]). The dots are coloured by friction velocity (u_*) to show that potentially large fluxes likely occurring later in the day could be missed out in eddy covariance because of low values of u_* (corresponding to black – dark blue). Error bars denote an estimated 30% error in obtaining VMRs using an empirical sensitivity derived from relative transmission (see Sect. 2.2).

from drift tube reaction kinetics and proton transfer reaction rate constants (up to 100%) (e.g. Steinbacher et al., 2004) and was estimated at 30% by Taipale et al. (2008).

3.2 Estragole fluxes

Previous PTR-MS measurements over Ponderosa pines (*Pinus ponderosa)* showed concentrations of estragole to correlate closely with 2-methyl-3-butenol (MBO) (Bouvier-Brown et al., 2009a, b; Holzinger et al., 2005). However, MBO was not observed at the oil palm plantation, implying different biochemistries of conifer leaf and oil palm floral emissions. Therefore the method suggested by Bouvier-Brown et al. (2009a) for inferring estragole emissions from correlations with MBO is not applicable for oil palm. A comparison of fluxes reported from other environments is shown in Table 2. The observed fluxes above oil palms are the highest reported so far, and for the first time reported from tropical oil palms. The flux time series is presented in Fig. 5 in relation to canopy temperature (T_c), which is the most likely driver for estragole emission (or deposition). Estragole net emission can be decreased by periods of estragole deposition, which can be affected by delayed temperature response, and local gradients caused by possibly slightly different release times of particular inflorescences. Night time emission and deposition are uncertain as the flux was generally below the detection limit and the turbulence was insufficient (small u_*). However, the small estragole concentrations observed in the shallow night-time boundary layer confirm that night-time

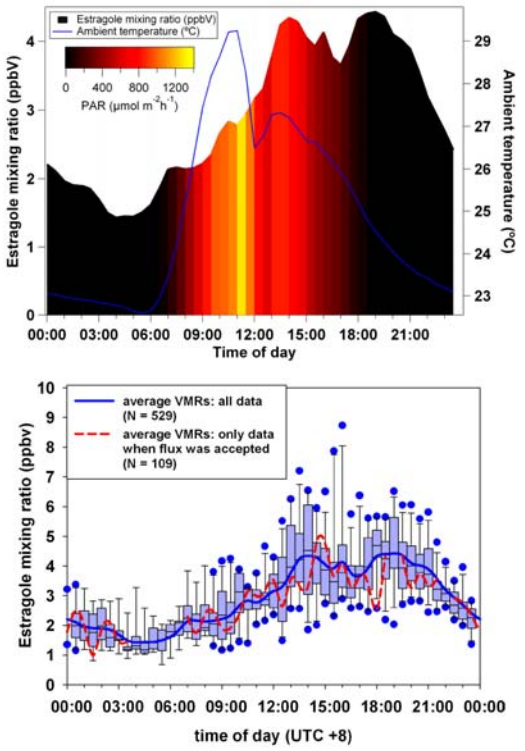

Fig. 4. Average diurnal cycles of estragole mixing ratios (left axis): **(a)** average in relation to temperature (right axis) and PAR (colour scale); **(b)** Box-and-Whisker plot of day-to-day variability, showing averages (blue line), median with 25th and 75th percentile (box), 5th and 95th percentiles (whiskers) and outliers (dots).

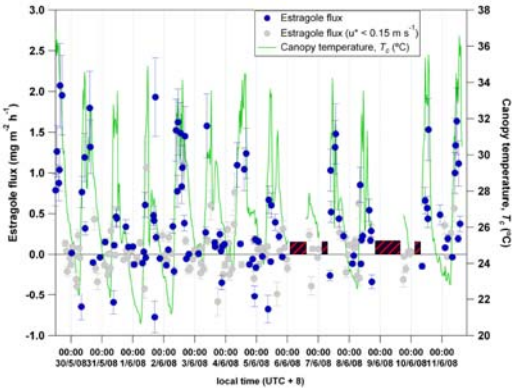

Fig. 5. Estragole flux with uncertainty bars (mean error estimated at 35%), and canopy temperature. Black/red areas refer to power interruptions.

Table 2. Comparison of estragole fluxes.

Site/date /source	PTR-MS vDEC (ambient 15 m)	GC-MS (flowers)	GC-MS (fronds)	GC-FID and PTR-MS (branch level)
Borneo (Oil palm) / 29-05-2008 – 11/06/2008 (this work)	0.81 mg m^{-2} h^{-1} [a] 0.44 mg m^{-2} h^{-1} [b]			
Borneo (Oil palm) / 25-05-2008 (this work)			~1 µg g^{-1} h^{-1}	
Blodget Forest (ponderosa pine)/ (Bouvier-Brown et al., 2009b)				0.20 mg m^{-2} h^{-1} [c]
Borneo (Oil palm)/ 15/52009 – 17/5/2009 (this work)		Female flowers ~ 0.2 mg m^{-2} h^{-1} [d]		

[a] mid-day mean 10:00–14:00 ($N = 26$); [b] 24-h average of 12 days of validated flux ($N = 109$) [c] converted from basal rate of 1.37 µmol m^{-2} h^{-1} (Bouvier-Brown et al., 2009a); [d] expected to be underestimated (explanation in Sect. 3.4); the value was estimated assuming 150 trees ha^{-1} average global density although the actual density at the site was smaller (124 trees ha^{-1}).

Table 3. Comparison of empirical constants between G06 for isoprene and modified G06 for estragole.

Parameter	Type of activity factor	Original G06 for isoprene	Modified G06 for estragole
C_{T1} (Eq. 5)	γ_T	95	131
C_{T2} (Eq. 5)	γ_T	542	230
b_1 (Eq. 6)	γ_P	0.004	0.031
b_2 (Eqs. 6, 7)	γ_P	0.0005	0.0030
b_3 (Eq. 7)	γ_P	0.0468	0.0453
b_4 (Eq. 8)	γ_T	0.6	-0.32
b_5 (Eq. 9)	γ_T	2.034	1.812
b_6 (Eq. 9)	γ_T	0.05	−0.21
T_b (Eq. 8)	γ_T	313 K	307 K
P_0 (Eq. 7)	γ_P	200 µmol m^{-2} s^{-1} (sun leaves) 50 µmol m^{-2} s^{-1} (shade leaves)	200 µmol m^{-2} s^{-1}

emissions are very small. The highest fluxes were normally observed during the middle of the day, peaking at approximately 2 mg m^{-2} h^{-1}. There were also periods of apparent deposition for estragole, which is, however, less certain being often at the edge of the rejection thresholds and could be driven by varying gradients caused by different opening times of male and female flowers. On the averaged diurnal graph (Fig. 6a) one can see the estragole flux in comparison with T_c and PAR (on the colour scale). Although in the mixing ratios there was a delayed correlation observed with temperature, it seems that there is not a large shift in the flux compared with the T_c but the afternoon peak is disproportionally higher in relation to T_c and PAR. This is because most of the flux is transported by turbulent eddies, and thus as soon as mixing within the PBL decreases it appears that there is an accumulation of estragole, which slowly decays overnight. However, also because of the laminar conditions it is possible that the true flux at night time might not be captured by eddy covariance. It would be interesting to study if estragole can be taken up by palms during the night, whether it can penetrate into the soil, and to better understand its ventilation and chemistry at night. The Box-and-Whisker plot in Fig. 6b shows high day-to-day variability, probably due to periods of deposition but also because the strength of the particular flower sources operating in a 5 day pollination cycle (Syed, 1979) can be varied as more flowers on the spikelets/inflorescences are becoming active/inactive.

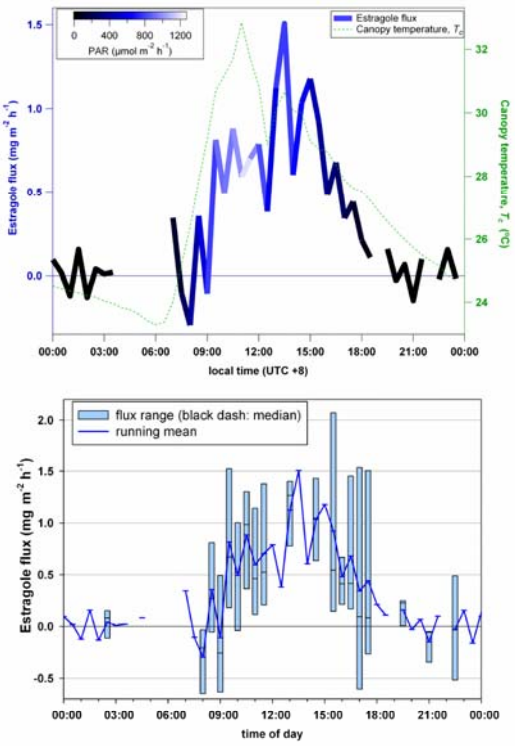

Fig. 6. Average diurnal cycles of the estragole flux: **(a)** in comparison with canopy temperature (right axis), and shaded by PAR; **(b)** Box-and-Whisker plots showing day-to-day variability.

3.3 Contribution of estragole from oil palms to global emissions

The 24-h average canopy flux of estragole for the period 29 May–11 June 2008 (12 days of measurement) including both emission and deposition was 0.44 mg m^{-2} h^{-1}. Given the total area of oil palm plantations worldwide of 13.9 million hectares (FAO, 2009) and assuming that this net flux is representative for the annual average (oil palms produce flowers and fruit all year) this average flux would yield 535 Gg (10^9 g) of globally emitted estragole per year, with the regional 60% contribution for Indonesia and Malaysia of 321 Gg y^{-1}. This is a very large flux in terms of regional contribution, and probably the highest global floral emission source, which is however three orders of magnitudes lower than estimates of global isoprene emission.

3.4 Investigating emissions of estragole from male and female inflorescences of oil palm

A semi-quantitative approach was used to confirm that oil palm flowers are indeed the source of estragole in the atmosphere above oil palm plantations. Six different inflorescences which were typical in appearance and health (based on visual inspection) were randomly selected for enclosures within a commercial oil palm plantation. Three inflorescences were male, and three were female.

Female inflorescences yielded estragole concentrations in the sample tubes ranging from 0.31 to 1.69 µg L^{-1} taking account of the approximate 50% free air-space in the 80-litre bag, which accumulated in the static enclosure over the sampling periods. This corresponds to an accumulated concentration over an hour ranging from ~0.26 to 1.39 ppm. Concentrations were higher in the morning than later in the day. However, the third female inflorescence gave sample concentrations which were in excess of 77 µg L^{-1} in the morning (~60 ppm). It is possible that the sample tubes for this female flower actually touched the source of estragole in the inflorescence, and contaminated the steel case. In contrast, male inflorescences gave lower concentrations in the sample tubes ranging from 0.02 to 0.18 µg L^{-1} (up to ~0.15 ppm). Concentrations tended to be higher in the middle part of the day. Generally, male and female inflorescences weigh about 0.5 kg and 1 kg, respectively. Therefore differences in mass do not entirely account for the different concentrations found in samples from male and female inflorescences. Because the concentrations in some of the samples saturated the GC-MS detector, it is likely that the true concentrations are underestimated by an unknown factor.

The concentrations of estragole were assumed to accumulate over the sampling period, and therefore an approximate emission rate from each inflorescence could be estimated simply by dividing the concentration (µg L^{-1}) by time (h) to give emission rates expressed as (µg estragole inflorescence^{-1} h^{-1}). It is recognised that size of inflorescence varies, and at best, these estimates are semi-quantitative with the aim of showing that oil palm flowers were a significant source of estragole. Consequently, although it is not possible to report accurate quantitative fluxes of estragole from oil palm flowers, if an average of 15 female inflorescences per tree is assumed, and a global planting density of 150 trees ha^{-1}, one derives a semi-quantitative estimate of up to 0.2 mg m^{-2} h^{-1} emission of estragole from female flowers. The actual density of palms at the measurement site was 124 trees ha^{-1}, so lower than recommended by FAO. The flux upscaled from enclosures is approximately half of the total-flux value derived from the PTR-MS (0.44 mg m^{-2} h^{-1}). This could be explained by the different sampling period, underestimation of flux from GC cartridges due to detector saturation (see above) or enclosure sampling losses. However, this confirms that oil palm flowers are the most likely source of the estragole in the atmosphere

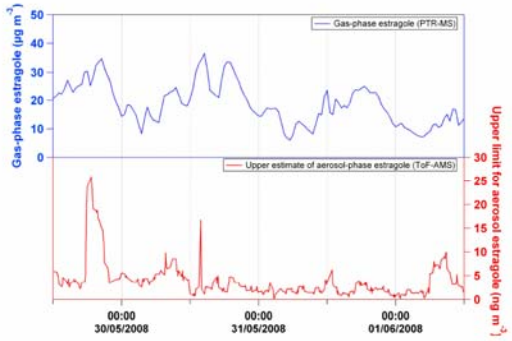

Fig. 7. Estragole in gas phase as measured by PTR-MS (blue) and upper limit in the aerosol phase (measured by AMS) as estimated from typical fragmentation patterns for estragole.

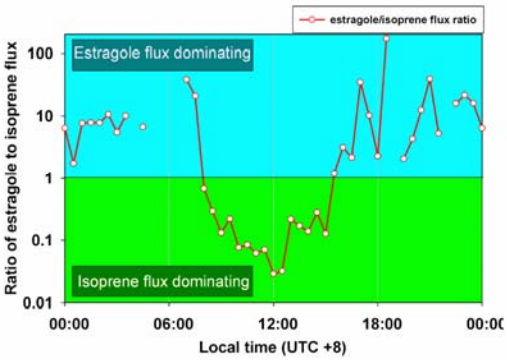

Fig. 8. Diurnal trend of the ratios of estragole to isoprene flux, showing the morning and afternoon times when estragole flux dominated over the isoprene flux, which was very high during the day. The fluxes of these two compounds had similar values at around 08:00 and 15:30 h local time (UTC+8).

above oil palm plantations, although the possibility of another source within the plantation biota cannot be excluded.

3.5 Estragole partitioning in the aerosol phase

Estragole has a relatively high aerosol partition coefficient, log K_{oa} octanol-air partition coefficient of 5.194, as estimated by KOAWIN^{TM} v1.10 (EPA, 2007), and in certain conditions can partition into the aerosol phase. To evaluate whether estragole could be detected with the HR-ToF-AMS, nebulised estragole was sampled into the instrument under laboratory conditions, with the main peaks at *m/z* 53 (2), 70 (10), 77 (10), 91 (10), 115 (8) and 147 (6), selected as likely fragments for estragole aerosol). In brackets are given relative percentages of the most dominant peak at *m/z* 15. This peak could be the methyl fragment disconnected from the chavicyl ether moiety, but it was not included in the list of potential estragole fragments due to expected contributions at this *m/z* from other compounds. Although, under field conditions, each of these peaks has contributions from many other compounds, an upper estimate of the aerosol estragole concentration can be obtained by summing the signals at these *m/z*. A ratio of the fragment sum for estragole and *m/z* 15 (0.46) was used to convert to the actual estragole concentrations (in $\mu g\,m^{-3}$) and thus potentially leading to an additional overestimation due to likely contributions from other sources at the plantation. For this reason, the absolute values for aerosol estragole should be treated as a total upper threshold of an estimate. In Fig. 7 the comparison between this upper estimate of estragole in the aerosol phase and the PTR-MS gas-phase measurement is presented. The morning peak, related to a rise in aerosol fraction, can be seen on particular days by AMS and the late peak is generally dominated by PTR-MS. Overall, the gas phase concentration exceeds the potential aerosol mass by a factor of 1×10^3 to 1×10^4, which cannot be determined more accurately from the available data.

3.6 Parameterisations for estragole flux

It is worth noting the uniqueness of estragole emissions, for example in comparison with isoprene, which was the most abundant BVOC at the plantation and whose response to temperature and PAR was instantaneous rather than delayed. In Fig. 8 the ratio of estragole to isoprene flux is presented on a diurnal graph, which shows the dominance of isoprene emissions during midday, whereas estragole flux takes over after about 15:30 h. This skewness of estragole emission response to PAR and temperature towards later in the day placed severe constraints on the parameterisation using empirical method such as the G06 algorithm. The modelled emission is compared with the measured flux in Fig. 9. The modelled flux was derived as described in Sect. 2.5 with the fitted parameters given in Table 3. As the measured canopy flux is the net eddy covariance flux, a part of this predominantly positive (upward) flux may be lost in deposition. In the case of estragole some deposition can be expected due to the nature of the molecule, its lifetime, and because of several validated deposition points from a larger pool of the points that did not pass the quality criteria (for example night time or rain episodes). Detailed modelling would require the deposition term or loss-in-emission term to be included in the model so that the net flux escaping the canopy is appropriately represented. A first attempt was made to estimate the actual total loss in emission by inclusion of a deposition term following the resistance approach of Eq. (2), which was fitted to the available deposition data (not shown). The deposition component was relatively small (16.5% of the total flux) and is subject to large uncertainties mainly related to the small number of validated deposition points used in deriving mean R_c and our lack of mechanistic understanding of

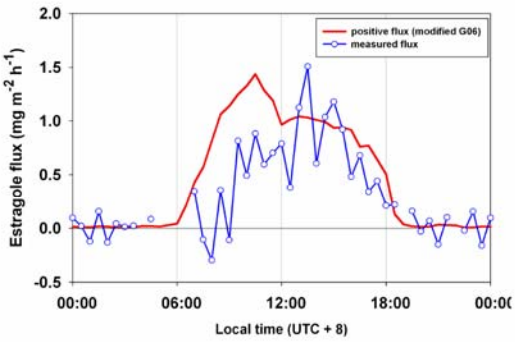

Fig. 9. Diurnal patterns for measured estragole flux (blue) in relation to modelled emission by modified G06 (red).The current G06 algorithm is unable to accurately represent the second peak of estragole (occurring at 13:00–18:00 h), which could be due to possible thermogenesis and/or specific circadian control of emission. The whole dataset was used to constrain the algorithm, so that the morning peak is overestimated by the modelled emissions.

the deposition pathways.

The overall average of the total flux predicted by the emission-only model amounted to 0.49 mg m^{-2} h^{-1} which is only 0.05 mg m^{-2} h^{-1} higher than the actual measurement. Although the parameterised emission for isoprene gave an almost identical fit with measurements above the canopy (Misztal et al., 2010), the same parameterisation for estragole was unable to fully resolve the late peak of emissions, which is underestimated and which in turn results in an overestimation of the morning peak of emissions due to the G06-algorithm parameters being constrained by the whole measurement dataset. Nevertheless, bearing in mind that flowers are governed by different, often complex, mechanisms from leaves with stomata (e.g., different production, mechanical release), the overall agreement is rather impressive. This could be further improved if the model was adjusted to contain other factors such as thermogenesis.

It is possible that inflorescences of *E. guineensis* are thermogenic as has been reported for other oil palm species (Knudsen et al., 2001). Thermogenesis presumably helps to volatilise floral scents (in this case estragole) and serves as a cue for pollinators (Ervik et al., 1999). However, although not explicitly tested during this study, thermogenic volatilisation after the decrease in ambient temperature could explain the delayed peak of estragole concentrations with temperature (Terry et al., 2004).

4 Conclusions

Using data from this study it is estimated that approximately 500 Gg of estragole are emitted from oil palm plantations annually. Although three orders of magnitude less than global isoprene emissions from vegetation, these estragole emissions are probably the highest single floral contribution of reactive carbon to global atmospheric chemistry. Estragole is probably present also in the aerosol phase as well as the gas phase and is also subject to deposition as well as emission. Since estragole emissions are likely to make a regionally-important contribution to BSOA, whether by directly partitioning into the aerosol phase or after reacting to more condensable oxidation products, it is possible that estragole emissions may have an important influence on regional climate. Although the processes driving floral emissions are less well understood than for foliar emissions, we have shown that the former can also be described by a modification of the G06 algorithm.

A number of uncertainties accompany the above conclusions, including: a comparatively short measurement period; not always the same period of measurement for the different techniques; seasonal variations in emissions; calibration precision; flux errors; and influence of high humidity on measurement sensitivity. Despite these caveats, it is estimated that the overall measurement error should be within a factor of 2 for the PTR-MS concentrations and fluxes, smaller for the in situ GC-MS results, but much larger for data from the enclosures. Clearly, more research is required to understand the mechanisms of estragole formation, its biotic and abiotic controls, and to quantify its emission rates from other tropical species.

Acknowledgements. This work was funded by the UK Natural Environment Research Council (NERC) through the ACES (Aerosol Coupling in the Earth System) project of the APPRAISE (Aerosol Properties, PRocesses and InfluenceS on the Earth's climate) research programme. Pawel Misztal thanks his supervisors J. Neil Cape and Mathew R. Heal, and the Centre for Ecology & Hydrology and the School of Chemistry, University of Edinburgh, for funding his PhD. We are grateful to the Sabahmas Plantation of PPB Oil Palms Bhd., and in particular to Mr. Foo Koh Kei (senior manager) and Mr. Chang Sip Woon (group manager) for the provision of lodging, transport and site infrastructure. This is paper number 505 of the Royal Society's South East Asian Rainforest Research Programme.

Edited by: R. MacKenzie

References

Altshuller, A. P.: Review – Natural volatile organic-substances and their effect on air-quality in the United-States, Atmos. Environ., 17, 2131–2165, 1983.

Binnie, J., Cape, J. N., Mackie, N., and Leith, I. D.: Exchange of organic solvents between the atmosphere and grass – the use of open top chambers, Sci. Total Environ., 285, 53–67, 2002.

Blake, R. S., Monks, P. S., and Ellis, A. M.: Proton-Transfer Reaction Mass Spectrometry, Chem. Rev., 109, 861–896, doi:10.1021/cr800364q, 2009.

Bouvier-Brown, N. C., Holzinger, R., Palitzsch, K., and Goldstein, A. H.: Quantifying sesquiterpene and oxygenated terpene emissions from live vegetation using solid-phase microextraction fibers, J. Chromatography A, 1161, 113–120, 2007.

Bouvier-Brown, N. C., Goldstein, A. H., Worton, D. R., Matross, D. M., Gilman, J. B., Kuster, W. C., Welsh-Bon, D., Warneke, C., de Gouw, J. A., Cahill, T. M., and Holzinger, R.: Methyl chavicol: characterization of its biogenic emission rate, abundance, and oxidation products in the atmosphere, Atmos. Chem. Phys., 9, 2061–2074, doi:10.5194/acp-9-2061-2009, 2009a.

Bouvier-Brown, N. C., Holzinger, R., Palitzsch, K., and Goldstein, A. H.: Large emissions of sesquiterpenes and methyl chavicol quantified from branch enclosure measurements, Atmos. Environ., 43, 389–401, doi:10.1016/j.atmosenv.2008.08.039, 2009b.

Buchmann, N., Guehl, J. M., Barigah, T. S., and Ehleringer, J. R.: Interseasonal comparison of CO2 concentrations, isotopic composition, and carbon dynamics in an Amazonian rainforest (French Guiana), Oecologia, 110, 120–131, 1997.

Culf, A. D., Fisch, G., Malhi, Y., Carvalho Costa, R., Nobre, A. D., de O. Marques Filho, A., Gash, J. H. C., and Grace, J.: Carbon dioxide measurements in the nocturnal boundary layer over Amazonian forest, Hydrol. Earth Syst. Sci., 3, 39–53, doi:10.5194/hess-3-39-1999, 1999.

Davison, B., Taipale, R., Langford, B., Misztal, P., Fares, S., Matteucci, G., Loreto, F., Cape, J. N., Rinne, J., and Hewitt, C. N.: Concentrations and fluxes of biogenic volatile organic compounds above a Mediterranean macchia ecosystem in western Italy, Biogeosciences, 6, 1655–1670, doi:10.5194/bg-6-1655-2009, 2009.

de Gouw, J., Warneke, C., Karl, T., Eerdekens, G., van der Veen, C., and Fall, R.: Sensitivity and specificity of atmospheric trace gas detection by proton-transfer-reaction mass spectrometry, Int. J. Mass Spectrom., 223–224, 365–382, 2003.

DeCarlo, P. F., Kimmel, J. R., Trimborn, A., Northway, M. J., Jayne, J. T., Aiken, A. C., Gonin, M., Fuhrer, K., Horvath, T., Docherty, K. S., Worsnop, D. R., and Jimenez, J. L.: Field-deployable, high-resolution, time-of-flight aerosol mass spectrometer, Anal. Chem., 78, 8281–8289, doi:10.1021/ac061249n, 2006.

Ervik, F., Tollsten, L., and Knudsen, J. T.: Floral scent chemistry and pollination ecology in phytelephantoid palms (Arecaceae), Plant Syst. Evol., 217, 279–297, 1999.

FAOSTAT: Online Statistical Service. Item: Oil palm fruit; element: area harvested; year: 2007; country: World, South East Asia, Malaysia, Indonesia, online available at: http://faostat.fao.org (last access: April 2009), 2009.

Foken, T. and Wichura, B.: Tools for quality assessment of surface-based flux measurements, Agr. Forest Meteorol., 78, 83–105, 1996.

Geron, C., Guenther, A., Sharkey, T., and Arnts, R. R.: Temporal variability in basal isoprene emission factor, Tree Physiol., 20, 799–805, 2000.

Geron, C., Owen, S., Guenther, A., Greenberg, J., Rasmussen, R., Hui Bai, J., Li, Q.-J., and Baker, B.: Volatile organic compounds from vegetation in southern Yunnan Province, China: Emission rates and some potential regional implications, Atmos. Environ., 40, 1759–1773, 2006.

Guenther, A., Hewitt, C. N., Erickson, D., Fall, R., Geron, C., Graedel, T., Harley, P., Klinger, L., Lerdau, M., McKay, W. A., Pierce, T., Scholes, B., Steinbrecher, R., Tallamraju, R., Taylor, J., and Zimmerman, P.: A global-model o fnatural volatile organic-compound emissions, J. Geophys. Res.-Atmos., 100, 8873–8892, 1995.

Guenther, A., Baugh, B., Brasseur, G., Greenberg, J., Harley, P., Klinger, L., Serça, D., and Vierling, L.: Isoprene emission estimates and uncertainties for the Central African EXPRESSO study domain, J. Geophys. Res., 104, 30625–30639, doi:10.1029/1999jd900391, 1999.

Guenther, A., Karl, T., Harley, P., Wiedinmyer, C., Palmer, P. I., and Geron, C.: Estimates of global terrestrial isoprene emissions using MEGAN (Model of Emissions of Gases and Aerosols from Nature), Atmos. Chem. Phys., 6, 3181–3210, doi:10.5194/acp-6-3181-2006, 2006.

Guenther, A. B., Zimmerman, P. R., Harley, P. C., Monson, R. K., and Fall, R.: Isoprene and monoterpene emission rate variability - model evaluations and sensitivity analyses, J. Geophys. Res.-Atmos., 98, 12609–12617, 1993.

Hanson, D. T. and Sharkey, T. D.: Rate of acclimation of the capacity for isoprene emission in response to light and temperature, Plant Cell Environ., 24, 937–946, 2001.

Hartley, C. W. S.: The oil palm (*Elaeis guineensis* Jacq.), 3rd ed., Tropical Agriculture Series, Longman Scientific & Technical, Harlow, 1988.

Heiden, A. C., Kobel, K., Komenda, M., Koppmann, R., Shao, M., and Wildt, J.: Toluene Emissions from Plants, Geophys. Res. Lett., 26, 1283–1286, 1999.

Helmig, D., Ortega, J., Guenther, A., Herrick, J. D., and Geron, C.: Sesquiterpene emissions from loblolly pine and their potential contribution to biogenic aerosol formation in the Southeastern US, Atmos. Environ., 40, 4150–4157, 2006.

Henderson, A.: A Review of Pollination Studies in the Palmae, Botan. Rev., 52, 221–259, 1986.

Hewitt, C. N., Lee, J. D., MacKenzie, A. R., Barkley, M. P., Carslaw, N., Carver, G. D., Chappell, N. A., Coe, H., Collier, C., Commane, R., Davies, F., Davison, B., DiCarlo, P., Di Marco, C. F., Dorsey, J. R., Edwards, P. M., Evans, M. J., Fowler, D., Furneaux, K. L., Gallagher, M., Guenther, A., Heard, D. E., Helfter, C., Hopkins, J., Ingham, T., Irwin, M., Jones, C., Karunaharan, A., Langford, B., Lewis, A. C., Lim, S. F., MacDonald, S. M., Mahajan, A. S., Malpass, S., McFiggans, G., Mills, G., Misztal, P., Moller, S., Monks, P. S., Nemitz, E., Nicolas-Perea, V., Oetjen, H., Oram, D. E., Palmer, P. I., Phillips, G. J., Pike, R., Plane, J. M. C., Pugh, T., Pyle, J. A., Reeves, C. E., Robinson, N. H., Stewart, D., Stone, D., Whalley, L. K., and Yin, X.: Overview: oxidant and particle photochemical processes above a south-east Asian tropical rainforest (the OP3 project): introduction, rationale, location characteristics and tools, Atmos. Chem. Phys., 10, 169–199, doi:10.5194/acp-10-169-2010, 2010.

Holzinger, R., Lee, A., Paw, K. T., and Goldstein, U. A. H.: Observations of oxidation products above a forest imply biogenic emissions of very reactive compounds, Atmos. Chem. Phys., 5, 67–75, doi:10.5194/acp-5-67-2005, 2005.

Hussein, M. Y., Lajis, N. H., Kinson, A., and Teo, C. B.: Laboratory and field evaluation on the attractancy of *Elaeidobius kamerunicus* Faust to 4-allylanisole, Porim Bull., 18, 20–26, 1989.

Hussein, M. Y., Lajis, N. H., and Ali, J. H.: Biological and chemical factors associated with the successful introduction of *Elaeidobius kamerunicus* Faust, the oil palm pollinator in Malaysia, Acta Hort. (ISHS) 288, 81–87, 1991.

Jayne, J. T., Leard, D. C., Zhang, X. F., Davidovits, P., Smith, K. A., Kolb, C. E., and Worsnop, D. R.: Development of an aerosol mass spectrometer for size and composition analysis of submicron particles, Aerosol Sci. Technol., 33, 49–70, 2000.

Jimenez, J. L., Jayne, J. T., Shi, Q., Kolb, C. E., Worsnop, D. R., Yourshaw, I., Seinfeld, J. H., Flagan, R. C., Zhang, X. F., Smith, K. A., Morris, J. W., and Davidovits, P.: Ambient aerosol sampling using the Aerodyne Aerosol Mass Spectrometer, J. Geophys. Res.-Atmos., 108, 8425 doi:10.1029/2001jd001213, 2003.

Karl, T. G., Spirig, C., Rinne, J., Stroud, C., Prevost, P., Greenberg, J., Fall, R., and Guenther, A.: Virtual disjunct eddy covariance measurements of organic compound fluxes from a subalpine forest using proton transfer reaction mass spectrometry, Atmos. Chem. Phys., 2, 279–291, doi:10.5194/acp-2-279-2002, 2002.

Kim, S., Karl, T., Helmig, D., Daly, R., Rasmussen, R., and Guenther, A.: Measurement of atmospheric sesquiterpenes by proton transfer reaction-mass spectrometry (PTR-MS), Atmos. Meas. Tech., 2, 99–112, doi:10.5194/amt-2-99-2009, 2009.

Knudsen, J. T., Tollsten, L., and Ervik, F.: Flower scent and pollination in selected neotropical palms, Plant Biol., 3, 642–653, 2001.

Langford, B., Davison, B., Nemitz, E., and Hewitt, C. N.: Mixing ratios and eddy covariance flux measurements of volatile organic compounds from an urban canopy (Manchester, UK), Atmos. Chem. Phys., 9, 1971–1987, doi:10.5194/acp-9-1971-2009, 2009.

Lee, A., Goldstein, A. H., Keywood, M. D., Gao, S., Varutbangkul, V., Bahreini, R., Ng, N. L., Flagan, R. C., and Seinfeld, J. H.: Gas-phase products and secondary aerosol yields from the ozonolysis of ten different terpenes, J. Geophys. Res.-Atmos., 111, D07302, doi:10.1029/2005jd006437, 2006a.

Lee, A., Goldstein, A. H., Kroll, J. H., Ng, N. L., Varutbangkul, V., Flagan, R. C., and Seinfeld, J. H.: Gas-phase products and secondary aerosol yields from the photooxidation of 16 different terpenes, J. Geophys. Res.-Atmos., 111, D17305, doi:10.1029/2006jd007050, 2006b.

Lindinger, W., Hansel, A., and Jordan, A.: On-line monitoring of volatile organic compounds at pptv levels by means of proton-transfer-reaction mass spectrometry (PTR-MS) - Medical applications, food control and environmental research, Int. J. Mass Spectrom., 173, 191–241, 1998.

Mahbob, A.: The Pollinator *E. Camerunicus* is Nature's little helper, Global Oil & Fats Business Magazine, 5, 58–59, 2008.

Misztal, P. K., Nemitz, E., Langford, B., Coyle, M., Ryder, J., DiMarco, C., Phillips, G., Oram, D., Owen, S., Heal, M. R., and Cape, J. N.: First direct ecosystem fluxes of VOCs from oil palms in SE Asia, in preparation, 2010.

Monson, R. K., Harley, P. C., Litvak, M. E., Wildermuth, M., Guenther, A. B., Zimmerman, P. R., and Fall, R.: Environmental and developmental controls over the seasonal pattern of isoprene emission from aspen leaves, Oecologia, 99, 260–270, 1994.

Nemitz, E., Loubet, B., Lehmann, B. E., Cellier, P., Neftel, A., Jones, S. K., Hensen, A., Ihly, B., Tarakanov, S. V., and Sutton, M. A.: Turbulence characteristics in grassland canopies and implications for tracer transport, Biogeosciences, 6, 1519–1537, doi:10.5194/bg-6-1519-2009, 2009.

Nemitz, E., Phillips, G. J., Di Marco, C. F., Siong, J., Farmer, D., Kimmel, J., Jimenez, J., and Fowler, D.: Concentrations and fluxes of submicron aerosol components above an oilpalm plantation in Sabah, Malaysia, in preparation, 2010.

Petron, G., Harley, P., Greenberg, J., and Guenther, A.: Seasonal temperature variations influence isoprene emission, Geophys. Res. Lett., 28, 1707–1710, 2001.

Rinne, H. J. I., Guenther, A. B., Warneke, C., de Gouw, J. A., and Luxembourg, S. L.: Disjunct eddy covariance technique for trace gas flux measurements, Geophys. Res. Lett., 28, 3139–3142, 2001.

Rinne, J., Taipale, R., Markkanen, T., Ruuskanen, T. M., Hellén, H., Kajos, M. K., Vesala, T., and Kulmala, M.: Hydrocarbon fluxes above a Scots pine forest canopy: measurements and modeling, Atmos. Chem. Phys., 7, 3361–3372, doi:10.5194/acp-7-3361-2007, 2007.

Rosenstiel, T. N., Potosnak, M. J., Griffin, K. L., Fall, R., and Monson, R. K.: Increased CO_2 uncouples growth from isoprene emission in an agriforest ecosystem, Nature, 421, 256–259, doi:10.1038/nature01312, 2003.

Sharkey, T. D., Singsaas, E. L., Lerdau, M. T., and Geron, C. D.: Weather effects on isoprene emission capacity and applications in emissions algorithms, Ecol. Appl., 9, 1132–1137, 1999.

Spirig, C., Neftel, A., Ammann, C., Dommen, J., Grabmer, W., Thielmann, A., Schaub, A., Beauchamp, J., Wisthaler, A., and Hansel, A.: Eddy covariance flux measurements of biogenic VOCs during ECHO 2003 using proton transfer reaction mass spectrometry, Atmos. Chem. Phys., 5, 465–481, doi:10.5194/acp-5-465-2005, 2005.

Steinbacher, M., Dommen, J., Ammann, C., Spirig, C., Neftel, A., and Prevot, A. S. H.: Performance characteristics of a proton-transfer-reaction mass spectrometer (PTR-MS) derived from laboratory and field measurements, Int. J. Mass Spectrom., 239, 117–128, 2004.

Sutton, M. A., Burkhardt, J. K., Guerin, D., Nemitz, E., and Fowler, D.: Development of resistance models to describe measurements of bi-directional ammonia surface-atmosphere exchange, International Conference on Atmospheric Ammonia – Emissions, Deposition and Environmental Impacts, Culham, England, ISI:000072633600029, 473–480, 1995.

Syed, R. A.: Studies on oil palm pollination by insects, Bull. Ent. Res., 69, 1979.

Taipale, R., Ruuskanen, T. M., Rinne, J., Kajos, M. K., Hakola, H., Pohja, T., and Kulmala, M.: Technical Note: Quantitative long-term measurements of VOC concentrations by PTR-MS – measurement, calibration, and volume mixing ratio calculation methods, Atmos. Chem. Phys., 8, 6681–6698, doi:10.5194/acp-8-6681-2008, 2008.

Tandon, R., Manohara, T. N., Nijalingappa, B. H. M., and Shivanna, K. R.: Pollination and Pollen-pistil Interaction in Oil Palm, Elaeis guineensis, Ann. Bot., 87, 831–838, doi:10.1006/anbo.2001.1421, 2001.

Terry, I., Moore, C. J., Walter, G. H., Forster, P. I., Roemer, R. B., Donaldson, J. D., and Machin, P. J.: Association of cone thermogenesis and volatiles with pollinator specificity in Macrozamia cycads, Plant Syst. Evol., 243, 233–247, doi:10.1007/s00606-003-0087-x, 2004.

Test Plan for Estragole: http://www.epa.gov/HPV/pubs/summaries/

estragole/c14022tp.pdf, (last access: 21 April 2009), 2002.

US Environmental Protection Agency Estimation Program Interface (EPI): Suite v3.2: http://www.epa.gov/opptintr/exposure/pubs/episuite.htm, (last access: 21 September 2009), 2007.

Wang, Y. F., Owen, S. M., Li, Q. J., and Penuelas, J.: Monoterpene emissions from rubber trees (Hevea brasiliensis) in a changing landscape and climate: chemical speciation and environmental control, Glob. Change Biol., 13, 2270–2282, 2007.

White, M. L., Russo, R. S., Zhou, Y., Ambrose, J. L., Haase, K., Frinak, E. K., Varner, R. K., Wingenter, O. W., Mao, H., Talbot, R., and Sive, B. C.: Are biogenic emissions a significant source of summertime atmospheric toluene in the rural Northeastern United States?, Atmos. Chem. Phys., 9, 81–92, doi:10.5194/acp-9-81-2009, 2009.

II-I Pike, R. C., … , Misztal, P.,et al.: Can a global model chemical mechanism reproduce NO, NO2, and O3 measurements above a tropical rainforest?, Atmos. Chem. Phys. Discuss., 9, 27611-27648, 2009

Atmos. Chem. Phys. Discuss., 9, 27611–27648, 2009
www.atmos-chem-phys-discuss.net/9/27611/2009/

Atmospheric Chemistry and Physics Discussions

This discussion paper is/has been under review for the journal Atmospheric Chemistry and Physics (ACP). Please refer to the corresponding final paper in ACP if available.

Can a global model chemical mechanism reproduce NO, NO_2, and O_3 measurements above a tropical rainforest?

R. C. Pike[1], J. D. Lee[2], P. J. Young[1,*], S. Moller[3], G. D. Carver[1,4], X. Yang[1], P. Misztal[5,6], B. Langford[7], D. Stewart[8,], C. E. Reeves[8], C. N. Hewitt[7], and J. A. Pyle[1,4]**

[1]Centre for Atmospheric Science, Department of Chemistry, University of Cambridge, Lensfield Road, Cambridge, CB2 1EW, UK
[2]National Centre for Atmospheric Science (NCAS), University of York, Heslington, York, YO10 5DD, UK
[3]Department of Chemistry, University of York, Heslington, York, YO10 5DD, UK
[4]National Centre for Atmospheric ScienceClimate, University of Cambridge, Lensfield Road, Cambridge, CB2 1EW, UK
[5]Centre for Ecology and Hydrology Edinburgh, Bush Estate, Penicuik, Midlothian, EH26 0QB, UK
[6]The University of Edinburgh, School of Chemistry, Joseph Black Building, West Mains Road, Edinburgh, EH9 3JJ, UK

[7] Lancaster Environment Centre, Lancaster University, Lancaster, LA1 4YQ, UK
[8] School of Environmental Sciences, University of East Anglia, Norwich, NR4 7TJ, UK
[*] now at: NOAA Earth System Research Laboratory, 325 Broadway, Boulder, CO, 80501, USA
[**] now at: Department of Chemistry, University of Reading, Whiteknights, Reading, RG6 6AH, UK

Received: 24 November 2009 – Accepted: 30 November 2009
– Published: 21 December 2009

Correspondence to: R. C. Pike (rachel.pike@atm.ch.cam.ac.uk)

Published by Copernicus Publications on behalf of the European Geosciences Union.

Abstract

A cross-platform field campaign, OP3, was conducted in the state of Sabah in Malaysian Borneo between April and July of 2008. Among the suite of observations recorded, the campaign included measurements of NO_x and O_3–crucial outputs of any model chemistry mechanism. We describe the measurements of these species made from both the ground site and aircraft. We examine the output from the global model p-TOMCAT at two resolutions for this location during the April campaign period. The models exhibit reasonable ability in capturing the NO_x diurnal cycle, but ozone is overestimated. We use a box model containing the same chemical mechanism to explore the weaknesses in the global model and the ability of the simplified global model chemical mechanism to capture the chemistry at the rainforest site. We achieve a good fit to the data for all three species (NO, NO_2, and O_3), though the model is much more sensitive to changes in the treatment of physical processes than to changes in the chemical mechanism. Indeed, without some parameterization of the nighttime boundary layer-free troposphere mixing, a time dependent box model will not reproduce the observations. The final simulation uses this mixing parameterization for NO and NO_2 but not O_3, as determined by the vertical structure of each species, and matches the measurements well.

1 Introduction

A four month field campaign, part of the NERC-funded "Oxidant and Particle Photochemical Processes" (OP3)[1], was conducted in the Malaysian state of Sabah, on the island of Borneo, between April and July of 2008 (for more information, see Hewitt et al., 2009b). There were two intensive periods of observation, the first between 8 April and 3 May, and the second between 25 June and 23 July. A key goal of the project is to assess our understanding of photochemical processes above a rainforest and their

[1]More information on OP3 can be found online at: http://www.es.lancs.ac.uk/op3/

impacts on various scales; to this end, the campaign utilized simultaneous ground, airborne, and satellite measurements (for a full list of instrumentation see Hewitt et al., 2009b). A further aim is to understand the scale relationships of these measurements as they are used by and contribute to mesoscale, regional, and global models.

Atmospheric oxidation above a tropical rainforest is complex (e.g. Kuhn et al., 2007; Lelieveld et al., 2008), and it is therefore beyond current computational resources to represent it explicitly in a global model. Furthermore, the horizontal resolution of the current generation of global models is 2–5° (approximately equivalent to 220 and 550 km at the equator, Stevenson et al., 2006), which limits their ability to model subgrid scale processes such as emission variability. At the same time, these models attempt to simulate the production and destruction of ozone, which is dependent on local chemical conditions (Crutzen, 1973; Sillman et al., 1990; Jenkin and Clemitshaw, 2000). Ozone is important for radiation (Gauss et al., 2006), and at high concentrations is detrimental to both human (Wilkins et al., 2001; Jerrett et al., 2009) and crop health (van Dingenen et al., 2009). Our understanding of the future impacts of ozone very often relies on the output of global models (Forster et al., 1996; Fuglestvedt et al., 1999; Stevenson et al., 2006) and it is therefore essential to understand how global chemical mechanisms perform in relation to the local measurements which help to constrain them.

Production of tropospheric ozone is non-linear (Liu et al., 1987; Jenkin and Clemitshaw, 2000), and depends largely on local concentrations of volatile organic compounds (VOC), the hydroxyl radical (OH), and the oxides of nitrogen ($NO + NO_2 = NO_x$) (e.g. Sillman, 1995). NO and NO_2 act as catalysts in many oxidation cycles in the atmosphere due to their rapid interconversion; the availability of NO_x largely determines whether ozone production or destruction dominates in a specific region of the tropical boundary layer (Liu et al., 1987), and the impact of NO_x on ozone production in the observation region has been previously described (Hewitt et al., 2009a). Photolysis of NO_2 is the only known production mechanism for ozone, while loss occurs through photochemical reaction with other trace gases and deposition to surfaces such

as the ocean or vegetation. Ozone can also be entrained into the troposphere from the ozone-rich stratosphere (Holton et al., 1995). The lifetime of tropospheric ozone is a few weeks to a month, depending on location in the atmosphere (e.g. Stevenson et al., 2006; Wild, 2007), and as such transport from the free troposphere may influence local boundary layer measurements of ozone.

Nitrogen oxides are emitted both by natural processes and human activities. Of the natural sources, emission from soils (Yienger and Levy II, 1995; Delon et al., 2008) and formation during lightning storms (Franzblau and Popp, 1989; Schumann and Huntrieser, 2007) are the major contributors. Fossil fuel combustion, biomass burning and aircraft emissions are the major anthropogenic sources (Kasibhatla, 1993; Levy II et al., 1999; Toenges-Schuller et al., 2006). Though fluxes from tropical areas are not yet well constrained, the work of Bakwin et al. (1990) suggested significant emissions from tropical forested areas. Jaeglé et al. (2004) reported that soil emissions could be as large as biomass burning emissions in Africa. In these remote tropical areas the potential for NO_x species to influence local chemistry is significant due to low background NO_x and high concentrations of both the hydroxyl radical and biogenic VOC (Steinkamp et al., 2009). An increase in the frequency and spatial distribution of tropical NO_x measurements will help quantify local tropical fluxes and sources. But global models will largely play the role of quantifying the impact of these fluxes on a regional and global scale. For this reason, it is important to understand how global models relate to local measurements.

Here, we present measurements of NO, NO_2, and O_3 taken over two four-week periods in a remote rainforest location from ground and aircraft platforms. We use a global model chemical mechanism implemented in both a global model and a box model to explore the variables that are most important for capturing the diurnal variation of key constituent concentrations at the rainforest site.

In Sect. 2 we present a summary of the measurement techniques and the data. Section 3 examines our ability to reproduce the measurements in two different chemical modelling frameworks. In Sect. 3.1, we use the global model p-TOMCAT at two

different resolutions. In Sect. 3.2, we introduce a box model with the same chemical mechanism as p-TOMCAT and describe sensitivity experiments that investigate uncertainties related to the chemistry and physics. Section 3.3 describes the parameters that give the best fit to the measurements. Finally, Sect. 4 summarizes the study and the results.

2 Measurements

2.1 Methods

Nitrogen oxides and ozone measurements were taken at the Bukit Atur Global Atmospheric Watch (GAW) station (04°58′53″, 117°50′37″, and elevation 426 m). NO measurements were made by chemiluminescence using an Ecophysics CLD 780 TR nitric oxide analyzer, with an Ecophysics PLC 762 NO_2 photolytic converter connected to allow conversion of NO_2 to NO. NO and NO_2 concentrations were measured from an inlet situated at 5 m above ground level through quarter-inch PFA tubing. Measurements were run on continuous sampling except during calibrations and when running zeros. The analyzer was calibrated using an Eco Physics PAG003 pure air generator, an Environs calibration gas blender S6100 and a cylinder of 450 ppbv NO in nitrogen. The photolytic converter efficiency is also determined as part of the calibration. Zero air was run through the system on several occasions to allow more accurate determination of the systematic artefact and detection limit.

Each measurement cycle lasted for 1 min and consisted of 12 s of NO measurement, 12 s of NO_2 measurement and 24 s of interference determination. The remaining 12 s allowed for switching between the different modes and purging of the reaction cell. The 1σ limit of detection for 10 min frequency data was approximately 2.8 pptv for NO and 7 pptv for NO_2.

Ozone concentrations were measured using a Thermo Environmental Instruments (TEI) 49i UV absorption ozone analyzer. The data was internally averaged to one minute frequency and the detection limit was 0.6 ppbv.

On board the FAAM BAe 146 aircraft, NO and NO_2 were measured using the University of East Anglia (UEA) NO_{xy} instrument, which employed the same technique as the ground based instrument described above. Zeros were carried out at the beginning of level runs during the flights and calibrations took place during transit to and from the airport. Detection limits of the UEA NO_{xy} are on the order of 3 pptv for NO and 15 pptv for NO_2 for 10s data, with estimated accuracies of 10% for NO at 1 ppbv and 10% for NO_2 at 1 ppbv. The instrument is described in detail by Brough et al. (2003). Ozone was measured on board the aircraft using a TEI 49C UV absorption analyser.

Isoprene fluxes, used in our box modelling experiments, were measured using a PTR-MS instrument at the Bukit Atur site. Its response was optimized so as to achieve the best compromise between the optimal detection limit for VOCs and the minimization of the impact of high relative humidity. The operational details of the instrument have been presented elsewhere (e.g. Lindinger et al., 1998; de Gouw et al., 2003; Blake et al., 2009) whereas the experimental setup and methodology for OP3 are described in this special issue (Langford et al., 2009).

2.2 Discussion

Time series of NO, NO_2, and O_3 data are shown in Fig. 1. Although the frequency of data collection is 1 min (Sect. 2.1), it is shown here with a running average of 10 min for smoothing purposes. NO levels were typically below 0.1 ppbv, although there were regular spikes above this level which reached up to 0.4 ppbv. NO_2 levels were higher, generally below 0.4 ppbv but reaching 0.8 ppbv. Ozone concentrations ranged from near zero up to 30 ppbv, but were only consistently above 20 ppbv on three days (11–13 April).

Figure 2 shows the median diurnal profiles for the entire April measurement period for all three species[2]. The 25–75 quartile limit is shown in shaded regions around each of the profiles. The ozone diurnal cycle shows a minimum of approximately 6 ppbv around 07:00 h followed by a rise through the morning. Ozone concentrations of approximately 11 ppbv remain until the evening, when concentrations slowly fall to their minimum in the morning. NO_2 concentrations exhibit the most amplified diurnal cycle, which peaks at midnight around 240 pptv and reaches a low of 80 pptv in mid-afternoon. The loss of NO_2 between midnight and midday occurs less rapidly than the buildup between late afternoon and evening. An NO peak of around 70 pptv is observed at 08:00 h and quickly recovers to a fairly constant level between 30 and 40 pptv. This persists until 18:00 h when a further drop to 20 pptv occurs. Non-zero NO concentrations between 15–20 pptv persist throughout the night.

In July, an aircraft joined the campaign in order to make dedicated measurements above the site and over the surrounding areas. On the right side of Fig. 2, the diurnal cycles of NO, NO_2, and O_3 from the ground site at the Bukit Atur GAW tower are shown for this second observation period. These diurnal cycles are sampled only for the four days for which equivalent aircraft data is also available. The average measurements made in profile flight patterns directly over the site are plotted as whiskered points and show values for both boundary layer and free troposphere.

O_3 shows little vertical structure compared to ground measurements. A diurnal structure in the ground based O_3 observations is not clear, with the values around 9 ppbv. Morning aircraft measurements are slightly higher (10–12 ppbv) than the ground based. Aircraft measurements of ozone levels rise slightly to approximately 13 ppbv in the late afternoon, though boundary layer and free troposphere values remain indistinguishable (within uncertainty) from each other.

Boundary layer NO_2 matches the ground based measurements closely, which remain in the range of 100–200 pptv for most of the day. NO_2 measurements show a

[2]A version of this Figure appeared in Hewitt et al. (2009b). The Figure that appears here has higher temporal resolution (10 min data) than the previous version (1 h data).

similar structure (rise until midnight and subsequent decrease afterwards) to the first campaign, but because only four days are sampled here the full diurnal cycle is not shown. NO_2 measurements of around 20 pptv in the free troposphere are much lower than those in the boundary layer and at the surface, demonstrating that NO_2 has a strong vertical structure. NO displays a similar pattern to NO_2 with boundary layer values of 80–200 pptv, that resembles ground-based measurements well, and free tropospheric values that are much lower (less than 10 pptv). The diurnal cycle of NO also bears significant resemblance to that of the first campaign, (i.e. a rise in early morning followed by a slow tapering into the afternoon).

For comparison, the NO concentrations at the ground site in both measurement periods are in between measurements made in the Amazon Rainforest of 20 pptv (Lelieveld et al., 2008) and 100 pptv (Karl et al., 2009). Ozone, on the other hand, is lower at the Borneo site than in reported values for the Amazon for both the boundary layer (19 ppbv) and the free troposphere (37 ppbv) (Lelieveld et al., 2008).

3 Model simulations

In this section, we describe two sets of model simulations. In Sect. 3.1, a global model is used to simulate the diurnal cycle of the three measured species NO, NO_2, and ozone. In Sect. 3.2, we use a box model to explore the chemical and physical parameters influencing the mechanism's performance in replicating observations.

3.1 Global model

3.1.1 Model description

We use the Cambridge global chemistry transport model (CTM) p-TOMCAT to simulate the diurnal cycles of NO, NO_2, and O_3 observed during the April measurement period. The model uses a chemical mechanism implemented in the ASAD chemistry

package (Carver et al., 1997), which is based on the mechanism described in Arnold et al. (2005), has been used in the UM_CAM global model (Zeng et al., 2008; Young et al., 2009), and has recently been incorporated into the United Kingdom Chemistry and Aerosol Model (UKCA, Morgenstern et al., 2008, 2009; O'Connor et al., 2009). It is a medium-size chemistry for a global model, simulating the oxidation of methane, ethane, propane, and isoprene. Isoprene chemistry is simulated using the Mainz isoprene mechanism (MIM) of Pöschl et al. (2000). 81 tracers are carried through 154 bimolecular and 18 termolecular reactions.

The Cambridge p-TOMCAT global CTM is described in more detail in Cook et al. (2007) and Hamilton et al. (2008). The model was used for this study in both a high horizontal resolution mode ($0.56^\circ \times 0.56^\circ$, approximately 62 km in the tropics) and a low resolution mode ($2.8^\circ \times 2.8^\circ$, approximately 310 km in the tropics). Both have 31 levels in the vertical, from the surface to 10 hPa. Both are driven by 6 hourly operational analyses of wind, temperature, and humidity from the European Centre for Medium-range Weather Forecasting (ECMWF). The boundary layer height is diagnosed from input ECMWF operational analyses using the non-local scheme of Holtslag and Boville (1993).

The p-TOMCAT model considers the photolysis of 37 reactions. Photolysis rates are determined by using the Cambridge 2-D model (Law and Pyle, 1993) with the scheme of Hough (1988). This takes account of multiple scattering by clouds using a climatological cloud cover dataset and a fixed aerosol profile. Emissions of NO_x, CO, ethane, propane and isoprene are included. NO_x emissions are added according to the recommendations used in the TAR of the IPCC (Prather et al., 2001) and include industrial, biomass burning, soil, aircraft and lightning emissions. The lightning emissions are scaled to produce 5 Tg N yr^{-1}. A seasonal variation is applied to the biomass burning emissions. Isoprene emissions are taken from the GEIA inventory of Guenther et al. (1995) and have a diurnal cycle applied in the model. Dry deposition velocities are calculated from tabulated velocities based on data from Ganzeveld and Lelieveld (1995) and Zhang et al. (2003) according to the method of Giannakopoulos (1998).

3.1.2 Global model results

Monthly mean diurnal variations for NO, NO_2, and ozone in the boundary layer are shown for both model resolutions in Fig. 3. Both resolutions show a fit for NO which matches the data well; the model reaches a maximum of 65 pptv in the morning around 08:00 h, when the measurement data also peaks (at 60 pptv). At low resolution, there is a dip in midday values to 40 pptv, which was not recorded in the measurements. NO drops to zero around 18:00 h in p-TOMCAT, coinciding with the point when measurement values also drop. As described above, residual NO concentrations of approximately 20 pptv are present throughout the night, and these values are not captured by the global model at either resolution.

The fit to measurements for NO_2 is reasonable for both global models, though the amplitude of the diurnal cycle is slightly too high at 250 pptv, compared with 200 pptv in the measured data. The low resolution version of the model shows constant NO_2 concentrations at night, while the high resolution version of the model shows an increase in NO_2 until dawn. At higher altitude in the model (not shown), NO_2 concentrations are lower (less than 50 pptv) than in the boundary layer levels, which is consistent with the observed vertical profile (Sect. 2.2). We argue below that the measurements, especially during the second half of the night (24:00 to 06:00 h), reflect a large component of free tropospheric character due to mixing during this time. It seems possible that mixing between boundary layer and free tropospheric air in the global model is not sufficient to capture the nighttime decrease in NO_2 shown in the measurements. In addition, the diurnal pattern in both resolutions of the model is slightly too narrow, with a more precipitous decrease in concentrations in the morning and a stronger rise in the evening. In contrast, the measurements show a smoother rise and fall throughout the day and night. Both models capture the rise between 14:00 and 18:00 well.

Finally, the modelled ozone is much too high in both versions of the global model. Concentrations in the low resolution model are around 25 ppbv. The higher resolution model performs slightly better with values of approximately 20 ppbv. In contrast,

measured mixing ratios are between 6 and 11 ppbv. Despite this, the diurnal cycle of the model seems to capture the observed data well. Deposition is an important loss process for ozone and variation in the land surface type, which helps control the deposition rate, can be captured better in the high resolution model. The high resolution version of the model has a much higher resolution land sea mask, and also shows a much stronger land-sea gradient in ozone concentrations than the low resolution version of the model (Fig. 10, Sect. 5, Hewitt et al., 2009b).

3.2 Box model

3.2.1 Model description

We use a stationary box model fitted with the same chemical mechanism as the global model to run a series of sensitivity studies. The chemistry is the same in the two models. Dry deposition in the box model uses the same tabulated values as the global model, but only six species are deposited: NO, NO_2, O_3, peroxy acetyl nitrate (PAN), peroxy-methacrylic nitric anhydride (MPAN), and a lumped nitrate species representing the products from isoprene oxidation (ISON, see Pöschl et al., 2000). The photolysis follows the scheme of the Master Chemical Mechanism (MCM, Saunders et al., 2003). As those photolysis rate constants are originally for July, at 45° N for clear sky conditions, the rate constant for J_{NO_2} was reduced by 50% to account for clouds and aerosol.

Only NO and isoprene are emitted into the box. NO emissions were 600 pptv day^{-1} (the flux is constant) unless otherwise mentioned. Isoprene emissions into the model are taken from ground based flux measurements. Occasionally, flux measurements were not available due to power outages; in these instances, we used linear interpolation to fill in the gaps. In the absence of NO flux measurements at the site, we were not able to constrain NO emissions to a diurnal pattern. NO flux measurements were made in a nearby site underneath the canopy layer Dorsey et al. (2009). In contrast, the Bukit Atur GAW station was in a clearing, and therefore canopy flux measurements are not representative of this site, as there can be a strong difference between below- and

above-canopy fluxes of NO_x (e.g. Duyzer et al., 2004). For these reasons, we assume that NO is emitted constantly into the model; this is also consistent with the emissions used in the global model.

The box model boundary layer height is fixed to a set value during the day (06:00 to 18:00 h) and fixed to a different value at night. For the first set of sensitivity experiments, the daytime boundary layer height was set to 1000 m, and the nighttime height was set to 200 m. The boundary layer height is effectively a mixing depth, and therefore controls the range over which emissions are mixed into the model, and the rate of sinks via deposition.

We set temperature to 25 °C and pressure to a surface value of 1013 mb in the box, appropriate to the conditions of the rainforest site. A 5 °C variation in temperature showed negligible impact on box model output (not shown), so a constant temperature was used. Initial concentrations of chemical species in the box model are set to the values shown in Table 1. NO, NO_2, and O_3 are initialized to their midnight values from the diurnal cycle in the measurements. All other species are initialized to zero.

For the following model-measurement comparisons, both the model and the data are sampled for 15 days to account for day to day variability in isoprene flux measurements.

3.2.2 The base case

Figure 3 shows the initial results from the box model (dark blue line). The box model overestimates NO concentrations (80 pptv instead of 60 pptv), though the structure is decently captured. The shape of the NO_2 curve is very different from the measurements, with NO_2 building up throughout the night. This occurs because any NO emitted into the model reacts with ozone to form NO_2. Ozone is also overestimated in the box model. The box model calculates values of approximately 30 ppbv, with an 8 ppbv diurnal cycle; measurements of 6–11 ppbv are far below this level.

To obtain the "base case" box model run (Fig. 3, light blue line), one key adjustment was made to the original box model output. A dilution parameter was introduced to simulate mixing with the free troposphere resulting from a collapse of the boundary

layer at night. This "venting parameter" removes a small fraction—between 0 and 4 percent—of chemical tracers at each 10 min timestep between 24:00 h and 06:00 h. Doppler lidar measurements of the backscatter from aerosol (Pearson et al., 2009) provide strong evidence for dilution of aerosol in the boundary layer during this period. These measurements were made in a valley next to the Bukit Atur GAW site used for NO_x and ozone measurements in an area of complex topography; the elevation of the lidar measurement site was 198 m (Pearson et al., 2009) compared with 426 m for the Bukit Atur site. The median boundary layer height dropped to approximately 200 m according to these measurements, suggesting that on some nights the Bukit Atur site may have effectively been in the free troposphere. The venting parameter is a simple way to simulate the mixing between the boundary layer box and the free troposphere by parameterizing dilution of species which are concentrated in the boundary layer. As is evident in Fig. 3, the box model was not able to capture the diurnal structure of NO_2 before the introduction of the venting parameter.

The base case (shown in both Figs. 3 and 4) shows both the strengths and weaknesses of the box model with venting. A good fit to the data for NO is obtained, simulating the morning rise in concentration due in part to the onset of photolysis of NO_2. During the day modelled NO follows a similar decay pattern to the measured data, an improvement over the model without venting. Similar to the global model, nighttime NO measurements are not replicated by the box model.

NO_2 measurements and model simulations are in good agreement following the addition of the venting parameter (the base case) and the buildup of NO_2 until midnight and subsequent reduction in concentrations is well captured. At sunrise, when the boundary layer begins to grow, a steep drop in NO_2 concentrations appears around 06:00 h in the box model due to the onset of photolysis. The largest divergence between modelled and measured values occurs in the afternoon, between 12:00 and 16:00 h, though this is still relatively small. Base case modelled and measured ozone display similar diurnal cycles. Both show minima between 07:00 and 08:00 h and maxima in the late afternoon, though the measurements have more structure in the

afternoon than the modelled ozone. However, the box model underestimates the total concentration of ozone, simulating values of 0–8 ppbv instead of 6–11 ppbv.

In summary, the "base case" box model run performs reasonably well, although ozone is too low. The inclusion of the venting parameter, which parameterizes dilution of boundary layer air between 24:00 and 06:00 h, seems necessary in order to simulate the structure of NO_2 measurements at night.

In the next two sections, we describe a series of sensitivity studies in which we explore changes to this base model.

3.2.3 Chemical sensitivities

We have performed a range of sensitivity experiments to explore the model performance. First, a series of emissions sensitivities were carried out (not shown.) In order to determine if the nighttime NO concentration could be captured if emissions were altered, a sensitivity study was performed in which emissions of NO were tripled to 1.8 ppbv day^{-1}. This did not improve the agreement between the modelled and measured values at night. Nonzero nighttime NO could arise from emission taking place very near to the measurement inlet, which is not reproduced by the box model as NO quickly reacts with O_3 to form NO_2 in a zero dimensional model.

We also examined the sensitivity of the model to changing isoprene emissions (not shown). Doubling the emission fluxes into the model reduced NO and NO_2 by approximately 12 pptv during the day, due to sequestration into organic NO_y species. However, the ozone concentration was relatively unaffected. Overall, the diurnal patterns were very similar between the two runs, and between these two studies we determined that the regime was likely not emissions controlled. Although it has been proposed that some chemistry in high-VOC environments might be explained by the presence of unknown reactive hydrocarbons (see Di Carlo et al., 2004, and references therein), any VOC with similar reactivity to that of isoprene seems to be unable to explain any divergence in the model-measurement comparison.

A summary of the various chemical sensitivity runs is shown in Table 2, with corresponding results plotted in Fig. 4. Generally, the diurnal cycle was modelled reasonably well for all the chemical parameters tested and was relatively insensitive to chemical changes. The overall diurnal structure for NO is well captured, with the maxima at 08:00 h. With the inclusion of the venting parameter, the NO_2 diurnal structure is also always well simulated. All the chemical sensitivities capture the cycle of ozone but not the magnitude.

In the first chemical sensitivity test (Fig. 4, aqua line), the photolysis rate of O_3 was reduced by a factor of three. The chemical mechanism shows very little sensitivity to J_{O_3}, barely changing from the base case run. In the second test, ozone deposition velocities (both daytime and nighttime values) were reduced by 75% (Fig. 4, orange line). For ozone, this simulation has the most impact of any of the chemical sensitivity studies, but still does not increase the concentration enough to match measured values. The change in deposition velocities also alters the shape of the diurnal cycle, as nighttime deposition velocities approach a limit of zero.

In an attempt to keep ozone production values high by increasing the concentration of NO_x in the system, an additional simulation was carried out. Recycling of NO_x from the reaction of ISON with OH was modified by increasing the ISON + OH rate constant from 1.3×10^{-11} cm^3 s^{-1} (Chen et al., 1998; Pöschl et al., 2000) to 4.5×10^{-11} cm^3 s^{-1} (Horowitz et al., 2007) (Fig. 4, green line). We also performed an experiment in which NO_x concentrations would decrease; in this sensitivity study, ISON deposition velocity was increased to match nitric acid (Fig. 4, yellow line). Neither experiment has an impact on the modelled values of O_3.

Two computational tests were also performed. In the first, the model species concentrations were reinitialized each day at midnight, rather than using the values calculated by the model the previous day (Fig. 4, red line). This introduced a stronger bias in NO and NO_2 around 06:00 h, the first time photochemistry turns on after reinitialization. A second study reinitializes the model at an artificially high value of ozone, and this too displays a similar model bias at sunrise (Fig. 4, purple line). These two experiments

give confidence that the model sensitivity to initial conditions is eliminated by reusing the concentrations calculated from the previous day.

The six studies discussed emphasize that the results from the UKCA chemical mechanism are relatively robust to chemical, photolytic, and deposition rate changes. As models with this level of complexity, particularly for isoprene oxidation, seem to perform relatively similarly (Archibald et al., 2009; Emmerson and Evans, 2009), it seems plausible that this is not an artefact of the model mechanism itself. From our analysis, it appears likely that the regime is more sensitive to physical processes and parameterizations than chemical ones. In order to assess the impact of these chemistry factors in relation to physical parameters controlling the processes of emission, mixing and deposition, we conducted a further series of experiments based on physical variables.

3.2.4 Physical sensitivities

As shown in Fig. 2, the aircraft data show vertical structure in both NO and NO_2 which display much lower concentrations in the free troposphere compared with the boundary layer. The venting parameter simulates exchange with free tropospheric air at night and assumes that this incoming air has lower concentrations of NO, NO_2, and ozone. However, O_3 displays little to no vertical structure in the measurements. For this reason, a simulation was run in which venting of ozone was turned off while all other species continued to be diluted. Not venting O_3 is the numerical equivalent of removing O_3 and introducing an equal amount during the same amount of time, such that a collapse of the boundary layer and mixing with the free tropospheric air may well bring in "new" ozone, but the concentrations will be similar to the boundary layer air it is replacing. This is reinforced by the difference between the species in their distribution of sources and sinks; NO_x has a source which is largely surface dominated at a remote rainforest location (higher in the troposphere, lightning can contribute as well), whereas ozone has a significant surface sink due to deposition.

Figure 5 shows the results of the box model when ozone is not vented, which displays much better agreement with the measurements. The amplitude of the diurnal cycle of ozone is dampened when O_3 is no longer vented, as the nighttime sinks are reduced. This dampened cycle more closely matches the measured diurnal profile. NO_2 changes little when ozone is not vented, but NO is significantly improved, particularly in the early daytime hours. By keeping O_3 in the box during the night, the chemical sink for NO remains higher, and the elevated values of NO in the morning are correspondingly reduced.

Three variables are used to further test the physical boundaries of the box model: the exact quantity of material lost at night (the venting parameter), the height of the boundary layer during the day, and the height of the boundary layer at night. In order to obtain the best value for these three parameters, a cost function analysis was used:

$$CF_x = \frac{1}{t} \sum_t \frac{(|\text{model}_x - \text{measured}_x|)}{\text{measured}_x} \quad (1)$$

where for each species (denoted by x) and at each timestep (t), the difference between modelled and measured values of NO, NO_2, O_3 are evaluated and averaged over a 24 h day and 15 experiment days. The cost function gives the average devation of the model from the measurements expressed as a fraction, where zero is a perfect match. The NO cost function is only evaluated between 06:00 and 18:00 h due to the mechanism's inability to capture nighttime NO concentrations, so that results are not skewed because of nighttime values. The results of the three cost functions are shown in Fig. 6, where a lower value of the cost function represents better agreement between measured and modelled concentrations.

The NO cost function shows a dependence on the venting fraction until the value of 2% per timestep, at which point model and measured data converge to a reasonable agreement of less than 30% difference in value. At the zero value for venting, NO shows almost no dependence on the nighttime boundary layer height, reflecting the fact that we only evaluate the cost function during daytime hours. NO matches the

measurements best (values less than 0.20) for high values of the daytime boundary layer height, though the gradient of dependence on daytime boundary layer height decreases with increasing venting fraction.

At a 0% value for the venting parameter, the NO_2 cost function shows values of 0.30 to 0.80. With venting, the levels are lower (values less than or equal to 0.30), which suggests that the best fit requires at least some material to be removed at night. Between 1% and 4% for the venting parameter, however, NO_2 displays little variation in the cost function, and the entire cost function "space" is valued under 0.30. NO_2 also shows very little dependence on the nighttime boundary layer height, demonstrating that venting is a more important loss process than deposition. The height of the boundary layer during the day is important only at heights less than approximately 700 m.

Ozone was not vented in these experiments, so the cost function for ozone is relatively stable in relation to venting parameter. Ozone shows a very high sensitivity to the boundary layer height during the day (with values ranging between 0.10 and 1.0), presumably due to deposition, and little dependence at night except below 500 m.

3.3 Best fit to measurements

Figure 7 shows the best fit to the measurements obtained using the box model. The values for the venting parameter (2%), boundary layer height during the day (1200 m) and night (750 m) were taken from the cost function analysis minima. The results show good agreement between measured and modelled values, capturing the majority of structure and diurnal variation for all three measured species. NO matches particularly well, though the model is still not able to simulate the residual concentrations at night. These could arise from a highly stratified boundary layer, or rapid mixing times up from the soil to the measurement inlet before chemical reaction[3]. In either case, these

[3]The presence of nighttime NO concentrations will be the subject of a forthcoming paper by Lee et al. (2009). A discussion of nighttime NO can also be found in Pugh et al. (2009)

processes are very small scale, and beyond the capability of a global model (with a resolution of tens to hundreds of kilometres) to capture physically.

Modelled NO_2 is slightly higher than the measured values but captures the structure of the measurements effectively. In particular, the nighttime structure of NO_2 is well simulated once venting was included in the box model. Afternoon NO_2 concentrations are slightly higher in the model than measurements. Since our analysis shows that transport and physical processes dominate the diurnal structure, perhaps this afternoon discrepancy arises from afternoon convection. Ozone looks very similar to measurements, though the rapid rise in the morning is not entirely captured. Nevertheless, the magnitude and basic form of the diurnal cycle are simulated well.

It is possible to crudely adjust the boundary layer scheme in the global model to attempt to reproduce the night time decline in NO_2, a parameterization similar to the box model "venting parameter". The boundary layer in p-TOMCAT varies diurnally in a similar fashion to that seen by the lidar measurements close to Bukit Atur. During daytime the observed boundary layer extends to approximately 1 km but falls to 200 m or less at night (Pearson et al., 2009). In p-TOMCAT, the boundary layer height is similar during the day but at night falls to less than 100 m. The model boundary layer is constrained for numerical stability to be no shallower than the bottom model layer (approximately 30 m). Of course, the global model simulation does not resolve the small scale topography around the measurement site, so we introduced idealized nighttime mixing to simulate the exchange of near surface air with air from above the boundary layer. This new simulation was performed with the diffusion coefficient for the boundary layer increased between midnight and 06:00 h for the bottom three model levels (from the surface to ~300 m) for the gridcell containing the measurement site. Results (not shown) do produce a decrease in NO_2 from midnight, as seen in the box model and the data, as expected, though not for the entire 6 h period. We have not attempted to optimize the mixing; it is nevertheless clear that influx of free tropospheric air could explain the observations in the global model as well as in the box model.

4 Summary

Changes in tropical processes, including land use, biogenic VOC emissions, and soil NO_x emissions are important drivers of global change. To assess these changes, we generally have to run global models at moderate resolutions. In contrast, validation of the global models requires comparison with data representative of much smaller spatial scales.

Data collected during the NERC OP3 field campaign in Sabah, Borneo, present a major opportunity to explore these questions of model validation. How well can a global model chemical mechanism capture the detailed measurements? Here we have used new ground and aircraft data of NO, NO_2, and ozone to address this question. We have compared these measurements with results from a chemical transport model, p-TOMCAT, and the same chemical mechanism included in a box model.

The observed diurnal cycle of NO at the Bukit Atur GAW site showed concentrations between 40 and 60 pptv throughout most of the day, with lower (15–20 pptv) concentrations at night. NO_2 displayed a distinct rise and fall during nighttime, with a peak at midnight. NO_2 concentrations ranged between 100 and 300 pptv. Ozone showed a diurnal pattern with a maximum in the afternoon and a minimum in the early morning. Ozone concentrations were between 6 and 11 ppbv.

The global model displayed decent comparison to the diurnal patterns of NO and NO_2. Residual concentrations of NO at night could not be simulated by any model studied. NO_2 was overestimated during the evening and, especially, before dawn. For ozone, the diurnal cycle was well captured although the concentrations were generally too high. The high resolution model, with a more accurate representation of the land surface and therefore deposition, performed better than the low resolution version of the model, particularly for ozone.

To explore the cause of any differences between p-TOMCAT and the observations, we have used a box model in which a range of chemical and physical sensitivity experiments were performed. These experiments demonstrated that the chemical

mechanism was relatively insensitive to a range of chemical parameters but that modifying the representation of physical processes had a much larger impact. We conclude that the chemical mechanism in our global model, p-TOMCAT, is sufficient to represent the behaviour of the three species considered in detail (NO, NO_2, and ozone), but that discrepancies between model and observations arise from the difficulty of representing physical processes accurately in the global model (especially those related to boundary layer structure). Aerosol backscatter data and the NO_2 nighttime measurements suggest that the surface measurements at the GAW site, when the boundary layer collapses, are influenced significantly by the free troposphere (indeed the site may effectively be in the free troposphere). We cannot expect that the boundary layer scheme, even in the high resolution p-TOMCAT integrations, can capture the details of the boundary layer structure in an area of complex topography, although a preliminary experiment suggests that increased mixing could help replicate the data. The vertical gradient of NO_2, in both the model and the observations, suggests that transport down from the free troposphere is required to explain the observations. In the box model we attempted to represent this by a "venting" parameter and were then able to capture successfully the drop in NO_2 between 24:00 and 08:00 h. In addition, in experiments in which ozone is not vented (because the vertical gradient of ozone is negligible), ozone is reproduced well. Our final "best fit" simulation using the box model closely matches the measurements.

Acknowledgements. The authors would like to acknowledge the OP3 team for their help. We acknowledge the Malaysian and Sabah Governments for permission to conduct research in Malaysia and the Malaysian Meteorological Department (MMD) for access to the Bukit Atur Global Atmosphere Watch tower. We thank the National Environment Research Council for their financial support of the OP3 campaign. B. L. and P. M. thank Brian Davison for his help in transporting and managing equipment. We also acknowledge the National Centre for Atmospheric Science for their support in the development of the model. RCP acknowledges the Gates Cambridge Trust for funding.

References

Archibald, A., Jenkin, M., and Shallcross, D.: An isoprene mechanism intercomparison, Atmos. Environ., doi:10.1016/j.atmosenv.2009.09.016, in press, 2009. 27627

Arnold, S. R., Chipperfield, M. P., and Blitz, M. A.: A three-dimensional model study of the effect of new temperature-dependent quantum yields for acetone photolysis, J. Geophys. Res., 110, D22305, doi:10.1029/2005JD005998, 2005. 27620

Bakwin, P. S., Wofsy, S. C., Fan, S., Keller, M., Trumbore, S. E., and Costa, J. M. D.: Emission of nitric oxide (NO) from tropical forest soils and exchange of NO between the forest canopy and atmospheric boundary layers, J. Geophys. Res., 95, 16755–16764, 1990. 27615

Blake, R. S., Monks, P. S., and Ellis, A. M.: Proton-Transfer Reaction Mass Spectrometry, Chem. Rev., 109, 861–896, 2009. 27617

Brough, N., Reeves, C. E., Penkett, S. A., Stewart, D. J., Dewey, K., Kent, J., Barjat, H., Monks, P. S., Ziereis, H., Stock, P., Huntrieser, H., and Schlager, H.: Intercomparison of aircraft instruments on board the C-130 and Falcon 20 over southern Germany during EXPORT 2000, Atmos. Chem. Phys., 3, 2127–2138, 2003, http://www.atmos-chem-phys.net/3/2127/2003/. 27617

Carver, G. D., Brown, P. D., and Wild, O.: The ASAD atmospheric chemistry integration package and chemical reaction database, Comput. Phys. Commun., 105, 197–215, doi:10.1016/S0010-4655(97)00056-8, 1997. 27620

Chen, X., Hulbert, D., and Shepson, P. B.: Measurement of the organic nitrate yield from OH reaction with isoprene, J. Geophys. Res., 103, 25563–25568, 1998. 27626

Cook, P. A., Savage, N. H., Turquety, S., Carver, G. D., O'Connor, F. M., Heckel, A., Stewart, D., Whalley, L. K., Parker, A. E., Schlager, H., Singh, H. B., Avery, M. A., Sachse, G. W., Brune, W., Richter, A., Burrows, J. P., Purvis, A. C., Lewis, A. C., Reeves, C. E., Monks, P. S., Levine, J. G., and Pyle, J. A.: Forest fire plumes over the North Atlantic: p-TOMCAT model simulations with aircraft and satellite measurements from the ITOP/ICARTT campaign, J. Geophys. Res., 112, D10S43, doi:0.1029/2006JD007563, 2007. 27620

Crutzen, P. J.: A discussion of the chemistry of some minor constituents in the stratosphere and troposphere, Pure Appl. Geophys., 106, 1385–1399, doi:10.1007/BF00881092, 1973. 27614

de Gouw, J., Warneke, C., Karl, T., Eerdekens, G., van der Veen, C., and Fall, R.: Sensitivity and specificity of atmospheric trace gas detection by proton-transfer-reaction mass spectrometry,

Int. J. Mass Spectrom., 223–224, 365–382, 2003. 27617

Delon, C., Reeves, C. E., Stewart, D. J., Serça, D., Dupont, R., Mari, C., Chaboureau, J.-P., and Tulet, P.: Biogenic nitrogen oxide emissions from soils impact on NO_x and ozone over West Africa during AMMA (African Monsoon Multidisciplinary Experiment): modelling study, Atmos. Chem. Phys., 8, 2351–2363, 2008, http://www.atmos-chem-phys.net/8/2351/2008/. 27615

Di Carlo, P., Brune, W. H., Martinez, M., Harder, H., Lesher, R., Ren, X., Thornberry, T., Carroll, M. A., Young, V., Shepson, P. B., Riemer, D., Apel, E., and Campbell, C.: Missing OH reactivity in a forest: Evidence for unknown reactive biogenic VOCs, Science, 304, 722–724, doi:10.1126/science.1094392, 2004. 27625

Dorsey, J. R. and Gallagher, M. W.: Observations of soil NO_x emission from a Southeast Asian rainforest: a technique to assess biological controls, Atmos. Chem. Phys. Discuss., in preparation, 2010. 27622

Duyzer, J. H., Dorsey, J. R., Gallagher, M. W., Pilegaard, K., and Walton, S.: Oxidized nitrogen and ozone interaction with forests. II: Multi-layer process-oriented modelling results and a sensitivity study for Douglas fir, Q. J. Roy. Meteorol. Soc., 130, 1957–1971, 2004. 27623

Emmerson, K. M. and Evans, M. J.: Comparison of tropospheric chemistry schemes for use within global models, Atmos. Chem. Phys., 9, 1831–1845, 2009, http://www.atmos-chem-phys.net/9/1831/2009/. 27627

Forster, P. M. D., Johnson, C. E., Law, K. S., Pyle, J. A., and Shine, K. P.: Further estimates of radiative forcing due to tropospheric ozone changes, Geophys. Res. Lett., 23, 3221–3324, 1996. 27614

Franzblau, E. and Popp, C. J.: Nitrogen oxides produced from lightning, J. Geophys. Res., 94, 11089–11104, 1989. 27615

Fuglestvedt, J. S., Berntsen, T. K., Isaksen, I. S. A., Mao, H., Liang, X.-L., and Wang, W.-C.: Climatic forcing of nitrogen oxides through changes in tropospheric ozone and methane; global 3D model studies, Atmos. Environ., 33, 961–977, doi:10.1016/S1352-2310(98)00217-9, 1999. 27614

Ganzeveld, L. and Lelieveld, J.: Dry deposition parametisation in a chemistry general circulation model and its influence on the distribution of reactive trace gases, J. Geophys. Res., 100, 20999–21012, doi:10.1029/95JD02266, 1995. 27620

Gauss, M., Myhre, G., Isaksen, I. S. A., Grewe, V., Pitari, G., Wild, O., Collins, W. J., Dentener, F. J., Ellingsen, K., Gohar, L. K., Hauglustaine, D. A., Iachetti, D., Lamarque, J.-F., Mancini,

E., Mickley, L. J., Prather, M. J., Pyle, J. A., Sanderson, M. G., Shine, K. P., Stevenson, D. S., Sudo, K., Szopa, S., and Zeng, G.: Radiative forcing since preindustrial times due to ozone change in the troposphere and the lower stratosphere, Atmos. Chem. Phys., 6, 575–599, 2006, http://www.atmos-chem-phys.net/6/575/2006/. 27614

Giannakopoulos, C.: Modelling the impact of physical and removal processes on tropospheric chemistry, Ph.D. thesis, University of Cambridge, 1998. 27620

Guenther, A., Hewitt, C. N., Erickson, D., Fall, R., Geron, C., Graedel, T., Harley, P., Klinger, L., Lerdau, M., McKay, W. A., Pierce, T., Scoles, B., Steinbrecher, R., Tallaamraju, R., Taylor, J., and Zimmerman, P.: A global model of natural volatile organic compound emissions, J. Geophys. Res., 100, 8873–8892, 1995. 27620

Hamilton, J. F., Allen, G., Watson, N. M., Lee, J. D., Saxton, J. E., Lewis, A. C., Vaughan, G., Bower, K. N., Flynn, M. J., Crosier, J., Carver, G. D., Harris, N. R. P., Parker, R. J., Remedios, J. J., and Richards, N. A. D.: Observations of an atmospheric chemical equator and its implications for the tropical warm pool region, J. Geophys. Res., 113, D20313, doi: 10.1029/2008JD009940, 2008. 27620

Hewitt, C. N., MacKenzie, A. R., Di Carlo, P., Di Marco, C. F., Dorsey, J. R., Evans, M., Fowler, D., Gallagher, M. W., Hopkins, J. R., Jones, C. E., Langford, B., Lee, J. D., Lewis, A. C., Lim, S. F., McQuaid, J., Misztal, P., Moller, S. J., Monks, P. S., Nemitz, E., Oram, D. E., Owen, S. M., Phillips, G. J., Pugh, T. A. M., Pyle, J. A., Reeves, C. E., Ryder, J., Siong, J., Skiba, U., and Stewart, D. J.: Nitrogen management is essential to prevent tropical oil palm plantations from causing ground-level ozone pollution, Proc. Natl. Acad. Sci. USA, 106, 18447–18451, doi:10.1073/pnas.0907541106, 2009a. 27614

Hewitt, C. N., Lee, J., Barkley, M. P., Carslaw, N., Chappell, N. A., Coe, H., Collier, C., Commane, R., Davies, F., DiCarlo, P., Di Marco, C. F., Edwards, P. M., Evans, M. J., Fowler, D., Furneaux, K. L., Gallagher, M., Guenther, A., Heard, D. E., Helfter, C., Hopkins, J., Ingham, T., Irwin, M., Jones, C., Karunaharan, A., Langford, B., Lewis, A. C., Lim, S. F., MacDonald, S. M., MacKenzie, A. R., Mahajan, A. S., Malpass, S., McFiggans, G., Mills, G., Misztal, P., Moller, S., Monks, P. S., Nemitz, E., Nicolas-Perea, V., Oetjen, H., Oram, D., Palmer, P. I., Phillips, G. J., Plane, J. M. C., Pugh, T., Pyle, J. A., Reeves, C. E., Robinson, N. H., Stewart, D., Stone, D., and Whalley, L. K.: Oxidant and particle photochemical processes above a south-east Asian tropical rain forest (the OP3 project): introduction, rationale, location characteristics and tools, Atmos. Chem. Phys., submitted, 2009b. 27613, 27614, 27618,

27622

Holton, J. R., Haynes, P. H., McIntyre, M. E., Douglass, A. R., Rood, R. B., and Pfister, L.: Stratosphere-troposphere exchange, Rev. Geophys., 33, 403–439, 1995. 27615

Holtslag, A. and Boville, B.: Local Versus Nonlocal Boundary-Layer Diffusion in a Global Climate Model, J. Climate, 6, 1825–1842, 1993. 27620

Horowitz, L. W., Fiore, A. M., Milly, G. P., Cohen, R. C., Perring, A., Wooldridge, P. J., Hess, P. G., Emmons, L. K., and Lamarque, J.-F.: Observational constraints on the chemistry of isoprene nitrates over the eastern United States, J. Geophys. Res., 112, D12S08, doi: 10.1029/2006JD007747, 2007. 27626, 27641

Hough, A.: The calculation of photolysis rates for use in global tropospheric modelling studies, AERE Report 13259, At. Energy Res. Estab., Harwell, UK, 1988. 27620

Jaeglé, L., Martin, R. V., Chance, K., Steinberger, L., Kurosu, T. P., Jacob, D. J., Modi, A. I., Yobou, V., Sigha-Nkamdjou, L., and Galy-Lacaux, C.: Satellite mapping of rain-induced nitric oxide emissions from soils, J. Geophys. Res., 109, D21310, doi:10.1029/2004JD004787, 2004. 27615

Jenkin, M. E. and Clemitshaw, K. C.: Ozone and other secondary photochemical pollutants: Chemical processes governing their formation in the planetary boundary layer, Atmos. Environ., 34, 2499–2527, doi:10.1016/S1352-2310(99)00478-1, 2000. 27614

Jerrett, M., Burnett, R. T., Pope, C. Arden, I., Ito, K., Thurston, G., Krewski, D., Shi, Y., Calle, E., and Thun, M.: Long-Term Ozone Exposure and Mortality, N. Engl. J. Med., 360, 1085–1095, 2009. 27614

Karl, T., Guenther, A., Turnipseed, A., Tyndall, G., Artaxo, P., and Martin, S.: Rapid formation of isoprene photo-oxidation products observed in Amazonia, Atmos. Chem. Phys., 9, 7753–7767, 2009, http://www.atmos-chem-phys.net/9/7753/2009/. 27619

Kasibhatla, P. S.: NO_y from Sub-Sonic Aircraft Emissions: A Global Three-Dimensional Model Study, Geophys. Res. Lett., 20, 1707–1710, 1993. 27615

Kuhn, U., Andreae, M. O., Ammann, C., Araújo, A. C., Brancaleoni, E., Ciccioli, P., Dindorf, T., Frattoni, M., Gatti, L. V., Ganzeveld, L., Kruijt, B., Lelieveld, J., Lloyd, J., Meixner, F. X., Nobre, A. D., Pöschl, U., Spirig, C., Stefani, P., Thielmann, A., Valentini, R., and Kesselmeier, J.: Isoprene and monoterpene fluxes from Central Amazonian rainforest inferred from tower-based and airborne measurements, and implications on the atmospheric chemistry and the local carbon budget, Atmos. Chem. Phys., 7, 2855–2879, 2007,

http://www.atmos-chem-phys.net/7/2855/2007/. 27614
Langford, B., Misztal, P., Nemitz, E., Davison, B., Helfter, C., Lee, J., MacKenzie, A. R., and Hewitt, C. N. Fluxes of volatile organic compounds from a south-east Asian tropical rainforest, Atmos. Chem. Phys. Discuss., in preparation, 2010. 27617
Law, K. S. and Pyle, J. A.: Modeling trace gas budgets in the troposphere 1. Ozone and odd nitrogen, J. Geophys. Res., 98, 18377–18400, 1993. 27620
Lee, J. et al.: NO_x above a tropical rainforest, in preparation, Atmos. Chem. Phys., 2009. 27629
Lelieveld, J., Butler, T. M., Crowley, J. N., Dillon, T. J., Fischer, H., Ganzeveld, L., Harder, H., Lawrence, M. G., Martinez, M., Taraborrelli, D., and Williams, J.: Atmospheric oxidation capacity sustained by a tropical forest, Nature, 452, 737–740, doi:10.1038/nature06870, 2008. 27614, 27619
Levy II, H., Moxim, W. J., Klonecki, A. A., and Kasibhatla, P. S.: Simulated tropospheric NO_x : Its evaluation, global distribution and individual source contributions, J. Geophys. Res., 104, 26279–26306, 1999. 27615
Lindinger, W., Hansel, A., and Jordan, A.: On-line monitoring of volatile organic compounds at pptv levels by means of proton-transfer-reaction mass spectrometry (PTR-MS) medical applications, food control and environmental research, Int. J. Mass Spectrom. Ion Proc., 173, 191–241, 1998. 27617
Liu, S. C., Trainer, M., Fehsenfeld, F. C., Parrish, D. D., Williams, E. J., Fahey, D. W., Hübler, G., and Murphy, P. C.: Ozone production in the rural troposphere and the implications for regional and global ozone distributions, J. Geophys. Res., 92, 4191–4207, 1987. 27614
Morgenstern, O., Braesicke, P., Hurwitz, M. M., O'Connor, F. M., Bushell, A. C., Johnson, C. E., and Pyle, J. A.: The World Avoided by the Montreal Protocol, Geophys. Res. Lett., 35, L16811, doi:10.1029/2008GL034590, 2008. 27620
Morgenstern, O., Braesicke, P., O'Connor, F. M., Bushell, A. C., Johnson, C. E., Osprey, S. M., and Pyle, J. A.: Evaluation of the new UKCA climate-composition model Part I: The stratosphere, Geoscientific Model Development, 2, 43–57, 2009. 27620
O'Connor, F. M., Johnson, C. E., Morgenstern, O., and Collins, W. J.: Interactions between tropospheric chemistry and climate model temperature and humidity biases, Geophys. Res. Lett., 36, L16 801, 2009. 27620
Pearson, G., Davies, F., and Collier, C.: Remote sensing of the tropical rain forest boundary layer using pulsed Doppler lidar, in preparation, Atmos. Chem. Phys., 2009. 27624, 27630
Pöschl, U., von Kulhmann, R., Poisson, N., and Crutzen, P. J.: Development and

intercomparison of condensed isoprene oxidation mechanisms for global atmospheric modelling, J. Atmos. Chem., 37, 29–52, doi:10.1023/A:1006391009798, 2000. 27620, 27622, 27626
Prather, M., Ehhalt, D., Dentener, F., Derwent, R., Dlugokencky, E., Holland, E., Isaksen, I., Katima, J., Kirchoff, V., Matson, P., Midgley, P., and Wang, M.: Climate Change 2001: The Scientific Basis, chap. Atmospheric chemistry and greenhouse gases, Cambridge University Press, Cambridge, UK, 239–287, 2001. 27620
Pugh, T. A. M., MacKenzie, A. R., Hewitt, C. N., Langford, B., Edwards, P. M., Furneaux, K. L., Heard, D. E., Hopkins, J. R., Jones, C. E., Karunaharan, A., Lee, J., Mills, G., Misztal, P., Moller, S., Monks, P. S., and Whalley, L. K.: Simulating atmospheric composition over a South-East Asian tropical rainforest: Performance of a chemistry box model, Atmos. Chem. Phys., in preparation, 2009. 27629
Saunders, S. M., Jenkin, M. E., Derwent, R. G., and Pilling, M. J.: Protocol for the development of the Master Chemical Mechanism, MCM v3 (Part A): Tropospheric degradation of non-aromatic volatile organic compounds, Atmos. Chem. Phys., 3, 161–180, 2003, http://www.atmos-chem-phys.net/3/161/2003/. 27622
Schumann, U. and Huntrieser, H.: The global lightning-induced nitrogen oxides source, Atmos. Chem. Phys., 7, 3823–3907, 2007, http://www.atmos-chem-phys.net/7/3823/2007/. 27615
Sillman, S.: The use of NO_y, H_2O_2, and HNO_3 as indicators for ozone-NO_x-hydrocarbon sensitivity in urban locations, J. Geophys. Res., 100, 14175–14188, 1995. 27614
Sillman, S., Logan, J. A., and Wofsy, S. C.: The sensitivity of ozone to nitrogen oxides and hydrocarbons in regional ozone episodes, J. Geophys. Res., 95, 1837–1851, 1990. 27614
Steinkamp, J., Ganzeveld, L. N., Wilcke, W., and Lawrence, M. G.: Influence of modelled soil biogenic NO emissions on related trace gases and the atmospheric oxidizing efficiency, Atmos. Chem. Phys., 9, 2663–2677, 2009, http://www.atmos-chem-phys.net/9/2663/2009/. 27615
Stevenson, D. S., Dentener, F. J., Schultz, M. G., Ellingsen, K., van Noije, T. P. C., Wild, O., Zeng, G., Amann, M., Atherton, M., Bell, N., Bergmann, D. J., Bey, I., Bulter, T., Cofala, J., Collins, W. J., Derwent, R. G., Doherty, R. M., Drevet, J., Eskes, H. J., Fiore, A. M., Gauss, M., Hauglustaine, D. A., Horowitz, L. W., Isaksen, I. S. A., Krol, M. C., Lamarque, J.-F., Lawrence, M. G., Montanaro, V., Müller, J. F., Pitari, G., Prather, M. J., Pyle, J. A., Rast, S., Rodriguez, J. M., Sanderson, M. G., Savage, N. H., Shindell, D. T., Strahan, S. E., Sudo, K., and Szopa,

S.: Multimodel ensemble simulations of present-day and near-future tropospheric ozone, J. Geophys. Res., 111, D08301, doi:10.1029/2005JD006338, 2006. 27614, 27615

Toenges-Schuller, N., Stein, O., Rohrer, F., Wahner, A., Richter, A., Burrows, J. P., Beirle, S., Wagner, T., Platt, U., and Elvidge, C. D.: Global distribution pattern of anthropogenic nitrogen oxide emissions: Correlation analysis of satellite measurements and model calculations, J. Geophys. Res., 111, D05312, doi:10.1029/2005JD006068, 2006. 27615

van Dingenen, R., Dentener, F. J., Raes, F., Krol, M. C., Emberson, L., and Cofala, J.: The global impact of ozone on agricultural crop yields under current and future air quality legislation, Atmos. Environ., 43, 604–618, 2009. 27614

Wild, O.: Modelling the global tropospheric ozone budget: exploring the variability in current models, Atmos. Chem. Phys., 7, 2643–2660, 2007, http://www.atmos-chem-phys.net/7/2643/2007/. 27615

Wilkins, C. K., Clausen, P. A., Wolkoff, P., Larsen, S., Hammer, M., Larsen, K., Hansen, V., and Nielsen, G. D.: Formation of strong airway irritants in mixtures of isoprene/ozone and isoprene/ozone/nitrogen dioxide, Environ. Health Persp., 109, 937–941, 2001. 27614

Yienger, J. J. and Levy II, H.: Empirical model of global soil-biogenic NO_x emissions, J. Geophys. Res., 100, 11477–11464, 1995. 27615

Young, P., Arneth, A., Schurgers, G., Zeng, G., and Pyle, J. A.: The CO_2 inhibition of terrestrial isoprene emission significantly affects future ozone projections, Atmos. Chem. Phys., 9, 2793–2803, 2009, http://www.atmos-chem-phys.net/9/2793/2009/. 27620

Zeng, G., Pyle, J. A., and Young, P. J.: Impact of climate change on tropospheric ozone and its global budgets, Atmos. Chem. Phys., 8, 369–387, 2008, http://www.atmos-chem-phys.net/8/369/2008/. 27620

Zhang, L., Brook, J. R., and Vet, R.: A revised parametisation for gaseous dry deposition in air-quality models, Atmos. Chem. Phys., 3, 2067–2082, 2003, http://www.atmos-chem-phys.net/3/2067/2003/. 27620

Table 1. Initial concentrations of six species used in the box model.

Species	Concentration
CO	130 ppbv
HOOH	3 ppbv
C_2H_6	500 pptv
C_3H_8	50 pptv
HCHO	1 ppbv
CH_3COCH_3	50 pptv

Table 2. Summary of chemical sensitivity tests

Short name	Fig. Colour	Description
Base	Light Blue	The base case
O3 phot	Aqua	J_{O_3} divided by 3
Vd O3	Orange	Ozone deposition velocities reduced by 75%
Horowitz	Green	NO_x recycling rates as Horowitz et al. (2007)
ISON dep	Yellow	ISON tracer deposition velocities set equal to those of PAN
Reinit	Red	Reinitialized the model each day at midnight
Init O3=9	Purple	Reinitialized at midnight with 9 ppbv O_3

27641

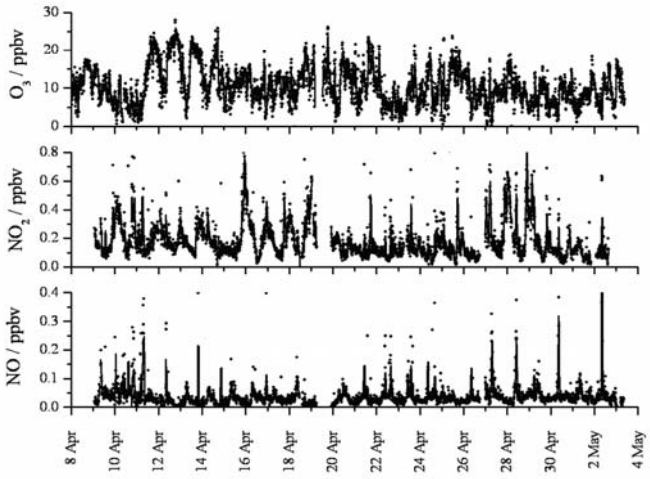

Fig. 1. Time series of measured NO, NO_2, and O_3 at the Bukit Atur GAW ground site, plotted versus local time (GMT + 8).

27642

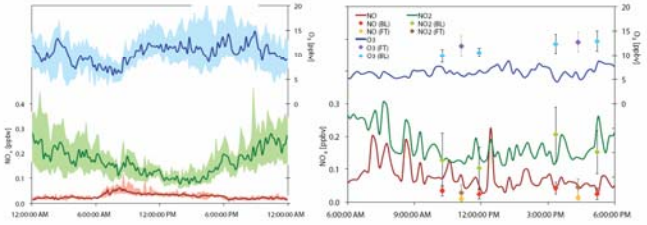

Fig. 2. Left: Median diurnal cycle of ground-based measured NO (dark red), NO_2 (dark green), and O_3 (dark blue) in April. The corresponding 25–75 quartile interval is shown with each measurement: NO in pink, NO_2 in light green, and O_3 in light blue. Right: median diurnal measurements in July, shown only for the days when corresponding flight data is available between 06:00 and 18:00 h; diurnal profiles are the same color. Average flight data for morning and afternoon profiles above the site are shown as whiskered points and are separated by height. NO boundary layer measurements are show in red (boundary layer) and yellow (free troposphere). NO_2 is shown in light green (boundary layer) and brown (free troposphere). O_3 is shown in light blue (boundary layer) and purple (free troposphere).

27643

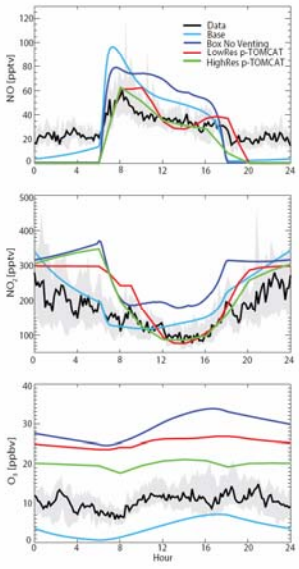

Fig. 3. Global and box model comparison to diurnal cycle of NO, NO_2, and O_3 from the median diurnal cycle in the measurements (black, with 25–75 quartile in grey). The global model is shown in red (low resolution) and green (high resolution) for the lowest model level, and the box model is shown dark blue (without venting) and light blue (the "base case").

27644

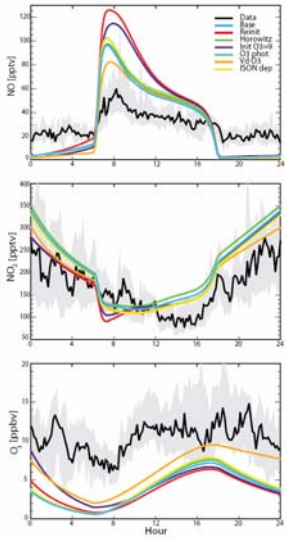

Fig. 4. 15 day average diurnal **(a)** NO [pptv], **(b)** NO_2 [pptv], **(c)** and O_3 [ppbv] from measurements (black) with 75% confidence intervals shown in the shaded grey. Seven model experiments are overlaid in various colours: the base run is shown in light blue, reduction of ozone photolysis rate is shown in dark blue, reduction of ozone deposition velocities is shown in orange, adjustment of NO_x recycling rates is shown in green, ISON deposition change is shown in yellow, reinitialisation at midnight is shown in red, and reinitialisation with high ozone is shown in purple.

27645

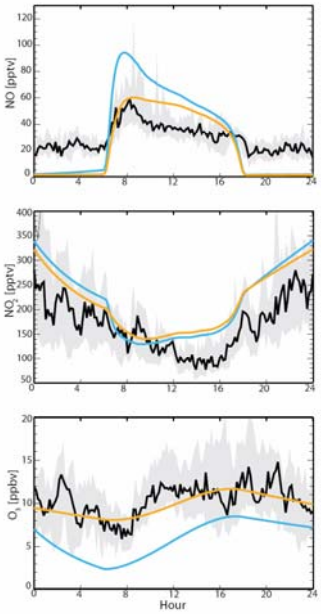

Fig. 5. Model comparison to diurnal cycle of NO **(a)**, NO_2 **(b)**, and O_3 **(c)** without (orange) and with (the base case, blue) venting ozone.

27646

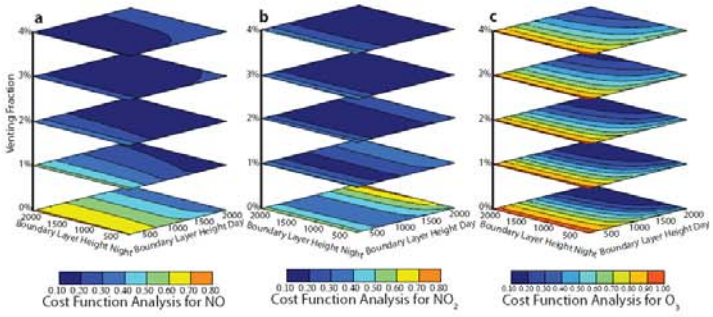

Fig. 6. Cost function [|%| difference] of model-measurement comparison to diurnal average **(a)** NO, **(b)** NO_2, and **(c)** O_3. See text for a description of the cost function.

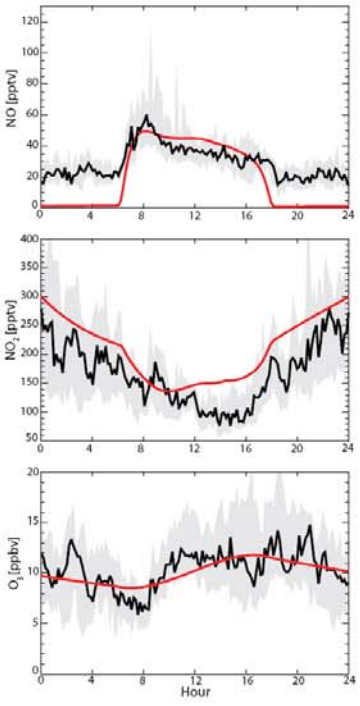

Fig. 7. Red: Best fit box model comparison to diurnal average medians of **(a)** NO, **(b)** NO_2, and **(c)** O_3after adjustments to the venting parameter and boundary layer heights.

II-J Pugh, T. A. M., … , Misztal, P., et al. : Simulating atmospheric composition over a South-East Asian tropical rainforest: performance of a chemistry box model, Atmos. Chem. Phys., 10, 279-298, 2010.

Source: http://www.atmos-chem-phys.net/10/279/2010/acp-10-279-2010.html

Atmos. Chem. Phys., 10, 279–298, 2010
www.atmos-chem-phys.net/10/279/2010/

Atmospheric Chemistry and Physics

Simulating atmospheric composition over a South-East Asian tropical rainforest: performance of a chemistry box model

T. A. M. Pugh[1], A. R. MacKenzie[1], C. N. Hewitt[1], B. Langford[1], P. M. Edwards[2], K. L. Furneaux[2,†], D. E. Heard[2], J. R. Hopkins[3], C. E. Jones[4], A. Karunaharan[5], J. Lee[3], G. Mills[6], P. Misztal[7,8], S. Moller[4], P. S. Monks[5], and L. K. Whalley[2]

[1]Lancaster Environment Centre, Lancaster University, Lancaster, UK
[2]School of Chemistry, University of Leeds, Leeds, UK
[3]National Centre for Atmospheric Science, University of York, York, UK
[4]Department of Chemistry, University of York, York, UK
[5]Department of Chemistry, University of Leicester, Leicester, UK
[6]School of Environmental Sciences, University of East Anglia, UK
[7]Centre for Ecology and Hydrology Edinburgh, U.K.
[8]School of Chemistry, The University of Edinburgh, U.K.
[†]Sadly passed away on 28 July 2009

Received: 28 August 2009 – Published in Atmos. Chem. Phys. Discuss.: 16 September 2009
Revised: 11 December 2009 – Accepted: 4 January 2010 – Published: 14 January 2010

Abstract. Atmospheric composition and chemistry above tropical rainforests is currently not well established, particularly for south-east Asia. In order to examine our understanding of chemical processes in this region, the performance of a box model of atmospheric boundary layer chemistry is tested against measurements made at the top of the rainforest canopy near Danum Valley, Malaysian Borneo. Multivariate optimisation against ambient concentration measurements was used to estimate average canopy-scale emissions for isoprene, total monoterpenes and nitric oxide. The excellent agreement between estimated values and measured fluxes of isoprene and total monoterpenes provides confidence in the overall modelling strategy, and suggests that this method may be applied where measured fluxes are not available, assuming that the local chemistry and mixing are adequately understood. The largest contributors to the optimisation cost function at the point of best-fit are OH (29%), NO (22%) and total peroxy radicals (27%). Several factors affect the modelled VOC chemistry. In particular concentrations of methacrolein (MACR) and methyl-vinyl ketone (MVK) are substantially overestimated, and the hydroxyl radical (OH) concentration is substantially underestimated; as has been seen before in tropical rainforest studies. It is shown that inclusion of dry deposition of MACR and MVK and wet deposition of species with high Henry's Law values substantially improves the fit of these oxidised species, whilst also substantially decreasing the OH sink. Increasing OH production arbitrarily, through a simple OH recycling mechanism , adversely affects the model fit for volatile organic compounds (VOCs). Given the constraints on isoprene flux provided by measurements, a substantial decrease in the rate of reaction of VOCs with OH is the only remaining option to explain the measurement/model discrepancy for OH. A reduction in the isoprene+OH rate constant of 50%, in conjunction with increased deposition of intermediates and some modest OH recycling, is able to produce both isoprene and OH concentrations within error of those measured. Whilst we cannot rule out an important role for missing chemistry, particularly in areas of higher isoprene flux, this study demonstrates that the inadequacies apparent in box and global model studies of tropical VOC chemistry may be more strongly influenced by representation of detailed physical and micrometeorological effects than errors in the chemical scheme.

Correspondence to: T. A. M. Pugh
(t.pugh@lancs.ac.uk)

Published by Copernicus Publications on behalf of the European Geosciences Union.

1 Introduction

Global emissions of non-methane biogenic volatile organic compounds (BVOCs) are estimated to total 1150 Tg C yr^{-1} (Guenther et al., 1995) and exceed those of their anthropogenic counterparts by a factor of 10 (WMO, 1995). Furthermore BVOCs typically have much shorter atmospheric lifetimes than anthropogenic VOCs and hence are believed to play a dominant role in the chemistry of the planetary boundary layer (PBL) and lower troposphere (Fuentes et al., 2000). A modelling study by Poisson et al. (2000) found that BVOCs could affect the composition of the entire troposphere due to the formation of longer-lived intermediates (e.g. CO), with strong increases in O_3 and depletion in boundary layer OH concentrations being observed. Convection of BVOC oxidation products is a major source of HO_x in the upper atmosphere (Poisson et al., 2000; Tan et al., 2001), whilst relatively long-lived oxides of nitrogen such as PAN can influence remote tropospheric NO_x, and hence ozone chemistry. Much work has been carried out on defining the reactions of these species (Jenkin et al., 2007; Saunders et al., 2003; Pinho et al., 2005), however, due to the number of compounds and complexity of the reaction schemes involved, their precise roles in controlling chemical budgets and processes in the atmosphere are poorly understood.

Over half the world's forests are found in the tropics, and, due to the prevailing high temperatures and solar fluxes, they are believed to account for almost half of all BVOC emissions to the atmosphere (Guenther et al., 1995). In recent years knowledge of tropical BVOC emissions and chemistry has been greatly increased by several measurement studies (e.g., Kuhn et al., 2004, 2007; Karl et al., 2007) and modelling studies (e.g., Lelieveld et al., 2008; Butler et al., 2008; Ganzeveld et al., 2008; Kubistin et al., 2008). In particular, flaws have been suggested in the current understanding of the reaction of isoprene and OH under low [NO_x] conditions, resulting in questions about current understanding of global oxidant budgets.

Rapid land-use change makes it imperative to understand the chemistry of tropical forests, both for a holistic understanding of natural processes, and to predict the effect of such land-use changes on local/regional photochemistry and climate change. Therefore it is important to test current atmospheric chemistry models, currently optimised for the polluted mid-latitudes, in this relatively pristine environment. Reproducing measurements at box-model level is an important step towards generating accurate predictions from global and regional models.

This study tests the performance of the CiTTyCAT box model of atmospheric chemistry against measurements made at Bukit Atur, Sabah, Malaysian Borneo, as part of the Oxidant and particle photochemical processes above a South-East Asian tropical rain forest (OP3-Danum-08) field campaign (Hewitt et al., 2010). Forest in Borneo, including the Bukit Atur measurement site, is principally lowland evergreen broadleaf rainforest (Schmitt et al., 2008). Structurally and floristically, it is very different to the rainforest of Amazonia (Hewitt et al., 2010). Seasonal cycles are weak, with dry periods of greater than 1 month absent or rare, cf. to Amazonia or Equatorial Africa where most of the rainforest experiences a significant dry season (Walsh, 1996). The average peak daytime temperature of 27 °C is less than observations in Amazonia of 28–32 °C (Karl et al., 2007) and >30 °C (Kuhn et al., 2007). The analysis herein pays particular attention to the replication of the concentrations of BVOCs and their oxidants under the low NO_x conditions observed. First, the measurement site (Sect. 2) and model parametrisation (Sect. 3) are outlined. Then the model is used to generate estimates of biogenic emissions from the site (Sect. 4) and the resultant model output is compared to observations and improvements suggested (Sect. 5). This is followed by an investigation of the relationship between isoprene and OH (Sect. 6).

2 Measurement site description

The OP3-Danum-08 field campaign was carried out in three phases: (i) ground-based measurements only, during April/May 2008 (OP3-1), (ii) a reduced set of flux and concentration measurements at a nearby oil palm estate during May/June (OP3-2), and (iii) both ground and aircraft measurements, during June/July 2008 (OP3-3). We focus here on measurements made during OP3-1. Ground-based measurements of atmospheric composition were primarily made at the Bukit Atur Global Atmospheric Watch (GAW) station (4°58′59″ N, 117°50′39″ E) (Hewitt et al., 2010). These measurements included concentrations of NO, NO_2, NO_y, HONO (OP3-3 only), O_3, OH, HO_2 (OP3-3 only), HO_2+RO_2, PAN, organic nitrates, isoprene, total and speciated monoterpenes and oxygenated organic compounds (formaldehyde and glyoxal). Fluxes of isoprene, total monoterpenes, O_3, latent and sensible heat were also measured. Physical parameters measured included relative humidity, wind, mixing height and $J(O^1D)$. A detailed description of the site and measurements is given in Hewitt et al. (2010).

The Bukit Atur (BA) GAW site is situated at an altitude of 437 m a.m.s.l., on a small hill approximately 260 m above the surrounding valley floor. The top of the hill features a small grassy clearing approximately 150 m by 50 m surrounded by secondary rainforest, rising to ∼10 m on three sides. The surrounding rainforest is either virgin or has not been logged since 1988 (Tangki and Chappell, 2008). A 100 m high steel-framed measurement tower has been erected in the centre of the clearing as part of the World Meteorological Organisation Global Atmospheric Watch site that has been established at BA. The measurements used in this report were made at ∼5 m above ground level in this clearing, with the exception of PTR-MS measurements of BVOC concentrations

and fluxes which were made at 75 m, and PAN measurements which were made at 30 m. References to measurement heights in this paper are always relative to the top of the hill.

It is possible that the 5-m measurements are effectively within the canopy. To ascertain whether this is indeed the case NO_x measurements made at a nearby under-canopy site (4°58′50″ N, 117°51′19″ E) are compared with those made in the boundary layer by an aircraft and those made at 5 m at BA. The in-canopy measurements (8 m above soil surface) display significantly higher levels of NO (316 pptv as opposed to 37 pptv in the median at midday). However the aircraft and 5-m measurements of NO and NO_2 show good agreement (Hewitt et al., 2009), suggesting that the 5-m measurements may indeed be regarded as representative of the well-mixed boundary layer during daytime. Unlike NO_x, isoprene measurements during OP3-1 are on average 36% lower at 75 m than at 5 m, indicating that isoprene does show a gradient in the surface layer. This is because the ratio of emission rate to chemical loss rate is much greater for isoprene than for NO. No such gradient is discernible for monoterpenes which have a lower emission rate. Good agreement is seen for 75-m and boundary layer aircraft measurements of isoprene Hewitt et al. (2009). Model calculations suggest that, at most, OH concentrations would increase by 30% between 5 m and 75 m as a result of the gradient. An increase of this magnitude is within the uncertainty of the measurements and, since it is an increase, would not adversely affect the analysis carried out in this study. As explained in Sect. 6, there is considerable uncertainty over whether isoprene is a significant net OH sink at all. 5-m and aircraft measurements of OH concentration show close agreement, supporting the assertation that for most species (i.e. those lacking strong surface emission) the 5-m measurement height on top of the hill is representative of, the daytime mixed layer. At nighttime, stratification within the clearing (Pugh et al., 2010) means that these measurements cannot be assumed to represent the nocturnal boundary layer. This paper concentrates on the daytime measurements, drawing only limited comparisons with measurements made during the night.

3 Model description and parametrisation

The CiTTyCAT atmospheric chemistry model (Wild et al., 1996; Evans et al., 2000; Emmerson et al., 2004; Donovan et al., 2005) was run in stationary-box mode at ground level over the Bukit Atur GAW site. Unless otherwise stated, all model species are allowed to evolve freely and are not constrained to observations. Hence, the model provides a bridge between 0D constrained box studies (e.g., Emmerson et al., 2007, and other papers this issue) and global models (e.g., Cook et al., 2007, and other papers this issue). Model runs were carried out for 8-day periods to achieve a nearly steady diurnal cycle, with all model-data comparisons being made using output from the last day. The model was initialised using average measured midnight concentrations, however the results are insensitive to the initial conditions. Isoprene chemistry follows the MIM2 scheme (Taraborrelli et al., 2009) and monoterpene chemistry is split equally between the α-pinene (Jenkin, 1996) and d-limonene (Stockwell et al., 1997) schemes, representing the approximately equal split between more- and less-reactive monoterpenes seen in GC-FID measurements at Bukit Atur. The average diurnal temperature variation measured at Bukit Atur is used. Photon fluxes are calculated using the on-line photolysis scheme (Wild et al., 1996). As no direct measurements of cloud cover were made, model cloud cover is adjusted such that the generated diurnal variation of the photolysis frequency of ozone to form excited oxygen atoms, $J(O^1D)$, fits the average measured by a filter radiometer at the site. With this adjusted cloud cover the model reproduces the measured photolysis frequency of NO_2 well, leading to the conclusion that photolysis rates are effectively simulated across the wavelength band of interest for boundary layer photochemistry.

Surface emissions of BVOCs, NO, CO and CH_4 were emitted into the box at each timestep and are assumed to be mixed instantaneously throughout the box. CH_4 and CO are emitted following Ohara et al. (2007), whilst BVOC and NO emissions are described in Sect. 4. All mentions in this paper of emissions into the model refer to above-canopy emissions. Studies of of in-canopy chemistry (Fuentes et al., 2007; Farmer and Cohen, 2008) have indicated that some oxidation of BVOCs may occur within the canopy, resulting in a net emission of oxidation products above the canopy. These studies show that the photolytic source of OH is substantially reduced within the canopy due to the reduced photolytic flux density and hence oxidation by ozone and/or NO_3 becomes important. Farmer and Cohen (2008) infer very high levels of OH in the canopy of a pine forest which they attribute to the ozonolysis of very reactive organic compounds emitted within the canopy, such as those implied by Holzinger et al. (2005). However the forest in which these measurements were conducted experiences high levels of ozone, with Murphy et al. (2007) finding average 8 hour maximum ozone mixing ratios >60 ppbv. This is compared to the very low ozone (4–8 ppbv) mixing ratios measured within at the OP3 in-canopy site. Likewise the study of Fuentes et al. (2007) reports significant oxidation by NO_3, which is unlikely during OP3 due to the low [NO_x] observed. In another modelling study over tropical rainforest Ganzeveld et al. (2008) calculate that about 90% of their modelled isoprene flux exits the rainforest canopy. The missing 10% is not all reacted, with soil uptake also playing a role (Cleveland and Yavitt, 1997; Pegoraro et al., 2006). Given that oxidation products themselves may be deposited before exiting the canopy, the above canopy-flux of oxidation products will be a relatively small proportion of the whole. Hence an explicit coverage of in-canopy chemistry is neglected here.

The box height is defined during the day by the height of the well-mixed PBL, which vertical velocity variance measurements from a pulsed Doppler LIDAR (light detection and ranging) indicate to be 800 m between 10:00–18:00 LT (Pearson et al., 2010). As measurements of vertical velocity variance are a direct measurement of the turbulent mixing process, they are the most useful data for the estimation of mixing height during convective conditions (Tucker et al., 2009). This estimation of mixing height also agrees closely with that derived from aerosol backscatter, which may be considered an indicator of the vertical extent of mixing. Aircraft profiles over the rainforest during OP3-3 indicated that the region of $d\theta/dh$=0 rarely extended above 1000 m above ground-level, whilst NO_x mixing ratios dropped off rapidly above ~800 m. A mixing layer height of 800 m is significantly less than the 1200–1500 m indicated in some studies of the Amazon (Martin et al., 1988; Krejci et al., 2005; Eerdekens et al., 2009). However it is comparable with the measurements of Fisch et al. (2004) who measured a mean maximum convective boundary layer height of 1002 m (standard deviation 195 m) during the Amazonian wet season, using sonde profiles. The specification of wet season is important as the 1200–1500-m measurements were all made in the dry season when boundary layer heights have been observed to be higher than in the wet season (Fisch et al., 2004). As OP3 typically experienced daily rainfall episodes, a comparison against measurements made during the Amazonian wet season is most appropriate.

Upon collapse of the well-mixed boundary layer at 18:00 LT, the box is split into two separate layers, the lower one representing the inversion-capped nocturnal boundary layer (NBL), and the upper one representing the residual layer. These layers are integrated separately throughout the night with no mixing between them. When LIDAR measurements show turbulent mixing to be re-initiated between 08:00–10:00 LT the following morning (Pearson et al., 2010), the residual layer concentrations are gradually mixed into the lower box as the mixing height rises, until the lower box has engulfed the residual layer, following the parametrisation,

$$C_L(i,t) = C_U(i,t-1) + \left((C_U(i,t-1) - C_L(i,t-1)) \times \frac{m(t)}{h(t)} \times T \right) \quad (1)$$

where C_L and C_U are the concentrations of species i at time t in the lower and upper box respectively, h is the mixing height (height of the lower box), m is the rate of mixing height rise and T is the model timestep. In the absence of reliable measurements, the nighttime PBL height is set at 200 m following sensitivity studies of the measurement fit. The aim of this optimisation is to gain the best fit to the daytime measurements and therefore comparisons of the modelled nighttime concentrations to the measurements should be made with caution, especially for the lower box. No other mixing or entrainment processes are permitted.

Dry deposition is included for O_3, NO_x, N_2O_5, HNO_3, HO_2NO_2, H_2O_2, HCHO, CH_3CHO, CH_3OOH, CH_3CO_3H, PANs and isoprene nitrates using the values listed in Evans et al. (2000). The deposition velocity for isoprene nitrates is assumed to be as for HNO_3 following Horowitz et al. (2007). Wet deposition is considered in Sect. 5.2.

4 Emissions optimisation

Hewitt et al. (2010) report an average midday NO_x mixing ratio of 200 pptv. In such a remote NO_x-limited regime, accurate emissions of NO are vital to effective modelling. However above-canopy measurements of NO fluxes at Bukit Atur are not available. Therefore it is necessary to make an estimate of the above-canopy emission from the available ambient concentration data. This estimation process was also used to estimate isoprene and total monoterpene fluxes, as a cross-check. A tri-variate sensitivity study of 384 runs was carried out, varying 24-h average NO emissions from 0.002 to 0.008 mg N m^{-2} h^{-1} and monoterpene and isoprene emissions from 0.06 to 0.24 and 0.14 to 0.37 mg m^{-2} h^{-1} respectively. The selection of these ranges was informed by previous coarser resolution sensitivity studies, covering a much wider range of values. The isoprene emission followed a diurnal cycle defined by its characteristic light dependence (Guenther et al., 2006). Monoterpene emission was set to follow a the same diurnal cycle as isoprene, following the findings of Kuhn et al. (2004) and the OP3 measurements, which also suggested very little monoterpene emission during the night. A cost function was then run over the model output to locate the optimum emission fluxes that replicate the concentrations observed in the field. The cost function uses OP3-1 campaign-median values for each hour of a 24-h cycle for OH, NO, NO_2, O_3, isoprene, monoterpenes and HO_2+RO_2, in the form,

$$C_{total} = \sum_{t=10}^{t=18} \sum_{i=1}^{n} \left(w(i) \frac{|x_i(t) - \hat{x}_i(t)|}{\hat{x}_i(t)} \right) \quad (2)$$

where C_{total} is the total cost, a dimensionless metric where small numbers indicate a better fit, t is the hour of the day, n is the number of species used in the fitting, $\hat{x}_i$ is the campaign median measured concentration of a species for each hour of the day and x_i is the modelled concentration of that species, w is a weighting function for that species (typically w=1). Only 10:00–18:00 LT concentrations were used, as LIDAR measurements give confidence that the flux tower is fully enveloped by the PBL during that period, and hence the well-mixed assumption of the model is valid. Median values are selected to represent the "typical" day, and eliminate the influence of extreme events. To reflect the fact that the OH and HO_2+RO_2 measurements may carry more uncertainty, the function was also run with w=0.5 for these species. The result returned was virtually identical, indicating a robust fit with respect to the observations.

The best-fit cost function result of $C_{total} = 2.20$ was found at a 24-h-average monoterpene emission of 0.15 mg m^{-2} h^{-1}, isoprene emission of 0.23 mg m^{-2} h^{-1} and NO emission of 0.005 mg N m^{-2} h^{-1}. It can been seen from Fig. 1 that the region of values below C_{total}=2.3 (coloured dark blue) is quite broad. The best fit is located at the furthest-right point of this dark blue area (black dot in Fig. 1), however this quite broad general minima indicates that monoterpene emissions can be traded on an approximately 1:1 basis for isoprene emissions for only a small penalty in fit. This is not altogether surprising given the broadly comparable atmospheric chemistry and lifetimes of these species, at least as far as the model is concerned. It was not possible to use observations of methacrolein (MACR) or methyl-vinyl ketone (MVK), which are oxidation products unique to isoprene, to distinguish between isoprene and monoterpene chemistry, as the strong model overestimation of MACR and MVK (see Sect. 5), suggests these products are not being treated correctly in the model.

The best-fit isoprene and monoterpene emissions show excellent agreement with the measured eddy-covariance fluxes, following the median measurement very closely throughout the day (Fig. 2). It should be noted that these isoprene emissions are much less than the 1.7 mg m^{-2} h^{-1} predicted for the region by Müller et al. (2008) for the year 2001. The 24-h average measured isoprene (monoterpene) emission for the "typical" day was 0.28 (0.19) mg m^{-2} h^{-1} (Langford et al., 2010). The model-data agreement gives confidence in the estimated NO emission. It also suggests that this method may be useful in estimating emissions in other campaigns where flux measurements are not available, assuming the the local chemistry and mixing is adequately understood. As the model generated fluxes can only account for what remains or is reacted in the boundary layer, it is possible that much of the 18% difference between model estimated and measured emissions may be explained by venting to the free troposphere. If venting out of the top of the boundary layer is occurring, then comparisons against the eddy-covariance fluxes, which measure the total flux from the surface, only necessitate that the model generated net flux into the PBL be less.

The model-estimated above-canopy NO emission compares very well with the yearly average above-canopy flux estimate of 0.005 mg N m^{-2} h^{-1} given for the area in April by the Yienger and Levy (1995) database. Monthly values in this database range from 0.002 in February to 0.012 mg N m^{-2} h^{-1} in July. Given the minimal variability of the seasonal climate cycle in Borneo (Chappell et al., 2001; Hewitt et al., 2010) these minima and maxima nicely bracket the estimated emission. Anthropogenic contributions to the local NO_x budget are small in comparison to soil NO_x in this very remote location.

However, the model-estimated NO emission is 26 times smaller than the soil flux of 0.13 mg N m^{-2} h^{-1} (J. Dorsey, personal communication, 2009) measured via the chamber method (van Dijk and Duyzer, 1999) at a nearby under-canopy site (4°58′ 50″ N, 117°51′ 19″ E). As the PBL can be considered well-mixed during the day, then the model estimate may be considered to be representative of the above-canopy NO flux over a fairly large locality. The difference between the model estimate and under-canopy measurements is 96%, compared to the 75% and 50% canopy reduction estimated for tropical rainforest by Yienger and Levy (1995) and Ganzeveld et al. (2002) respectively.

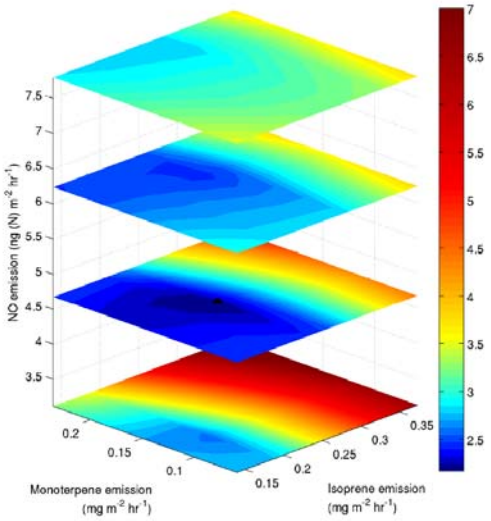

Fig. 1. Cost function surface generated to find the optimum emissions of isoprene, monoterpenes and NO to fit measurements of OH, NO, NO_2, O_3, isoprene, monoterpenes and HO_2+RO_2. Lower values indicate a better fit, with the minima marked by a black dot.

To test the impact of higher NO fluxes, the model was run with the measured soil NO_x emissions, using a canopy reduction of 75%. This resulted in a 400% overestimation of midday [NO_2] and 180% overestimation of [NO] compared to the measurements. Furthermore NO_y mixing ratios were hugely overestimated at greater than 2 ppbv. Such high emissions exiting the canopy are clearly not consistent with the measurements, unless some very large loss of NO_y is not accounted for in the model. Possible losses of NO_y are tested below.

Probably the most poorly understood NO_y loss in this scenario is via organic nitrates, particularly isoprene nitrates. However the 10% average alkyl nitrate yield in the MIM2 mechanism from the RO_2+NO reaction (Taraborrelli et al., 2009), is already at the high end of the spectrum of 4–12% suggested in the literature (Carter and Atkinson, 1996; Chen et al., 1998; Sprengnether et al., 2002; Paulot et al., 2009).

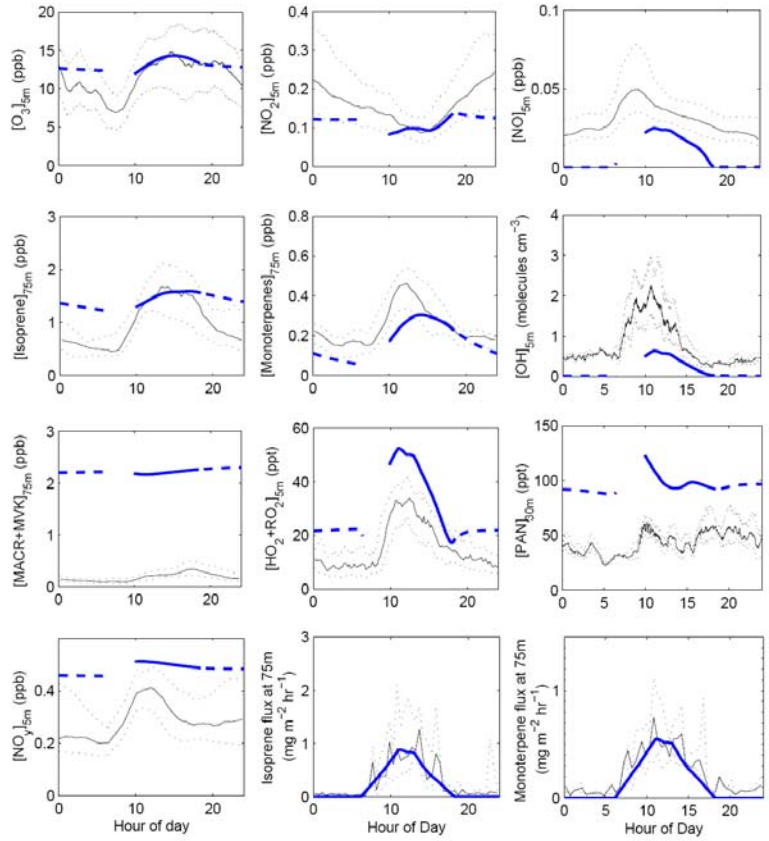

Fig. 2. Comparison of model best fits (blue line) against the OP3-1 average measurement at Bukit Atur (black line). Upper and lower quartiles for the measurements are marked by grey dots. Measurement height is shown in subscript. The solid blue line represents the well-mixed daytime box, whilst the dashed line shows the nighttime residual layer concentrations. The discontinuity between 08:00 and 10:00 LT is due to the mixing between the two layers during this period.

Furthermore the dry deposition velocity applied here to the isoprene nitrates is at the upper end of the range suggested in the literature (0.4–5 cm s^{-1}, Shepson et al., 1996; Rosen et al., 2004; Giacopelli et al., 2005; Horii et al., 2006). Hence the recycling of isoprene nitrates back into NO_x is small. The NO_3+isoprene→alkyl nitrate channel can be neglected due to the very low levels of NO_x and hence NO_3 during OP3. Treves et al. (2000) have shown hydroxy alkyl nitrates, similar to those formed from isoprene, to be very soluble, with Henry's Law constants equal to 1.7×10^4 M atm^{-1} at 298 K. Therefore the model is run with wet deposition enabled. Although the reduction in modelled afternoon [NO_y] is striking, at its minimum value it is still more than twice the measurements. Furthermore, NO_x concentrations are barely altered. For details on the wet deposition parametrisation see Sect. 5.2.

Another possibility is that increased PAN deposition, as observed by Turnipseed et al. (2006), could draw more NO_x through PAN formation to maintain equilibrium as the PAN is deposited. To test this the model is run with $V_{d(PAN)}$=1.0 cm s^{-1} and $V_{d(higherPAN)}$=1.5 cm^{-1} following the average maximum observed by Turnipseed et al. (2006). NO_y concentration is indeed reduced, however the reduction of 16% is nowhere near sufficient for the modelled concentrations to approach the measurements. In another test $V_{d(HNO_3)}$ is increased to 5.0 cm s^{-1}, the very upper

end of the literature range. This also results in a 16% reduction in [NO_y], but virtually no change in [NO_x]. Finally the NO_2 deposition velocity is doubled to give maximum $V_{d(NO_2)}$=1.0 cm s^{-1}. Only a 7% decrease in [NO_y] is achieved.

Even combining all these processes in a single run leaves the minimum in modelled [NO_y] almost twice the measured value, and the concentrations in the morning, before substantial rainfall, are highly unrealistic. Modelled NO_2 and NO concentrations remain overestimated by 320% and 180% respectively. Assuming that there is no canopy loss unaccounted for in the studies of Yienger and Levy (1995) and Ganzeveld et al. (2002), there are three factors which could explain the difference between measured and modelled [NO_x] fluxes. Firstly, the measurements of NO_x which the model is constrained against, were made 5 m above grass in a rainforest clearing. It is possible that the soil in the clearing will have a different characteristic NO emission to the surrounding rainforest. However, as explained in Sect. 2, comparison of 5-m and aircraft measurements supports the hypothesis that the measured 5-m [NO_x] was representative of the mixed boundary layer during the day. Hence this possibility is discarded. Second, it is possible that a significant amount of NO_x is lost from the boundary layer by entrainment into the free troposphere. However dilution on this scale would have a very large impact on concentrations of other tracers such as isoprene, which are modelled well without an entrainment factor. Finally, natural soils demonstrate considerable heterogeneities. Measured soil emissions between the chambers varied by more than an order of magnitude. Hence attempting to scale up such values is fraught with error as the heterogeneity of the soil at the canopy scale cannot be accurately determined.

5 Comparison of best-fit model concentrations with measurements

A comparison of the output generated by running the model with the emissions defined in Sect. 4, against the in-situ measurements made at Bukit Atur during OP3-1, is shown in Fig. 2. As mentioned in Sect. 4, due to the nighttime meteorology, the comparison is most valid between 10:00–18:00 LT, hence concentrations from the surface box are only shown between these times. Concentrations modelled in the nighttime residual layer (dashed blue line) are also shown for context, although direct comparison should not be made between modelled residual layer concentrations and 5-m level measurements. No concentrations are shown between 08:00–10:00 LT as the concentrations observed at this point will depend strongly on the height of the observer in the boundary layer. Table 1 lists the individual contributions, C_i, to the total cost, C_{total}, between 10:00–18:00 LT. It also lists the mean-bias error (MBE) as a percentage of the average 10:00–18:00 LT concentration. This statistic gives the average percentage by which the model under- or over-predicts the measurements. It is calculated using Eq. (2), but without taking the absolute value of the numerator.

Table 1. Individual contributions, C_i, to the total cost, C_{total}, and % mean-bias error (MBE), between 10:00–18:00 LT for the best fit scenario generated in Sect. 4.

Species	C_i	% of C_{total}	% MBE
NO	0.48	22	−48
NO_2	0.13	6	−10
O_3	0.05	2	+5
OH	0.64	29	−64
HO_2+RO_2	0.59	27	+58
Isoprene	0.08	4	+5
Total monoterpenes	0.24	11	−24
Total	2.20	100	

Good agreement in particular is seen for O_3, and NO_2 with MBEs of +5% and −10% respectively. This robust fit to O_3 and NO_x was also observed by Pike et al. (2009). The relatively poor fit of NO compared to the other two variables is attributable to the overestimation of peroxy radical concentrations (MBE of +58%). The interaction of peroxy radicals and NO control the cycling of NO to NO_2 and HO_2 to OH via Reaction (R1), as well as conversion of RO_2 to HO_2.

$$HO_2 + NO \rightarrow OH + NO_2 \quad \text{(R1)}$$

As discussed in Sect. 5.2, when wet deposition is turned on, modelled peroxy radical concentrations come into close agreement with the measurements. Consequently the simulated [NO] increases to within the bounds of the observations, due to a decrease in the rate of cycling of NO to NO_2 via Reaction (R1). Conversely, constraining daytime [NO] to the measurements results in a serious deterioration of the fit to NO_2, NO_y and O_3 concentrations. NO_y concentrations are overestimated in the model. As mentioned in Sect. 4, wet deposition can play a role for many NO_y species, and indeed later analysis including the effects of wet deposition (see e.g. Fig. 6) yields concentrations close to the measurements. The behaviour of O_3, NO and NO_2 during the night will be the focus of a subsequent paper (Pugh et al., 2010).

Modelled OH concentrations are around 2–3 times less than those measured with an MBE of −64%. As HONO photolysis has been observed to contribute as much as 56% of OH production in some forested environments (Kleffmann, 2007), it appears possible that a model underestimation of HONO could explain the missing OH. However measurements of HONO during OP3-3 indicate mixing ratios <10 pptv. At a midday HONO photolysis rate of 8.7×10^{-4} s^{-1}, as calculated by CiTTyCAT, 10 pptv of HONO would generate 2.0×10^5 molecules OH cm^{-3} s^{-1}, ∼3% of the modelled OH source at that time. This

demonstrates that HONO photolysis was not important during OP3-3, although it is possible that HONO concentrations were higher during the OP3-1 period upon which our model analysis is based. This will be investigated further by Whalley et al. (2010b).

Analysis of modelled OH loss mechanisms concludes that 70% of OH loss at midday is attributable to isoprene or its direct oxidation products, with a further 11% due to monoterpenes and their oxidation products. Constraining the model to measured daytime OH concentrations results in a strong increase in peroxy radical concentrations to more than twice the measured values, whilst decreasing [NO] and [NO_2]. Interestingly the concentration of HO_2 is insensitive to the model being constrained to OH. Hence the increase in total peroxy radicals is due to RO_2 from the increased oxidation of VOC under the higher [OH] conditions. Given the constraints on emission fluxes provided by measurements, it appears something may be amiss within the isoprene oxidation scheme, as hypothesised by Lelieveld et al. (2008). This possibility will be explored in more detail in Sect. 6. Morning monoterpene concentrations are somewhat underestimated by the model. The reason for this is not entirely clear, but may be due to uncertainty in the speciation of monoterpenes at the canopy level, meaning the split between monoterpene schemes used here may not be ideal. Routing monoterpene concentrations entirely though the α-pinene or d-limonene schemes results in changes of +14% and −15% respectively.

During the night, modelled residual layer concentrations of HO_2+RO_2 are 2–3 times larger than measured at 5 m, suggesting that something is depleting peroxy radical concentrations near the surface during the night. It is likely that this is linked to the relatively high nighttime [NO] at 5 m, which would react with HO_2 and RO_2, leading to the formation of the relatively high nocturnal [OH] observed at 5 m (see e.g., Geyer and Stutz, 2004). Further discussion of this issue is beyond the scope of this paper, but will be addressed in Whalley et al. (2010a).

5.1 Dry deposition of MACR and MVK

Whilst daytime modelled isoprene and monoterpene concentrations are quite close to the measurements, there is a substantial overestimation, by 5–10 times, of modelled MACR and MVK concentrations, compared to the measurements. This is much larger than the measurement uncertainty of a factor of two. As these products are principally formed through the reaction of OH+isoprene, this lends further credence to the idea that something may be wrong with the way isoprene oxidation is represented. Indeed Peeters et al. (2009) suggest that current yield for the reaction of isoprene peroxy radicals with NO may produce 50% too much MACR and MVK in these low [NO_x] conditions. However, this alone cannot account for the overestimation seen. Such large overestimations are not apparent in other oxidation products, such as HO_2+RO_2 or PAN (Fig. 2).

Another possibility is that MACR and/or MVK undergoes significant dry deposition. The existence of a substantial dry deposition flux of MACR/MVK has been suggested before by Karl et al. (2004), following measurements made in Costa Rica. Using eddy-covariance measurements and taking account for the effects of chemistry and dew, they measure an average deposition velocity ($V_{d(MACR+MVK)}$) of 1.6 cm s^{-1}. However, they also calculate a possible deposition velocity over the Amazon of 2–4 cm s^{-1} utilising data published by Andreae and Merlet (2001). More recently, measurements during the AMAZE field study indicated $V_{d(MACR+MVK)}$=2.4 cm s^{-1} (Karl et al., 2009b), and measurements made over a strongly isoprene emitting oil palm plantation during OP3-2 showed $V_{d(MACR+MVK)}$=1–2 cm s^{-1} (Misztal et al., 2010)

Such high deposition rates cannot be explained by current theory. For instance, Zhang et al. (2002) estimate daytime deposition velocities over evergreen deciduous forest of 0.341 and 0.499 cm s^{-1} for MACR and MVK respectively, using a dry deposition model calibrated using measurements of O_3 and SO_2. However they note that very little data is available to evaluate these values. Interestingly Zhang et al. (2002) also predict deposition velocities for PAN species ∼0.5 cm s^{-1}, whereas recent measurements by Turnipseed et al. (2006) showed deposition of PAN species up to 1.5 cm s^{-1}. In a recent modelling study Ganzeveld et al. (2008), using a similar approach to estimating dry deposition velocities to Zhang et al. (2002), overestimate MACR+MVK by 2–3 times compared to concentrations measured over Suriname during the GABRIEL campaign. Such a range of literature values illustrates that MACR and MVK deposition rates are currently poorly characterised, yet they may be large enough to significantly impact upon concentrations.

To test the importance of MACR/MVK deposition for the Danum Valley regime, a model run was carried out with $V_{d(MACR+MVK)} = 2.0$ cm s^{-1}. This deposition velocity can explain much of the difference between the model and measurements, causing a 63% reduction in midday mixing ratio to 0.8 ppbv, about twice the magnitude measured. MACR/MVK flux measurements over the rainforest show no clear net flux. However, it is quite likely that any dry deposition flux is masked in the measurements due to the spatial variation of MACR and MVK chemical sources and sinks within the PBL.

The above dry deposition of MACR and MVK decreases the OH sink, increasing modelled peak [OH] by 18% to 7.5×10^6 molecules cm^{-3}. This increase in [OH] in turn increases modelled isoprene and monoterpene loss rates, hence decreasing their concentrations significantly below measurements. Re-computing a new best-fit then increases isoprene and monoterpene emissions, in order to maintain a fit to observed isoprene and monoterpene concentrations, consequently reducing [OH] back to similar levels to those in Fig. 2. This illustrates the importance of correctly characterising MACR/MVK deposition velocities to simulating PBL

chemistry, and raises the possibility that deposition of other important intermediate species might lead to significant errors in model studies.

5.2 Wet deposition

The model runs above also show a large build-up of organic peroxides (ROOH) to >5 ppbv over the 8 day period, These are produced as part of isoprene oxidation, typically by the reaction of organic peroxy radicals (RO_2) with the hydrogen peroxy radical (HO_2). Some of these higher peroxides have reaction rates with OH similar to that of isoprene with OH ($\sim 10^{-10}$ cm^3 molecule^{-1} s^{-1}) and hence may contribute substantially to the OH sink. However organic peroxides typically have high Henry's Law coefficients $>1\times10^6$ M atm^{-1}, and hence are very susceptible to wet deposition processes.

In this study wet deposition has been simulated using the S-WET2 scheme described in Real et al. (2008). This scheme has been extended to cover all appropriate species in the organic schemes used here. Henry's Law constants have been taken from Sander (2009) and Treves et al. (2000) where available. For those species lacking a measured value for Henry's Law, the most structurally similar compound with available measurements has been utilised. The pH of rainwater in this remote region is assumed to be 5.6. Notable species aside from ROOH which undergo wet deposition in the scheme are HCHO, HO_2, H_2O_2, HNO_3, HO_2NO_2, CHOCHO, CH_3CHO and isoprene nitrates. The rain rates supplied to the model are the diurnal averages of those measured at Danum Valley Field Centre (4°57′42″ N 117°48′12″ E) during the course of OP3-1. This profile gives no rain during the morning, but a strong peak of $\sim$3 mm h^{-1} at 15:00 LT, with levels circa 0.5 mm h^{-1} persisting throughout the afternoon and evening. All rainfall is assumed to be convective.

Applying this wet deposition parametrisation to the model run shown in Fig. 2 leads to an 88% reduction in modelled midday [ROOH] to $\sim$0.7 ppbv. This is much closer to aircraft measurements made during OP3-3 of $\sim$0.2 ppbv. Furthermore the tendency of ROOH to accumulate in the box is greatly reduced. Peak HCHO mixing ratios are reduced from $\sim$4 ppbv to $\sim$1.5 ppbv, with almost no HCHO persisting in the afternoon. Clearly wet deposition is a very important loss process for several BVOC oxidation products in this environment.

The photolysis of HCHO is an important source of HO_2, so a reduction in HCHO concentrations will play a role in the 25% reduction in modelled peroxy radical concentrations yielding a negative impact on OH production. However, overall, the change in the OH sink cancels out this decrease in production. Closer inspection reveals that the wet deposition of NO_y, in particular isoprene nitrates, leads to a substantial reduction in ambient [NO_x]. When the NO emission is increased to cancel out this effect the decrease in [HO_2+RO_2] is almost unchanged, but an increase in peak [OH] of 72% is revealed with a consequent decrease in peak isoprene concentration of 31%, showing that when [NO_x] is maintained the change in OH sink caused by wet deposition is substantial. Hence consideration of wet deposition is also an important factor in correctly modelling the oxidising capacity of the tropical boundary layer. The importance of correct deposition velocities of intermediates for the OH sink is also highlighted in Edwards et al. (2010).

5.3 Residual layer MACR and MVK

In their paper describing modelling of atmospheric chemistry over rainforest in Guyana and Suriname, Ganzeveld et al. (2008) report a modelled increase in residual layer MACR and MVK concentrations during the night, which they believe was a contributor to their overestimation of the daytime concentrations of these species. Although this study focuses upon daytime measurements for reasons explained in Sect. 3, some analysis of this problem is possible here.

CiTTyCAT also observes a small increase in the upper box MACR and MVK concentrations during the night. The small magnitude is likely due to the lower concentrations of ozone and isoprene during this study cf. Ganzeveld et al. (2008). It is possible, although absolute confirmation cannot be made, that the 75-m observations are within the residual layer during the night. If this is the case, the decrease observed during the night in average total MACR+MVK mixing ratios from 335 pptv at 18:00 LT to 91 pptv at 06:00 LT, suggests the model is incorrectly modelling production and/or loss during the night. Nighttime measurements of isoprene concentration at 75 m are around 50% of those modelled in the residual layer. Therefore, if these measurements really are in the residual layer, it is clear that $\sim$50% too much nighttime production of MACR and MVK is being modelled. Note that this does little to affect the model overestimation of [MACR+MVK] as most of the modelled increase takes place during the day. However, the model overestimation of [MACR+MVK] also means its loss rate to its reaction with ozone is being overestimated many more times than its production. When MACR and MVK concentrations overall are reduced by deposition, the net nighttime production in the residual layer is increased as gross production is virtually unchanged, but loss to ozone is reduced (see Fig. 6).

This lends support to the hypothesis of Ganzeveld et al. (2008) that intermittent nocturnal transport events may be connecting the residual layer with the surface, allowing some deposition from the residual layer. In CiTTyCAT such effects are implicitly accounted for in that by defining the NBL height, which controls deposition rates, by a sensitivity study optimised to daytime concentrations, what is actually defined is an effective NBL height with the aim of producing the correct concentrations at the end of the night. The idea that an optimised NBL height implicitly incorporates mixing with the residual layer has been suggested before by Strong et al. (2009). Indeed, the net change in [MACR+MVK] averaged over both boxes during the night

is negative when $V_{d(MACR+MVK)}$=1.5 cm s^{-1} is applied. As a box model cannot reproduce the chemical gradients caused by limited mixing in a stable boundary layer, this solution is adequate for the purposes of this study. However, assuming the 75-m nighttime measurements are in the residual layer, it would appear that any model attempting to accurately recreate residual layer concentrations will need to account for such nocturnal transport events.

6 Isoprene and OH

The cause of [OH] underestimation over tropical rainforest is currently unknown, although such model underestimations of [OH] measurements have been observed before. Tan et al. (2001), measuring over a North American deciduous forest, found that observations of [OH] were on average 2.7 times greater than the modelled concentrations. However the modelled and measured HO_2 were in good agreement. Carslaw et al. (2001) similarly found that modelled OH concentrations over a forest in Northern Greece were on average, half the measured concentrations. For both these studies observed concentrations of isoprene were >1 ppbv. More recently Ren et al. (2008) found observed [OH] was as much as 4 times larger than modelled OH in the boundary layer over North America. They also found that higher model underestimation was clearly correlated to increased concentrations of isoprene. In the only other studies to date incorporating [OH] measurements over a tropical rainforest, Lelieveld et al. (2008) and Martinez et al. (2008) report very much higher observed concentrations of OH than predicted using their chemical model. A notable feature of all these studies is the low [NO_x] observed at the sites, and that the model:measurement discrepancy is greater at lower NO_x. In a different study Thornton et al. (2002) show that they are unable to close their HO_x budgets at low [NO_x] based upon current knowledge.

In contrast urban modelling studies have typically agreed well with, or overestimated [OH] compared to the measurements (e.g. George et al., 1999; Konrad et al., 2003; Emmerson et al., 2005, 2007), although Emmerson et al. (2005) did find some days when they significantly underpredicted OH concentrations. Ren et al. (2006) also modelled measured OH and HO_2 concentrations well in a rural environment where isoprene concentrations were typically <1 ppbv. Similarly Kanaya et al. (2007) overestimate both OH and HO_2 significantly in a model:measurement comparison for Japanese coniferous forests. Whilst Kanaya et al. (2007) measured 200–400 pptv of monoterpenes, they make no mention of isoprene concentrations, which are typically relatively low for coniferous forests (Guenther et al., 2006).

The above literature supports the hypothesis that the underestimation of [OH] is related to isoprene, or an unaccounted for compound that is emitted following the same pattern. It has been suggested (e.g. Tan et al., 2001; Karl et al., 2007) that the reaction of terpenes and ozone could produce sufficient OH to bridge the gap between models and measurements. However Ganzeveld et al. (2008) concluded that this pathway alone could not explain the model deficiencies. Modifying the model here such that each reaction of a terpene with O_3 produces one OH molecule, can only generate [OH] within the bounds of measurements at terpene emission rates much greater than those of isoprene. This test was carried out utilising the rate constant of the sesquiterpene β-caryophyllene, which, compared to most monoterpenes, has a very fast reaction with O_3 and a relatively slow reaction with OH (Atkinson and Arey, 2003). Thornton et al. (2002) and Lelieveld et al. (2008) noted that errors in the photochemical rate constants could be responsible, particularly those for the dissociation of higher peroxides. However Kubistin et al. (2008) found no evidence for this.

6.1 OH recycling

Several recent studies (Lelieveld et al., 2008; Butler et al., 2008; Kubistin et al., 2008) have noted the apparent correlation between OH and isoprene concentrations, and hypothesised that, under low-NO_x conditions, there is an as-yet-unknown pathway in the isoprene oxidation process that is responsible for recycling OH. Their suggestion is supported to some extent by the experimental work of Hasson et al. (2004), Jenkin et al. (2007) and Dillon and Crowley (2008), who found that OH could be produced by the reaction of HO_2 with organic peroxy radicals containing a carbonyl group. Following this, Lelieveld et al. (2008) and Butler et al. (2008) utilised an OH recycling mechanism of,

$$\mathrm{ISOPROO} + \mathrm{HO_2} \rightarrow \mathrm{ISOPROOH} + \mathrm{nOH} \quad \text{(R2)}$$

where ISOPROO are peroxy radicals formed from the reaction of isoprene with OH, ISOPROOH is the resulting peroxide, and n is the number of OH produced. Lelieveld et al. (2008) found values of n=2−4 gave the best fit to their measurements.

The proposed chemistry behind this recycling hypothesis was tested by modifying the model chemistry scheme following the results of Dillon and Crowley (2008). All reactions of HO_2 with carbonyl containing peroxy radicals in the isoprene and monoterpene schemes were altered to include a further reaction channel producing OH. The branching coefficient assigned to the new channel depended on the position of the carbonyl group on the peroxy radical. If the carbonyl group was on the same carbon as the peroxy group a branching coefficient of 0.5 was applied, following the result for CH_3CO_3 in Dillon and Crowley (2008). For all other positions of the carbonyl group relative to the peroxy group, a coefficient of 0.15 was applied, following $CH_3C(O)CH_2O_2$ in Dillon and Crowley (2008). Non-carbonyl containing peroxy radicals are assumed not to display this reaction channel. Considering this extra source of OH involving the carbonyl groups

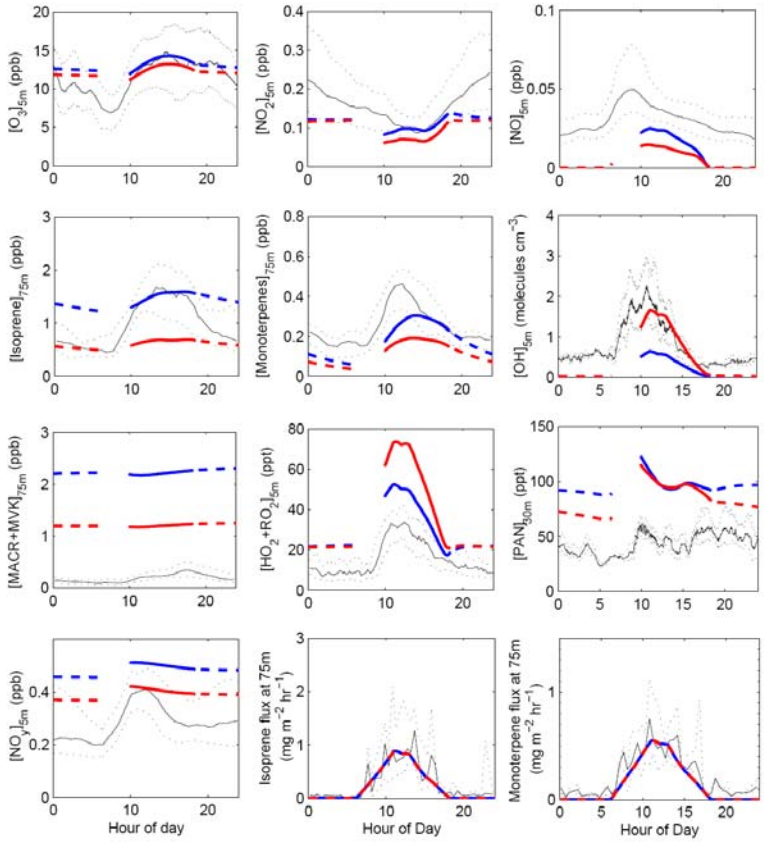

Fig. 3. Comparison of model output with (red line) and without (blue line) OH recycling of m=3.0 against the OP3-1 average measurement at Bukit Atur (black line). Upper and lower quartiles for the measurements are marked by grey dots. Emissions are the same for both scenarios.

resulted in only a 4% increase in the peak [OH], with a similarly small decrease in isoprene and monoterpene concentrations. Hence it may be concluded that recycling of OH via the reaction of carbonyl containing peroxy radicals is only able to produce a very small fraction of the missing OH.

In order to test the hypothesis that unknown OH recycling within the isoprene oxidation scheme could improve the model fit, a tetra-variate sensitivity study was carried out, varying OH recycling, isoprene, monoterpene and NO emissions. Rather than assume a method for OH recycling, the generic reaction,

$$\text{ISOPRENE} + \text{OH} \rightarrow \text{ISOPROO} + \text{mOH} \qquad \text{(R3)}$$

was used. The cost function unambiguously returned a minimum at m=0.0, showing that "artificial" OH recycling did not improve the model fit to the measurements.

To try and understand this lack of improvement, a run was carried out with m=3.0, which was sufficient to give good agreement between measured an modelled [OH], and utilising the emissions derived in Sect. 4. Figure 3 compares the results of this run with those shown in Fig. 2 and the observations. Once again the improved OH fit is at the cost of the isoprene and monoterpene profiles, whose concentrations are heavily reduced. Increasing the isoprene and monoterpene emission can bring these profiles back into line with the best fit previously achieved. However, this requires isoprene and monoterpene emissions to exceed the measured values.

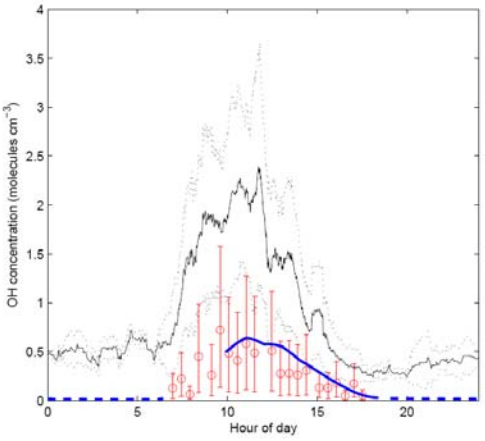

Fig. 4. Comparison of model output for OH, for a run with the best fit emissions generated in Sect. 4 and no OH recycling (blue line), the OP3-1 median measurements (black line, upper and lower quartiles marked by grey dots) and the OP3-1 median [OH] as computed from isoprene fluxes and concentrations following Karl et al. (2007) (red dots, propagated error shown by bars).

Furthermore, this reduces the OH concentration almost back to the levels of no recycling, whilst the HO_2+RO_2 levels increase still further. A similar test is also carried out by constraining the model to measured [OH]. This reduces the peak isoprene mixing ratio to 0.6 ppbv.

A recent theoretical paper by Peeters et al. (2009) postulates an alternative mechanism which may result in significant OH recycling via the reactions of the ISOPROO channel. The details of the Peeters et al. (2009) scheme have not been implemented here, but for the purposes of this study, it is expected to behave similarly to the simpler schemes described above. Using measurements of oxidised VOC made over the Amazon, Karl et al. (2009a) also suggest that the overall HO_x recycled via this mechanism can only be 33% of that suggested by Peeters et al. (2009), in order to remain consistent with their measurements. Interestingly in regimes of intermediate NO mixing ratios, in the 100 s of pptv, it appears the Lelieveld et al. (2008) scheme may prove unable to produce significant amounts of OH (Hofzumahaus et al., 2009), whereas Peeters et al. (2009) expect their mechanism to be important up to NO mixing ratios approaching 1 ppbv.

Hofzumahaus et al. (2009) hypothesise a rather different method of OH recycling due to increased cycling of peroxy radicals into OH, via an unknown compound with a similar reduction capacity to NO; a potentially convenient solution here, given the model overestimation of [HO_2+RO_2]. This was also tested in the model by adding a compound with the same concentration and reaction rate with peroxy radicals as NO. The result was a >100% increase in OH concentration for a 10% decrease in peroxy radical concentration. However the problem of modelled isoprene and OH concentrations not matching the measurements simultaneously is still observed. Hence for the purposes of this study this simply represents another possible method for OH recycling.

6.2 Mass balance analysis

OH concentrations may be calculated indirectly from the isoprene flux and concentrations after Karl et al. (2007) using,

$$F_s - F_e = (k_{OH} \times [OH] + k_{O_3} \times [O_3]) \times C_{mean} \times z_{mix} \quad (3)$$

where F_s is the surface flux of isoprene and F_e is the entrainment flux of isoprene from the top of the PBL into the free troposphere, C_{mean} is the mean concentration of isoprene, z_{mix} is the height of the PBL, and k_{OH} and k_{O_3} are the rate constants for the reaction with isoprene of OH and O_3 respectively. Concentrations were only derived for the daytime due to the lack of mixing at night. The resultant [OH] is compared to measurements and the optimum model output (without OH recycling) in Fig. 4. This suggests an OH concentration in line with that provided by the model, suggesting that the main features of the modelled relationship between isoprene and OH can be represented by Eq. (3), and hence allowing a more simplified analysis of the isoprene and OH problem.

Measured values are available for the isoprene and O_3 concentrations and the isoprene flux. Due to low concentrations and slow kinetics, the isoprene+O_3 reaction is relatively unimportant. In order to increase [OH] in line with measurements we can reduce the net isoprene flux into the PBL by venting out of the top of the box. However this also results in a reduction in isoprene concentration, below the bounds of the measurements. Another possibility is the mixing height (z_{mix}). Following Eq. (3), a decrease in the mixing height would negate the need for a decrease in the isoprene concentration with a decreased flux. However, z_{mix} may be estimated quite accurately from the lidar measurements. Furthermore halving the daytime z_{mix} from 800 m to 400 m, whilst appropriately reducing the emitted fluxes, realises only a 4% [OH] increase.

The only remaining possibility is the rate of reaction. The utilised rate constants for the reactions of isoprene with OH and O_3 ($1.0\pm0.2\times10^{-10}$ and $1.27\pm0.25\times10^{-17}$ cm^3 molecule^{-1} s^{-1} at 298 K respectively) are the result of numerous studies (IUPAC, 2009). Assuming a well mixed atmosphere, such well defined rates give very little room for manoeuvre, unless an outside process can influence the rate of reaction.

6.3 BVOC segregation

Following the work of Krol et al. (2000), Butler et al. (2008) argue that the segregation of isoprene into distinct plumes

may result in a depletion in OH within those plumes. This would invalidate the well-mixed assumption of box models and lead to a lower effective rate constant. Butler et al. (2008) suggest utilising a 50% reduction in rate constant, which, when combined with OH recycling, improves their isoprene and OH fits.

The importance of segregation can be assessed using the Damköhler number (Da) following Krol et al. (2000),

$$\mathrm{Da} = \frac{\tau_{\mathrm{mix}}}{\tau_{\mathrm{chem}}} \quad (4)$$

where τ_{chem} is the chemical lifetime and τ_{mix} is the mixing timescale. If Da$\approx$ 1 then segregation effects are likely to be most prominent. Using average midday [OH] during OP3-1, yields an isoprene lifetime (τ_{chem}) of ~80 min. τ_{mix} can be approximated by the convective velocity timescale,

$$t_* = \frac{z_i}{w_*} \quad (5)$$

where,

$$w_* = \left[\frac{g \times z_i}{T_{\mathrm{v}}} F_{\mathrm{H}}\right]^{\frac{1}{3}} \quad (6)$$

where z_i is the height of the boundary layer, g is acceleration due to gravity, T_{v} is the virtual temperature and F_{H} is the kinematic heat flux. Using average values yields w_*=1.4 m s^{-1} at midday, giving t_*=9 min. In this case Da=0.1, suggesting that the role of segregation at Bukit Atur may be limited. However the range of OH measurements is large, with peak concentrations $>6\times10^6$ molecules cm^{-3} recorded on some days. An OH concentration of this magnitude would result in an isoprene lifetime of ~28 min, and hence a Damköhler number much closer to unity. In comparison, Butler et al. (2008) suggest an isoprene lifetime of <30 min over the Guyanas, which is comparable to the estimated convective mixing timescale during their campaign of 8–16 min. In order to definitively prove the segregation hypothesis, high-frequency, co-located measurements of VOCs and OH are required. These are not available from the OP3 or other campaigns.

In order to ascertain whether reducing the rate constant could improve the model fit, the sensitivity study outlined in Sect. 4 was carried out with a 50% reduction in the effective rate constant of OH+isoprene. As any physical process affecting the OH+isoprene rate would also likely affect the OH+monoterpene rate, reduction factors are also applied to these reactions. Applying the cost function defined in Eq. (2) to this run generated a minima of C_{total}=1.83 at a 24 h average monoterpene emission of 0.15 mg m^{-2} h^{-1}, an isoprene emission of 0.18 mg m^{-2} h^{-1} and NO emission of 0.005 mg N m^{-2} h^{-1}.

Model output using these settings is shown in red in Fig. 5. The green line shows a model run with the same emission rates, but without the change in effective rate constant, so as to show the effect of the rate constant reduction more clearly. OH concentrations are ~50% higher, whilst the fit to isoprene is maintained. A substantial decrease in modelled isoprene emission is required to generate this fit. A possible justification for this could be venting out of the boundary layer, as the previous reason for not lowering isoprene emission, its concentration falling too low, is no longer relevant. However no data regarding isoprene flux out of the boundary layer is available to test this theory.

O_3 and NO_x concentrations are largely unaffected by this model scenario. The reduced quantity of oxidised VOC is evident in the modelled MACR/MVK concentrations which are reduced by 33% at midday, and in the HO_2+RO_2 and PAN concentrations, both of which are closer to the measurements. Some care however, must be taken in using the modelled MACR/MVK concentrations as support for the rate constant reduction due to the poorly understood loss processes for these compounds. Furthermore, it is possible that any physical process which impacts upon the rate of the OH+isoprene reaction may also affect the MACR/MVK+OH reaction.

At this point it is worth considering that, whilst OH recycling alone was shown not to be able to reconcile OH and isoprene concentrations in Sect. 6.1, in conjunction with a reduced rate of reaction, it might be able to consume some of the missing isoprene flux, that would otherwise have to be vented out of the boundary layer. If the standard reaction rate between isoprene/monoterpenes and OH is indeed too high, the extra isoprene loss this causes would have masked the need for some OH recycling in Sect. 6.1. This will be addressed further in Sect. 6.4.

6.4 Further discussion

In the analysis presented herein, isoprene concentrations are relatively low compared to other studies over a tropical rainforest. For example, Karl et al. (2007) report an average noon isoprene flux of 7.8 mg m^{-2} h^{-1}, around seven times larger than that during OP3-1, leading to a peak measured isoprene mixing ratio of ~7 ppbv. Modelled isoprene concentration for OP3-1 is approaching steady state after 8 days and is very close to the observations. However, entering the Karl et al. (2007) flux into the CiTTyCAT model causes mixing ratios of isoprene to accumulate to highly unrealistic levels of over 100 ppbv, clearly indicating an underestimation of the isoprene sinks. Note that this is not an attempt to simulate the Karl et al. (2007) regime, as differences in temperature, boundary layer dynamics, etc are not considered, and to do so would be beyond the scope of this paper. However, the extent of the isoprene accumulation can be explained by considering the relative contributions to OH production. Making the assumptions that every reaction of isoprene and OH regenerates one OH radical and other OH production is dominated by Reaction (R1),

$$O(^1D) + H_2O \rightarrow 2OH \quad (R4)$$

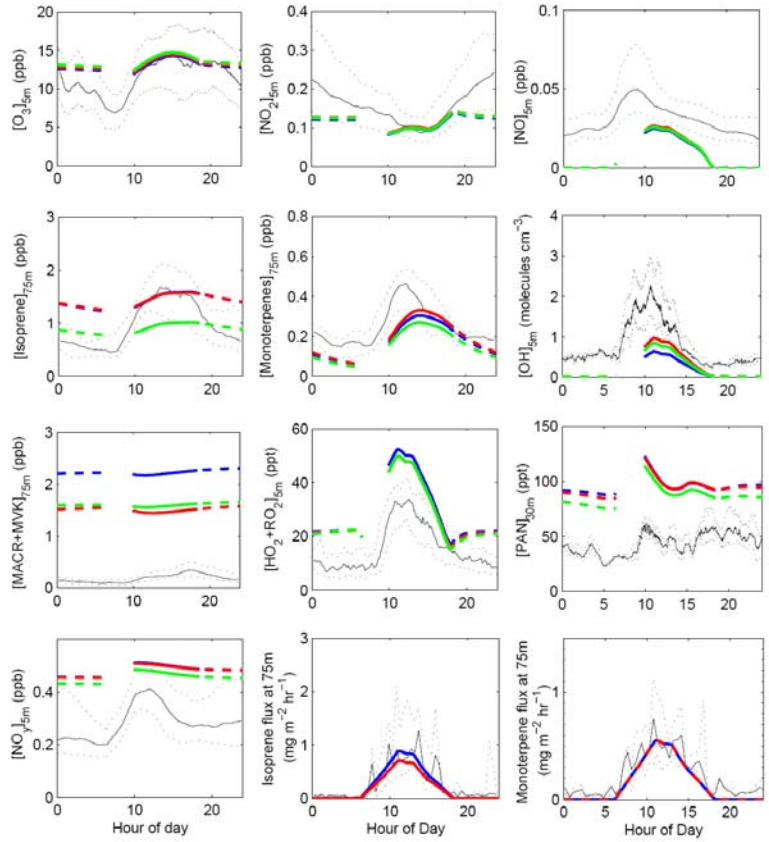

Fig. 5. Comparison of model output with the OP3-1 average measurements at Bukit Atur (black line). The blue line is the run shown in Fig. 2. The red line is a run with the isoprene+OH rate constant reduced by 50% and the emissions adjusted as per the best fit. The green line shows the effect of the emissions change alone.

it is possible to estimate the potential contribution of OH recycling to the overall OH production using,

$$\frac{\mathrm{OH_{prod}}}{dt} = 2(k_1[\mathrm{O^1D}][\mathrm{H_2O}]) + k_2[\mathrm{HO_2}][\mathrm{NO}] + k_3[\mathrm{Iso}][\mathrm{OH}] \quad (7)$$

where k_1, k_2 and k_3 are the rate constants for the respective reactions. Entering average midday measured concentrations (except for $O(^1D)$ and HO_2 where modelled concentrations are used in the absence of measurements), shows that 4.1×10^6 molecules OH cm^{-3} s^{-1} are contributed by Reactions (R4) and (R1), whilst 7.4×10^6 molecules OH cm^{-3} s^{-1} are contributed by isoprene+OH. Hence OH recycling via isoprene would contribute 64% of OH_{prod}. However, with an isoprene mixing ratio of 7 ppbv, and all other concentrations remaining equal, OH recycling via isoprene would contribute 32.2×10^6 molecules OH cm^{-3} s^{-1} or 89% of OH_{prod}. Of course these percentages will vary depending on the yield of OH assumed.

Hence OH recycling has the potential to dominate OH_{prod} in high isoprene environments, such as observed by Karl et al. (2007), where neglecting to consider it would be to potentially ignore the principal source of OH production. However, considering that a reduced effective rate constant for isoprene+OH may reduce the contribution of OH recycling by half, its effect in the regime measured during OP3-1 may be greatly reduced. Overall, it is clear from the results presented above, that whilst there may be an important role for unknown OH recycling in moderating modelled isoprene to reasonable levels in the most isoprene-rich tropical

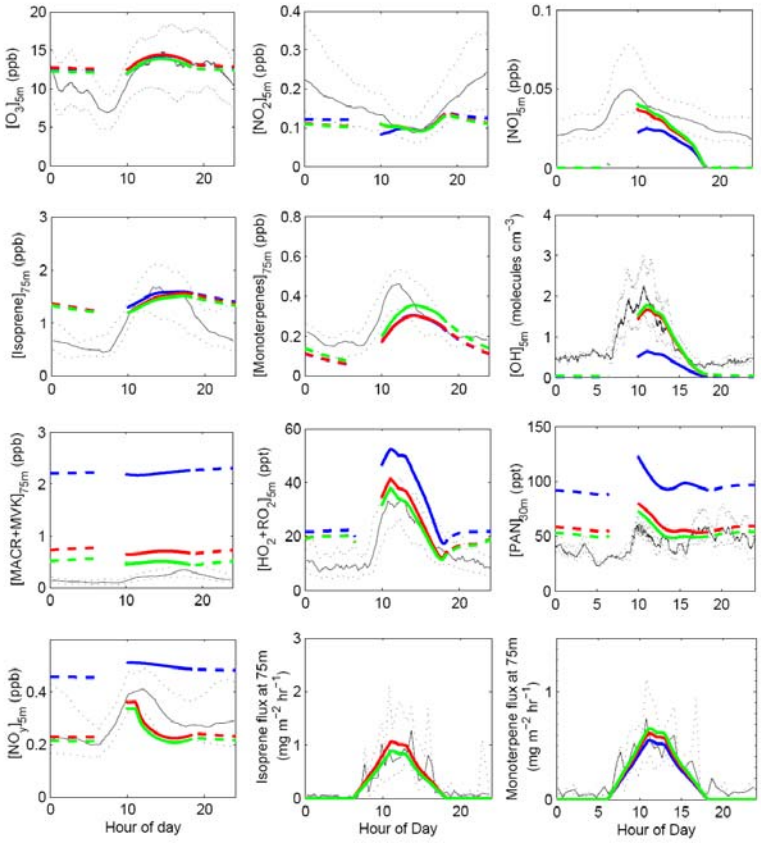

Fig. 6. Comparison of model output with the OP3-1 average measurements at Bukit Atur (black line). The blue line is the run shown in Fig. 2. The red line is shows S1 and the green line shows S2, as described in Sect. 6.4.

environments, it is not able to fully explain the modelled underestimation of [OH] in all cases.

Given that several factors presented herein have been able to affect the VOC+OH chemistry, a final sensitivity study of 10 000 runs is carried out, varying the effective rate of isoprene/monoterpenes+OH, $V_{d(MACR+MVK)}$, OH recycling via Reaction (R3) and emissions of isoprene, monoterpenes and NO. Wet deposition is also enabled. Two potential best fits are found in the parameter space. The reason for this behaviour being that both OH recycling in the isoprene oxidation scheme and greater deposition of MACR and MVK result in the required increase in OH. Therefore more information is required to determine the exact position of this balance.

The fit returned at $C_{total} = 1.11$, referred to below as S1, gives an effective rate for isoprene/monoterpenes+OH 50% of the IUPAC value, $V_{d(MACR+MVK)}$=1.5 cm s^{-1} and m=0.25. Emissions of isoprene and monoterpenes were 0.28 and 0.17 mg m^{-2} h^{-1} respectively, and those for NO, 0.007 mg N m^{-2} h^{-1}. The fit returned at C_{total} = 0.99, referred to below as S2, has the same rate constant reduction of 50% and the same NO emssion, but $V_{d(MACR+MVK)}$=2.5 cm s^{-1} and m=0.0. Emissions of isoprene and monoterpenes were 0.26 and 0.18 mg m^{-2} h^{-1} respectively. Analysis of the output concentrations shown in Fig. 6 demonstrates that both give a good fit within the measurement uncertainty.

There is a 71% (72%) reduction in the contribution of OH to C_{total} for S1 (S2), giving an MBE for OH of −9% (−5%), well within measurement uncertainty, whilst maintaining

isoprene and monoterpene fits. In Sect. 2 it was demonstrated that the 5-m OH measurements may underestimate boundary layer OH by up to 30%. The optimised model fit would still lie in the uncertainty bounds of the OH measurements for both S1 and S2 even if such a gradient in OH exists. Notably secondary species such as HO_2+RO_2, PAN and NO_y also show improved fits to the measurements, further demonstrating the importance of the physical processes considered to accurate simulations of the chemistry.

Although this study is unable to precisely define the relative contributions of MACR/MVK deposition and OH recycling, these results offer an improved explanation in many respects. Regardless of whether S1 or S2 is chosen, the measured emissions of isoprene and monoterpenes are fully accounted for, whilst the rate constant reduction of 50% required to generate the improved OH fit is the same as that suggested by Butler et al. (2008). Although such a reduction in rate is substantial, Krol et al. (2000) find rate reductions between a reactive hydrocarbon (RH) and OH up to 29.4% using a Large Eddy Simulation model with heterogeneous NO and VOC emissions. As the rate they utilise for the reaction of OH+RH is approximately one quarter of that between isoprene and OH at 298K (IUPAC, 2009), it is reasonable that even stronger segregation may exist for the latter reaction. Vinuesa and Vilà-Guerau de Arellano (2005) suggest a reduction of 40.5% for a reaction of OH+RH with a similar rate to isoprene+OH. When the stated 20% error in the isoprene+OH rate constant (IUPAC, 2009) is taken into account, the reductions here do not appear unreasonable. It is important to note that whilst the agreement with Butler et al. (2008) is good, this by no means infers that 50% rate constant reductions for isoprene/monoterpenes+OH should be applied in every situation. A different forest landscape, for instance one with a less varied distribution of NO or VOC emitting species or different turbulent mixing characteristics, might be expected to experience a different intensity of segregation.

An OH recycling fit of between m=0.0 and m=0.25 is small, demonstrating the magnitude of recycling required in this scenario is much less than has been suggested in other studies. However, it is close to the yield of m=0.22, calculated by Karl et al. (2009a) when they adjust the Peeters et al. (2009) mechanism to fit their field observations. Detailed analysis as to the source of such OH recycling is left to other papers in this issue. As for the rate constant reductions, these results are representative of the region studied and it is not necessarily the case that an unaccounted for yield of OH recycling should be the same for all regions. For instance the Hofzumahaus et al. (2009) recycling hypothesis mentioned earlier is based upon an as yet unidentified reduction agent similar to NO. The global or regional distribution of such an agent might vary considerably. In the case of an omission in the isoprene oxidation scheme (e.g. Lelieveld et al., 2008; Peeters et al., 2009), under the subtly different temperature and chemical conditions encountered in different regions, the yield along such a pathway might vary considerably.

7 Summary and conclusions

To our knowledge, this is the first modelling study of the chemistry occurring in the tropical rainforest PBL to utilise such a wide suite of ground-based measurements, including both [OH] measurements and VOC fluxes, to inform the modelling. It is also the first detailed model:measurement comparison over the relatively unstudied South-East Asian rainforest. The ability of the CiTTyCAT model to represent the broad features of atmospheric composition above a tropical rainforest has been demonstrated. In particular the model appears to perform robustly with respect to NO_x and O_3 chemistry. The potential to generate net fluxes of compounds into the PBL, utilising ambient concentration measurements has also been shown, and the technique may be applied to estimate fluxes where measurements are not available, or PBL venting where they are, assuming a sufficient knowledge of the local chemistry and mixing. However modelling chemistry above the South-East Asian rainforest is shown to suffer the same problems with reconciling BVOC and OH concentrations highlighted in other tropical modelling studies.

It has been shown that both dry and wet deposition of intermediate VOC oxidation products can have a very significant influence on both their concentrations and the oxidation capacity of the boundary layer. It is critical that further investigation into deposition processes over tropical forests is carried out, in order to reduce the uncertainties in these regions. The importance of considering micrometerological mixing processes when modelling compounds of intermediate atmospheric lifetime such as isoprene has also been highlighted.

In the light of the work presented here, it appears that inadequacies apparent in box and global model studies of tropical VOC chemistry may be more strongly influenced by representation of detailed physical and micrometeorological effects than by errors in the chemical scheme. Further measurement work is required to fully understand the nature of these processes, so that they may be accounted for effectively in future studies.

Acknowledgements. This work was funded by the Natural Environment Research Council (award NE/D0 02117/1). The authors would like to thank Brian Davison for organising the campaign logistics and Glen Reynolds and the Royal Society for the support they provided prior to and during the campaign. They also thank, T. Karl, L. Ganzeveld, J. Vila, R. Cohen, E. Browne, N. Carslaw and an annoymous reviewer for their comments on the manuscript and F. Davies and G. Pearson for their advice regarding the LIDAR measurements. They would also like to acknowledge all the members of the OP3 team who provided advice and discussion during this work. The cooperation of the Malaysian Meteorological Service in providing the Bukit Atur site is very gratefully appreciated. This is paper number 503 of the Royal Society's South East Asian Rainforest Research Programme.

Edited by: W. T. Sturges

References

Andreae, M. and Merlet, P.: Emissions of trace gases and aerosols from biomass burning, Global Biogeochem. Cy., 15, 955–966, 2001.

Atkinson, R. and Arey, J.: Gas-phase tropospheric chemistry of biogenic volatile organic compounds: a review, Atmos. Environ., 37, S197–S219, 2003.

Butler, T. M., Taraborrelli, D., Brühl, C., Fischer, H., Harder, H., Martinez, M., Williams, J., Lawrence, M. G., and Lelieveld, J.: Improved simulation of isoprene oxidation chemistry with the ECHAM5/MESSy chemistry-climate model: lessons from the GABRIEL airborne field campaign, Atmos. Chem. Phys., 8, 4529–4546, 2008, http://www.atmos-chem-phys.net/8/4529/2008/.

Carslaw, N., Creasey, D. J., Harrison, D., Heard, D. E., Hunter, M. C., Jacobs, P. J., Jenkin, M. E., Lee, J. D., Lewis, A. C., Pilling, M. J., Saunders, S. M., and Seakins, P. W.: OH and HO_2 radical chemistry in a forested region of north-western Greece, Atmos. Environ., 35, 4725–4737, 2001.

Carter, W. P. L. and Atkinson, R.: Development and evaluation of a detailed meachanism for the atmospheric reactions of isoprene and NO_X, Int. J. Chem. Kinet., 28, 497–530, 1996.

Chappell, N., Bidin, K., and Tych, W.: Modelling rainfall and canopy controls on net-precipitation beneath selectively-logged forest, Plant Ecol., 153, 215–229, 2001.

Chen, X., Hulbert, D., and Shepson, P. B.: Measurement of the organic nitrate yield from OH reaction with isoprene, J. Geophys. Res., 95, 22319–22341, 1998.

Cleveland, C. C. and Yavitt, J. B.: Consumption of atmospheric isopene in soil, Geophys. Res. Lett., 24, 2379–2382, 1997.

Cook, P., Savage, N., Turquety, S., Carver, G., O'Connor, F., Heckel, A., Stewart, D., Whalley, L., Parker, A., Schlager, H., Avery, H. S. M., Sachse, G., Brune, W., Richter, A., Burrows, J., Purvis, R., Lewis, A., Reeves, C., Monks, P., Levine, J., and Pyle., J.: Forest fire plumes over the North Atlantic: p-TOMCAT model simulations with aircraft and satellite measurements from the ITOP/ICARTT campaign, J. Geophys. Res., 112, D10S43, doi:10.1029/2006JD007563, 2007.

Dillon, T. J. and Crowley, J. N.: Direct detection of OH formation in the reactions of HO_2 with $CH_3C(O)O_2$ and other substituted peroxy radicals, Atmos. Chem. Phys., 8, 4877–4889, 2008, http://www.atmos-chem-phys.net/8/4877/2008/.

Donovan, R., Hope, E., Owen, S., Mackenzie, A., and Hewitt, C.: Development and Application of an Urban Tree Air Quality Score for Photochemical Pollution Episodes Using the Birmingham, United Kingdom, Area as a Case Study, Environ. Sci. Technol., 39, 6730–6738, 2005.

Edwards, P., Whalley, L. K., Heard, D. E., et al.: OH reactivity measurements in a South-East Asian tropical Rainforest, Atmos. Chem. Phys. Discuss., in preparation, 2010.

Eerdekens, G., Yassaa, N., Sinha, V., Aalto, P. P., Aufmhoff, H., Arnold, F., Fiedler, V., Kulmala, M., and Williams, J.: VOC measurements within a boreal forest during spring 2005: on the occurrence of elevated monoterpene concentrations during night time intense particle concentration events, Atmos. Chem. Phys., 9, 8331–8350, 2009, http://www.atmos-chem-phys.net/9/8331/2009/.

Emmerson, K. M., MacKenzie, A. R., Owen, S. M., Evans, M. J., and Shallcross, D. E.: A Lagrangian model with simple primary and secondary aerosol scheme 1: comparison with UK PM_{10} data, Atmos. Chem. Phys., 4, 2161–2170, 2004, http://www.atmos-chem-phys.net/4/2161/2004/.

Emmerson, K. M., Carslaw, N., Carpenter, L. J., Heard, D. E., Lee, J. D., and Pilling, M. J.: Urban Atmospheric Chemistry during the PUMA Campaign, 1: Comparison of Modelled OH and HO_2 Concentrations with Measurements, J. Atmos. Chem., 52(2), 143–164, 2005.

Emmerson, K. M., Carslaw, N., Carslaw, D. C., Lee, J. D., McFiggans, G., Bloss, W. J., Gravestock, T., Heard, D. E., Hopkins, J., Ingham, T., Pilling, M. J., Smith, S. C., Jacob, M., and Monks, P. S.: Free radical modelling studies during the UK TORCH Campaign in Summer 2003, Atmos. Chem. Phys., 7, 167–181, 2007, http://www.atmos-chem-phys.net/7/167/2007/.

Evans, M., Shallcross, D., Law, K., Wild, J., Simmonds, P., Spain, T., Berrisford, P., Methven, J., Lewis, A., McQuaid, J., Pilling, M., Bandy, B., Penkett, S., and Pyle, J.: Evaluation of a Lagrangian box model using field measurements from EASE (Eastern Atlantic Summer Experiment) 1996, Atmos. Environ., 34, 3843–3863, 2000.

Fisch, G., Tota, J., Machado, L. A. T., Silva Dias, M. A. F., da Lyra, R. F., Nobre, C. A., Dolman, A. J., and Gash, J. H. C.: The convective boundary layer over pasture and forest in Amazonia, Theor. Appl. Climatol., 78(1–3), 47–59, doi:10.1007/s00704-004-0043-x, 2004.

Farmer, D. K. and Cohen, R. C.: Observations of HNO_3, ΣAN, ΣPN and NO_2 fluxes: evidence for rapid HOx chemistry within a pine forest canopy, Atmos. Chem. Phys., 8, 3899–3917, 2008, http://www.atmos-chem-phys.net/8/3899/2008/.

Fuentes, J., Lerdau, M., Atkinson, R., Baldocchi, D., Bottenheim, J., Ciccioli, P., Lamb, B., Geron, C., Gu, L., Guenther, A., Sharkey, T., and Stockwell, W.: Biogenic hydrocarbons in the atmospheric boundary layer: A review, B. Am. Meteor. Soc., 81, 1537–1575, 2000.

Fuentes, J. D., Wang, D., Bowling, D. R., Potosnak, M., Monson, R. K., Goliff, W. S., and Stockwell, W. R.: Biogenic Hydrocarbon Chemistry within and Above a Mixed Deciduous Forest, J. Atmos. Chem., 56, 165–185, 2007.

Ganzeveld, L. N., Lelieveld, J. Dentener, F. J., Krol, M. C., Bouwman, A. J., and Roelofs, G.-J.: Global soil-biogenic NO_X emissions and the role of canopy processes, J. Geophys. Res., 107(D16), 4298, doi:10.1029/2001JD001289, 2002.

Ganzeveld, L., Eerdekens, G., Feig, G., Fischer, H., Harder, H., Königstedt, R., Kubistin, D., Martinez, M., Meixner, F. X., Scheeren, H. A., Sinha, V., Taraborrelli, D., Williams, J., Vilà-Guerau de Arellano, J., and Lelieveld, J.: Surface and boundary layer exchanges of volatile organic compounds, nitrogen oxides and ozone during the GABRIEL campaign, Atmos. Chem. Phys., 8, 6223–6243, 2008, http://www.atmos-chem-phys.net/8/6223/2008/.

George, L. A., Hard, T. M., and O'Brien, R. J.: Measurement of free radicals OH and HO_2 in Los Angeles smog, J. Geophys. Res., 104, 11643–11655, 1999.

Geyer, A. and Stutz, J.: The vertical structure of OH-HO_2-RO_2 chemistry in the nocturnal boundary layer: A one-dimensional model study, J. Geophys. Res., 109, D16301, doi:{10.1029/2003JD004425}, 2004.

Giacopelli, P., Ford, K., Espada, C. and Shepson, P. B.: Comparison of the measured and simulated isoprene nitrate distri-

butions above a forest canopy, J. Geophys. Res., 110, D01304, doi:10.1029/2004JD005123, 2005.

Guenther, A., Hewitt, C., Erickson, D., Fall, R., Geron, C., Graedel, T., Harley, P., Klinger, L., Lerdau, M., McKay, W., Pierce, T., Scholes, B., Steinbrecher, R., Tallamraju, R., Taylor, J., and Zimmerman, P.: A global model of natural volatile organic compound emissions, J. Geophys. Res., 100, 8873–8892, 1995.

Guenther, A., Karl, T., Harley, P., Wiedinmyer, C., Palmer, P. I., and Geron, C.: Estimates of global terrestrial isoprene emissions using MEGAN (Model of Emissions of Gases and Aerosols from Nature), Atmos. Chem. Phys., 6, 3181–3210, 2006, http://www.atmos-chem-phys.net/6/3181/2006/.

Hasson, A., Tyndall, G., and Orlando, J.: A product yield study of the reaction of HO_2 radicals with ethyl peroxy ($C_2H_5O_2$), acetyl peroxy ($CH_3C(O)O_2$), and acetonyl peroxy ($CH_3C(O)CH_2O_2$) radicals, J. Phys. Chem. A, 108, 5979–5989, doi:{10.1021/jp048873t}, 2004.

Hewitt, C. N., Lee, J. D., MacKenzie, A. R., Barkley, M. P., Carslaw, N., Carver, G. D., Chappell, N. A., Coe, H., Collier, C., Commane, R., Davies, F., Davison, B., DiCarlo, P., Di Marco, C. F., Dorsey, J. R., Edwards, P. M., Evans, M. J., Fowler, D., Furneaux, K. L., Gallagher, M., Guenther, A., Heard, D. E., Helfter, C., Hopkins, J., Ingham, T., Irwin, M., Jones, C., Karunaharan, A., Langford, B., Lewis, A. C., Lim, S. F., MacDonald, S. M., Mahajan, A. S., Malpass, S., McFiggans, G., Mills, G., Misztal, P., Moller, S., Monks, P. S., Nemitz, E., Nicolas-Perea, V., Oetjen, H., Oram, D. E., Palmer, P. I., Phillips, G. J., Pike, R., Plane, J. M. C., Pugh, T., Pyle, J. A., Reeves, C. E., Robinson, N. H., Stewart, D., Stone, D., Whalley, L. K., and Yin, X.: Overview: oxidant and particle photochemical processes above a south-east Asian tropical rainforest (the OP3 project): introduction, rationale, location characteristics and tools, Atmos. Chem. Phys., 10, 169–199, 2010, http://www.atmos-chem-phys.net/10/169/2010/.

Hewitt, C. N., MacKenzie, A. R., Di Carlo, P., Di Marco, C. F., Dorsey, J. R., Evans, M., Fowler, D., Gallagher, M. W., Hopkins, J. R., Jones, C. E., Langford, B., Lee, J. D., Lewis, A. C., Lim, S. F., McQuaid, J., Misztal, P., Moller, S. J., Monks, P. S., Nemitz, E., Oram, D. E., Owen, S. M., Phillips, G. J., Pugh, T. A. M., Pyle, J. A., Reeves, C. E., Ryder, J., Siong, J., Skiba, U., and Stewart, D. J.: Nitrogen management is essential to prevent tropical oil palm plantations from causing ground-level ozone pollution, P. Natl. Acad. Sci. USA, 106, 18447–18451, 2009.

Hofzumahaus, A., Rohrer, F., Lu, K., Bohn, B., Brauers, T., Chang, C.-C., Fuchs, H., Holland, F., Kita, K., Kondo, Y., Li, X., Lou, S., Shao, M., Zeng, L., Wahner, A., and Zhang, Y.: Amplified Trace Gas Removal in the Troposphere, Science, 324, 1702–1704, doi:{10.1126/science.1164566}, 2009.

Holzinger, R., Lee, A., Paw, K. T., and Goldstein, U. A. H.: Observations of oxidation products above a forest imply biogenic emissions of very reactive compounds, Atmos. Chem. Phys., 5, 67–75, 2005, http://www.atmos-chem-phys.net/5/67/2005/.

Horowitz, L. W., Fiore, A. M., Milly, G. P., Cohen, R. C., Perring, A., Wooldridge, P. J., Hess, P. G., Emmons, L. K., and Lamarque, J.-F.: Observational constraints on the chemistry of isoprene nitrates over the eastern United States, J. Geophys. Res., 112, doi:{10.1029/2006JD007747}, 2007.

Horii, C. V., Munger, J. W., Wofsy, S. C., Zahniser, M., Nelson, D., and McManus, J. B.: Atmospheric reactive nitrogen concentration and flux budgets at a northeastern US forest site, Agric. For. Meteorol., 136, 159—174, 2006.

IUPAC: Evaluated kinetic data, http://www.iupac-kinetic.ch.cam.ac.uk/, last access: 19th March 2009, 2009.

Jenkin, M.: Chemical Mechanisms forming condensable material, Tech. Rep. AEA/RAMP/2001 0010/002, AEA, 1996.

Jenkin, M. E., Hurley, M. D., and Wallington, T. J.: Investigation of the radical product channel of the $CH_3C(O)O_2$+HO_2 reaction in the gas phase, Phys. Chem. Chem. Phys., 9, 3149–3162, doi:{10.1039/b702757e}, 2007.

Kanaya, Y., Cao, R., Kato, S., Miyakawa, Y., Kajii, Y., Tanimoto, H., Yokouchi, Y., Mochida, M., Kawamura, K., and Akimoto, H.: Chemistry of OH and HO_2 radicals observed at Rishiri Island, Japan, in September 2003: Missing daytime sink of HO_2 and positive nighttime correlations with monoterpenes, J. Geophys. Res., 112, D11308, doi:10.1029/2006JD007987, 2007.

Karl, T., Potosnak, M., Guenther, A., Clark, D., Walker, J., Herrick, J., and Geron, C.: Exchange processes of volatile organic compounds above a tropical rain forest: Implications for modeling tropospheric chemistry above dense vegetation, J. Geophys. Res., 109, D18306, doi:{10.1029/2004JD004738}, 2004.

Karl, T., Guenther, A., Yokelson, R. J., Greenberg, J., Potosnak, M., Blake, D. R., and Artaxo, P.: The tropical forest and fire emissions experiment: Emission, chemistry, and transport of biogenic volatile organic compounds in the lower atmosphere over Amazonia, J. Geophys. Res., 112, D18302, doi:{10.1029/2007JD008539}, 2007.

Karl, T., Guenther, A., Turnipseed, A., Tyndall, G., Artaxo, P., and Martin, S.: Rapid formation of isoprene photo-oxidation products observed in Amazonia, Atmos. Chem. Phys., 9, 7753–7767, 2009, http://www.atmos-chem-phys.net/9/7753/2009/.

Karl, T.: Interactive comment on "Simulating atmospheric composition over a South-East Asian tropical rainforest: Performance of a chemistry box model" by T. A. M. Pugh et al., Atmos. Chem. Phys. Discuss., 9, C6470–C6473, 2009.

Kleffmann, J.: Daytime Sources of Nitrous Acid (HONO) in the Atmospheric Boundary Layer, Chem. Phys. Chem., 8, 1137–1144, 2007.

Konrad, S., Schmitz, Th., Buers, H.-J., Houben, N., Mannschreck, K., Mihelcic, D., Müsgen, P., Pätz, H.-W., Holland, F., Hofzumahaus, A., Schäfer, H.-J., Schröder, S., and Volz-Thomas, A.: Hydrocarbon measurements at Pabstthum during the BERLIOZ campaign and modelling of free radicals, J. Geophys. Res., 108, 8251, doi:10.1029/2001JD000866, 2003.

Krejci, R., Ström, J., de Reus, M., Williams, J., Fischer, H., Andreae, M. O., and Hansson, H.-C.: Spatial and temporal distribution of atmospheric aerosols in the lowermost troposphere over the Amazonian tropical rainforest, Atmos. Chem. Phys., 5, 1527-1543, 2005, http://www.atmos-chem-phys.net/5/1527/2005/.

Krol, M., Molemaker, M., and de Arellano, J.: Effects of turbulence and heterogeneous emissions on photochemically active species in the convective boundary layer, J. Geophys. Res., 105, 6871–6884, 2000.

Kubistin, D., Harder, H., Martinez, M., Rudolf, M., Sander, R., Bozem, H., Eerdekens, G., Fischer, H., Gurk, C., Klüpfel, T., Knigstedt, R., Parchatka, U., Schiller, C. L., Stickler, A.,

Taraborrelli, D., Williams, J., and Lelieveld, J.: Hydroxyl radicals in the tropical troposphere over the Suriname rainforest: comparison of measurements with the box model MECCA, Atmos. Chem. Phys. Discuss., 8, 15239–15289, 2008, http://www.atmos-chem-phys-discuss.net/8/15239/2008/.

Kuhn, U., Rottenberger, S., Biesenthal, T., Wolf, A., Schebeske, G., Ciccioli, P., Brancaleoni, E., Frattoni, M., Tavares, T., and Kesselmeier, J.: Seasonal differences in isoprene and light-dependent monoterpene emission by Amazonian tree species, Glob. Change Biol., 10, 663–682, doi:{10.1111/j.1529-8817.2003.00771.x}, 2004.

Kuhn, U., Andreae, M. O., Ammann, C., Araújo, A. C., Brancaleoni, E., Ciccioli, P., Dindorf, T., Frattoni, M., Gatti, L. V., Ganzeveld, L., Kruijt, B., Lelieveld, J., Lloyd, J., Meixner, F. X., Nobre, A. D., Pöschl, U., Spirig, C., Stefani, P., Thielmann, A., Valentini, R., and Kesselmeier, J.: Isoprene and monoterpene fluxes from Central Amazonian rainforest inferred from tower-based and airborne measurements, and implications on the atmospheric chemistry and the local carbon budget, Atmos. Chem. Phys., 7, 2855–2879, 2007, http://www.atmos-chem-phys.net/7/2855/2007/.

Langford, B., Davison, B., Nemitz, E., and Hewitt, C. N.: Mixing ratios and eddy covariance flux measurements of volatile organic compounds from an urban canopy (Manchester, UK), Atmos. Chem. Phys., 9, 1971–1987, 2009, http://www.atmos-chem-phys.net/9/1971/2009/.

Langford, B., Misztal, P., Nemitz, E., Davison, B., Helfter, C., Lee, J., MacKenzie, A. R., and Hewitt, C. N.: Fluxes of volatile organic compounds from a south-east Asian tropical rainforest, Atmos. Chem. Phys. Discuss., in preparation, 2010.

Lelieveld, J., Butler, T. M., Crowley, J. N., Dillon, T. J., Fischer, H., Ganzeveld, L., Harder, H., Lawrence, M. G., Martinez, M., Taraborrelli, D., and Williams, J.: Atmospheric oxidation capacity sustained by a tropical forest, Nature, 452, 737–740, doi:{10.1038/nature06870}, 2008.

Martin, C. L., Fitzjarrald, D., Garstang, M., Oliveira, S. P., Greco, S., and Browell, E.: Structure and growth of the mixing layer over the Amazonian rain forest, J. Geophys. Res., 93, 1361–1375, 1988.

Martinez, M., Harder, H., Kubistin, D., Rudolf, M., Bozem, H., Eerdekens, G., Fischer, H., Gurk, C., Klüpfel, T., Königstedt, R., Parchatka, U., Schiller, C. L., Stickler, A., Williams, J., and Lelieveld, J.: Hydroxyl radicals in the tropical troposphere over the Suriname rainforest: airborne measurements, Atmos. Chem. Phys. Discuss., 8, 15491–15536, 2008, http://www.atmos-chem-phys-discuss.net/8/15491/2008/.

Misztal, P. K., Nemitz, E., Langford, B., Coyle, M., Ryder, J., DiMarco, C., Phillips, G., Oram, D., Owen, S., and Cape, J. N.: First direct ecosystem fluxes of VOCs from oil palms in SE Asia, Atmos. Chem. Phys. Discuss., in preparation, 2010.

Murphy, J. G., Day, D. A., Cleary, P. A., Wooldridge, P. J., Millet, D. B., Goldstein, A. H., and Cohen, R. C.: The weekend effect within and downwind of Sacramento – Part 1: Observations of ozone, nitrogen oxides, and VOC reactivity, Atmos. Chem. Phys., 7, 5327–5339, 2007, http://www.atmos-chem-phys.net/7/5327/2007/.

Müller, J.-F., Stavrakou, T., Wallens, S., De Smedt, I., Van Roozendael, M., Potosnak, M. J., Rinne, J., Munger, B., Goldstein, A., and Guenther, A. B.: Global isoprene emissions estimated using MEGAN, ECMWF analyses and a detailed canopy environment model, Atmos. Chem. Phys., 8, 1329–1341, 2008, http://www.atmos-chem-phys.net/8/1329/2008/.

Ohara, T., Akimoto, H., Kurokawa, J., Horii, N., Yamaji, K., Yan, X., and Hayasaka, T.: An Asian emission inventory of anthropogenic emission sources for the period 19802020, Atmos. Chem. Phys., 7, 4419–4444, 2007, http://www.atmos-chem-phys.net/7/4419/2007/.

Paulot, F., Crounse, J. D., Kjaergaard, H. G., Kroll, J. H., Seinfeld, J. H., and Wennberg, P. O.: Isoprene photooxidation: new insights into the production of acids and organic nitrates, Atmos. Chem. Phys., 9, 1479–1501, 2009, http://www.atmos-chem-phys.net/9/1479/2009/.

Pearson, G. and et al.: Remote sensing of the tropical rain forest boundary layer using pulsed Doppler lidar, Atmos. Chem. Phys. Discuss., in preparation, 2010.

Peeters, J., Nguyen, T. L., and Vereecken, L.: HO_X radical regeneration in the oxidation of isoprene, Phys. Chem. Chem. Phys., 11, 5935–5939, doi:{10.1039/b908511d}, 2009.

Pegoraro, E., Rey, A., Abrell, L., Vanharen, J. and Lin, G.: Drought effect on isoprene production and consumption in Biosphere 2 tropical rainforest, Glob. Change Biol., 12, 456–469, doi:10.1111/j.1365-2486.2006.01112.x, 2006.

Pike, R. C., Lee, J. D., Young, P. J., Moller, S., Carver, G. D., Yang, X., Misztal, P., Langford, B., Stewart, D., Reeves, C. E., Hewitt, C. N., and Pyle, J. A.: Can a global model chemical mechanism reproduce NO, NO_2, and O_3 measurements above a tropical rainforest?, Atmos. Chem. Phys. Discuss., 9, 27611–27648, 2009, http://www.atmos-chem-phys-discuss.net/9/27611/2009/.

Pinho, P., Pio, C., and Jenkin, M.: Evaluation of isoprene degradation in the detailed tropospheric chemical mechanism, MCM v3, using environmental chamber data, Atmos. Environ., 39, 1303–1322, doi:{10.1016/j.atmosenv.2004.11.014}, 2005.

Poisson, N., Kanakidou, M., and Crutzen, P.: Impact of non-methane hydrocarbons on tropospheric chemistry and the oxidizing power of the global troposphere: 3-dimensional modelling results, J. Atmos. Chem., 36, 157–230, 2000.

Pugh, T. and et al.: Nocturnal profiles of NO_X and O_3 over a South-East Asian rainforest, in preparation, 2010.

Real, E., Law, K. S., Schlager, H., Roiger, A., Huntrieser, H., Methven, J., Cain, M., Holloway, J., Neuman, J. A., Ryerson, T., Flocke, F., de Gouw, J., Atlas, E., Donnelly, S., and Parrish, D.: Lagrangian analysis of low altitude anthropogenic plume processing across the North Atlantic, Atmos. Chem. Phys., 8, 7737–7754, 2008, http://www.atmos-chem-phys.net/8/7737/2008/.

Ren, X., Brune, W.H., Oliger, A., Metcalf, A.R., Simpas, J.B., Shirley, T., Schwab, J.J., Bai, C., Roychowdhury, U., Li, Y., Cai, C., Demerjian, K.L., He, Y., Zhou, X., Gao, H., and Hou, J.: OH, HO_2, and OH reactivity during the PMTACS-NY Whiteface Mountain 2002 campaign: Observations and model comparison, J. Geophys. Res., 111, D10S03, doi:10.1029/2005JD006126, 2006.

Ren, X., Olson, J. R., Crawford, J. H., Brune, W. H., Mao, J., Long, R. B., Chen, Z., Avery, M. A., Sachse, G. W., Barrick, J. D., Diskin, G. S., Huey, L. G., Fried, A., Cohen, R. C., Heikes, B., Wennberg, P. O., Singh, H. B., Blake, D. R. and Shetter, R. E.: HO_X chemistry during INTEX-A 2004: Observation, model calculation, and comparison with previous studies, J. Geophys.

Res., 113, D05310, doi:10.1029/2007JD009166, 2008.

Rosen, R. S., Wood, E. C., Wooldridge, P. J., Thornton, J. A., Day, D. A., Kuster, W., Williams, E. J., Jobson, B. T., and Cohen, R. C.: Observations of total alkyl nitrates during Texax Air Quality Study 2000: Implications of O_3 and alkyl nitrate photochemistry, J. Geophys. Res., 109, D07303, doi:10.1029/2003JD004227, 2004.

Sander, R.: Compilation of Henry's Law Constants for Inorganic and Organic Species of Potential Importance in Environmental Chemistry (Version 3), online available at: http://www.henrys-law.org, 2009.

Saunders, S. M., Jenkin, M. E., Derwent, R. G., and Pilling, M. J.: Protocol for the development of the Master Chemical Mechanism, MCM v3 (Part A): tropospheric degradation of non-aromatic volatile organic compounds, Atmos. Chem. Phys., 3, 161–180, 2003, http://www.atmos-chem-phys.net/3/161/2003/.

Schmitt, C., Belokurov, A., Besancon, C., Boisrobert, L., Burgess, N. D., Campbell, A., Coad, L., Fish, L., Gliddon, D., Humphries, K., Kapos, V., Loucks, C., Lysenko, I., Miles, L., Mills, C., Minnemeyer, S., Pistorius, T., Ravilious, C., and Winkel, G.: Global Ecological Forest Classification and Forest Protected Area Gap Analysis: Analyses and Recommendations in view of the 10% target for forest protection under the Convention on Biological Diversity (CBD), Freiburg University Press, Freiburg, Germany, 2008.

Shepson, P. B., Mackay, E., and Muthuramu, K.: Henry's law constants and removal processes for several atmospheric β-hydroxy alkyl nitrates, Enivron. Sci. Technol., 30, 3618–3623, 1996.

Sprengnether, M., Demerjian, K. L., Donahue, N. M., and Anderson, J. G.: Product analysis of the OH oxidation of isoprene and 1,3-butadiene in the presence of NO, J. Geophys. Res., 107, 4269, doi:10.1029/2001JD000716, 2002.

Stockwell, W., Kirchner, F., Kuhn, M., and Seefeld, S.: A new mechanism for regional atmospheric chemistry modeling, J. Geophys. Res., 102, 25847–25879, 1997.

Strong, J., Whyatt, J. D., Hewitt, C. N. and Derwent, R. G.: Development and application of a Lagrangian model to determine the origins of ozone episodes in the UK, Atmos. Environ., doi:10.1016/j.atmosenv.2009.11.019, in press, 2009.

Tan, D., Faloona, I., Simpas, J., Brune, W., Olson, J., Crawford, J., Avery, M., Sachse, G., Vay, S., Sandholm, S., Guan, H., Vaughn, T., Mastromarino, J., Heikes, B., Snow, J., Podolske, J., and Singh, H.: OH and HO_2 in the tropical Pacific: Results from PEM-Tropics B, J. Geophys. Res., 106, 32667–32681, 2001.

Tangki, H. and Chappell, A.: Biomass variation across selectively logged forest within a 225-km^2 region of Borneo and its prediction by Landsat TM, Forest Ecol. Manag., 256, 1960–1970, 2008.

Taraborrelli, D., Lawrence, M. G., Butler, T. M., Sander, R., and Lelieveld, J.: Mainz Isoprene Mechanism 2 (MIM2): an isoprene oxidation mechanism for regional and global atmospheric modelling, Atmos. Chem. Phys., 9, 2751–2777, 2009, http://www.atmos-chem-phys.net/9/2751/2009/.

Thornton, J. A., Wooldridge, P. J., Cohen, R. C., Martinez, M., Harder, H., Brune, W. H., Williams, E. J., Roberts, J. M., Fehsenfeld, F. C., Hall, S. R., Shetter, R. E., Wert, B. P., and Fried, A.: Ozone production rates as a function of NO_X abundances and HO_X production rates in the Nashville urban plume, J. Geophys. Res., 107(D12), 4146, doi:10.1029/2001JD000932, 2002.

Treves, K., Shragina, L., and Rudich, Y.: Henry's Law Constants of some β-, γ-, and δ-Hydroxy Alkyl Nitrates of Atmospheric Interest, Environ. Sci. Technol., 34, 1197–1203, 2000.

Tucker, A. C., Brewer, W. A., Banta, R. M., Senff, C. J., Sandberg, S. P., Law, D. C., Weickmann, A. M. and Hardesty, R. M.: Doppler Lidar Estimation of Mixing Height Using Turbulence, Shear, and Aerosol Profiles, J. Atmos. Ocean Tech., 26, 673–688, 2009.

Turnipseed, A. A., Huey, L. G., Nemitz, E., Stickel, R., Higgs, J., Tanner, D. J., Slusher, D. L., Sparks, J. P., Flocke, F., and Guenther, A.: Eddy covariance fluxes of peroxyacetyl nitrates (PANs) and NO_y to a coniferous forest, J. Geophys. Res., 111, D09304, doi:10.1029/2005JD006631, 2006.

van Dijk, S. and Duyzer, J.: Nitric oxide emissions from forest soils, J. Geophys. Res., 104, 15955–15961, 1999.

Vinuesa, J.-F. and Vilà-Guerau de Arellano, J.: Introducing effective reaction rates to account for the inefficient mixing of the convective boundary layer, Atmos. Environ., 39, 445–461, 2005.

Walsh, R. P. D.: Climate, The Tropical Rain Forest, edited by: Richards, P. W., Cambridge University Press, Cambridge, 159–205, 352 pp., 1996.

Whalley, L. K., Furneaux, K. L., Edwards, P. E., Heard, D. E.: The chemistry of OH and HO_2 in a tropical rainforest, Atmos. Chem. Phys. Discuss., in preparation, 2010a.

Whalley, L. K., Furneaux, K. L., Edwards, P. E., and Heard, D. E.: Resolving the missing OH source in forested regions, Geophys. Res. Lett., in preparation, 2010b.

Wild, O., Law, K., McKenna, D., Bandy, B., Penkett, S., and Pyle, J.: Photochemical trajectory modeling studies of the North Atlantic region during August 1993, J. Geophys. Res., 101, 29269–29288, 1996.

WMO: Scientific assessment of ozone depletion: 1995 Global Ozone Research and Monitoring Project, Geneva, Switzerland, 1995.

Yienger, J. and Levy, H.: Empirical model of global soil biogenic NO_X emissions, J. Geophys. Res., 100, 11447–11464, 1995.

Zhang, L., Moran, M., Maker, P., Brook, J., and Gong, S.: Modelling gaseous dry deposition in AURAMS: a unified regional air-quality modelling system, Atmos. Environ., 36, 537–560, 2002.